

Reactions of Hydrosilanes with Transition Metal Complexes and Characterization of the Products

Joyce Y. Corey*

Department of Chemistry and Biochemistry, University of Missouri—St. Louis, Missouri 63121

Received November 4, 2009

Contents

1. Introduction	864	5.3.5. $[\text{RuH}_2\{\eta^2\text{-HSiMe}_2\}_2\text{X}](\text{PCy}_3)_2$ ($\text{X} = \text{C}_6\text{H}_4$, 3-127) and $\text{RuH}_3(\text{SiMeCl}_2)(\text{PPh}_3)_3$, 3-124 : Interpreting Longer-Range Ru—H...Si Interactions	976
2. Background	865	5.3.6. $\text{Cp}_2\text{Nb}(\text{H})(\text{SiMe}_2\text{H})(\text{SiMe}_2\text{Cl})$: IHI, Another Interpretation of Long-Range Interactions, The Role of Calculations, and Persistence of Interactions in Solution	976
3. Reactions of Hydrosilanes with Transition Metal Complexes	867	5.4. Complexes with Si—H...TM Interactions	977
3.1. Types of Ligands at the Metal and Substituents at Silicon	923	5.4.1. σ -Complexes	977
3.2. Ligand Loss	926	5.4.2. α -, β -, and Other Long-Range Agostic Interactions	997
3.2.1. Phosphines	927	5.4.2.1. α -Agostic Interactions	997
3.2.2. Carbonyl(s) or Carbonyl Units	928	5.4.2.2. β -Agostic Interactions	998
3.2.3. Olefin or Acetylene	930	5.4.2.3. γ -Agostic Interactions and Beyond	1000
3.2.4. Coordinated Solvent	932	5.5. M—H...Si Interactions	1001
3.2.5. H_2	932	5.5.1. IHI Interactions	1001
3.3. Exchange of Anionic Ligands: Preparation from TM—R, TM—H, and TM—Si	933	5.5.2. SISHA Interactions	1004
3.3.1. TM—R Precursors	933	5.5.3. Hydrides That Span Metal—Silicon Multiple Bonds	1007
3.3.2. TM—H Precursors	936	5.6. Miscellaneous Examples and Unclassified Cases	1008
3.3.3. TM—Si Precursors	937	5.6.1. Additional SISHA Examples	1008
3.4. Addition of Silanes to Metals and to Low-Valent Metal Complexes	939	5.6.2. SiH_4 and M_{atoms}	1009
3.5. Reactions of Polynuclear Metal Complexes with Silanes	941	5.6.3. Unclassified Complexes	1010
3.6. Miscellaneous Methods	943	5.7. Summary	1011
3.6.1. Reactions Providing Polynuclear Metal Complexes from Mononuclear Systems	944	6. Solution Processes Determined from NMR Data	1011
3.6.2. Formation of Silylene Complexes	946	6.1. Monometallic Hydride Complexes	1011
3.6.3. Reactions of Silanes and Other Substrates with $[\text{TM}]=\text{X}$	949	6.1.1. $\text{H}_b\text{—}[\text{TM}]\text{—SiH}_{a(\text{term})} \rightleftharpoons \text{H}_a\text{—}[\text{TM}]\text{—SiH}_{b(\text{term})}$ and Related Intramolecular RE in $\text{H—}[\text{TM}]\text{—SiR}_3$ Cases (Intramolecular Processes)	1012
3.6.4. Reactions at Silyl Substituents	950	6.1.2. $\text{H}_a[\text{TM}](\sigma\text{-H}_b\text{—Si}) \rightleftharpoons \text{H}_b[\text{TM}]\text{M}(\sigma\text{-H}_a\text{—Si})$	1013
3.7. Transfer of Hydride from Si to TM	951	6.1.3. $\text{H}[\text{TM}]\text{SiH} < \rightleftharpoons [\text{TM}] + \text{H}_2\text{Si} <$	1015
3.8. Summary	953	6.1.4. $\text{H}_a[\text{TM}]\text{H}_b$ or $[\text{TM}]\text{H}_a\text{H}_b\text{Si}$ Exchange	1016
4. Solid-State Structures	954	6.1.5. $[\text{TM}]\text{—}\sigma\text{-H}_a\text{—Si—H}_{b(\text{term})} \rightleftharpoons [\text{TM}]\text{—}\sigma\text{-H}_b\text{—Si—H}_{a(\text{term})}$ or Two Diastereotopic $\text{SiH}_{(\text{term})}$	1017
5. Nonclassical Interactions	971	6.1.6. $\text{H—}[\text{TM}]\text{—Si} \rightleftharpoons \text{Si—}[\text{TM}]\text{—H}$	1018
5.1. General Comments on X-ray Data	972	6.2. Bimetallic Metal Hydride Complexes	1018
5.2. General Comments for NMR and IR Data	973	6.2.1. Si— H_{term} and Si— $\text{H}_{\text{br}}\text{—M}$ Exchange	1018
5.3. Categories of Nonclassical Interactions and Selected Examples	973	6.2.2. M— H_{term} and Si— $\text{H}_{\text{br}}\text{—M}$ exchange	1019
5.3.1. Tautomeric Equilibrium between η^2 -Silane and OA.	974	6.2.3. Si— $\text{H}_{\text{br}}\text{—M}$ and M— $\text{H}_{\text{br}}\text{—M}$ Exchange	1019
5.3.2. $\text{Tp}(\text{PPh}_3)\text{Ru}''\text{H}_2\text{SiR}_3''$ [$\text{Tp} = \text{hydridotris}(\text{pyrazolyl})\text{borate}$]: $\text{Ru}(\eta^2\text{-H}_2)$ or $\text{Ru}(\eta^2\text{-H-Si})$?	974	6.2.4. Exchange of M— $(\text{H}_{\text{br}})_2\text{—M}$	1020
5.3.3. $[\text{Cp}(\text{Me}_3\text{P})_2\text{Ru}(\eta^2\text{-H—SiCl}_3)]^+[\text{BAR}_4^f]$, Ru—H, or $\eta^2\text{-H—Si}$ and the Role of the $^2J_{(\text{SiH})}$ Coupling Constant	975	6.3. Miscellaneous Processes	1020
5.3.4. $\text{Cp}^*(\text{dmpe})\text{Mo}(\text{H})(\text{SiR}_2)$, ($\text{R} = \text{Et}$, 2-10): What Is the Role of the Hydride?	975	6.3.1. Exchange of a Classical Silyl Ligand with Added Silane	1020
		6.3.2. Exchange through M=Si Intermediates	1020

* E-mail: corey@umsl.edu.

6.3.3. Hindered M—Si Rotation	1022
6.3.4. Isomerization in Square-Planar Complexes	1022
6.3.5. Isomerization in 5- and 6-Coordinate Geometries	1023
7. Bonding and Calculations	1023
7.1. σ -Complexes: Comparison of H ₂ and HSi	1023
7.2. Long-Range Bonding Interactions	1024
7.3. Theoretical Calculations: Specific Cases	1024
7.3.1. Ti Triad	1024
7.3.2. V Triad	1025
7.3.3. Cr Triad	1028
7.3.4. Mn Triad	1031
7.3.5. Fe Triad	1033
7.3.6. Cobalt Triad	1039
7.3.7. Nickel Triad	1042
7.3.7.1. Mononuclear Complexes	1042
7.3.7.2. Dinuclear Complexes	1044
7.3.7.3. Oxidative Addition and Reductive Elimination	1045
7.3.7.4. Silylene Complexes	1047
7.3.7.5. Cases from Tables 1, 2, and 3	1048
7.3.8. Cu	1049
8. Oxidative Addition Reactions of Other Si—X Bonds	1050
8.1. Lanthanides/Actinides	1050
8.1.1. Silyl Complexes of Lanthanides/Actinides	1050
8.1.2. Reactions That Involve Transfer of Hydride from Hydrosilanes	1050
8.1.3. Complexes with β -H...Si interactions	1052
8.1.4. Theoretical Calculations	1054
8.2. Oxidative Additions of Other Si—El Bonds	1055
8.2.1. Si—Si Bonds	1055
8.2.2. Si—C bonds	1058
8.2.3. Si—El (El = Sn, B, S)	1060
8.2.4. SiX (X = Halogen)	1060
9. Conclusion	1061
10. Acknowledgments	1063
11. Supporting Information Available	1063
12. References	1063

1. Introduction

Hydrosilanes are used as versatile coreactants in the generation of silyl—metal complexes. Since organohydrosilanes may contain one, two, or three SiH bonds as tertiary, secondary, and primary silanes, respectively, there are many product variations upon their reaction with transition metal (TM) complexes.¹ The interaction of a SiH bond with the transition metal center may range from a weak σ -interaction (generally a three-centered bond), where hydrogen forms a bonding interaction with both the silicon and the metal center, to full oxidative addition, where there are two-electron—two-centered bonds between the metal and both the hydrogen and the silicon. Thus, the most widely employed approach to the formation of complexes that contain a silicon-to-transition metal bond involves reaction of a hydrosilane precursor. This review will summarize the publications that concern the reaction of hydrosilanes with transition metal complexes as reported during the years 1998–2008 in Chemical Abstracts.

A coordinatively unsaturated metal precursor is required for oxidative addition to lead to the isolation of stable H[TM]Si complexes. However, straightforward oxidative



Joyce Y. Corey completed a B.S. in Chemistry and an M.S. in Organic Chemistry at the University of North Dakota and a Ph.D. in Inorganic Chemistry at the University of Wisconsin—Madison in 1964 under the direction of Robert West. After a four year period at Villa Madonna College in Covington, KY, she joined the faculty at the University of Missouri—St. Louis, was promoted to Professor in 1980, and retired from classroom teaching in 2008. Over a 45 year period, she directed research in various aspects of organosilicon chemistry varying from the synthesis of silicon analogues of drugs to the development of transition metal promoted reactions of hydrosilanes including homocoupling and hydrosilylation reactions.

addition may not be the only pathway taken during the interaction of HSi with a metal complex. For example, R[TM] (where R is an organic group) can react with HSiR₃ with elimination of RH and formation of R₃Si[TM]. The product may arise from oxidative addition of HSi followed by elimination of RH, or it could occur through a σ -bond metathesis pathway, although this reaction route appears to be less common for electron-rich metals. For the most part, the emphasis of this review update will continue to be on complexes that have been isolated and characterized. However, in some cases, the products of reaction of [TM] with HSiR₃ were too unstable to be isolated but could be adequately characterized spectroscopically, and such examples are also included.

Other synthetic routes have been utilized to generate silyl—transition metal complexes, and a few examples that have been published during the current review period will be included as illustrations in the Background section. Section 3, the synthesis section, will focus on the complexes formed with primary, secondary, and tertiary silanes as well as from silane itself. Characterization data for representative complexes from a given publication are summarized in Tables 1–3 and are organized in the tables according to the metal triad, starting with the early transition metals. If more than one complex of a single type was reported, additional derivatives will be found listed in the footnotes to the tables. The rare examples of the corresponding silyl—lanthanide complexes will be found at the end of Table 1. Silyl complexes with both 2c/2e bonds as well as those with 3c/2e bonds are included in Tables 1–3. Complexes that have been reported to contain more remote HSi...TM (β - through ε -interactions) are also rare and, during this review period, occur primarily for early transition metals and lanthanides. The examples found for lanthanides are summarized later in section 8 of the review. The representations of these weak interactions have not been standardized and are generally shown in this review as depicted by the original author. Occasionally the hydrosilane reactant acts as a reducing agent

Sc	Ti	V	Cr	Mn	Fe	Co	Ni	<i>Cu</i> ^a	<i>Zn</i> ^b
Y	Zr	Nb	Mo	<i>Tc</i> ^c	Ru	Rh	Pd	<i>Ag</i> ^c	<i>Cd</i> ^b
<i>La</i> ^d	<i>Hf</i> ^a	Ta	W	Re	Os	Ir	Pt	Au	Hg

a. No new examples during the review period. b. Observed in matrix studies. c. No known examples. d. Only complexes containing β -H-Si interactions have been reported (Table 17).

Figure 1. Transition metal complexes that react with hydrosilanes to form isolable silyl-metal compounds as reported during this review period.

and produces a metal hydride. Examples of this type of reactivity are provided in Table 5.

In section 4, the solid state structures are summarized, and Table 6 provides information for the [TM]–H, Si–H, and [TM]–Si bond distances for all complexes in Tables 1, 2, and 3 that were crystallographically characterized, including examples from the footnotes to the indicated tables. Footnotes to Table 6 give TM–Si bond distances for any additional derivatives not prepared from hydrosilanes that were characterized by X-ray crystallography in the references associated with Tables 1–3 as well as for complexes prepared by other routes and reported in the Cambridge Structural Database. When the structure cannot be reasonably deduced from the formula provided, depiction of selected examples appear at the end of Tables 1–3 and 9. Many of the complexes that appear in Tables 1–3 exhibit both σ -type (η^2 -HSiR₃) and β - through ϵ -agostic (M–X–Si–H) interactions where NMR data including coupling constants become a key factor in the structural assignment. These data will be summarized in section 5 (and in Table 9). Also discussed in section 6 are complexes that exhibit fluxional behavior as demonstrated by variable-temperature NMR experiments, and when provided, a proposed mechanism for the fluxional behavior will be presented.

One of the aspects in the study of silyl-metal complexes that has changed since the previous review is the prevalence of calculations that appear not only in synthesis and characterization papers but also in reports that are devoted solely to calculations. These are both included in section 7, and Tables 1–3 and 9 also indicate reports of calculations in the “other characterization” column in the tables. Some calculations are included in section 5 where support for a particular Si···H···TM interaction was required.

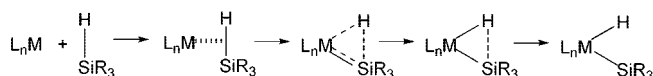
Although the current review is focused on the oxidative addition reactions of SiH bonds with transition metal complexes, there are other Si–X bonds that also appear to undergo oxidative addition to metal centers. Examples include Si–C, Si–X (X = halogen), Si–Si, and Si–El (El = heteroatom) bonds, and these are included in section 8 and in Table 18.

The study of the reactivity of hydrosilanes with transition metal complexes is an active area as reflected in the approximately 800 references that cover an 11-year period and are found at the end of the review.

2. Background

The versatility of hydrosilane reactants as precursors to silyl-metal complexes is illustrated by Figure 1. Silyl-metal complexes formed from hydrosilanes and elements that are in bold type in Figure 1 will be found in Tables 1–3. Of the transition metals illustrated, Hf and Cu complexes also react with hydrosilanes,¹ but no new examples were reported during the current review period. Occasionally, reaction of

Scheme 1



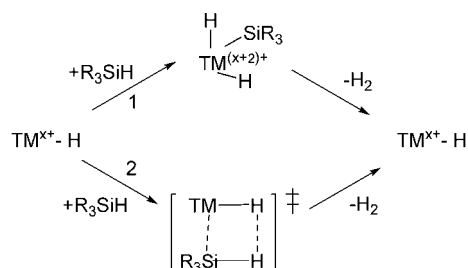
a metal complex with a hydrosilane results in formation of a metal hydride with no [TM]–Si bonds. These cases are summarized in Table 4.

When a hydrosilane oxidatively adds to a metal center, the oxidation state of the metal increases as does the coordination number.² The reverse process, reductive elimination of a hydrosilane, may also occur, lowering the oxidation state and opening a coordination site. Both of these classes of reactions have been invoked in many catalytic and stoichiometric reactions, particularly those that involve H–H, C–H, or Si–H bonds. Oxidative addition reactions of hydrosilanes are more facile than those of hydrocarbons and will often occur at room temperature. With late metals such as Pt, the Pt–Si bonds are stronger than Pt–C bonds and provide part of the driving force for the oxidative addition reaction. Although the sp^3 Si–H bond tends to be weaker than those of an sp^3 C–H, the Si–H bond strength ranges over ~ 25 kcal/mol (75–100 kcal/mol) depending on the other substituents present at silicon.³ It is likely that the Si[TM] bond strength varies across the transition metal series, but the available bond energy data are insufficient to support this suggestion.

An idealized sequence for the reaction of a hydrosilane with a transition metal center is summarized in Scheme 1. The final reaction product could be the classical 2c/2e product shown or an intermediate stage of interaction exemplified in the “nonclassical” 3c/2e forms in Scheme 1. The nonclassical interaction represents an arrested addition of the Si–H bond to the metal center. Such interactions have also been referred to as σ -complexes or agostic interactions. The σ -complex may be a transition state, an intermediate in the oxidative addition reaction, or, as will be illustrated in Tables 1, 2, and 3, can be present in an isolated complex. Schubert has proposed that the Si–H unit approaches the metal center, then pivots to place the Si atom near the metal, increasing the TM–Si interaction and weakening the Si–H bond.⁴ Another nonclassical interaction, referred to as a hypervalent interligand interaction, has also been proposed to account for the structural features present in the sequence H[TM]–(SiCl). Several commentaries and reviews have been published relatively recently describing these nonclassical interactions⁵ and will be discussed later in section 5.

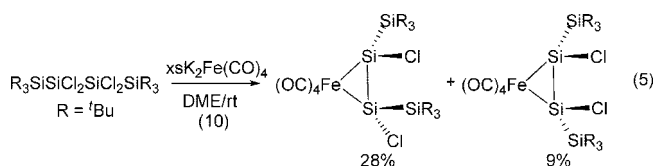
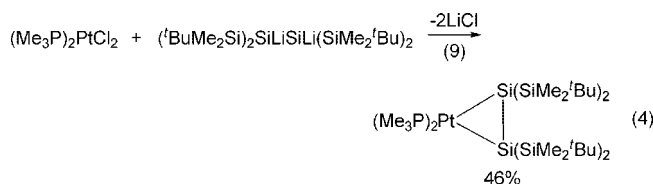
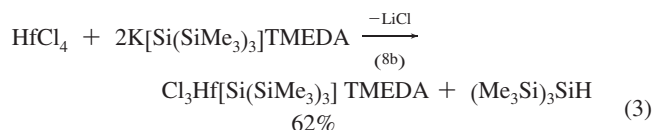
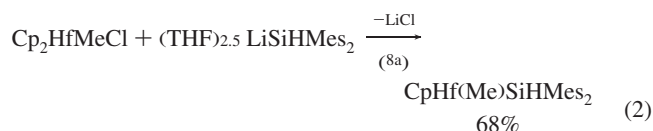
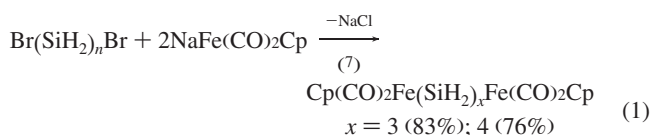
The interaction between an empty metal d-orbital and the Si–H σ -bonding orbital gives rise to the nonclassical interaction. The greater basicity of the Si–H bond relative to a H–H or to a C–H bond is a factor that makes the Si–H unit a better donor.⁶ However, the Si–H σ^* -antibonding orbital can overlap with a donor d-orbital of π -symmetry and is a better π -type acceptor than either C–H or H–H. The nature of the donor/acceptor ability of the Si–H bond can be tuned by the substituents on silicon. If strong π -backbonding from the metal to the Si–H σ^* -antibonding orbital occurs, then weakening of the Si–H bond results and ultimately may result in full oxidative addition of the Si–H bond to the metal center. As will be demonstrated in later sections, electron-withdrawing groups at silicon seem to provide oxidative addition products particularly if the substituents at silicon are relatively small. Increased electron density at the metal center also increases $d\pi$ -backbonding and promotes oxidative addition.

Scheme 2

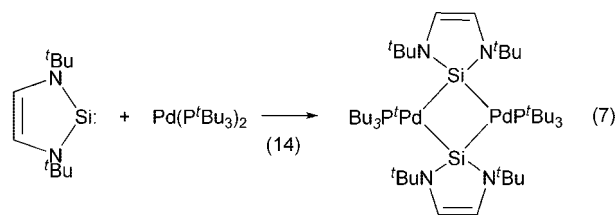
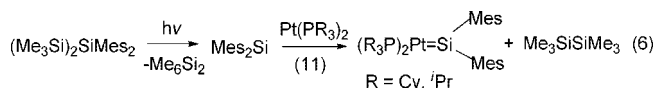


The actual end product obtained in the reaction of a hydrosilane with a transition metal complex will obviously depend on the nature of the metal (primarily the group number) as well as the remaining substituents on the metal and on silicon. The most common ligands present in the metal complexes that are reacted with hydrosilanes are 2-electron bases such as a carbonyl, phosphine, chloride, hydride, or an organic group. If oxidative addition is to occur to a metal center, the metal must be able to undergo an increase in oxidation number. Therefore an oxidation state at least two units less than the maximum number for that particular metal is one requirement. Consequently, oxidative addition is not possible for Ti(IV) or V(V) and another reaction pathway will be necessary. A complex with a 16-electron count or lower could undergo oxidative addition if a coordination site is available. Loss of a carbonyl or a phosphine usually either thermally or photochemically can provide an open coordination site for reaction with a silane. However, once the oxidative addition occurs, subsequent reaction to eliminate HCl, H₂, or RH could occur, thus losing these units from the original metal complex. In addition to an oxidative addition pathway, a metathesis route for reaction of the metal with a hydrosilane is also possible. A comparison of these two pathways (oxidative addition, path 1, and σ -bond metathesis, path 2) is shown in Scheme 2. It should be noted that [TM]–Cl bonds can also be reduced by hydrosilanes to [TM]–H, and examples of this process will be given in Table 4. Such a reduction then allows reactions related to those of metal hydrides.

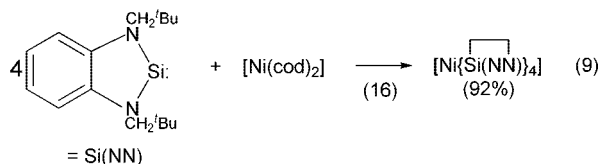
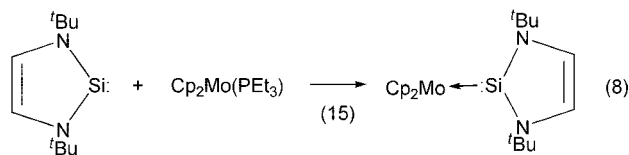
Other synthetic methods will lead to the formation of a silyl–transition metal derivative, although these tend to be less versatile. Selected examples that have been published during the review period will be briefly summarized in this section. Salt metathesis between either a silyl halide and a sodium metallate (eq 1) or a silyllithium and a metal halide (eqs 2 and 3) can provide derivatives with silicon–metal bonds. The silyllithium reagent shown in eq 2 is one of the few known that contains a SiH bond. The salt metathesis route is, of course, limited by the range of transition metal anions and the range of silyllithium reagents that are available. The salt metathesis route from silyllithium as well as from a transition metal anion has also been utilized to form η^2 -disilene complexes as shown in eqs 4 and 5.



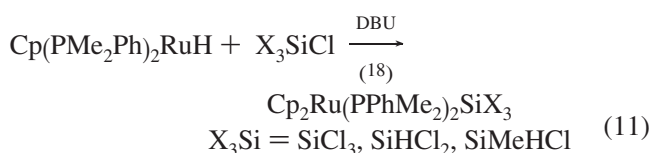
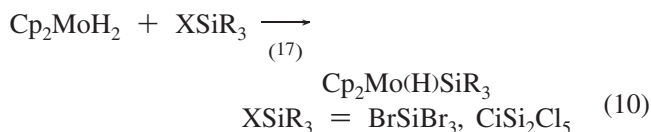
Another route that has been exploited more recently is the reaction of a suitable metal complex with a silylene. This can now be done either by generating the silylene in situ and trapping with a metal(0) complex (eq 6^{11,12}) or through the reaction of a stable, isolable silylene with a metal(0) complex that can lose a ligand(s) (eqs 7, 8^{13,14,16}). When Pd(P^tBu₃)₂ was reacted with more than 1 equiv of the unsaturated silylene (shown in eq 7), a homoleptic monomer, Pd[Si(^tBuNCH=CHN^tBu)]₃ (not isolated), as well as a dimer as shown in eq 7 was produced.¹⁴ However, the monomer, Pd[Si(^tBuNCH=CHN^tBu)]₃, could be isolated from the reaction of Pd(COD)Me₂ with the silylene,¹⁴ which indicates that a different chemistry can be observed from Pd(0) and Pd(II) precursors. The first Mo–silylene complex with a tricoordinate Si(II) center was formed from Cp₂Mo(PEt₃) and Si(^tBuNCH=CHN^tBu) (eq 8).¹⁵ The chemistry of the saturated silylene analogue has also been studied, and reaction of Pd(P^tBu₃)₂ with Si(^tBuNCH₂CH₂N^tBu) gave Pd[Si(^tBuNCH₂CH₂N^tBu)]₄, which converted to a silylene bridged dimer on workup.¹⁴ Reaction of a related stable silylene with a Ni(0) complex is shown in eq 9.



A seemingly new method for the preparation of metal–silyls using a metal hydride and a halosilane has been reported, although the details have not been published for the example utilizing Cp₂MoH₂ shown in eq 10. A similar strategy was



used for $\text{Cp}(\text{R}_3\text{P})_2\text{RuH}$ in eq 11, although an acid acceptor was also added.



The objective in forming silyl–metal derivatives in which there is a useful functional group such as SiH or SiCl is to provide a possible entry into other silyl–metal complexes through substitution at silicon. Such reactions may provide an entry into complexes that are not easily accessible through oxidative-addition reactions of a hydrosilane. Examples of the utility of functional groups at silicon in silyl–metal complexes will be provided in a later section.

A listing of stable silyl–metal complexes that have been formed on reaction of a hydrosilane and a transition metal precursor are detailed in section 3. In most cases, the complexes have been isolated, but examples of complexes that appear to be stable only in solution are also included. The silyl–metal complexes are included in the tables irrespective of the bonding interaction between [TM]–H–Si. The syntheses of complexes with nonclassical interactions between [TM]–H–Si have been merged in the discussion of section 3. The tables are divided according to the type of hydrosilane reactant: SiH_4 and RSiH_3 (Table 1), R_2SiH_2 (Table 2), and R_3SiH (Table 3). Entries occur in sequence from the early transition metal groups to the late transition metal groups and within each group from 3d to 4d to 5d transition metals. Published characterization data also appear in Tables 1–3, and each compound is numbered according to the sequence of appearance within a given table (i.e., 1-4, 2-5, etc.), and this number is used to identify an individual compound in the text. Within a triad, complexes are listed in order of complexity starting with mononuclear derivatives through polynuclear (if reported). The ligands bound to the metal center are written first in the formula for the complex followed by the metal then the silyl group. The ligand sequence for the groups at the metal center are approximately in the following order without regard to the oxidation state of the metal: $\eta^5\text{-Cp} > \eta^5\text{-Cp}^* > \text{Cp}' > \eta^6\text{-C}_6\text{R}_6 > \text{CO} > \text{PR}_3 > \text{PP} > \text{other} > \text{H}$. For phosphines, the order is given on the basis of increasing complexity of the R groups, and for groups on silicon, the order is also in increasing complexity (alkyl > aryl > halide > alkoxy). In cases where the structure of the complex is not evident from

the formula, a structure diagram is provided at the end of the table and an asterisk appears by the number of the compound in the table. Abbreviations are used for some ligands, and a listing of the abbreviations is provided at the end of each table before the footnotes.

The characterization data found in Tables 1–3, 6, and 9 provide the following information (if listed in the reference or the supporting information associated with the reference): reactants, yield, color, melting point, if elemental analyses were obtained, NMR solvents, and temperature for collection of NMR data (if other than ambient temperature was reported). ^1H chemical shifts (and coupling constants for M–H and Si–H resonances when relevant), ^{29}Si chemical shifts (and coupling constants to metals when relevant), and a listing of other techniques used to characterize the complex are also included. In a number of cases, several derivatives were prepared by the same general route and may differ only by groups attached to silicon (for example, Me_3Si vs PhMe_2Si) or by a phosphine ligand (Ph_3P vs Me_3P). Because of the volume of entries reported in the tables, one representative example of a structure type is generally provided for an individual reference, and additional complexes are provided in footnotes to the table. Expansion of data for nonclassical systems appears in Table 9.

Structural data are provided in Table 6 for the compounds listed in Tables 1–3, and the derivatives appear with their identification number as reported in Tables 1–3. If compounds listed in the footnotes to Tables 1–3 have been structurally characterized, these are also included in Table 6. In the footnotes to Table 6 are TM–Si distances for compounds reported in the Cambridge Structural Database (CSD) for silyl–metal complexes prepared by other routes and appearing in the CSD (through version 5.30) during the review period. The original reference is provided for all these bond distances.

3. Reactions of Hydrosilanes with Transition Metal Complexes

The products that contain a Si–[TM] from hydrosilanes with a range of transition metal complexes are summarized in Tables 1 (SiH_4 and primary silanes),^{19–76} 2 (secondary silanes),^{77–137} and 3 (tertiary silanes).^{138–303} In some cases, the hydrosilane reacts to transfer hydride to the transition metal complex and there is no Si–[TM] bond in the final product. Examples of this type of reactivity are tabulated in Table 5^{304–332} in section 3.7. Structural representations of selected complexes (indicated by an asterisk preceding the complex in the body of the table) appear at the end of the table.

Section 3 is organized initially to provide a general description of the types of ligands in the metal complexes and the types of substituents at silicon (section 3.1) in complexes that were published during the review period. The remaining subsections are organized in terms of the ligand on the metal center that was eliminated upon reaction with the silane: section 3.2, loss of neutral ligands (PR_3 , CO, alkenes, alkynes, solvent, or H_2); section 3.3, loss of anionic ligands in TM–R (R = organic substituent), TM–H, or TM– SiR_3 ; section 3.4, oxidative addition to a low-valent metal (without loss of original ligands); section 3.5, reactions of dinuclear or metal cluster precursors that maintain the integrity of the dinuclear complex or the cluster; section 3.6, miscellaneous reactions; and section 3.7, reactions of silanes leading to MH complexes.

Table 1. Complexes Formed from Reaction of SiH₄ and RSiH₃ with Transition Metal Complexes (Structures Are Shown at the End of the Table for Compounds Marked with an Asterisk)^{a,‡}

compound	reactants	% yield, color m.p., °C	solvent (temp.) ²	NMR			other ^d	ref
				¹ H M–H ³	¹ H Si–H ³	²⁹ Si ^{1,3}		
Reactions of SiH ₄								
1-1 Cp ₂ (Me ₃ P)TiSiH ₃ ⁵	Cp ₂ TiMe ₂ + PMe ₃ + SiH ₄	76 purple	6		7		X-ray EPR	19
1-2a HTi(μ-H) ₂ SiH ₃ ⁸ (cis and trans)	Ti ₂ (acac) ₂ + SiH ₄ + Ar (a) hν = 500 nm (b) hν = 500 nm then 410 nm						IR UV-vis calc	20a
1-2b HTi(μ-H) ₂ Si ⁸	Cr ⁰ + SiH ₄						IR calc	21a
1-3a HCr–SiH ₃	Mo ⁰ + SiH ₄						IR calc	21a
1-3b H ₃ Mo≡SiH	W ⁰ + SiH ₄						IR calc	21a
1-3c H ₃ W≡SiH							³¹ P IR EA calc	21b
1-3d + 1-3e (OC)(depe) ₂ -Mo(η ² -SiH ₄) ¹⁰	[Mo(CO)(depe) ₂] ₂ (μ-N ₂) + SiH ₄	59 lemon-yellow	C ₇ D ₈ (–5)	–7.57(s)(MoH, OA) ¹⁰ –8.23(s)J _{SiH} = 35 (η ² -H–Si) ¹⁰	4.56(s) J _{SiH} = 164 (SiH ₃ , η ³) ¹⁰ 3.48(s) J _{SiH} = 143 (SiH ₃ , OA) ¹⁰			
1-4 Cp*(Pr ₃ P)Os(H)(Br)(SiH ₃)	Cp*(Pr ₃ P)OsBr + SiH ₄	76 yellow	CD ₂ Cl ₂	–15.35(d)	3.59 (s) J _{SiH} = 175	72.97 (gdd) J _{SiH} = 176 J _{SiH} = 10	¹³ C ³¹ P EA	22
1-5 HN(SiH ₃) ₃ ⁸	Ni ₂ (acac) ₂ + SiH ₄ + Ar hν						IR UV-vis calc	23
1-6 trans-(Cy ₃ P) ₂ HP(SiH ₃)	Zn ₂ (acac) ₂ + SiH ₄ + Ar						IR UV-vis calc	24a,b
1-7 HZnSiH ₃ ⁸								25
reactions of RSiH ₃								
Sc triad								
1-8 Cp* ₂ ScSiH ₂ Me ¹²	[Cp* ₂ ScMe] + H ₃ SiMe	59 bright yellow 175–176	C ₆ D ₆		4.35 (s)	–71.0 J _{SiH} = 135	¹³ C EA IR	26a,b
1-9 Cp* ₂ ScSiH ₂ SiPh ₃ ¹³	[Cp* ₂ ScMe] + H ₃ SiSiPh ₃	55 yellow 175–176	C ₆ D ₆		3.47 (s) J _{SiH} = 128	–3.75(SiH ₂ SiPh ₃) –113.8 (SiH ₂ SiPh ₃)	¹³ C IR EA X-ray	26b
1-10a (Cp*Y) ₄ (μ-H) ₇ (μ-SiH ₂ Ph)	(Cp*Y) ₄ (μ-H) ₇ (C ₈ H ₉) + PhSiH ₃						X-ray ¹⁴	26c
1-10b (C ₃ Me ₂ SiMe ₃ Y) ₄ (μ-H) ₇ -(μ-SiH ₂ Ph)	{(C ₃ Me ₂ SiMe ₃ Y) ₄ (μ-H) ₇ -(C ₈ H ₉) ¹⁴ + H ₃ SiPh							76
Ti triad								
1-11 Cp ₂ (py)TiSiPhH ₂	Cp ₂ TiMe ₂ + py + H ₃ SiPh	dark violet					EPR	27
1-12 Cp ₂ (Me ₃ P)TiSiPhH ₂ ¹⁵	Cp ₂ (Me ₃ P)TiH or Cp ₂ (Me ₃ P)Ti(η ² -H–SiPhH ₂) (1-11) or Cp ₂ Ti(PMe ₃) ₂ or Cp ₂ (Me ₃ P)TiPPh ₂ + 2 equiv H ₃ SiPh	bright purple					EPR	28
1-13 Cp ₂ (Me ₃ P)Ti(η ² -H–SiPhH ₂) ¹⁶	Cp ₂ Ti(PMe ₃) ₂ + xs H ₃ SiPh	dark brown	C ₇ D ₈ (–55)	–4.02 (d)	5.70 (br s)		³¹ P	28
1-14a Cp ₂ Ti(η ² -H–SiH ₂ Ph)-(η ² -H–Bcat–4 ⁷ Bu)	Cp ₂ Ti(PMe ₃) ₂ + xs H ₃ SiPh	65 yellow	C ₇ D ₈ (–80)	–4.99 –6.78	5.11 5.33		¹¹ B 2D-NMR IR	29a
1-14b (dmpe) ₂ Ti(Si ₃ H ₃ Ph ₃) + PhMeSiH ₂	Cp ₂ Ti(HBcat–4 ⁷ Bu) ₂ + H ₃ SiPh (dmpe) ₂ TiMe ₂ + H ₃ SiPh (3.9 equiv; 4 h)	44 purple (100% in soln)	C ₇ D ₈ (–20)	¹ H{ ³¹ P} Ti–H–Si 4.75 (td) 4.50 (dd)	¹ H{ ³¹ P} Ti–Si–H 6.35 (d) 6.25 (d) Si–H 3.27		³¹ P	29b
*1-14c (dmpe) ₂ Ti(Si ₄ H ₆ Ph ₄)	(dmpe) ₂ TiMe ₂ + H ₃ SiPh (5 equiv; 16 weeks)	44 purple	C ₇ D ₈ (–20)	Ti–H–Si 4.27 (dd) J _{SiH} = <40 4.19 (dd) J _{SiH} = <40	Ti–Si–H 6.57 (d) J _{SiH} = 127 6.31 (d) J _{SiH} = 133 Si–H 4.95 (d) J _{SiH} = 186 4.50 (d) J _{SiH} = 189		³¹ P X-ray	29b

Table 1a. Continued

compound	reactants	% yield, color m.p., °C	solvent (temp.) ²	NMR			ref
				¹ H M–H ³	¹ H Si–H ³	²⁹ Si/ ¹³ other ^d	
1-15 [Cp ₂ Zr(Si(CH ₃ Ph) ₂) ₂] ²⁺ 2 [BBu _n (C ₆ F ₅) _{4–n}] ^{2–} + H ₃ SiCH ₂ Ph	[Cp ₂ Zr(SiPhH ₃) ₂] ²⁺ 2 [BBu _n (C ₆ F ₅) _{4–n}] ^{2–} + H ₃ SiCH ₂ Ph	80 yellow	C ₆ D ₆ C ₆ D ₆		5.95 (s) (SiH) –3.15 (s) (μ–SiH) 5.80 (s) –3.38 (s)	105	30 31
*1-16 [(Cp ₂ Zr(SiH ₂ Ph) ₂) ₂] ²⁺ [B(C ₆ F ₅) ₄] ₂	[Cp ₂ Zr(η ² (C ₆ N)-CH ₂ CHMe (6-methyl-2-pyridyl))] + [B(C ₆ F ₅) ₄] + H ₃ SiPh						
V triad 1-17a Cp(dmpe)VSiH ₂ Mes	Cp(dmpe)VSMe + H ₃ SiMes	64					31b
1-17b Cp(ArN=)Nb(PMe ₃) ₂ (H)– (SiPhH ₂) Ar = 2,6-Pr ₂ C ₆ H ₃	Cp(ArN=)Nb(PMe ₃) ₂ + H ₃ SiPh	65	C ₆ D ₆	2.30 (d)	5.84 (s) 5.64 (s)		32a
1-17c Cp(Me)HTa[PhSiH ₂ – N(C ₆ H ₃ Me) ₂ (NSiMe ₃)]	Cp*(Me)Ta[=N(C ₆ H ₃ Me) ₂ NSiMe ₃] + H ₃ SiPh	58 white 148–149 (d)	C ₆ D ₆	17.15 (s)	5.29 (d) ¹ J _{SiH} = 179 ² J _{HH} = 9.6 4.68 (d) ¹ J _{SiH} = 184 ² J _{HH} = 9.6 5.46 (d) ¹ J _{SiH} = 195 ² J _{HH} = 9.8		32b
1-18 Cp*(C)HTa[PhSiH ₂ – N(C ₆ H ₃ Me) ₂ (NSiMe ₃)]	Cp*(C)Ta[=N(C ₆ H ₃ Me) ₂ –N–SiMe ₃] + H ₃ SiPh	60 pale yellow 138–141 (d)	C ₆ D ₆	20.44 (s)			32b
1-19 Cp(C)HTa[PhSiH ₂ – N(C ₆ H ₃ Me) ₂ (NSiPhHCl)]	Cp*(C)Ta[=N(C ₆ H ₃ Me) ₂ NSiMe ₃]/ CH ₂ Cl ₂ + H ₃ SiPh	84 pale yellow 156–159(d)	CD ₂ Cl ₂ (H) C ₆ D ₆ (13C, ²⁹ Si)	14.85 (d) ⁴ J _{HH} = 6.0	–26.9 (t) ¹ J _{SiH} = 208 (PhSiH ₂ N) –66.8 (d) ¹ J _{SiH} = 272 (SiHClPh)		32b
1-20a Cp(ArN=)Ta ₂ H ₂ – (μ–ArNSiHPh) Ar = 2,6-Pr ₂ C ₆ H ₃	Cp*(ArN=)HTa–Si(SiMe ₃) ₃ + H ₃ SiPh	(A) 18 yellow	(A) C ₆ D ₆ (73)	10.5 (br s) 0.2 (br s)	9.7 (br)		33
1-20b Cp(H ₂ Ta ₂ (μ–ArNSiHPh) ₂) Ar = 2,6-Pr ₂ C ₆ H ₃	Cp*(ArN=)HTa–Si(SiMe ₃) ₃ + H ₃ SiPh	(B) 71 dark green	(B) C ₆ D ₆	11.63 (term) –0.99 (pt; bridging)	14.2 –7.6		33
*1-20c {Cp*Ta[N(Pr)C(Me)– N(Pr)SiH ₂ Ph]} ₂ (η ¹ –η ¹ –μ– N ₂)(Cp*Ta [N(Pr)C(Me)–N(Pr)H])	{Cp*Ta[N(Pr)C(Me)–N(Pr)] ₂ (η ¹ , η ¹ –μ–N ₂) + H ₃ SiPh	54 orange	C ₆ D ₆		unassigned		34b
1-20d {Cp*Ta[N(Pr)C(Me)N(Pr)– (=NSiH ₂ Ph)](μ–N)–(Cp*Ta– (Pr)NC(Me)N(Pr)H)}	{Cp*Ta[N(Pr)C(Me)N(Pr)] ₂ (μ–η ¹ : η ¹ –N) ₂ + H ₃ SiPh	55 colorless	C ₆ D ₆		unassigned		34b

Table 1b. Continued

compound	reactants	% yield, color m.p., °C	solvent (temp.) ²	NMR				ref
				¹ H M-H ³	¹ H Si-H ³	²⁹ Si/ ¹ 3	other ⁴	
*1-21 ([NPN]Ta) ₂ (μ-NSiH ₂ Bu) ₂ ¹⁸	([NPN]Ta) ₂ (μ-H) ₂ (μ-η ¹ :η ² -N ₂) + 2H ₃ SiBu	63	C ₆ D ₆		4.91 (s)	8.79 (d) -1.74 (dd)	³¹ P EA X-ray ¹³ C ³¹ P EA X-ray	34a
*1-22 [NPN]HTa(μ-H) ₂ -(μ-η ¹ :η ² -BuH ₂ SiNN)Ta-[NPN] ¹⁹	([NPN]Ta) ₂ (μ-H) ₂ (μ-η ¹ :η ² -N ₂) + H ₃ SiBu	99	C ₇ D ₈ (-60 °C)	11.21, 11.23 (ddd, TaHTa) 14.27 (dd, TaH ₁)	5.05, 3.97 (d, ² J _{HH} = 11.7, SiH ₂ Bu)	-14.96 (NSiH ₂ Bu) 11.17 (d), 8.98 (d), 8.79 (d), 8.49 (d)	³¹ P EA X-ray	34b
Cr triad 1-23 Cp ₂ (H)Mo[SiH ₂ C ₃ Me ₄ H] ²⁰	Cp ₂ MoH ₂ + H ₃ Si(C ₃ Me ₄ H) (hv)	73	C ₆ D ₆	-8.42 (s)	4.65 (d) ¹ J _{SiH} = 168	14.1	¹³ C IR MS EA X-ray ³¹ P IR EA X-ray	35
1-24 Cp*(dmpe)(H)Mo=Si(H)Ph	Cp*(dmpe)Mo(η ³ -CH ₂ Ph) + H ₃ SiPh ²¹	69 dark green	C ₆ D ₆	-9.96 (td) ² J _{SiH} = 30	9.45 (m) ² J _{SiH} = 130	250	¹³ C X-ray ³¹ P IR EA X-ray	36a
1-25a Cp*(dmpe)(H)Mo(SiH ₂ Ph) ₂ ²²	Cp*(dmpe)(H)MoSi(H)Ph + H ₃ SiPh Δ	61 yellow	C ₆ D ₆	-7.27 (t)	5.00 (d) ² J _{SiH} = 165 4.97 (d) ² J _{SiH} = 158	10.1	¹³ C X-ray ³¹ P HMQC IR EA X-ray ³¹ P VT IR X-ray	36a
*1-25b (ArN)(PMc ₃)(PhH ₂ Si)Mo-(η ³ -NAr-SiHPh-H) Ar = 2,6-Pr ₂ C ₆ H ₃	(ArN=) ₂ Mo(PMc ₃) ₃ + 2PhSiH ₃	77 brown	C ₇ D ₈ -50 °C		4.35 (bm) ²³ ¹ J _{SiH(a)} = 113 6.03 (bd) ¹ J _{SiH(b)} = 245 5.68 (s), 5.97 (s) ¹ J _{SiH(cd)} = 245 4.36 (m) ²⁴ (Si-H _a) 6.12 (m) (Si-H _b) 5.97 (bs) 5.64 (bs) (Si-H _c H _d)	-72.9 (dd) (SiH _a H _b Ph) 1.2 (t) (SiH _c H _d Ph)	³¹ P IR EA X-ray ³¹ P VT IR X-ray	36b
*1-25c (ArN)(PMc ₃)(<i>m</i> -Tol)H ₂ Si)Mo(η ³ -NAr-SiHPh-H) Ar = 2,6-Pr ₂ C ₆ H ₃ ²⁵	(ArN)(PMc ₃)(PhH ₂ Si)Mo-(η ³ -NAr-SiHPh-H) + H ₃ Si(<i>m</i> -Tol)	43	C ₆ D ₆ -50 °C				HMBC-GP	36b
*1-26 [H ₃ Mo]([Ph ₂ PCH ₂ CH ₂ P(Ph)-C ₆ H ₄ -o]-(Ar)Si-P,P,P,Si)] Ar = <i>o</i> -CH ₃ C ₆ H ₄ ²⁶	(dppe) ₂ MoH ₄ + H ₃ Si(C ₆ H ₄ CH ₃ - <i>o</i>) Δ	75 pale yellow-green	C ₇ D ₈	-4.05 (br t) -4.38 (br quint)			³¹ P IR EA	37a,b
1-27 [MoH ₂ (Ar)]([Ph ₂ PCH ₂ CH ₂ P(Ar)C ₆ H ₄ - <i>o</i>](Ar)Si-P,P,P,Si)] Ar = Ph ²⁷	(dppe) ₂ MoH ₄ + xs H ₃ SiPh Δ	78 yellow	C ₆ D ₆	-4.50 (br m) -5.40 (br m)	4.20(2)		³¹ P IR [EA] X-ray ²⁸	37b
1-28 Cp*(OC) ₃ WSiH ₂ -[C(SiMe ₃) ₃] ²⁹	Cp*W(CO) ₃ Me + H ₃ SiC(SiMe ₃) ₃ (hv)	50 orange	C ₆ D ₆		4.37 (s) ¹ J _{SiH} = 179.3	-27.2	¹³ C IR EA	38a
1-29a Cp(OC) ₃ (H)W=Si(H)-[C(SiMe ₃) ₃] ³⁰	Cp*W(CO) ₃ Me + H ₃ Si[C(SiMe ₃) ₃] (hv)	44 orange	C ₆ D ₆	-10.67 (d) ¹ J _{WH} = 65 ² J _{SH} = 28.3 ³ J _{HH} = 1.7	10.42 (d) ¹ J _{SH} = 155.1 ² J _{WH} = 13.7 ³ J _{HH} = 1.7	-3.6 (SiMe) 275.1 (WSi) ¹ J _{WSi} = 109.9	¹³ C VT IR EA X-ray calc	38a
1-29b <i>cis</i> -Cp*(OC) ₂ (HW=SiHPh)·THF (THF = tetrahydrofuran)	Cp*(OC) ₃ WMe + H ₃ SiPh hv	70 pale yellow	THF- <i>d</i> ₈	-9.91 (d) ¹ J _{WH} = 67.7 ³ J _{HH} = 4.3	7.23 (d) ³ J _{WH} = 4.3 ¹ J _{SiH} = 178.4	117.1 ¹ J _{WSi} = 103.3	¹³ C IR EA	38b

Table 1c. Continued

compound	reactants	% yield, color m.p., °C	NMR				other ^d	ref
			solvent (temp.) ²	¹ H M–H ³	¹ H Si–H ³	²⁹ Si/ ¹ 3		
1-30 [Cp ⁺ (dmpe)(H) ₂ W=Si(H)Dipp] ⁺ [B(C ₆ F ₅) ₄] ^{−31}	[<i>η</i> ⁷ -C ₅ Me ₃ (CH ₂) ₂ (dmpe)–W(H) ₂][B(C ₆ F ₅) ₄] [−] + H ₃ SiDipp	57 orange	C ₆ H ₅ F	−4.1 (m)	10.83 (s) <i>J</i> _{SiH} = 167	286 <i>J</i> _{SiH} = 167	¹³ C ³¹ P IR EA ³¹ P IR	39
1-31 (OC) ₃ (R ₃ P) ₂ HWSiPhH ₂ ³² R = C ₆ H ₁₁	(OC) ₃ (R ₃ P) ₂ W + H ₃ SiPh	bright yellow (≤ −45)	C ₇ D ₈ (−45) ³³	−4.51 (t) <i>J</i> _{HW} = 28	5.79 (s) <i>J</i> _{SiH} = 177		³¹ P IR	40
Mn triad 1-32 (DippN=) ₃ ReSiH ₂ Ph ³⁴ Dipp = 2,6-Pr ₂ C ₆ H ₃ –	(DippN=) ₃ ReSiMe ₃ + H ₃ SiPh (1 equiv)		C ₆ D ₆		6.59 (s) <i>J</i> _{SiH} = 201	−16.52 (tt) ¹ <i>J</i> _{SiH} = 201 ⁴ <i>J</i> _{SiH} = 7	¹³ C IR EA ³⁴	41
Fe Triad *1-33a Cp(Pr ₂ MeP)Fe(H) ₂ SiH ₂ Ph ³⁵	Cp(Pr ₂ MeP)Fe(BH ₄) + H ₃ SiPh/NEt ₃	80 yellow oil	C ₆ D ₆	−15.24 (d + sat) <i>J</i> _{SiH} = 19.8	5.39 (s + sat) <i>J</i> _{SiH} = 183.4	−13.8 (m)	¹³ C ³¹ P IR	42a
1-33b Cp ⁺ (OC) ₂ FeSi(CHPh ₂)H ₂ ³⁶	Cp ⁺ (OC) ₂ FeMe + 1/2 H ₃ Si(CHPh ₂)	41 yellow	C ₆ D ₆		4.65 (d)		¹³ C IR EA	42b
*1-34 (1-15⁺) Cp ₂ (OC) ₂ Fe ₂ (μ-CO)(μ-Si(CHR ₂) ₂)H] R = Ph ³⁷	Cp(OC) ₂ FeSiMe ₃ + H ₃ Si(CHPh ₂) (hv)	62 (cis) <1 (trans) ³⁸ red	C ₆ D ₆		7.49 (d)	227.4	¹³ C IR MS EA	43a
1-35 (1-16) Cp ₂ (OC) ₂ Fe ₂ (μ-CO)–[μ-Si(CHPh ₂) ₂]H]	Cp ⁺ (OC) ₂ FeMe + 1/2 H ₃ Si(CHPh ₂)	8 orange–red	C ₆ D ₆		7.48 (d)	252.6	¹³ C IR MS EA X-ray	42b
1-36 (¹⁸ PDI)Fe(<i>η</i> ² -HSiH ₂ Ph) ₂	(¹⁸ PDI)Fe(N ₂) ₂ + 2H ₃ SiPh	—green	C ₆ D ₆ C ₇ D ₈ (−40)		−6.69 (s) (<i>η</i> ² -SiH, basal) −6.80 (s) (<i>η</i> ² -SiH, basal) 0.05 (s) (<i>η</i> ² -SiH, apical) 6.11 (s) (SiH ₂ , basal) 2.78 (s) (SiH ₂ , apical)	(−80 °C, tol-d ₈) 50.23 (apical) ¹ <i>J</i> _{SiH} = 54 ³⁹ ¹ <i>J</i> _{SiH} = 196 −44.6 (basal) ¹ <i>J</i> _{SiH} = 119 ³⁹ ¹ <i>J</i> _{SiH} = 220	gCOSY ROESY NOESY HMBC UV-vis <i>μ</i> _{eff} X-ray	44a
*1-37 [{PhB(CH ₂ P ^{Ph}) ₃]Fe(H)(<i>η</i> ³ -H ₃ SiPhMe) ⁴⁰ (hybrid: σ-complex/silylene complex)	[PhB(CH ₂ P ^{Ph}) ₃ FeMe] + H ₃ SiPh	65% red	C ₆ D ₆	−13.45 (m) ¹ <i>J</i> _{SiH} = 68 ⁴¹		162	¹³ C ³¹ P IR EA calc X-ray ¹³ C ³¹ P IR EA	45
1-38a (¹⁸ PNP)FeH(SiH ₂ Ph)N ₂	(¹⁸ PNP)FeH ₂ (N ₂) + H ₃ SiPh	81 orange	C ₆ D ₆	−13.12 (t)	4.94 (t)		X-ray ¹³ C ³¹ P IR EA	46a
*1-38b Cp ₃ Fe ₃ (CO) ₄ SiN(SiMe ₃) ₂	2CpFe(CO) ₂ SiMe ₃ + H ₃ SIN(SiMe ₃) ₂ hv (in hexane)	10 black	C ₆ D ₆ (¹ H) CDCl ₃ (²⁹ Si)			−0.96, 2.40 (SiMe ₃) 426.3 426.3	¹³ C IR EA X-ray	46b
*1-38c Cp ₂ Fe ₂ (CO) ₂ (μ-CO)(μ-SiN(SiMe ₃)SiMe ₂ CH ₂)	2CpFe(CO) ₂ SiMe ₃ + H ₃ SIN(SiMe ₃) ₂ hv (in hexane)	22 red	C ₆ D ₆			−1.33, (SiMe ₃) 11.25 (SiMe ₂) 220.1 (silylene)	¹³ C IR EA X-ray	

Table 1d. Continued

compound	reactants	% yield, color m.p., °C	solvent (temp.) ²	NMR			other ^d	ref
				¹ H M-H ³	¹ H Si-H ³	²⁹ Si ^{1,3}		
* 1-38d Cp ₂ Fe ₃ (μ ₂ -SiH(SiMe ₃) ₂)- {(μ ₃ -CO)SiH ₂ N(SiMe ₃) ₂ }- {(μ ₃ -η ² -C ₂ O ₂ -SiHN(SiMe ₃) ₂)}	2 CpFe(CO) ₂ SiMe ₃ + H ₃ SiN(SiMe ₃) ₂ (in toluene)	22 brown	C ₆ D ₆			-45.6 (O ₂ Si) -17.36 (OSi) 2.18 (SiMe ₃) 2.95 (SiMe ₃) 4.99 (SiMe ₃) 6.98 (SiMe ₃) 176.2 (silylene)	¹³ C EA X-ray	46b
1-38e Cp*(OC) ₂ Ru- [SiH ₃ C(SiMe ₃) ₃]	Cp*(Ru)(CO) ₂ Me + H ₃ SiC(SiMe ₃) ₃ hν (5 °C)	76					X-ray	393a
1-38f Cp*(OC)(py)RuSiH ₂ - [SiH ₂ C(SiMe ₃) ₃]	Cp*(OC)(py)RuMe + H ₃ SiC(SiMe ₃) ₃						X-ray	393a
1-39a [Cp*(Me ₃ P) ₂ HRuSiH ₂ SiPh ₃][BPh ₄] ⁻⁴²	Cp*(Me ₃ P) ₂ Ru=Si(SEt) ₂ ⁺ BPh ₄ ⁻ + H ₃ SiSiPh ₃	24	CD ₂ Cl ₂	-10.10 (t)	3.77 (vt)		¹³ C 31P [EA]	47a
* 1-39b [Cp*(κ-P,N-2-Me ₂ N-3- <i>P</i> Pr ₂ -indene)- (H) ₂ Ru=SiHPh] ⁺ X ⁻ X ⁻ = SO ₃ CF ₃ ⁻⁴³	[Cp*(κ-P,N-2-Me ₂ N-3- <i>P</i> Pr ₂ -indene) RuCl] ⁺ SO ₃ CF ₃ ⁻ + H ₃ SiPh	95 off-white	C ₆ D ₃ Br	-10.38 (d) -11.74 (app dd)	5.10 (app t)	107.2 ⁴⁴ ¹ J _{SiH} = 195	¹³ C 31P EA	47b
* 1-39c [C ₃ H ₄₉ PNSiRul][B(C ₆ F ₅) ₄] (isomer of cation in 1-39b) (See structure for 1-39c)	[Cp*(κ-P,N-2-Me ₂ N-3- <i>P</i> Pr ₂ -indene)(H) ₂ Ru = [SiHPh] ⁺ [B(C ₆ F ₅) ₄] ⁻ in Et ₂ O-d ₁₀		Et ₂ O-d ₁₀	-10.60 (d) -11.37 (app dd)	5.63(m)	111.6 ¹ J _{SiH} = 192 ⁴⁵	¹³ C X-ray 31P	47b
* 1-39d [C ₃ H ₄₉ PNSiRul][SO ₃ CF ₃] (isomer of cation in 1-39c) (See structure for 1-39d)	1-39b in CH ₂ Cl ₂ (48 hrs)	95 off-white	C ₆ D ₃ Br	-10.38 (d) -11.74 (app dd)	5.10 (app t)	107.2 ¹ J _{SiH} = 195	¹³ C 31P EA	47b
* 1-39e C ₃ H ₄₃ OPRu (See structure for 1-39e)	1a ₂ N ₂ ⁴⁶ + H ₃ SiPh	95 orange	C ₆ D ₆	-11.14 (d) -11.92 (app dd)	6.61 (m)	60.4 ¹ J _{SiH} = 199.7 ² J _{SiH} = 9.4 -17.2	¹³ C 31P EA X-ray	47c
1-40 Tp(Ph ₃ P)HRu(η ² -H-SiPhH ₂) (σ-complex) ⁴⁷	Tp(Ph ₃ P)(CH ₃ CN)RuH + H ₃ SiPh	55	C ₆ D ₈ O	-10.32 (d) ¹ J _{SiH} = 27	5.22 (d) ¹ J _{SiH} = 196		³¹ P T ₁ VTNMR IR MS calc [EA] ¹³ C ⁴⁹ 31P VT HRMS IR	48a
* 1-41 (Me ₃ P) ₃ H ₂ Ru(SiH ₂ Ph) ₂ ⁴⁸	(Me ₃ P) ₃ (H) ₃ RuSiMe ₃ + xs H ₃ SiPh	83 pale yellow	C ₆ D ₆ C ₇ D ₈ (-48)	-8.00 (br s) -9.20 (d) -6.95 (dm)	5.18 (br q) 4.81 (br q) 5.57 (sept)	-15.8 (br s)	¹³ C 31P T ₁ VTNMR IR MS calc [EA] ¹³ C ⁴⁹ 31P VT HRMS IR	49
* 1-42 [(1,3-CH ₃ ² PBu ₂) ₂ C ₆ H ₃]- (N ₂)Ru(SiCIPhH) ₂ ⁵⁰	[RuHCl]([1,3-CH ₃ ² PBu ₂ -C ₆ H ₄]) + H ₃ SiPh + N ₂	75	C ₇ D ₈		5.37 ¹ J _{SiH} = 206	31.5 (t)	X-ray ¹ H(³¹ P) 31P T ₁ IR EA	50
* 1-43 [(Cp*Ru) ₂ (H)(μ-H)(μ-η ² -H- SiR)(μ-ClSi(BuNCH=CHN(Bu)) R = Hex ⁵¹	Cp* [†] η ¹ -Si(BuNCH=CHN(Bu))RuCl + H ₃ SiPh	85 red-orange 120–122 (d)	C ₆ D ₆	-7.17 (d) ¹ J _{SiH} = 40 ² J _{HH} = 3 (RuHSi) (RuHSi) (RuH) -12.92 (s) -13.21 (d) ² J _{HH} = 3 (μ-H) -14.82 (ddd)		154.6 (μ-η ² -SiH) 33.1	X-ray ¹³ C IR EA X-ray	51a
1-44 Cp*(Pr ₃ P)Cl(H)OsSiPhH ₂ ⁵²	Cp*(Pr ₃ P) ₂ OsCl + H ₃ SiPh	61 yellow	C ₆ D ₆		5.47 (dd)		³¹ P IR MS EA	52

Table 1e. Continued

compound	reactants	% yield, color m.p., °C	solvent (temp.) ²	NMR			ref
				¹ H M–H ³	¹ H Si–H ³	²⁹ Si ^{1,3}	
1-45 Cp*(Pr ₃ P)Br(H)OsSiPhH ₂ ⁵³	Cp*(Pr ₃ P)OsBr + H ₃ SiPh	81 yellow 163–165	C ₆ D ₆	–14.8 (d) ² J _{SiH} = 4	6.60 (d) ¹ J _{SiH} = 189 ² J _{HH} = 4 4.71 (vq) ¹ J _{SiH} = 182 5.48 (dd) ¹ J _{SiH} = 200	–26.0	53,22a
1-46 (1-38) Cp*(Pr ₃ P)Br(H)Os[Si(C ₆ F ₅)H ₂] ⁵⁴	Cp*(Pr ₃ P)OsBr + H ₃ SiC ₆ F ₅	77 orange	CD ₂ Cl ₂	–15.05 (d) ² J _{SiH} = 5		–62.2 (d) (INEPT)	22a
1-47 Cp*(Pr ₃ P)Br(H)Os[Si(trip)H ₂] Trip = 2,4,6-Pr ₃ C ₆ H ₂	Cp*(Pr ₃ P)OsBr + H ₃ Si(trip)	85	CD ₂ Cl ₂	–15.07 (d)	4.96 (d) ¹ J _{SiH} = 205 4.83 (d) ¹ J _{SiH} = 205	–53.0	54
1-48 (1-39) Cp*(Pr ₃ P)Br(H)Os[SiH ₂ Si(SiMe ₃) ₃] ⁵⁵	Cp*(Pr ₃ P)OsBr + H ₃ SiSi(SiMe ₃) ₃	81 yellow	C ₆ D ₆	–14.9 (d)	3.62 (s) ¹ J _{SiH} = 171 5.12 (s) ¹ J _{SiH} = 179	–8.3 (SiMe ₃) –83.5 (d) (SiOs) –134 (Si(SiMe ₃) ₃) (gHMBC) –20	22a
*1-49 Cp*Pr ₃ P(H)OsCH ₂ C ₆ H ₂ (SiH ₂)Me ₂ ⁵⁶	Cp*(Pr ₃ P)OsCH ₂ Ph + H ₃ SiMes	86 pale orange 149–152	C ₆ D ₆	–15.8 (d)	6.38 (t)		55
1-50 Cp*(Pr ₃ P)(H)Os=SiH(trip) ^{57,58}	Cp*(Pr ₃ P)OsCH ₂ Ph + H ₃ Si(trip)	orange 69 158–160	C ₆ D ₆	–16.0 (dd) ² J _{SiH} = 7.7	12.1 (s) ¹ J _{SiH} = 144	229	55
*1-51 [(Bu ₂ PC ₂ H ₄ CHC ₂ H ₄ P'Bu) ₂] [–] H ₃ Os(=SiH ₂)SiCPh ₂	[OsH ₂ Cl][CH(C ₂ H ₄ P'Bu ₂) ₂] + 2H ₃ SiPh	83	C ₆ D ₆	–9.70 (ddt)	4.74 (dd) ¹ J _{SiH} = 179.3	30.4 (dd)	50
*1-52 [(2,6-H ₂ CP'Bu ₂) ₂ C ₆ H ₃](H ₃ Os- (=SiPhCl) (2 rotamers) ⁵⁹	[OsH ₂ Cl][2,6-(CH ₂ P'Bu ₂) ₂ C ₆ H ₃] + H ₃ SiPh	60 yellow	C ₇ D ₈ (–70 °C)	(a) –7.50, –6.33 (b) –7.34, –6.98		(a) 239.3 (b) 246.5	50
*1-53 [(η ⁵ -C ₃ H ₄ CH ₂ CH ₂ P(Bu) ₂)(Bu) ₂] [–] HCOsSiH ₂ Ph	(η ⁵ -C ₃ H ₄ CH ₂ CH ₂ P(Bu) ₂)(Co(η ² -C ₂ H ₄) + H ₃ SiPh	85 yellow 122–123	C ₇ D ₈	–16.89 (dd)	5.10 (ddd) ¹ J _{SiH} = 86.6 ⁶⁰ 5.50 (dd) ¹ J _{SiH} = 79.2 ⁶¹ 5.93 (d) (silylene) 5.75 (br s) 5.70 (br s) 5.54 (br s) 5.31 (br s) 5.99 (d)	(280 K) 33.2 (s) 8.2 (s) 1.7 (s) –16.0 (s) –30.1 (s) (263 K) 22.2 (d) ¹ J _{SiH} = 162 10.0 (s) 2.7 (s) –18.9 (d) ¹ J _{SiH} = 195 –28.4 (br s)	56
*1-54a [(κ ² -Bu ₂ PCH ₂ Me ₂ SiN- SiMe ₂ CH ₂ P'Bu ₂)(H)Si=] [–] Co(H) ₃ (SiH ₂ Ph) ₂ ⁶²	^t BuPNPCo + 4.1H ₃ SiPh	100 ⁶³	C ₆ D ₆	–11.29 (s)			57a,b
*1-54b [(κ ² -Bu ₂ PCH ₂ Me ₂ SiN- SiMe ₂ CH ₂ P'Bu ₂)(H)- Si=Co(H) ₃ (SiHPh ₂) (silylene) ⁶⁴	^t BuPNPCo + 2H ₃ SiPh	100 brown oil	Tol-d ₈	–11.46 (s)			57a,b
*1-55a [Cp*Co(P(OMe) ₃)](H)(η ² -H- SiPhH ₂)](B(AtF) ₄) ⁶⁵	Cp*[(MeO) ₃ P]HC(η ² -H ₂) ⁺ [B(AtF) ₄] [–] + H ₃ SiPh		CD ₂ Cl ₂ (H, rt) (²⁹ Si, –30)	–12.34 (d, Co*H) (η ² -HSi) ¹ J _{SiH(obs)} = 29.0 ⁶⁶	4.69 (s, 2H, SiH _{term}) ¹ J _{SiH} = 218		57c

Table 1f. Continued

compound	reactants	% yield, color m.p., °C	NMR			other ^d	ref
			¹ H M—H ³	¹ H Si—H ³	²⁹ Si ^{1,3}		
*1-55b [Cp*Co(PMe ₃)(H)(η ² -H-SiPhH ₂)](BAr ₄) ⁶⁷	Cp*Me ₃ P[HC(η-H) ₂] ⁺ [B(Ar ₄) ₄] [−] + H ₃ SiPh		−13.14 (d, Co*H)/(η ² -HSi) ¹ J _{SiH(obs)} = 30	4.69 (s, 2H, SiH _{term}) ¹ J _{SiH} = 218	−27.7 (d)		57c
1-56 (tmp)RhSiPhH ₂ ^{68,69}	(tmp)RhCl + H ₃ SiPh	82 orange				¹³ C IR HRMS EA	62a
1-57 (Et ₃ P) ₃ (H) ₂ Ir[Si(C ₆ H ₃ Mes-2,6)(Cl)H]	(Et ₃ P) ₃ IrCl + H ₃ Si(C ₆ H ₃ Mes-2,6)	63 off-white 150–152	−14.5 (ddd) −13.8 (ddd)	6.41 (ddd) ¹ J _{SiH} = 188	−7.1 (dt)	¹³ C ³¹ P IR	58
1-58 (Et ₂ PhP) ₃ (H) ₂ Ir[Si(CI)CH ₂ (C ₆ H ₂ -Mes-2,4)(C ₆ H ₃ (Mes))]	(Et ₂ PhP) ₃ IrCl + H ₃ Si(C ₆ H ₃ Mes-2,6)	63 off-white 162–163			−0.8 (dt)	X-ray ³¹ P IR EA	59
1-59a [PhB(CH ₂ PPH ₂) ₃](H)Ir-SiAr(c-C ₈ H ₁₃) ⁷⁰	[PhB(CH ₂ PPH ₂) ₃](H)Ir(η ³ -C ₈ H ₁₃) + H ₃ SiAr	75 tan 240–44 (d)	−10.00 (dm)		274.2	X-ray ¹³ C ³¹ P IR	60a,b
1-59b (PNP)(H)Ir(SiMesH ₂) ⁷¹	(PNP)IrH ₂ + H ₃ SiMes	73 brt orange	−20.87 (t)	5.02 (t) ¹ J _{SiH} = 156 −2.16 (s) ¹ J _{SiH} = 203	−70.5	X-ray EA ¹³ C EA	61
1-59c (tmp)IrSiPhH ₂ ⁷²	(tmp)IrCl(CO) + H ₃ SiPh	34 purple				¹³ C HRMS (FAB)	62b
*1-59d [NSiN]IrSiH ₂ Ph ₂ (NCMe) ₂] ⁺ [OSO ₂ CF ₃] ^{−3}	(NSiN)Ir(H)(OTf)(coe) + H ₃ SiPh (CH ₃ CN solvent)	77 yellow		3.84 (d) ¹ J _{SiH} = 169 3.39 (d) ¹ J _{SiH} = 171	2.2 (s) (SiMe) −51.6 (s) (SiH ₂ Ph)	¹³ C ¹⁹ F IR EA	57d
Ni Triad							
1-60 (dmpe)[Ni{(SiH ₂) ₂ C ₆ H ₄ }] ⁷⁴	(dmpe) ₂ Ni + 1,2-(H ₃ Si) ₂ C ₆ H ₄ (2.5 equiv)	81 white		4.75–5.10 (m)	−0.35 (dd) 4.62 (t)	³¹ P IR MS EA X-ray	63
*1-61 {(dmpe)Ni[(H ₂ Si) ₂ C ₆ H ₄]} ₂ - (μ-dmpe) ⁷⁴	(dmpe) ₂ Ni + 1,2-(H ₃ Si) ₂ C ₆ H ₄ (0.67 equiv)	42 light yellow		5.28–5.38 (m)	−7.7 (t)	³¹ P IR EA X-ray	63
1-62 [(1,2-C ₆ H ₄ (SiH ₂) ₂ (SiH)) ₂ - Ni ₂ (dmpe) ₂]	1-61 + Δ	34 orange 134–152				IR EA	64
*1-63 [(1,2-C ₆ H ₄ (SiH ₂)(SiH)) ₂ - Ni ₂ (depe) ₂]	(depe)Ni(PEt ₃) ₂ ⁷⁵ + 1,2-(H ₃ Si) ₂ C ₆ H ₄	49 orange 150–157 (dec)			−52.0 (ddd) (SiH ₂) 92.2 (quasi dt) (μ-SiH) −48.5 ⁷⁶ (SiH ₂) 79.9 (μ-SiH)	X-ray ³¹ P CPMAS EA X-ray	64
*1-64 (depe)Ni[(η ² -H-SiH(C ₆ H ₄ SiH ₂)]	(depe)Ni(PEt ₃) ₂ + [(2-H ₃ Si)C ₆ H ₄] ₂ SiH ₂	77 light brown		2.61 (br s, 5H) 5.67 (t, 1H) J = 17 −6.70 (1H) 4.79 (4H)	−2.3 (dept) (sextet t) ¹ J _{SiH} = 80 34.4 (dt) ¹ J _{SiH} = 173 23.8 (dd) (CSiH) −31.4 (dd) (PdSiH ₂ SiH ₂) −61.8 (s) (SiH ₂ SiH) −23.88 (tt) 79.8 (tt)	³¹ P IR EA X-ray DFT	65
*1-65 [R ₂ P(CH ₂) ₂ PR ₂][Pd(SiH- (C ₆ H ₄ -o-SiH ₂ SiH(C ₆ H ₄))] ⁷⁷ R = Cy	(Et ₃ P) ₂ Pd + R ₂ P(CH ₂) ₂ PR ₂ + [(2-H ₃ Si)C ₆ H ₄] ₂ SiH ₂	86	−80			X-ray	66a
1-66a { [R ₂ P(CH ₂) ₂ PR ₂][Pd] ₂ - [Si(C ₆ H ₄ -o-SiH ₂ SiH ₂)] ₂ } ⁷⁸ R = Me	2Pd(PEt ₃) ₄ + 2R ₂ P(CH ₂) ₂ PR ₂ + [(2-H ₃ Si)C ₆ H ₄] ₂ SiH ₂	81 yellow				X-ray	66a
1-66b (dmpe)Pd[(1,2-C ₆ H ₄ - (SiMe ₂)(SiH ₂))] ⁷⁹	Pd(PEt ₃) ₂ (dmpe) + 1-(H ₃ Si)-2-(HMMe ₂ Si)C ₆ H ₄	72 pale brn		5.57 (t) J _{SiH} = 158	−17.7 (d) J _{SiH} = 158 (SiH ₂) 31.8 (d) (SiMe ₂)	³¹ P EA	66b

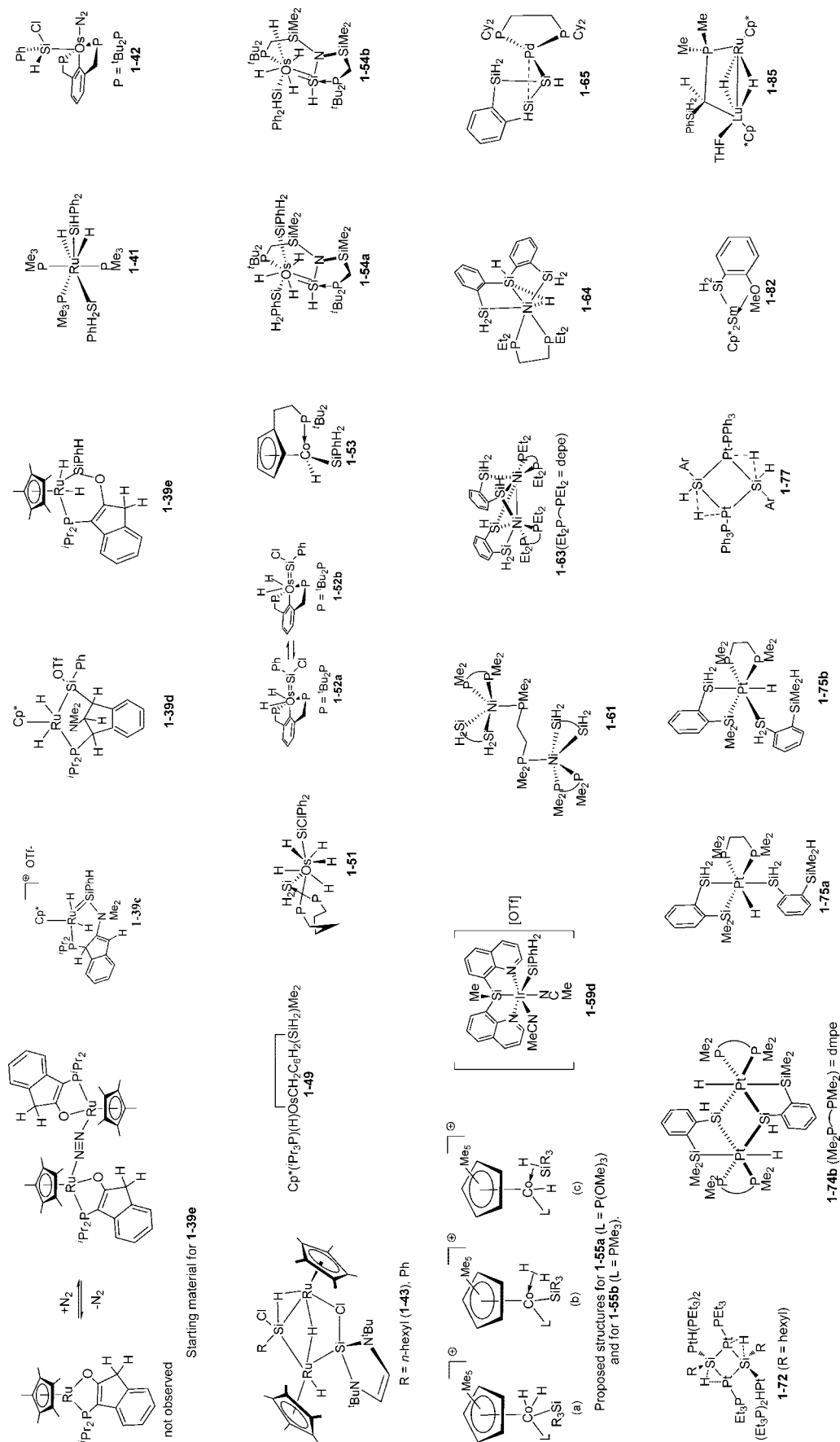
Table 1g. Continued

compound	reactants	% yield, color m.p., °C	solvent (temp.) ²	NMR			other ^d	ref
				¹ H M–H ³	¹ H Si–H ³	²⁹ Si ^{1,3}		
1-67 (Ph ₃ P) ₂ HP(SiAr)H ₂ ⁷⁹ Ar = 2,6-(Me) ₂ C ₆ H ₃	(Ph ₃ P) ₃ Pt + H ₃ SiAr	38 colorless 68–71	C ₆ D ₆	–3.40 dd	4.58 (dd) ¹ J _{SiH} = 166	–54.9 (dd)	¹³ C ³¹ P IR	67
1-68 (Ph ₃ P) ₂ HPt{Si[C ₆ (C ₆ H ₅) ₅]H ₂ } ⁸⁰	(Ph ₃ P) ₂ Pt(η ² -C ₂ H ₄) + H ₃ Si[C ₆ (C ₆ H ₅) ₅]	76 off-white	C ₆ D ₆	–1.81 dd	4.26 (pt) ¹ J _{SiH} = 182	–45.4 ¹ J _{Psi} = 1155	X-ray ³¹ P IR [EA]	68a,b
1-69 (Ph ₃ P) ₂ Pt[Si(<i>p</i> -Tol)H ₂] ⁸¹	(Ph ₃ P) ₂ Pt(η ² -C ₂ H ₄) + H ₃ Si(<i>p</i> -Tol)	88 yellow	C ₆ D ₆		5.08 (m) ¹ J _{SiH} = 177		³¹ P	68a,b
1-70 [(Et ₃ P) ₂ Pt(μ-Si(Hex)H)] ₂ ⁸²	(Et ₃ P) ₃ Pt + H ₃ SiHex	yellow	C ₆ D ₆		4.01 (app pent) (trans) 3.55 (m) (cis)	–93 (tt) ¹ J _{Psi} = 667 (trans) –66 (tt) ¹ J _{Psi} = 676 (cis)	³¹ P ¹⁹⁵ Pt IR	69
1-71 (Pr ₃ P) ₂ Pt{[μ-Si(Hex)H]} ₂ ⁸³	(Pr ₃ P) ₃ Pt + H ₃ SiHex	40 yellow	C ₆ D ₆		3.89 (app sept) (trans) ¹ J _{SiH} = 159 3.54 (br) (cis)	–94 (tt) (trans) –66 (cis)	¹³ C ³¹ P ¹⁹⁵ Pt X-ray	69
*1-72 {(Et ₃ P)Pt(μ-η ² -H-Si(Hex))Pt(H)(PEt ₃) ₂ }] ₂ ⁸⁴ (σ-complex)	(Et ₃ P) ₃ Pt + H ₃ SiHex	22 yellow	C ₆ D ₆	–2.23 dd ¹ J _{PtH} = 998	1.03–1.05 (q) ¹ J _{SiH} = 30	194 (app tm) ¹ J _{Psi} = 1080	³¹ P ¹⁹⁵ Pt EA	69
1-73 (1-35) {(Ph ₃ P)Pt[μ-η ² -H-Si(Ar)H]} ₂ ⁸⁵ Ar = 2,4,6-(MeO) ₃ C ₆ H ₂ (σ-complex)	(Ph ₃ P) ₂ Pt(η ² -C ₂ H ₄) + H ₃ SiAr	79 white	C ₆ D ₆		2.44 (br d) (μ-η ² -H) (trans) 8.95 (s) SiH(TMP) ¹ J _{SiH} = 159 2.38 (br d) (μ-η ² -H) (cis) 8.65 (s) SiH(TMP) ¹ J _{SiH} = 160 5.53 (d) ¹ J _{SiH} = 159	125 126	³¹ P X-ray VTNMR IR EA	68a
1-74a [(1,2-C ₆ H ₄ (SiMe ₂)(SiH ₂))–Pt(dmpe)]	(Et ₃ P) ₂ Pt(dmpe) ⁸⁷ + 1,2-C ₆ H ₄ (SiMe ₂ H)(SiH ₃) (1:1 ratio)	92 colorless 1-74a / 1-74b = 95/5	THF- <i>d</i> ₈				1-74a ³¹ P	66c
*1-74b [(dmpe)(H)Pt] ^{IV} {1,2-C ₆ H ₄ (SiMe ₂)(μ-SiH)} ₂ ⁸⁶	(Et ₃ P) ₂ Pt(dmpe) ⁸⁷ + 1,2-C ₆ H ₄ (SiMe ₂ H)(SiH ₃) (1:1 ratio)	92 colorless 1-74a / 1-74b = 95/5	THF- <i>d</i> ₈	–8.61		–94.0 (quasi-sep)	1-74b ³¹ P ²⁹ Si (CP-MAS) X-ray mixture [EA] thermodynamic parameters	66c

Table 1h. Continued

compound	reactants	% yield, color m.p., °C	solvent (temp.) ²	NMR			other ^d	ref
				¹ H M–H ³	¹ H Si–H ³	²⁹ Si ^{1,3}		
* 1-75a [(1,2-C ₆ H ₄ (SiMe ₂ H)- (SiH ₂))(1,2-C ₆ H ₄ (SiMe ₂)- (SiH ₂))(H)PtIV(dmpe)] (mixture of isomers, 1-75a and 1-75b) ⁸⁸	(Et ₃ P) ₂ Pt(dmpe) + 1,2-C ₆ H ₄ (SiMe ₂ H)(SiH ₃) (1:2 ratio)	78 light yellow(5:3)	C ₆ D ₆	-10.03 (br d) 1-75a -8.30 (t) 1-75b	4.30–5.35 (m, SiH ₂)	1-75a -48.8 (dd) <i>J</i> _{PtSi} = 685 1-75b -34.8 (t) <i>J</i> _{PtSi} = 592 (SiH ₂) -19.2 (s) (SiMe ₂ H) 8.2 (dd) <i>J</i> _{PtSi} = 641 (SiMe ₂ Pt) 1-75b -37.5 (dd) <i>J</i> _{PtSi} = 746 -25.4 (dd) <i>J</i> _{PtSi} = 643 (SiH ₂) -19.0 (s) SiMe ₂ H 6.5 (dd) <i>J</i> _{PtSi} = 671 SiMe ₂ Pt 1-76a -26.6 (t) <i>J</i> _{PtSi} = 657 (SiH ₂) 6.9 (dd) <i>J</i> _{PtSi} = 668 (SiMe ₂ Pt) 174	mixture ³¹ P EA 1-75b X-ray	66c
1-76a [(1,2-C ₆ H ₄ (SiMe ₂)(SiH ₂)) ₂ - PtIV(dmpe)] (mixture of isomers, 1-76a and 1-76b) ⁹⁰	1-75a + 1-75b + Δ	77 colorless	C ₇ D ₈		4.05–4.65 (mixture)		³¹ P X-ray mixture [EA]	66c
* 1-77 [(Ph ₃ P) ₂ Pt(μ-η ² -H- Si(Ar)H)] ₂ ⁸⁵ Ar = 2,3,4,5,6-(Ph) ₅ C ₆ (<i>o</i> -complex)	(Ph ₃ P) ₂ Pt(η ² -C ₂ H ₄) + H ₃ SiAr	97 cream	CD ₂ Cl ₂		0.35 (d) (μ-η ² -H) <i>J</i> _{SiH} = 48 <i>J</i> _{SiH} = 650 <i>J</i> _{PtH} = 7.48 (s) SiHAr		³¹ P IR EA X-ray	68a
1-78 [(Ph ₃ P) ₂ Pt(μ-η ² -HSi(Ar)H)] ₂ Ar = 2-Pr-6-Me-C ₆ H ₂ (cis/trans = 1/3)	(Ph ₃ P) ₂ Pt(η ² -C ₂ H ₄) + H ₃ SiAr or Pt(PPh ₃) ₄ + H ₃ SiAr	83 off-white	C ₆ D ₆	2.17 Pt(η ² -H-Si) (cis and trans)	8.42 (br s) <i>J</i> _{PtH} = 137, 78 Pt(η ² -H-Si) (cis) (trans) 8.92 (br s) <i>J</i> _{SiH} = 216 <i>J</i> _{PtH} = 137, 72 Pt(η ² -H-Si) (trans) <i>J</i> _{SiH} = 169	126 (cis) 131 (trans)	³¹ P VTNMR IR EA X-ray	68b
1-79 [(Me ₂ PhP) ₂ Pt(μ-Si(Ar)H)] ₂ Ar = 2-(Pr)-6-(CH ₃)C ₆ H ₃	(Me ₂ PhP) ₂ Pt(CH ₃) ₂ + H ₃ SiAr	26 yellow	C ₆ D ₆			-134.2	³¹ P 2D- NMR VT- NMR IR EA X-ray	70
Cu triad 1-80 RSi on Au surface R = Hex ⁹¹	Au surface + H ₃ SiR	91					RAIRS XPS	71a
lanthanides 1-81 [Cp* ₂ SmSiH ₃] ₂ ⁹²	Cp* ₂ SmCH(SiMe ₃) ₂ + H ₃ SiPh [Cp* ₂ Sm(μ-H)] ₂ + H ₃ Si(C ₆ H ₄ OMe- <i>o</i>)	35–56 orange 210 (d) ¹⁵	C ₆ D ₆ or C ₇ D ₈ C ₆ D ₆				IR EA IR	72 73
* 1-82 Cp* ₂ Sm[Si(C ₆ H ₄ OMe- <i>o</i>)H] ₂ ⁹⁴								

Table 1j. Continued



²⁹Si may have been determined by direct observation, INEPT, or DEPT, or 2D ²⁹Si-¹H correlation. These methods are not distinguished in the table. ² Deuterated solvent key: toluene, C₇D₈; methylene chloride, CD₂Cl₂; benzene, C₆D₆; fluorobenzene, C₆H₅F; tetrahydrofuran, C₄D₈O. Ambient temperature unless otherwise noted. Temperatures in °C. ³ In ppm. Coupling constants in Hz. Assignments: s, singlet; d, doublet; t, triplet; q, quartet; quin, quintet; m, multiplet; br, broad; vt = virtual triplet. ⁴ Will contain other characterization methods including spectroscopic, X-ray, and calculations if reported. If elemental analyses were reported, this will be indicated by EA. If analysis is outside ±0.5% of calculated percentage value for carbon, this will be indicated by the symbolism [EA]. The ¹³C NMR data are proton decoupled unless otherwise indicated otherwise. ⁵ In the absence of PMe₃, an insoluble, pyrophoric powder was produced. ⁶ Not specified. ⁷ Only broad resonances were observed, consistent with a paramagnetic species. ⁸ Observed only in a matrix. ⁹ Laser-ablated metal was reacted with SiH₄ (or SiD₄) in excess argon or neon during condensation at 4 K. In the reaction of Mo, the intermediate HMo-SiH₃ was observed, which underwent α-H transfers to produce the silylidyne complex. The intermediate was not observed in the reaction of W. ¹⁰ In solution, an equilibrium mixture of the σ-complex, **1-3d**, and the hydrosilyl tautomer MoH(SiH₃)(CO)(depe), **1-3e** (OA product), exists. ¹¹ Compound prepared previously from reaction of (C₅H₅)₂PH₂ and SiH₄ (X-ray structure reported) (see ref 24b). ¹² With SiH₄ and primary silanes such as PhSiH₃, C₆H₁₁SiH₃, 3,5-Me₂-C₆H₃SiH₃, and MeSiH₃, Cp*₂ScH was produced. Reaction of Cp*₂ScPh with PhSiH₃ gave Cp*₂ScH as the major Sc-product in ~60% yield as well as Ph₂SiH₂, and with MeSiH₃, equivalent amounts of **1-8** and C₂H₆ were produced. ¹³ Additional derivative prepared from [Cp*₂ScMe] + H₃SiSi(SiMe₃)₃. See also Table 2. ¹⁴

Table 1k. Continued

¹⁴ C₆H₉ is a styrenyl ligand.⁷⁶ Spectroscopic and X-ray analysis are claimed, but structure was not deposited and spectroscopic data are not available.¹⁵ Characterized in solution (not isolated).^{28, 16} Observed in solution in solution ≤ -50 °C.^{28, 17} Stereochemically rigid from -60 to 95 °C.^{33, 18, 19} The analogue, **1-22**–¹⁵N, also reported.^{34b, 19} Also reported from *o*-Me₂NCH₂C₆H₄SiH₃.^{35, 21} Reaction with C₆F₅SiH₃ and PhSiH₄ led to decomposition products. Additional derivatives successfully prepared from MesSiH₃ and PhCH₂SiH₃.^{36a} In this case, a nearly statistical distribution of deuterium at all 4 Si–H positions was observed.^{36b, 28} See structure of **1-25b** in structure section for proton assignments.^{36b, 24} Reaction of **1-25b** with PhSiD₃ was also described, but in this case, a nearly statistical distribution of deuterium at all 4 Si–H positions was observed.^{36b, 28} See structure of **1-25c** in structure section for proton assignments.^{36b, 24} Full paper describes reaction with *p*-MeC₆H₄SiH₃, *o*-MeC₆H₄SiH₃, *p*-C₆H₄SiH₃, and *n*-C₆H₁₃SiH₃.^{37a, 27} Additional derivative formed from *p*-MeC₆H₄SiH₃.^{37b, 27} Preparation of **1-28** involved photolysis with no periodic removal of the volatile components. When CO and CH₄ were removed by periodic freeze–pump–thaw cycles, **1-29** was the major product.^{38a, 39} Additional derivative with Cp' = Cp*.^{38a, 39} Also reported were [Cp*(dmpe)(H)₂W=SIRr][B(C₆F₅)₄] (R = R', Me (X-ray); R = Ph, R' = Me) as well as [Cp*(dmpe)(D)₂W=SiPh₂][B(C₆F₅)₄] (characterized in solution only) reported in Table 2.^{39, 32} Characterized in solution. Additional derivative, R = R' = Ph, Me (X-ray); R = Ph, R' = Me) as well as [Cp*(dmpe)(D)₂W=SiPh₂][B(C₆F₅)₄] (characterized in solution only) reported in Table 2.^{39, 32} Characterized in solution. Additional derivative, R = R' = Ph, Me (X-ray); R = Ph, R' = Me) as well as [Cp*(dmpe)(D)₂W=SiPh₂][B(C₆F₅)₄] (characterized in solution only) reported in Table 2.^{39, 32} Characterized in solution. Additional derivative, R = R' = Ph, Me (X-ray); R = Ph, R' = Me) as well as [Cp*(dmpe)(D)₂W=SiPh₂][B(C₆F₅)₄] (characterized in solution only) reported in Table 2.^{39, 32} Characterized in solution. Additional derivative, R = R' = Ph, Me (X-ray); R = Ph, R' = Me) as well as [Cp*(dmpe)(D)₂W=SiPh₂][B(C₆F₅)₄] (characterized in solution only) reported in Table 2.^{39, 32} Characterized in solution. Additional derivative, R = R' = Ph, Me (X-ray); R = Ph, R' = Me) as well as [Cp*(dmpe)(D)₂W=SiPh₂][B(C₆F₅)₄] (characterized in solution only) reported in Table 2.^{39, 32} Characterized in solution. Additional derivative, R = R' = Ph, Me (X-ray); R = Ph, R' = Me) as well as [Cp*(dmpe)(D)₂W=SiPh₂][B(C₆F₅)₄] (characterized in solution only) reported in Table 2.^{39, 32} Characterized in solution. Additional derivative, R = R' = Ph, Me (X-ray); R = Ph, R' = Me) as well as [Cp*(dmpe)(D)₂W=SiPh₂][B(C₆F₅)₄] (characterized in solution only) reported in Table 2.^{39, 32} Characterized in solution. Additional derivative, R = R' = Ph, Me (X-ray); R = Ph, R' = Me) as well as [Cp*(dmpe)(D)₂W=SiPh₂][B(C₆F₅)₄] (characterized in solution only) reported in Table 2.^{39, 32} Characterized in solution. Additional derivative, R = R' = Ph, Me (X-ray); R = Ph, R' = Me) as well as [Cp*(dmpe)(D)₂W=SiPh₂][B(C₆F₅)₄] (characterized in solution only) reported in Table 2.^{39, 32} Characterized in solution. Additional derivative, R = R' = Ph, Me (X-ray); R = Ph, R' = Me) as well as [Cp*(dmpe)(D)₂W=SiPh₂][B(C₆F₅)₄] (characterized in solution only) reported in Table 2.^{39, 32} Characterized in solution. Additional derivative, R = R' = Ph, Me (X-ray); R = Ph, R' = Me) as well as [Cp*(dmpe)(D)₂W=SiPh₂][B(C₆F₅)₄] (characterized in solution only) reported in Table 2.^{39, 32} Characterized in solution. Additional derivative, R = R' = Ph, Me (X-ray); R = Ph, R' = Me) as well as [Cp*(dmpe)(D)₂W=SiPh₂][B(C₆F₅)₄] (characterized in solution only) reported in Table 2.^{39, 32} Characterized in solution. Additional derivative, R = R' = Ph, Me (X-ray); R = Ph, R' = Me) as well as [Cp*(dmpe)(D)₂W=SiPh₂][B(C₆F₅)₄] (characterized in solution only) reported in Table 2.^{39, 32} Characterized in solution. Additional derivative, R = R' = Ph, Me (X-ray); R = Ph, R' = Me) as well as [Cp*(dmpe)(D)₂W=SiPh₂][B(C₆F₅)₄] (characterized in solution only) reported in Table 2.^{39, 32} Characterized in solution. Additional derivative, R = R' = Ph, Me (X-ray); R = Ph, R' = Me) as well as [Cp*(dmpe)(D)₂W=SiPh₂][B(C₆F₅)₄] (characterized in solution only) reported in Table 2.^{39, 32} Characterized in solution. Additional derivative, R = R' = Ph, Me (X-ray); R = Ph, R' = Me) as well as [Cp*(dmpe)(D)₂W=SiPh₂][B(C₆F₅)₄] (characterized in solution only) reported in Table 2.^{39, 32} Characterized in solution. Additional derivative, R = R' = Ph, Me (X-ray); R = Ph, R' = Me) as well as [Cp*(dmpe)(D)₂W=SiPh₂][B(C₆F₅)₄] (characterized in solution only) reported in Table 2.^{39, 32} Characterized in solution. Additional derivative, R = R' = Ph, Me (X-ray); R = Ph, R' = Me) as well as [Cp*(dmpe)(D)₂W=SiPh₂][B(C₆F₅)₄] (characterized in solution only) reported in Table 2.^{39, 32} Characterized in solution. Additional derivative, R = R' = Ph, Me (X-ray); R = Ph, R' = Me) as well as [Cp*(dmpe)(D)₂W=SiPh₂][B(C₆F₅)₄] (characterized in solution only) reported in Table 2.^{39, 32} Characterized in solution. Additional derivative, R = R' = Ph, Me (X-ray); R = Ph, R' = Me) as well as [Cp*(dmpe)(D)₂W=SiPh₂][B(C₆F₅)₄] (characterized in solution only) reported in Table 2.^{39, 32} Characterized in solution. Additional derivative, R = R' = Ph, Me (X-ray); R = Ph, R' = Me) as well as [Cp*(dmpe)(D)₂W=SiPh₂][B(C₆F₅)₄] (characterized in solution only) reported in Table 2.^{39, 32} Characterized in solution. Additional derivative, R = R' = Ph, Me (X-ray); R = Ph, R' = Me) as well as [Cp*(dmpe)(D)₂W=SiPh₂][B(C₆F₅)₄] (characterized in solution only) reported in Table 2.^{39, 32} Characterized in solution. Additional derivative, R = R' = Ph, Me (X-ray); R = Ph, R' = Me) as well as [Cp*(dmpe)(D)₂W=SiPh₂][B(C₆F₅)₄] (characterized in solution only) reported in Table 2.^{39, 32} Characterized in solution. Additional derivative, R = R' = Ph, Me (X-ray); R = Ph, R' = Me) as well as [Cp*(dmpe)(D)₂W=SiPh₂][B(C₆F₅)₄] (characterized in solution only) reported in Table 2.^{39, 32} Characterized in solution. Additional derivative, R = R' = Ph, Me (X-ray); R = Ph, R' = Me) as well as [Cp*(dmpe)(D)₂W=SiPh₂][B(C₆F₅)₄] (characterized in solution only) reported in Table 2.^{39, 32} Characterized in solution. Additional derivative, R = R' = Ph, Me (X-ray); R = Ph, R' = Me) as well as [Cp*(dmpe)(D)₂W=SiPh₂][B(C₆F₅)₄] (characterized in solution only) reported in Table 2.^{39, 32} Characterized in solution. Additional derivative, R = R' = Ph, Me (X-ray); R = Ph, R' = Me) as well as [Cp*(dmpe)(D)₂W=SiPh₂][B(C₆F₅)₄] (characterized in solution only) reported in Table 2.^{39, 32} Characterized in solution. Additional derivative, R = R' = Ph, Me (X-ray); R = Ph, R' = Me) as well as [Cp*(dmpe)(D)₂W=SiPh₂][B(C₆F₅)₄] (characterized in solution only) reported in Table 2.^{39, 32} Characterized in solution. Additional derivative, R = R' = Ph, Me (X-ray); R = Ph, R' = Me) as well as [Cp*(dmpe)(D)₂W=SiPh₂][B(C₆F₅)₄] (characterized in solution only) reported in Table 2.^{39, 32} Characterized in solution. Additional derivative, R = R' = Ph, Me (X-ray); R = Ph, R' = Me) as well as [Cp*(dmpe)(D)₂W=SiPh₂][B(C₆F₅)₄] (

Table 2. Complexes Formed from Reaction of R_2SiH_2 with Transition Metal Complexes (Structures Are Shown at the End of the Table for Compounds Marked with an Asterisk)^{†,‡}

compound	reactants	% yield,color m.p., °C	NMR			other	ref	
			solvent ^{1,3} (temp., °C) ²	¹ H M–H	¹ H Si–H			²⁹ Si
Sc triad								
2-1 Cp [*] ₂ ScSiH(SiMe ₃) ₂ ⁶	Cp [*] ₂ ScMe + H ₂ Si(SiMe ₃) ₂	52 163–166			2.53 (s) ¹ J _{SiH} = 115	–6.41 (SiMe ₃) ₂ –108.2 (SiH)	¹³ C IR EA X-ray	26b
Ti triad								
2-2 Cp ₂ (py)TiSiPh ₂ H ⁷	Cp ₂ TiMe ₂ + py + H ₂ SiPh ₂	87 violet					[EA] X-ray EPR	27, 77 ⁸
V triad								
2-3a Cp(dmpe)VSiHPh ₂	Cp(dmpe)VMe + Ph ₂ SiH ₂	74 red–brown					IR EA μ_{eff} X-ray ³¹ P IR	31b
2-3b Cp(ArN)(PMe ₃)HNb-SiHMePh Ar = 2,6-C ₆ H ₃ iPr ₂ (a mixture of two isomers) ¹⁰	Cp(ArN)Nb(PMe ₃) ₂ + H ₂ SiMePh	100 yellow–brn oil		1st isomer 2.02 (d) 2nd isomer 2.24 (d)	1st isomer 5.96 (h) 2nd isomer 5.96 (q)	2nd isomer 13.3 ¹ J _{SiH} = 156 ² J _{SiH} < 14 ? ¹ J _{SiH} = 180 ² J _{SiH} = 14		32a
2-3c Cp(ArN)(PMe ₃)HTa-SiHMePh Ar = 2,6-C ₆ H ₃ iPr ₂	Cp(ArN)Ta(PMe ₃) ₂ + H ₂ SiMePh	98 cherry-red		5.87 (dd)	6.18 (q)	¹³ C ³¹ P EA IR		78a
2-4 Cp [*] (Me)HTa[(CH ₂) ₃ SiHN-(C ₆ H ₃ Me) ₂ NSiMe ₃] ¹¹	Cp [*] (Me)Ta[=N(C ₆ H ₃ Me) ₂ N-SiMe ₃] + H ₂ Si(CH ₂) ₃	60 off-white		17.02 (s)	5.14 (m)	DFT ¹³ C IR		32b
2-5 (RCH ₂) ₃ Ta=C(SiR'PhH)R ¹² R = SiMe ₃ , R' = Me	(RCH ₂) ₃ (PMe ₃) ₂ Ta=CHR + H ₂ SiMePh	red-orange oil			4.9 (q)	0.08 (CH ₂ SiMe ₃) –13.2 (=CSiMe ₃) –49.9 (=CSiPhMeH) 0.4	[EA] ¹³ C	79
*2-6 (Me ₃ P) ₂ [=CRSiR'PhCR=]Ta-(CH ₂ R) ¹³ R = SiMe ₃ , R' = Me	(Me ₃ P) ₂ (RCH ₂)(RCH=) ₂ Ta + H ₂ SiMePh	78 yellow				¹³ C ³¹ P 2D NMR X-ray		79
Cr triad								
2-7 (OC) ₃ Cr=Si(CH=CH ₂)(C ₆ H ₄ -CH ₂ NMe ₂ -o) ¹⁴	Cr(CO) ₆ + H ₂ Si(C ₆ H ₄ CH ₂ NNMe ₂ -o)-(CH=CH ₂) (hv) Cr(CO) ₆ + H ₂ SiPh ₂	43		–11.17 ¹ J _{SiH} = 108 (Cr–H–Si)	6.02 ¹ J _{SiH} = 234 (Cr–Si–H)			80a
2-8 (OC) ₅ Cr(η^2 -H ₂ SiPh ₂) ¹⁵						VT		81

Table 2a. Continued

compound	reactants	% yield, color m.p., °C	NMR				other	ref
			solvent ^{1,3} (temp., °C) ²	¹ H M-H	¹ H Si-H	²⁹ Si		
2-9 Cp ₂ (H)Mo[Si(C ₃ Me ₄ H) ₂ H]	Cp ₂ MoH ₂ + H ₂ Si(C ₃ Me ₄ H) ₂ (hν)	47	C ₆ D ₆	-8.11 (s)	5.07 (s) ¹ J _{SiH} = 177	26.2	¹³ C IR MS	17, 35
2-10 Cp*(dmpe)(H)Mo=SiEt ₂ ¹⁶ (silylene)	Cp*(dmpe)Mo(η ³ -CH ₂ Ph) + H ₂ SiEt ₂	67 red	C ₆ D ₆	-13.91 ¹ J _{SiH} = 44		273 (m)	X-ray ¹³ C ³¹ P IR EA X-ray	36a
2-11 Cp*(dmpe)(H)Mo=Si(Cl)Mes silylene	Cp*(dmpe)Mo(η ³ -CH ₂ Ph) + H ₂ SiMes(Cl)	88 dark red	C ₆ D ₆	-12.50 (t; ¹ J _{Hsi} = 38)		182	ND ¹³ C ³¹ P IR EA X-ray	82a
2-12 (OC) ₃ Mo(η ² -H ₂ SiPh ₂) ¹⁷	Mo(CO) ₆ + H ₂ SiPh ₂		CD ₂ Cl ₂ -88	-6.49 ¹ J _{SiH} = 111 (Mo-H-Si)	6.04 ¹ J _{SiH} = 232 (Mo-Si-H)			81, 83a
2-13 (2-6c) (OC)(depe) ₂ Mo- (η ² -H-SiHPh ₂)	[Mo(CO)(depe) ₂] ₂ (μ-N ₂) + H ₂ SiPh ₂	lemon-yellow 61	C ₆ D ₆	-7.57 (d) ¹ J _{SiH} = 8.1 ¹ J _{SiH} = 50.6 (Mo(η ² -H-Si))	6.78 (d) ¹ J _{SiH} = 8.2 ¹ J _{SiH} = 172 (SiH)		³¹ P IR EA X-ray	21b
2-14 (OC)(^t Bu ₂ PC ₂ H ₄ P ^t Bu) ₂ Mo- (η ² -HSiHPh ₂)	Mo(CO)(^t Bu ₂ PCH ₂ - CH ₂ P ^t Bu) ₂ + H ₂ SiPh ₂	¹⁸	C ₆ D ₃ CD ₃	-7.48 (d) ¹ J _{SiH} = 7.5 ¹ J _{SiH} = 49 (Mo(η ² -HSi))	6.72 (d) ¹ J _{SiH} = 7.5 ¹ J _{SiH} = 168 ¹⁹		calc ³¹ P VT	21b
*2-15 [H ₃ Mo{[Ph ₂ PCH ₂ CH ₂ P(Ph)- C ₆ H ₄ -o](Ph)(R)Si- P,P,P,P,Si} R = Ph ²⁰	(dppe) ₂ MoH ₄ + H ₂ SiPh ₂	87 yellow	C ₆ D ₆	-5.20 (d quart)			³¹ P IR	37ab
2-16 [{Mo(μ-η ² -H- SiEt ₂)(CO) ₄ } ₂]	Mo(CO) ₆ + H ₂ SiEt ₂	~98 brown	C ₇ D ₈ (-30)	-8.33(s)		207.7(dg) ¹ J _{SiH} = 58 ² J _{SiH} = 41	X-ray ¹³ C ⁹⁵ Mo IR	84
2-17 <i>trans</i> -Cp*(OC) ₂ (py)W- SiPh ₃ H ²¹	Cp*(OC) ₃ WMe + py + H ₂ SiPh ₂ (hν)	34 ²² yellow	C ₆ D ₆		5.96 ¹ J _{SiH} = 176	22.4 ¹ J _{Wsi} = 38	X-ray ¹³ C IR MS HRMS	85a ⁵
2-18 <i>cis</i> -Cp*(OC) ₂ (py-d ₅)W- SiPh ₂ H ²³	Cp*(OC) ₃ WMe + py-d ₅ + H ₂ SiPh ₂ (hν)		C ₅ D ₅ N ²⁹ Si (-35)		6.79 ¹ J _{SiH} = 177	100.0 ¹ J _{Wsi} = 81	X-ray ¹³ C	85a ⁵
2-19 Cp*(OC) ₂ (H)W=SiMePh •py-d ₅ ²⁴	Cp*(OC) ₂ (H)W=SiEt ₂ • py-d ₅ + H ₂ SiMePh	100 ²⁵	C ₅ D ₃ N					85a ⁵
2-20 Cp*(OC) ₂ (H)W=SiR ₂ •py R = Ph ²⁶	Cp*(OC) ₃ WMe + py + CH ₃ CN + H ₂ SiPh ₂ (hν)	78 orange	C ₆ D ₆	-7.70 (s) ¹ J _{WH} = 65		94.0 ¹ J _{Wsi} = 111	¹³ C IR MS HRMS X-ray	85a ⁵

Table 2b. Continued

compound	reactants	% yield, color m.p., °C	NMR				other	ref
			solvent ^{1,3} (temp., °C) ²	¹ H M–H	¹ H Si–H	²⁹ Si		
2-21 [Cp*(dmpe)(H) ₂ W=SiMe ₂] ⁺ [B(C ₆ F ₅) ₄] ²⁷	(<i>η</i> ⁶ -C ₅ Me ₃ CH ₂)(dmpe)W(H)Cl + Li(Et ₂ O) _{2.5} B(C ₆ F ₅) ₄ + H ₂ SiMe ₂	65 orange	FC ₆ H ₅ ²⁸	–5.90 J _{WH} = 48		314 ² J _{SiH} = 7	¹³ C ³¹ P <i>T</i> ₁ IR EA X-ray calc	39 86 475
2-23 (OC) ₃ W(<i>η</i> ² -H ₂ SiPh ₂) ⁵	[(<i>η</i> ⁷ -C ₅ Me ₃ (CH ₂) ₂ (dmpe)- W(H) ₂][B(C ₆ F ₅) ₄] + H ₂ SiMe ₂ W(CO) ₆ + H ₂ SiPh ₂	65 orange	CD ₂ Cl ₂	–6.40 J _{SiH} = 98 J _{WH} = 39 (W–H–Si) 4.62 (dd)	6.50 J _{SiH} = 236 (W–Si–H)			81
2-24a Cp*(dmpe)H(Cl)WSiPh ₂ H ²⁹	(<i>η</i> ⁶ -C ₅ Me ₃ CH ₂)(dmpe)W- (H)Cl + H ₂ SiPh ₂	61 lt orange	CD ₂ Cl ₂		5.44 (s)	9.3 J _{SiH} = 157 (HMQC)	¹³ C ³¹ P IR EA ¹³ C	39
2-24b (OC) ₃ (<i>η</i> ⁴ -nbd)(H)W(<i>μ</i> -H- SiEt ₂)	(OC) ₄ W(<i>η</i> ⁴ -nbd) + H ₂ SiEt ₂	C ₆ D ₁₂	C ₆ D ₆ (²⁹ Si)	–8.33 (d) J _{WH} = 52 J _{SiH} = 29.1				87b
*2-25 (<i>μ</i> -SiPh ₂)[W ₂ (CO) ₁₀]	W(CO) ₆ + H ₂ SiPh ₂ (1:1) hν ³⁰	80 orange	CDCl ₃	–11.47 (d) J _{WH} = 38.1		211.3 J _{SiW} = 211	¹³ C IR [EA] X-ray ¹³ C	87a, 87b
2-26a [{W(<i>μ</i> - <i>η</i> ² -H–SiPh ₂ (CO) ₄) ₂] ³¹	W(CO) ₆ + H ₂ SiPh ₂ (1:1) hν or (OC) ₄ W(<i>η</i> ⁴ -nbd) + H ₂ SiPh ₂ W(CO) ₆ + 1.4H ₂ SiEt ₂ hν	– yellow mixture	C ₇ D ₈	–7.50 J _{WH} = 33 J _{SiH} = 41		194		87b
2-26b [{W(<i>μ</i> - <i>η</i> ² -H–SiEt ₂)(CO) ₄] ₂ + [(<i>μ</i> -SiEt ₂){W(CO) ₅] ₂]	W(CO) ₆ + 1.4H ₂ SiEt ₂ hν	– yellow mixture	C ₇ D ₈ (–30)	–9.31 (s) J _{WH} = 40 J _{SiH} = 34		184	¹³ C IR X-ray ¹³ C IR	87c
intermediates identified: [W(<i>μ</i> - <i>η</i> ² -H–SiEt ₂)(CO) ₅]				–8.05 (d) J _{WH} = 38 J _{SiH} = 93	5.10 (dq) J _{SiH} = 217	239 J _{WSi} = 49		
[(OC) ₅ W(<i>μ</i> - <i>η</i> ² -H–SiEt ₂)(<i>μ</i> -H)W(CO) ₅]				–8.25 (d) J _{WH} = 35 J _{SiH} = 37				
*2-26c (OC) ₄ W(<i>μ</i> - SiPh ₂) ₂ W(CO) ₄	W(CO) ₆ + H ₂ SiPh ₂ hν ³²	40 orange 147–147.5	C ₆ D ₆	–10.39 (d) J _{WH} = 32			¹³ C IR MS EA ³¹ P X-ray	88
*2-27 (OC) ₃ (¹ Pr ₃ P)W- (<i>μ</i> -H–SiPh ₂) ₂ W(¹ Pr ₃)(CO) ₃ (<i>σ</i> -complex)	(OC) ₃ (¹ Pr ₃ P) ₂ W + H ₂ SiPh ₂	34 orange	C ₄ D ₈ O ²⁹ Si (–20)	–7.26 (m)		146 (brd) J _{SiH} = 52		40

Table 2c. Continued

compound	reactants	% yield, color m.p., °C	NMR				other	ref
			solvent ^{1,3} (temp., °C) ²	¹ H M–H	¹ H Si–H	²⁹ Si		
2-28 Cp(OC)Fe(μ -CO)- [μ -Si(CHPh ₂)H]WCp(CO) ₂	Cp(OC) ₃ WMe + [H ₂ Si(CHPh ₂) ₂][Fe(Cp*)(CO) ₂] (h ν)	44 red	C ₆ D ₆		8.08 (d)	228.1	¹³ C IR MS EA X-ray	42b
Mn triad 2-29 (η^5 -C ₅ H ₄ Me)(OC) ₂ Mn- (η^7 -HSiHPPh ₂)	(η^5 -C ₅ H ₄ Me)Mn(CO) ₃ + H ₂ SiPh ₂ ³³						T ₁ ND X-ray calc ¹³ C EI-MS [EA] VTNMR IR MS HRMS EA X-ray	89a,d
2-30 η -Cp(OC) ₂ Mn=Si[2-Me ₂ N- CH ₂ C ₆ H ₄]Me	CpMn(CO) ₃ + H ₂ Si[C ₆ H ₄ CH ₂ N(CH ₃) ₂]CH ₃	36	CDCl ₃					90
2-31 (OC) ₂ Re(μ -C ₃ H ₄ -C ₃ H ₄)- (μ -SiPh ₂)Re(CO) ₂	FvRe ₂ (CO) ₆ + H ₂ SiPh ₂ (h ν)	22 yellow 190 (d)	C ₇ D ₈ ³⁴					91
Fe triad 2-32 (η^5 -C ₅ H ₄ Me)(H) ₂ - Fe(SiCl ₂ H) ₂ ³⁵	(C ₆ H ₅ Me) ₂ Fe ³⁶ + H ₂ SiCl ₂	1–2 yellow	C ₆ D ₆	–18.6 (t)	6.07 (t) <i>J</i> _{SiH} = 281		[EA] X-ray	92
2-33 Cp(OC)Fe(μ -CO)- [μ -Si(CHPh ₂)H]FeCp(CO) ³⁷	Cp(OC) ₂ FeSiMe ₃ + [H ₂ Si(CHPh ₂) ₂][Fe(Cp*)(CO) ₂]	57 red	CD ₃ CN C ₆ D ₆	–18.66 (t) <i>2J</i> _{SiH} = 17.6	5.86 (t) <i>3J</i> _{HH} = 4.8 7.38 (d)	239.8	¹³ C MS EA	42b
*2-34 (Cp*Fe) ₂ (μ -H) ₂ - (μ - η^2 : η^2 -H ₂ Si ^t Bu ₂) ³⁸	(Cp*Fe) ₂ (μ -H) ₄ + H ₂ Si ^t Bu ₂	89 dk gm	C ₄ D ₈ O	–16.25 (br s) ³⁹		71.5	X-ray ¹³ C VTNMR IR	93, 94
*2-35 (Cp*Fe) ₂ (μ -H) ₂ - (μ -SiPh ₂)	(Cp*Fe) ₂ (μ -H) ₄ + H ₂ SiPh ₂ or (Cp*Fe) ₂ (μ -H) ₂ (μ - η^2 : η^2 -H ₂ - Si ^t Bu ₂) + H ₂ SiPh ₂ Cp(OC) ₂ FeCH ₃ + H ₂ Si[Cp(OC) ₂ Fe] ₂ (h ν)	dk gm	–110 C ₆ D ₆	–5.28, –27.12 –23.71 (s)		293	EA X-ray ¹³ C X-ray	93, 94
*2-36a [Cp ₂ (OC) ₂ (μ_2 -CO)Fe ₂][Si- (3 isomers: a/b/c = 4:76:20)]	Cp(OC) ₂ FeH	57 dk red 158	C ₆ D ₆		8.15 (a) 8.53 (b) <i>1J</i> _{SiH} = 143 7.49 (c)	293.7 (b) 276.3 (c)	¹³ C 2DNMR IR	95a
*2-36b Fe ₂ (μ -H)(edt)(SiPh ₂ H)- (CO) ₃ (dppbz) ⁴⁰	Fe ₂ (edt)(CO) ₃ dppbz + H ₂ SiPh ₂ (h ν)	72 orange	CDCl ₃	–12.27 (t)			³¹ P IR FD-MS EA DFT X-ray	95c

Table 2d. Continued

compound	reactants	% yield,color m.p., °C	NMR				other	ref
			solvent ^{1,3} (temp., °C) ²	¹ H M-H	¹ H Si-H	²⁹ Si		
*2-36c Fe ₂ (<i>η</i> -H ₂ SiPh ₂)(edt)(CO) ₂ -(dppv) ⁴¹	Fe ₂ (edt)(CO) ₂ dppv + H ₂ SiPh ₂ (hv)	16.5 brown	CDCl ₃	-14.67 (t) -11.81 (s)			³¹ P VTNMR IR DFT FD-MS X-ray ¹³ C ³¹ P EA ¹³ C ³¹ P EA	95c
*2-36d [Cp*Ru(<i>κ</i> - <i>P,N</i> -2-Me ₂ <i>N</i> -3- <i>P</i> Pr ₂ -indene)(H) ₂ Ru=SiPh ₂] ⁺ X ⁻ X ⁻ = B(C ₆ F ₅) ₄ ⁻⁴²	[Cp*Ru(<i>κ</i> - <i>P,N</i> -2-Me ₂ <i>N</i> -3- <i>P</i> Pr ₂ -indene)RuCl] ⁺ [B(C ₆ F ₅) ₄] ⁻ + H ₂ SiPh ₂	82 off white	CD ₂ Cl ₂	-10.24 (d)		106.7 ² J _{SiH} = 3.0	X-ray ¹³ C ³¹ P	47b
*2-36e C ₃₀ H ₄₃ OPSiRu (see structure for 2-36e)	1a ₂ ·N ₂ ⁴³ + H ₂ SiPh ₂	95 peach	C ₆ D ₆	-11.02 (d)		57.4 ² J _{SiH} = 9.8	EA ³¹ P EA	47c
*2-36f C ₃₀ H ₅₀ PNSiRu (kinetic product, KP)	Cp*Ru(<i>κ</i> ³ - <i>P,C,C'</i>)-complex ⁴⁴ + H ₂ SiPh ₂		C ₆ D ₆	KP -9.90 (d)	KP 5.10 (s)		X-ray TP ¹³ C ³¹ P EA X-ray	47d
C ₃₀ H ₅₀ PNSiRu (thermodynamic product, TP) (see structures for 2-36f) 2-37 Tp(Ph ₃ P)(H)Ru(<i>η</i> ² -H-SiEt ₂ H) ⁴⁵	Tp(Ph ₃ P)(CH ₃ CN)RuH + H ₂ SiEt ₂	91 (TP) yellow 61 orange	C ₆ D ₆	KP -9.90 (d) TP -9.40 (d) -10.93 (dd) J _{SiH} = 24		TP 9.8 16.9	TP EA X-ray	48a
2-38a (Me ₃ P) ₄ (H)RuSiPh ₂ H ⁴⁶	(Me ₃ P) ₄ RuH ₂ + H ₂ SiPh ₂ (hv)		C ₇ D ₈	(a) -10.3 (dq) (b) -9.5 (m)	(a) 5.9 (tt) (b) 6.7 (m) ¹ J _{SiH} = 64.5	(a) ⁴⁷ (b) -10.4 (br s)	calc (a) ³¹ P (b) ³¹ P	96
2-38b (Me ₃ P) ₃ (H) ₃ RuSiPh ₂ H ⁴⁶								
2-39 (Me ₃ P) ₄ (H)RuSiMe ₂ H	(Me ₃ P) ₄ RuH ₂ + H ₂ SiMe ₂ (hv)	80	C ₆ D ₆	-10.96 (dq)	4.60 (m)	94.3 (dtd)	¹³ C ³¹ P EA	97
2-40 (Me ₃ P) ₃ (H) ₂ Ru(SiPh ₂ H) ₂ ⁴⁸	(Me ₃ P) ₃ (H) ₃ RuSiMe ₃ + H ₂ SiPh ₂	85 colorless	C ₆ D ₆	-7.71 (br s)	5.84 (br s)		X-ray ¹³ C ³¹ P VT IR EA ¹³ C IR EA	49
2-41 {Cp*Ru(<i>μ</i> -H)} ₂ (<i>μ</i> -SiMeEt) ⁴⁹	Cp*Ru(<i>μ</i> -H) ₂ RuCp* + Me(CH ₂ =CH)SiH ₂	28 red	C ₇ D ₈ C ₆ D ₆	-8.34 (dt) -7.13 (dt) -14.7 (d) -14.6 (d)	5.66 (dt) 6.19 (t)	310.8	IR EA ¹³ C IR EA	98
*2-42a [(OC) ₆ Ru ₂ (<i>μ</i> -dppm)-(<i>μ</i> -Si(<i>p</i> -Tol) ₂)]	(dppm)Ru ₃ (CO) ₁₀ + H ₂ Si(<i>p</i> -Tol) ₂	46 yellow	C ₆ D ₆			172.6 (t)	X-ray ¹³ C ³¹ P IR EA	99
*2-42b (CO) ₅ Ru ₂ [Si(<i>p</i> -Tol) ₂ H]-(<i>μ</i> -dppm)-[<i>μ</i> - <i>η</i> ² -H-Si(<i>p</i> -Tol) ₂]		24 yellow-orange	C ₆ D ₆	-8.87(d) J _{SiH} = 36.0	5.91(d) J _{SiH} = 178.5	11.5 (d, Si(<i>p</i> -Tol) ₂ -H) 150.4 (dd) (Si _{br})	X-ray ¹³ C ³¹ P IR EA	

Table 2e. Continued

compound	reactants	% yield, color m.p., °C	NMR				other	ref
			solvent ^{1,3} (temp., °C) ²	¹ H M–H	¹ H Si–H	²⁹ Si		
2-43a (OC) ₃ Ru ₂ [Si(<i>p</i> - ^t BuC ₆ H ₄) ₂ H]– (μ-dppm)–[μ-η ² -H–Si(<i>p</i> -Tol) ₂] ⁵⁰	2-42a + xs H ₂ Si(<i>p</i> - ^t BuC ₆ H ₄) ₂		C ₆ D ₆	–8.87 (d) (d, 1H) (Ru–H–Si)	5.92 (d, 1H)	10.3 (d), Si(<i>p</i> - ^t Bu C ₆ H ₄) ₂ H 150.2 (dd) Ru–Si–Ru	³¹ P	99
+ 2-43b {(OC) ₂ Ru[Si(<i>p</i> - ^t Bu- <i>u</i> - C ₆ H ₄) ₂ H] ₂ (μ-dppm)– [μ-η ² :η ² -H ₂ Si(<i>p</i> -Tol) ₂]} ratio of 2-43a / 2-43b = 1/4								
*2-44 {(OC) ₂ Ru[Si(<i>p</i> -Tol) ₂ H]} ₂ – (μ-dppm)–[μ-η ² :η ² -H ₂ Si– (<i>p</i> -Tol) ₂ H]	2-42a / 2-42b mixture with xs H ₂ Si(<i>p</i> -Tol) ₂	67 yellow	C ₆ D ₆	–8.44 (m-2H) (Ru–H–Si) –8.44 ⁵¹ <i>J</i> _{SiH} = 24.4	5.88 (m, 2H)	12.3 (d) Si(<i>p</i> - ^t Bu–C ₆ H ₄) ₂ H 154.6 Ru–Si–Ru	³¹ P	99
*2-45 (C ₃ P) ₂ (H) ₂ Ru(SiH ₄)Ru(H) ₂ – (PCy ₃) ₂ ²²	(Cy ₃ P) ₂ (H ₂) ₂ RuH ₂ + H ₂ SiMePh	32 white	C ₆ D ₆ (23)	–7.89 (pt) <i>J</i> _{SiH} = 36	5.85 (m) <i>J</i> _{SiH} = 177	13.7 (t) (Si _{tem}) 154.8 (t) (Si _{br}) 290.2 (s) ⁵³ <i>J</i> _{SiH} = 36	¹³ C ³¹ P IR EA X-ray ³¹ P IR [EA] calc	100, 101
2-46 Cp*(Pr ₃ P)– (Cl)HOsSiPh ₂ H ⁵⁴	Cp*(Pr ₃ P) ₂ OsCl + H ₂ SiPh ₂ or Cp*(Pr ₃ P)Cl(H)OsSiPh ₃ + H ₂ SiPh ₂	67 yellow	C ₇ D ₈ (20) C ₃ D ₈ (–80) C ₆ D ₆	–7.67 (pt) –6.0 (br) –8.6 (br) –14.43 (dd)	6.77 (d)	–	³¹ P IR MS EA X-ray ¹³ C ³¹ P EA X-ray	52
2-47 Cp*(Pr ₃ P)(Br)HOs– SiMe ₃ H	Cp*(Pr ₃ P)OsBr + H ₂ SiMe ₂	92 yellow–orange	C ₆ D ₆	–15.28 (d)	6.16 (m) <i>J</i> _{SiH} = 178	–23.9	³¹ P IR MS EA X-ray ¹³ C ³¹ P EA X-ray	22
2-48 Cp*(Pr ₃ P)(Br)HOs–SiPh ₂ H	Cp*(Pr ₃ P)OsBr + H ₂ SiPh ₂	78 yellow	CD ₂ Cl ₂ (²⁹ Si, HMBC) C ₆ D ₆	–14.15 (d)		–10.65 (d)	¹³ C ³¹ P IR MS EA X-ray	22
Co triad 2-50 (η ⁵ -C ₅ H ₄ CH ₂ CH ₂ P(^t Bu) ₂)– (H)CoSiHMePh ⁵⁵	(η ⁵ -C ₅ H ₄ CH ₂ CH ₂ P(^t Bu) ₂)– Co(η ² -C ₂ H ₄) + H ₂ SiMePh	57 ⁵⁶ orange	C ₆ D ₆	–17.12 (d)	4.35–5.43 (br m) <i>J</i> _{SiH} = 82.7 ⁵⁷		¹³ C ³¹ P VT-NMR IR MS EA X-ray ¹³ C ³¹ P IR VTNMR HR-MS X-ray	56
2-51 (η ⁵ -C ₅ H ₄ CH ₂ CH ₂ P(^t Bu) ₂)– (H)CoSiHPh ₂ ⁵⁸	(η ⁵ -C ₅ H ₄ CH ₂ CH ₂ P(^t Bu) ₂)– Co(η ² -C ₂ H ₄) + H ₂ SiPh ₂	79 orange 142	C ₇ D ₈	–17.02 (d)	5.73 (dd) <i>J</i> _{SiH} = 89 <i>J</i> _{HH} = 1.6		¹³ C ³¹ P IR VTNMR HR-MS X-ray	56

Table 2f. Continued

compound	reactants	% yield,color m.p., °C	NMR				other	ref
			solvent ^{1,3} (temp., °C) ²	¹ H M–H	¹ H Si–H	²⁹ Si		
2-52a Cp [*] (H) ₂ Co(SiPh ₂ H) ₂ ⁵⁹	Cp [*] Co(η ² -C ₂ H ₄) ₂ + 10H ₂ SiPh ₂	72 white	C ₆ D ₆	–15.51 (s)	5.92 (s)		¹³ C X-ray calc	103
2-52b [Cp [] Co{P(OMe) ₃ }(H)- (η ² -H–SiPh ₂ H)][B(Ar _F) ₄] ⁶⁰	Cp [*] {(MeO) ₃ P}HCo(η ² -H ₂) ⁺ [B(Ar _F) ₄] [–] + H ₂ SiPh ₂		CD ₂ Cl ₂ –30	–12.14 (d, Co [*] H)(η ² -HSi) ¹ J _{SiH(obs)} = 31.5	5.71 (s, 2H, SiH _{term}) ¹ J _{SiH} = 222	–2.5		57c
2-52c [Cp [] Co(PMe ₃)(H)- (η ² -H–SiPh ₂ H)][B(Ar _F) ₄] ⁶¹	Cp [*] {[Me ₃ P]HCo(η ² -H ₂) ⁺ [B(Ar _F) ₄] [–] + H ₂ SiPh ₂		CD ₂ Cl ₂ –30	–13.07 (d, Co [*] H)(η ² -HSi) ¹ J _{SiH(obs)} = 30	5.80 (s, 2H, SiH _{term}) ¹ J _{SiH} = 222	0.72		57c
*2-53a {κ ² -Bu ₂ PCH ₂ Me ₂ Si- NSiMe ₂ CH ₂ Bu ₂ P(H)Si=}– Co(H) ₄ (SiHPh ₂)	^{rb} PNPCo + 2PhSiH ₃	100 brown oil	Tol- <i>d</i> ₈	–11.46 (s)	5.99 (d)	(263 K) 22.2 (d) ¹ J _{SiH} = 162	³¹ P VT	57a,b
also in Table 1 as 1-55b								
*2-54 (OC) ₆ (μ-OC)Co ₂ [μ-SiMeH- (CH ₂) ₂ SiMeH] ⁶²	Co ₂ (CO) ₈ + H ₂ MeSi(CH ₂) ₂ SiMeH ₂	62	C ₆ D ₆		3.36 (m)	10.0 (s) 2.7 (s) –18.9 (d) ¹ J _{SiH} = 195	¹³ C IR	104
*2-55 [(OC) ₃ Co] ₂ – [μ-SiMe(CH ₂) ₂ SiMe] ⁶³	Co ₂ (CO) ₈ + 2H ₂ MeSi(CH ₂) ₂ SiMeH ₂	70 pale yellow	CDCl ₃ (¹ H) C ₆ D ₆ (¹³ C, ²⁹ Si)			210	¹³ C IR IR MS X-ray	104, 105
*2-56 [(CO) ₉ Co ₃][SiFe(CO) ₂ Cp] ⁶⁴	Co ₂ (CO) ₈ + H ₂ Si[Fe(CO) ₂ Cp] ₂	51						95a,b
2-57a Cp(Me ₃ P)(H)RhSiEt ₂ H ⁶⁵	Cp(Me ₃ P)Rh(C ₂ H ₄) + H ₂ SiEt ₂		C ₆ D ₆	–14.6 (dd) ¹ J _{RhH} = 32.1	3.94 (d)		³¹ P	106
2-57b CpRh(C ₂ H ₃ CO ₂ Bu)HRh- SiHEt ₂ ⁶⁶ 2 isomers	CpRh(C ₂ H ₃ CO ₂ Bu) ₂ + H ₂ SiEt		C ₇ D ₈	–13.60 (d) ¹ J _{RhH} = 31	3.83	26.0(d) ¹ J _{RhH} = 18 ² J _{SiH} = 16	¹³ C ¹⁰³ Rh VTNMR	102
2-58 (Me ₃ P) ₄ RhSiPh ₂ H ⁶⁷	(Me ₃ P) ₄ RhMe + H ₂ SiPh ₂ hν	62 orange 100–102 (d)	C ₆ D ₆ (rt) C ₇ D ₈ (–60)	–14.68 (d) ¹ J _{RhH} = 34	4.05 5.50 (s)		³¹ P VTNMR IR	107
2-59 <i>mer</i> -(Me ₃ P) ₃ (Cl)(H)Rh- [Si(C ₆ H ₄ X- <i>p</i>) ₂ H] X = H ⁶⁸	[(Me ₃ P) ₄ Rh]Cl + H ₂ SiPh ₂	96 yellow	C ₆ D ₆	–8.85 (ddt)	5.30 (dt)	14.9 (ddt)	EA ¹³ C ³¹ P IR EA X-ray ¹³ C ³¹ P IR X-ray EA	108
2-60 <i>fac</i> -(Me ₃ P) ₃ (H)Rh[Si(H)- (Mes)C ₆ H ₃ Me ₂ CH ₂]	(Me ₃ P) ₃ RhMe + H ₂ SiMes ₂	69 off-white 145–150 (d)	C ₆ D ₆	–9.90 (dq)	5.76 (m)			107
2-61 (Me ₃ P) ₃ (Ar ₅)HRhSiAr ₂ H Ar = Ar' = Ph ⁷⁰	(Me ₃ P) ₃ Rh(SAr) + H ₂ SiPh ₂	79 colorless	C ₆ D ₆	–8.97 (ddt) ¹ J _{RhH} = 16	5.47 (dt)			109
2-62 (Me ₃ P) ₃ (Ar ₅)HRhSiAr ₂ H Ar = C ₆ H ₄ OMe- <i>p</i> ⁷¹ Ar' = C ₆ H ₄ Me- <i>p</i>	(Me ₃ P) ₃ Rh(SC ₆ H ₄ OMe- <i>p</i>) + H ₂ Si(C ₆ H ₄ Me- <i>p</i>) ₂	72 colorless	C ₆ D ₆	–8.94 (ddt)	5.51 (dt)			110

Table 2g. Continued

compound	reactants	% yield, color m.p., °C	NMR				other	ref
			solvent ^{t,3} (temp., °C) ²	¹ H M–H	¹ H Si–H	²⁹ Si		
2-63 [PhB(CH ₂ PPr ₂) ₃](H) ₂ – (Me ₃ P)RhSiHPh ₂	[κ ² -PhB(CH ₂ PPr ₂) ₃]Rh– (PMe ₃) ₂ + H ₂ SiPh ₂	44 pale yellow	C ₆ D ₆	–11.0 (m) –10.25 (m)	5.81 (br s) ¹ J _{SiH} = 152	19.6 (brd) ¹ J _{SiRh} = 239	¹¹ B ¹³ C ³¹ P EA X-ray ³¹ P	111
2-64 (Ph ₃ P) ₂ (Cl)(H)RhSi(ⁿ Hex) ₂ H	[(Ph ₃ P) ₂ Rh(μ-Cl)] ₂ + H ₂ Si(ⁿ Hex) ₂	yellow	C ₆ D ₆	–14 (dt) ¹ J _{Rh-H} = 22	3.60 (br s) (ω _{1/2} ≈ 40)	⁷²	EA X-ray ³¹ P	112
2-65a (Pr ₃ P) ₂ OTf(H)RhSiPh ₂ H	[Rh(Pr ₃ P) ₂ OTf] + H ₂ SiPh ₂ (1:1) –30 °C	100 ⁷⁴	C ₇ D ₈	–21.85 (ddt)	5.44 (ddt)	19 (dt) ¹ J _{RhSi} = 62	³¹ P	113a
2-65b [(ⁱ Pr ₃ P) ₂ RhSiPh ₂ OTf] ⁷³	2:1 ratio	⁷⁵	C ₇ D ₈			71.3 (dt) ¹ J _{RhSi} = 106	³¹ P	
2-66a Rh(tpp)SiPh ₂ H ⁷⁶	Rh(tpp)Cl or Rh(ttp)Me + H ₂ SiPh ₂	72(67) orange	CDCl ₃	–1.28 (d)			¹³ C HRMS EA ³¹ P	62a 113b
*2-66b (NacNac)(H)Rh(SiHPh ₂)– (PPhPh ₂)	Rh(NacNac)(C ₈ H ₁₄)N ₂ + H ₂ SiPh ₂	43	C ₆ D ₆	–13.5 (dd) ¹ J _{RhH} = 15.4	(not assigned)	21.4 (dd) ¹ J _{RhH} = 23.5 ¹ J _{RhH} = 34.1	³¹ P	114
*2-67 [(dippe)Rh] ₂ – [μ-SiMePh] ₂ ⁷⁷	[(dippe)Rh] ₂ (μ-H) ₂ + 2H ₂ SiMePh	65 orange	C ₆ D ₆				³¹ P EA X-ray ³⁹ (trans) ³¹ P	114
2-68 [(dippe)Rh] ₂ – [μ-SiMe(<i>p</i> -Tol)] ₂ ⁷⁸	[(dippe)Rh] ₂ (μ-H) ₂ + H ₂ SiMe(<i>p</i> -Tol)	76 red bm	C ₆ D ₆ (¹ H) C ₇ D ₈ (²⁹ Si)	–6.00		157–166 (br m)	EA ³¹ P	114
*2-69 [(dippe)HRh] ₂ – [μ-η ² -H–SiMe ₂] ₂	[(dippe)Rh] ₂ (μ-H) ₂ + 2H ₂ SiMe ₂	62 yellow	C ₇ D ₈ (¹ H) C ₆ D ₆ (³¹ P)	–11.59 (m)	⁷⁹		EA ³¹ P	114
2-70 [CH ₂ (η ⁵ -C ₅ H ₄) ₂][RrH– (μ-SiEt ₂) ₂] ⁸⁰	[CH ₂ (η ⁵ -C ₅ H ₄) ₂] ₂ – [Rr(C ₂ H ₄) ₂] ₂ + xs Et ₂ SiH ₂ λ (exhaustive)		C ₆ D ₆	–14.40 (m)		205.9(t) ¹ J _{RhSi} = 37	X-ray ¹³ C ¹⁰³ Rh	115
2-71a Cp(Me ₃ P)(H)Ir[SiMes(H)– (η ² -C ₆ H ₂)(CH ₃) ₂ (CH ₂)] ⁺ [OTf] [–]	Cp*(Me ₃ P)(OTf)IrMe + H ₂ SiMes ₂			–14.56 (d)	5.03 (s)	–10.6 (dd) ¹ J _{SiH} = 10	¹³ C ¹⁹ F ³¹ P	116, 117a
2-71b [Cp*(Me ₃ P)Hr=SiMes] ⁺ [OTf] ^{–81}		72 yellow		–15.90 (d)			¹³ C ¹⁹ F ³¹ P	
2-72 <i>fac</i> -(Me ₃ P) ₃ (Me)Hr– (SiMes ₂ H)	(Me ₃ P) ₄ IrMe + H ₂ SiMes ₂	73 colorless 124–127	C ₆ D ₆	–11.47 (dt)	5.93 (m)	–46.7 (d) ¹ J _{SiH} = 151	IR EA ¹³ C ³¹ P	60a,b
2-73 (Me ₃ P) ₂ Cl(H)Ir– [η ² -SiMesH(CH ₂) ₂ PPh ₂] ⁸²	[(OC)(Me ₃ P) ₄ Ir]Cl + H ₂ SiMes(CH ₂ CH ₂ PPh ₂)	80 white	C ₆ D ₆	–9.41 (dt)	4.77 (dd) ³ J _{HH} = 6.4, 20.1	–19.8 (ddd)	IR EA ¹³ C ³¹ P	118
2-74 [PhB(CH ₂ PPh ₂) ₃](H) ₂ Ir=SiR ₂ R = Mes ⁸³	[PhB(CH ₂ PPh ₂) ₃](H)Ir– (η ³ -C ₈ H ₁₃) + H ₂ SiR ₂ ⁸⁴	67	C ₆ D ₆	–9.47 (m)		241.2 (dt)	X-ray ¹³ C ³¹ P	60a,b 61

Table 2h. Continued

compound	reactants	% yield, color m.p., °C	NMR				other	ref
			solvent ^{1,3} (temp., °C) ²	¹ H M–H	¹ H Si–H	²⁹ Si		
2-75a [PhB(CH ₂ PPh ₂) ₃](H) ₃ Ir- (SiHEt ₂) (+ COD)	[PhB(CH ₂ PPh ₂) ₃](H)Ir- (η^3 -C ₈ H ₁₃) + Et ₂ SiH ₂	96 off-white	C ₆ D ₆	–12.21 (m)	5.78 (br s)	–19.8 (br q)	IR EA X-ray ¹³ C ³¹ P	111
*2-75b [NSiN]Ir(SiHPh ₂ - (NCMe ₂) ⁺][OSO ₂ CF ₃] ^{–85}	(NSiN)Ir(H)(OTf)(coe) + H ₂ SiPh ₂ (CH ₃ CN solvent)	82 yellow	CD ₃ CN		4.33 (s) ¹ J _{SiH} = 173	2.8 (s) (SiMe) –25.0 (s) (SiHPh ₂)	EA X-ray ¹³ C ¹⁹ F	57d
2-75c (tp)IrSiPhMeH	(tp)IrCl(CO) + H ₃ SiPhMe	34 purple	CDCl ₃		–2.24 (q) ¹ J _{SiH} = 200		IR EA ¹³ C HRMS (FAB)	62b
Ni triad 2-76 [(1,2-C ₆ H ₄ (SiH ₂)(SiH)) ₂] ^{2–} Ni ₂ (dmpe) ₂] (see also 1-62)	{(dmpe)Ni[C ₆ H ₄ - (SiH ₂) ₂] ₂ (μ -dmpe) + heat ⁸⁶	34 orange 134–152 (dec)					IR EA X-ray	64
2-77 (dtbpe)Ni(μ -H)SiHAr ₂ Ar = 2,4,6-Me ₃ C ₆ H ₂ ⁸⁷	[(dtbpe)Ni] ₂ (C ₆ H ₆) + 2H ₂ SiAr ₂	65% yellow	THF-d ₈		–0.17 (t, SiH ₂) ⁸⁸	53.36 (T)	¹³ C ³¹ P VTNMR	119
2-78a (dcpe)Pd(H){SiH(^t Bu) ₂ } ⁸⁹	[(dcpe) ₂ Pd] + H ₂ Si ^t Bu ₂		C ₇ D ₈ (–80)	–1.86 (dd)	4.80 (dd)	33.5	IR X-ray ³¹ P HMQC VT(²⁹ Si)	120a
2-78b (dmpe)Pd(SiPh ₂ H) ₂	(dmpe)PdMe ₂ + H ₂ SiPh ₂	91 pale yellow	C ₆ D ₆		5.69 (appt)	–4.5 (dd)	calc ¹³ C ³¹ P	120b
2-79a [(Me ₃ P)Pd](μ - η^2 -H–SiPh ₂) ₂ - (σ -complex) *2-81	(Me ₃ P) ₂ PdEt ₂ + H ₂ SiPh ₂	63% red 109 (dec)	C ₇ D ₈ (²⁹ Si) –50 CD ₂ Cl ₂ (25)		0.59 (br) ¹ J _{SiH} = 79		IR EA ³¹ P	121a 121b
*2-79b [(1,2-C ₆ H ₄ (SiMe ₂)(SiH))]- Pd(dmpe) ₂	(dmpe)Pd[(1,2-C ₆ H ₄ - (SiMe ₂)(SiH ₂))] ≥ 90 °C (44 h), 95 °C (51 h), 100 °C (47 h)	~39 colorless <i>meso/dl</i> = 72/28	C ₆ D ₆		5.62 (ddd) (<i>dl</i>) 5.86 (ddd) (<i>meso</i>)		VTNMR ⁹⁰ X-ray ³¹ P X-ray	66b
*2-79c C ₃₆ H ₆₄ P ₄ Pd ₃ Si ₆ DME ⁹¹		~23 orange–red	C ₄ D ₈ O		(unassigned)	–2.11 (d) 25 (s) 38.7 (d) 130–132 (m) 173 (d) 211 (ddd)	³¹ P IR EA X-ray DFT	

Table 2i. Continued

compound	reactants	% yield, color m.p., °C	NMR				other	ref
			solvent ^{1,3} (temp., °C) ²	¹ H M-H	¹ H Si-H	²⁹ Si		
*2-79d C ₃₄ H ₇₂ Si ₅ P ₆ Pd ₄ ⁹¹			C ₄ D ₈ O		6.06 (tt) (SiH ₂) 7.76–7.93 (br m) (SiH) 1.77 (s) ¹ J _{SiH} = 77	102–104 (m, SiH ₂) 138–140 (m, SiH)	³¹ P X-ray	
2-81 [(Me ₃ P)Pd] ₂ (μ-η ² -H-SiPh ₂) ₂ + 2-79a ⁹²	(Me ₃ P) ₂ PdEt ₂ + H ₂ SiPh ₂ or (Me ₃ P) ₂ Pd(η ² -CH ₂ =CHPh)	3 pale yellow 105 (dec)	CD ₂ Cl ₂		(br m) (SiH) 1.77 (s) ¹ J _{SiH} = 77		³¹ P VTNMR EA	121ab
2-82 [(Et ₃ P)Pd] ₂ (μ-η ² -H-SiPh ₂) ₂	(Et ₃ P) ₂ PdEt ₂ + H ₂ SiPh ₂	60 pale yellow	CD ₂ Cl ₂		1.76 (br d) ¹ J _{SiH} = 78		³¹ P VTNMR ⁹³ EA	121b
2-83 [(Cy ₃ P)Pd] ₂ (μ-η ² -H-SiPh ₂) ₂ ⁹⁴	(Cy ₃ P) ₂ Pd + 2 H ₂ SiPh ₂	80 yellow	C ₆ D ₆	2.07 (app t)			X-ray ¹³ C ³¹ P EA	122
*2-84 Pd[<i>o</i> -(HSi)(H ₂ Si)C ₆ H ₄] ₂ -[<i>o</i> -(HSi)C ₆ H ₄](depe) ₂ ⁹⁵	(depe)Pd[<i>o</i> -(H ₂ Si)C ₆ H ₄] + heat	44 red	C ₇ D ₈		4.16 (brd s, 2H) 5.18–5.73 (overlap of d + brd, 6H)	–12.9 (dd, J _{HSi} = 182, SiH) –11.3 (s, J _{HSi} = 184, SiH ₂)	X-ray ³¹ P VTNMR IR X-ray	123
2-85 <i>cis</i> -(Me ₃ P) ₂ Pt(CZ=CSiPh ₂ H)(SiPh ₂ H)(SiPh ₂ H) ⁹⁶ Z = COOMe (γ-complex)	0.67(Me ₃ P) ₂ Pt(SiPh ₂ H) ₂ + 2.01H ₂ SiPh ₂ + 0.67 ZC≡CZ or (Me ₃ P) ₂ PtSiPh ₂ CZ=CSiPh ₂ H + H ₂ SiPh ₂	93 pale orange	C ₆ D ₆ (¹ H, ³¹ P) CD ₂ Cl ₂ (²⁹ Si)	5.45 (app t, PtSiH) ² J _{PH} = 40 6.35 (s, CSiH) ¹ J _{SiH} = 197 ⁴ J _{PH} = 19		–20 (ddd, J _{HSi} = 187, SiH) –13.3 (ap t, CSi) ³ J _{PHSi} = 121 –2.51 (dd, PtSi) ¹ J _{PHSi} = 1169	³¹ P IR [EA]	124 454
2-86 <i>trans</i> -(Me ₃ P) ₂ Pt(CZ=CSiPh ₂ H)(SiPh ₂ H)(SiPh ₂ H) Z = COOMe (γ-complex)	0.14 <i>cis</i> -(Me ₃ P) ₂ Pt(CZ=CSiPh ₂ H)- (SiPh ₂ H) (2-85) Z = COOMe + 1.41H ₂ SiPh ₂	57 yellow	C ₆ D ₆ (¹ H, ³¹ P) CDCl ₃ (¹³ C, ²⁹ Si)	4.98 (t, PtSiH) 6.21 (s, CSiH) ⁴ J _{PH} = 14 ¹ J _{SiH} = 196		–16.9 (t, PtSi) ¹ J _{PHSi} = 83 –12.5 (t, CSi) ³ J _{PHSi} = 33	¹³ C ³¹ P IR [EA] X-ray	124 454
2-87 <i>trans</i> -(Me ₃ P) ₂ Pt(SiPh ₂ H) ₂ ⁹⁷	<i>cis</i> -(Me ₃ P) ₂ PtEt ₂ + 2H ₂ SiPh ₂	90 colorless	C ₆ D ₆	5.29 (t, trans) 5.60 (app t, cis)			¹³ C ³¹ P VTNMR	125
*2-88 (Me ₃ P) ₂ Pt(SiPh ₂ C(=CH-C ₆ H ₄ F-4)CH ₂)(SiPh ₂ H) (cyclic)	(Me ₃ P) ₂ Pt(SiPh ₂ C(=CH-C ₆ H ₄ F-4)CH ₂) + H ₂ SiPh ₂ ⁹⁸ (cyclic)	34 colorless	CD ₂ Cl ₂ C ₆ D ₆ (¹ H, ³¹ P) CD ₂ Cl ₂ (¹³ C, ²⁹ Si)	4.81 (t, trans) 4.90 (app t, cis)		11.5 (dd)	EA X-ray (trans) ¹³ C ³¹ P EA	126
2-89 (Ph ₃ P) ₂ Pt(SiAr ₂ H) ₂ Ar ₂ = C ₁₂ H ₈ ⁹⁹	(Ph ₃ P) ₂ Pt(η ² -C ₂ H ₄) + H ₂ SiAr ₂	52 pale yellow	C ₇ D ₈ 223	5.04 (s) ¹ J _{SiH} = 176 ¹⁰⁰		–17.2 (dd)	X-ray ³¹ P IR EA	127c

Table 2j. Continued

compound	reactants	% yield,color m.p., °C	NMR				other	ref
			solvent ^{1,3} (temp., °C) ²	¹ H M–H	¹ H Si–H	²⁹ Si		
2-90 <i>cis</i> -(Me ₂ -PhP) ₂ Pt(SiPh ₂ H)-(SiPh ₂ Me) ¹⁰¹	<i>cis</i> -(PhMe ₂ P) ₂ Pt(SiPh ₂ Me) ₂ + 20H ₂ SiPh ₂	93 colorless	C ₆ D ₆				³¹ P	128
2-91 <i>cis</i> -(Et ₃ P) ₂ Pt(SiPh ₂ H) ₂ ¹⁰²	(Et ₃ P) ₄ Pt + 2H ₂ SiPh ₂		C ₆ D ₆		5.46 (t, trans) 5.70 (app t, cis)		¹³ C ³¹ P EA X-ray ³¹ P	125
2-92 <i>cis</i> -(Ph ₃ P) ₂ Pt(H)(SiPh ₂ H) ¹⁰³	(Ph ₃ P) ₂ Pt(η ² -C ₂ H ₄) + H ₂ SiPh ₂	¹⁰³	C ₇ D ₈ 223	−0.96 (dd) ¹ J _{PH} = 1008	4.82 (m)	9.6 (dd) ¹ J _{PSi} = 1113	³¹ P	127c
2-93 <i>cis</i> -(Ph ₃ P) ₂ Pt(H)(SiAr ₂ H) Ar = C ₁₂ H ₈ ¹⁰⁴	(Ph ₃ P) ₂ Pt(η ² -C ₂ H ₄) + H ₂ SiAr ₂	¹⁰⁴	C ₇ D ₈ 223	−1.61 (br d) ¹ J _{PH} = 945	6.56 (br s) ² J _{PH} = 56	−20.7 (br)	³¹ P	127c 132 134
2-94 <i>cis</i> -(Cy ₃ P) ₂ (H)PtSiHPh ₂ ¹⁰⁵	(Cy ₃ P) ₂ Pt + H ₂ SiPh ₂	55 white	C ₇ D ₈	−3.1 (ddd) J _{PH} = 838 J _{HSiPH} = 10	5.37 (s) J _{SiH} = 164	3.43 J _{SiPt} = 1206 (2D-HMQC)	³¹ P ¹⁹⁵ Pt VTNMR EXSY IR EA MS(FAB)	129
2-95 <i>cis</i> -(Cy ₃ P) ₂ HPtSiMes ₂ H ¹⁰⁶	(Cy ₃ P) ₂ Pt + H ₂ SiMes ₂	48 159 (dec)	C ₆ D ₆ C ₇ D ₈	−3.98 (br dd) ¹ J _{PH} = 1050	5.86 (br)		¹³ C ³¹ P 2DNMR IR	11 12
2-96a <i>cis</i> -(Cy ₃ P) ₂ Pt(SiHEt ₂)(H) ¹⁰⁷ (rt)	(Cy ₃ P) ₂ Pt + H ₂ SiEt ₂	—	C ₆ D ₆	−3.39 (dd) J _{PH} = 870 ¹⁰⁸	4.41 (m)	188.1 (appt)	[EA] ³² P	127a
*2-96b [(Cy ₃ P)Pt(μ-η ² -HSiEt ₂)] ₂ (80 °C)		91 white	C ₇ D ₈ (80)				¹³ C ³¹ P IR EA X-ray ¹³ C ³¹ P	
*2-96c [(Cy ₃ P)Pt(μ-η ² -HSiPhMe)] ₂ <i>trans/cis</i> = 98:2 ¹⁰⁹	[(Cy ₃ P)Pt(μ-η ² -HSiEt ₂)] ₂ + H ₂ SiMePh	88 pale yellow	C ₇ D ₈	<i>trans</i> ¹¹⁰			EA X-ray ¹³ C ³¹ P	127a
*2-96d [Pt(PCy ₃)] ₂ (μ-η ² -HSiPh ₂)-(μ-η ² -HSiEt ₂) (50 pts) +	[(Cy ₃ P)Pt(μ-η ² -HSiEt ₂)] ₂ + H ₂ SiPh ₂ (3 h, rt)		C ₇ D ₈ ¹ H (25) ¹³ C (80) ²⁹ Si (45) ³¹ P (25)	¹¹⁰			X-ray 2-96d ¹³ C ³¹ P X-ray	127a 127b
*2-96e [Pt(PCy ₃)] ₂ (μ-η ² -η ² -H ₂ SiEt ₂)-(μ-SiPh ₂) (45 pts) +								
*2-96f [(Cy ₃ P)Pt(μ-η ² -HSiPh ₂)] ₂ ¹⁰⁹ (5 pts) ¹¹¹							2-96e ¹³ C ³¹ P IR EA X-ray	
2-96f (Ph ₃ P) ₂ (H) ₂ Pt(SiAr ₂ H) ₂ ¹¹² Ar = C ₁₂ H ₈	(Ph ₃ P) ₂ Pt(η ² -C ₂ H ₄) + H ₂ SiAr ₂	¹¹²	C ₇ D ₈	−9.1 (br s)	6.01 (m)	J _{PSi} = 1180	³¹ P	127c

Table 2k. Continued

compound	reactants	% yield,color m.p., °C	solvent ^{1,3} (temp., °C) ²	NMR				other	ref
				¹ H M-H	¹ H Si-H	²⁹ Si			
2-97a <i>trans</i> -(Et ₃ P) ₂ IPt(SiMePhH)	<i>trans</i> -(Et ₃ P) ₂ (O)PtSiMe ₃ + 2H ₂ SiMePh	93 white 105–107	C ₆ D ₆		4.21 (qt)	–22.7 ¹ J _{PtSi} = 1318		¹³ C ³¹ P IR EA ¹³ C ³¹ P ¹⁹⁵ Pt IR ESI-MS EA ³¹ P IR	130a
*2-97b [CIPt(<i>o</i> - ⁱ Pr ₂ -PC ₆ H ₄) ₂ SiH]Pt]	<i>trans</i> -(Me ₂ S) ₂ Pt(Me)Cl + H ₂ Si(<i>o</i> - ⁱ Pr ₂ PC ₆ H ₄) ₂	62 colorless	C ₆ D ₆		5.75(br s) ¹ J _{SiH} = 183	12.3 (t) ¹ J _{SiPt} = 1190			130b
*2-98 [(Ph ₃ P) ₂ Pt(μ-η ² -HSiPh ₂) ₂] ¹¹³ (σ-complex)	(a) (Ph ₃ P) ₂ Pt(η ² -C ₂ H ₄) + H ₂ SiPh ₂ or (b) 2-99 + Ph ₂ SiH ₂	(a) 70 white (b) 28 pale yellow	CD ₂ Cl ₂	2.84 (s) ¹ J _{PtH} = 624 ² J _{PtH} = 111					127c 127d
2-99 [(Ph ₃ P) ₂ Pt(μ-η ² -HSiAr ₂) ₂] ₂ Ar ₂ = C ₂₀ H ₂₄ ¹¹⁴ (σ-complex)	2-103 + Δ		CD ₂ Cl ₂ (–50)	2.80 (s) ¹ J _{PtH} = 620				³¹ P IR X-ray ³¹ P X-ray	127c
2-100 [(Ph ₃ P) ₂ Pt(μ-η ² -HSiAr ₂) ₂] ₂ Ar ₂ = SiC ₁₂ H ₈ O ¹¹⁵ (σ-complex)	(Ph ₃ P) ₂ Pt(η ² -C ₂ H ₄) + H ₂ SiAr ₂	71 gold- yellow	C ₇ D ₈ 360	3.27 (s) ¹ J _{PtH} = 696 ² J _{PtH} = 119					131
2-101 [(Ph ₃ P) ₂ Pt(μ-η ² -HSiAr ₂) ₂] ₂ Ar ₂ = SiC ₁₃ H ₁₁ N (σ-complex)	(Ph ₃ P) ₂ Pt(η ² -C ₂ H ₄) + H ₂ SiAr ₂	55 yellow	CD ₂ Cl ₂	3.25 (s) ¹ J _{PtH} = 691 ² J _{PtH} = 136 2.36		128		³¹ P IR [EA] ³¹ P EA	131
2-102a [(Cy ₃ P) ₂ Pt(μ-η ² -HSiPh ₂) ₂] ₂ (σ-complex)	(Cy ₃ P) ₂ PtMe ₂ + H ₂ SiPh ₂ Δ	24	C ₆ D ₆	2.47 (app t) ¹ J _{PtH} = 604.5 ² J _{PtH} = 87.5				X-ray ¹³ C ³¹ P IR	121b 122
*2-102b [(Pt(dmpe)) ₂ (μ-SiPh ₂) ₂] ¹¹⁶	[(Cy ₃ P) ₂ Pt(μ-η ² -HSiPh ₂) ₂ + 2Me ₂ PCH ₂ CH ₂ PMe ₂	98 yellow	THF- <i>d</i> ₆ 25 (¹ H, ³¹ P) 55 (¹³ C)			–95.5 ¹ J _{PtSi} = 789 (CPMAS)		¹ H ¹³ C ³¹ P EA	127a
*2-103 (Ph ₃ P) ₂ (H)Pt(μ-SiC ₂₀ H ₂₄)- (μ-η ² -HSiC ₂₀ H ₂₄)Pt(PPh ₃) (σ-complex) ¹¹⁷	(Ph ₃ P) ₂ Pt(η ² -C ₂ H ₄) + H ₂ SiC ₂₀ H ₂₄	86 brt orange 186–192	C ₇ D ₈ (–50)	–5.2 (t) ¹ J _{PtH} = 572 ² J _{PtH} = 90	1.93 (d)	164 (d) ^{1/8} 154 (m)		X-ray ³¹ P VTNMR EA	132 127c
2-104 (Ph ₃ P) ₂ (H)Pt(μ-SiAr ₂)- (μ-η ² -HSiAr ₂)Pt(PPh ₃) Ar ₂ = C ₁₃ H ₉ Br ₂ N ¹¹⁹ (σ-complex)	(Ph ₃ P) ₂ Pt(η ² -C ₂ H ₄) + H ₂ SiAr ₂	51 orange	C ₇ D ₈	–6.34 (t, ¹ J _{PtH} = 564	2.91 (d)	136? 137?		X-ray ³¹ P COSY HMQC IR [EA]	131
*2-105 [(dmpe)Pt(Me ₂ SiC ₆ H ₄ SiH- <i>μ</i> -) ₂ - Pt(dmpe)]	(dmpe)Pt{[1,2-C ₆ H ₄ - (SiMe ₂)(SiH ₂)] ¹²⁰	65 yellow	CD ₂ Cl ₂ (¹ H) C ₇ D ₈ (²⁹ Si)		4.70–5.40 (m) 6.64–6.90 (m)	84.62 (ddd, ¹ J _{PtSi} ≈ 550) 96.07 (quasi t, ¹ J _{PtSi} ≈ 690) Dept, SiH		X-ray ³¹ P EA X-ray	133

Table 2m. Continued

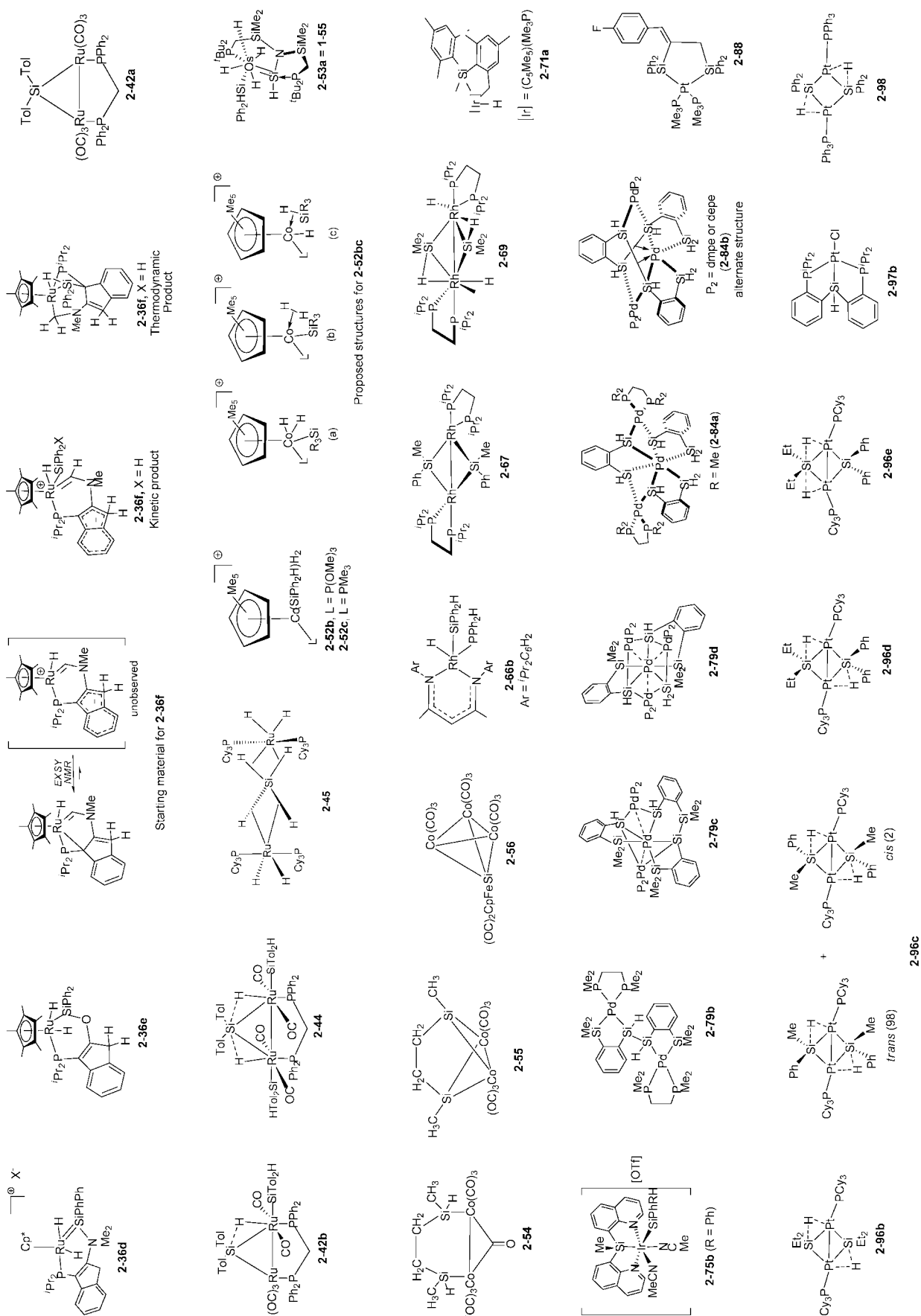
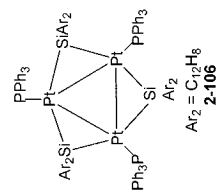
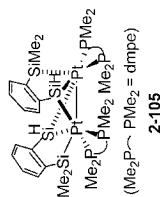
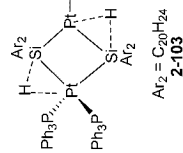
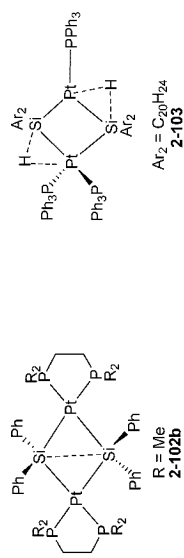


Table 2n. Continued



¹ ²⁹Si may have been determined by direct observation, INEPT or DEPT, or 2D ²⁹Si-¹H correlation. These methods are not distinguished in the table. ² Ambient temperature unless otherwise noted. Temperatures in °C. ³ In ppm. Coupling constants in Hz. Assignments: s, singlet; d, doublet; t, triplet; q, quartet; quintet; m, multiplet; br, broad; vt = virtual triplet. ⁴ Will contain other characterization methods including spectroscopic, X-ray, and calculations if reported. If elemental analyses were reported, this will be indicated by EA. If analysis is outside ±0.5% of calculated percentage value for carbon, this will be indicated by the symbol [EA]. The ¹³C NMR data are proton decoupled unless indicated otherwise. ⁵ Some data have been retrieved from the Supporting Information associated with the indicated reference. ⁶ Attempts to react Mes₂SiH₂ with Cp*₂ScMe failed. However, with smaller secondary silanes such as Ph₂SiH₂, Me₂SiH₂, and Et₂SiH₂, reaction produced Cp*₂SeH.^{26b} ⁷ Contains 0.25 equiv of pyridine solvate. Additional derivatives included the deuterated analogue of **2-2** and Cp₂TiSiHMePh(py), which decomposed to Cp₂Ti(μ-NC₄H₄)(μ-H)TiCp₂.^{27,77} ⁸ The full paper also describes competition of hydrosilylation and hydrogenation of pyridine.⁷⁷ ⁹ SiH signal was not observed, and the other signals were broad and shifted. Reactions of Ph₂SiH₂ with Cp(Me₃P)₂VMe₂, Cp(Me₃P)(V)(CH₂CMe₂)₂, and Cp(dmpe)V(=CHCMe₂) did not proceed at room temperature, and at 60 °C, decomposition was observed.^{31a} ¹⁰ Additional derivative reported for reaction of Cp(Ar'N)Nb(PMe₃)₂ (Ar' = 2,6-C₆H₃Me₂) and H₂SiMePh.^{32b} ¹¹ For additional derivatives from primary silanes, see **1-17c**, **1-18**, and **1-19** in Table 1. ¹² Additional derivative with R' = Ph.¹³ Additional derivative with R = SiMe₃, R' = Ph.¹⁴ ¹⁵ In a subsequent full paper, it is stated that compound **2-7** could not be prepared from H₂Si(μ-Me₂NC₄H₄)(Vin) as polymerization of the alkenylsilane occurs. However, **2-7** was generated from reaction of VinMgBr with [C₆H₄CH₂N(CH₃)₂-2](Cl)Si=Cr(CO)₃ as well as from [C₆H₄CH₂N(CH₃)₂-2](Vin)SiCl₂ and K₂Cr(CO)₃.⁹⁰ ¹⁶ Complex not isolated. ¹⁷ SiH₂Ph₂; K = 20.3 (278 K), 12.2 (288 K), 5.2 (298 K), 2.5 (308 K), 0.65 (328 K), 0.37 (338 K); equilibrium constants were determined from ³¹P NMR integration data.^{21b} ¹⁸ Unbound SiH of the bound H₂SiPh₂.^{21b} ¹⁹ Additional derivative with R = Me.²⁰ Product formed with shorter irradiation times than those reported for formation of **2-20**. Parameters also reported for the py-*d*₅ analogue.^{85c} Reaction also generates compound **2-18**.^{85a} ²² Isolated complex; 80% yield by NMR at 96% conversion.^{95c} ²³ Observed only in solution. Reaction proceeds through Cp*(OC)₂(CH₃CN)WMe. *cis*-**2-18** isomerizes to *trans*-**2-17-d₅**.^{85a} ²⁴ Observed only in solution. Reaction also reported for Cp*(OC)₂(H)W=SiEt₂·py-*d*₅ with PhMe₂SiH₂, resulting in nearly quantitative release of Et₂Si₂.^{85a} ²⁵ At 90% conversion of the metal complex.^{85a} ²⁶ Additional derivatives with R₂ = PhMe (**2-19**), Et₂. Reaction proceeds through Cp(OC)₂(CH₃CN)WMe.^{85a} Related THF adduct, *cis*-Cp*(OC)₂(H)W=SiPh₂·THF, was reported in 2006 by Sakaba and coworkers in ref 477. ²⁷ Additional derivatives prepared from reaction with PhMeSiH₂ and also with Ph₂SiH₂.³⁹ See also **1-30**. ²⁸ Cp₂D₆ added for lock.^{39b} ²⁹ Additional derivative from reaction with PhMeSiH₂.³⁹ Also prepared with (p⁷-C₆H₄)Fe(H)₂(SiMeCl)₂.³² ³⁰ Prepared from co-condensation of Fe vapor and toluene.⁹² ³¹ Additional or related derivatives: **1-34**, **1-35**, and **2-28**.^{42b} ³² Analogue of **2-34** prepared from ¹Pr₂SiH₂.⁹³ ³³ w_{1/2} = 68 Hz.⁹³ ³⁴ Additional derivative with dpvp replacing dpvp.^{95c} Reaction of Fe₂(edt)(CO)₂dpvpz with PhSiH₃ appears to give complexes spectroscopically similar to **2-36b** and **2-36c**.⁴¹ Additional derivative with dpvp replacing dpvp.^{95c} Derivative formed from Ph₂SiH₂ but with X⁻ = SO₃CF₃ (X-ray) also reported as the SO₃CF₃⁻ salt of **1-39b** (X-ray structure).^{47b} ⁴³ See equilibrium involving Ia₂·N₂ and unobserved monomer depicted in structure section of Table 1.^{47c} ⁴⁴ See structure of starting material deduced from EXSY NMR as well as the product produced in structure section for Table 2.^{47d} ⁴⁵ Additional derivative: Tp(Ph₃P)HRu(η²-HSiHPh₂).^{48a} ⁴⁶ Observed only in solution. Initial ratio **2-38a**/**2-38b** = 1/4.5. After prolonged photolysis, ratio becomes ~1/1. ⁴⁷ Data not provided. ⁴⁸ Additional derivative, **1-41**.⁴⁹ Related derivative prepared from Cp*Ru(μ-H)₂Ru(Cp*) + Ph(CH₂=CH)SiH₂.⁵⁰ ⁴⁹ Observed only in solution as a mixture of **2-43a** and **2-43b**. After 1 day at room temperature, formation of Ru₂(CO)₅[Si(p-Tol)₂H(μ-dppm)(μ-η²-HSi(p-Tol)₂H)] is 1/4.⁹⁹ ⁵¹ AA'XX'YY' multiplet.⁹⁹ ⁵² When 2 equiv of H₂SiPhMe were used, the products identified were **2-45**, RuH₂(η²-H₂)(η²-HSiPh₃)(PCy₃)₂, HSiPh₂Me, and HSiMe₂Ph in a 1:1.3:2.2:3.4 ratio. Additional derivatives: (Pr₃P)₂(H₂)Ru(SiH₂)Ru(H)₂(PPh₃)₂ (X-ray).^{100,101} ⁵³ The ²⁹Si(INEPT)(C₆D₆) spectrum taken at 15 °C shows a nonet.¹⁰¹ ⁵⁴ Additional derivatives from reaction of HSiEt₃ (**3-149**), HSi(CH₂CH=CH₂)Me₂, HSiPh₃, and H₂SiPh₂ (**1-44**).⁵² ⁵⁵ Isolated as an 8:5 mixture of diastereomers.⁵⁶ For additional derivatives, see also **1-53** and **3-164**. Related complexes were formed from Ph₂SiH₂, Ph₂GeH₂, and Bu₃SnH.⁵⁶ As a mixture of diastereomers in 8:5 ratio. ⁵⁷ Additional couplings reported: ³J_{SiH,COH} = 3.7, ³J_{Si,CH} = 6.4.⁵⁸ Additional derivative with Ph₂GeH₂.⁵⁶ When 5 equiv of Ph₂SiH₂ was reacted with Cp*Co(η²-C₂H₂)₂ at 70 °C for 15 min, the initial product formed was Cp*(H₂)Co(SiHPh₂)(SiPh₂Et) (not isolated). A similar reaction was observed starting from **1-55ab** in the structure section for Table 1 for related structures. Additional complexes prepared from HSiEt₃, H₂SiMePh (VT studies), and H₂SiPh (see Table 1) (studied in solution).^{57c} ⁵⁸ Studied in solution only. See proposed structures for **1-55ab** in the structure section for Table 1 for related structures. Additional complexes prepared from HSiEt₃, H₂SiMePh, and H₂SiPh (see Table 1) (studied in solution).^{57c} ⁵⁹ Compound **2-54** not isolated. Broad signals in ¹H NMR spectrum due to paramagnetism. Product **2-54** observed when excess silane used.¹⁰⁴ ⁶⁰ Air-sensitive and thermally sensitive but stable at -20 °C under N₂ for several weeks.¹⁰⁴ Additional derivatives with H₂SiPh₂ and Co₂(CO)₈ and H₂SiPh₂ (all three characterized by X-ray).¹⁰⁴ ⁶¹ **2-56** was reported by Malisch and coworkers in 1982 from Cp(CO)₂FeSiH₃ and Co₂(CO)₈.¹⁰⁶ ⁶² Observed only in solution.¹⁰² ⁶³ Compound **2-58** is in equilibrium with (Me₃P)₃RhSiHPh₂ + PMe₃.¹⁰⁷ ⁶⁴ Additional derivatives: X = Me, OMe, F, CF₃. X-ray structures obtained for OMe, F, and CF₃ derivatives. Heating a solution of **2-59** gave two products *fac*-L₃(H₂)Rh(SiPh₂Cl) and *mer*-L₃(Cl)HRh(SiPh₂Cl) where Cl transferred from Rh to Si. In addition, **2-59** reacted with H₂Si(C₆H₄X-p)₂ to generate an equilibrium with *mer*-RhCl(H)SiH(C₆H₄X-p)₂L₃.¹⁰⁸ ⁶⁵ Experimental given for preparation of **2-60** from (Me₃P)₃RhCl + (THF)₂LiSiMe₃H (75% yield). The paper states that reaction of Mes₂SiH₂ + (Me₃P)₄RhMe also affords **2-60**, but no experimental detail was given. Reaction with D₂SiMe₂ was also performed. Scrambling of D into Si-H, RhH, RhCH₃, and *ortho*-Me positions was observed.¹⁰⁷

Table 20. Continued

⁷⁰ Additional derivatives: Ar' = *p*-Tol, Ar = *p*-Tol or *p*-C₆H₄OMe; Ar' = *m*-Tol, Ar = Ph or *p*-C₆H₄OMe; Ar' = *p*-Tol, Ar = Ph, Ar' = *p*-C₆H₄F, Ar = *p*-Tol. No reductive elimination of H₂SiAr'^{102, 103}.
⁷¹ Additional derivatives: Ar = C₆H₄OMe-*p*, Ar' = C₆H₄Me-*p*, C₆H₄F-*p*, C₆H₄CF₃-*p* (Co-19).¹¹⁰ Deuterium labeling experiments were performed with Ph₃SID₂ and (ArSi)Rh(PMe₃)₃, where Ar = C₆H₄OMe-*p* and C₆H₄Me-*p*.^{110, 112, 29} [1H] signal was not observed at room temperature in C₆D₆. Complex decomposes in solution.^{112, 73} Route to **2-65b** is unknown.^{113a, 74} No
decomposition above 0 °C.^{113a, 75} **2-65b** was treated with a 10-fold excess of PhMeSiH₂, a 92% yield of HPhMeSiSiMePhH was obtained.¹¹³ Additional derivative reported from Rh(tmp)Cl + Ph₂SiH₂, Rh(tmp)I + Ph₂SiH₂. When
as by the exchange reaction between Rh(tmp)SiEt₃ and H₂SiPh₂. The analogue of **2-66**, Rh(tmp)SiPhMeH, was prepared from Rh(tmp)SiPhMeH. Rh(tmp)SiPhMeH was also prepared from
Rh(tmp)SiPhMeH and PhMeSiH₂.^{62a, 77} Mixture of cis and trans isomers. Additional derivative with Ph₂SiH₂, MePhSiH₂, and Me₂SiH₂,^{114, 80} Si-Me groups are inequivalent.^{114, 80} **2-70** was
formed from the kinetic product, cyclometallated IR(V) alkyl hydride, [Cp*(Me)₂P]Ir(H)(μ²-SiH(MeSi)(2-CH₂-4,6-Me₂C₆H₃))][OTf] which isomerizes to give the Ir=Si complex over
the course of 12 h.^{116, 82} Compound (**2-73**) undergoes photolysis to give trans isomer (X-ray).^{118, 83} Additional derivatives characterized in solution only: R = Ph, Et, Me.⁶¹ The addition of silane is reversible
and no reaction was observed with the related allyl complex [PhBPz₃]Ir(H)(OTf)(coe) + H₂SiPh₂ was conducted in benzene solvent, the complexes formed were (NSiN)PhIr(SiPh₂OTf)
and (NSiN)PhIr(HSiPhOTf), produced from redistribution of H₂SiPh₂.^{57d, 86} Formation also speculated from (dmpe)Ni(SiH₂C₆H₄SiH₂) via dehydrogenative dimerization.^{64, 87} Additional derivatives prepared
from (dmpe)Ni(SiH₂C₆H₄SiH₂) and H₂SiPh₂ Me (footnote 240, Table 3).^{119, 88} **2-77** exhibits fluxional behavior at 298 K, and a static solution structure was not observed upon
cooling.^{119, 88} Equilibrium between the OA product and the starting materials precluded isolation of the complex.^{120a, 90} Temperature-dependent spectra of compound show dynamic behavior of molecule with
exchange of phosphine ligands. At -90 °C, the spectra indicate a structure analogous to that observed in the solid-state X-ray structure.^{121a, 91} See structure figures for Table 2. ⁸² Additional derivative with
X-ray structure. ^{121b, 92} No change in NMR spectra from 25 to -90 °C.^{121b, 94} Also prepared from reaction of (dmpe)Pt(SiPh₂H)₂ + Pd(PCy₃)₂ along with [(Cy₃P)Pt(μ²-H₂SiPh₂)₂]Pd(PCy₃)₂ and
[(dmpe)Pt(μ²-SiPh₂)₂] (see Table 3).^{122, 86} Similar derivative prepared from (dmpe)Pd[μ²-(H₂Si)₂C₆H₄]₂.^{123, 95} When **2-86** is dissolved in hexane, partial conversion to (Me₂P)₂Pt(SiPh₂CZ=CZ) and PhSiH₂ occurs.
(X-ray) also observed from reaction of (Me₂P)₂Pt(SiPh₂H)₂ with (MeCO)₂C≡C(CO)₂Me in 85% yield. A related derivative, (dmpe)Pt(SiPh₂H)(CZ=CZSiPh₂H), was
prepared from reaction of (dmpe)Pt(SiPh₂H)₂ and (MeCO)₂C≡C(CO)₂Me in 61% yield (X-ray).^{124, 97} When solid was redissolved, a mixture of trans and cis isomers was
obtained: C₂D₆ (50:50 trans/cis), CD₂Cl₂ (23:77 trans/cis), C₆H₆O (26:74 trans/cis). VT-NMR (-50 to +10 °C range in C₆H₆O) shows temperature-dependent change in peak intensities between isomers,
indicating cis and trans isomers are equilibrated (similar behavior in CD₂Cl₂, but negligible temperature-dependent change observed in C₆D₆).^{125, 98} Also prepared from reaction of Pt(SiHPh₂)₂(PMMe₃)₂ and
C₆H₄(4-fluorophenyl)allene at 50 °C for 18 h.^{126, 99} Ar = C₆H₄ represents silafluorene. Additional derivative prepared from (Ph₃P)₂Pt(η²-C₂H₄) + H₂SiAr₂ (Ar = C₂₀H₂₄, 3,7-di-*tert*-butylsilafluorene) also identified
but observed only in solution.^{127c, 100} Data from [1H] NMR spectrum.^{127c, 100} Exchange reactions of (Ph₃PCH₂CH₂SiMe₂)₂Pt(PPh₃)(SiPh₂) with H₂SiPh₂ was also observed, but the ³¹P NMR resonances for both compounds could
not be assigned unequivocally due to signal overlap.^{128, 102} Trans-to-cis ratio 6:94. Additional derivative with H₂Si(C₆H₄F-*p*).^{125, 103} **2-92** was reported earlier without spectroscopic data. [Eaborn, C.; Ratcliff, B.;
Arbuckle, J. *J. Organomet. Chem.* **1974**, *65*, 181. Eaborn, C.; Pidcock, A.; Ratcliff, B. *J. Organomet. Chem.* **1972**, *43*, C5.] **2-92** was observed in solution only.^{127c, 104} **2-93** was observed only in solution. Ar
= C₁₂H₈ represents silafluorene. Additional derivative prepared from (Ph₃P)₂Pt(η²-C₂H₄) + H₂SiAr₂ (Ar = C₂₀H₂₄, 3,7-di-*tert*-butylsilafluorene) also observed only in solution.^{127c, 105} Additional derivative
prepared in the same manner from Et₂SiH₂. **2-94** was also generated from the reaction of *cis*-(Cy₃P)₂(H)PtSiPh₂ with Ph₂SiH₂, and the Et₂SiH₂ was generated similarly. *Trans*-**2-94** was generated by photolysis
of *cis*-**2-94**, and *trans*-(Cy₃P)₂(H)PtSiHEt₂ was similarly generated from the corresponding cis isomer. The Pt-H resonances in the trans isomers generally shift downfield relative to the cis isomers, and the
coupling constants are smaller in the trans isomers. Additional derivatives reported from tertiary silanes in Table 3.^{129, 106} **2-95** is the exclusive product initially but isomerizes to trans isomer slowly at
90 °C, where decomposition is more rapid. Trans isomer generated from reaction of H₂ with (Cy₃P)₂Pt=SiMe₂ is fluxional by NMR spectroscopy.^{111, 12} and the fluxional behavior is consistent with restricted
rotation about the Pt-Si bond.^{111, 12} Pt-H and Si-H exchange rapidly for **2-95**, and Pt-H exchanges with free Me₂SiH₂ (rate constant 23(4) Hz at 27 °C).^{11, 107} Analogue of **2-96a** and **2-96b** formed from
Pt-H-Si signals overlap with ligands.^{127a, 110} Pt-H-Si signal overlap with ligands.^{127a, 111} Leaving a solution of **2-96d/2-96e** = 6/94 for 2 weeks gave an equilibrium mixture of **2-96d** and **2-96e** in a 55/45 ratio. The reaction of
Pt-H-Si signals overlap with ligands.^{127a, 112} **2-96f** was not isolated (C₁₂H₈ represents silafluorene). Additional derivative from (Ph₃P)₂Pt(η²-C₂H₄) + H₂SiAr₂ (Ar₂ = C₂₀H₂₄, 3,7-di-*tert*-butylsilafluorene) also
reported previously with limited characterization data [Auburn, M.; Ciriano, M.; Howard, J. A. K.; Murray, M.; Pugh, N. J.; Spencer, J. L.; Stone, F. G. A.;
Woodward, P. J. *Chem. Soc., Dalton Trans.* **1980**, 659].¹¹⁴ Additional derivative prepared from reaction of dppe with [(Cy₃P)Pt(μ²-H₂SiPh₂)]₂ (X-ray).^{127a, 113} **2-98** was also reported.^{127a, 113} **2-98** was observed only in solution.^{127c, 113} **2-98** was reported previously with limited characterization data [Auburn, M.; Ciriano, M.; Howard, J. A. K.; Murray, M.; Pugh, N. J.; Spencer, J. L.; Stone, F. G. A.;
Woodward, P. J. *Chem. Soc., Dalton*

Table 3. Complexes Formed from Reaction of R_3SiH with Transition Metal Complexes (Structures Are Shown at the End of the Table for Compounds Marked with an Asterisk)^{†,‡}

compound	starting metal complex	% yield color m.p., °C	NMR			other ^d	ref ⁵
			solvent (temp., °C) ^f	¹ HM–H ²	²⁹ Si ^{2,3}		
Ti triad							
3-1 Cp ₂ (Me ₃ P)Ti(η ² -HSiMeCl ₂) ⁶ Cp = C ₅ H ₅ IHI	Cp ₂ Ti(PMe ₃) ₂ + HSiMeCl ₃	50 yellow	C ₆ D ₆	−4.35 (dd) <i>J</i> _{SiH} = 22		¹³ C ³¹ P IR EA X-ray calc	20b
3-2 Cp ₂ Ti[2-SiMe ₂ (C ₅ H ₄ N)]	Cp ₂ TiMe ₂ + HSiMe ₂ (2C ₅ H ₄ N)	63 deep purple	C ₇ D ₈		⁷	EA X-ray EPR	138
3-3 Cp ₂ Ti(RC ₂ SiMe ₂ H) R = Ph ⁸ (β-complex)	(A) Cp ₂ TiCl ₂ + Mg or (B) Cp ₂ Ti(η ² -Me ₃ SiC≡CSiMe ₃) + HSiMe ₂ (C≡CPh)	(A) 67 (B) 42 violet 125–130	C ₄ D ₈ O	−5.96 (sept)	21.0 ¹ <i>J</i> _{SiH} = 99	¹³ C ²⁹ SiCPMS MS IR EA	139
3-4 Cp ₂ Ti(HMe ₂ SiC ₂ SiMe ₂ H) (β-complex)	Cp ₂ Ti(η ² -Me ₃ SiC≡CSiMe ₃) + HMe ₂ SiC≡CSiMe ₂ H	61 violet 142–146	C ₇ D ₈ (83) C ₆ D ₆ (30) (C ₂ D ₅) ₂ O (30) (−108)	−0.96 (30) −8.04 ⁹ (−108)	−3.0 (C ₆ D ₆) ¹⁰ ¹ <i>J</i> _{SiH} = 152 −22.8 ¹ <i>J</i> _{SiH} = 186 (free)	¹³ C EA	139
3-5 Cp* ₂ Ti(RC≡CSiMe ₂ H) R = ^t Bu ¹¹ Cp* = C ₅ Me ₅	Cp* ₂ TiCl ₂ + Mg + HSiMe ₂ (C≡C ^t Bu)	51 yellow–brown 90–92	C ₆ D ₆	¹²	34.3 ¹ <i>J</i> _{SiH} = 92 (coord) −36.4	¹³ C IR EA	139
3-6 (THI) ₂ Ti(^t BuC≡CSiMe ₂ H)	(THI) ₂ TiCl ₂ /Mg + ^t BuC≡CSiMe ₂ H	66 red–brown oil	C ₆ D ₆	¹³	−35.4 ¹ <i>J</i> _{SiH} = 185	IR EA	139
3-7 [(Me ₂ Si(η ⁵ -C ₅ H ₄) ₂)Ti- (η ² - ^t BuC≡CSiMe ₂ H)] (β-complex)	[(Me ₂ Si(η ⁵ -C ₅ H ₄) ₂)TiCl ₂ /Mg + HSiMe ₂ (C≡C ^t Bu ¹)	71 violet	C ₇ D ₈	−6.54 ¹ <i>J</i> _{SiH} = 100	−16.6 (SiMe ₂) 7.4 (SiMe ₂ H)	¹³ C IR EA	139
3-8 Cp ₂ Zr(η ² -RC≡CSiMe ₂ H) R = ^t Bu ¹⁴ (β-complex)	Cp ₂ Zr(Me ₃ SiC≡CSiMe ₃)*THF + HSiMe ₂ (C≡C ^t Bu ¹)	68 yellow–brown 87–92	C ₆ D ₆	−3.74	16.1 ¹ <i>J</i> _{SiH} = 72	IR EA	139
3-9 Cp ₂ Zr(η ² -HMe ₂ SiC ₂ SiMe ₂ H) (β-complex) ¹⁵	Cp ₂ ZrCl ₂ + Mg + HMe ₂ SiC≡SiMe ₂ H	70 red–orange 45	C ₄ D ₈ O −56 C ₇ D ₈ 92 17	−3.69 0.5 ¹⁶ −4.35 ¹⁷ ¹ <i>J</i> _{SiH} = 70	18.2 ¹ <i>J</i> _{SiH} = 72 −21.8 34.8 ¹⁹	¹³ C X-ray	139
*3-10 [{η ⁵ -C ₅ H ₄ (SiMe ₂ H)}- ZrCl ₃] ₂ ²⁰ (linear agostic interaction) V triad	ZrCl ₄ + (HSiMe ₂) ₂ C ₅ H ₄	50 pale yellow	C ₆ D ₆ CDCl ₃	−4.40 ¹⁸ ¹ <i>J</i> _{SiH} = 69 ²¹	−21.6 35.3 ¹⁹	¹³ C EA X-ray	140
3-11a Cp(OC) ₃ V(η ² -H–SiEt ₃) ²²	CpV(CO) ₄ + HSiEt ₃ hν					IR calc	141 165b
3-11b Cp(dmpe)VSIClPh ₂	Cp(dmpe)VSiHPh ₂ + HSiClPh ₂	82 red–purple	C ₆ D ₆			[EA]	31b
3-11c Cp(ArN=)V(H)(SiMeCl ₂) Ar = 2,6-C ₆ H ₃ Pr ₂	Cp(ArN=)V(PMe ₃) ₂ + HSiMeCl ₂	45 green	C ₆ D ₆	2.60 (d)		¹³ C IR EA	32a
3-12a Cp ₂ (H)NbSiMe ₂ Cl(H) ²³ (Si central)	Cp ₂ NbH ₃ + HSiMe ₂ Cl or [Cp ₂ NbBH ₄] + HSiMe ₂ Cl	70–78 lt. beige or colorless	C ₆ D ₆	(a) −4.80 (s)	(a) 83.9	(a) ¹³ C EA	142
3-12b Cp ₂ (H) ₂ Nb(η ² -H–SiMe ₂ Cl) ²³ (Si lateral; IHI complex)				(b) −4.42 (s) −4.61	(b) 88.7	(b) ¹³ C X-ray calc	
3-13 Cp ₂ (H)NbSiCl ⁱ Pr ₂ (H) ²⁴	Cp ₂ NbBH ₄ + HSiCl ⁱ Pr ₂ + NEt ₃	72 yellow	C ₆ D ₆	−4.64 (s)		¹³ C IR EA X-ray	143
3-14 Cp ₂ (H) ₂ Nb(SiMe ₂ OEt) ²⁵	Cp ₂ NbH ₃ + xs HSiMe ₂ OEt	58 yellow	C ₆ D ₆	−5.38 (s)		EA	144
3-15 Cp ₂ (H) ₂ NbSi(OEt) ₃ ^{22,26}	[Cp ₂ NbBH ₄] + NEt ₃ HSi(OEt) ₃	82 yellow	C ₆ D ₆	−5.12 (s) ²⁷		¹³ C EA	142
3-16 Cp ₂ (H)Nb(SiMe ₂ Cl) ₂ ²⁸ (IHI complex)	(a) Cp ₂ NbH ₃ + HSiMe ₂ Cl or (b) Cp ₂ Nb(H)(η ² -CH ₂ =CHPh) +	(a) 84 (b) 61	C ₇ D ₈	−5.15 (br s)	90.0	¹³ C IR	142 144

Table 3a. Continued

compound	starting metal complex	% yield color m.p., °C	NMR				other ^d	ref ⁵
			solvent (temp., °C) ^f	¹ H M-H ²	²⁹ Si ^{2,3}			
	HSiMe ₂ Cl	lt. beige	CDCl ₃	−4.93 (s)			EA X-ray ND ¹³ C ³¹ P IR EA X-ray calc	145a
*3-17 [Cp(Me ₃ P)ClNb{η ³ -N-(Ar)SiMe ₂ -H}] ²⁹ Ar = 2,6- ⁱ Pr ₂ C ₆ H ₃ (β-agostic)	Cp(Me ₃ P) ₂ Nb=NAr + HSiMe ₂ Cl	97 dk-green	C ₆ D ₆	−5.67 (s)	−52.1 ¹ J _{SiH} = 97		¹³ C EA DFT	146 147a 32a
*3-18 [Cp(Me ₃ P)ClNb{η ³ -N-(Ar)SiMe ₂ -H}] Ar = 2,6- ⁱ Pr ₂ C ₆ H ₃ (isomer of 3-17) (β-agostic) ratio 3-17 / 3-18 = 10:1			C ₆ D ₆	−3.76 (s)			¹³ C EA DFT	146 147a 32a
*3-19 [Cp(Me ₃ P)ClNb{η ³ -N-(Ar')SiMe ₂ -H}] Ar' = 2,6-Me ₂ C ₆ H ₃ ³⁰ (β-agostic)	Cp(Me ₃ P) ₂ Nb=NAr' + HSiMe ₂ Cl	79 dk-green	C ₆ D ₆	−3.41 (s)	−68 ¹ J _{HSi} = 116		¹³ C ³¹ P IR EA X-ray ³¹	147a 32a
3-20 Cp(RN)(Cl)(PR'Me ₂)Nb-(SiHMe ₂) ³² R = Ar, Ar'; R' = Me, Ph	CpNb=NR(PR'Me ₂) ₂ + HSiMe ₂ Cl							148
3-21 Cp(Me ₃ P)(H)Nb(=NAr)-SiPh ₂ Cl ³³ Ar = 2,6- ⁱ Pr ₂ C ₆ H ₃	Cp(Me ₃ P) ₂ Nb=NAr + HSiPh ₂ Cl	77 beige		2.86 (d)			¹³ C ³¹ P EA IR X-ray	149 32a
3-22 (Cp(Me ₃ P)(Cl)Nb(=NAr)-SiMeClH) ³⁴ Ar = 2,6- ⁱ Pr ₂ C ₆ H ₃	Cp(Me ₃ P) ₂ Nb=NAr + HSiMeCl ₂	63		³⁵	— ¹ J _{SiH} = 207		IR EA	149
3-23 Cp ₂ Ta(H)(SiMe ₂ SiMe ₃) ₂	<i>endo</i> -Cp ₂ Ta(H)(η ² -C ₃ H ₆) + HSiMe ₂ SiMe ₃ + Δ	85 yellow 8	C ₆ D ₆	−3.03	−8.7 −14.9		IR	150
3-24 Cp ₂ Ta(H)(SiMe ₂ SiMe ₂ -OMe) ₂	<i>endo</i> -Cp ₂ Ta(H)(η ² -C ₃ H ₆) + HSiMe ₂ SiMe ₂ OMe + Δ	yellow 8	C ₆ D ₆	−3.10	−9.9 19.5		IR	150
3-24b Cp ₂ Ta{SiMe ₂ ...OMe...SiMe ₂ }		yellow 7		³⁶	127.8		X-ray	
3-25a [Cp(Me ₃ P)Ta(NAr)(H)-(SiMe ₂ Cl)] ³⁷ Ar = 2,6- ⁱ Pr ₂ C ₆ H ₃ (IHI complex)	Cp(Me ₃ P) ₂ Ta=NAr + HSiMe ₂ Cl	61 lt. pink	C ₆ D ₆	5.13 (d)	91.7 ¹ J _{SiH} = 33		³¹ P X-ray calc	146 147ab
3-25b Cp(ArN=)Ta(PMe ₃)-(ClSiMePh...H) Ar = 2,6-C ₆ H ₃ ⁱ Pr ₂	Cp(ArN=)Ta(PMe ₃) ₂ + HSiClMePh	51 yellow	C ₆ D ₆	5.78 (d) 5.34 (d)	88.3		¹³ C ³¹ P DFT	147b
3-26a [Cp(Me ₃ P)Ta(NAr)(H)-(SiMeCl ₂)] ³⁸ Ar = 2,6- ⁱ Pr ₂ C ₆ H ₃ (IHI complex)	Cp(Me ₃ P) ₂ Ta=NAr + HSiMeCl ₂	51	C ₆ D ₆	6.14 (d)	105 ¹ J _{SiH} = 40		¹³ C ³¹ P EA X-ray	78a
3-26b Cp(Ar'N=)Ta(PMe ₃)-(ClSiMeCl...H) ³⁹ (Ar' = 2,6-Me ₂ C ₆ H ₃)	Cp(Ar'N=)Ta(PMe ₃) ₂ + HSiMeCl ₂	46 yellow	C ₆ D ₆	6.00	106.1 ¹ J _{SiH} = −41		¹³ C ³¹ P IR EA X-ray	147b
Cr triad								
3-27 Cp(OC) ₂ Cr{(SiMe ₂)...OMe... (SiMe ₂)}	Cp(OC) ₃ CrMe + HSiMe ₂ SiMe ₂ OMe (hν)	⁴⁰	C ₆ D ₆		129		¹³ C IR MS EA X-ray	151
3-28 (η ⁶ -C ₆ H ₆)(OC) ₂ Cr(η ² -H-SiEt ₃)	(η ⁶ -C ₆ H ₆)Cr(CO) ₂ (THF) + HSiEt ₃						IR UV-vis KineticBE ⁴¹	152
3-29 (OC) ₅ Cr(η ² -H-SiR ₃) ⁴² R = Et ⁴³	Cr(CO) ₆ + HSiR ₃ (hν)		CD ₂ Cl ₂	−13.58 (−33) ¹ J _{SiH} = 95			¹³ C IR	83a 81
3-30a <i>trans</i> -(OC) ₄ (PMe ₃)Cr(η ² -H-SiEt ₃) +	(OC) ₅ (Me ₃ P)Cr + HSiEt ₃		CD ₂ Cl ₂ (−63)	−12.47 ¹ J _{SiH} = 102			³¹ P	81
3-30b <i>cis</i> -(OC) ₄ (PMe ₃)Cr(η ² -H-				−14.18			³¹ P	

Table 3b. Continued

compound	starting metal complex	% yield color m.p., °C	NMR				other ^d	ref ⁵
			solvent (temp., °C) ^f	¹ H M–H ²	²⁹ Si ^{2,3}			
SiEt ₃) 3-31 Cp ₂ (H)MoSiR ₃ R = Et ⁴⁴	Cp ₂ MoH ₂ + HSiEt ₃ (hν)	59	C ₆ D ₆	<i>J</i> _{SiH} = 99 −7.39 (s)	35.2	¹³ C MS [EA]	35 17	
3-32 Cp(OC) ₂ Mo{(SiMe ₂) ^{•••} OMe ^{•••} (SiMe ₂) ⁴⁵	Cp(OC) ₃ MoMe + HSiMe ₂ SiMe ₂ OMe (hν)	33% yellow	C ₆ D ₆		118	¹³ C IR MS EA X-ray	151	
3-33 Cp*(OC) ₂ (Me ₃ Si)Mo= SiMes ₂ Cp* = C ₅ Me ₅	Cp*(OC) ₃ MoMe + HSiMe ₂ SiMeMes ₂	54 orange	C ₆ D ₆		35.0 (SiMe ₃) 414.1 (SiMes ₂)	¹³ C IR EA X-ray	153	
3-34 Cp(OC) ₂ HMo{κ ² (<i>Si_i</i> , <i>Si</i>)- xantsil}	Cp*(OC) ₃ MoMe + xantsilH ₂ (hν, 20 min)	78 white	C ₇ D ₈	−5.65 ² <i>J</i> _{SiH} = 37	15.2	¹³ C IR MS EA	154	
3-35 Cp(OC)HMo{κ ² (<i>Si_i</i> , <i>Si</i> , <i>O</i>)- xantsil}	Cp*(OC) ₃ MoMe + xantsilH ₂ (hν, 70 min)	88 orange	C ₇ D ₈	−2.30	32.7	¹³ C IR EA	154	
3-36 (OC) ₅ Mo(η ² -H-SiR ₃) ⁴² R = Et	Mo(CO) ₆ + HSiEt ₃ (hν)		CD ₂ Cl ₂	−8.36 ¹ <i>J</i> _{SiH} = 96 ¹ <i>J</i> _{SiH} = 97		¹³ C IR X-ray	83a 81 155a	
3-37a (Me ₃ P) ₂ (ArN=)ClMo- [N(SiMe ₂ H)Ar'] Ar' = 2,6-Me ₂ C ₆ H ₃ ⁴⁶ β-agostic interaction	(Ar'N) ₂ Mo(PMe ₃) ₃ + HSiClMe ₂	?						
*3-37b <i>trans</i> -[(R'MeSi)(η ⁵ -R- C ₅ H ₃)Mo(CO) ₃] ₂ R' = CH ₂ Ph, R = ^t Bu	Mo(CO) ₆ + C ₅ Me ₄ HSiPhMeH	6 colorless 242 °C (dec)	CDCl ₃			IR EA X-ray	155c	
3-38 Cp ₂ (H)WSiCl ₃	Cp ₂ WH ₂ + HSiCl ₃ (hν)	20 brt. orange	C ₆ D ₆	−11.69		¹³ C MS	35	
3-39 Cp*(OC) ₂ W(=SiMe ₂)- SiMe ₃	Cp*(OC) ₃ WMe + HSiMe ₂ SiMeMes ₂	40 pale yellow	C ₆ D ₆		22.1 (SiMe ₃) ¹ <i>J</i> _{W–Si} = 30.5	¹³ C MS EA X-ray	156	
3-40a Cp(OC) ₂ W{(κ ² - <i>Si_i</i> , <i>C</i>)- SiMe ₂ NMe ₂ (<i>o</i> -C ₆ H ₄) ⁴⁷	Cp*(OC) ₃ WMe + (<i>o</i> -HMe ₂ Si)C ₆ H ₄ (NMe ₂) hν	76 orange	C ₆ D ₆		380.9 (SiMe ₂) (¹ <i>J</i> _{WSi} = 154.9) 115.0 <i>J</i> _{Wsi} = 103	¹³ C IR EI-MS EA X-ray	157a	
3-40b Cp*(OC) ₂ W{κ ² -(<i>C,N</i>)- C(Me)=N(Si(<i>p</i> -Tol) ₃) ⁴⁸	Cp*(OC) ₂ W(NCMe)Me + HSi(<i>p</i> -Tol) ₃	59 red	C ₆ D ₆		−17.9	¹³ C IR EI-MS [EA] X-ray	157b	
3-41 Cp*(OC) ₂ ArW=SiMe ₂ · DMAP Ar = C ₆ H ₅ ⁴⁹	Cp*(OC) ₃ WMe + HSiMe ₂ Ar + DMAP hν	42 yellow	C ₆ D ₆		86.7 ¹ <i>J</i> _{Wsi} = 71	IR X-ray	158	
3-42 Cp*(OC) ₂ W- (η ³ -Me ₂ SiCHCMe ₂)	Cp*(OC) ₂ W(NCMe)Me + HSiMe ₂ (CH=CMe ₂) (hν)	54 yellow	C ₆ D ₆		8.8	¹ H (NOE) ¹³ C IR HRMS X-ray	159a	
*3-43 (C ₅ Me ₄ Et)(OC) ₂ W(μ-η ¹ :η ³ - C≡C'Bu)(SiPh ₂) ⁵⁰ (silylene hybrid)	(C ₅ Me ₄ Et)(OC) ₂ (MeCN)WMe + HSiPh ₂ C≡C'Bu	64 orange–brown	C ₇ D ₈ (−70)		−47.8 ¹ <i>J</i> _{Wsi} = 38	¹³ C IR EA X-ray	160a	
3-44 Cp(OC) ₂ HW{κ ² (<i>Si_i</i> , <i>Si</i>)- xantsil}	Cp*(OC) ₃ WMe + xantsilH ₂	80 white	C ₆ D ₆ (¹ H) C ₇ D ₈ (²⁹ Si)	−3.95 ¹ <i>J</i> _{WH} = 83 ² <i>J</i> _{SiH} = 24	10.8 ¹ <i>J</i> _{Wsi} = 14)	IR MS EA X-ray ⁵¹	154	
3-45 Cp(OC)HW{κ ² (<i>Si_i</i> , <i>Si</i> , <i>O</i>)- xantsil}	Cp*(OC) ₃ WMe + xantsilH ₂	92 orange	C ₇ D ₈	0.78		IR X-ray	154	
*3-46 [Cp'(CO) ₂ W(=SiMe ₂)- (SiMe ₃) ₂] ₂ ⁵² Cp' = C ₅ Me ₄ Et	(Cp')(OC) ₃ WMe + HSiMe ₂ SiMe ₃ (hν)	54 yellow	C ₇ D ₈		20.1 (s) ¹ <i>J</i> _{Wsi} = 54.3 ⁵³	IR MS EA X-ray	156	
3-47 Cp(OC) ₂ W(μ-SiMe ₂)- (μ-H)Re(CO) ₂ Cp* ⁵⁴	Cp*(OC) ₂ (MeCN)WMe + HSi[ReCp*(CO) ₂ H]Me + (hν)	72	C ₇ D ₈ (−50)	−11.37	168.3	¹³ C IR MS EA	161	

Table 3c. Continued

compound	starting metal complex	% yield color m.p., °C	NMR				
			solvent (temp., °C) ^l	¹ H—H ²	²⁹ Si ^{2,3}	other ^d	ref ⁵
3-48 (η^6 -PhSiHPh ₂)W(CO) ₃ ⁵⁵	W(CO) ₆ + HSiPh ₃ (hν)	70	CDCl ₃		−16.4	¹³ C IR UV-vis X-ray ¹³ C	162
3-49 (OC) ₅ W(η^2 -HSiR ₃) ⁴² R = Et ⁵⁶	W(CO) ₆ + HSiEt ₃ (hν)		CD ₂ Cl ₂	−8.55 <i>J</i> _{SiH} = 86 <i>J</i> _{WH} = 36		IR	81
3-50 (OC) ₅ WPPH ₂ CH ₂ CH ₂ SiR ₂ H R = Me ⁵⁷	W(CO) ₆ + HSi(CH ₂ CH ₂ PPh ₂)Me ₂ (hν)		C ₆ D ₆	3.97 (SiH)		³¹ P	163
*3-51 (OC) ₄ W(η^2 -HSiRR'- CH ₂ CH ₂ PPh ₂) R = R' = Me ⁵⁸	W(CO) ₆ + HSi(CH ₂ CH ₂ PPh ₂)RR' (hν)		C ₆ D ₆	−8.18 (s, br) ¹ <i>J</i> _{SiH} = 95 ¹ <i>J</i> _{WH} = 36		³¹ P	163
*3-52a (OC) ₄ W=C(NHR)- SiMe ₂ H R = Me ⁵⁹ (β -complex)	(OC) ₅ W=C(NHR)SiMe ₂ H (hν)	73	C ₆ D ₆	−2.61 (s) ¹ <i>J</i> _{SiH} = 104		¹³ C IR calc	164
3-52b (OC) ₃ (η^4 -nbd)(H)WSiCl ₃	(OC) ₄ W(η^4 -nbd) + HSiCl ₃		C ₆ D ₁₂	−2.07 (s) ¹ <i>J</i> _{HW} = 16 ² <i>J</i> _{Hsi} = 31.1	47.8 ¹ <i>J</i> _{SiW} = 214	¹³ C IR	87b
*3-52c <i>trans</i> -[(R'MeSi)(η^5 - RC ₅ H ₃)W(CO) ₃] ₂ R' = CH ₂ Ph, R = 'Bu ⁶⁰ Mn triad	W(CO) ₆ + C ₅ Me ₄ HSiPhMeH	7 colorless	CDCl ₃			IR EA X-ray	155c
3-53 Cp(OC) ₂ (H)MnSiEt ₃	CpMn(CO) ₃ + HSiEt ₃ (hν)					IR calc	165a
*3-54 Cp'(OC) ₂ Mn(η^2 -H- SiPh ₂ SiPh ₂ H) Cp' = C ₅ H ₄ Me ⁶¹	Cp'Mn(CO) ₃ + HPH ₂ SiSiPh ₂ H (hν)	9 76 (d)	C ₆ D ₆	−10.71 <i>J</i> _{SiH} = 57 ⁶²	−27.4 (SiPh ₂ H) −2.62 (MnSiPh ₂)	¹³ C IR EA	166
3-55 Cp'(OC)(Me ₃ P)Mn- (η^2 -HSiMe ₂ SiXSiMe ₂ H) X = 1,2-C ₆ H ₄ ⁶³ Cp' = C ₅ H ₄ Me	Cp'Mn(CO) ₂ (PMe ₃) + HSiMe ₂ XSiMe ₂ H	14 yellow	C ₆ D ₆	−11.71 (br d) ⁶⁴	26.1 (MnSi) −24.2 (SiMe ₂ H)	¹³ C ³¹ P IR	167
3-56 Cp'(OC) ₂ Mn(η^2 -H-SiPhMe- SiPhMeH- η^2)Mn(CO) ₂ Cp' Cp' = C ₅ H ₄ Me ⁶⁵	Cp'Mn(CO) ₃ + HSiPhMeSiPhMeH (hν)	23 pale yellow 88 (d)	C ₆ D ₆	−11.16 (s, <i>J</i> _{SiH} = 57)	−3.6 −2.8	¹³ C IR EA	166
3-57 [(OC) ₃ P ₂ Mn(η^2 -HSiR ₃)] P = P(OCH ₂) ₃ CMe R = Et ⁶⁶	[<i>mer</i> -(OC) ₃ (P(OCH ₂) ₃ CMe) ₂ - Mn(ClCH ₂ Cl)][BARf] + HSiEt ₃		CD ₂ Cl ₂ (−78)	−16.75 (t) −16.1		³¹ P	168
3-58 Cp(OC) ₂ (H)ReSiEt ₃	CpRe(CO) ₃ + HSiEt ₃ (hν)					IR calc	165
3-59 Cp(OC) ₂ (H) ReSiPh ₂ SiPh ₂ H ⁶⁷	Cp(OC) ₂ Re(THF) + HSiPh ₂ SiPh ₂ H	22 colorless 79	C ₆ D ₆	−9.06 (s) ⁶⁸	−25.6 (SiH) −19.1 (ReSi)	¹³ C IR EA	166
3-60 [(OC) ₅ Re(η^2 -HSiEt ₃)] ⁺ - [B(C ₆ F ₅) ₄] [−]	(OC) ₅ ReCl + [Et ₃ Si][B(C ₆ F ₅) ₄] + HSiEt ₃		C ₆ H ₅ F (−23)	−10.73 ⁶⁹ <i>J</i> _{SiH} = 55			81
3-61 [(OC) ₄ (R ₃ P)Re(η^2 -H- SiEt ₃)] ⁺ [BARf] [−] R = Ph ⁷⁰	[(OC) ₄ (R ₃ P)Re] ₂ (μ -H)] ⁺ - [BARf] [−] + HSiEt ₃		CD ₂ Cl ₂ (−40)	−8.89 (d) <i>J</i> _{SiH} = 60.9		³¹ P	170 165
3-62 [(OC) ₄ (P) ₂ Re(η^2 -HSiEt ₃)] ⁺ - [BARf] [−] P = P(OCH ₂) ₃ CMe ⁷¹	[(OC) ₄ (P) ₂ Re (CH ₂ Cl ₂)] ⁺ - [BARf] [−] + HSiEt ₃		CD ₂ Cl ₂ (0)	−10.68 (brd)		³¹ P	171
3-63 [<i>fac</i> -(OC) ₃ (P) ₂ Re- (η^2 -H-SiEt ₃)] ⁺ [BARf] [−] P = P(OCH ₂) ₃ CMe	[<i>fac</i> -(OC) ₃ (P) ₂ Re(CH ₂ Cl ₂)] ⁺ - [BARf] [−] + HSiEt ₃	69 colorless	CD ₂ Cl ₂	−10.43 (t) <i>J</i> _{SiH} = 66		¹³ C IR EA	171
*3-64 (Ph ₃ P) ₂ H ₆ Re[η^1 -(SiMe ₂ - C ₂ B ₁₀ H ₁₀ (SiMe ₂ H)-Si)]	Re(PPh ₃) ₂ H ₇ + 1,2-(HMe ₂ Si) ₂ C ₂ B ₁₀ H ₁₀	75 yellow 153–155 (dec)	CDCl ₃	−5.28 (t) ⁷² ² <i>J</i> _{HH} = 19		¹³ C ³¹ P IR EA X-ray	172
*3-65 (PPh ₃) ₂ H ₃ Re[η^1 : η^1 - (SiMe ₂) ₂ -C ₂ B ₁₀ H ₁₀ -Si, Si]	(Ph ₃ P) ₂ H ₆ ReSiMe ₂ C ₂ B ₁₀ H ₁₀ -2- (SiMe ₂ H) + Δ	68 colorless 166–168 (dec)	CDCl ₃	−6.75 (t) ² <i>J</i> _{HH} = 19		¹³ C ³¹ P IR EA X-ray	172
3-66a (OC) ₅ ReSiPh ₃	Re ₂ (CO) ₈ [μ -C(H)(H) ^a Bu]- (μ -H) + HSiPh ₃ 97 °C	13 colorless	CD ₂ Cl ₂			IR EA X-ray	173
*3-66b (OC) ₆ Re ₂ (μ - η^7 -SiPh ₃)- (μ -H)		10		−18.45 (s)		IR MS EA X-ray	
*3-66c (OC) ₈ Re ₂ (μ -SiPh ₂)(SiPh ₃)- (μ -H)		30 colorless		−9.43 (s) ¹ <i>J</i> _{SiH} = 44		IR EA X-ray	

Table 3d. Continued

compound	starting metal complex	% yield color m.p., °C	NMR				other ^d	ref ⁵
			solvent (temp., °C) ^f	¹ H M—H ²	²⁹ Si; ^{2,3}			
3-67 (OC) ₈ Re ₂ (μ-SiPh ₂) ₂ ⁷³	Re ₂ (CO) ₈ [μ-C(H)(C(H) ⁿ Bu)- (μ-H) + HSiPh ₃ + 125 °C	44 yellow	CD ₂ Cl ₂				IR EA X-ray	173
Fe triad								
3-68a Cp(ⁱ Pr ₂ MeP)FeH ₂ SiMeCl ₂ ⁷⁴	Cp(ⁱ Pr ₂ MeP)Fe(BH ₄) + HSiMeCl ₂ /NEt ₃	80 yellow	C ₆ D ₆	−15.06 (s + sat; <i>J</i> _{SiH} = 18.3)	70.0 (dt) <i>J</i> _{SiH} = 19.2	¹³ C ³¹ P IR DFT X-ray		42a
3-68b Cp*(OC) ₂ FeSiMe ₂ NPh ₂	Cp*(OC) ₂ FeMe + HSiMe ₂ NPh ₂ , hν	48 yellow	C ₆ D ₆		47.3	¹³ C IR EA MS X-ray		174b
3-69 Cp*(OC)(Me ₃ Si)Fe=Si- Mes ₂ ^{75, 76}	Cp*(OC)(py)FeMe ⁷⁷ + HMe ₂ SiSiMes ₂ Me or Cp*Fe(CO) ₂ Me + HMe ₂ SiSiMeMes ₂ (hν)	70 (40) orange	C ₆ D ₆		28.4 (SiMe ₃) 365.8 (Fe=Si)	¹³ C IR MS EA X-ray		175 22b
3-70 (C ₆ H ₅ CH ₃)(H) ₂ Fe- (SiMeCl ₂) ₂ ⁷⁸	Fe _(atom) + C ₇ H ₈ + HSiMeCl ₂	~2	CD ₃ CN	−18.87 (s) ² <i>J</i> _{SiH} = 17.2				92
3-71 (3-38) [(OC) ₄ (H)FeSiMe ₂] ₂ NH	Fe(CO) ₅ + (HSiMe ₂) ₂ NH (hν)	18 white				IR [EA]		176
3-72a (OC) ₄ (H)FeSiMe ₂ OEt ⁷⁹	Fe(CO) ₅ + HSiMe ₂ OEt hν	45	C ₆ D ₆	−9.45 (s)	48.4			177a
*3-72b <i>cis</i> -[(OC) ₄ Fe(xantsil)]	Fe(CO) ₅ + H ₂ [Xantsil]	53 colorless	C ₆ D ₆		9.0	¹³ C IR FAB-MS X-ray		177b
*3-72c (OC) ₄ Fe[8-Br-1,6- (Me ₂ Si) ₂ C ₆ H ₃]	Fe ₂ (CO) ₉ + 1,6-(HMe ₂ Si) ₂ -BrC ₆ H ₃ + Δ	22 colorless 115–117 16 ⁸⁰	—		46.7 39.1	EA IR X-ray		177c
3-73 (CO) ₃ (H)Fe{SiMe ₂ ⋯O(2- C ₅ H ₄ N)⋯SiMe ₂ }	Fe(CO) ₅ + HSiMe ₂ O- (2-C ₅ H ₄ N) (hν)		C ₆ D ₆	−9.95 (s)	74.9 96.0	¹³ C IR MS		177a
3-74 (OC) ₃ (Me ₃ Si)(H)Fe=Si- (SiMe ₃) ₂ ⁸¹	Fe(CO) ₅ + HSi(SiMe ₃) ₃ (hν)							178a
3-75a <i>mer</i> -(OC) ₃ (Ph ₃ P)HFe- SiPh ₂ SiPh ₂ H ⁸²	<i>mer</i> -(OC) ₃ (Ph ₃ P)HFeSiMe ₃ + HPh ₂ SiSiPh ₂ H	78 beige 87 (d)	C ₆ H ₆	−8.42 (d)	−26.3 (SiPh ₂ H) 9.6 (d)	¹³ C ³¹ P IR EA		166 163
3-75b [(SiP ^{Ph} ₃)FeMes] ⁸³	Fe ₂ Mes ₄ + H[SiP ^{Ph} ₃]	46 red	C ₆ D ₆ 23 °C C ₇ D ₈ −60 °C			¹³ C ³¹ P VT IR EA UV-vis μ _{eff} = 0 X-ray		178b
*3-75c [(SiP ^{Pr} ₃)FeCl] ⁸⁴	FeCl ₂ + MeMgCl + H[SiP ^{Pr} ₃]	60 orange	C ₆ D ₆			¹³ C ³¹ P IR EA UV-vis μ _{eff} = 3.3μ _B X-ray		178b
*3-76 [Cp(OC)HFe] ₂ - [μ ₂ -SiMe ₂ OSiR ₂] ₂ R = <i>p</i> -Tol ⁸⁵	Cp(OC) ₂ FeSiMe ₂ (OSiHR ₂) hν	beige 10% 179	C ₆ D ₆	−12.54 (s) ² <i>J</i> _{HFeSi} = 24	46.7 (SiMe ₂) ⁸⁵	¹³ C IR EA X-ray		179
3-77 Cp(OC) ₂ FeSi(Me) (OSiMe ₂) ₂ Fe(CO)(H)Cp	Cp(OC) ₂ FeCH ₃ + (HSiMe ₂ O) ₂ (Me)SiFeCp*(CO) ₂ (hν)							180
3-78 Cp*(OC)(H)Fe- [(SiMe ₂ O) ₂ SiMe]- Fe(CO) ₂ Cp (2 isomers)	Cp(OC) ₂ FeCH ₃ + (HSiMe ₂ O) ₂ MeSiFe- Cp*(CO)H (hν)							180
3-79 [Cp*Ru(η ⁶ -C ₆ H ₅ SiPh ₂ - OCH ₃) ⁺][BPh ₄] [−]	(a) [Cp*Ru(H ₂ O)(NBD)]BF ₄ + HSiPh ₃ ⁸⁶ (b) NaBPh ₄ + MeOH	65 white	CDCl ₃			MS-(TOF) EA X-ray		181a
3-80 [Cp(Me ₃ P) ₂ Ru-(η ² -H- SiCl ₃) ⁺][BAr ^f ₄] ^{−87} (σ-complex)	Cp(Me ₃ P) ₂ RuSiCl ₃ + [H(OEt) ₂][BAr ^f ₄] Ar ^f = 3,5-C ₆ H ₃ (CF ₃) ₂	80–85 white	CD ₂ Cl ₂	rt −9.87 (t) −65 −10.13 (t)	30.6 (t) ¹ <i>J</i> _{SiH} = 48	³¹ P VT EA X-ray		182

Table 3e. Continued

compound	starting metal complex	% yield m.p., °C	NMR				other ^d	ref ⁵
			solvent (temp., °C) ^f	¹ H M—H ²	²⁹ Si ^{2,3}			
3-81a Cp(PhMe ₂ P) ₂ RuSiMeH-Cl ^{88, 89}	Cp(PhMe ₂ P) ₂ RuH + HSiMeCl ₂ + DBU	— pale yellow 80–90	CD ₂ Cl ₂	⁹⁰	68.4 (dt) <i>J</i> _{SiH} = 165.1		¹³ C ³¹ P [EA]	18
3-81b [Cp(ⁱ Pr ₃ P)(H) ₂ RuSiMe ₂ Cl] ⁹¹	[Cp(ⁱ Pr ₃ P)Ru(H) ₃] + HSiMe ₂ Cl	65 yellow	C ₇ D ₈	−12.46 (d + sat) <i>J</i> _{SiH} = 12.2			¹⁴ C ³¹ P IR EA X-ray	181c
3-81c [Cp(Ph ₃ P)(PhMe ₂ P)Ru-(SiMeCl ₂)]	[Cp(Ph ₃ P)(PhMe ₂ P)RuCl] + HSiMeCl ₂	88 yellow	C ₆ D ₆				¹³ C ³¹ P EA	181c
3-81d [Cp(ⁱ Pr ₂ MeP)(SiMeCl ₂) ₂ -RuH]	[Cp(Ph ₃ P)(ⁱ Pr ₂ MeP)RuH] + HSiMeCl ₂	70 yellow	C ₆ D ₆	−10.7 (d + sat) <i>J</i> _{SiH} = 19.7			¹³ C ³¹ P IR	181c
3-82 Cp(Ph ₂ MeP) ₂ RuSiCl ₃ ⁹²	Cp(Ph ₂ MeP) ₂ RuMe + HSiCl ₃ (neat; Δ)	92 yellow	CD ₂ Cl ₂		33.36 (s)		¹³ C ³¹ P [EA]	18
3-83 Cp*(Me ₃ P) ₂ RuSiR ₃ R = Cl ⁹³	Cp*(Me ₃ P) ₂ RuCH ₂ SiMe ₃ + HSiCl ₃	22 yellow	C ₆ D ₆		42.7		¹³ C ³¹ P IR EA	47a
3-84 Cp*(Me ₃ P) ₂ Ru(Si ⁱ Pr ₂ Cl)	Cp*(Me ₃ P) ₂ RuCH ₂ SiMe ₃ + HSi(ⁱ Pr ₂)Cl	76 yellow	?		102.1		¹³ C ³¹ P IR EA	183
3-85 Cp*(Me ₃ P) ₂ Ru[Si(SPh) ₃]	Cp*(Me ₃ P) ₂ RuCH ₂ SiMe ₃ + HSi(SPh) ₃	64 yellow	(?) CD ₂ Cl ₂ (²⁹ Si)		48.8		¹³ C ³¹ P IR EA	183
3-86 Cp*[(pyl) ₃ P](H) ₂ Ru-SiMe ₂ Ph	Cp*[(pyl) ₃ P]Ru(H) ₃ + HSiMe ₂ Ph + heat	76 white	C ₆ D ₆	−10.6 (d)	18.4 (s) ⁹⁴ <i>J</i> _{SiH} = 17		³¹ P IR EA X-ray	184
3-87 Cp*(Ph ₃ P)(H) ₂ RuSiMe ₂ Cl (IHI complex)	Cp*(Ph ₃ P) ₂ RuCl + xs HSiMe ₂ Cl		C ₆ H ₁₂	−11.6 (d)	57.7		¹³ C ³¹ P X-ray	185
3-88 Cp*(ⁱ Pr ₃ P)(H) ₂ RuSiMe ₂ Cl ⁹⁵ (IHI complex)	Cp*(ⁱ Pr ₃ P)RuH ₃ + xs HSiMe ₂ Cl Δ	30 colorless	C ₆ D ₆	−12.23 (d) <i>J</i> _{SiH} = 11.7	63.3		¹³ C ³¹ P IR EA X-ray	186
3-89a Cp*(Me ₂ ⁱ PrP)(H) ₂ Ru-SiMe ₂ Cl	Cp*(Me ₂ ⁱ PrP)RuH ₃ + xs HSiMe ₂ Cl	white (1:1 mix)	C ₆ D ₆	−12.13 (d) <i>J</i> _{SiH} = 12.9	61.9		¹³ C ³¹ P IR EA X-ray	186
3-89b Cp*(Me ₂ ⁱ PrP)(H) ₂ Ru-SiMeCl ₂ ⁹⁶				−11.5 <i>J</i> _{SiH} = 11	68.2		¹³ C ³¹ P IR X-ray	
3-90 Cp*(ⁱ Pr ₃ P)(H) ₂ RuSiMeCl ₂ (double IHI interaction) ⁹⁷	Cp*(ⁱ Pr ₃ P)RuH ₃ + xs HSiMeCl ₂ + NEt ₃ Δ	18 lt green	C ₆ D ₆	−11.6	69.9		¹³ C ³¹ P IR EA X-ray	186
3-91a Cp*(ⁱ Pr ₃ P)(H)ClRu-SiMeCl ₂ ⁹⁸	Cp*(ⁱ Pr ₃ P)RuH ₃ + HSiMeCl ₂ Δ	47 lt yellow	C ₇ D ₈	−9.51	61		¹³ C ³¹ P IR EA	186
3-91b Cp*(ⁱ Pr ₃ P)(H) ₂ Ru-SiMeClH ⁹⁹							¹³ C ³¹ P IR EA	
3-92 Cp*(ⁱ Pr ₃ P)ClRu-(η^2 -H-SiMe ₂ Cl) (SiH + Cl⋯SiCl IHI)	Cp*(ⁱ Pr ₃ P)RuCl + xs HSiMe ₂ Cl	¹⁰⁰ orange—yellow	C ₇ D ₈ (−40)	−9.65 <i>J</i> _{Hsi} = 33.5			¹³ C ³¹ P IR EA X-ray	187
3-93 Cp*(ⁱ Pr ₃ P)(H)ClRuSiCl ₃ ¹⁰¹	Cp*(ⁱ Pr ₃ P)RuCl + HSiCl ₃ ¹⁰²	~100 red—orange	C ₆ D ₆	−9.47			¹³ C ³¹ P IR EA	186
3-94 Cp*(ⁱ Pr ₃ P)(H) ₂ RuSiCl ₂ H ¹⁰³	Cp*(ⁱ Pr ₃ P)RuH ₃ + xs HSiCl ₃ + NEt ₃		C ₆ D ₆	−11.4 ¹⁰⁴			¹³ C ³¹ P	186
3-95a Cp*(ⁱ Pr ₃ P)(H) ₂ RuSiClH ₂	Cp*(ⁱ Pr ₃ P)RuH ₃ + NEt ⁱ Pr ₂ + HSiCl ₃ ¹⁰⁵ Δ	62 gray	C ₆ D ₆	−12.2 (dt) ¹⁰⁶			¹³ C ³¹ P IR	186
*3-95b C ₄₅ H ₅₄ PNSiRu (kinetic product, KP)	Cp*Ru(κ^3 -P,C,C′)-complex ¹⁰⁷		C ₆ D ₆	KP −9.21 (d)			¹³ C ³¹ P EA	47d

Table 3f. Continued

compound	starting metal complex	% yield m.p., °C	color	NMR				other ^d	ref ⁵
				solvent (temp., °C) ^f	¹ HM—H ²	²⁹ Si ^{2,3}			
C ₄₅ H ₅₄ PNSiRu (thermodynamic product, TP) (see structures 3-95b) 3-96a Cp*(OC)(py)Ru-SiMe ₂ NPh ₂ ¹⁰⁸	Cp*(OC)(Py)RuMe + HSiMe ₂ NPh ₂	TP 93 yellow 29 orange		C ₆ D ₆		TP 30.6 37.8		¹³ C IR EA ¹³ C	188
3-96b Cp*(OC)HRu{κ ² (Si, C)-SiMe ₂ N(O-C ₆ H ₄)(Ph)} ¹⁰⁹		31 light yellow		C ₆ D ₆ (25)	−10.53 (br)	52.2		IR EA ¹³ C	
3-97 Cp*(OC)(py)RuSiMe ₂ NEt ₂	Cp*(OC)(Py)RuMe + HSiMe ₂ NEt ₂ + py	38 yellow		C ₇ D ₈ C ₆ D ₆	−10.53 (s)	41.5		IR EA ¹³ C	188
*3-98 Cp*Ru[η ⁵ -C ₅ H ₅ Si ^t (Bu)H] ¹¹⁰	[Cp*RuCl] ₄ or [Cp*RuOMe] ₄ + H ^t (Bu)[SiC ₅ H ₆] + nBuLi	45 dk orange 82–85 86 white 143–146		C ₆ D ₆	¹¹¹	−33.7		[EA] ¹³ C IR EA ¹³ C	189a
*3-99a Cp'(Me ₃ P)(H)Ru(η ² -1,4-Si ₂ C ₄ Me ₆) Cp' = C ₅ Me ₄ Et	Cp'(Me ₃ P) ₂ RuCH ₂ SiMe ₃ + 1,4-H ₂ Si ₂ C ₄ Me ₆			C ₆ D ₆	−12.6 (d)	44.0 (d) (trans to PMe ₃) 31.5 (d) (cis to PMe ₃)		IR EA X-Ray calc ¹³ C ³¹ P	189a
3-99b [(η ⁵ -indenyl)(Ph ₃ P)- (HCy ₂ P)RuSiEt ₃]	[(η ⁵ -indenyl)(Ph ₃ P)Ru=PCy ₂] + HSiEt ₃	21 yellow		CDCl ₃				IR EA X-ray ¹³ C ³¹ P	189b
3-100 (C ₆ H ₆)(Ph ₃ P)Ru(SiCl ₃) ₂ ^{112,113}	(Ph ₃ P) ₃ RuCl ₂ + xs HSiCl ₃ + CH ₂ =CHC ₆ H ₁₃ + C ₆ H ₆	75–85 orange		CD ₂ Cl ₂		¹¹⁴		X-ray ¹³ C ³¹ P	190
3-101 (C ₆ H ₆)(Ph ₃ P)Ru(SiMe ₂ Cl) ₂ (7 pts) + (C ₆ H ₆)(Ph ₃ P)Ru(SiMeCl ₂)- (SiMe ₂ Cl) (12 pts) + (C ₆ H ₆)(Ph ₃ P)Ru- (SiMeCl ₂) ₂ (1 pt) ¹¹⁵	(Ph ₃ P) ₃ RuCl ₂ + xs HSiMe ₂ Cl + CH ₂ =CHC ₆ H ₁₃ + C ₆ H ₆	off white		CD ₂ Cl ₂		72.31 (d) 73.27 (d) 79.31 (d)		X-ray ³¹ P	190
3-102 (<i>p</i> -cymene)Cl ₂ (H)RuSiPh ₃ ¹¹⁶ 3-103 Tp(Ph ₃ P)(H)Ru(η ² -H—SiR ₃) R = Et ¹¹⁷	[(<i>p</i> -cymene)RuCl ₂] ₂ + HSiPh ₃ Tp(Ph ₃ P)(H)Ru(NCCH ₃) + HSiR ₃	41 orange		CDCl ₃ C ₄ D ₈ O	−10 −11.62 (d) ¹¹⁸ <i>J</i> _{SiH} = 23.3	24.7		³¹ P VTNMR IR MS calc ¹³ C	191 48a
3-104 (3-51) (OC) ₄ Ru(Xantsil)	Ru ₃ (CO) ₁₂ + H ₂ Xantsil	34 colorless		C ₆ D ₆		−8.2		VTNMR IR EI-MS X-ray ¹³ C	192 177b
*3-105 (Xantsil)(H)(CO)Ru{SiMe ₂ ... O'Bu...SiMe ₂ } ¹¹⁹	(Xantsil)(OC)Ru(η ⁶ -C ₆ H ₅ CH ₃) + HSiMe ₂ SiMe ₂ O'Bu	84% colorless		CD ₂ Cl ₂	−2.23 (s)	15.4 (Si _{3,4}) 107.6 (Si _{1,2})		IR MS EA X-ray ¹³ C ³¹ P	193a,b
3-106 (3-52) (OC) ₂ HRu{SiMe[(CH ₂) _x PPh ₂] ₂ } <i>x</i> = 3 ¹²⁰	Ru ₃ (CO) ₁₂ + MeSi(CH ₂ CH ₂ CH ₂ PPh ₂) ₂ H (CO) ₃ (Ph ₃ P) ₂ Ru + biPSiH	8 yellow 100		CDCl ₃ (?) C ₆ D ₆	−6.29 −6.73 (t) ¹²³	−1.1 ¹²³		EA X-ray ¹³ C ¹²³ ³¹ P ¹²³	194 195a
*3-107 (OC) ₂ HRu(biPSi) ¹²¹ (<i>syn</i> and <i>anti</i> isomers) ¹²²				C ₄ D ₈ O CDCl ₃	−7.06 (t) ¹²³				
3-108 (OC)(PPh ₃) ₂ ClRuSiMeCl ₂	(OC)(PPh ₃) ₃ ClRuH + HSiMeCl ₂ Δ or (OC)(PPh ₃) ₂ ClRuPh + HSiMeCl ₂	95 yellow 230 °C (d)						¹ H ¹³ C IR EA	196
3-109 (OC)(etp)(H)RuSiEt ₃ ¹²⁴	(OC)(etp)RuH ₂ + HSiEt ₃ <i>hν</i>			C ₄ D ₈ O	−8.00 (m)	18.1 (dt)		³¹ P	197
3-110 (OC)(Ph ₃ P) ₂ (Cl)Ru-SiMe ₂ Ph ¹²⁵	(a) (OC)(Ph ₃ P) ₂ ClRu(R ¹ C=C-HR ²) + HSiMe ₂ Ph	(a) not isolated		−16	(ddd)				198 199 200
¹²⁶	(b) (OC)(Ph ₃ P) ₃ ClRuH + CH ₂ =CH(SiMe ₂ Ph)	(b) 37 orange		CDCl ₃				³¹ P IR EA ¹³ C	201
3-111 (OC)(Ph ₃ P) ₂ ClRu- {SiMe ₂ ...NMe ₂ ...SiMe ₂ } ¹²⁷	(OC)(Ph ₃ P) ₂ ClRuSiMe ₂ Cl + xs HSiMe ₂ NMe ₂	34		C ₇ D ₈		59.8 (dd)		IR EA ¹³ C	201
3-112 (OC)(Ph ₃ P) ₂ HRu- {SiMe ₂ ...NMe ₂ ...SiMe ₂ } ¹²⁷	(OC)(Ph ₃ P) ₂ ClRuSiMe ₂ Cl + xs HSiMe ₂ NMe ₂	40		C ₇ D ₈ (¹ H) CH ₂ Cl ₂ - C ₆ D ₆ (²⁹ Si) CDCl ₃	−6.78 (t)	65.9 (dd)		IR EA X-ray ¹ H	201 202
3-113 (OC)(Ph ₃ P) ₂ (κ ² -S ₂ CNMe ₂)-	RuH(κ ² -S ₂ CNMe ₂)(CO)-	94							

Table 3g. Continued

compound	starting metal complex	% yield color m.p., °C	NMR				other ^d	ref ⁵
			solvent (temp., °C) ^f	¹ H M-H ²	²⁹ Si ^{2,3}			
RuSiClPh ₂	(PPh ₃) ₂ + xs HSiClPh ₂	pale yellow					¹³ C IR EA X-ray	
3-114 [Cy ₃ PH][(OC)(PCy ₃)ClRu-(SiCl ₃) ₂]	(OC)(Cy ₃ P) ₂ ClRuH + 2.4 equiv HSiCl ₃	85 pale yellow	CD ₂ Cl ₂				¹³ C ³¹ P IR X-ray	203
3-115 (OC)(biPSi)RuCl ¹²⁸	<i>mer</i> -(OC)(Ph ₃ P) ₃ (Cl)RuH + HSi(Me)(CH ₂ CH ₂ CH ₂ PPh ₂) ₂	70 brt yellow	C ₆ D ₆		53.7 (t)		¹³ C ³¹ P IR EA X-ray	204
3-116 (Me ₃ P) ₄ (Me)RuSiMe ₃	(Me ₃ P) ₄ RuMe ₂ + HSiMe ₃ (1:1 ratio)	12.7 white	C ₆ D ₆				¹³ C ³¹ P VT EA X-ray	97
3-117 (Me ₃ P) ₄ (H)RuSiMe ₃ ¹²⁹	(Me ₃ P) ₄ RuMe ₂ + HSiMe ₃ (1:6 ratio)	89 white	C ₆ D ₆	−11.17 (dtd)	7.9 (dtd)		¹³ C ³¹ P EA IR X-ray	97
3-118 (Me ₃ P) ₄ (H)RuSiEt ₃	(Me ₃ P) ₃ Ru(η ² -CH ₂ PMe ₂)H + HSiEt ₃ hν	37 light brown	C ₆ D ₁₂ C ₆ D ₆	−11.33 (dtd) −11.04 (dq)			¹³ C ³¹ P EA IR X-ray	97
3-119a <i>cis</i> -(Me ₃ P) ₄ (H)Ru-CH ₂ SiMe ₂ Cl	<i>cis</i> -(Me ₃ P) ₄ Ru(H)SiMe ₃ + HSiMe ₂ CH ₂ Cl	100 white	C ₆ D ₆	−9.8 (dq) <i>J</i> _(H,Si) < 12 ¹³⁰	40.9 (dd)		¹³ C ³¹ P IR HRMS-(Cl) X-ray	205
*3-119b <i>fac</i> -(Me ₃ P) ₃ (Cl)Ru-(CH ₂ SiMe ₂ -H-μ) (β-complex)	3-119a + hν or Δ	82 yellow	C ₆ D ₆	−7.85 (dt) <i>J</i> _{SiH} = 75	−19.4 (dd)		¹³ C ³¹ P IR EA X-ray	
*3-119c <i>mer</i> -(Me ₃ P) ₃ (Cl)Ru-(CH ₂ SiMe ₂ -H-μ) (β-complex)		7 yellow	C ₆ D ₆	−6.0 (dt) <i>J</i> _{SiH} = 77.5	−19.8		¹³ C ³¹ P HRMS X-ray	
3-120 (Me ₃ P) ₃ (H) ₃ Ru(SiMe ₃) ¹³¹	<i>cis</i> -(Me ₃ P) ₄ RuH ₂ + HSiMe ₃ (~1:10 ratio) hν	89 colorless	(a) C ₆ D ₆ (b) C ₆ D ₁₂	(a) −10.18 (br m) (b) −10.34 (br m)	(a) −10.8 (q)		¹³ C ³¹ P <i>T</i> ₁ IR EA X-ray ¹³²	97
3-121 (Me ₃ P) ₃ (H) ₃ Ru-(SiMe ₂ CH ₂ SiMe ₃)	(Me ₃ P) ₃ (H) ₃ RuSiMe ₃ + HSiMe ₂ CH ₂ SiMe ₃	~100	(a) C ₆ D ₆ (b) C ₆ D ₁₂	(a) −10.15 (br m) ¹³³ <i>J</i> _{HSi} = 25 (b) −10.37 (s) ¹³³	(a) −0.9 (SiMe ₃) −9.2 (q) (b) −10.27 (br m) −19.29 (q)		¹³ C ³¹ P IR EA X-ray	49
*3-122 (Me ₃ P) ₃ (H) ₂ Ru-(Me ₂ SiCH ₂ CH ₂ SiMe ₂)	<i>cis</i> -(Me ₃ P) ₃ (H) ₃ RuSiMe ₃ + HMe ₂ SiCH ₂ CH ₂ SiMe ₂ H	85 colorless	C ₇ D ₈ CD ₃ C ₆ D ₁₁ (−123)	−10.37 (s) ¹³³ −10.53 (s)			¹³ C ³¹ P IR [EA] X-ray	49
3-123 (Me ₃ P) ₃ (H) ₂ Ru(SiMe ₃) ₂	[(Me ₃ P) ₃ (H)Ru(SiMe ₃) ₂ N ₂ + xs HSiMe ₃	¹³⁴	CD ₃ C ₆ D ₁₁ (−118)	−9.56 (br m) −7.48 (br m)			³¹ P VTNMR	49
3-124 (Ph ₃ P) ₃ H ₃ RuSiMeCl ₂ (σ-complex) ¹³⁵	(Ph ₃ P) ₃ RuCl ₂ ¹³⁶ + xs HSiMeCl ₂	83 near colorless	CD ₂ Cl ₂	−9.76	34.6 (q) <i>J</i> _{SiH} = 38		¹³ C ³¹ P <i>T</i> ₁ IR EA X-ray	206
3-125a (Cy ₃ P) ₂ (H) ₂ (η ² -H ₂)Ru-(η ² -H-SiMe ₂ Cl)	(Cy ₃ P) ₂ (H) ₂ Ru(H ₂) ₂ + HSiMe ₂ Cl		C ₇ D ₈ (15)	−8.51 (br, 5RuH) ¹³⁷	38 (s) ¹³⁷		³¹ P <i>T</i> ₁	207a
3-125b (Cy ₃ P) ₂ (H) ₂ Ru-(η ² -H-SiMe ₂ Cl) ₂			C ₇ D ₈ (−40)	−7.90 (br t; RuHSi) −10.69 (AA'XX') ¹³⁸	29 (s) ¹³⁷		³¹ P	
3-125c (Cy ₃ P) ₂ Cl(η ² -H ₂)Ru-(SiMe ₂ Cl)			C ₇ D ₈ (15)	−13.75 (br t)	85.7 (s) ¹³⁷		³¹ P	

Table 3h. Continued

compound	starting metal complex	% yield color m.p., °C	NMR				other ^d	ref ⁵
			solvent (temp., °C) ^f	¹ HM–H ²	²⁹ Si ^{2,3}			
3-126a (Cy ₃ P){(η ² -C ₆ H ₈)PCy ₂ }- (H)Ru(η ² -H–SiMe ₂ Cl) (SISHA)	(Cy ₃ P) ₂ (H) ₂ Ru(H ₂) ₂ + C ₂ H ₄ + HSiMe ₂ Cl	24 orange	C ₇ D ₈ (20)	–11.98 (dd, RuH ₂) –9.06 (t, RuHSi)	46.2 ¹³⁹ <i>J</i> _{SiH(1)} = 37.3 <i>J</i> _{SiH(2)} = 24.1 72.6	³¹ P EA X-ray calc <i>T</i> ₁ ³¹ P EA X-ray DFT ³¹ P VTNMR EA X-ray calc ³¹ P VTNMR calc ³¹ P X-ray calc ³¹ P <i>T</i> ₁ IR EA X-ray	207a 452	
3-126b (Cy ₃ P) ₂ (η ² -H ₂)(Cl)Ru- (SiMeCl ₂) ¹⁴⁰	(Cy ₃ P) ₂ (η ² -H ₂)(Cl)RuH + HSiMeCl ₂	— orange	C ₇ D ₈	–12.14 (br) (η ² -H ₂)			207b	
*3-127 [(Cy ₃ P) ₂ (H) ₂ Ru-{(η ² - HSiMe ₂) ₂ X}] X = C ₆ H ₄ ¹⁴¹	(Cy ₃ P) ₂ (H) ₂ Ru(H ₂) ₂ + 1,2-(HSiMe ₂) ₂ C ₆ H ₄	94 white	C ₆ D ₆	–7.74 (SiH) –12.3 (RuH)	4.8 <i>J</i> _{SiH} = 65		208 209	
*3-128 [(Cy ₃ P) ₂ (H) ₂ Ru- {(η ² -HSiR ₂) ₂ O}] R = Me ¹⁴²	(Cy ₃ P) ₂ (H) ₂ Ru(H ₂) ₂ + HMe ₂ SiOSiMe ₂ H	72 white	C ₆ D ₆	–9.48 (SiH)	–5.6 <i>J</i> _{SiH} = 22		208 209	
3-129 (Cy ₃ P) ₂ (H) ₂ (η ² -H ₂)Ru- (η ² -HSiPh ₃) (SISHA) ¹⁴³	(Cy ₃ P) ₂ (H) ₂ Ru(H ₂) ₂ + HSiPh ₃	40 beige	C ₆ D ₆	–8.45 (br s)			210a 101	
*3-130a [(Cy ₃ P) ₂ (H) ₂ Ru{η ⁴ -H- SiMe ₂ (CH=CHMe)}] (β-complex)	(Cy ₃ P) ₂ H ₂ Ru(H ₂) ₂ + HSiMe ₂ (CH ₂ =CHCH ₂)	61 white	C ₇ D ₈ (¹ H)	–12.46 (dt) RuH	–11.3 (d) ¹⁴⁴ <i>J</i> _{SiH} = 106	³¹ P <i>T</i> ₁ IR EA X-ray	211a 212	
*3-130b Ru(PPh ₂ CH ₂ OSiMe ₂ H) ₃ ¹⁴⁵	RuH ₂ (H ₂) ₂ (PCy ₃) ₂ + HMe ₂ SiOCH ₂ PPh ₂ (3 equiv)	36 grey	C ₆ D ₆ (²⁹ Si) (0) C ₇ D ₈ –5 (¹ H) –42 (²⁹ Si)	–9.46 (dt) –7.74 (s) <i>J</i> _{SiH} = 105 4.07 (sept) (SiH)	8.2 (d) ¹ <i>J</i> _{SiH} = 200	¹³ C ³¹ P EA DFT X-ray ³¹ P [EA]	211b	
3-131 [(pyl ₃ P) ₂ (H) ₂ Ru{(η ² -H- SiMe ₂) ₂ X}] X = C ₆ H ₄ ¹⁴⁶	Ru(cod)(cot) + Ppyl ₃ + 1,2-(HSiMe ₂) ₂ C ₆ H ₄	70 white	C ₆ D ₆ (15) (¹ H)	–6.47 (SiHRu)	66.8 (s) <i>J</i> _{SiH} = 26 8.8 <i>J</i> _{SiH} = 61		208	
*3-132 [(Cy ₃ P) ₂ H ₂ Ru-{(η ² - HSiMe ₂) ₂ NH}] (σ-complex)	RuH ₂ (H ₂)(PCy ₃) ₂ + (HMe ₂ Si) ₂ NH	72 colorless	C ₇ D ₈	–8.83 (RuH) –9.80 (br s)		³¹ P VTNMR IR EA X-ray calc ³¹ P EA	212	
*3-133 [(Ph ₃ P) ₂ (H) ₂ Ru{(η ² -H- SiMe ₂) ₂ X}] X = C ₆ H ₄ ¹⁴⁷	Ru(cod)(cot) + PPh ₃ + 1,2-(HSiMe ₂) ₂ C ₆ H ₄	86 white		–7.10 (SiHRu) –10.46 (RuH)	8.1 <i>J</i> _{SiH} = 63		208	
*3-134a <i>fac</i> -[PSiP](Ph ₃ P)RuCl	RuCl ₂ (PPh ₃) ₃ + Et ₃ N H[PSiP]	89 red	CD ₂ Cl ₂ 300 K 183 K		–61.8	¹³ C ³¹ P EA VTNMR X-ray ³¹ P VTNMR	213a	
*3-134b H ₂ Ru{η ² -HSiMe ₂ CH ₂ - (<i>o</i> -C ₆ H ₄)PPh ₂] ₂ <i>ε</i> -agostic	(Cy ₃ P) ₂ (η ² -H ₂)RuH ₂ + HSiMe ₂ [CH ₂ (C ₆ H ₄)PPh ₂ - <i>o</i>]	— orange	C ₇ D ₈ –80	–10.45 (AA'XX') –5.16 (br s) <i>J</i> _{SiH} = 27.8 –9.77 (t) <i>J</i> _{SiH} = 67	8.30	³¹ P VTNMR	213c	
*3-134c Ru[η ² -H–SiMe ₂ - (CH(C ₆ H ₄)PPh ₂) ₂] β- and ε-agostic	Ru(COD)(COT) + 2Ph ₂ P- (<i>o</i> -C ₆ H ₄)CH ₂ SiMe ₂ H	92 yellow	C ₆ D ₆ C ₇ D ₈ –80		–4.37 (s)	¹³ C ³¹ P EA X-ray DFT ³¹ P DFT	213c	
*3-134d RuH{η ² -H–SiMe ₂ CH ₂ - (<i>o</i> -C ₆ H ₄)PPh ₂ }{η ² -H- SiMe ₂ CH(<i>o</i> -C ₆ H ₄)PPh ₂ } + 3-134b + 3-134c	Ru(COD)(COT) + H ₂ 2HSiMe ₂ [CH ₂ (C ₆ H ₄)PPh ₂ - <i>o</i>]	yellow mixture	C ₇ D ₈	–6.04 (br s) <i>J</i> _{SiH} = 76 –8.00 (pt) <i>J</i> _{SiH} = 27 –9.36 (dd) <i>J</i> _{SiH} = 40 –17.76 (s)	–80 –9.36 (dd) carbometallated 11.00 (s) nonmetallated		213c	
3-134b/3-134c/3-134d = 1:13:5								
3-134e [N ₃]Ru(H)(Cl){Si(NN)}	{[N ₃]Ru} ₂ (μ-N ₂) + H(Cl)Si(NN)	77 red	C ₆ D ₆		126.9	VT NMR IR X-ray	213b	
*3-134f [RuH] ¹⁴⁸	[Ru(cod)(cot)] + HMe ₂ Si(OSi≡)		¹ H MAS	–8.3		IR EXAFS TEM	213d	
3-134g [{Ru(CO) ₄] ₂ {μ- (Me ₂ Si) ₄ TTF}]} ¹⁴⁹	Ru ₃ (CO) ₁₂ + (HMe ₂ Si) ₄ TTF	72 orange–brown	¹ H (CDCl ₃)			IR EA	213e	

Table 3i. Continued

compound	starting metal complex	% yield m.p., °C	color	NMR				other ^d	ref ⁵
				solvent (temp., °C) ^f	¹ H—H ²	²⁹ Si ^{2,3}			
*3-135a {Cp*Ru(μ -H)} ₂ (μ -SiPh ₂)	Cp*Ru(μ -H) ₄ RuCp* + Ph ₃ SiH	(a) — red		C ₄ D ₈ O (¹ H) C ₆ D ₆ (²⁹ Si)	−13.51 (s)	265.0		¹³ C IR FD-MS EA X-ray ¹³ C	98
*3-135b (3-66b) {Cp*Ru(μ -SiPh ₂)(μ -H)} ₂ ¹⁵⁰		(b) 56 red		C ₇ D ₆ (¹ H) C ₆ D ₆ (²⁹ Si)	−19.7	109.8			
3-136 {Cp*Ru(μ -SiPhMe)(μ -H)} ₂ (mixture of diastereomers: <i>syn/anti</i> ≈ 55:45)	Cp*Ru(μ -H) ₄ RuCp* + Ph ₂ MeSiH	84 ¹⁵¹ orange		C ₄ D ₈ O (¹ H, 60) (¹ H, −40)	<i>syn</i> : −20.4 (br) −21.01 (d) −19.77 (d)	<i>anti</i> : 108.2 108.7		¹³ C (anti) IR FDMS	97
*3-137a <i>trans</i> -[(R'MeSi)(η^5 -R-C ₅ H ₃)Ru(CO) ₂] ₂ R' = Ph, R = H ¹⁵²	Ru ₃ (CO) ₁₂ + HSi(RC ₅ H ₄)R'Me	10 colorless >300 °C		C ₆ D ₆ (²⁹ Si) CDCl ₃				IR EA X-ray	155c
3-137b <i>trans</i> -[(R'MeSi)(η^5 -R-C ₅ H ₃)Ru(CO) ₂] ₂ R' = CH ₂ Ph, R = H	Ru ₃ (CO) ₁₂ + HSi(RC ₅ H ₄)R'Me	9 colorless 190–192 °C (dec)		CDCl ₃				IR EA	155c
+									
*3-137c [(η^2 -C ₅ H ₇)SiMeR'-Ru(CO) ₃] ₂ R' = CH ₂ Ph		11 yellow 98–99 °C		CDCl ₃				IR EA X-ray	
*3-137d [PhMeSi)(η^5 -C ₅ Me ₄)]-Ru ₂ (CO) ₆	Ru ₃ (CO) ₁₂ + HSi(C ₅ Me ₄ H)PhMe	19 yellow 130–132 °C		CDCl ₃				IR X-ray	155c
*3-137e Cp*Ru(μ -H) ₂ (μ -H) ₂ (μ -Si-PhMe)(μ -SiMe ₂)	Cp*Ru(μ -H) ₄ RuCp* + PhMe ₂ SiH	(e) 80 dk red		C ₄ D ₈ O (¹ H, 70) (¹ H, −60)	−20.80 (s) −21.13 (d) −20.44 (d)	112.3 (SiMe ₂) 107.9 (SiPhMe)		(e) ¹³ C FD-MS [EA] X-ray	97
*3-137f {Cp*Ru(μ -SiMe ₂)(μ -H)} ₂		(f) 5		C ₆ D ₆ (²⁹ Si) C ₄ D ₈ O (−60)	−21.16 (s)			FD-MS	
*3-138 {Cp*Ru(μ -H)} ₂ { μ - η^2 : η^2 -H-SiMe ₂ (CH=CH ₂)} ¹⁵³	Cp*Ru(μ -H) ₄ RuCp* + HSiMe ₂ (CH=CH ₂)	100 dk red		C ₇ D ₈	−14.50 (br, w _{1/2} =1275)	−8 (d, <i>J</i> _{SiH} = 31) ¹⁵⁴		¹³ C VTNMR IR FDMS [EA] X-ray	214
				(¹ H, 23)					
				C ₇ D ₈ /C ₄ D ₈ O (¹ H, −70)	−9.28 (br) <i>J</i> _{SiH} = 36.3				
					−14.54 (br, Ru—H—Ru) −20.22 (br, Ru—H—Ru)				
*3-139 (μ_2 , η^3 : η^5 -4,6,8-trimethyl-4,5-dihydroazulene)Ru ₂ (CO) ₅ + HSiMe ₂ Ph		yellow 60 196 (d)		C ₄ D ₈ O (²⁹ Si, −70) C ₆ D ₆		−8.6 (d, <i>J</i> _{SiH} = 54) ¹⁵⁵ 22.3, 27.4		¹³ C IR [EA] X-ray	215
3-140 [(OC) ₄ RuSiMe ₂ Ph] ₂	Ru ₃ (CO) ₁₂ + 3 equiv HSiMe ₂ Ph	65–70 yellow		CDCl ₃		5.3		¹³ C	216
3-141 −[SiRR'Ru(CO) ₄ Ru(CO) ₄ -SiRR'(C ₆ H ₄) _n]- R = R' = Me C ₆ H ₄ = 1,3-C ₆ H ₄ ¹⁵⁷	2/3Ru ₃ (CO) ₁₂ + (1,3-HSiMe ₂) ₂ C ₆ H ₄	24 yellow		CDCl ₃		5.4 (s)		IR X-ray IR UV-vis <i>M</i> _w ¹⁵⁸	216
3-142 [Ru ₂ (μ -Cl)(μ -H)(SiEt ₃) ₂ -(CO) ₂ (P'Pr ₃) ₂]	[Ru(<i>E</i> -CH=CH'Bu)Cl(CO)-(P'Pr ₃) ₂] + xs HSiEt ₃	29 red		C ₆ D ₈	−12.86 (t)			¹³ C ³¹ P IR EA X-ray	217
*3-143 [Ru(SiMe ₂ ...NMe ₂ ...SiMe ₂)(CO)-(μ -{SiMe ₂) ₂ (μ -Cl)RuH ₂ -(CO)(PPh ₃)] (+ 3-111)	(OC)(Ph ₃ P) ₂ (Cl)RuSiMe ₂ Cl + xs HSiMe ₂ NMe ₂	20 orange		C ₇ D ₈ CH ₂ Cl ₂ /C ₇ D ₈ (²⁹ Si)	−6.37 (d)	71.05 (term Si) 148.60 (d) (br Si)		¹³ C EA X-ray	201
*3-144a Ru ₂ H ₂ (μ - η^2 : η^2 -H ₂ -Si(OMe) ₂) ₂ (PCy ₃) ₂ + Si(OMe) ₄ (σ -complex)	Ru ₂ H ₄ (μ - η^2 : η^2 : η^2 -SiH ₄)-(PCy ₃) ₄ + xs HSi(OMe) ₃	65 white		C ₆ D ₆	−9.94 (d)	85.5 (nonet) ¹⁵⁹ <i>J</i> _{SiH} = 22		³¹ P ¹⁶⁰ IR EA X-ray calc	101

Table 3j. Continued

compound	starting metal complex	% yield m.p., °C	NMR				other ^d	ref ⁵
			solvent (temp., °C) ⁱ	¹ H M-H ²	²⁹ Si ^{2,3}			
*3-144b [(OC) ₁₀ Ru ₃ (Xantsil)(μ-H) ₂] + 3-72b ¹⁶¹	Ru ₃ (CO) ₁₂ + H ₂ [Xantsil]	19 ¹⁶² red	C ₆ D ₆	−16.27 (s) −14.94 (s)	7.2	¹³ C VT IR FABMS X-ray ¹³ C		177b
		3-72 (19)						
*3-145 (μ ₃ ,η ² :η ³ :η ⁵ -acenaphthylene)Ru ₃ H(SiR ₃)(CO) ₆ SiR ₃ = SiMe ₂ Ph ¹⁶³	(μ ₃ ,η ² :η ³ :η ⁵ -acenaphthylene)- Ru ₃ (CO) ₇ + HSiMe ₂ Ph	61	CDCl ₃	−15.21 (s)	29.5	¹³ C IR TLC		218
3-146 (H)(OC) ₆ Ru ₃ (μ ₃ ,η ⁵ :η ⁵ -4,6,8-trimethyl-4,5-dihydroazulene)(SiMe ₂ Ph)	(OC) ₇ Ru ₃ (μ ₃ ,η ⁵ :η ⁵ -4,6,8-trimethylazulene) + HSiMe ₂ Ph	155–156 (d) 50 red m.p. 134 (d)	C ₆ D ₆	−13.6	42.2	¹³ C IR FABMS EA X-ray ¹³ C ³¹ P		215
*3-147 [Ru ₄ (μ-Cl) ₂ (μ-H) ₂ (μ-SiEt ₂) ₂ (CO) ₄ (P ^{<i>i</i>} Pr ₃) ₄] ¹⁶⁴	[Ru(<i>E</i> -CH=CH ^{<i>t</i>} Bu)Cl(CO)-(P ^{<i>i</i>} Pr ₃) ₂] + xs HSiEt ₃	21 dark red	C ₇ D ₈	−14.35 (t)		¹³ C ³¹ P X-ray IR EA X-ray ³¹ P		217
*3-148 (a) (OC) ₁₄ Ru ₅ (SiEt ₃)(μ ₅ -C)(μ-H) b. (OC) ₁₅ Ru ₅ (SiEt ₃)(μ ₅ -C)(μ-H)	Ru ₅ (CO) ₁₅ (μ ₅ -C) + Et ₃ SiH	(a) 11 (b) 4	CDCl ₃	(a) −22.83 (b) −22.35		¹³ C X-ray ³¹ P		219
3-149 Cp(^{<i>i</i>} Pr ₃ P)(Cl)(H)OsSiR ₃ R = Et ¹⁶⁵	Cp(^{<i>i</i>} Pr ₃ P) ₂ OsCl + HSiEt ₃	51 yellow	C ₆ D ₆	−13.45 (d)		¹³ C MS EA ¹³ C ³¹ P X-ray ¹³ C IR EI-MS EA X-ray ¹³ C ³¹ P		52
3-150 Cp*(Me ₃ P) ₂ OsSi ^{<i>i</i>} Pr ₂ Cl	Cp*(Me ₃ P) ₂ OsCH ₂ SiMe ₃ + HSi ^{<i>i</i>} Pr ₂ Cl	85 pale yellow	CD ₂ Cl ₂		61 (HMBC)	¹³ C ³¹ P EA X-ray ¹³ C IR EI-MS EA X-ray ¹³ C ³¹ P		220
3-151a <i>cis</i> -(OC) ₄ Os(Xantsil)	Os ₃ (CO) ₁₂ + H ₂ [Xantsil]	87 colorless	C ₆ D ₆		−31.7	¹³ C IR EI-MS EA X-ray ¹³ C ³¹ P		177b
3-151b (OC) ₂ (Ph ₃ P) ₂ HOs-Si{OCH ₂ CH ₂ } ₃ N ¹⁶⁶	(OC) ₂ (Ph ₃ P) ₃ Os + HSi(OCH ₂ CH ₂) ₃ N	83 colorless 220–223	CDCl ₃	−9.64 (dd) (isomer c) −7.63 (t) (isomer a) −7.12 (dd) (isomer b) ¹⁶⁶ −9.03 (brd) (−60) −8.82 (tt) ¹⁶⁷ −9.20 (m)	−39.1 (t) (isomer a)	¹³ C ³¹ P IR HRMS EA ¹³ C ³¹ P T ₁ IR EA X-ray ¹³ C ³¹ P T ₁ IR EA		221
3-152 (OC)(Ph ₃ P) ₂ (H) ₃ OsSiMe ₃	(OC)(Ph ₃ P) ₂ (Cl)OsPh + Me ₃ SiH	7 off-white 133–135	CDCl ₃	−9.03 (brd) (−60) −8.82 (tt) ¹⁶⁷ −9.20 (m)		¹³ C ³¹ P T ₁ IR EA X-ray ¹³ C ³¹ P T ₁ IR EA		222
3-153 (OC)(Ph ₃ P) ₂ (H) ₃ OsSiR ₃ R = Et ¹⁶⁸	(OC)(Ph ₃ P) ₂ (H) ₃ OsSiMe ₃ + HSiEt ₃	46 colorless 138–140	CDCl ₃	−8.92 (brd, 1H) −9.81 (brd, 2H) (−20) −9.04 (tt) ¹⁶⁷ −9.85 (m)		¹³ C ³¹ P T ₁ IR EA		222
3-154 (OC)(Ph ₃ P) ₂ (Me ₂ NCS ₂)Os-SiCl ₃ ¹⁶⁹	(OC)(Ph ₃ P) ₂ (Me ₂ NCS ₂)OsH + HSiCl ₃	70 colorless	CDCl ₃			¹³ C ³¹ P IR EA X-ray ¹³ C ³¹ P		223
3-155 (OC)(Ph ₃ P) ₂ ClOsSi(OEt) ₃	(OC)(Ph ₃ P) ₂ ClOsPh + HSi(OEt) ₃	86 brt -yellow	CDCl ₃		−61.1(t)	¹³ C ³¹ P IR HRMS EA X-ray ¹³ C ³¹ P		224
3-156 (OC)(Ph ₃ P) ₂ ClOs-Si{OCH ₂ CH ₂ } ₃ N ¹⁷⁰	(OC)(Ph ₃ P) ₂ ClOsPh + HSi{OCH ₂ CH ₂ } ₃ N	94 brt yellow 214–217	CDCl ₃		−65.0	¹³ C ³¹ P IR [EA] X-ray ¹ H ¹³ C IR EA		225
3-157 (OC)(PPh ₃) ₂ ClOsSiMeCl ₂	(OC)(PPh ₃) ₂ ClOsPh + HSiMeCl ₂ Δ	93 yellow–orange 240 °C (d)	CDCl ₃			¹³ C ¹ H ¹³ C IR EA		196

Table 3k. Continued

compound	starting metal complex	% yield color m.p., °C	NMR				ref ⁵
			solvent (temp., °C) ^f	¹ H M-H ²	²⁹ Si ^{2,3}	other ^d	
3-158 (OC)(Ph ₃ P) ₂ (Cl)Os- {SiMe ₂ ···NMe ₂ ···SiMe ₂ } ¹⁷¹	(Ph ₃ P) ₂ (OC)(Cl)OsSiMe ₂ Cl + xs HSiMe ₂ NMe ₂ + heat	40 colorless	C ₇ D ₈ (¹ H) CH ₂ Cl ₂ - C ₆ D ₆ (²⁹ Si)		37.8 (dd)	¹³ C IR EA X-ray	201
3-159 (OC)(Ph ₃ P) ₂ (H)Os- {SiMe ₂ ···NMe ₂ ···SiMe ₂ } ¹⁷¹	(Ph ₃ P) ₂ (OC)(Cl)OsSiMe ₂ Cl + xs HSiMe ₂ NMe ₂ + heat	45	C ₆ D ₆ (¹ H) CH ₂ Cl ₂ - C ₆ D ₆ (²⁹ Si)	-7.69 (t)	39.6 (dd)	¹³ C IR EA X-ray	201
3-160 (Ph ₃ P) ₃ H ₃ Os- Si{OCH ₂ CH ₂ } ₃ N	(Ph ₃ P) ₃ OsH ₄ + N{OCH ₂ CH ₂ } ₃ SiH	63 colorless 175–179	CDCl ₃	-11.19 (m)	-15.2 (q)	¹³ C ³¹ P T ₁ IR HRMS EA X-ray	221
3-161 (OC) ₉ H ₃ Os ₃ (SiEt ₃) ₃ (mixture of isomers)	(OC) ₁₀ Os ₃ H ₂ + HSiEt ₃ ¹⁷²	— colorless	CD ₂ Cl ₂	-16.31(s)		IR	226
*3-162a Os ₃ (μ-H)(μ-SiPh ₃)- (CO) ₉ (μ-dppm) ¹⁷³	Os ₃ (μ-H){μ ₃ -Ph ₂ PCH ₂ PPh-(C ₆ H ₄)}(CO) ₈ + HSiPh ₃	a. 45 orange	CD ₂ Cl ₂	a. -18.32 (app d)		a. ³¹ P X-ray	227
*3-162b Os ₃ (μ-H) ₂ (μ-SiPh ₃)- {μ ₃ -Ph ₂ PCH ₂ PPh(C ₆ H ₄)}- (CO) ₇		(b) 50 yellow		(b) -12.43 (dd) -15.05 (d)		(b) ³¹ P IR EA	
Co triad 3-164a (η ⁵ -C ₅ H ₄ CH ₂ CH ₂ - P(Bu) ₂)(H)CoSiPh ₃ ¹⁷⁴	(η ⁵ -C ₅ H ₄ CH ₂ CH ₂ P(Bu) ₂)- Co(η ² -C ₂ H ₄) + HSiPh ₃	54 deep red 138	C ₆ D ₆	-16.53 (d) J = 47.6		¹³ C ³¹ P VTNMR IR HR-MS	56
*3-164b [Cp*Co{P(OMe) ₃ }(H)- (η ² -H-SiEt ₃)] [B(Ar _F) ₄] ¹⁷⁵	Cp*[(MeO) ₃ P]HCo(η-H ₂) ⁺ - [B(Ar _F) ₄] ⁻ + HSiEt ₃		CD ₂ Cl ₂	-13.3 (d, (¹ H, -25) (²⁹ Si, -30) ¹ J _{SiH(obs)} = 29.0	20.9 (br s)		57c
*3-164c [Cp*Co(PMe ₃)(H)(η ² -H- SiEt ₃)] [B(Ar _F) ₄]	Cp*(Me ₃ P)HCo(η-H ₂) ⁺ - [B(Ar _F) ₄] ⁻ + HSiEt		CD ₂ Cl ₂	-13.96 (d, (¹ H, -19) (²⁹ Si, -30) ¹ J _{SiH(obs)} = 29 ¹⁷⁷	20.7 (d)		57c
3-165 (OC) ₄ CoSiMe ₂ Ph ¹⁷⁶	(OC) ₄ Co[C(O)OCH ₃] + HSiMe ₂ Ph	91				¹ H ¹³ C IR	228
3-166 (OC) ₄ CoSiEt ₂ Ph ¹⁷⁸	Co ₂ (CO) ₈ + 2 HSiEt ₂ GePh ₃					IR	229
3-167 (OC) ₄ CoSiPh ₃	Co ₂ (CO) ₈ + HSiPh ₃ ¹⁷⁹	61 white 158–160	CDCl ₃			¹ H ¹³ C IR	229
3-168a (OC) ₄ CoSiCl ₂ Me	Co ₂ (CO) ₈ + HSiCl ₂ Me	90 pale yellow	CDCl ₃		66.4	X-ray ¹³ C IR [EA]	230a
3-168b [tripod (H) ₂ CoSiPh ₃] ¹⁸⁰	[“tripodCo ⁰ ”] ¹⁸¹ + HSiPh ₃	62 yellow	CD ₂ Cl ₂	-13.12 (br s, 2H)		¹³ C ³¹ P MS(FAB) MS(LIFD) UV-vis E _A ^p DSC-TGA EA X-ray	230b
*3-169 (OC) ₄ Co[Si(Me)Fe- (η ⁵ -C ₅ H ₄) ₂]	Co ₂ (CO) ₈ + NEt ₃ + Fe(η ⁵ -C ₅ H ₄) ₂ SiMeH	23 red	C ₆ D ₆		24.3	¹³ C MS HRMS [EA] X-ray	231
3-170 (OC) ₄ Co-SiR ₂ FeCp(CO) ₂ R = Me ¹⁸²	Co ₂ (CO) ₈ + HR ₂ SiFe(CO) ₂ Cp						232
*3-171 [(OC) ₇ Co ₂ Si(R)- (η ⁵ -C ₅ H ₄)Fe(η ⁵ -C ₅ H ₅) R = Me ¹⁸³	Co ₂ (CO) ₈ + HSiMe[Fe(η-C ₅ H ₄) ₂]	45 lt. orange	C ₆ D ₆		137.5	¹³ C IR MS HRMS X-ray	231
3-172 (OC) ₃ Co(μ-SiMe ₂) ₂ - Co(CO) ₃ ¹⁸⁴	Co ₂ (CO) ₈ (2 equiv) + HSi(SiMe ₃) ₃	22 blk	C ₆ D ₆		213.4 (HMBC)	¹³ C EA X-ray	233
*3-173 [Co ₂ (CO) ₇ (SiMe ₂) ₂ NH ₂] ⁺ - [Co(CO) ₄] ⁻	Co ₂ (CO) ₈ + HN(SiMe ₂ H) ₂	38 red	CDCl ₃			¹ H ¹³ C EA UV	176

Table 3l. Continued

compound	starting metal complex	% yield color m.p., °C	NMR				other ^d	ref ⁵
			solvent (temp., °C) ^f	¹ H M—H ²	²⁹ Si ^{2,3}			
3-174 [(OC) ₄ CoSiMe ₂ (CH ₂) ₃] ₄ Si	Co ₂ (CO) ₈ + [HMe ₂ Si(CH ₂) ₃] ₄ Si		C ₆ D ₆				¹ H IR MS EA	234
3-175 [(OC) ₄ Co] ₈ Si ₈ O ₁₂	4 Co ₂ (CO) ₈ + H ₈ Si ₈ O ₁₂	87 colorless			−55 ¹⁸⁵		IR Raman MS EA X-ray IR	235
3-176 Cp(OC)HRhSiEt ₃ ¹⁸⁶	CpRh(CO) ₂ + HSiEt ₃ hν							236
3-177 Cp(Ph ₃ P)(H)RhSi(ⁱ Pr) ₃ ¹⁸⁷	Cp(Ph ₃ P)Rh(η ² -C ₂ H ₄) + HSi(ⁱ Pr) ₃	60 dk yellow	C ₇ D ₈	−13.60 (dd) ¹ J _{RhH} = 28	47.4 (dd) ¹ J _{RhSi} = 9.8		¹³ C ³¹ P MS EA X-ray	237
3-178 Cp(Me ₃ P)(H)RhSi(ⁱ Pr) ₃ ¹⁸⁸	Cp(Me ₃ P)Rh(η ² -C ₂ H ₄) + HSi(ⁱ -Pr) ₃	yellow	C ₆ D ₆	−14.6(dd) J _{RhH} = 29.8			³¹ P X-ray	106
3-179 CpRh(C ₂ H ₃ CO ₂ ^t Bu)HRh- SiEt ₃ ¹⁸⁹ 2 isomers	CpRh(C ₂ H ₃ CO ₂ ^t Bu) ₂ + HSiEt ₃		C ₇ D ₈	−13.80 (d) J _{RhH} = 32 −14.74 (d) J _{RhH} = 35	39.8 ¹ J _{RhSi} = 22 ² J _{SiH} = 20 41.7 ¹ J _{RhSi} = 20 ² J _{SiH} = 18		¹³ C ¹⁰³ Rh VTNMR	102
3-180 [Cp*(Me ₃ P)(MeCN)Rh- SiPh ₃] ⁺ [BAr' ₄] ^{−190} Ar' = 3,5-C ₆ H ₃ (CF ₃) ₂	Cp*(Me ₃ P)(MeCN)RhMe + HSiPh ₃	93 orange	CD ₂ Cl ₂ (−20)				¹³ C ³¹ P	238
3-181a [Cp*(Me ₃ P)Rh(SiEt ₃)- (η ² -HSiEt ₃)] ⁺ [BAr' ₄] [−] (−60 °C) ¹⁹¹	[Cp*(Me ₃ P)(Me)Rh- (ClCH ₂ Cl)][BAr' ₄] Ar' = 3,5-C ₆ H ₃ (CF ₃) ₂ + HSiEt ₃	(a) >90	CD ₂ Cl ₂ (−60)	(a) −12.39 (dd) ¹ J _{RhH} = 36 ¹ J _{SiH(obs)} = 28 ¹ J _{SiH(η)} = 56			³¹ P	239
3-181b [Cp*(Me ₃ P)(H) ₂ Rh- (SiEt ₃)] ⁺ [BAr' ₄] (−40 °C)		(b) ~15		(b) −11.38 (dd) ¹ J _{RhH} = 27				
3-182a [Cp*(Me ₃ P)(ClCD ₂ Cl)Rh- (SiPh ₃)] ⁺ [BAr' ₄] (−80 °C) ^{192,193}	[Cp*(Me ₃ P)(Me)Rh- (ClCH ₂ Cl)][BAr' ₄]/CD ₂ Cl ₂ Ar' = 3,5-C ₆ H ₃ (CF ₃) ₂ + HSiPh ₃	(a) ¹⁹⁵	CD ₂ Cl ₂				(a) ³¹ P	239
3-182b [Cp(Me ₃ P)Rh[C ₆ H ₄ - (η ² -HSiPh ₂)] ⁺ [BAr' ₄] [−] (> −40 °C) ¹⁹⁴		(b) 90%		(b) −8.95 (dd, J _{RhH} = 28; ¹ J _{SiH} = 84)			(b) ¹³ C ³¹ P	
3-183 (Me ₃ P) ₄ RhSi(OEt) ₃ ¹⁹⁶	(Me ₃ P) ₄ RhMe + HSi(OEt) ₃	92 ¹⁹⁷	C ₆ D ₆ (¹ H, C ₇ D ₈ ³¹ P, −93)				¹ H ³¹ P	240 241
3-184 <i>cis-fac</i> -(Et ₃ P) ₃ (H) ₂ Rh- SiPh ₃ ¹⁹⁸	(Et ₃ P) ₄ RhH + HSiPh ₃	— colorless	C ₇ D ₈	−10.74 (m)			³¹ P IR EA X-ray	241
3-185 <i>mer</i> -(Me ₃ P) ₃ ClHRh- SiMe ₂ Ph	(Me ₃ P) ₃ RhCl + HSiMe ₂ Ph	100						242
3-186 <i>mer</i> -(Me ₃ P) ₃ ClHRhSiPh ₃	(Me ₃ P) ₃ RhCl + HSiPh ₃	21 colorless	C ₆ D ₆	−9.49 (ddt) ¹⁹⁹			VTNMR IR EA X-ray	243
3-187 <i>mer</i> -(Me ₃ P) ₃ ClHRh- SiPh ₂ Cl	[Rh(PMe ₃) ₄]Cl + HSiPh ₂ Cl	70 pale yellow	C ₆ D ₆	−8.78 (ddt)	41.7 (ddt)		¹³ C ³¹ P	108
3-188 <i>fac</i> -(Me ₃ P) ₃ (H) ₂ Rh- SiMe ₂ Ph ²⁰⁰	(Me ₃ P) ₄ RhH + HSiMe ₂ Ph	97 yellow—white	C ₆ D ₆	−10.12 (d of pseudo t)			³¹ P	240
3-189a <i>mer</i> -(Me ₃ P) ₃ ClHRh- SiAr ₃ ²⁰¹	(Me ₃ P) ₃ RhCl + HSi(<i>p</i> -CF ₃ C ₆ H ₄) ₃	12 colorless	C ₆ D ₆	−17.29 (ddt) ¹ J _{RhH} = 21			³¹ P EA X-ray	243
3-189b <i>fac</i> -(Me ₃ P) ₃ (H) ₂ Rh- SiAr ₃ ²⁰¹ Ar = C ₆ H ₄ -4-CF ₃		78 colorless	C ₆ D ₆	−10.47 (m)			³¹ P EA X-ray	
3-190 <i>fac</i> -(Me ₃ P) ₃ (H) ₂ Rh- SiAr ₂ Cl Ar = Ph ²⁰²	(Me ₃ P) ₃ RhCl + <i>cis</i> -(Me ₃ P) ₂ Pt(SiAr ₂ H) ₂	5					¹ H ³¹ P	244
3-191 <i>fac</i> -(Me ₃ P) ₃ HRh- [Si(OEt) ₃] ₂ ²⁰³	(Me ₃ P) ₄ RhMe + 2HSi(OEt) ₃ ²⁰⁴	²⁰⁵ brown oil	C ₆ D ₆	−10.76 (d of pseudo q)			³¹ P	240
3-192 <i>mer</i> -(Me ₃ P) ₃ (ArS)HRh- SiPh ₃ ²⁰⁵ Ar = C ₆ H ₅	(Me ₃ P) ₃ Rh(SPh) + HSiPh ₃	80 yellow	C ₆ D ₆	−8.79 (ddt)			³¹ P [EA] X-ray	109

Table 3m. Continued

compound	starting metal complex	% yield color m.p., °C	NMR				
			solvent (temp., °C) ^f	¹ H—H ²	²⁹ Si ^{2,3}	other ^d	ref ⁵
3-193 <i>mer</i> -(Me ₃ P) ₃ (ArS)HRh-SiCl ₃ ²⁰⁶ Ar = Ph	(Me ₃ P) ₃ Rh(SPh) + HSiCl ₃	71 yellow	C ₆ D ₆	−9.24 (ddt)		³¹ P IR EA	109
3-194 <i>mer</i> -(Me ₃ P) ₃ (ArS)(H)Rh-Si(OMe) ₃ Ar = Ph ²⁰⁷	(Me ₃ P) ₃ Rh(SPh) + HSi(OMe) ₃	26 yellow	C ₆ D ₆	−9.33 (ddt)		³¹ P IR EA	109
3-195 (PP ₂)RhSi(SET) ₃ ²⁰⁸	(PP ₂)RhMe + HSi(SET) ₃	80 (25- isolated) deep red	C ₆ D ₆			X-ray ³¹ P [EA] X-ray ³¹ P	245
3-196 (PP ₂)(H) ₂ RhSi(SET) ₃	(PP ₂)RhH + HSi(SET) ₃	85 brown vis liq	C ₆ D ₆	−9.05 (dddt) ¹ J _{RhH} = 15.2 −9.25 (m) ¹ J _{RhH} = 13.7			245
3-197 (Me ₃ P) ₂ (Cl)HRh-[SiMe ₂ (CH ₂) ₂ PPh ₂]	(Me ₃ P) ₃ RhCl + HMe ₂ Si (CH ₂) ₂ PPh ₂	90 ivory	C ₆ D ₆	−9.32 (pseudo dq) ¹ J _{RhH} = 15	40.4 (dddd) ¹ J _{RhSi} = 26	¹³ C ³¹ P EA X-ray ¹³ C ³¹ P	242 246
3-198a [PSiP]RhPPh ₃ ²⁰⁹	(Ph ₃ P) ₃ RhCl + H[PSiP] PhCH ₂ K	49 orange	C ₆ D ₆		73.4	¹³ C ³¹ P EA X-ray ³¹ P	213a
3-198b (Ph ₃ P) ₂ ClHRhSiEt ₃ ²¹⁰	(Ph ₃ P) ₃ RhCl + HSiEt ₃		C ₆ D ₅ Cl (−18)	−14.6 (dt) J _{HRh} = 23	69.4 (d) J _{SiRh} = 38	³¹ P	247
3-199a (Me ₃ P) ₂ HRh(SiMe ₂ Ph)-[SiMe ₂ (CH ₂) ₂ PPh ₂] ²¹¹	(Me ₃ P) ₂ Rh[SiMe ₂ (CH ₂) ₂ PPh ₂] + 6 HSiMe ₂ Ph	²¹²	C ₇ D ₈ (−20)	−10.30 (pseudo dq) ¹ J _{RhH} = 16		³¹ P	246
3-199b (Ph ₃ P) ₂ (H) ₃ Rh(SiMe ₂ -C ₆ H ₄ SiMe ₂) ²¹³	(Ph ₃ P) ₄ RhH or (Ph ₃ P) ₃ RhCl + <i>o</i> -(HMe ₂ Si) ₂ C ₆ H ₄		C ₇ D ₈	rt −8.4 (brd)	−70 20.5 (dd) J _{SiRh} = 71.2	¹³ C ³¹ P	242 247b
*3-199c [(Ph ₃ P) ₂ (H)Rh(SiMe ₂ -C ₆ H ₄ SiMe ₂)	(Ph ₃ P) ₄ RhH + 2.5 <i>o</i> -(HMe ₂ Si) ₂ C ₆ H ₄	58 orange 133 °C (dec)	C ₆ D ₆	−6.90 (2H, br s) T ₁ = 2002 ms −7.31 (ddd) T ₁ = 926 ms RhH	40.4 (dd)	¹³ C ³¹ P IR EA X-ray	247b [Co-18(08)]
	or						
*3-199d [(Ph ₃ P)Rh(SiMe ₂ C ₆ H ₄ -SiMe ₂)(<i>η</i> ⁴ HSiMe ₂ C ₆ H ₄ -SiMe ₂) ²¹⁴	(Ph ₃ P) ₃ RhCl + 10 <i>o</i> -(HMe ₂ Si) ₂ C ₆ H ₄	68 orange	C ₆ D ₆	−0.26 (br s) J _{SiH} = 112 Rh—H—Si		¹³ C ³¹ P IR X-ray ¹³ C ³¹ P	248
3-200 <i>trans</i> -(Et ₃ P) ₂ (Cl)(H)Rh-[Si(Pr) ₂ OH] ²¹⁵	(Et ₃ P) ₃ RhCl or [(Et ₃ P) ₂ RhCl] ₂ + HSi(Pr) ₂ OH		C ₆ D ₆	−16.49 (dt) ¹ J _{RhH} = 27.2	58.1 (dt) ¹ J _{RhSi} = 31.4	³¹ P	249
3-201 (Pr ₃ P) ₂ (Cl)HRh-[Si(CH ₂ CH ₂ Ph) ₃] ²¹⁶	[(Pr ₃ P) ₂ RhCl + HSi(CH ₂ CH ₂ Ph) ₃	yellow	C ₆ D ₆	−16.63 ¹ J _{RhH} = 22		³¹ P	245
3-202 (Et ₃ P) ₂ (Cl)HRhSi(SET) ₃	(Et ₃ P) ₃ RhCl + HSi(SET) ₃	100 yellow—orange vis liq	C ₆ D ₆	−15.85 (dt) ¹ J _{RhH} = 23.7		³¹ P	250
3-203 (Ph ₃ P) ₂ (Cl)HRhSiR ₃ ²¹⁷ R ₃ Si = PhMe ₂ Si	(Ph ₃ P) ₃ RhCl + HSiR ₃			−15.27 (dt) ¹ J _{RhH} = 22		³¹ P	251
3-204 (Ph ₃ P) ₂ (Cl)HRhSiMe ₂ Ph ²¹⁸	(Ph ₃ P) ₃ RhCl + HSiMe ₂ Ph		CDCl ₃	−15.27 (dt)		¹³ C	252
3-205 (Ph ₃ P) ₂ (Cl)HRhSi(OEt) ₃ ²¹⁹	(Ph ₃ P) ₃ RhCl + HSi(OEt) ₃	79 pale yellow	C ₆ D ₆ (¹ H, ¹³ C, ³¹ P) CD ₂ Cl ₂ (²⁹ Si, −50 °C)	−13.98 (dt) ¹ J _{RhH} = 24	−34.0 ¹ J _{RhH} = 49	¹³ C ³¹ P X-ray	252
3-206 (Ph ₃ P) ₂ (I)HRhSi(OEt) ₃	(Ph ₃ P) ₃ RhI + HSi(OEt) ₃	86 pale yellow	C ₆ D ₆ (¹ H, ¹³ C, ³¹ P) CD ₂ Cl ₂ (²⁹ Si, −50 °C)	−10.89 (dt) ¹ J _{RhH} = 26	−39.78 ¹ J _{RhH} = 49	¹³ C ³¹ P IR EA X-ray ¹³ C ³¹ P	252
3-207 (Ph ₃ P) ₂ (I)HRh-(SiMe ₂ OSiMe ₃)	(Ph ₃ P) ₃ RhI + HMe ₂ SiOSiMe ₃	88 pale yellow	C ₆ D ₆ (¹ H, ¹³ C, ³¹ P) CD ₂ Cl ₂ (²⁹ Si, −50 °C)	−11.27 (dt) ¹ J _{RhH} = 25	44.4 ¹ J _{RhH} = 29	¹³ C ³¹ P IR EA X-ray ³¹ P	253
3-208 [(Ar ₁) ₃ P] ₂ (Cl)HRhSiCl ₃ ²²⁰ Ar ₁ = <i>p</i> -(F ₁₃ C ₆ CH ₂ CH ₂ -SiMe ₂)C ₆ H ₄ —	[(Ar ₁) ₃ P] ₃ RhCl + HSiCl ₃		C ₆ D ₆	−14.2 (dt) ¹ J _{RhH} = 19		¹³ C ³¹ P	254
3-209 (Ph ₃ P)(Cl)HRh[NSiN]	(Ph ₃ P) ₃ RhCl + HSi(C ₉ H ₆ N) ₂ Me	yellow 62%	CD ₂ Cl ₂	−15.9 (d, J _{RhH} = 24, of d)	40.3	¹³ C ³¹ P EA	254

Table 3n. Continued

compound	starting metal complex	% yield color m.p., °C	NMR				
			solvent (temp., °C) ^f	¹ H M-H ²	²⁹ Si ^{2,3}	other ^d	ref ⁵
3-210 (COD)Rh[NSiN]	(COD)Rh(η^3 -CH ₂ Ph) + HSi(C ₆ H ₆ N) ₂ Me	dark brown 92	C ₆ D ₆		35.2 (d) ¹ J _{RhSi} = 33	¹³ C EA	254
3-211 [NSiN]Rh(SiPh ₃)(H) ²²¹	[NSiN]Rh(COD) + HSiPh ₃		C ₆ D ₆	−13.2 (d) ¹ J _{RhH} = 28	36.6 (d) ¹ J _{SiRh} = 55 (SiMe) 18.1 (d) ¹ J _{SiRh} = 55 (SiPh ₃) 36.7 (d) ¹ J _{SiRh} = 69 (SiMe) −0.32 (d) ¹ J _{SiRh} = 86 (Si(OMe) ₃)	¹³ C EA	254
3-212a [NSiN]Rh(C ₈ H ₁₃)- Si(OSiMe ₃) ₃ ^{222, 223}	[NSiN]Rh(COD) + HSi(OSiMe ₃) ₃ + COD	>95 (NMR) 42 (isolated) dark yellow	C ₆ D ₆		42/5 ² J _{SiH} = 3	¹³ C EA	254a
3-212b [CyPSiP]RhHCl	1/2[Rh(COE) ₂ Cl] ₂ + [CyPSiP]H	85 brt yellow	C ₆ D ₆	−18.80 (dt)		¹³ C ³¹ P EA X-ray	254b
3-212c (PNP)(H)Rh(SiClMe ₂)	(PNP)Rh[S(ⁱ Pr) ₂ + HSiMe ₂ Cl]	62 orange	C ₆ D ₆	−15.6 (dt) ² J _{SiH} = 31	49.3 ² J _{SiH} = 31 ¹ J _{RhSi} = 23	¹³ C ³¹ P X-ray	254c
3-213 (PyInd)(H) ₂ Rh(SiEt ₃) ₂ ²²⁴	(PyInd)Rh(η^2 -C ₂ H ₄) ₂ + HSiEt ₃	71 oily, red solid	C ₆ D ₆	−15.32 (dd) ¹ J _{RhH} = 28.5 ² J = 9.0	63.0 ¹ J _{RhSi} = 26.8 gHMBC: 63.0 (¹ J _{SiH} = 8.1, 6.2)	¹³ C IR EA	255
*3-214 [(ⁱ Pr ₃ P)(H) ₂ Rh](μ -SiR ₂) ₂ ²²⁵ R = CH ₂ CH ₂ Ph	[(ⁱ Pr ₃ P)] ₂ RhCl + HSi(CH ₂ CH ₂ Ph) ₃	22 yellow	C ₆ D ₆	−7.09 (dd)		³¹ P EA X-ray	249
3-215a [CH ₂ (η^5 -C ₅ H ₄) ₂]- [Rh(C ₂ H ₄) ₂][HRh(C ₂ H ₄)- (SiEt ₃)] ²²⁶	[CH ₂ (η^5 -C ₅ H ₄) ₂][Rh(C ₂ H ₄) ₂] + xsHSiEt ₃ h ν	3-166a , major product ²²⁷	C ₆ D ₆	−14.62 (d) ¹ J _{SiH} = 14	41.35 (d) ¹ J _{RhSi} = 23	¹³ C ¹⁰³ Rh	115
3-215b [CH ₂ (η^5 -C ₅ H ₄) ₂]- [HRh(C ₂ H ₄)(SiEt ₃) ₂]			C ₆ D ₆	−14.65 (d) ¹ J _{SiH} = 14	41.43 (d) ¹ J _{RhSi} = 23	¹³ C ¹⁰³ Rh	
*3-216 [L(H)RhSiAr ₃] ₂ (μ -H)- (μ -Cl) ²²⁷ L = P(ⁱ Pr) ₃ ; Ar = −C ₆ H ₄ F- <i>p</i>	[L(H)RhSiPh ₃] ₂ (μ -H)(μ -Cl) ²²⁸ + 10HSiAr ₃	78 yellow	C ₆ D ₆	−12.55 (tt) (μ -H) −16.07 ²²⁹ (Rh-H)		³¹ P EA X-ray	256 257
*3-217 [L(H)RhSiAr ₃] ₂ (μ -Cl) ₂ ²³⁰ L = P(ⁱ Pr) ₃ ; Ar = CH ₂ Ph	[L ₂ Rh(Cl)] + 1.5HSi(CH ₂ Ph) ₃	40 yellow	C ₆ D ₆	−19.17 (dd)		³¹ P EA X-ray	249
*3-218 [(Me ₃ P)(Ar ₂ HSi)Pt]- (μ -H)(μ - η^2 -H-SiAr ₂)- [Rh(PMe ₃) ₃] Ar = C ₆ H ₄ F- <i>p</i>	(Me ₃ P) ₃ RhMe + <i>cis</i> -(Me ₃ P) ₂ Pt(SiHAr ₂) ₂	48	C ₄ D ₈ O (−90)	−12.9 (d) (Si-H-Rh) ¹ J _{RhH} = 148 −7.69 (d) (Pt-H-Rh) ¹ J _{RhH} = 70 ¹ J _{PtH} = 356 4.47 (d) (Si-H)		³¹ P EA X-ray	258 244
3-219 [(Me ₃ P)(ClAr ₂ Si)Pt]- (μ -H)(μ - η^2 -H-SiAr ₂)- [Rh(PMe ₃) ₃] ²³¹ Ar = C ₆ H ₄ F- <i>p</i>	(Me ₃ P) ₃ RhCl + <i>cis</i> -(Me ₃ P) ₂ Pt(SiHAr ₂) ₂	58	CD ₂ Cl ₂ (−90)	−7.47 (d, μ -H) ¹ J _{RhH} = 63 ¹ J _{PtH} = 358 −13.1 (d, Si-H-Rh) ¹ J _{RhH} = 143		³¹ P VTNMR [EA] X-ray ²³²	258 244
3-220 (tmp)RhSiPh ₂ Me ^{233, 234}	(tmp)RhCl + HSiPh ₂ Me	26 orange	CDCl ₃			¹³ C HRMS EA X-ray	62
3-221 [(NSiN)RhCl] ₂ ²³⁵	RhCl ₃ (NCCH ₃) ₃ + NEt ₃ + HSi(C ₆ H ₆ N) ₂ Me	62 yellow	DMSO		51.6 (d) ¹ J _{SiRh} = 22	¹³ C EA X-ray	254a
3-222 Cp*(L)PhIrSiPh ₂ F ²³⁶ L = PMe ₃	Cp*(Me ₃ P)Ir(CH ₃) ₂ + [Cp ₂ Fe][PF ₆] + HSiPh ₃	83 white	CD ₂ Cl ₂ (¹ H) C ₆ D ₆ (¹³ C, ¹⁹ F)			¹ H ¹³ C ¹⁹ F ³¹ P [EA] X-ray	259
3-223 Cp*(Me ₃ P)HIr- [Si(OEt) ₂ OTf] ²³⁷	Cp*(Me ₃ P)(OTf)IrMe + 2HSi(OEt) ₃	85% ²³⁸ yellow oil	? CD ₂ Cl ₂	−18.13 (d)	−29.2 (d)	¹³ C ¹⁹ F ³¹ P IR HRMS	117a

Table 3o. Continued

compound	starting metal complex	% yield color m.p., °C	NMR				other ^d	ref ⁵
			solvent (temp., °C) ^f	¹ H M-H ²	²⁹ Si ^{2,3}			
3-224 {Cp*(Me ₃ P)(H)Ir- [SiPh ₂ C ₆ H ₄]} ⁺ [BAR ₄] ⁻ Ar = C ₆ F ₅	Cp*(Me ₃ P)(Ph)Ir(SiPh ₂ OTf) + NaBAR ₄	81 pale yellow		-12.7 (d)	-62.5 (br s)	¹³ C ¹⁹ F ³¹ P IR EA X-ray	116 117a	
3-225 Cp*(Me ₃ P)Ir(SiPh ₂ Cl)Cl	Cp*(Me ₃ P)(OTf)IrMe + HSiClPh ₂ + PPnCl	49 yellow-orange	? CD ₂ Cl ₂		6.7	¹³ C ³¹ P IR EA X-ray	117a	
3-226 Cp*(Me ₃ P)Ir(SiMe ₂ OTf)- [SiMe(SiMe ₃) ₂]	Cp*(Me ₃ P)(OTf)IrMe + HSi(SiMe ₃) ₃	82 ²³⁹ peach foam 138-140 (dec)	? CD ₂ Cl ₂		62.2 (d) (SiMe ₂ OTf) -15.5 (s) (SiMe ₃) -79.0 (d) [Si(SiMe ₃) ₂ Me] -12.4 (d)	¹ H ¹³ C ¹⁹ F ³¹ P IR EA X-ray	117a	
3-227 {Cp*(Me ₃ P)Ir[κ ² Si(S ^t Bu) ₂ - S ^t Bu]} ⁺ [OTf] ^{-240,241}	Cp*(Me ₃ P)(OTf)IrMe + HSi(S ^t Bu) ₃	88 brt yellow 116-120 (dec)	? CD ₂ Cl ₂			¹ H ¹³ C ¹⁹ F ³¹ P IR EA X-ray	117a	
3-228 Cp*(H) ₂ Ir[η ¹ :η ¹ -(SiMe ₂)- BC ₂ B ₉ H ₁₀ -Si ^t Bu] ²⁴²	(Cp*IrCl ₂) ₂ + NEt ₃ - (HSiMe ₂)(C ₂ B ₁₀ H ₁₁)	60 colorless 163-165	CDCl ₃	-14.88 (br) -14.99 (br)	-31.9	¹¹ B ¹³ C IR EA X-ray calc	172	
3-229 Cp*(H) ₂ Ir[η ¹ :η ¹ -(SiMe ₂)- C ₂ B ₁₀ H ₁₀ -Si ^t Si] ²⁴³	1/2(Cp*IrCl) ₂ + NEt ₃ - (HSiMe ₂) ₂ (C ₂ B ₁₀ H ₁₀)	62 colorless 181-183	CDCl ₃	-16.15 (s)	14.0	¹¹ B ¹³ C IR EA calc	172	
3-230 <i>trans</i> -Cp*(Cl)(H)Ir- [SiMe ₂ C ₆ H ₄ SiMe ₂] ²⁴⁴	1/2(Cp*IrCl) ₂ + NEt ₃ - 1,2-(HSiMe ₂) ₂ C ₆ H ₄	43 172-173 (d)	CDCl ₃	-16.06 (s)	5.25	¹³ C IR EA X-ray ²⁴⁵	172	
3-231 <i>trans</i> -Cp*(H) ₂ Ir- [SiMe ₂ C ₆ H ₄ SiMe ₂] ²⁴⁶	1/2(Cp*IrCl) ₂ + NEt ₃ - 1,2-(HSiMe ₂) ₂ C ₆ H ₄	29 yellow 165-167 (d)	CDCl ₃	-16.30 (s)	1.05	¹³ C IR EA X-ray calc	172	
3-232 Cp'(H) ₃ Ir(SiEt ₃) Cp' = C ₃ H ₄ CH ₂ CH ₂ OMe ^{247, 248}	[Cp'IrCl(μ-Cl)] ₂ + xs HSiEt ₃ (5 h)	90 orange-red oil	C ₇ D ₈ (20 °) C ₇ D ₈ (-80)	-16.29 (s) -16.25 (d, <i>J</i> = 6.6) -15.72 (t, <i>J</i> = 6.6)		¹³ C VT (¹ H) IR EA MS-FAB	260	
3-233 Cp'(H) ₂ Ir(SiEt ₃) ₂ Cp' = C ₃ H ₄ CH ₂ CH ₂ OMe ²⁴⁹	[Cp'IrCl(μ-Cl)] ₂ + xs HSiEt ₃	78 red oil	C ₇ D ₈	-17.20 (s)		¹³ C IR MS-FAB EA ³¹ P	260	
3-234 (OC)(Ph ₃ P) ₂ (H) ₂ Ir- [Si(ⁱ Pr) ₂ OH] ²⁴⁹	(OC)(Ph ₃ P) ₃ IrH + HSi(ⁱ Pr) ₂ OH		C ₆ D ₆	-9.33 (ddd) -10.88 (ddd)		³¹ P	248	
3-235 (OC)Cl(H)Ir(biPSi) ²⁵⁰	<i>trans</i> -[OC(Ph ₃ P) ₂ IrCl] + biPSiH	66 white	CDCl ₃ (¹³ C, ³¹ P)	-18.2 (t)		¹³ C ³¹ P IR EA X-ray	194	
3-236a (OC)(Ph ₃ P)ClIr- {κ ² -(Si ⁱ P)-Me ₂ SiCH ₂ PPh ₂ }	OC(Ph ₃ P) ₂ IrCl + HMe ₂ SiCH ₂ PPh ₂						261a	
3-236b (OC)(Ph ₃ P) ₂ Ir- {κ ² -(Si ⁱ P)-Me ₂ SiCH ₂ PPh ₂ }								
3-237a (Me ₃ P) ₃ (H)IrSiMe ₂ - (CH=CH ₂)	(Me ₃ P) ₃ (η ² -C ₈ H ₁₄)IrMe + HMe ₂ SiCH=CH ₂	90 orange	C ₃ D ₆ O	-12.53 (ddd)		¹³ C ³¹ P EA	261b	
3-237b (Me ₃ P) ₃ (H)IrSiMe ₂ - (CH=CMe ₂)	(Me ₃ P) ₃ (η ² -C ₈ H ₁₄)IrMe + HMe ₂ SiCH=CMe ₂	91 lt. orange	C ₃ D ₈ O	-12.47 (ddd)		¹³ C ³¹ P EA X-ray	261b	
3-237c (Me ₃ P) ₃ (H)IrSiMe ₂ - (CH=CH-CH=CH ₂) (E-isomer) ²⁵²	(Me ₃ P) ₃ (η ² -C ₈ H ₁₄)IrMe + HMe ₂ SiCH=CH-CH=CH ₂ (E-isomer)	79 orange	C ₆ D ₆	-12.18 (ddd)		¹³ C ³¹ P EA	261b,c	

Table 3p. Continued

compound	starting metal complex	% yield m.p., °C	color	NMR				other ^d	ref ⁵
				solvent (temp., °C) ^f	¹ H M-H ²	²⁹ Si ^{2,3}			
3-237d (Me ₃ P) ₃ (H)(Cl)IrSiMe ₂ - (CH=CMc-CMe=CH ₂) (<i>mer</i> -E) ²⁵³	(Me ₃ P) ₃ (η ² -C ₈ H ₁₄)IrCl + HMe ₂ SiCH=CMc-CMe=CH ₂ (E isomer)	79	yellow	C ₆ D ₆	−10.37 (dt)			¹³ C ³¹ P EA HRES-MS	261c
3-237e (Me ₃ P) ₃ (H)(Me)IrSiMe ₂ - (CH=CMc-CMe=CH ₂) (<i>fac</i> -E) ²⁵⁴	(Me ₃ P) ₃ (η ² -C ₈ H ₁₄)IrMe + HMe ₂ SiCH=CMc-CMe=CH ₂ (E isomer)	83	yellow	C ₆ D ₆	−12.14 (ddd)			¹³ C ³¹ P EA X-ray	261c
3-237f (κ ¹ -NSiN)Ir(H)(Me)- (PMe ₃) ₃	(Me ₃ P) ₄ IrMe + Qn ₂ SiHMe	71	orange	C ₆ D ₆	−11.3 (d)	−9.4 (m)		¹³ C ³¹ P IR EA X-ray	57d
*3-237f (Me ₃ P) ₂ HIr[SiMe ₂ - (CH ₂) ₂ PPh ₂][SiMe ₂ - (<i>p</i> -MeC ₆ H ₄)]	(Me ₃ P) ₂ (H)MeIr[SiMe ₂ - (CH ₂) ₂ PPh ₂] + 2HSiMe ₂ (<i>p</i> -MeC ₆ H ₄)	82	colorless	C ₆ D ₆	−12.41 (dt)			¹³ C ³¹ P IR MS EA X-ray	262
3-238a [PhB(CH ₂ PPh ₂) ₃](H) ₃ - IrSiR ₃ ²⁵⁵ R = Me	[PhB(CH ₂ PPh ₂) ₃]Hir- (η ³ -C ₈ H ₁₃) + HSiR ₃	66	tan 191–197 (dec) 213–220 (melt)	C ₆ D ₆	−10.6 (dm)	−21.4		¹³ C ³¹ P EA X-ray	60b
3-239 <i>fac</i> -(PP ₂)Me(H)IrSi(SET) ₃	(PP ₂)IrMe + HSi(SET) ₃		off-white	C ₆ D ₆	−12.38 (ddd)			¹³ C ³¹ P EA X-ray	245
3-240a (Et ₃ P) ₂ (Cl)(H)Ir- [Si(^t Pr) ₂ OH]	<i>trans</i> -(Et ₃ P) ₂ Ir(Cl)(η ² -C ₂ H ₄) + OH HSi(^t Pr) ₂	100	yellow	C ₆ D ₆	−20.82 (t)	19.6 (t)		¹³ C ³¹ P IR EA X-ray	248a
3-240b [(η ² -SNC ₅ H ₄)(PPh ₃) ₂ (H)Ir- SiMePh ₂]	[(PPh ₃) ₂ (η ² -SNC ₅ H ₄)Ir] + MePh ₂ SiH	63	yellow	C ₆ D ₆	−19.60 (dd)			³¹ P EA X-ray	248b
3-241 [(Me ₃ P)(cod)(CH ₃ CN)(H)- Ir[Si(OMe) ₃]] ⁺ [BF ₄] ^{−256}	[(Me ₃ P)(cod)Ir(NCCH ₃)] [BF ₄] + HSi(OMe) ₃	61	pale yellow	CD ₂ Cl ₂ (20)	−17.36 (d)			¹³ C ³¹ P IR EA X-ray	263
3-242a (Tp ^{Me2})(H) ₃ IrSiEt ₃ ²⁵⁷	(Tp ^{Me2})(H) ₂ Ir(SC ₄ H ₄) + HSiEt ₃ ²⁵⁸	> 90		C ₆ D ₆ (¹ H) CDCl ₃ (¹³ C, ²⁹ Si)	−18.30 (s)	−75.2 (m) <i>J</i> _{SiH} = 6		¹³ C VTNMR <i>T</i> ₁ IR EA X-ray	264
3-242b <i>mer</i> -(H)(C ₆ F ₅)(ArNC) ₃ - IrSiPh ₃ (S and Si <i>trans</i>)	[Ir ₂ (SC ₆ F ₅) ₂ (cod) ₂] + HSiPh ₃	53	colorless	C ₆ D ₆	−8.55 (s)			¹³ C ³¹ P IR EA X-ray	264b
3-243 Cl(H)Ir(biPSi)	[Ir(cod)Cl] ₂ + biPSiH	95	yellow	CDCl ₃ (¹³ C, ³¹ P)	−22.38 (t)			¹³ C ³¹ P IR EA X-ray	194
3-244 [PyInd](H) ₂ Ir(SiR ₃) ₂ R ₃ = Ph ₂ Me ²⁵⁹	K[PyInd] + 0.5[(coe) ₂ IrCl] ₂ + 2R ₃ SiH	82	red–orange	C ₆ D ₆	−16.59 (d) ² <i>J</i> = 2.5	7.2 <i>J</i> _{SiH} = 11.7 <i>J</i> _{SiH'} = 14.2 (gHMBC)		¹³ C IR EA X-ray	255
3-245a (coe)Cl(H)Ir(NSiN)	1/2[(coe) ₂ IrCl] ₂ + HSiMe(C ₉ H ₆ N) ₂	87 ²⁶⁰	yellow	CD ₂ Cl ₂	−15.6	−4.8		¹³ C IR EA X-ray	265
*3-245b [NSiN]Ir(SiPh ₃)(OTf)] ↔ [NSiN]PhIr(SiPh ₂ (OTf)] ²⁶¹	(NSiN)Ir(H)(OTf)(coe) + HSiPh ₃ (benzene solvent)	88	orange	C ₆ D ₆		54 (s) (SiPh ₂ OTf)		¹³ C ¹⁹ F EA X-ray	57d
3-245c [NSiN]Ir(SiPh ₃)(NCMe) ₂] ⁺ - [OTf] [−]	(NSiN)Ir(H)(OTf)(coe) + HSiPh ₃ (acetonitrile solvent)	56	yellow	CD ₃ CN		−8.4 (SiMe) −1.2 (s) (SiMe) −25.3 (s) (SiPh ₃)		¹³ C ¹⁹ F EA X-ray	57d
3-245d (ttp)Ir[Si(OEt) ₃] ²⁶²	(ttp)IrCl(CO) + HSi(OEt) ₃	54	purple	CDCl ₃				¹ H ¹³ C HRMS (FAB) EA X-ray	62b
3-245e [(POCOP)Ir(H)(η ¹ - HSiEt ₃)] ⁺ [B(C ₆ F ₅) ₄] [−]	[(POCOP)Ir(H)(acetone)] ⁺ [B(C ₆ F ₅) ₄] [−] + HSiEt ₃			−44.2	−44.2 (t) IrH −4.9 ¹ <i>J</i> _{SiH} = 79			VTNMR DFT X-ray	266a

Table 3q. Continued

compound	starting metal complex	% yield color m.p., °C	NMR				ref ⁵
			solvent (temp., °C) ^f	¹ H—H ²	²⁹ Si ^{2,3}	other ^d	
3-246a [CyPSiP]IrHCl	1/2[Ir(COE) ₂ Cl] ₂ + [CyPSiP]H	75 brt yellow	C ₆ D ₆	Ir····H····Si −23.79 (t)	7.7 ² J _{SiH} = 3	¹³ C ³¹ P EA X-ray	254b
3-246b [(1,5-COD)(O ₂ CQuin)- (H)IrSiPh ₃] ²⁶³	[(1,5-COD)Ir(O ₂ CQuin)] + HSiPh ₃	77 yellow–orange	CDCl ₃	−15.33 (s)	−8.98	IR EA ¹³ C	266b
3-247 [C \cap N]Cl(H)(CH ₃ CN)Ir- SiMe ₂ Ph ²⁶⁴	[C \cap N](Cl)Ir(COD) + HSiMe ₂ Ph	45 lt yellow	CD ₃ CN	−19.78		MS EA X-ray	267
Ni triad							
*3-248 (Et ₃ P) ₂ Ni- [SiMe ₂ (C ₂ B ₁₀ H ₁₀)SiMe ₂]	(Et ₃ P) ₄ Ni + HMe ₂ Si(C ₂ B ₁₀ H ₁₀)SiMe ₂ H	86 dark red	C ₆ D ₆		43.2 (t)	¹³ C ³¹ P MS EA X-ray	268 269
3-249 [(Ph ₃ P) ₂ Ni{Si(OEt) ₃ }] ₂ ²⁶⁵	Ni(PPh ₃) ₂ { η^2 -CH ₂ =CHPh} + HSi(OEt) ₃	black–red	C ₆ D ₆			¹³ C	270
*3-250 (dmpe)Ni- [SiH(SiMe ₂ C ₆ H ₄)] ₂ ²⁻	[Ni(dmpe) ₂] + 1-SiMe ₂ H- 2-SiH ₃ (C ₆ H ₄) (2 equiv)	21 yellow 178–183 (dec)				IR EA X-ray	64
3-251 (dtbpe)Ni(H)SiClPh ₂ ²⁶⁶	[(dtbpe)Ni] ₂ (C ₆ H ₆) + 2HSiClPh ₂	84 brt yellow	THF- <i>d</i> ₈ (298 K)	−8.29 (t, br) ¹ J _{SiH} = 5.0	59.22 (t)	¹³ C ³¹ P IR	271
3-252 [{(η -CH ₂ =CHSiMe ₂) ₂ O}- Ni{Si(OC ₂ H ₅) ₃ }] ₂	[Ni{(η -CH ₂ =CHSiMe ₂) ₂ O}- (η -CH ₂ =CHPh)] + HSi(OEt) ₃	red oil	C ₇ D ₈ (200 K) C ₆ D ₆			¹ H ¹³ C	272
3-253 (Cp*Al) ₃ (H)NiSiEt ₃	Ni(AlCp*) ₃ + HSiEt ₃	80 yellow 98 (dec)	C ₆ D ₆	−12.80 (s)		¹³ C ²⁷ Al EA MS X-ray	273
3-254 (dippe)(H)PdSiPh ₃ ²⁶⁷	[(μ -dippe)Pd] ₂ + HSiPh ₃	84 beige	C ₆ D ₆	−1.75		IR [EA] ¹³ C ³¹ P	274
3-255 (dcpe)(H)PdSiPh ₃ ²⁶⁸	[(μ -dcpe)Pd] ₂ + HSiPh ₃	64 beige	C ₆ D ₆	−1.81 (t)	5.25 (t) ¹ J _{SiH} = 27	VTNMR IR [EA] X-ray ¹³ C ³¹ P	274
3-256a (3-133c *) (Cab ^{Si,P}) ₂ Pd ²⁶⁹ <i>trans/cis</i> = 2/1	Pd ₂ (dba) ₃ + 2HMe ₂ Si(B ₁₀ C ₂ H ₁₂)PR ₂ R = Me	34 225–228 (dec)	CDCl ₃			EA IR EA X-ray ¹³ C ³¹ P	275 276a
3-256b <i>cis</i> -(κ -NSiN) ₂ Pd	(tmeda)PdMe ₂ + HSi(C ₆ H ₆ N) ₂ Me	44	C ₆ D ₆		13.2	¹ H ¹³ C EA X-ray ¹³ C ³¹ P	276b
3-257a (Cab ^{Si,P}) ₂ Pd ²⁷⁰	Pd ₂ (dba) ₃ + 2HMe ₂ Si(B ₁₀ C ₂ H ₁₂)PR ₂ R = Ph	65 yellow 225–227 (d)	CDCl ₃			EA X-ray ¹³ C ³¹ P	276a
3-257b [PSiP]PdCl	[PdCl(C ₃ H ₅)] ₂ + H[PSiP]	96 pale yellow	CDCl ₃		60	EA X-ray ¹³ C ³¹ P	213a
3-258 (PN)Pd(SiCl ₃) ₂ ²⁷¹ R = Ph ²⁷²	(PN)PdCl ₂ + xs HSiCl ₃	84	CDCl ₃		19.3 (Si <i>trans</i> to P) 14.3 (Si <i>trans</i> to N)	EA ¹³ C ³¹ P [EA] X-ray calc	277
3-259 [(NN)(Me)Pd(η^2 -H- SiEt ₃)] ₂ [BARF] ^{273, 274}	[(NN)(MeO)Pd(Me)] ₂ [BARF] + HSiEt ₃		CD ₂ Cl ₂	−9.87			278
*3-260a (Et ₃ P)Pt(μ - η^2 -HSiPh ₂) ₂ - Pd(PEt ₃) ²⁷⁵	(Et ₃ P) ₃ Pd + (HSiPh ₂) ₂ Pt(PEt ₃) ₂	(a) 34 yellow	(a) C ₆ D ₆	2.71 (d) (Pd–H–Si) ² J _{HPt} = 99 2.06 (d) (Pt–H–Si) ¹ J _{HPt} = 650		(a) ¹³ C ³¹ P EA X-ray	279

Table 3r. Continued

compound	starting metal complex	% yield color m.p., °C	NMR				ref ⁵
			solvent (temp., °C) ^f	¹ H M-H ²	²⁹ Si ^{2,3}	other ^d	
*3-260b (Et ₃ P) ₂ Pt(μ - η^2 -HSiPh ₂) ₂ ⁻ - Pd(PEt ₃)		(b) 25 orange	(b) CD ₂ Cl ₂	2.03 (Pd-H-Si) ² J _{HPt} = 65 ¹ J _{SiH} = 28 1.28 ²⁷⁶		(b) ¹³ C ³¹ P EA X-ray	
*3-260c [{Pd(dmpe)} ₂ (μ -SiPh ₂) ₂] ²⁷⁷	(dmpe)Pd(SiPh ₂ H) ₂ + Δ	24 yellow	CD ₂ Cl ₂ (-90) C ₆ D ₆	-8.61 (t) (PtH) ¹ J _{PH} = 550	-51.0	[EA] X-ray	120b
3-261 (Et ₃ P) ₂ HPtSiAr ₃ Ar = Ph ²⁷⁸	(Et ₃ P) ₄ Pt + (<i>i</i> -Pr ₃ P) ₂ Cl(H)RhSiAr ₃	60 white	CPMAS ²⁹ Si C ₆ D ₆	-2.43 (dd) ¹ J _{PH} = 873		³¹ P EA X-ray	280
3-262 <i>trans</i> -(Et ₃ P) ₂ XPtSiMe ₂ Ph X = Br ²⁷⁹	<i>trans</i> -(Et ₃ P) ₂ (X)PtSiMe ₃ + HSiMe ₂ Ph	69 white 80-82	C ₆ D ₆		-12.6	¹³ C ³¹ P IR EA	130
3-263 <i>cis</i> -(PhMe ₂ P) ₂ Pt(SiMe ₂ Ph) (SiPh ₃) ²⁸⁰	<i>cis</i> -(PhMe ₂ P) ₂ Pt(SiPh ₃) ₂ + HSiMe ₂ Ph	97	CD ₂ Cl ₂			¹³ C ³¹ P	281
3-264 <i>cis</i> -(PhMe ₂ P) ₂ Pt- (SiMePh ₂) ₂			CD ₂ Cl ₂			³¹ P VTNMR	282a,b
3-265 <i>cis</i> -(PhMe ₂ P) ₂ Pt(SiPh ₂ F) ₂	<i>cis</i> -(PhMe ₂ P) ₂ (Me)PtSiPh ₃ + 10HSiPh ₂ F	72 white	CD ₂ Cl ₂			X-ray ¹ H ¹³ C ³¹ P	281
3-266 <i>cis</i> -(R ₃ P) ₂ Pt- [Si(OMe) ₃] ₂ ^{282,283} R ₃ P = PhMe ₂ P	(R ₃ P) ₂ Pt(SiMe ₂ Ph) ₂ + xs HSi(OMe) ₃		C ₆ D ₆			EA ³¹ P	128 283
*3-267 (Me ₃ P) ₂ Pt{SiPh ₂ C(=CH- C ₆ H ₄ F-4)CH ₂] (cycle)	(HPh ₂ Si) ₂ Pt(PMe ₃) ₂ + CH ₂ =C=CH(C ₆ H ₄ F-4)	34 colorless	C ₆ D ₆			¹³ C ³¹ P EA	126
*3-268 (Me ₃ P) ₂ Pt[SiPh ₂ C(=CH- C ₆ H ₄ F-4)CH ₂ SiPh ₂] (cycle)	(HPh ₂ Si) ₂ Pt(PMe ₃) ₂ + CH ₂ =C=CH(C ₆ H ₄ F-4) + Δ	48 colorless	C ₆ D ₆		11.5 (dd)	X-ray ¹³ C ³¹ P EA	126
3-269a <i>cis</i> -[(Ph ₃ P) ₂ HPt- {SiMe(CH ₂ SPh) ₂ }] ²⁸⁴	(Ph ₃ P) ₂ Pt(η^2 -C ₂ H ₄) + HSiMe(CH ₂ SPh) ₂	90 yellow	CDCl ₃ (-30)	-2.66 (dd) ¹ J _{PH} = 972		X-ray ¹³ C, ³¹ P ¹⁹⁵ Pt IR EA	284a,b
3-269b <i>cis</i> -(Ph ₃ P) ₂ Pt(SiPh ₂ SiPh ₂ H)(H) (-60 °C)	(Ph ₃ P) ₂ Pt(C ₂ H ₄) + HSiPh ₂ SiPh ₂ H		C ₇ D ₈ (-60)	(3-269b) -1.83 (dd) ¹ J _{PH} = 923 (PtH) [5.71 (s) (SiH)]		X-ray ³¹ P	284c
3-269c <i>cis</i> -(Ph ₃ P) ₂ Pt(SiPh ₂ H) ₂ ²⁸⁵ (-30 °C)		45 yellow	(-30)	(3-269c) [5.80 (t) (SiH)]		³¹ P EA X-ray	
3-269d (Ph ₃ P) ₂ Pt(SiPh ₂ H)(H) (-10 to -5 °C)		37 colorless	CD ₂ Cl ₂ (-50)	-1.89 (ddd) ¹ J _{PH} = 996 (PtH) 4.00 (ddd) (SiH)		(3-269d) ³¹ P IR EA X-ray	
3-270 ClPt{SiPh[(CH ₂) ₂ PCy ₂]- [(CH ₂) ₂ PPh ₂]}	(cod)PtCl ₂ + NEt ₃ + HSiPh(CH ₂ CH ₂ PPh ₂)- (CH ₂ CH ₂ PCy ₂)	75 off-white	CDCl ₃			¹³ C ³¹ P	194
3-271 ClPt[SiMe(CH ₂ CH ₂ PCy ₂) ₂] ²⁸⁶	(cod)PtCl ₂ + NEt ₃ + HSiMe(CH ₂ CH ₂ PCy ₂) ₂	84 off-white	CDCl ₃			[EA] ¹³ C ³¹ P	194
3-272 ClPt[SiMe[(CH ₂) ₃ PPh ₂] ₂] ²⁸⁷	Pt(cod)Cl ₂ + NEt ₃ + HSiMe[(CH ₂) ₃ PPh ₂] ₂	73 cream	CDCl ₃			EA ¹³ C ³¹ P	194
3-273 [R' ₂ P(CH ₂) ₂ PR' ₂][Pt(SiR ₃) ₂] ²⁸⁸ R' = Ph; R = OMe	[R' ₂ P(CH ₂) ₂ PR ₂][Pt(SiMe ₂ Ph) ₂ + 2HSiR ₃		C ₆ D ₆			X-ray ³¹ P	283
*3-274 (Ph ₃ P) ₂ Pt- [SiMe ₂ (C ₂ B ₁₀ H ₁₀)SiMe ₂]	(Ph ₃ P) ₂ Pt(η^2 -C ₂ H ₄) + HMe ₂ Si(C ₂ B ₁₀)SiMe ₂ H ²⁸⁹	82 yellow 175-180 (dec)	CDCl ₃		39.6 (dd) ¹ J _{PSi} = 1282	¹³ C ³¹ P EA X-ray	285 286
3-275 (Ph ₃ P) ₂ Pt{ η^2 - <i>o</i> -(SiMe ₂) ₂ - TTFMe ₂ }	(Ph ₃ P) ₂ Pt(η^2 -C ₂ H ₄) + (<i>o</i> -HSiMe ₂) ₂ TTF(Me ₂ - <i>o</i>)	75 yellow	CDCl ₃			¹ H ³¹ P EA	287

Table 3s. Continued

compound	starting metal complex	% yield color m.p., °C	NMR				other ^d	ref ⁵
			solvent (temp., °C) ^f	¹ HM–H ²	²⁹ Si ^{2,3}			
3-276a <i>cis</i> -(Et ₃ P) ₂ Pt(H)- Me ₂ SiOSiMe ₂ (H)Pt(PEt ₃) ₂ ²⁹⁰	(Et ₃ P) ₃ Pt + (HSiMe ₂ Si) ₂ O 2/3 ratio	75	C ₆ D ₆	–1.96 (dd) ¹ J _{PH} = 1020			¹³ C ³¹ P	288
3-276b [(Et ₃ P) ₂ Pt{(SiMe ₂) ₂ O}]	(Et ₃ P) ₃ Pt + (HSiMe ₂ Si) ₂ O 1/5 ratio	71					¹³ C ³¹ P X-ray	
3-277 <i>trans</i> -(Cy ₃ P) ₂ Pt(H)- (SiCl ₂ Me) ²⁹¹	(Cy ₃ P) ₂ Pt + HSiCl ₂ Me	²⁹²	C ₇ D ₈	–4.5 ¹ J _{PH} = 628			³¹ P	129
3-278a <i>cis</i> -(Cy ₃ P) ₂ (H)PtSiPh ₃ ²⁹³	(Cy ₃ P) ₂ Pt + HSiPh ₃	47 white	C ₇ D ₈ –23	–4.0 ¹ J _{PH} = 784			³¹ P ¹⁹⁵ Pt IR [EA] MS (FAB)	129
*3-278b [Pt{Ga(dpp)} ₂ (H)(SiEt ₃)]	[Pt(1,3-cod){Ga(dpp)} ₂] + HSiEt ₃	49 orange	C ₆ D ₆	–5.63 (t) ¹ J _{PH} = 530			¹³ C VT EA X-ray	298a
*3-279 (Ph ₃ P)HPt- [SiMe ₂ (C ₂ B ₁₀ H ₁₂)PPh ₂]	(Ph ₃ P) ₂ Pt(η ² -C ₂ H ₄) + HSiMe ₂ (C ₂ B ₁₀ H ₁₂)PPh ₂	89 colorless 198 (dec)	CDCl ₃	–0.75 (ddd) ¹ J _{PH} = 1119	41.0 (ddd) ¹ J _{PSi} = 1013		¹³ C ³¹ P IR X-ray	275
3-280 {κ ² -(Hpz)BHpz* ₂ }(H) ₂ - PtSiEt ₃ } ⁺ [BAr' ₄] ^{–294} Ar' = 3,5-(CF ₃) ₂ C ₆ H ₃	{κ ² -(Hpz*)BHpz* ₂ }- (H)Pt(solv)}[BAr' ₄] + 1.8Et ₃ SiH solv = Et ₂ O	80 lt. pink	CD ₂ Cl ₂ (–70)	–16.69 (s) ¹ J _{PH} = 1049			¹³ C ³¹ P IR EA X-ray	289
*3-281 [(C ₂ B ₁₀ H ₁₂)PPh ₂]HPt- SiMe ₂ (C ₂ B ₁₀ H ₁₂)PPh ₂	(cod) ₂ Pt + Ph ₂ PC ₂ B ₁₀ H ₁₂ + HSiMe ₂ (C ₂ B ₁₀ H ₁₂)PPh ₂	82 colorless 225 (dec)	CDCl ₃	–1.33 (ddd) ¹ J _{PH} = 1122			¹³ C ³¹ P IR X-ray	275
3-282a [Me ₂ N(CH ₂) ₃ PPh ₂](Me)- Pt(SiPh ₂ Me) ²⁹⁵	(Me ₂ N(CH ₂) ₃ PPh ₂)PtMe ₂ + HSiPh ₂ Me		C ₆ D ₆		(a) –10.6 (s)		(a) ¹ H ³¹ P ¹⁹⁵ Pt	290
3-282b (3-151b) [Me ₂ N(CH ₂) ₃ PPh ₂](Ph)Pt- (SiPhMe ₂) ²⁹⁶					(b) –21.6 (s)		(b) ¹ H ³¹ P ¹⁹⁵ Pt	
3-283 [Me ₂ N(CH ₂) ₃ PPh ₂](Me)Pt- (SiEt ₃) ²⁹⁷	(Me ₂ N(CH ₂) ₃ PPh ₂)PtMe ₂ + HSiEt ₃		C ₆ D ₆		15.7		¹ H calc	290
3-284a [Me ₂ N(CH ₂) ₂ PMe ₂](Me)- PtSi(OMe) ₃ ²⁹⁸	(Me ₂ N(CH ₂) ₂ PMe ₂)Pt(Me) ₂ + 3.5 equiv HSi(OMe) ₃		C ₆ D ₆		–43.7 (d) ¹ J _{PSi} = 2479		¹³ C ³¹ P	291
3-284b [Me ₂ N(CH ₂) ₂ PMe ₂]Pt- [Si(OMe) ₃] ₂ ²⁹⁹					–3.41 (d, Si trans to P) ¹ J _{PSi} = 2308 –44.94 (d, Si cis to P) ¹ J _{PSi} = 2226 –1.38 (d, Si cis to P) ¹ J _{PSi} = 1510 30.04 (d, Si trans to P) ¹ J _{PSi} = 1490		X-ray	
3-285 [Me ₂ N(C ₆ H ₄)PMe ₂]Pt- [SiMe ₂ C ₆ H ₄ SiMe ₂] ²⁹⁹	[Me ₂ N(C ₆ H ₄)PMe ₂]Pt(Me) ₂ + 1,2-(HMe ₂ Si)C ₆ H ₄ ³⁰⁰	84 pale yellow	(CD ₃) ₂ CO				¹³ C ³¹ P EA X-ray	292 293
3-286a (P∩N)(Me)PtSiR ₃ 3-286b (P∩N)Pt(SiR ₃) ₂ ³⁰¹ 3-286c [PSiP]PtCl	(P∩N)PtMe ₂ + HSiR ₃ PtCl ₂ (SEt) ₂ + H[PSiP]	95 pale yellow	CDCl ₃		35.6		¹³ C ³¹ P EA ¹³ C ³¹ P IR EA X-ray	213a
*3-287 <i>trans</i> -(Cab ^{Si,P}) ₂ Pt R = Me ³⁰²	(Ph ₃ P) ₂ Pt(η ² -C ₂ H ₄) + 2HMe ₂ Si(B ₁₀ C ₂ H ₁₂)PR ₂ ³⁰³	73 colorless/yellow 235–237 (dec)	CDCl ₃				¹³ C ³¹ P IR EA X-ray ³⁰⁴	275 276a
3-288 <i>trans</i> -(Cab ^{Si,P}) ₂ Pt R = Ph	(cod) ₂ Pt + 2HMe ₂ Si(B ₁₀ C ₂ H ₁₂)PR ₂ R = Ph	43 ³⁰⁵ 245–248	CDCl ₃				calc ¹ H ¹³ C ³¹ P IR EA X-ray	276a
3-289 Tp'(H) ₂ PtSiEt ₃	Tp'(H)Pt(Me) ₂ + HSiEt ₃	24 off-white	CD ₂ Cl ₂	–20.15			¹³ C IR EA X-ray	295
3-290a [(NN)Me(H)PtSiEt ₃] ⁺ - [BAr _F] ₃ ³⁰⁶ 3-290b ClPt(NSiN) ³⁰⁷	[(NN)PtMe][BAr _F] + HSiEt ₃ (COD)PtCl ₂ + HSi(C ₉ H ₆ N) ₂ Me	83 lt yellow 32 yellow	CD ₂ Cl ₂ (–10 °C) CD ₂ Cl ₂	–17.31 (s)	14.9		¹ H ¹³ C EA X-ray	278 276b

Table 3t. Continued

compound	starting metal complex	% yield color m.p., °C	NMR				other ^d	ref ^e
			solvent (temp., °C) ^f	¹ HM–H ²	²⁹ Si ^{2,3}			
*3-290c <i>cis</i> -[(κ -NSiN) ₂ Pt]	(tmeda)PtMe ₂ + 2HSi(C ₆ H ₆ N) ₂ Me	64 yellow	CD ₂ Cl ₂		–6.0 ¹ J _{PtSi} = 1670	¹ H ¹³ C EA		276b
*3-290d (NSiN)PtH ₂ (Cl)	(COD)PtCl ₂ + 2.1HSi(C ₆ H ₆ N) ₂ Me	54 yellow	CD ₂ Cl ₂	–18.3 (s) ¹ J _{PtH} = 1274	6.7 (s) ¹ J _{PtSi} = 928	¹³ C EA		276b
3-290e (NSiN)Pt(Me) ₂ OTf ³⁰⁸	1/4[Me ₃ PtOTf] + HSi(C ₆ H ₆ N) ₂ Me	83 yellow	CD ₂ Cl ₂		7.4 ¹ J _{PtSi} = 1223	¹ H ¹³ C ¹⁹ F EA X-ray		276b
3-291 (cod)Pt(SiMeCl ₂) ₂ ^{309,310}	(cod)PtCl ₂ + 2cod + 4HSiMeCl ₂ ³¹¹	95 colorless	CDCl ₃		35.0 ¹ J _{PtSi} = 2110	¹ H ¹³ C ¹⁹⁵ Pt X-ray		296
3-292 <i>cis</i> -[(Ph ₃ P) ₂ HPt- {Si(Me)(CH ₃ SPh) ₂ }- Re(Br)(CO) ₃]	(Ph ₃ P) ₂ Pt(η^2 -C ₂ H ₄) + (CO) ₃ BrRe(SPhCH ₂) ₂ SiMeH ²¹²							
3-293 [(Ph ₃ P) ₂ Pt- {(R ₂ Si) ₂ TTF(SiR ₂) ₂ }- Pt(PPh ₃) ₂] R = Me ³¹³ (TTF = tetrathiafulvalene)	(Ph ₃ P) ₂ Pt(η^2 -C ₂ H ₄) + TTF(SiR ₂ H) ₄	70 yellow	CDCl ₃			³¹ P EA		297
3-294 [R ₃ Si(μ -Cl)(η^2 -cod)Pt] ₂ R = Et ³¹⁴	(cod)PtCl ₂ + cod + 2 HSiR ₃		CDCl ₃		22.9	¹ H ¹³ C ¹⁹⁵ Pt ³¹ P		296
3-295 [(dmpe)Pt(μ -SiPh ₂) ₂]	Pd(PCy ₃) ₂ (dmpe)Pt(SiPh ₂ H) ₂							
*3-296 [(dmpe)Pt(μ -SiAr ₂) ₂] (Ar = C ₆ H ₄ F- <i>p</i>)	(dmpe)PdMe ₂ (Me ₃ P) ₂ Pt(SiAr ₂ H) ₂	21 pale yellow	C ₆ D ₆			¹ H ³¹ P X-ray		244
*3-297a {[C(Cy ₃ P)Pt](μ - η^2 -H- SiPh ₂) ₂ Pd(PCy ₃)}	Pd(PCy ₃) ₂ (dmpe)Pt(SiPh ₂ H) ₂	28 pale yellow	C ₆ D ₆ (40)	2.49 (d, Pd–H) ² J _{PtH} = 73 1.70 (d, Pt–H) ¹ J _{PtH} = 601		¹³ C ³¹ P IR EA X-ray		122
3-297b [(Ph ₃ P) ₂ Pt(H)(μ -SiMe ₂)- (μ -SiHMe ₂)Pt(PPh ₃)] ³¹⁵	<i>cis</i> -(Ph ₃ P) ₂ Pt(SiMe ₂ H) ₂ (rt)	53 colorless	CD ₂ Cl ₂ (–70)	0.70 (d) (Si–H–Pt) –7.05 (t) ¹ J _{PtH} = 553		³¹ P VT HMBC (¹ H– ³¹ P) EA X-ray		284c
3-298a {[C(Cy ₃ P)Pt](μ -SiPh ₂) ₂ }] ₃	<i>cis</i> -(Me ₃ P) ₂ Pt(SiPh ₂ H) ₂ Δ	(a) 28 red	C ₆ D		279.4 ¹ J _{PtSi} = 945	(a) ³¹ P ¹⁹⁵ Pt EA X-ray calc		241 298
3-298b (Me ₃ P) ₂ Pt(SiPh ₂ OSiPh ₂)] ³¹⁶		(b) 34 yellow				(b) ³¹ P		298
3-299 [Pt ₃ {Si(OSiMe ₃) ₃ }- (μ -PPh ₂) ₃ (PPh ₃) ₂ }] ³¹⁷	[Pt ₃ Ph](μ -PPh ₂) ₃ (PPh ₃) ₂ + xs HSi(OSiMe ₃) ₃	47 dk red	ClC ₆ H ₅ –C ₆ D ₆			³¹ P X-ray ³¹⁸		299
3-300 [Pt ₃ (SiPh ₃)(μ -PPh ₂) ₃ - (PEt ₃) ₂]	[Pt ₃ H(μ -PPh ₂) ₃ (PEt ₃) ₃] + HSiPh ₃	75 dark red	CD ₂ Cl ₂			¹³ C ³¹ P X-ray		135
3-301a [Pt ₃ (SiMe ₂ C ₆ H ₄ SiMe ₂ H)- (PEt ₃) ₂ (μ -PPh ₂) ₃]] ^{319,320}	[Pt ₃ H(PEt ₃) ₃ (μ -PPh ₂) ₃] + 1,4-(HMe ₂ Si) ₂ C ₆ H ₄ 2/3 ratio	87 red	C ₆ D ₆	³²²		¹³ C ³¹ P IR EA X-ray		300
3-301b [(Et ₃ P) ₂ (μ -PPh ₂) ₃ Pt ₃ - (SiMe ₂ C ₆ H ₄ SiMe ₂)Pt ₃ - (PEt ₃) ₂ (μ -PPh ₂) ₃]] ³²¹	1:1 ratio	71 red	C ₆ D ₆			³¹ P EA X-ray		
3-302 SiO on Au	Au + Si ₈ H ₈ O ₁₂ + uhv						XPS RAIRS calc	301
3-303 AuSi	Au + <i>cis</i> -[PtCl ₂ (PhCH=CH ₂) ₂] + –(RSiH) _x –							302
Zn triad								
3-304 ⁷ BuHgSi(SiMe ₂ SiMe ₃) ₃	⁷ Bu ₂ Hg + HSi(SiMe ₂ SiMe ₃) ₃ (~1:1 ratio)	85 yellow	C ₆ D ₆		–91.4 (SiHg) –30.5 (SiMe ₂) –16.3 (SiMe ₃)	¹³ C ¹⁹⁹ Hg UV-Vis		303
3-305 (3-164) (Me ₂ SiMe ₂ Si) ₃ SiHg	⁷ Bu ₂ Hg + HSi(SiMe ₂ SiMe ₃) ₃ (~2:1 ratio)	67 red	C ₆ D ₆		–49.6, –46.0 (SiHg)	¹³ C ¹⁹⁹ Hg		303

Table 3u. Continued

compound	starting metal complex	% yield color m.p., °C	NMR				other ^d	ref ⁵
			solvent (temp., °C) ^f	¹ HM–H ²	²⁹ Si ^{2,3}			
HgSi(SiMe ₂ SiMe ₃) ₃					–30.7 –30.4 (SiMe ₂) –14.7, –13.0 (SiMe ₃) ³²³		UV-Vis X-ray	

[†] Definitions: **Alkyl groups and alkanes:** Me = methyl, CH₃; Et = ethyl, C₂H₅; ⁱPr = isopropyl, –CHMe₂; Bu = butyl, C₄H₉; ^tBu = *tert*-butyl, –CMe₃; Hex = C₆H₁₃; Cy = cyclohexyl, *c*-C₆H₁₁; pyl = *N*-pyrrolyl, NC₄H₄; DBU = 1,8-diazabicyclo[5.4.0]undec-7-ene. **Aryl groups and arenes:** Ph = phenyl, C₆H₅; Mes = 2,4,6-mesityl, 2,4,6-Me₃C₆H₂; py = pyridine, NC₅H₅; dipp = 2,6-diisopropylphenyl, 2,6-ⁱPr₂C₆H₃–; Ar^F = 3,5-C₆H₃(CF₃)₂; *p*-Tol = *p*-tolyl, *p*-CH₃C₆H₄; trip = 2,4,6-tri-isopropylphenyl, 2,4,6-ⁱPr₃C₆H₂; *p*-cymene = 4-isopropyltoluene; Fv = fulvalene; THI = tetrahydroindenyl; Xantsil = (9,9-dimethylxanthene-4,5-diyl)bis(dimethylsilyl) pyInd = 2-(2'-pyridyl)indolide; DMAP = 4-dimethylaminopyridine; Si(NN) = *N,N'*-bis(neopenyl)-1,2-phenylenedi(amino)silylene. **Olefins:** NBD = norbornadiene; COD = cyclooctadiene, C₈H₁₂; COE = cyclooctene, C₈H₁₄. **Cp ligands:** Cp = C₅H₅; Cp* = C₅Me₅; Cp'' = C₅Me₄SiMe₃; Cp' = C₅Me₄Et. **Miscellaneous:** dpp = 2-[(2,6-diisopropylphenyl)amino]–4-[(2,6-diisopropylphenyl)imino]–2-pentene. **Monodentate phosphines:** dimethylphenylphosphine, Me₂PhP; diethylphenylphosphine, Et₂PhP; trimethylphosphine, Me₃P; triphenylphosphine, Ph₃P; tri-isopropylphosphine, ⁱPr₃P; tripropylphosphine, Pr₃P. **Chelates:** **dmpe** = Me₂PCH₂CH₂PMe₂; **depe** = Et₂PCH₂CH₂PEt₂; **dppe** = Ph₂PCH₂CH₂PPh₂; **diippe** = 1,2-(diisopropylphosphino)ethane; **dcpe** = dicyclohexylphosphinoethane; **Tp'** = hydridotris(pyrazolyl)borate, [HB{NHN(Me)}₃][–]; ***t*-BuPNP** = {^tBu₂PCH₂SiMe₂}₂N[–]; (ⁱPr₂CH₂)₂(C₅H₃N), bis(diisopropylphosphino)pyridine; [**PSiP**] [^κ3-(2-Ph₂PC₆H₄)₂SiMe][–]. [**CyPSiP**][–] = [^κ-(2-Cy₂PC₆H₄)₂SiMe][–]; [**NSiN**] = bis(8-quinolyl)(methyl)silyl, [(C₉H₆N)₂CH₃Si]; [**PNSiP**] = PhN(SiMe₂CH₂)₂PPh; **tpp** = 5,10,15,20-tetramesitylporphyrinato; **ttp** = 5,10,15,20-tetratolylporphyrinato; **PpSiPP** = {[Ph₂PCH₂CH₂P(Ph)C₆H₄-*o*]₂Si-*P,P,P,P*,*Si*}; **^{tr}PDI** = ((2,6-CHMe₂)₂C₆H₃N=CMe)₂C₅H₃N; **Cab^{SiP}** = HMe₂Si(B₁₀C₂H₁₂)PMe₂; C₂B₁₀H₁₀ = *ortho*-dicarborane; **NN** = 1,4-bis(methoxypropyl)-2,3-dimethyl-1,4-diazabutadiene; **dba** = dibenzylideneacetone; **PN** = dichloro-1-[(R)-1-[(S)-2-(diphenylphosphino)-*κ*P]ferrocenyl]ethyl-3-phenyl-5-methyl-1*H*-pyrazole-*κ*N]; **etp** = PhP(CH₂CH₂PPh₂)₂; (*o*-HSiMe₂)₂TTF(Me₂-*o*) = 3,4-dimethyl-3',4'-(dimethylsilyl)tetrathiafulvalene. **PP₂** = ⁱPr₂P(CH₂)₃P(Ph)(CH₂)₃PⁱPr₂; **biPSiH** = HSi(Me)[(CH₂)₃PPh₂]₂ (*x* = 2, 3); **PfN** = R₂N–R'–PPh₂; ^κ2-SiMe₂C₆H₄NMe₂-*o*–; {^κ(*Si,Si,O*)-Xantsil}[SiP^R₃][–] = [(2-R₂PC₆H₄)₃Si][–] (R = Ph, ⁱPr); [**N₃**] = 2,6-(MesN=CMe)₂C₅H₃N; [**CfN**] = [*N-n*-butyl-*N'*-(2-pyridylmethyl)-4,5-dichloroimidazole-2-ylidene]. **Tripod** = CH₃C(CH₂PPh₂)₃. **Counteranions:** [BAR_F][–] = [BAR_F^F][–], [3,5-(CF₃)₂C₆H₃]₄B][–]; OTf[–] = triflate, CF₃SO₃[–]. [‡]

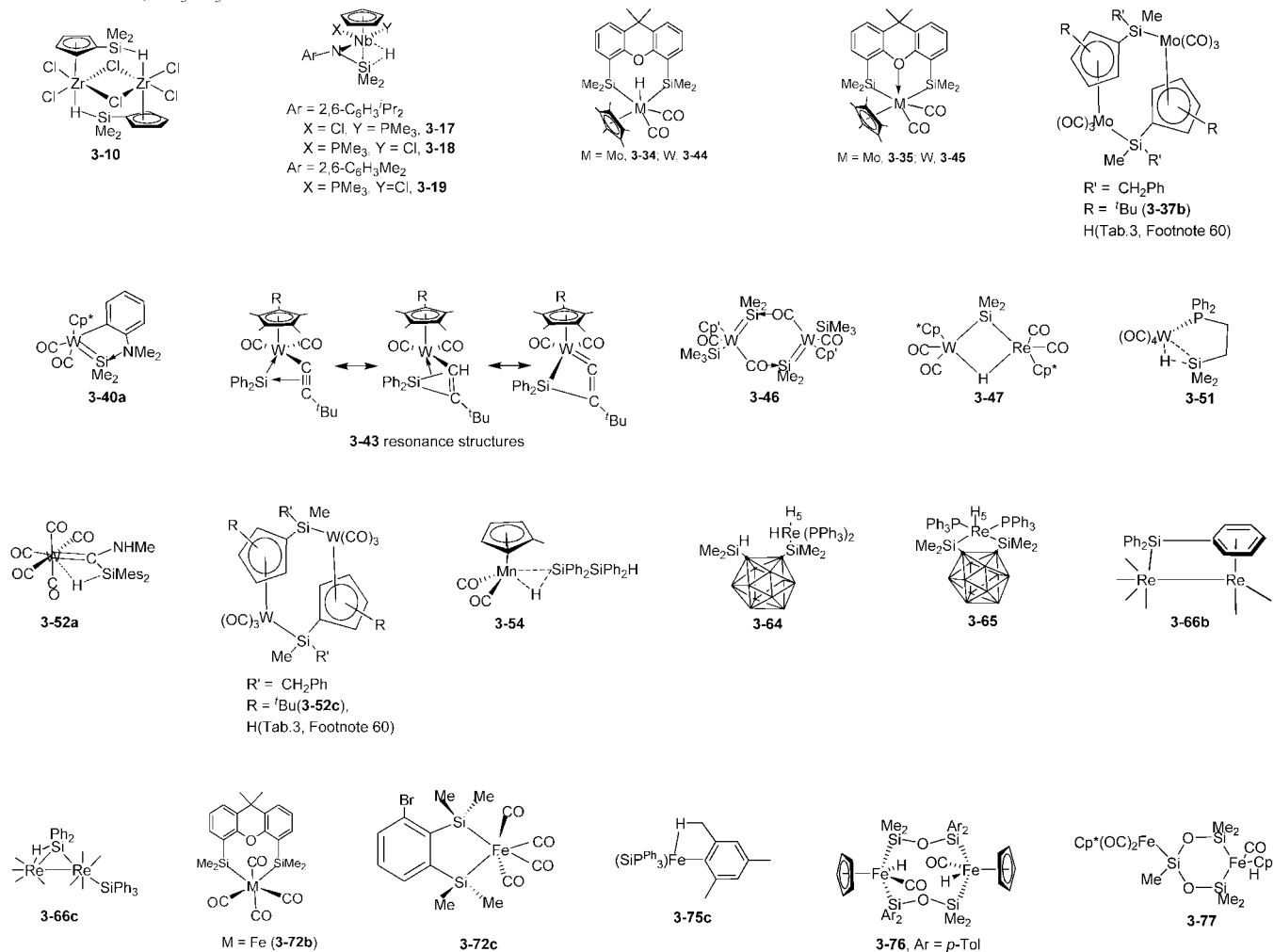


Table 3v. Continued

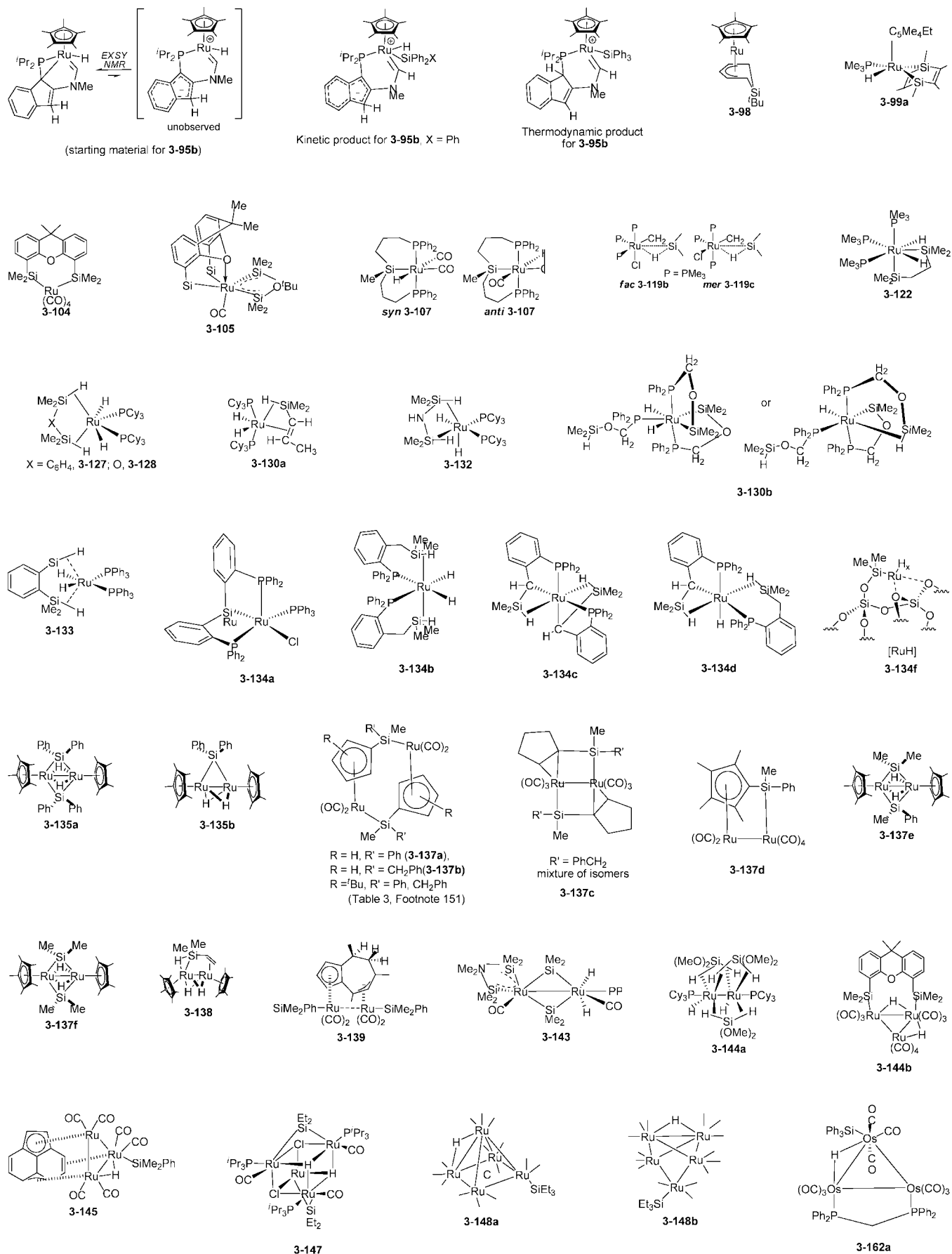
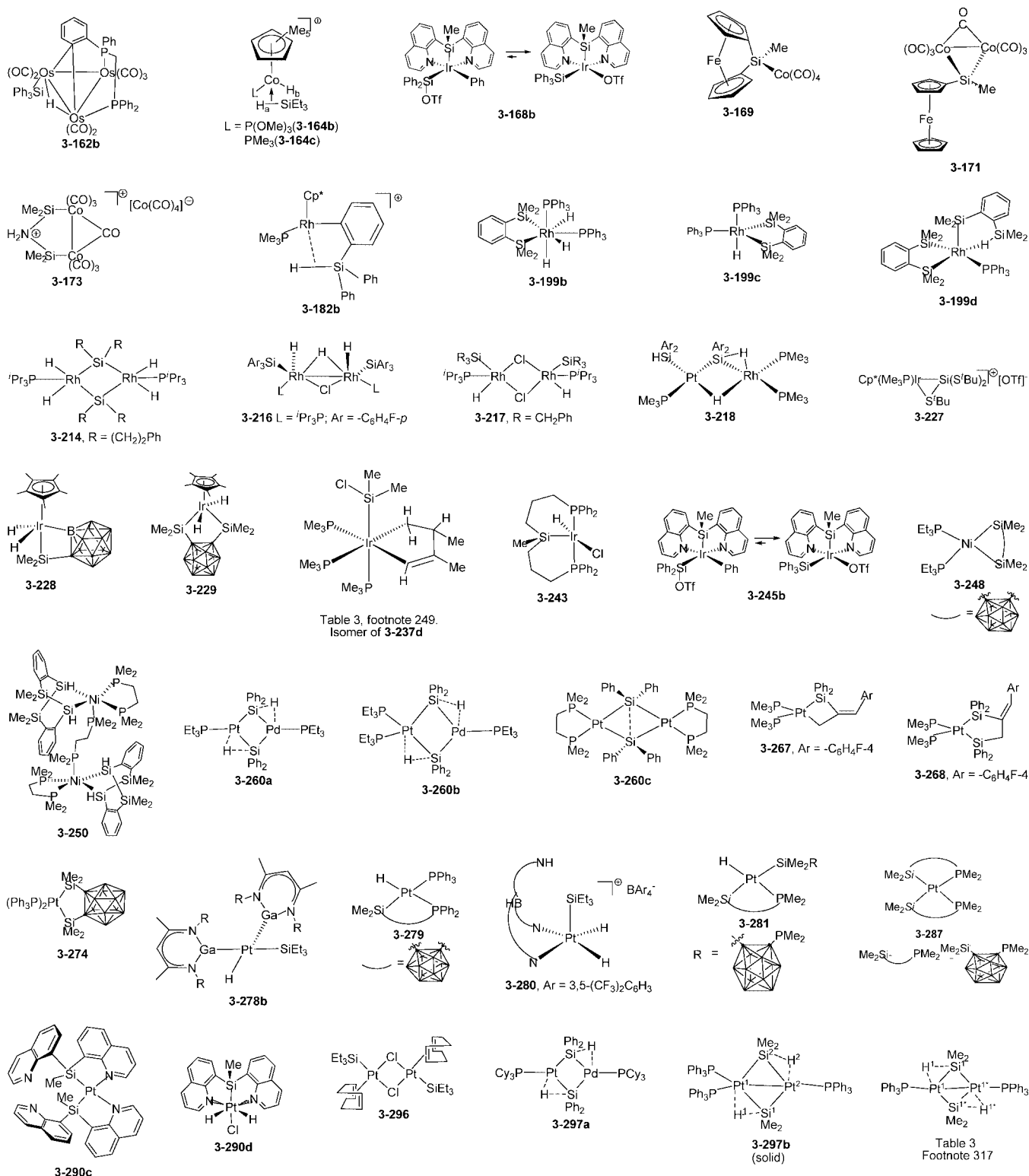


Table 3w. Continued



¹ Ambient temperature unless otherwise noted. Temperatures in °C. ² In ppm. Coupling constants in Hz. Assignments: s, singlet; d, doublet; t, triplet; q, quartet; quin, quintet; sept, septet; m, multiplet; br, broad; vt = virtual triplet. ¹J_{SiH} coupling constants were determined either from ²⁹Si satellites in the proton spectrum or from proton-coupled ²⁹Si NMR data. The former appear in the SiH column, and the latter appear in the ²⁹Si column. ³ ²⁹Si may have been determined by direct observation, INEPT or DEPT, or 2D ²⁹Si–¹H correlation. These methods are not distinguished in the table. ⁴ Will contain other characterization methods including spectroscopic, X-ray, and calculations if reported. If elemental analyses were reported, this will be indicated by EA. If analysis is outside ±0.5% of calculated percentage value for carbon, this will be indicated by the symbolism [EA]. ⁵ Some data have been retrieved from the Supporting Information associated with the indicated reference. ⁶ Additional derivatives produced from reaction of Cp₂Ti(PMe₃)₂ with HSiMe₂Cl, HSiMePhCl (X-ray), HSiClPh₂, and HSiCl₃ (X-ray).^{20b} ⁷ No discernable signals.¹³⁸ ⁸ Additional derivative, Cp₂Ti(BuC₂SiMe₂H) (X-ray). ²⁹Si NMR spectrum of solid Cp₂Ti(BuC₂SiMe₂H) exhibited a resonance at 16.7 ppm at 291 K and at 16.1 at 320 K (both assigned to SiMe₂H). The NMR spectrum of a solution spectrum of Cp₂Ti(BuC₂SiMe₂H) in C₇D₈ exhibited a resonance at 17.6 (193 K) and at –0.5 (303 K).¹³⁹ ⁹ Uncoordinated SiH: ¹H [(C₂D₅)₂O], 4.58 ppm.¹³⁹ ¹⁰ Averaged signal.¹³⁹

Table 3x. Continued

¹¹ Additional derivative, $\text{Cp}^*(\text{HMe}_2\text{SiC}\equiv\text{CSiMe}_2\text{H})$.^{139, 12} Uncoordinated SiH: ^1H (C_6D_6), 4.47 (s, $^1J_{\text{SiH}} = 183$).^{139, 13} Uncoordinated SiH: ^1H (C_6D_6), 3.97.^{139, 14} Additional derivatives prepared from $\text{PhC}_2\text{SiMe}_2\text{H}$ and $\text{Me}_3\text{SiC}_2\text{SiMe}_2\text{H}$.^{139, 15} The THF adduct of **3-9** was also prepared and exhibited no β -agostic interaction.^{139, 16} Averaged signal for free and coordinated HSi.^{139, 17} Uncoordinated SiH: ^1H (C_7D_8 , 17°C), 4.98 ($^1J_{\text{SiH}} = 190$).^{139, 18} Uncoordinated SiH: ^1H (C_7D_8 , -27°C), 5.05 ($^1J_{\text{SiH}} = 187$).^{139, 19} Agostic HSiMe_2 .^{139, 20} Lewis acids such as ZrCl_4 cleave a Si–C bond in silylcyclopentadiene compounds.^{140, 21} SiH ^1H resonance appears at 4.50 (sept, C_6D_6) and 4.49 (sept, CDCl_3), indicating that the agostic interaction does not persist in solution.^{140, 22} Observed in solution only.^{141, 23} **3-12a** and **3-12b** were formed in a 1:1.2 ratio and could not be isolated by the usual crystallization techniques. Crystals suitable for X-ray studies were composed only of **3-12b**. **3-12b** is the thermodynamic isomer.^{142, 24} Complex is most likely formed after removal of BH_3 by complexation with NEt_3 .^{143, 25} Formation of complexes **3-14** and **3-16** most likely involves elimination of H_2 from Cp_2NbH_3 followed by oxidative addition of the silane.^{144, 26} Process involves elimination of H_2 followed by oxidative addition of the silane. Additional derivative prepared from $[\text{Cp}_2\text{NbBH}_4]$ and HSiPhMe_2 .^{142, 27} Efforts to obtain Si,H coupling constants failed since the hydride and silicon resonances are broad (down to -100°C) due to the quadrupolar ^{93}Nb nucleus.^{142, 28} Additional derivative, $\text{Cp}_2(\text{H})\text{Nb}(\text{SiMe}_2\text{Ph})_2$.¹⁴² The formation of an inseparable mixture of $\text{Cp}_2\text{Nb}(\text{SiMe}_2\text{Cl})_2\text{H}$ and $\text{Cp}_2\text{Nb}(\text{C}_2\text{H}_3\text{Ph})\text{SiMe}_2\text{Cl}$ from reaction of Cp_2NbH_3 with $\text{CH}_2=\text{CHPh}$ followed by HSiMe_2Cl at $65-70^\circ\text{C}$ in toluene was also reported. $\text{Cp}_2\text{NbH}(\text{SiCl}_3)_2$ was prepared from the reaction of Cp_2NbH_3 and SiCl_4 .^{144, 29} As an isomeric ratio of 10:1. Data are given for the major isomer **3-17**.^{146, 147a} Additional derivative, $\text{Ar} = 2,6\text{-C}_6\text{H}_3\text{Me}_2$.^{147a} Reaction of $[\text{NbCp}(\text{Nbu}')(\text{PMe}_3)_2]$ with HSiMe_2Cl gave $[\text{NbCp}(\mu\text{-Nbu}')\text{Cl}]_2$. No reaction of $[\text{NbCp}(\text{NAr})(\text{PMe}_3)_2]$ occurred with the following silanes: HClSiPr_2 , ClSiMe_3 , Cl_2SiMe_2 , or HSiMe_2Ph under conditions comparable to those that gave **3-17**.^{147a} **3-17** and **3-18** are isomers that differ in position of the Me_2P and Cl ligands.³⁰ Additional derivative made with HSiClMePh and another made with HSiMe_2Cl and with PhMe_2P replacing PMe_3 (X-ray).^{32a, 31} X-ray structure was only of sufficient quality to establish overall geometry.^{147a} Additional derivative reported from reaction with HSiCl_3 .^{148, 33} Similar derivative prepared from $\text{CpNb}(\text{NAr})(\text{PMe}_3)_2$ and HSiCl_3 (X-ray), HSiMeCl_2 , HSiMe_2Cl , HSiMePhCl .^{32a, 149} Reaction proceeds through $\text{CpNb}(\text{ArN})(\text{PMe}_3)(\text{H})(\text{SiMeCl}_2)$ which could be isolated after 15–30 min reaction time. **3-22** was isolated after a few hours.^{149, 35} SiH resonance observed at 6.24 ppm as a quartet.^{149, 36} The OMe ^1H resonance for **3-24a** was observed at 3.33 ppm, whereas the OMe ^1H resonance is shifted upfield to δ 2.73 in **3-24b**, which is characteristic of methoxy-bridged silyl(silylene) complexes.^{150, 37} No reaction occurred between $[\text{CpTa}(\text{NAr})(\text{PMe}_3)_2]$ and HSiMe_2Ph .^{146, 38} Additional derivatives prepared from reaction of $[\text{CpTa}(\text{NAr})(\text{PMe}_3)_2]$ with H_2SiPhMe (Table 2) and HSiCl_3 .^{78a, 39} Related complexes prepared from HSiMe_2Cl and HPh_2Cl . The reaction with HSiPhMeCl was studied by NMR methods.^{147b, 40} Information not supplied.¹⁵¹

⁴¹ Kinetic measurements provided a bond dissociation enthalpy for **3-28** of 24.3 ± 1.2 kcal/mol.^{152, 42} Complex not isolated.^{81, 83a, 43} Additional derivative prepared from $\text{M}(\text{CO})_6 + \text{HSiPr}_3$.^{83a} Complex $\text{Cr}(\text{CO})_5(\eta^2\text{-HSiPh}_3)$ also reported.^{81, 44} Additional derivatives with $\text{R} = \text{Cl}$ and OEt .^{35, 45} Additional derivative prepared from $\text{Cp}(\text{OC})_3\text{MoMe} + \text{HSiMe}_2\text{SiMe}_2\text{NEt}_2$.^{151, 46} Additional derivative prepared from $(\text{Ar}'\text{N})_2\text{Mo}(\text{PMe}_3)_3 + \text{HSiCl}_2\text{Me}$ (X-ray).^{155a, 47} **3-40a** was also generated from $\text{Cp}^*(\text{OC})_2(\text{NCCD}_3)\text{WMe}$ in 86% yield as determined by NMR measurements.^{157a, 48} Additional derivative prepared from HSiEt_3 .^{157b, 49} Additional example prepared from $\text{HSiMe}_2(p\text{-Tol})$.^{158, 50} Derivative related to **3-43** was prepared from $(\text{Cp}^*)(\text{OC})_2(\text{MeCN})\text{W-Me} + \text{HSiPh}_2\text{C}\equiv\text{C}^t\text{Bu}$.^{160a, 51} A poor-quality crystal for **3-44** showed a piano-stool structure with *cis*-carbonyls and 2 Si centers.^{154, 52} Also prepared: $[\text{Cp}'\text{W}(\text{CO})_2(\text{SiMe}_2)(\text{SiMe}_3)_2]$ ($\text{Cp}' = \text{C}_5\text{Me}_5$).^{156, 53, 29} Si signal for $\text{W}=\text{SiMe}_2$ was not observed due to low solubility.¹⁵⁶

⁵⁴ Deuterium analogue, $\text{Cp}^*(\text{OC})_2\text{W}(\mu\text{-SiMe}_2)(\mu\text{-D})\text{-Re}(\text{CO})_2\text{Cp}^*$, also prepared.^{161, 55} A ditungsten complex in which two Ph groups of HSiPh_3 are coordinated to a $\text{W}(\text{CO})_3$ unit was observed in reaction mixtures ($\sim 7\%$ yield) but was not isolated.^{162, 56} Additional derivative: $(\text{OC})_5\text{W}(\eta^2\text{-HSiR}_3)$ ($\text{R}_3 = \text{Ph}_3$, HPh_2).^{81, 57} Additional derivative, $\text{R} = \text{Ph}$.^{163, 58} Additional derivatives, $\text{R} = \text{R}' = \text{Ph}$; $\text{R} = \text{Me}$, $\text{R}' = p\text{-Tol}$.^{163, 59} Additional derivative, $\text{R} = \text{Et}$.^{164, 60} Additional derivative prepared from $(\text{C}_3\text{H}_5)\text{PhMeSiH}$ (X-ray).^{155c, 61} Byproduct, $[\text{Cp}'(\text{OC})_2\text{Mn}(\eta^2\text{-HSiPh}_2\text{SiPh}_2\text{H})\text{Mn}(\text{CO})_2\text{Cp}']$ decomposes during chromatographic workup.^{166, 62} SiH resonance at 5.69 (s; $^1J_{\text{SiH}} = 173$).^{166, 63} Additional derivatives prepared from $\text{HMe}_2\text{SiXSiMe}_2\text{H}$, $\text{X} = -\text{CH}_2\text{CH}_2-$, O .^{167, 64} SiH resonance at 5.43 (br s).^{167, 65} Monosubstituted analogue of **3-54** decomposed on chromatographic workup, as did the product produced from $\text{Cp}'\text{Mn}(\text{CO})_3$ and $\text{HMe}_2\text{SiSiMe}_2\text{H}$.^{166, 66} Additional derivative, $\text{R}_3 = \text{PhH}_2$.^{168, 67} Additional derivatives: $\text{Cp}(\text{OC})_2\text{Re}(\text{H})(\text{SiPhMeSiPhMeH})$ as a 10:9 mixture of diastereomers; $\text{Cp}(\text{OC})_2\text{Re}(\text{H})(\text{SiPh}_2\text{SiMe}_3)$. Reaction of $\text{Cp}(\text{OC})_2\text{Re}(\text{THF})$ and $\text{HMe}_2\text{SiSiMe}_2\text{H}$ produced *cis*- and *trans*- $\text{Cp}(\text{OC})_2\text{Re}(\text{H})(\text{SiMe}_2\text{SiMe}_2\text{H})$ as well as $\text{Cp}(\text{OC})_2\text{Re}(\text{H})(\text{SiMe}_2\text{SiMe}_2\text{H})(\text{Re})(\text{CO})_2\text{Cp}$, all of which were identified spectroscopically.^{166, 68} SiH resonance observed at 5.65 (s, $^1J_{\text{SiH}} = 182.4$; $^2J_{\text{SiSiH}} = 8.6$).^{166, 69} Unresolved heptet.^{81, 70} Additional derivative, $\text{R} = c\text{-C}_6\text{H}_{11}$.^{170, 71} **3-62** observed only in solution and was thermally unstable, decomposing to $[\text{cis-Re}(\text{L})(\text{CO})_4]_2(\mu\text{-H})[\text{BAR}_f]$.^{171, 72} SiH resonance observed as a multiplet at 4.10 ppm.^{172, 73} Byproducts at this temperature were **3-66a** (25%) and **3-66b** (6%).^{173, 74} Additional derivative prepared from HSiCl_3 (X-ray), HSiMe_2Cl , HSiMe_2Ph .^{42a, 75} Improved preparation. The silylene **3-69** was also formed from $\text{Cp}^*(\text{OC})_2\text{FeSiMeMeSiMe}_2\text{Mes}$ or $\text{Cp}^*(\text{OC})_2\text{FeSiMe}_2\text{SiMe}_2\text{Mes}$ under fluorescent light.^{175, 76} Additional derivative generated from $\text{CpFe}(\text{CO})_2\text{Me}$, but the product was too unstable to isolate.^{22b, 77} $\text{Cp}^*(\text{OC})(\text{py})\text{FeMe}$ was prepared and isolated in 97% yield from reaction of $\text{Cp}^*(\text{OC})_2\text{FeMe}$ with py (photolysis).^{22b, 78} Additional derivatives: $(\text{C}_7\text{H}_8)(\text{H})_2\text{Fe}(\text{SiHCl}_2)_2$ (**2-32**), $(\text{C}_6\text{H}_6)(\text{H})_2\text{Fe}(\text{SiMeCl}_2)_2$.^{92, 79} Observed in solution. Additional examples reported for reaction with HSiMe_2OR ($\text{R} = \text{Me}$, $i\text{-Pr}$, $t\text{-Bu}$, Ph). $\text{SiMe}_2(\text{OR})_2$ was also identified in the product mixture. When the reaction of HSiMe_2OMe was conducted in the presence of HMPA, the complex $(\text{OC})_4\text{Fe}=\text{SiMe}_2\cdot\text{HMPA}$ (19%) was identified by comparison to literature values. For an isolated complex, see **3-73**.^{177a, 80} NMR yield was 41%.^{177a, 81} As HMPA adduct.^{178a, 82} Additional derivatives: *mer*-($\text{OC})_3(\text{Ph}_3\text{P})\text{Fe}(\text{H})(\text{SiPhMeSiPhMeH})$ as a 10:9 mixture of diastereomers and *mer*-($\text{OC})_3(\text{Ph}_3\text{P})\text{Fe}(\text{H})(\text{SiPh}_2\text{SiMe}_3)$.¹⁶⁶ Reaction of $\text{HMe}_2\text{SiSiMe}_2\text{H}$ and *mer*-($\text{OC})_3(\text{Ph}_3\text{P})\text{Fe}(\text{H})(\text{SiMe}_3)$ ultimately produced $(\text{OC})_3(\text{Ph}_3\text{P})\text{Fe}(\text{H})(\text{SiMe}_2\text{SiMe}_2\text{H})(\text{Fe})(\text{Ph}_3)(\text{CO})_3$ identified spectroscopically.⁸³ Complex **3-75b** contains a C–H agostic interaction from a Me group of the mesityl. **3-75b** was utilized in the preparation of $[(\text{SiPh}_3)_3\text{FeCl}]$ and $[(\text{SiPh}_3)_3\text{Fe}(\text{N}_2)]$.^{178b, 84} **3-75c** was used to prepare $[(\text{SiPh}_3)_3\text{Fe}(\text{N}_2)]$.^{178b, 85} Additional derivative, $\text{R} = \text{Me}$.¹⁷⁹ Signals for the ^{29}Si NMR resonance for $\text{Si}(p\text{-Tol})_2$ were not observed.⁸⁶ The product from step “a”, $[\text{Cp}^*\text{Ru}(\eta^6\text{-C}_6\text{H}_5\text{-SiPh}_2\text{-OH})\text{BF}_4]$, a yellow solid, was isolated in 86% yield and then reacted with the $\text{NaBPh}_4/\text{MeOH}$.^{181a, 87} Synthetic approach involves protonation of a TM–Si bond.^{182, 88} Additional derivatives were prepared from a similar reaction of $\text{Cp}(\text{PPhMe}_2)_2\text{RuH}$ and HSiCl_3 (with and without DBU) or H_2SiCl_2 (without DBU). Also prepared by this method were $\text{Cp}(\text{PPhMe}_2)_2\text{RuSiHCl}_2$ and $\text{Cp}(\text{PPhMe}_2)_2\text{RuSiH}_2\text{Cl}$.^{18, 89} Synthetic method involves elimination of HCl promoted by the base acceptor instead of reaction of the SiH bond.^{18, 90} SiH resonance observed at 5.52 ppm as a multiplet.^{18, 91} Additional derivatives, $\text{Cp}(\text{L})(\text{H})_2\text{RuSiMe}_2\text{Cl}$ ($\text{L} = \text{PPh}_3$) (X-ray), PPr_2Ph_2 , $\text{P}(\text{Pr})_2\text{Ph}$ (X-ray).^{181c, 92} A similar reaction with HSiMe_2Cl produced a mixture of products including $\text{Cp}(\text{PPhMe}_2)_2\text{RuH}$, $[\text{Cp}(\text{PPhMe}_2)_2\text{RuH}_2]^+$, and $\text{Cp}(\text{PPhMe}_2)_2\text{RuCl}$.^{18, 93} Additional derivatives: $\text{R}_3\text{Si} = (\text{Me}_2\text{N})_3\text{Si}$, $(\text{EtS})_3\text{Si}$, $(2\text{-NaphS})_3\text{Si}$, $\text{Si}(\text{SCH}_2)_3\text{SiPh}$, $\text{Si}(\text{SCy})_2\text{Cl}$, $\text{Si}(\text{SMes})_2\text{Cl}$.^{47a, 94, 29} ^{31}P and $^{29}\text{Si}\{^1\text{H}\}$ both recorded.^{184, 95} Additional derivative prepared from reaction of $\text{Cp}^*(\text{Me}'\text{Pr}_2)\text{RuH}_3$ and HSiMe_2Cl (X-ray; also an IHI complex).^{186, 96} The same type of mixture as **3-89a** and **3-89b** was generated starting with $\text{Cp}^*(\text{Me}_2\text{PhP})\text{RuH}_3$ and HSiMe_2Cl .¹⁸⁶ Disproportionation of HSiMe_2Cl provided HSiMeCl_2 (detected in solution).⁹⁷ Related derivative, $\text{Cp}^*(\text{Me}'\text{Pr}_2)(\text{H})_2\text{RuSiMeCl}_2$, was also prepared and isolated (X-ray; double IHI interaction). Reaction of $\text{Cp}^*(\text{Me}_2\text{PhP})\text{RuH}_3$ with HSiMeCl_2 gave a mixture of products including $\text{Cp}^*(\text{Me}_2\text{PhP})(\text{H})_2\text{RuMeCl}_2$ and $\text{Cp}^*(\text{Me}_2\text{PhP})(\text{H})_2\text{RuSiMeCl}_2$, but neither were isolated.^{186, 98} Related derivatives, $\text{Cp}^*(\text{Me}'\text{Pr}_2)(\text{H})\text{ClRuSiMeCl}_2$, $\text{Cp}^*(\text{Me}'\text{Pr}_2)(\text{H})\text{ClRuSiCl}_3$ (X-ray), and $\text{Cp}^*(\text{Me}_2\text{PhP})(\text{H})\text{ClRuSiCl}_3$ (X-ray), were also isolated.¹⁸⁶

⁹⁹ **3-91b** was the minor product and was not isolated.^{186, 100} No isolated yields were given, but an NMR study showed that **3-92** was formed quantitatively.^{187, 101} Similar derivatives were prepared and isolated from $\text{Cp}^*(\text{L})\text{RuH}_3$ [$\text{L} = \text{Me}'\text{Pr}_2\text{P}$ (X-ray), $\text{Me}_2'\text{PrP}$ (X-ray), Me_2PhP (X-ray)] and HSiCl_3 .^{186, 102} Also prepared from $\text{Cp}^*(\text{Pr}_3\text{P})\text{RuH}_3 + \text{HSiCl}_3$ at both room temperature and 90°C .^{186, 103} **3-94** could not be isolated from the mixture of products nor was the related derivative, $\text{Cp}^*(\text{Me}'\text{Pr}_2)(\text{H})_2\text{RuSiCl}_2\text{H}$, isolated from its product mixture.¹⁸⁶ The HSiCl_3 disproportionates in the presence of NEt_3 , providing H_2SiCl_2 .¹⁰⁴ SiH resonance, ^1H (C_6D_6), 6.89 (dt, $J_{\text{SiH}} = 255$).^{186, 105} The mixture of $\text{NEt}'\text{Pr}_2$ and HSiCl_3 was shown to generate H_2SiCl_2 . An NMR scale reaction showed that $\text{Cp}^*(\text{Pr}_3\text{P})(\text{H})_2\text{RuSiClH}_2$ was formed in 90% yield.^{186, 106} SiH resonance, ^1H (C_6D_6), 5.88 (t, $J_{\text{SiH}} = 204$).^{186, 107} See structure of starting material for **3-95b** in the structure section for Table 3.^{47d, 108} Reaction was also run between $\text{Cp}^*(\text{OC})(\text{Py})\text{RuMe} + \text{HSiMe}_2\text{N}(p\text{-Tol})_2$, which gave a 1:1 mixture of the analogues of **3-96a** and **3-96b**, but only the analogue of **3-96b** (X-ray) was isolated. **3-96a** was prepared from $\text{Cp}^*(\text{OC})(\text{Py})\text{RuMe} + \text{HSiMe}_2\text{NPh}_2$ in the presence of pyridine in 72% yield.^{188, 109} Possible route to **3-96b** could be loss of py from **3-96a** followed by insertion of Ru into the *o*-HC bond of NPh. Additional derivative from $\text{HMe}_2\text{N}(o\text{-Tol})_2$.^{188, 110} Reaction pathway includes the displacement of a RuCl with anionic silicon ligand, $[\text{C}_5\text{H}_5\text{SiH}(\text{Bu})]^-$.^{189a, 111} SiH resonance, ^1H (C_6D_6), 4.77 (br s, $J_{\text{SiH}} = 195$).^{189a}

Table 3y. Continued

¹¹² Additional derivative prepared from $(\text{Ph}_3\text{P})_3\text{RuCl}_2$ and xs HSiMeCl_2 in the presence of $\text{CH}_2=\text{CHC}_6\text{H}_{13}$ and C_6H_6 . Other arene derivatives reported from $(\text{Ph}_3\text{P})_3\text{RuCl}_2$ and xs HSiMeCl_2 in the presence of $\text{CH}_2=\text{CHC}_6\text{H}_{13}$ and arene (arene = *tol*, *o*-*xy*l, *m*-*xy*l, *p*-*xy*l, *mes*, *anisole*).¹⁹⁰

¹¹³ Reaction pathway must involve the equivalent of elimination of HCl from the metal center.¹⁹⁰ ¹¹⁴ Compound **3-100** was insufficiently soluble to obtain ²⁹Si NMR data.¹⁹⁰ ¹¹⁵ Isolated as a solid mixture. Spectroscopic data were reported for the mixture.¹⁹⁰ ¹¹⁶ Incompletely identified and characterized only in solution.¹⁹¹ ¹¹⁷ Additional derivatives, R = OEt, Ph.^{48a} ¹¹⁸ $T_1 = 593$ ms.^{48a} ¹¹⁹ Additional derivative prepared (Xantsil)(H)(CO)Ru{SiMe₂...OMe...SiMe₂}(X-ray).^{193b} ¹²⁰ Additional derivative, $x = 2$.¹⁹⁴ ¹²¹ *Syn/anti* = 4.5:1 at 295 K; 3.6:1 at 318 K.^{195a} *Syn*-isomer previously reported from $\text{Ru}_3(\text{CO})_{12} + \text{biPSiH}$.¹⁹⁴ ¹²² Reaction process involves oxidative addition of the silane and replacement of the 2 PPh₃ ligands by the 2 tethered phosphines of the silane.^{195a} ¹²³ *Anti*-isomer.^{195a} ¹²⁴ Not isolated.¹⁹⁷ ¹²⁵ Two additional derivatives prepared by route "b": (OC)(Ph₃P)₂ClRuSiMePh₂ and (OC)(Ph₃P)₂ClRuSiEt₃.¹⁹⁹ ¹²⁶ Process most likely involves elimination of R'CH=CHR₂ after oxidative addition of the silane.¹⁹⁹ ¹²⁷ Formed as a mixture of **3-111**, **3-112**, and **3-143**. **3-111** is maximized when the reaction is conducted in benzene at 70 °C for 18 h. **3-112** is maximized when the reaction is conducted in benzene at 80 °C for 24 h. **3-143** is isolated as a second crop of crystals after **3-112** is isolated.²⁰¹ ¹²⁸ *Syn*-diastereomer.²⁰⁴

¹²⁹ Additional derivative prepared from $(\text{PMe}_3)_4\text{RuMe}_2$ and excess $\text{HSiMe}_2\text{CH}_2\text{SiMe}_3$.⁹⁷ ¹³⁰ Determined from ¹H{³¹P} data.²⁰⁵ ¹³¹ Additional derivatives prepared from reaction of $(\text{PMe}_3)_4\text{Ru}(\text{SiMe}_3)\text{H}$ and $\text{HSiMe}_2\text{CH}_2\text{SiMe}_3$ and HSiEt_3 .⁹⁷ ¹³² Unpublished neutron diffraction study is also indicated.⁹⁷

¹³³ Data reported for ³¹P decoupled spectrum.⁴⁹ ¹³⁴ Observed only in solution mixed with starting complex and $(\text{Me}_3\text{P})_3\text{Ru}(\text{CH}_2\text{SiMe}_2)(\text{H})$.⁴⁹ ¹³⁵ Reaction process could involve exchange of MCl and SiH to give MH and SiCl (see section 3.7) followed by oxidative addition of HSiMeCl_2 . This could also be viewed as oxidative addition of the silane followed by elimination of MeSiCl_3 .²⁰⁶ ¹³⁶ Complex can also be prepared starting with RuHClL_3 or RuH_2L_4 (L = PPh₃).²⁰⁶ ¹³⁷ $T_{\text{min}} = 32$ ms (**3-60a**); fast exchange from 199 to 293 K.^{207a} ¹³⁸ ²⁹Si measurement was both proton and phosphorous decoupled. **3-125a** undergoes fast exchange from 199 to 293 K. T_{min} for **3-125c** was 29 s for the downfield signal at 253 K.^{207a} ¹³⁹ Signal coalescence at 20 °C.^{207a} ¹⁴⁰ ²⁹Si{¹H}{³¹P} data. Coupling constants were determined from the ²⁹Si{³¹P} spectrum.^{207a} ¹⁴¹ The reaction (NMR scale) of $(\text{Cy}_3\text{P})_2(\eta^2\text{-H}_2)(\text{Cl})\text{RuH}^+$ with D₂ gave $(\text{Cy}_3\text{P})_2(\eta^2\text{-D}_2)(\text{Cl})\text{RuD}$, which was then reacted with HSiMeCl_2 to give $(\text{Cy}_3\text{P})_2(\eta^2\text{-HD})(\text{Cl})\text{RuSiMeCl}_2$ (also conducted with HSiMe_2Cl and HSiCl_3). The observed J_{HD} value was 17.5 Hz (12.0 and 18.9 Hz).^{207b} ¹⁴² Additional derivatives, X = $-(\text{CH}_2)_2-$ (X-ray); $-(\text{CH}_2)_3-$; $-(\text{OSiMe}_2\text{O})-$ (X-ray).²⁰⁸ ¹⁴³ Additional derivative, $[\text{RuH}_2\{\eta^2\text{-HSiPh}_2\text{O}\}(\text{PCy}_3)_2]$, $[\text{RuH}_2\{\eta^2\text{-HSiMe}_2\text{O}\}(\text{PCy}_3)_2]$ (X = $-\text{CH}_2\text{CH}_2-$, $-\text{CH}_2\text{CH}_2\text{CH}_2-$, $-\text{Me}_2\text{SiOSiMe}_2\text{OSiMe}_2-$).²⁰⁸ ¹⁴⁴ **3-129** was reported previously.^{210a} ¹⁴⁵ ²⁹Si{³¹P} INEPT.^{210a} ¹⁴⁶ See structure section of Table 3 for proposed structures for **3-130b**.^{211b} ¹⁴⁷ Additional derivative, X = $-\text{CH}_2\text{CH}_2-$. Derivative with PPh₃, X = CH_2CH_2 (X-ray), also reported.²⁰⁸

¹⁴⁷ Additional derivative, X = $-\text{CH}_2\text{CH}_2-$ (X-ray).²⁰⁸ ¹⁴⁸ See structure section of Table 3. Average structure proposed for $[\text{RuH}][(\equiv\text{SiO})(\text{Me})_2\text{Si}-\text{Ru}(\text{H})_x(\equiv\text{SiOSi})_2]$.^{213d} ¹⁴⁹ TTF = tetrathiafulvalene.^{213e} ¹⁵⁰ $[\text{Cp}^*\text{Ru}(\mu\text{-SiPh}_2)(\mu\text{-H})_2]$ was removed by formation of insoluble $[\text{Cp}^*\text{Ru}(\mu\text{-}\eta^2\text{-HSiPh}_2)_2(\mu\text{-H})(\text{H})]$.⁹⁸ $[\text{Cp}^*\text{Ru}(\mu\text{-SiPh}_2)(\mu\text{-H})_2]$ has previously been prepared from $\text{Cp}^*\text{Ru}(\mu\text{-H})_4\text{RuCp}^*$ and Ph_2SiH_2 .⁹⁸ ¹⁵¹ Isolated as a mixture of *syn*- and *anti*-forms.⁹⁸ ¹⁵² Additional derivatives: **3-137b** and also complexes from $[\text{BuC}_5\text{H}_4\text{SiR}^+\text{MeH}]$ (R' = Ph, CH₂Ph).^{155c} ¹⁵³ Additional derivative prepared from VinSiPhMeH . Deuterated analogues prepared from reaction of DSiMe_2Vin with $\text{Cp}^*\text{Ru}(\mu\text{-H})_4\text{RuCp}^*$ to give **3-138** with *H/D* (hydride region) = 47/53 and with $\text{Cp}^*\text{Ru}(\mu\text{-D})_4\text{RuCp}^*$ to give **3-138**, *H/D* (hydride region) = 86/14.²¹⁴ ¹⁵⁴ Data collected at 23 °C.²¹⁴ ¹⁵⁵ Data collected at -70 °C.²¹⁴ ¹⁵⁶ Complex also generated from DSiMe_2Ph .²¹⁵ ¹⁵⁷ Additional derivatives, R = Me, R' = Ph, Ph = 1,4- C_6H_4 ; R = R' = Me, Ph = 1,4- C_6H_4 .²¹⁶ ¹⁵⁸ $M_w = 15\,000$; $P_D = 2.5$.²¹⁶ ¹⁵⁹ The ²⁹Si{INEPT}{¹HOMe}{³¹P} spectrum shows a nonet.¹⁰¹ ¹⁶⁰ ³¹P{¹H}{²⁹Si} NMR data also collected.¹⁰¹ ¹⁶¹ Also obtained from $\text{Xantsil-H}_2 + [\text{Ru}_3(\text{CO})_{10}(\text{NCMe})_2]$.^{177b} ¹⁶² **3-104** and **3-144b** are formed as co-crystals.^{177b} ¹⁶³ Additional derivatives, $\text{SiR}_3 = \text{Et}_3\text{Si}$, $(\text{PhCH}_2)_2\text{Me}_2\text{Si}$.²¹⁸ ¹⁶⁴ GCMS showed the presence of ClSiEt_3 , $\text{CH}_2=\text{CH}^t\text{Bu}$, SiEt_4 , and PPr_3 .²¹⁷ ¹⁶⁵ Additional derivatives, $-\text{Si}(\text{CH}_2\text{CH}=\text{CH}_2)_2\text{Me}_2$, SiPh_3 , SiHPh_2 (Table 2), SiH_2Ph (Table 1).⁵² ¹⁶⁶ Mixture contains 3 of the 6 possible isomers: (a) *cis*-CO's, *trans*-PPh₃'s (5 pts); (b) *cis*-CO's, *cis*-PPh₃'s (5 pts); (c) *cis*-PPh₃'s, *trans*-CO's (1 pt).²²¹ ¹⁶⁷ Proton *trans* to CO.²²² ¹⁶⁸ Additional derivative, R = Ph.²²² ¹⁶⁹ Additional derivative prepared from $(\text{OC})(\text{Ph}_3\text{P})_2(\text{Me}_2\text{NCS}_2)\text{OsH} + \text{HSiMeCl}_2$.²²³ ¹⁷⁰ Additional derivative, $(\text{OC})(\text{Ph}_3\text{P})_2\text{ClOsSi}\{\text{OCH}_2\text{CH}_2\}_3\text{N}$.²²⁵ ¹⁷¹ Mixture of **3-158** and **3-159** are formed. **3-158** is maximized when the reaction is conducted in benzene at 75 °C for 21 h. **3-159** is maximized when the reaction is conducted in benzene at 90 °C for 24 h.²⁰¹ ¹⁷² Initial products: $\text{H}_3\text{Os}_3(\text{CO})_{10}(\text{SiEt}_3)$ (79%), $\text{H}_3\text{Os}_3(\text{CO})_9(\text{SiEt}_3)$ (4.5%). After 2 days at room temperature, ¹H resonances for $\text{H}_2\text{Os}_3(\text{CO})_{10}(\text{SiEt}_3)_2$, -16.83 ppm (d), -17.57 ppm (d), $\text{H}_3\text{Os}_3(\text{CO})_9(\text{SiEt}_3)_3$, -16.18 ppm, $\text{H}_2\text{Os}_3(\text{CO})_{10}(\text{SiEt}_3)_2$, $\text{H}_2\text{Os}_3(\text{CO})_{10}$, and $\text{H}_2\text{Os}_3(\text{CO})_9(\text{SiEt}_3)$ were present.²²⁶ ¹⁷³ Related derivatives prepared from reaction of $\text{Os}_3(\mu\text{-H})\{\mu_3\text{-Ph}_2\text{PCH}_2\text{PPh}(\text{C}_6\text{H}_4)\}(\text{CO})_8$ with HSiEt_3 and HSiEtMe_2 . VT-NMR collected for the SiEt_3 analog.²²⁷ ¹⁷⁴ For additional derivatives, see **1-53**, **2-51**. Related compounds were formed from Ph_2GeH_2 , Bu_3SnH , and Ph_2GeH_2 .⁵⁶ ¹⁷⁵ Studied in solution only. For related derivatives of **3-164b**, see **1-55a** and **1-55b** in Table 1 as well as **2-52b** and **2-52c** in Table 2.^{57c} ¹⁷⁶ Reaction may involve oxidative addition of the silane followed by reductive elimination of $\text{H}(\text{O})\text{OCH}_3$ (observed).²²⁸

¹⁷⁷ ¹H, ¹³C, and IR data agree with published data.²²⁸ ¹⁷⁸ Identified in solution. Additional products included $\text{Ph}_2\text{Ge}[\text{Co}(\text{CO})_4]_2$ and $\text{Co}_4(\text{CO})_{12}$.²²⁹

¹⁷⁹ **3-167** was also prepared from reaction of $\text{Co}_2(\text{CO})_8$ with $\text{Ph}_3\text{SiSiPh}_2\text{H}$, $\text{HPh}_2\text{SiSiPh}_2\text{H}$, $\text{Ph}_3\text{GeSiPh}_2\text{H}$, or $\text{Ph}_3\text{SiSiPhMe}_2\text{H}$.²²⁹ ¹⁸⁰ Additional derivative prepared from HSiEt_3 .^{230b} ¹⁸¹ Product assumed from the reduction of $[\text{tripodcoCl}]$ with KC_8 in situ.^{230b} ¹⁸² Additional derivative with R = Cl.²³²

¹⁸³ Additional derivative, R = Et. Deuterium analogue of **3-171** (from Si-D) also prepared.²³¹ ¹⁸⁴ Previously reported from reaction of $\text{Co}_2(\text{CO})_8 + \text{HMe}_2\text{SiSiMe}_2\text{H}$ [Pakkanen, T.; Kerber, R. C. *Inorg. Chim. Acta* **1981**, 49, 47–52; Kerber, R. C.; Pakkanen, T. *Inorg. Chim. Acta* **1979**, 37, 61–65], but neither the structure nor the ²⁹Si NMR data were reported.²³³ ¹⁸⁵ Cp-MAS.²³⁵ ¹⁸⁶ Additional derivatives with $\text{C}_5\text{H}_4\text{Me}$ and C_5Me_5 .²³⁶ ¹⁸⁷ Additional derivative with HSiEt_3 .²³⁷ ¹⁸⁸ Additional derivatives were prepared from HSiMe_2Et , HSiMeEt_2 , $\text{HSi}(\text{OMe})_3$, and HSiEt_3 . See also Table 2, **2-57a**. Also, the same series of silanes was reacted with $\text{Cp}(\text{Ph}_3\text{P})\text{Rh}(\eta^2\text{-C}_2\text{H}_4)$ as well as $(\text{C}_5\text{H}_4\text{CF}_3)(\text{Me}_3\text{P})\text{Rh}(\eta^2\text{-C}_2\text{H}_4)$ to give $\text{Cp}(\text{Ph}_3\text{P})(\text{H})\text{RhSiR}_3$ and $(\text{C}_5\text{H}_4\text{CF}_3)(\text{Me}_3\text{P})(\text{H})\text{RhSiR}_3$, respectively.¹⁰⁶ ¹⁸⁹ Observed only in solution. Additional examples from reaction of $\text{CpRh}(\text{C}_2\text{H}_3\text{CO}_2\text{Bu})_2$ with HSiMe_3 , HSiEt_2H , $\text{HSi}(\text{OMe})_3$, and HSiMe_2Cl .²³⁸ ¹⁹⁰ Thermally sensitive, stored at -30 °C. Also prepared by reaction of $[\text{Cp}^*(\text{Me}_3\text{P})(\text{ClCH}_2\text{Cl})\text{RhMe}][\text{BAR}'_4]$ with HSiPh_3 followed by addition of MeCN at -40 °C.²³⁸ ¹⁹¹ Observed only in solution. Attempts to isolate solid material gave decomposition products. Analogues of **3-181a** and **3-181b** were also reported from reaction of HSiMe_3 . Also reported was the SiPh_3 analogue of **3-181b**.²³⁹

¹⁹² With excess Ph_3SiH , the reaction with $[\text{Cp}^*(\text{Me}_3\text{P})(\text{Me})\text{Rh}(\text{ClCH}_2\text{Cl})][\text{BAR}'_4]$ produced $[\text{Cp}^*(\text{PMe}_3)(\text{H})_2\text{Rh}(\text{SiPh}_3)][\text{BAR}'_4]$, which was also formulated in the nonclassical form, $[\text{Cp}^*(\text{PMe}_3)(\text{H})\text{Rh}(\eta^2\text{-HSiPh}_3)][\text{BAR}'_4]$.²³⁹ ¹⁹³ Reaction was conducted in CD_2Cl_2 ; thus, solvent exchange at the metal center also occurred.²³⁹ ¹⁹⁴ Orthometallation of **3-182a** and reductive elimination of SiH occurred prior to or with displacement of solvent.²³⁹ ¹⁹⁵ **3-182a** was the only observable species in solution. Estimated yield of **3-182b** was 90% by NMR.²³⁹ ¹⁹⁶ **3-183** was characterized in solution. Additional derivative with $\text{HSiMe}(\text{OMe})_2$.²⁴⁰ ¹⁹⁷ Not isolated; yield given based on NMR spectroscopy.²⁴¹ ¹⁹⁸ **3-184** was also generated from $\text{FRh}(\text{PET}_3)_3$.²⁴¹ ¹⁹⁹ In solution, *mer*-($\text{Me}_3\text{P})_3\text{Cl}(\text{H})\text{RhSiPh}_3$ and HSiPh_3 observed. Complex favored at lower temperature.²⁴² ²⁰⁰ Additional derivative with HSiPh_3 and $\text{HSi}(\text{OEt})_3$.²⁴⁰

²⁰¹ If reaction run on 1:1 (or 2:1) stoichiometry compounds, *mer*-($\text{Me}_3\text{P})_3\text{Cl}(\text{H})\text{Rh}(\text{SiAr}_3)$ (20% by NMR) and *fac*-($\text{Me}_3\text{P})_3(\text{H})_2\text{Rh}(\text{SiAr}_3)$ (33% by NMR) were formed. If reaction run on 3:1 ratio (Si/Rh), then by NMR 11% of *mer*-($\text{Me}_3\text{P})_3\text{Cl}(\text{H})\text{Rh}(\text{SiAr}_3)$, 78% of *fac*-($\text{Me}_3\text{P})_3(\text{H})_2\text{Rh}(\text{SiAr}_3)$, and 12% of $(\text{Me}_3\text{P})(\text{Cl})_2\text{Rh}(\text{H})_2$ were observed.²⁴³ ²⁰² Previously reported and prepared by thermolysis of *mer*-($\text{Me}_3\text{P})_3\text{Cl}(\text{H})\text{RhSiPh}_2\text{H}$ with *fac*-($\text{Me}_3\text{P})_3\text{Cl}(\text{H})\text{RhSiPh}_2\text{Cl}$ as co-product (refs 108 and 244). Major product in reaction is **3-218**.²⁰³ Byproduct from reaction was *fac*-($\text{Me}_3\text{P})_3(\text{H})_2\text{RhSi}(\text{OEt})_3$. Additional derivatives from reaction of $\text{HSiMe}(\text{OMe})_2$ with $\text{MeRh}(\text{PMe}_3)_4$ or $\text{PhRh}(\text{PMe}_3)_4$ with $\text{HSi}(\text{OMe})_3$.²⁴⁰ ²⁰⁴ Exact yield not given but stated as ~90–95%.²⁴⁰ ²⁰⁵ Additional derivative with Ar = *p*- MeC_6H_4 (X-ray). Reductive elimination of Ph_3SiH occurs in solution. Et_3SiH does not react.¹⁰⁹ ²⁰⁶ Additional derivative with Ar = C_6H_4 -*p*-Me.¹⁰⁹ ²⁰⁷ Additional derivatives with Ar = C_6H_4 -*p*-OMe and C_6H_4 -*p*-Me.¹⁰⁹ ²⁰⁸ Competition for Si–H vs. Si–S addition noted. Additional product observed, $(\text{PP}_2)\text{RhSEt}$ (ratio 1:4 favoring Rh–Si product).²⁴⁵ ²⁰⁹ Related complex, $[\text{PNP}]\text{Rh}(\text{COD})$, was prepared from $(\text{COD})\text{Rh}(\text{CH}_2\text{Ph})$ and H[PSiP] .^{213a} ²¹⁰ **3-155** was not isolated.²⁴⁷ ²¹¹ Not isolated, thermally unstable. After 20 h, a solution of $(\text{Me}_3\text{P})_2(\text{H})\text{Rh}(\text{SiMe}_2\text{Ph})[\text{SiMe}_2(\text{CH}_2)_2\text{PPh}_2]$ and PhMe_2SiH decomposed at room temperature (rt) to give $(\text{Me}_3\text{P})_2(\text{H})_2\text{Rh}[\text{SiMe}_2(\text{CH}_2)_2\text{PPh}_2]$ and $(\text{Me}_2\text{PhSi})_2$, each in 91% yield. Also prepared by reaction of $(\text{Me}_3\text{P})_2\text{Rh}[\text{SiMe}_2(\text{CH}_2)_2\text{PPh}_2]$ with 5 PhMe_2SiH .²⁴⁶

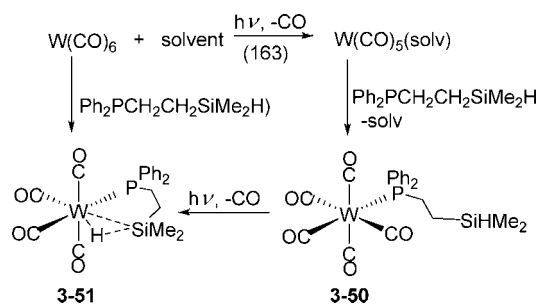
²¹² Quantitative by NMR spectroscopy.²⁴⁶ ²¹³ **3-199b** was not isolated due to facile elimination of H_2 .^{247b} ²¹⁴ From $(\text{Ph}_3\text{P})_3\text{RhH}$, the ratio of **3-199c** to **3-199d** after 6 h at 50 °C was 9:1. From $(\text{Ph}_3\text{P})_3\text{RhCl}$ at benzene reflux, the ratio of **3-199c** to **3-199d** was 2:7 after 1 h. Reaction of **3-199c** with 10 equiv of *o*-($\text{HMe}_2\text{Si})_2\text{C}_6\text{H}_4$ gave a 1:7 mixture of **3-199c**/**3-199d** after 1 h. **3-199c** but not **3-199d** could be isolated in pure form.^{247b} ²¹⁵ Characterized in solution only.²⁴⁸

Table 3z. Continued

²¹⁶ [(¹Pr₃P)₂ClRh(H)₂] also generated. Both species formed after 2 min. After 8 h, dinuclear species [(L)(H)₂Rh](μ-SiR₃)₂ was generated.^{249 217} Not isolated. Additional derivatives with MeEt₂SiH, Me₂EtSiH, and MePh₂SiH.^{250 218} Not isolated, decomposed within 30 min. Additional derivatives generated with Et₂MeSiH, Ph₂MeSiH, and EtMe₂SiH.^{251 219} Additional derivatives with HSiMe₂OSiMe₃, HSi(OEt)₂Me, and HSi(OEt)Me₂.^{252 220} Formed as mixture with P(Ar)₃, which was too soluble to isolate complex in pure form.^{253 221} **3-211** was observed in solution only.^{254a 222} Reaction of (NSiN)Rh(COD) + HSiPh₃ gave (NSiN)Rh(C₆H₁₃)SiPh₃, which was studied only in solution.^{254a 223} Oxidative addition of the hydrosilane followed by RhH addition to COD.^{254a 224} Other silanes did not provide the related derivative, (PyInd)(H)₂Rh(SiR₃)₂.^{255 225} Formed after 8 h.^{249 226} **3-215a** and **3-215b** were not isolated. Continued photolysis of **3-215a/3-215b** produced [CH₂(η⁵-C₅H₄)][HRh(C₂H₄)(SiEt₃)₂][CH₂(η⁵-C₅H₄)][CH₂(η⁵-C₅H₄)₂][CH₂(η⁵-C₅H₄)₂][HRu(μ-SiEt₂)₂], and [CH₂(η⁵-C₅H₄)₂][CH₂(η⁵-C₅H₄)₂][HRu(μ-SiEt₂)₂], all of which were characterized spectroscopically. Exhaustive photolysis gave [CH₂(η⁵-C₅H₄)₂][HRu(μ-SiEt₂)₂] (71%) and [CH₂(η⁵-C₅H₄)₂][HRu(μ-SiEt₂)₂] (neither was isolated). Analogues of **3-215a** and **3-215b** were prepared from HSiMe₃ and [CH₂(η⁵-C₅H₄)₂][Rh(C₂H₄)₂] and exhaustive photolysis gave [CH₂(η⁵-C₅H₄)₂][(Rh(SiMe₃))(RhH)(μ-SiMe₂)₂].^{115 227} Additional derivatives with Ar_{3-n}Ph_nSiH: *n* = 1 or 2, Ar = C₆H₄-*p*-F; *n* = 0, Ar = C₆H₄-*p*-CF₃¹³⁰ and Ar = C₆H₄-4-CH₃ (not isolated). When [L(H)RhSiPh₃]₂(μ-H)(μ-Cl) was treated with 4 equiv of HSiAr₃ (Ar = C₆H₄Me-*p*), [L(H)RhSiAr₃]₂(μ-H)(μ-Cl) (12 pts) and [L(H)SiAr₃Rh](μ-H)(μ-Cl)[RhH(SiPh₃)₂] (44 pts) and **3-216** (44 pts) formed.^{256 228} X-ray structure of [L(H)RhSiPh₃]₂(μ-H)(μ-Cl) (L = P(¹Pr)₃) reported in ref 256. ²²⁹ AAA' part of AA'MM'XX' pattern.^{256 230} Additional derivative with Ar = C₆H₄-*p*-Me. After 12 h, ClSi(CH₂Ph)₃ was observed.^{249 231} Isolated as 0.5 C₇H₈ solvate. Additional derivative with Ar = C₆H₅ (X-ray²⁴⁴). In addition, *mer*-(Me₂P)₃(H)₂RhSiAr₃Cl isolated in 5% yield (previously reported, see ref 108).^{258 232} As THF solvate.^{258 233} Additional product, (tmp)RhSiPhMeH was formed in 28% yield. Additional derivatives prepared from reaction of (tmp)RhCl or (tmp)RhI with HSiEt₃, HSi(OEt)₃, HSi¹Pr₃, HSiBnMe₂, HSiPhMe₂, and HSi¹BuMe₂ as well as from (tmp)RhCl with HSiEt₃, HSiBnMe₂, and HSiPhMe₂. The reactions of (por)RhMe with HSiEt₃, HSi(OEt)₃, HSiBnMe₂, HSiPhMe₂, and HSiPh₂Me also give the silyl-rhodium complexes, (por)RhSiR₃.^{62 234} Most likely, the reaction involves oxidative addition of the silane followed by elimination of HCl.^{62 235} Displacement of coordinated acetonitrile.^{254a 236} Additional derivatives with L = PMe₂Ph, PMePh₂, and PPh₃.^{259 237} The X-ray crystal structure of a related derivative, Cp*(Me₂P)(Ph)Ir(SiPh₂OTf), was reported in ref 117a.²³⁸ Sample was >95% **3-223**. Attempts to obtain a solid were unsuccessful.^{117a} X-ray quality crystals of **3-225** were obtained from CH₂Cl₂ at -35 °C.^{117a 240} Three inequivalent *tert*-butyl thiolato groups were observed at rt by ¹H NMR spectroscopy. Attempts to observe equilibration of these resonances at 60 °C resulted in decomposition.^{117a 241} Overall the reaction involves OA of the silane and displacement of OTf⁻ by a *S*Bu substituent at silicon.^{117a 242} Additional derivative with (HSiEt₂)(C₂B₁₀H₁₁).^{172 243} Additional derivative with (HSiEt₂)(C₂B₁₀H₁₁).^{172 244} Complexes **3-230** and **3-231** both formed in the reaction in a ratio of 1:1.5.^{172 245} Crystals obtained for X-ray crystal structural analysis were poor quality, but data established four-legged piano-stool geometry.^{172 246} Complexes **3-230** and **3-231** were both formed in the reaction in a ratio of 1:1.5.^{172 247} When the reaction of [Cp¹IrCl(Cl)(μ-Cl)]₂ + *xs* HSiEt₃ was conducted at -40 °C, a mixture of Cp¹(H)₂IrCl(SiEt₃), Cp¹(H)Ir(Cl)SiEt₃, and [Cp¹IrCl]₂(μ-H)(μ-Cl) in 60%, 20%, and 20%, respectively, was observed. Chromatographic separation of the mixture provided Cp¹(H)Ir(Cl)SiEt₃ in 18% yield. When **3-232** was heated in C₆D₆ for 1 day, **3-232-d₃** was obtained, and heating a sample for 9 days provided **3-232-d₇**.^{260 248} Reaction likely proceeds by a sequence of steps involving repetitive oxidative addition of the silane to the monomer and reductive elimination of ClSiR₃.^{260 249} Also prepared from reaction of *trans*-(Ph₃P)₂Ir(CO)Me with *xs* HSi(¹Pr)₂OH. A related complex, (OC)(Ph₃P)₂(H)₂Ir[Si(¹Bu)₂OH] (characterized in solution only), was formed from a similar reaction of *xs* HSi(¹Bu)₂OH with *trans*-(Ph₃P)₂Ir(CO)Me.^{248 250} Isolated as mono-CH₂Cl₂ solvate. Additional isomer observed with H *trans* to CO.^{194 251} Reaction involves exchange of phosphines at the metal center.^{261a 252} Z-HMe₂SiCH=CH-CH=CH₂ also gave a similar complex with retention of the Z-configuration.^{261c 253} When **3-237c** was dissolved in acetone, isomerization occurred to give (Me₂P)₃(H)(Cl)Me₂SiRCH=CMe-CMe=CH₂ (*fac* isomer; X-ray).^{261c} The Z-isomer of HMe₂SiCH=CMe-CMe=CH₂ gave the *mer*-Z-isomer of **3-237c**, which rearranged in THF to *fac*-(Me₂P)₃(H)(Cl)Me₂SiRCH=CMe-CMe=CH₂ (X-ray).^{261c 254} (Me₂P)₃(η²-C₈H₁₄)IrMe + HMe₂SiCH=CMe-CMe=CH₂ (Z-isomer) gave the *fac*-Z-isomer of **3-237e**. See structure in structure section for Table 3.^{261c 255} Additional derivative with R = Et.^{60b 256} Additional derivatives from HSiEt₃ and HSiPh₃. Reaction of **3-241** with *xs* HSi(OMe)₃ results in reductive elimination of (MeO)₃SiSi(OMe)₃.^{263 257} Reaction may involve OA of silane and elimination of HSC₄H₉.^{264 258} Reaction performed in sealed ampule at 80 °C for 24 h (quantitative yield, isolated yield >90%).^{264 259} Additional derivatives prepared from K[PyInd] + 0.5[(COE)₂IrCl]₂ + 2R₃SiH (R₃ = Et₃, Me₂Ph, Ph₃).^{255 260} Quantitative by NMR spectroscopy, isolated 87% as single diastereomer.^{265 261} Additional derivatives may be found in Tables 1 and 2. Reaction of (NSiN)Ir(H)(OTf)(coe) with HSi(OSiMe₃)₃ in benzene produced [NSiN]Ir(Si(OSiMe₃)₃(OTf))_n and in acetonitrile, [NSiN]Ir(Si(OSiMe₃)₃(NCMe)₂). Reaction of (NSiN)Ir(H)(OTf)(coe) and HSiEt₃ produced [NSiN]Ir(SiEt₃(NCMe)₂).^{57d 262} Related derivative formed from HSiBnMe₂ (X-ray). Additional examples may be found in Tables 1 and 2.^{62b 263} O₂CQuin = quinoline-2-carboxylate. Three other related carboxylate complexes, (O₂C)Pic, O₂Clsoq, and (O₂C)Pyraz), were studied in solution. The reaction was reversible, and isolation of the O₂CQuin example occurred only in the presence of excess Ph₃SiH.^{266b 264} [C¹N] is the carbene ligand, [N-*n*-butyl-N'-(2-pyridylmethyl)-4,5-dichloroimidazole-2-ylidene]. Additional derivative prepared from chloro[N-*n*-butyl-N'-(2-pyridylmethyl)imidazole-2-ylidene](1,5-cyclooctadiene)iridium(I) and HSiMe₂Ph.^{267 265} Intermediate [(Ph₃P)₂Ni(H)Si(OEt)₃] was not observed. However, in the reaction of [Ni(PPh₃)₂(η²-CH₂=CHPh)] with 1 equiv of HSiMe₂OSiMe₂OSiMe₃ showed the presence of [(Ph₃P)₂Ni(H)SiMe₂OSiMe₂OSiMe₃] as indicated by a ¹H resonance at -15.9 ppm. Addition of a second equivalent provided [(Ph₃P)₂Ni(SiMe₂OSiMe₂OSiMe₃)₂], although experimental details were not provided.^{270 266} Additional derivative prepared from HSiPh₂Me. See also **2-77** in Table 2 and accompanying footnote.^{271 267} Additional derivative from DSiPh₃.^{274 268} Additional derivative from DSiPh₃ (isolated); HSiPh₂Me, DSiPh₂Me, HSiPhMe₂, and HSiEt₃ (latter four observed in solution). VT and KIE experiments also performed.^{274 269} *Cis* and *trans* isomers formed. Ratio of *trans/cis* 2/1. Additional derivatives with R = OEt (60% *cis* only).^{275 270} *cis*-Isomer only.^{276a 271} (PN) = {1-[(R)-1,2-(diphenylphosphino-κP)ferrocenyl]ethyl}-3-phenyl-5-methyl-1H-pyrazole-κN}. Additional derivatives with one Me group in (PN) replaced by Me{1-[(R)-1,2-(diphenylphosphino-κP)ferrocenyl]ethyl}-3,5-dimethyl-1H-pyrazole-κN} and with two Me groups replaced by H; mesityl (X-ray) {1-[(R)-1-[(S)-2-(diphenylphosphino-κP)ferrocenyl]ethyl}-3-(2,4,6-trimethylphenyl)-1H-pyrazole-κN}.^{277 272} Reaction probably involves OA of the silane and reductive elimination of HCl.^{277 273} Not isolated. Decomposed when warmed to room temperature to give Et₃SiCl and Et₃SiOSiEt₃. Presumed (η²-H-Si) could be Pd(IV) silyl hydride.^{278 274} Reaction involves displacement of a coordinated methoxypropyl group of the 1,4-bis(methoxypropyl)-2,3-dimethyl-1,4-diazabutadiene ligand and OA of the silane.^{278 275} Deuterium analogues of **3-260a** and **3-260b** were also reported.^{279 276} Resonance does not exhibit Pt satellites at reasonable positions. The deuterium analogue exhibits signals at 2.15 ppm (²J_{PD} = 10 Hz) and 0.41 (¹J_{PD} = 106 Hz), the latter of which shows that Si-D-Pt bonding is present. Complex **3-260b** is fluxional.^{279 277} The K_e for 2(dmpe)Pd(SiPh₂H)₂ = {Pd(dmpe)₂(μ-SiPh₂)₂} + H₂SiPh₂ at 60 °C was 0.14.^{120b 278} Additional derivatives with Ar = C₆H₄-4-F, C₆H₄-4-Cl (X-ray). Complex formed from reductive elimination of HSiR₃ from (P₃P)₂Cl(H)RhSiAr₃ followed by oxidative addition of HSiR₃ to (Et₃P)₂Pt.^{280 279} Additional derivative with X = I.^{130 280} Compound could not be isolated in pure form.^{281 281} Prepared previously by salt elimination reaction involving (PhMe₂P)₂PtCl₂ with 2LiSiMePh₂; reports X-ray structure and VT-NMR (³¹P). Fluxional behavior is observed by NMR spectroscopy, which is attributed to a unimolecular twist-rotation via a pseudotetrahedral transition state.^{282a,b 282} Additional derivatives with R₃P = Ph₂MeP and Et₃P. Exchange reactions of (Ph₂PCH₂CH₂SiMe₂)Pt(PPh₃)(SiPh₃) with HSi(OMe)₃ were also reported and characterized by ³¹P NMR spectroscopy in solution only. Only exchange of the SiPh₃ group occurred.^{128 283} Rate of exchange of silyl groups correlates with the cone angle at phosphorus and decreases in the order PMePh₂ > PET₃ > PMe₂Ph. No exchange was observed with *trans*-(PhMe₂P)₂Pt(SiMe₂Ph)₂ and *xs* HSi(OMe)₃ or *xs* HMe₂Si-SiPh₃.^{283 284} Additional derivative: PtH{(PhSCH₂)₃Si}(PPh₃)₂.^{284b 285} By the same method, *cis*-(Ph₃P)₂Pt(SiMe₂H)₂ was prepared from HMe₂SiSiMe₂H (X-ray).^{284c 286} Additional derivatives with Me(Ph₂PCH₂CH₂)₂SiH and Ph(Cy₂PCH₂CH₂)₂SiH.^{194 287} Additional derivatives with Me(Cy₂P(CH₂)₃)SiH and Ph(Ph₂P(CH₂)₃)SiH.^{194 288} Additional derivatives with R = Me, Cy and R₃SiH = 1,2-(HMe₂Si)₂C₆H₄. Partially exchanged complexes not observed.^{283 289} Also prepared from reaction of (Ph₃P)₂Pt(η²-C₂H₄) with 2,3-(1,1,4,4-tetramethyldisilane)diylcarborane in 92% yield.^{285,286 290} Related derivative of **3-276a** was prepared from (Et₃P)₂Pt + HSiMe₂SiOSiMe₂OSiMe₂H (X-ray), but the ring closed platinumacycle analogous to **3-276b** was not formed.^{288 291} Product formed at -78 °C was *cis*-(Cy₃P)₂Pt(H)(SiCl₂Me), which isomerized to *trans*-**3-277** at room temperature.^{129 292} **3-277** was studied only in solution.¹²⁹

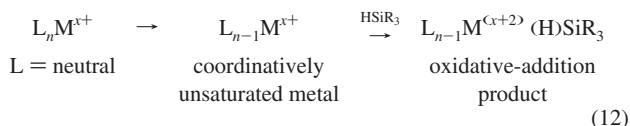
Table 3aa. Continued

²⁹³ Other tertiary silanes reacted with (Cy₃P)₃Pt included SiEt₃, SiMe₂Et, SiMe₂(CH₂CH=CH₂), SiPh₂OSiPh₂H, SiMe₂OSiMe₂H, SiMe(OSiMe₃)₂, SiMe₂OCH₂C(Me)=CH₂, and Si(OMe)₂CH₂CH=CH₂. Reaction of (Cy₃P)₃Pt with secondary silanes may be found in Table 2.^{129–294} Additional derivatives with Ph₃SiH and Ph₂SiH₂, as well as deuterium analogue from Et₃SiD.^{289–295} Additional products observed: [Me₂N(CH₂)₂PPH₂](Pt(Me)H and Ph₂SiMe₂).^{290–296} Characterized in solution only.^{290–297} Characterized in solution only. Additional products observed: immediate formation of MeSiEt₃ followed by [Me₂N(CH₂)₂PPH₂](Me)PtH, which reacted with HSiEt₃ to give **3-283**.^{290–298} Not isolated. Byproducts observed include MeSi(OMe)₃, Si(OMe)₄, and small amounts of [(MeO)₃Si]₂O and H(MeO)₂SiOSi(OMe)₃. Ratio of products changed over time. After 60 h, the ratio of **3-284a** to **3-284b** was 3.4/2.2.^{291–299} Additional derivatives with different PN chelate ligands including Me₂NCH₂PPH₂, Me₂N(CH₂)₂PPH₂, Me₂N(CH₂)₃PPH₂, and *o*-(Ph₂P)C₆H₄(CH₂NMe₂).^{292–300} Also prepared from reaction of 1,2-(HMe₂Si)C₆H₄ with [Me₂N(C₆H₄)PMe₂]₂Pt[OSiMe₂C₆H₄SiMe₂O].^{293–301} Observed in solution.^{294a} The results of the interactions of P,N chelates of Pt with selected silanes were summarized by Schubert in footnote 294.³⁰² *Trans* isomer only. Additional derivative with R = OEt. *Trans* isomer converted to *cis* (X-ray) by reaction with DMAD (dimethyl acetylenedecarboxylate) at 110 °C in 1 h, giving 92% yield.^{275–303} Reaction of Pt(COD)₂ with HMe₂Si(B₁₀C₂H₁₂)PR₂ (R = Me) gives *trans/cis* ratio of 2/1 in 59% yield; R = OEt gives *trans/cis* ratio of 1/1 in 51% yield; R = Ph gave *trans/cis* ratio of 1/6 in 43% yield.^{275–304} Both *cis* and *trans* isomers were structurally characterized by X-ray crystallography and DFT calculations.^{276a–305} Combined yield with *trans*-isomer (ratio of *cis/trans* 6:1).^{276a–306} Unstable at room temperature in solution.^{278–307} [(COD)PtR₂ (R = Me, Ph) did not react with HSi(C₆H₅N₂)Me and (Ph₃P)₂Pt(C₂H₄), Pt(PPH₃)₄, and Pt(dba)₂ reacted to give intractable mixtures.^{276b–308} Analogue of **3-290e** prepared from [Me₂SiPt]₄, (NSiN)Pt(Me)₂.^{276b–309} Additional derivative: (cod)Pt(SiCl₃)₂.^{296–310} A possible reaction sequence could be OA of the silane, and reductive elimination of HCl would give (cod)PtCl(SiMeCl₂). A second OA of silane and reductive elimination would give **3-291**.^{296–311} Also prepared from (a) [Cl₂MeSi(μ-Cl)(η²-cod)Pt]₂ + 2cod; (b) [Me₂ClSi(μ-Cl)(η²-cod)Pt]₂ + HSiMeCl₂.^{296–312} Also prepared by reaction of (Ph₃P)₂Pt(H)[SiMe(CH₂SPh)₂] with [Re(μ-Br)(CO)₃(thf)]₂.^{284a–313} Additional derivative prepared with R = Ph.^{297–314} Additional derivatives with R₃Si = Cl₂MeSi, ClMe₂Si, (EtO)₃Si, PhMe₂Si, Me₂SiOSiMe₂ (none isolated).^{296–315} If **3-297b** is left in solution for a few days at rt, colorless crystals of [(Ph₃P)Pt(μ-SiHMe₂)₂] form (X-ray). [(Ph₃P)Pt(μ-SiHMe₂)₂] was also formed from (Ph₃P)₂Pt(η²-C₂H₄) and H₂SiMe₂. The related complex, [(Ph₃P)Pt(μ-SiHPh₂)₂], was formed from (Ph₃P)₂Pt(η²-C₂H₄) and HSiPh₂SiPh₂H at rt.^{284c–316} Formation of **3-298b** probably occurs due to reaction of the disilene–Pt complex (generated in situ) with adventitious O₂. Satisfactory elemental analyses, NMR data, and an X-ray structure were obtained, but no data were supplied.^{298–317} Additional derivatives with R₃SiH (R = OMe, Ph, Et).^{299–318} X-ray structure not good quality.^{299–319} Related derivative, [Pt₃(SiMe₂fcSiMe₂H)(PEt₃)₂(μ-PPH₂)₃], was prepared similarly from [Pt₃H(PEt₃)₃(μ-PPH₂)₃] + 1,1'-bis(dimethylsilyl)ferrocene.^{300–320} Reaction probably occurs by oxidative addition of HSi followed by elimination of dihydrogen and a phosphine ligand.^{300–321} Related derivative, [(Et₃P)₂(μ-PPH₂)₃Pt₃(SiMe₂fcSiMe₂)Pt₃(PEt₃)₂(μ-PPH₂)₃] (X-ray).^{300–322} SiH resonance at 4.75 ppm (¹J = 183 Hz).^{300–323} ²⁹Si(C₆D₆, 60 °C): −48.7 (SiHg), −30.5 (SiMe₂), −14.8 (SiMe₃).³⁰³

Scheme 3

3.1. Types of Ligands at the Metal and Substituents at Silicon

Hydrosilanes react with a broad range of transition metal complexes. In general, the major pathway is by oxidative addition (OA). For an OA process to take place, the starting metal complex, in most cases that involve an electron-rich metal, forms (promoted thermally or photochemically) an electronically and coordinatively unsaturated species prior to reaction with the silane. Many starting metal complexes contain a mixture of neutral and anionic ligands coordinated to the metal center. A sequence for oxidative addition of the hydrosilane is shown in a simplified form in eq 12. In the case shown, both the hydrogen and silicon of the hydrosilane become bound to the metal center in the final product and the oxidation number of the metal increases by two.



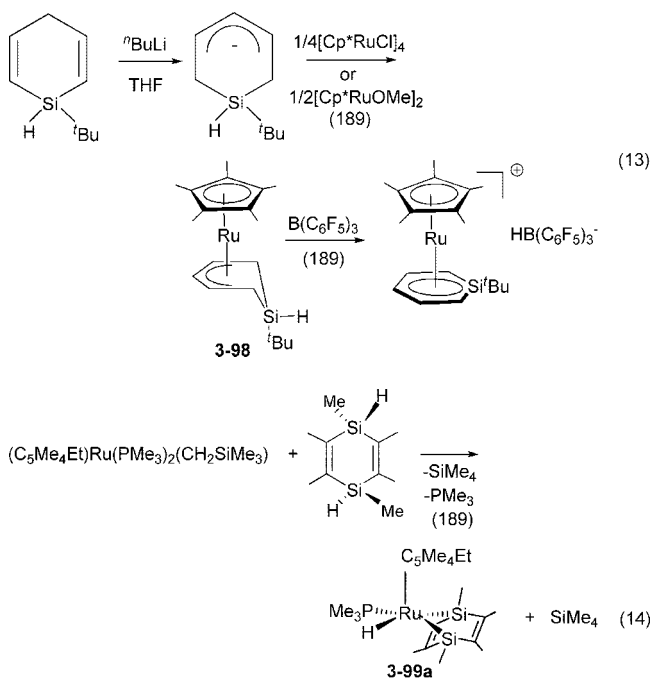
If one or more monoanionic ligands (L = X[−]) are present, subsequent loss of HX may occur and a silyl–metal complex is formed as shown in Path 1 of Scheme 2. This is particularly the case when X = H, R, or Si≡ and leads to the loss of H₂, RH, or HSi≡, respectively, which returns

the metal to the original oxidation state. The most common organic ligands, CH₃[−] and Ph[−], lead to elimination of CH₄ and C₆H₆, respectively. The loss of HSi≡ (when X is Si≡) constitutes a silane exchange reaction. In silane exchange, the Me₃Si group has the obvious advantage of elimination of Me₃SiH, which is a gas at room temperature and thus is easily removed. Although the most common reaction pathway appears to be OA (Path 1), another route is through σ-bond metathesis shown previously as Path 2 in Scheme 2 (section 2). The metathesis pathway requires an empty frontier orbital on the metal center and is most often speculated for reactions of early transition metals and rarely invoked for late transition metals.

For reaction of TM complexes with hydrosilanes, a desirable feature is the presence of a coordinated neutral ligand that may be readily lost from the metal center either during photolysis or in refluxing solvent. The most common precursor complexes thus contain CO or phosphines. However, as will be described in section 3.2, solvated complexes, and those containing unsaturated hydrocarbons (olefins or alkynes) as well as H₂ ligands, have also been employed. A second requirement for the metal center is an oxidation number less than the maximum for the triad (2 less for the most common cases), but the range can include M(0). Approximately 20% of the examples given for Cr through Ni triads in Tables 1, 2, and 3 involve M(0) precursors. Metal carbonyls, M_x(CO)_y, or mixed complexes of the type (OC)_mL_nM (L = a phosphine) from the Cr triad (formation of **1-31**, **2-12** to **2-14**, **2-16**, **2-23**, **2-25** to **2-27**, **3-29**, **3-30ab**, **3-36**, **3-37b**, **3-48** to **3-51**), from the Fe triad (formation of **2-42b**, **3-71** to **3-74**, **3-104**, **3-106**, **3-107**, **3-134g**, **3-137abcd**, **3-140**, **3-141**, **3-144b**, **3-151ab**), and the Co triad (formation of **2-54** to **2-56**, **3-166** to **3-168a**, **3-169** to **3-175**) have been employed as starting complexes. The metal(0) complex precursors are quite common for the Ni triad and are almost exclusively phosphine derivatives or a combination of a phosphine and another neutral ligand (especially olefins) (formation of **1-60**, **1-61**, **1-63** to **1-75**, **1-77** to **1-79**, **2-77**, **2-81**, **2-83**, **2-89**, **2-91** to **2-96f**, **2-98**, **2-100**, **2-101**, **2-103**,

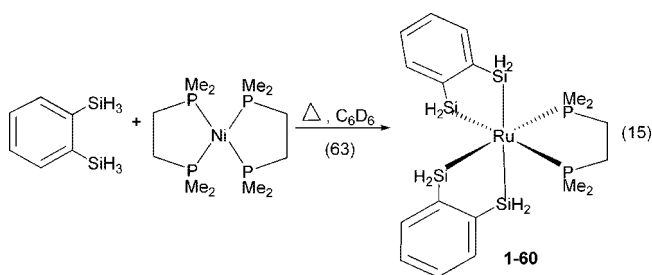
2-104, 2-106, 2-108, 3-248 to 3-251, 3-254 to 3-256a, 3-257a, 3-260ab, 3-261, 3-229abcd, 3-274 to 3-278a, 3-279, 3-287, 3-292, 3-293, 3-295, 3-297). Metal complexes with only olefin ligands are rarely used, although there are two ruthenium examples (formation of 3-131 and 3-133) and three examples in the Ni triad (formation of 3-252, 3-281, 3-288). The most obvious starting point could be the metal itself, however; in this case, the problem would be finding a suitable reaction medium. This can be solved by a gas-phase reaction (formation of 3-70 from Fe_(g)) or in a matrix that includes metal atoms (1-2ab, 1-3abc, 1-5, and 1-7), but in one case reaction with a gold surface (formation of 1-80) has been reported.

The range of hydrosilanes that have been employed in reactions with TM complexes is expanding slowly but is still dominated by those that are either commercially available or prepared from the reduction of commercial chlorosilanes. The common hydrosilanes tend to be Ph_xSiH_{4-x} ($x = 1, 2, 3$), Ph_xMe_{3-x}SiH ($x = 1, 2$), PhMeSiH₂, Me_xCl_{3-x}SiH ($x = 1, 2$), HSiR₃ (R = Et, Cl, OEt). The simplest hydrosilanes such as SiH₄, H₂SiCl₂, and Me_xSiH_{4-x} ($x = 1, 2, 3$) are gases at room temperature (rt) and are seldom employed as reactants. However, there were a few examples as illustrated in the formation of 1-1, 1-2ab, 1-5, 1-7 (SiH₄), 2-32 (H₂SiCl₂), 2-21 and 2-69 (Me₂SiH₂), 3-116 and 3-117, 3-120, 3-123, and 3-152 (Me₃SiH). It should be noted that disproportionation of HSiX₃ (X = Cl, OR) sometimes occurs to produce H₂SiX₂ in situ, although this appears to be fortuitous at this point and not exploited as a means of generating a secondary silane from a tertiary silane. Examples of the disproportionation will be introduced in section 3. Several substituted arylsilanes have been studied including many with substituents *ortho* to the silicon center. Some heterocyclic silanes have been synthesized to determine the possibility of π -complexation of novel systems such as silabenzene or disilabenzene as shown in eqs 13 and 14.

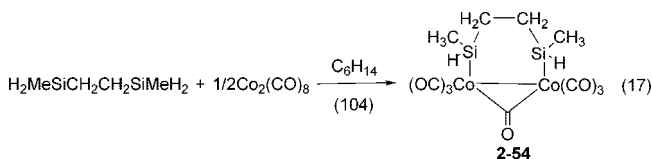
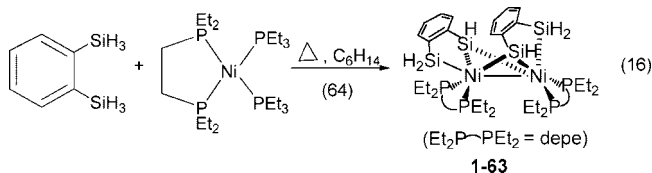


Chelating phosphine ligands are commonly used in the metal complexes that are employed in reactions with hydrosilanes. Selected examples of these phosphines and the silyl complexes produced include R₂PCH₂CH₂PR₂ (R = Ph,

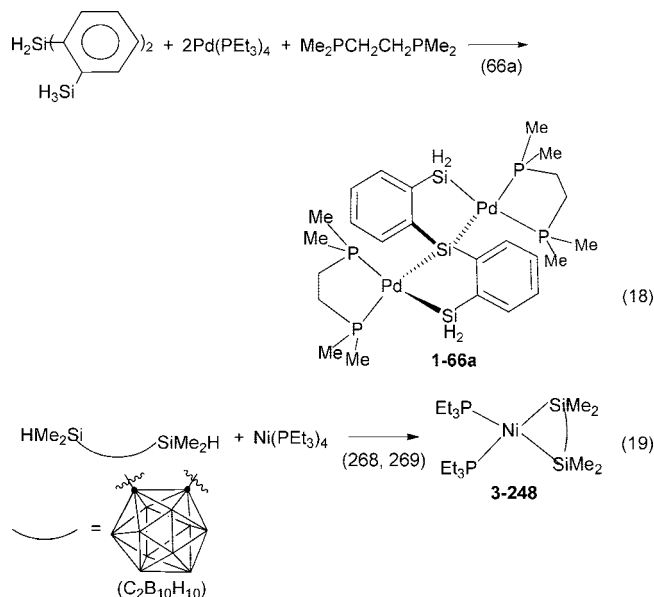
2-42a,b) and R₂PCH₂CH₂PR₂ [R = Ph (1-26, 1-27, 2-15, 3-273); Me (1-24, 1-25a, 1-30, 1-60, 1-61, 1-74ab, 1-75ab, 2-21, 2-24a, 2-76, 2-78b, 2-79bcd, 2-105, 3-250, 3-260c, 3-295 to 3-297; Et (1-63, 1-64, 1-65, 2-13); ^tPr (2-67 to 2-69, 3-254); Cy (1-65, 2-78a, 3-255); ⁱBu (2-77, 3-251)]. Chelating silanes have also been developed for reactions with transition metals including *o*-HRR'SiC₆H₄SiRR'H [R = R' = H (1-60, 1-61, 1-63), Me (3-127, 3-131, 3-133, 3-199bcd, 3-285, 3-301ab)], *o*-HMe₂SiC₆H₄SiH₃ (1-66b, 1-74ab, 3-250), H₂Si(C₆H₄SiH₃-*o*)₂ (1-64, 1-65, 1-66a), H₂MeSiCH₂-CH₂SiMeH₂ (2-54, 2-55), Cp*(OC)₂FeSiMe(OSiMe₂H)₂ (3-77), HMe₂Si(C₂B₁₀H₁₀)SiMe₂H (3-229, 3-248), 4,5-bis(dimethylsilyl)-9,9-dimethylxanthene (Xantsil; 3-104), and even HMe₂SiOSiMe₂H (3-128). The use of HR₂Si-X-SiR₂H as a chelate spanning *trans*-positions in ruthenium chemistry has been demonstrated by Sabo-Etienne and coworkers (section 3). The use of chelating silanes based on 1,2-disilylbenzenes and bis(2-silylphenyl)silane in reactions with group 10 transition metal complexes has been reviewed by Shimada and Tanaka,³³³ and those of 1,2-bis(dimethylsilyl)-carborane with group 10 has been reviewed by Kang, Lee, and Ko.³³⁴ Equations 15–19 illustrate the use of selected silane chelates. The complex 1-60 (eq 15) was the first reported tetrasilylnickel(IV) species isolated. Chelating silanes with SiH₃ or SiH₂ groups obviously can lead to complexes with more than one metal center as illustrated in eqs 16–18.



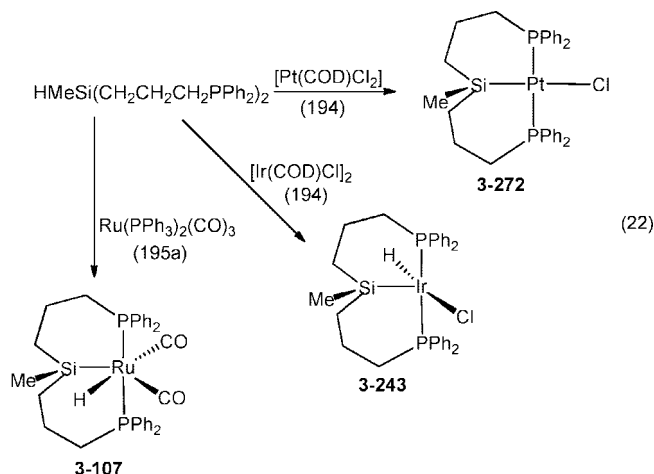
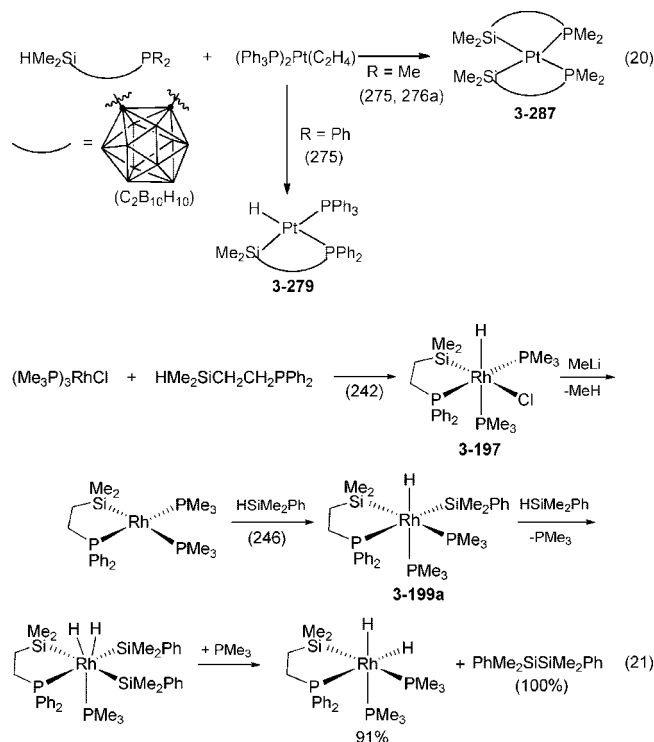
A more subtle form of chelation is derived from hydrosilanes that have phosphine tethers, and synthesis and reactivity of (phosphinoalkyl)silyl complexes has been reviewed by Okazaki and co-workers.³³⁵ The general systems (and selected examples) include HSiRR'CH₂CH₂PPh₂, viewed as



an analogue of diphos (R = H, R' = Mes, 2-73; R = R' = Me, 3-50, 3-51), HMeSi(CH₂)_xPPh₂)₂ (biPSiH, $x = 2, 194, 3, 195$ 3-107, 3-235, 3-243, 3-272), HPhSi(CH₂CH₂PPh₂)-(CH₂CH₂PCy₂)₂ (3-270), HSiMe(CH₂CH₂PCy₂)₂ (3-271), HMe₂Si(B₁₀C₂H₁₂)PR₂ (3-256a, 3-257a, 3-279, 3-281, and 3-287, 3-288), *o*-H₃SiC₆H₄OMe (1-82), and 2-HMe₂Si(C₅H₄N) (3-2). Schubert has demonstrated the chelate-assisted OA of SiH bonds through the sequence

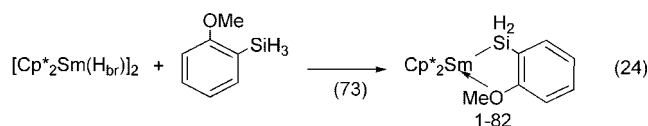
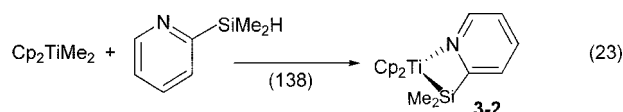


outlined in Scheme 3.¹⁶³ Coordination of the phosphine end of $\text{Ph}_2\text{PCH}_2\text{CH}_2\text{SiMe}_2\text{H}$ preceded the OA of the silane end. Equation 20 shows the reaction of $\text{HMe}_2\text{Si}(\text{B}_{10}\text{C}_2\text{H}_{12})\text{PR}_2$ with $(\text{PPh}_3)_2\text{Pt}(\text{C}_2\text{H}_4)$ and how the substituent at phosphorous can influence the nature of the product. Equation 21 illustrates the reaction of Wilkinson's catalyst with $\text{HMe}_2\text{SiCH}_2\text{CH}_2\text{PPh}_2$ and the sequence that led to dehydrogenative coupling of a tertiary silane. It is interesting to note that reaction of $\text{RhCl}(\text{PMe}_3)_3$ with HSiAr_3 occurred at room temperature (rt) to give *mer*- $[\text{RhCl}(\text{H})(\text{SiAr}_3)(\text{PMe}_3)_3]$ (**3-189a**) and no products of reductive elimination (such as $\text{Ar}_3\text{SiSiAr}_3$) were observed. Stobart and coworkers have developed the chemistry of the tridentate, $(\text{RSiH}(\text{CH}_2)_x\text{PR}')_2$ (when $\text{R} = \text{Me}$ and $\text{R}' = \text{Ph}$, $x = 2$ or 3, the ligand is abbreviated as biPSiH). With biPSiH ($x = 3$), the ligand provided distinguishable molecular faces at the metal center.¹⁹⁴ Selected examples are given in eq 22.

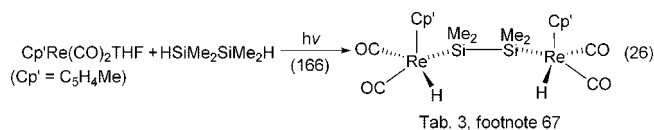
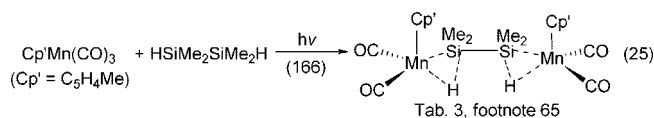


The strong and directed influence of the silyl group in the biPSi ligand was illustrated in the reaction between labeled ^{13}CO and $\text{Ru}(\text{biPSi})(\text{CO})\text{Cl}$. Entry of CO occurred only from the direction labeled "b" as shown in Figure 2.²⁰⁴ A kinetic study of the syn/anti stereomutation of **3-107** (eq 22) indicated that the process was nondissociative and intramolecular.^{195,204}

Although the chelating systems shown in Scheme 3 and eqs 20–22 contain 5- and 6-membered rings, it was also possible to observe formation of 4-membered ring chelates as shown in eq 23, and a related 5-membered ring is shown in eq 24.



Disilanes (or other silicon oligomers) with SiH bonds are rarely used as reactants, in part due to the complication resulting from insertion of the metal unit into the SiSi bond (section 8.2.1). However, complexes of the parent disilyl group have been prepared by reduction of $\text{MSiCl}_2\text{SiCl}_3$ (formed from salt metathesis) with LiAlH_4 , giving crystalline products of $\text{Cp}(\text{OC})_2\text{MSiH}_2\text{SiH}_3$ ($\text{M} = \text{Fe}, \text{Ru}$).^{336a} There have been attempts to determine whether β -H elimination in $\text{HSiR}_2\text{SiR}_2\text{H}$ could lead to a disilene coordinated to a metal center. Reaction of $(\eta^5\text{-C}_5\text{H}_4\text{Me})\text{Mn}(\text{CO})_3$ with $\text{HSiMe}_2\text{SiMe}_2\text{H}$ gave an unstable complex where each SiH is η^2 -bound to a different Mn center (eq 25), whereas the corresponding Re complex gives only OA products (eq 26). Thus, at least with these two metals, this strategy did not provide $\text{M}(\eta^2\text{-R}_2\text{Si}=\text{SiR}_2)$.¹⁶⁶



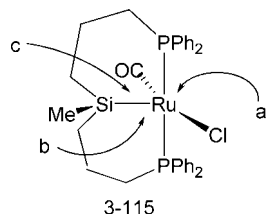
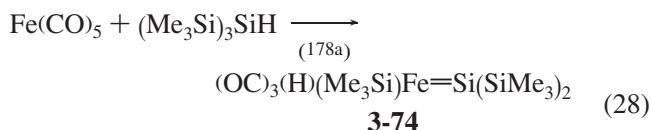
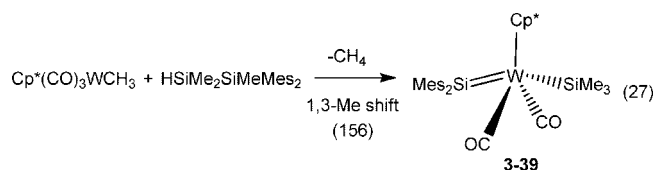
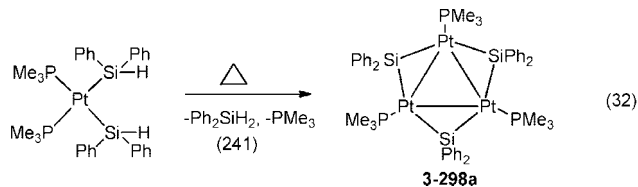
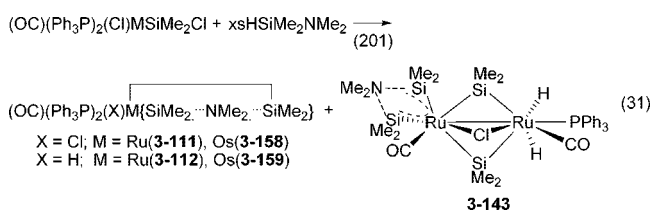
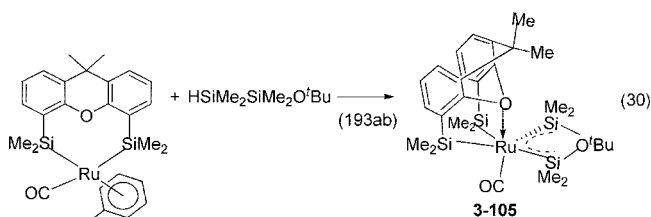
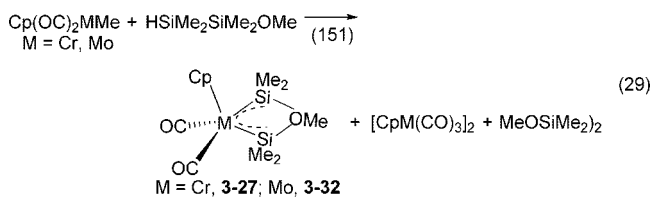


Figure 2. Three pathways for addition of CO to complex **3-115**.²⁰⁴

There are several interesting silylene complexes formed from precursors with HSiSi bonds, however, and these are shown in eqs 27 and 28. In both cases, migration of a group from silicon to the metal is required to account for the products. Compound **3-39** was the first donor-free silyl(silylene) complex with only alkyl and aryl groups at silicon to be reported.¹⁵⁶ When the disilane contained a donor substituent such as OR or NR₂, a donor-bridged bis-silylene product was formed as illustrated in eqs 29 and 30. The bis-silylene derivatives can also be prepared from a chlorodimethylsilyl ligand bound to a metal center as shown in eq 31.



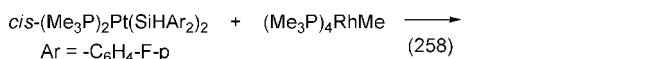
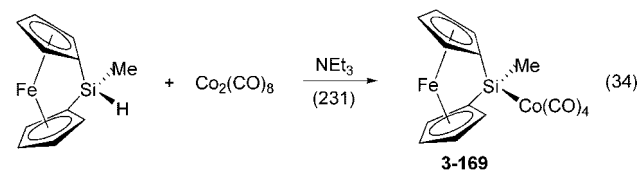
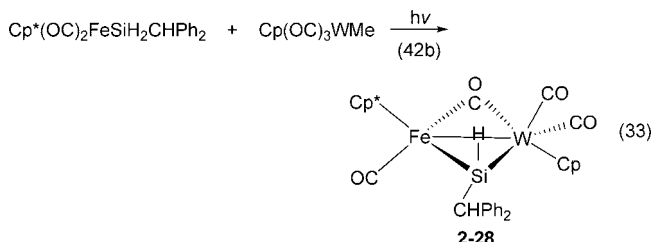
A related group 14 complex, Ph₂Ge[Co(CO)₄]₂, ultimately formed from the reaction of Ph₃GeSiEt₂H with Co₂(CO)₈, was believed to involve a 1,3-Ph shift from the intermediate Et₂Si=Co(GePh₃)(CO)₃²²⁹ to give Ph₂Ge=Co(CO)₃SiEt₂Ph. The extruded germylene was then trapped by Co₂(CO)₈.



Reaction of primary and secondary silanes, in principle, could lead to silyl complexes with residual hydrogens at the silicon center. However, a more complex outcome often resulted. For instance, silylene complexes, L_nM=SiR₂, can be obtained from reaction of RSiH₃ or of R₂SiH₂ with an appropriate TM complex, as illustrated in the formation of **1-29a**,³⁸ **1-29b**,^{38b} **1-30**,³⁹ **1-50**,⁵⁵ **1-51**,⁵⁰ **1-54ab**,^{57a,b} **1-59a**,^{60a,b} **2-10**,^{36a} **2-11**,⁸² **2-19**,^{85a} **2-20**,⁸⁵ **2-21**,^{39,86,475} **2-36d**,^{47b} **2-71b**,^{116,117a} and **2-74**.^{60,61} In many cases, dimer products were obtained presumably from further reaction of the residual silyl hydrogens of a hydrosilyl ligand (the mechanism or route to the dimer was not often determined). Many of the dimers contained bridging silyl groups or unsymmetrical bridging agostic M(η²-SiH)M units. Several examples of both cases were reported in Tables 1 and 2 and include the following: **1-70**,⁶⁹ **1-72**,⁶⁹ **1-73**,⁶⁹ **1-77**,^{68a} **1-78**,^{68b} **2-27**,⁴⁰ **2-69**,¹¹⁴ **2-80**,^{121b} **2-81**,^{121a,b} **2-82**,^{121b} and **2-83**.¹²² There are other interesting cases where an isolated M-SiH containing complex was utilized to make M-Si-M' (M = M' or M ≠ M') or where, on occasion, unexpected complex products were obtained. Some examples are shown in eqs 32–35.

3.2. Ligand Loss

In many examples in Tables 1–3, there was loss of a neutral ligand from the starting complex and oxidative addition of the hydrosilane to the coordinatively unsaturated intermediate as shown for a generalized example in eq 12. In the cases described in this section, there is an increase in

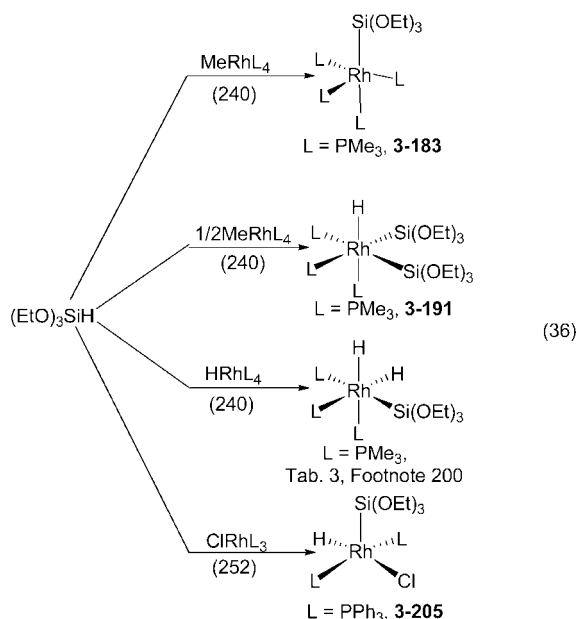


oxidation state and the ligand that is lost generally does not re-coordinate to the metal center. Typical ligands that may be lost include phosphines, carbonyls, olefins (alkynes),

Chart 1. Examples of Phosphine Loss from Metal Complexes during Oxidative Addition of Hydrosilanes (from Tables 1–3)

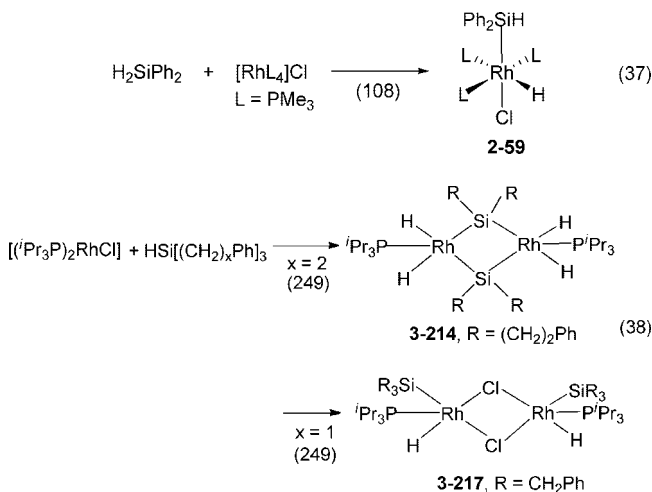
PMe₃: 1-12, 1-13, 2-3, 2-38b, 2-59, 2-63, 2-73, 3-1, 3-17 3-20, 3-25ab, 3-26ab, 3-99c, 3-119b, 3-120, 3-187, 3-188, 3-197, 3-219, 3-298a.
PEt₃: 1-63, 1-64, 1-65, 1-66, 1-70, 1-72, 1-74ab, 1-75, 2-91, 2-109, 3-184, 3-200, 3-202, 3-248, 3-260ab, 3-261, 3-276ab.
PPr₃ or Pⁱ(Pr)₃: 1-44, 1-67, 1-71, 2-27, 2-46, 3-149, 3-214, 3-217.
P(Cy)₃: 2-83, 3-114
PAr₃: 2-106, 3-87, 3-100, 3-101, 3-107, 3-115, 3-143, 3-151b, 3-198, 3-203, 3-204, 3-205 to 3-209, 3-234, 3-236ab.
Chelates: 1-60, 1-61, 3-250, 3-297ab

solvent molecules, and dihydrogen, although the first two ligands listed represent the majority of the examples. In most cases, the sequence of events leading from the reacting transition metal complex to the product has not been determined, but the type of sequence shown in eq 12 is usually assumed. In the following sections, the types of precursors that involve loss of PR₃, CO, olefin, solvent, and H₂ will be discussed in that order.

**3.2.1. Phosphines**

The majority of the precursor complexes that involve loss of phosphine from the initial starting material come from the cobalt and nickel triads; however, there are a few from the iron triad as well. Trialkylphosphines (PR₃, R = Me, Et, Pr, Cy,) are the most common phosphine ligands employed in the precursors to silyl–metal complexes, although there are several cases that involve PAr₃ (primarily Ar = Ph) (see Chart 1 for examples). Common starting materials for Rh(I) complexes have compositions that include [RhL₄]Cl, ClRhL₃, ClRhL₂, RRhL₄, and HRhL₄, where L represents a phosphine. Similar complexes for the nickel triad include ML₄ (M = Ni, Pd, Pt), PtL₃, and R₂PtL₂. There are no general studies that indicate how the nature (or size) of the substituents at phosphorous in the phosphine or the nature of the silane might influence the type of silyl–metal complex that is formed. Equation 36 shows the variation in products obtained from HSi(OEt)₃ and selected Rh(I) precursors, and eq 37 illustrates another variation produced in reaction with a secondary silane. The substituents on the silane can influence the product formed since the tertiary silane, HSi(C₆H₄CF₃-p)₃, reacted with L₃RhCl (L = PMe₃) to give a mixture of 11% *mer*-L₃H(Cl)Rh(SiAr₃) (H and Cl are *trans*) and 78% *fac*-L₃Rh(H)₂SiAr₃ (**3-189a** and **3-189b**), although no formal

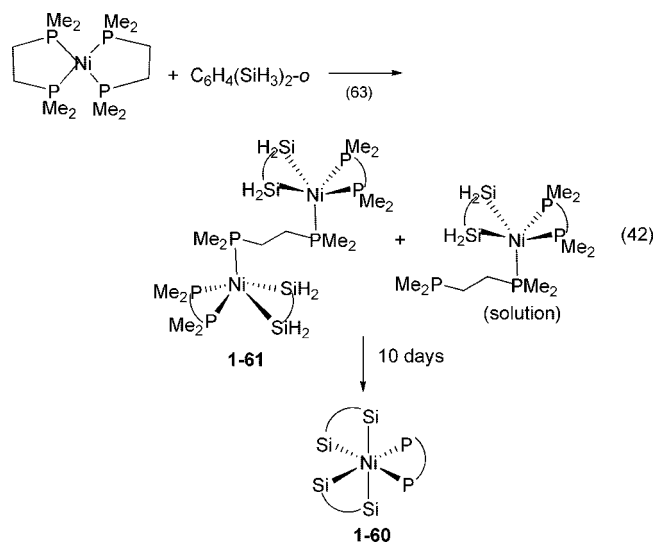
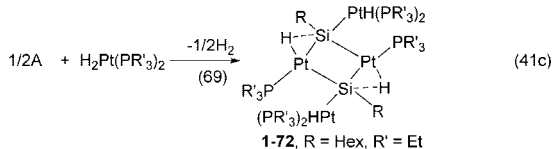
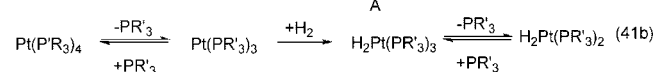
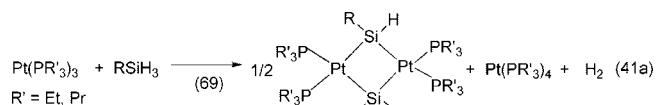
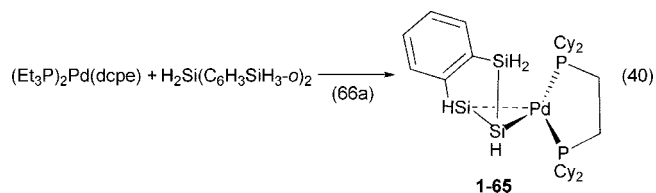
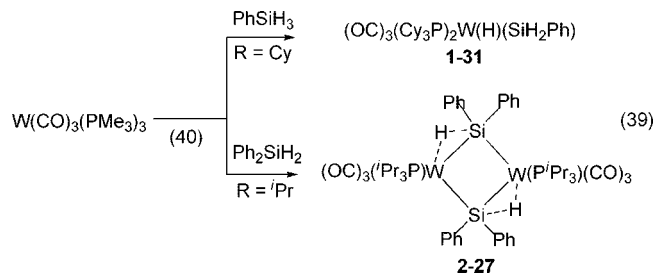
loss of phosphine occurred, as was the case depicted in eq 36.²⁴³ An additional variation starting with a Rh(I) precursor is shown in eq 38 in which dimers were produced.



Few investigators attempt to examine the reactivity of the same metal complex with different types of silanes. A rare example involves W(CO)₃(PⁱPr₃)₂ with related primary and secondary silanes as shown in eq 39.⁴⁰ The reaction with the primary silane induced simple oxidative addition (without loss of either CO or phosphine), but loss of phosphine in the reaction with the secondary silane did occur. The Cr analogue did not react with silanes.⁴⁰

Primary silanes can provide unpredictable products, especially if there are no bulky substituents on silicon. Examples of such unpredictable products were illustrated earlier in eqs 16 and 18 in the reaction of (Et₃P)₂Ni(depe) with 1,2-(H₃Si)₂C₆H₄ and of (Et₃P)₂Pd(dmpe) with H₂Si-(C₆H₃SiH₃-o)₂. Another variation of the latter reaction is shown in eq 40 where a dehydrocoupling of two silicon centers has occurred in the silicon ligand that becomes bound to Pd. One of the reasons that may contribute to the complexity of the reactions of primary silanes with relatively small substituents is illustrated in the sequence shown in eq 41 (a–c). If H₂ is formed in the reaction, Pt hydride species could be generated and provide additional reaction pathways.

It is generally not clear when the loss of phosphine ligand occurs during the reaction of a hydrosilane with a metal complex that contains a phosphine, but it most likely occurs prior to the reaction of the metal center with the silane. If a complex contains a chelating phosphine, it might be possible to “trap” a dissociated end of the chelate. This was demonstrated nicely in the reaction of *o*-(H₃Si)₂C₆H₄ with Ni(dmpe)₂ (eq 42). The structures of **1-61** and **1-60**, shown in eq 42, have been confirmed by X-ray structures.



3.2.2. Carbonyl(s) or Carbonyl Units

The use of carbonyl complexes in reactions with silanes is not as extensive as those for the phosphine complexes described in the previous section. The majority of the cases tend to be found in the Cr and Mn triads, where loss of CO precedes reaction with the hydrosilane. However, there are several examples of reactions of $\text{M}_x(\text{CO})_y$ where both substitution with retention of the M_x unit occurs (section 3.5) or breakdown to a single metal-containing complex was reported. It is this latter group that will be included in the current section. Loss of a CO in a complex such as $\text{L}_x(\text{OC})\text{MR}$ can lead to oxidative addition of HSiR'_3 [to give $\text{L}_x\text{M(H)R}(\text{SiR}'_3)$], which then eliminates RH to give the final product $\text{L}_x\text{MSiR}'_3$. Examples of this type of sequence will be included in this section. Consequently, there is some

overlap with section 3.3. Chart 2 summarizes the typical carbonyl precursors that have been utilized with hydrosilanes.

The photochemically induced loss of CO from $\eta^5\text{-CpM(CO)}_3$ ($\text{M} = \text{Mn, Re}$),^{165a} $\eta^5\text{-CpV(CO)}_4$,¹⁴¹ and M(CO)_6 ($\text{M} = \text{Cr, Mo, W}$),⁸³ in neat Et_3SiH under ambient conditions, has been studied with femtosecond pump–probe spectroscopic methods. The studies of the Mn and Re systems have been summarized by Harris and co-workers in an *Accounts of Chemical Research* article.^{165b} The reactive intermediates that were observed were modeled by density functional theory (DFT) and ab initio quantum chemical methods. The 295 nm photochemical reaction of CpMn(CO)_3 resulted first in the loss of CO to produce singlet and triplet states of CpMn(CO)_2 in an approximate 1:1 ratio, whereas CpRe(CO)_3 provided only the singlet dicarbonyl (see Scheme 4). After loss of CO, the dicarbonyl is solvated by Et_3SiH . The singlet dicarbonyl was preferentially solvated through the ethyl group of Et_3SiH and subsequently rearranged to give the final product with a nonclassical Si–H interaction for the Mn system and as the full oxidative addition product for the Re case. The two different products were suggested by ab initio calculations for the model system, $\text{CpM(CO)}_2(\text{H})\text{SiH}_2\text{CH}_3$, where the $r(\text{SiH})$ distance was calculated to be 1.90 Å ($\text{M} = \text{Mn}$) and 2.35 Å ($\text{M} = \text{Re}$) (MP2/lan/2dz). The decay of the triplet CpMn(CO)_2 partitioned between the formation of the singlet ethyl solvate and concerted spin crossover/SiH solvation to give the final product.

The reaction dynamics for the photochemical activation of CpV(CO)_4 in Et_3SiH were found to be similar to those just described for CpMn(CO)_3 .¹⁴¹ Both singlet and triplet CpV(CO)_3 species were formed with different geometries for the two different electronic states (eq 43). The data suggested that the triplet species reacted rapidly through a concerted spin crossover/solvation facilitated by the SiH bond of Et_3SiH (producing **3-11a**). Product formation from singlet ethyl-solvated CpV(CO)_3 was much faster than that of CpMn(CO)_2 . Calculations (DFT/B3LYP) again gave a slightly elongated Si–H distance (1.53 Å compared to a free silane SiH bond length of 1.49 Å), which may be a nonclassical $\eta^2\text{-SiH}$ interaction with V (as depicted in eq 43).

In a third report, Harris and co-workers described the SiH activation of M(CO)_6 ($\text{M} = \text{Cr, Mo, W}$) in the presence of HSiEt_3 and HSiPr^n_3 .^{83a} The 295 nm photolysis generated M(CO)_5 , which was rapidly solvated through the alkyl groups of the silane followed by rearrangement to the silyl hydride product. The authors proposed a dissociative rearrangement of the alkyl coordinated Et_3SiH (or HSiPr^n_3) and recoordination of SiH as originally proposed by Dobson and

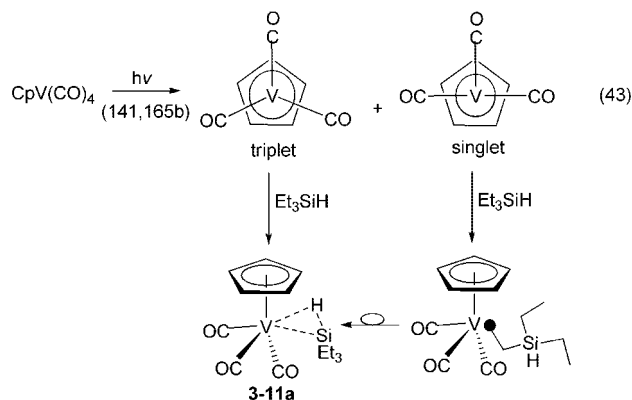
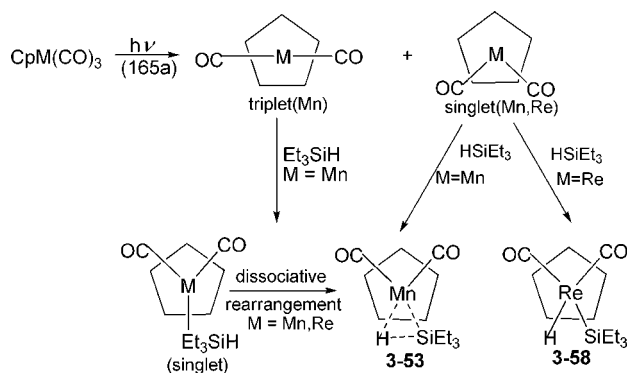


Chart 2. Examples of Loss of Carbonyl or Metal Carbonyl Units from Metal Complexes during Oxidative Addition of Hydrosilanes (from Tables 1, 2, and 3)

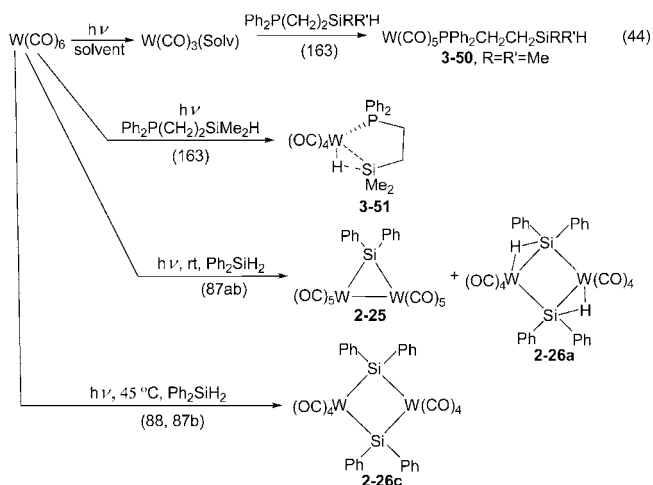
$M(CO)_y$: 2-7, 2-8, 3-29, 3-30ab (Cr); 2-12, 2-16 (Mo); 2-25, 2-26abc, 3-36, 3-37b, 3-49, 3-50, 3-51, 3-52abc (W); 3-71, 3-72abc, 3-73, 3-74 (Fe).
 $M_x(CO)_y$: 3-104, 3-106 (Ru); 3-166 to 3-168c, 3-169 to 3-175 (Co).
 $L_xM_y(CO)_z$: 3-52abc (W); 2-42ab, 3-107, 3-148ab (Ru);
 $Cp^*M(CO)_x$, $Cp^*M(CO)_2L$ or related: 3-11a (V); 2-29, 3-53 to 3-56 (Mn); 2-31, 3-58 (Re); 3-176 (Rh).
 $Cp^*M(CO)_yR$: 2-17, 2-18, 2-20, 2-28, 3-39, 3-40, 3-41, 3-44, 3-45 (W); 3-78 (Fe);
 $[Ir(CO)(PMe_3)_4]Cl$: 2-73

Scheme 4

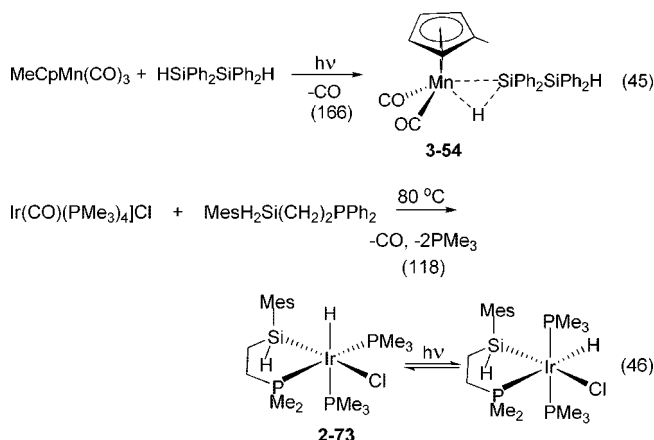


coworkers,^{83b} but in contrast to the chain-walk mechanism proposed by Simon and Xie.^{83c} In each of the three studies just described, data for the intermediate species formed from loss of a carbonyl ligand [$CpMn(CO)_2$, $CpRe(CO)_2$, $CpV(CO)_3$, and $M(CO)_5$ ($M = Cr, Mo, W$)] were obtained from fs-IR measurements. Although such detailed studies of the intermediate generated in the photolysis of metal carbonyls (in the presence of hydrosilanes) have not generally been performed, it has been assumed in reactions of other metal carbonyl precursors. Often, such reactions have been conducted in donor solvents and solvent molecules were presumed to replace the CO upon photolysis. Examples are shown in eqs 44–46, although eq 46 shows a thermally induced loss of CO as well as PMe_3 . The thermal reaction shown in eq 46 produced the isomer of **2-73** with *cis*-phosphines. Under photolysis, a photostationary state of *cis*-**2-73**/*trans*-**2-73** of 29:71 was produced.¹¹⁸

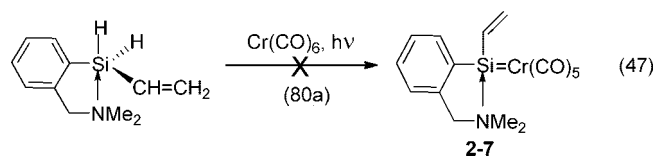
The reactions shown in eqs 44 and 45 include tertiary silanes and eqs 44 and 46 include secondary silanes, but the use of secondary silanes could lead to dimetallic species with bridging silylenes. As an example, photolysis of a mixture



of $W(CO)_6$ and Ph_2SiH_2 at 45 °C provided the bridged dimer



$[(OC)_4WSiPh_2]_2$ (see eq 44) presumably through the silylene intermediate, $[(OC)_5W=SiPh_2]$.⁸⁸ When the reaction of Ph_2SiH_2 and $W(CO)_6$ (1:1 ratio) was conducted at room temperature, the silylene was trapped by $W(CO)_5$ to give μ -diphenylsilylene(decacarbonyl)-ditungsten (also shown in eq 44).^{87a} A related reaction of the pentacoordinated silane (2- $Me_2NC_6H_4$)($CH_2=CH$) SiH_2 and $Cr(CO)_6$ presumably gave the 1-metalla-2-sila-1,3-diene shown in eq 47. However, a later report by the same group indicated that polymerization of the alkenylsilane was the actual reaction initiated by $Cr(CO)_6$.⁹⁰ The formation of $(OC)_3(H)(Me_3Si)Fe=Si(SiMe_3)_2$ (**3-74**) from $Fe(CO)_5$ and $(Me_3Si)_3SiH$ (eq 28) under photolysis probably occurred by loss of a CO group followed by oxidative addition of the silane. Loss of a second CO would open a coordination site and allow for migration of an $SiMe_3$ group from Si to Fe.^{178a}

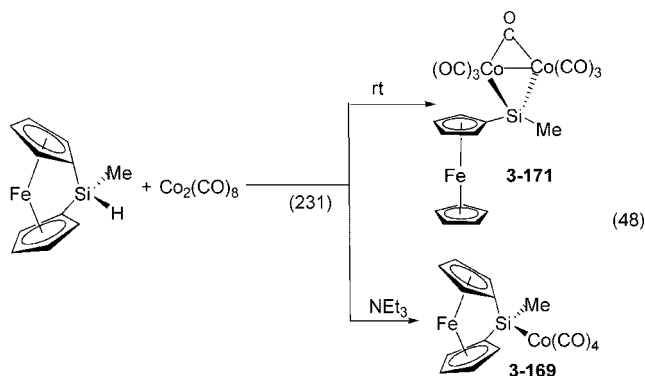


Carbonyl complexes can be dinuclear or polynuclear. The most commonly employed examples for reaction with silanes are $Co_2(CO)_8$ and $Ru_3(CO)_{12}$. In the reactions with hydrosilanes, both substitution and metal–metal bond cleavage products have been produced. The cobalt dimer, $Co_2(CO)_8$, is used to introduce a $Co(CO)_4$ unit, although the path is not necessarily straightforward. For instance, the disilane $HPh_2SiSiPh_2H$ reacted with $Co_2(CO)_8$ to ultimately give $Ph_3SiCo(CO)_4$ in 16% yield along with $Co_4(CO)_{12}$ (~10%) and unreacted $Co_2(CO)_8$ (16%). The reaction probably proceeds through $HPh_2SiSiPh_2[Co(CO)_4]$. Loss of CO would open a coordination site, and a sequence of 1,2- and 1,3-shifts would give $Ph_2Si=Co(CO)_3SiPh_3$. In this case, the silylene cobalt intermediate extruded the silylene and with re-entry of CO provided $Ph_3SiCo(CO)_4$ (also prepared from $Co_2(CO)_8$ and $HSiPh_3$; **3-167**).²²⁹ In the design of dendrimers,

Chart 3. Examples of Loss of Olefins or Acetylenes from Metal Complexes during Oxidative Addition of Hydrosilanes (from Tables 1, 2, and 3)

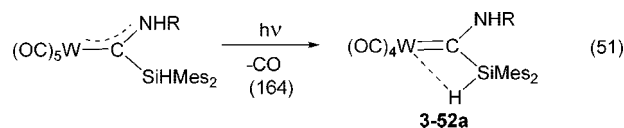
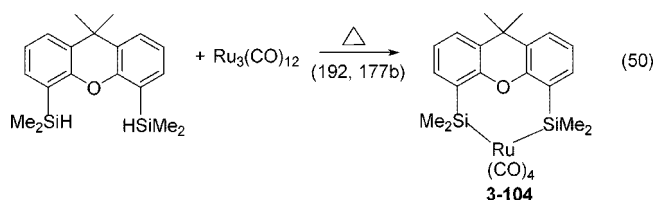
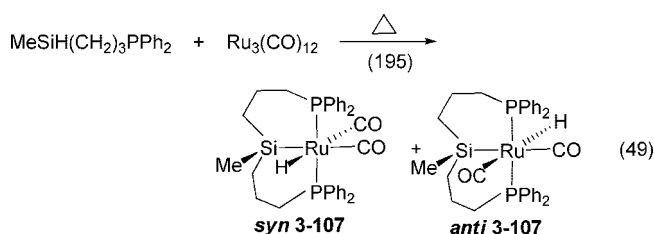
N_2 : **1-36** (Fe); **3-134e** (Ru)
 C_2H_4 : **2-50, 2-51, 2-52, 3-164** (Co); **2-57ab, 3-177, 3-178, 3-213, 3-215ab** (Rh); **3-240a** (Ir);
1-53 (Co); **1-68, 1-69, 1-73, 1-77, 2-92, 2-93, 2-96c, 2-98, 2-100, 2-101, 2-103, 2-104, 2-106, 2-108, 3-269abcd, 3-274, 3-275, 3-279, 3-287, 3-292, 3-293** (Pt).
 RCH=CH_2 : **3-16** (Nb); **3-252** (Ni) (R = Ph); **3-23** (R = Me).
 COD, COT, COE : **3-131, 3-133, 3-134cd** (Ru); **3-211, 3-212ab** (Rh); **3-243, 3-244, 3-245a, 3-246a, 3-247** (Ir); **3-270 to 3-272, 3-281, 3-288, 3-290bd, 3-291, 3-294** (Pt).
 $\text{RC}\equiv\text{CR}'$: **3-3, 3-4** (Ti); **3-8** (Zr).
 $\eta\text{-CH}_2\text{R}$: **2-11** (R = Ph); **3-118** (R = PMe_2)
 $\eta\text{-C}_8\text{H}_{13}$: **2-74, 2-75** (Ir)
 Arene : $\eta^6\text{-tol}$, **2-32** (Fe); **3-105** (Ru)

$\text{Co}_2(\text{CO})_8$ was reacted (in the dark) with $\text{Si}[(\text{CH}_2)_3\text{SiMe}_2\text{H}]_4$ to substitute all SiH bonds giving $[(\text{OC})_4\text{CoSiMe}_2(\text{CH}_2)_3]_4\text{Si}$ (**3-174**).²³⁴ Eight-fold functionalization of octasilsesquioxanes with $\text{Co}_2(\text{CO})_8$ to give $[(\text{OC})_4\text{CoSiO}_{1.5}]_8$ (**3-175**) has been reported in 87% yield.²³⁵ Two reaction pathways have been reported for $\text{Fe}(\eta^5\text{-C}_5\text{H}_4)_2\text{SiMeH}$ and $\text{Co}_2(\text{CO})_8$ (eq 48). In the absence of base, the Co_2 unit is retained, but when base is added, a $\text{Co}(\text{CO})_4$ unit becomes incorporated into the product (**3-169**).²³¹ Other examples (**2-55, 3-173**) where the Co_2 unit is retained will be found in section 3.7.



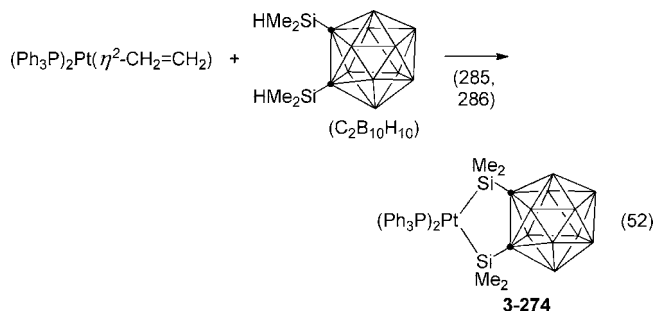
The ruthenium carbonyl, $\text{Ru}_3(\text{CO})_{12}$, has also been reacted with hydrosilanes. Examples where a single Ru center is transferred are shown in eqs 49 and 50. However, there are also examples of $\text{LRu}_x(\text{CO})_y$ substrates where CO loss occurs and a single hydrosilane is incorporated into the cluster. Such examples (**3-145**,²¹⁸ **3-146**,²¹⁵ **3-148ab**²¹⁹) are included in section 3.7. An unusual reaction that produced a $\beta\text{-SiH}$ agostic interaction occurred on photochemical loss of CO from $(\text{OC})_5\text{W}=\text{C}(\text{NHR})(\text{SiHMe}_2)$, as shown in eq 51.¹⁶⁴

A relatively common tactic for formation of complexes in which the metal ultimately retains the same oxidation state as in the starting complex is to utilize the sequence starting from $\text{L}_x(\text{OC})\text{MR}$, which, upon photolysis, loses CO to open a coordination site followed by oxidative addition of SiH to give $\text{L}_x\text{SiM}(\text{H})\text{R}$. Reductive elimination of RH returns the metal to its original oxidation state. Examples of this sequence will be presented in section 3.3.



3.2.3. Olefin or Acetylene

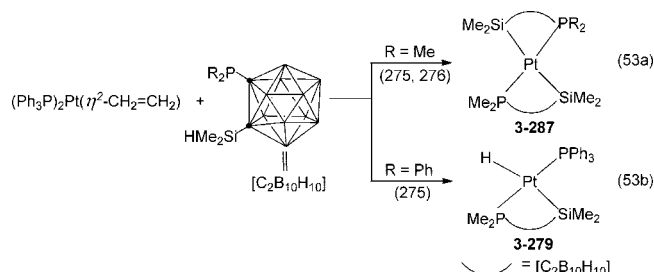
Although less common than the loss of phosphine or carbonyl ligands, loss of olefin or an alkyne from platinum centers in particular has been a useful synthetic strategy to open a coordination site. Examples from Tables 1, 2, and 3 are summarized in Chart 3. Further examples of olefin ligands appear in section 3.6, where reactions of low-valent complexes are included.



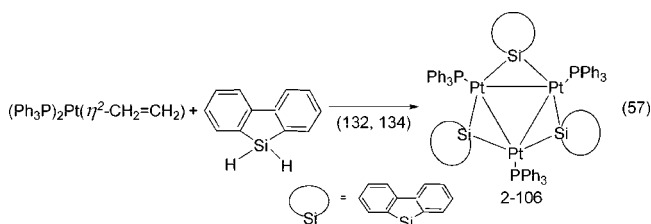
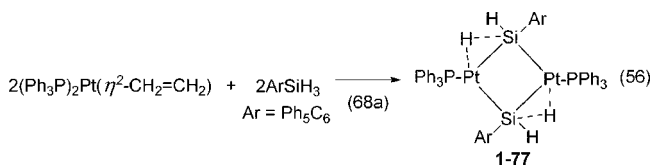
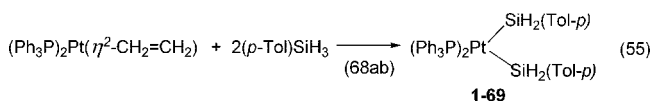
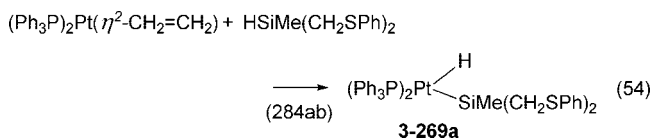
The most commonly employed olefin complexes in reactions with hydrosilanes are those of Pt and particularly the complex $(\text{Ph}_3\text{P})_2\text{Pt}(\eta^2\text{-CH}_2=\text{CH}_2)$. This is, in part, due to the commercial availability of this reagent. In reaction with a hydrosilane, it is the ethylene that is lost, thus providing two open coordination sites at Pt (in some cases, a phosphine may also be lost). This allows for reaction with chelating silanes as shown in eqs 52 and 53a or hydrosilanes with pendant phosphine groups. The *trans*-carborane complex

shown in eq 53a as isomerized to the *cis*-form in the presence of $\text{MeO}_2\text{CC}\equiv\text{CCO}_2\text{Me}$.²⁷⁵

The reactions of $(\text{Ph}_3\text{P})_2\text{Pt}(\eta^2\text{-CH}_2=\text{CH}_2)$ with primary or secondary silanes can be more complex. With the tertiary silane (nonchelating system), an expected oxidative addition pathway took place as shown in eq 54. However, a primary silane formed a bis-silyl complex (eq 55). If the primary silane, ArSiH_3 , contained an aryl substituent with groups in the *ortho*-position as shown for one example in eq 56, not only was ethylene lost from the Pt precursor but so also was a phosphine ligand (compare to the *p*-TolSiH₃ reaction shown

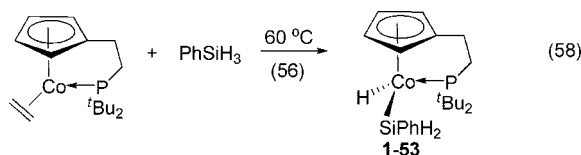


in eq 55). With a secondary silane in which the silicon is constrained in a ring system, a third variation was observed as shown in eq 57. The studies did not include $\text{L}_2\text{Pt}(\eta^2\text{-C}_2\text{H}_4)$ where L was a different phosphine, particularly one with a smaller cone angle; thus, it is not clear whether formations of dimers and trimers as illustrated in eqs 56 and 57 are general features of the reaction of Pt–ethylene complexes. The cobalt complex $[\text{CpCH}_2\text{CH}_2\text{P}^t\text{Bu}_2]\text{Co}(\eta^2\text{-C}_2\text{H}_4)$ also reacted with primary, secondary, and tertiary silanes through loss of ethylene. An example is shown in eq 58.

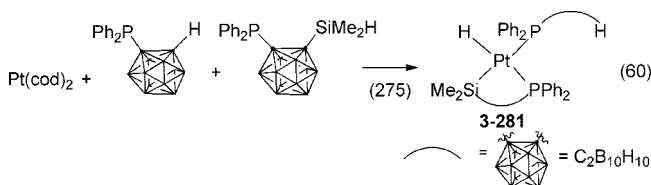
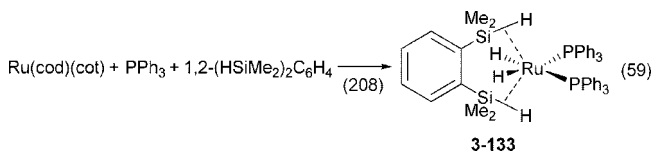


Another olefin complex of Pt(II) that has been used effectively in reactions with hydrosilanes is $[\text{Pt}(\text{cod})\text{Cl}_2]$. Stobart and coworkers have developed a tertiary silane with phosphine pendant groups, $\text{RSiH}[(\text{CH}_2)_x\text{PR}'_2]_2$ ($x = 2, 3$; biPSi) and examined the reactivity with $[\text{Pt}(\text{cod})\text{Cl}_2]$ as well as other metal complexes, and a Ru example was included earlier in eq 49. The silane where $\text{R} = \text{Me}$ and $\text{R}' = \text{Ph}$ has been abbreviated as biPSi, and the reaction with $[\text{Pt}(\text{cod})\text{Cl}_2]$

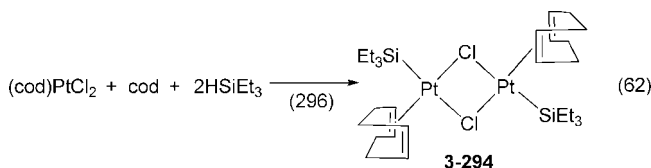
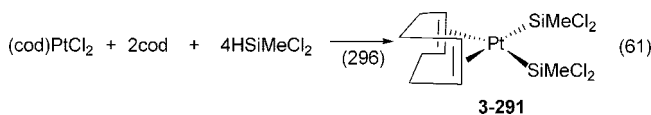
and $[\text{Ir}(\text{cod})\text{Cl}]_2$ was shown earlier in eq 22. If NEt_3 was not present in the reaction of the silylpropylphosphine with $[\text{Pt}(\text{cod})\text{Cl}_2]$, a mixture of products was obtained. When the HCl produced was removed as $\text{NEt}_3\text{H}^+\text{Cl}^-$, an 84% yield of the Pt product could be realized.



The M(0) complexes, $(\text{cod})_2\text{Pt}$ and $\text{Ru}(\text{cod})(\text{cot})$, were used in reactions with chelating hydrosilanes (and phosphines) to provide novel complexes with two $\text{Ru}(\eta^2\text{-HSi})$ interactions as shown in the selected example in eq 59 and a $\text{HMe}_2\text{SiXPPH}_2$ example where $(\text{X} = \text{C}_2\text{B}_{10}\text{H}_{10})$ in eq 60.

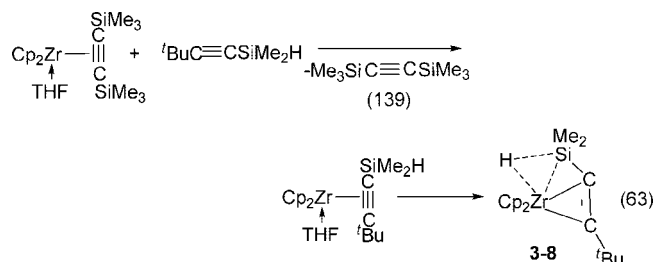


Usually the cod ligand is displaced when $(\text{cod})\text{PtCl}_2$ reacts with a hydrosilane, but two notable exceptions are found in eqs 61 and 62. The bis-silyl complex shown in eq 61 is stable only in the presence of excess cod. Since cod contains 2 olefin units, it can function as a “monodentate” or a “bidentate”. In the formation of **3-291** (eq 61), cod maintains its role as a bidentate. However, for the dimer (**3-294**) shown in eq 62, cod functioned as a monodentate. The dimer, **3-294**, decomposed in solution over several days. The bis-silyl complex showed catalytic activity in hydrosilylation reactions and was proposed as the actual catalyst in a Chalk-Harrod mechanism for hydrosilylation.²⁹⁶



Acetylene complexes of transition metals have been rarely reported as starting materials for reactions with hydrosilanes. One of the few exceptions can be found in the Ti and V triads. Replacement of the acetylene in the complex $\text{Cp}_2\text{M}(\text{L})(\eta^2\text{-Me}_3\text{SiC}\equiv\text{CSiMe}_3)$ ($\text{L} = \text{none}$, $\text{M} = \text{Ti}$; $\text{L} = \text{THF}$, $\text{M} = \text{Zr}$) with a second silylacetylene, $\text{RC}\equiv\text{CSiMe}_2\text{H}$, gave rise to a series of complexes that contained an agostic $\text{M}\cdots\text{H}\cdots\text{Si}$ interaction. One example is shown in eq 63. The complex $\{\text{Me}_2\text{Si}(1,2\text{-C}_2\text{B}_{10}\text{H}_{10})\text{SiMe}_2\}\text{Ni}(\text{PEt}_3)_2$ was found to be a good catalyst for the double silylation of alkynes, and the

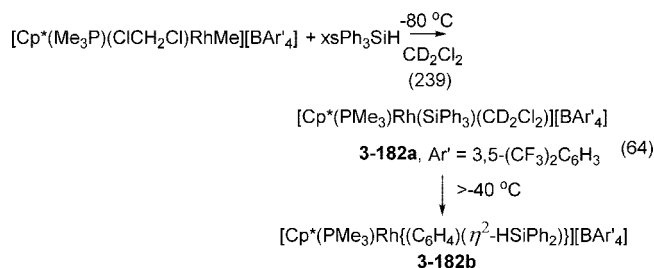
formation of $\{\text{Me}_2\text{Si}(1,2\text{-C}_2\text{B}_{10}\text{H}_{10})\text{SiMe}_2\}\text{Ni}(\eta^2\text{-RC}\equiv\text{CR}')\}$ was proposed as the first stage leading to the silylated product.²⁶⁹



3.2.4. Coordinated Solvent

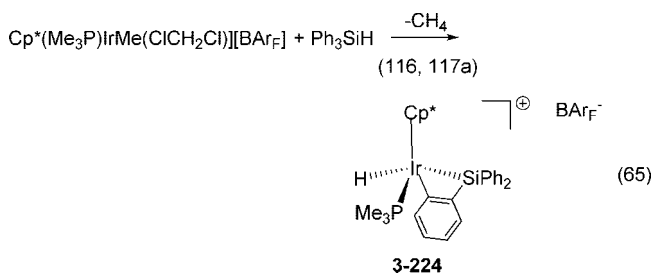
Loss of a ligand from a coordinatively saturated metal complex may result in a solvent molecule entering the coordination sphere of the metal, although this is not often demonstrated by suitable spectroscopic data. In this section, “solvated” complexes that have been isolated and characterized are the starting complexes for oxidative addition of silanes. The solvent molecule is generally weakly bound and is readily displaced by the incoming silane. The coordinated solvents in metal complexes include CH_3CN (**1-40**,^{48a} **2-37**,^{48a} **3-42**,^{159a} **3-47**,¹⁶¹ **3-103**,^{48a} **3-180**;²³⁸); CH_2Cl_2 (**3-57**,¹⁶⁸ **3-63**,¹⁷¹ **3-181a**,²³⁹ **3-181b**,²³⁹ **3-182a**,²³⁹ **3-182b**;²³⁹); THF (**3-59**;¹⁶⁶); and Et_2O (**3-280**;²⁸⁹).

When $\text{Cp}'(\text{OC})_3\text{WMe}$ was photolyzed in acetonitrile, the solid complex, $\text{Cp}'(\text{OC})_2\text{W}(\text{MeCN})\text{Me}$,^{159b} could be isolated after removal of the solvent. Sakaba and coworkers have reported a number of reactions of this solvate with hydrosilanes. However, most of these reactions also result in loss of CH_4 as well and will be discussed in 3.3.1. Another isolated solvate was $\text{TpRu}(\text{H})(\text{CH}_3\text{CN})(\text{PPh}_3)$.^{48b} In this case, the acetonitrile was replaced by HSiR_3 to give $\text{TpRu}(\text{PPh}_3)(\text{H})(\eta^2\text{-HSiR}_3)$ ($\text{R} = \text{Et}_3$, **3-103**), with a coordinated silane that may be considered a case of arrested addition to the ruthenium center.^{48a} Displacement of coordinated CH_3CN does not always occur, as was observed in the reaction of Ph_3SiH with the isolable complex $[\text{Cp}^*(\text{Me}_3\text{P})(\text{MeCN})\text{RhMe}]^+\text{BAR}'_4$ (produced by addition of CH_3CN to the solvate complex $\text{Cp}^*(\text{Me}_3\text{P})(\text{Me}_3\text{P})(\text{ClCH}_2\text{Cl})\text{RhMe}^+\text{BAR}'_4$ ($\text{Ar}' = 3,5\text{-C}_6\text{H}_3(\text{CF}_3)_2$ generated in situ).²³⁸ The product produced was the solvated rhodium silyl, $[\text{Cp}^*(\text{Me}_3\text{P})(\text{MeCN})\text{-RhSiPh}_3]^+\text{BAR}'_4$ (**3-180**; the Rh center retains the +3 oxidation state). The corresponding CH_2Cl_2 solvate, $[\text{Cp}^*(\text{Me}_3\text{P})(\text{CH}_2\text{Cl}_2)\text{RhSiPh}_3]^+\text{BAR}'_4$, could be generated but was not isolated because of a rearrangement reaction that occurred at $> -40^\circ\text{C}$, as shown in eq 64.^{238–239}

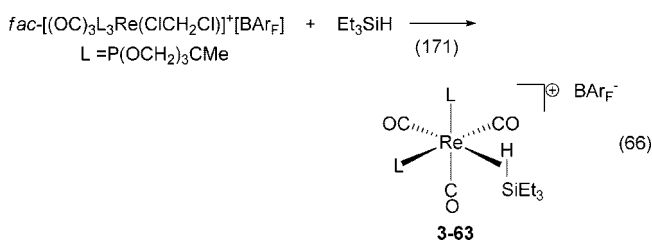


One of the earlier isolated CH_2Cl_2 solvates, $[\text{Cp}^*(\text{Me}_3\text{P})\text{Ir}(\text{Me})(\text{CH}_2\text{Cl}_2)]^+\text{BAR}'_4$,^{117b} activated both SiH and CH bonds as demonstrated in eq 65 and contrasted with the chemistry of the Rh analogue discussed previously. The product shown in eq 65 resulted from oxidation of Ir(III) to

Ir(V) and was the first structurally characterized and isolated Ir(V) arylhydride.¹¹⁶



Kubas and coworkers have utilized a “tied-back” phosphite, $[\text{MeC}(\text{OCH}_2)_3]\text{P}$ (L), in the preparation of CH_2Cl_2 complexes of Mn and Re. When $\text{trans-}[\text{L}_2(\text{OC})_3\text{MnMe}]$ was treated with $\text{Ph}_3\text{C}^+\text{BAR}'_4$, the Me group was abstracted and the solvated complex $\text{trans-}[\text{L}_2(\text{OC})_3\text{Mn}(\text{ClCH}_2\text{Cl})]^+\text{BAR}'_4$ was isolated.¹⁶⁸ The corresponding Re complex, $\text{fac-}[(\text{OC})_3\text{L}_2\text{Re}(\text{CH}_2\text{Cl}_2)]^+\text{BAR}'_4$, was isolated after protonation of $\text{fac-}[(\text{OC})_3\text{L}_2\text{ReMe}]$ by $[\text{H}(\text{OEt}_2)_2]^+\text{BAR}'_4$ to remove the Me group followed by addition of CH_2Cl_2 .¹⁷¹ Reaction of the manganese solvate with Et_3SiH gave $\text{trans-}[(\text{OC})_3\text{L}_2\text{Mn}(\eta^2\text{-H-SiEt}_3)]^+\text{BAR}'_4$ (**3-57**),¹⁶⁸ which was not isolated, but the Re solvate gave the isolated complex shown in eq 66. Two phosphines were required to stabilize the sigma complex as $\text{cis-}[(\text{OC})_3\text{L}_2\text{Re}(\eta^2\text{-H-SiEt}_3)]^+\text{BAR}'_4$, which was thermally unstable at room temperature.¹⁷¹

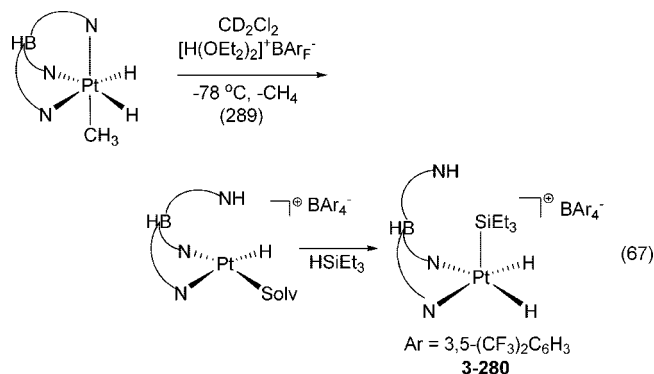


The photolysis of $\text{MeCpMn}(\text{CO})_3$ and $\text{HPh}_2\text{SiSiPh}_2\text{H}$ (2:1 ratio) gave a mixture of two complexes: $[\text{MeCp}(\text{OC})_2\text{Mn}(\eta^2\text{-H-SiPh}_2\text{SiPh}_2\text{H})]$ (**3-54**) and $[\text{MeCp}(\text{OC})_2\text{Mn}(\text{H})\text{SiPh}_2]_2$, but only the mononuclear complex was isolated.¹⁶⁶ If the irradiation of $\text{MeCpMn}(\text{CO})_3$ was conducted in THF, it was possible to monitor the quantitative formation of $[\text{MeCp}(\text{OC})_2\text{Mn}(\text{THF})]$ by IR spectroscopy. Addition of $\text{HPh}_2\text{SiSiPh}_2\text{H}$ resulted in formation of the mononuclear complex in higher yield. A faster reaction with higher yields of $\text{MeCp}(\text{OC})_2\text{Mn}(\eta^2\text{-HSiPh}_2\text{SiPh}_2\text{H})$ was realized with the more labile solvate, $\text{MeCpMn}(\text{CO})_2(\text{OEt}_2)$.¹⁶⁶ The corresponding rhenium complex, $\text{Cp}(\text{OC})_2\text{Re}(\text{THF})$ (formed in 50% yield from irradiation of $\text{CpRe}(\text{CO})_3$ in THF), also gave the mononuclear oxidative addition product, $\text{Cp}(\text{OC})_2(\text{H})\text{Re}(\text{SiPh}_2\text{SiPh}_2\text{H})$ (**3-59**).¹⁶⁶

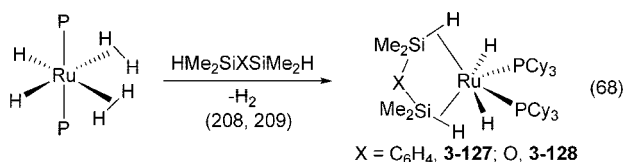
In a novel sequence of reactions, the protonation of a trispyrazolylborate complex of Pt(IV) led to the solvated cationic complex shown in eq 67 (which could be isolated as the acetonitrile adduct). Reaction of the intermediate cationic complex with HSiEt_3 provided a 5-coordinate Pt(IV) complex (**3-280**;^{289b}).

3.2.5. H_2

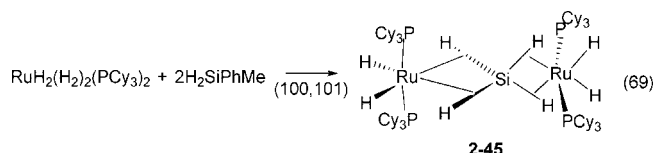
Dihydrogen complexes have been thoroughly reviewed by Kubas^{5c} but are still not commonly used as reagents for oxidative addition of hydrosilanes. A unique exception is the complex $\text{RuH}_2(\eta^2\text{-H}_2)_2(\text{PCy}_3)_2$, which has provided a



number of novel silyl–ruthenium complexes, some of which are summarized in Scheme 5. Both **3-129** and **3-130a**^{210,211a} were characterized by X-ray crystallography, and **3-125a,b,c** were characterized by NMR studies.²⁰⁷ When the ruthenium complex was reacted with chelating silanes, HMe₂Si–X–SiMe₂H, novel mononuclear ruthenium complexes were isolated with two Ru–(η²-H–Si) bonds as shown in eq 68.



One of the more interesting reactions of RuH₂(η²-H₂)₂(PCy₃)₂ involved the silane H₂SiMePh. In this case, the secondary silane disproportionated to provide SiH₄, which was then trapped by the Ru(II) complex as a novel Ru dimer (**2-45**) with an (μ-η²:η²:η²:η²-SiH₄) bridge as shown in eq 69.^{100,101} Additional silicon products resulting from the disproportionation were also identified and included HSiPh₃ (trapped as complex **3-129**), HSiPh₂Me, HSiMe₂Ph, an unidentified hydride product, and traces of the disilane, HMe₂SiSiMe₂H.¹⁰⁰ The bridged dimer **2-45** was also formed when the reaction was conducted with H₂SiEt₂.¹⁰⁰

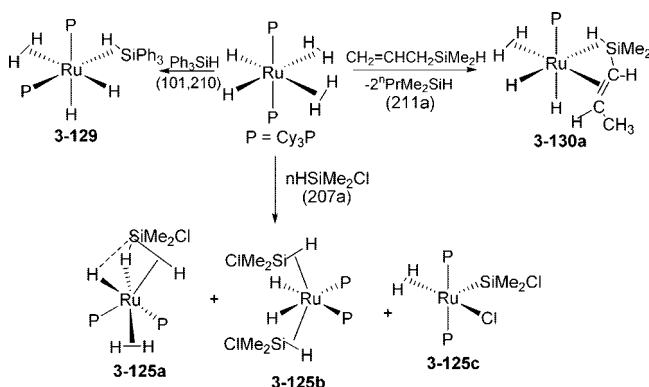


In this section, the loss of a variety of neutral ligands from the metal center followed by oxidative addition of a silane has been summarized. In the following three sections, loss of a neutral ligand may occur but an additional reaction, elimination of a small molecule HX (X = organic fragment (section 3.3.1), dihydrogen (section 3.3.2), or a silyl group (section 3.3.3), also occurred. Thus, there is no change in the oxidation state of the metal after the oxidative addition of the silane, and one may view the formation of the new silyl–metal complex as an “exchange” of a ligand at the metal with a silyl group (or a different silyl group).

3.3. Exchange of Anionic Ligands: Preparation from TM–R, TM–H, and TM–Si

In section 3.2, the transition metal precursors were assumed to lose a neutral ligand prior to oxidative addition of the silane. In this section, the reactions of the complex

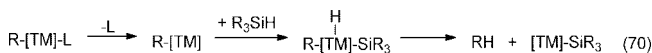
Scheme 5



will also involve loss of a neutral ligand and oxidative addition of the silane, but, in addition, elimination of a molecular fragment, RH, H₂, or HSiR₃, also occurs. The precursors and reactions are described in the order TM–R, TM–H, then TM–Si.

3.3.1. TM–R Precursors

Organotransition metal complexes that contain TM–R where R is an organic fragment (generally R is Me or Ph) can eliminate RH subsequent to the oxidative addition of the hydrosilane. A possible sequence for the reaction is shown in a general form in eq 70. The net effect is to replace an organic ligand with a silyl ligand.



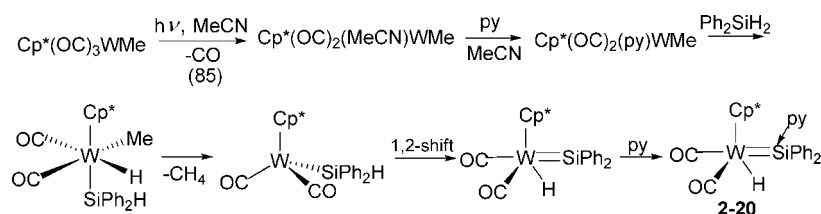
The majority of the transition metal precursors utilized in this approach contain Me substituents and tend to fit into two categories. The earlier transition metal complexes are of the type Cp(CO)_xMMe (x = 2, 3; Cp may be C₅H₅ or a Cp derivative), whereas the late transition metal complexes contain phosphine ligands in addition to one or two methyl groups. Examples of the basic systems are shown in Chart 4. The complexes of W and Fe that were exploited for reactions with silanes were primarily the 18-electron complexes CpW(CO)₃Me and CpFe(CO)₂Me, both of which lose a CO upon photolysis. The related Cp-substituted complexes of Ru and Os contain 2 PMe₃ ligands in place of the 2 CO groups, and the corresponding complexes of Rh and Ir contain one PMe₃ ligand and either an additional neutral ligand to produce an 18-electron metal cation or a second ligand that is anionic that completes the 18-electron count.

The facile replacement of a CO in CpW(CO)₃Me by CH₃CN to form the isolable CpW(CO)₂(MeCN)Me complex upon photolysis was previously described in section 3.2.4. The complex has been used as a starting material in reactions of hydrosilanes to provide a variety of products. Illustrated in Scheme 6 is a sequence that illustrates the use of Cp*(OC)₂(MeCN)WMe (an 18e complex) in the generation of a base-stabilized tungsten–silylene complex. The 1,2-rearrangement shown in Scheme 6 occurs when there is an open coordination site at the metal and can involve migration of groups other than hydrogen. Additional reactions starting with the isolated Cp*(OC)₂(MeCN)WMe complex are shown in Scheme 7.

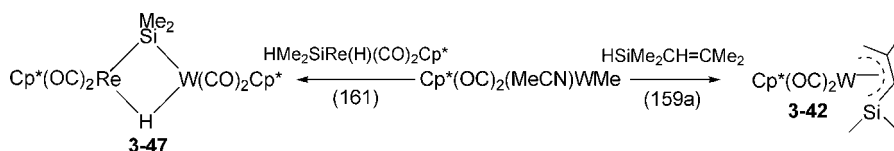
Chart 4. Selected Examples of Metal Complexes that Lose an Organic Group during the Oxidative Addition of Hydrosilanes (from Tables 1, 2, and 3) [Cp' Represents Both C₅H₅ and Substituted Cp Derivatives; L_x (x = 2, 3, 4) Represents Monodentate Ligands or a Chelate]

Cp'(OC)_{2,3}MMe or Cp'(OC)₂LMMe: 1-28, 1-29ab, 2-17, 2-18, 2-20, 2-28, 3-39 to 3-47 (W); 1-33b, 1-35, 2-36a, 3-68bc, 3-69, 3-77, 3-78, 3-82 (Fe).
 Cp'(OC)₂LWMe: 3-44, 3-45, 3-46, 3-47
 Cp*LiRMe₂, Cp*L(OTf)IrMe: 3-222, 3-223, 3-225 to 3-227
 [Cp*LL'RhMe]^{+,0}: 3-180, 3-181ab, 3-182ab
 Cp'LL'MR_x: 3-82, 3-96ab, 3-97 (R=Me; M=Ru); 3-83 to 3-85, 3-99, (R=CH₂SiMe₃, M=Ru, L=L'); 3-150 (R=CH₂SiMe₃; M=Os, L=L'); 3-180, (Me, M=Rh); 2-71ab, 3-223, 3-225 to 3-227 (Me; M=Ir; L'=OTf).
 Cp₂TiMe₂: 1-1, 1-11, 2-2, 3-2; Cp₂ZrR⁺, 1-16.
 Cp*₂ScMe: 1-8
 L₄MMe_x: 3-183, 3-191 (Rh, x = 1); 3-116, 3-117 (Ru, x = 2)
 L₃MMe: 2-60, 3-195, 3-218 (Rh).
 L₂MR₂ or LL'MR₂: 1-79, 3-282a,b, 3-283 (Pt, R=Me); 2-79a, 2-80, 2-82 (Pd, Et); 2-87 (Pt, Et); 2-102a (Pt, Ph)
 L₂PtMeR': 3-265 (R'=SiPh₃); Tp'(H)PtMe₂: 3-289
 L₂[Si∩P]IrMeH: 3-237
 [N∩P]PtMe₂: 3-283, 3-284a,b, 3-285, 3-286a,b
 Misc: LL'₂XOsPh: 3-152, 3-155 to 3-157

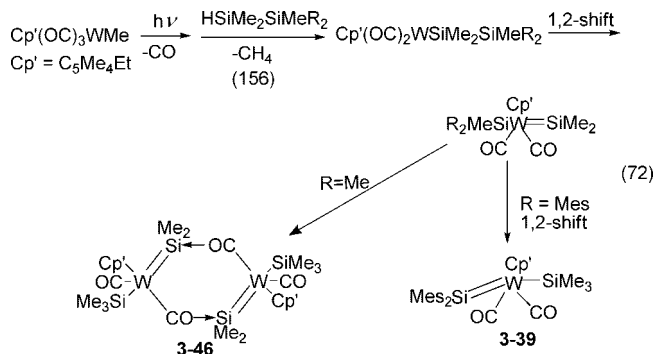
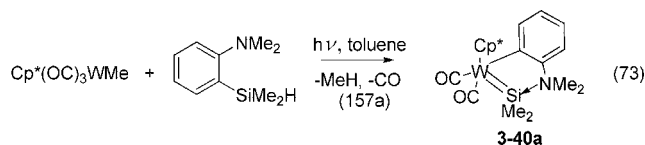
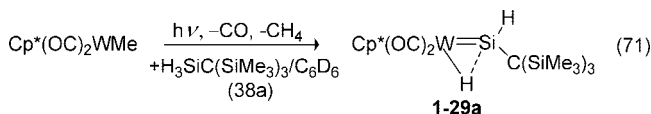
Scheme 6



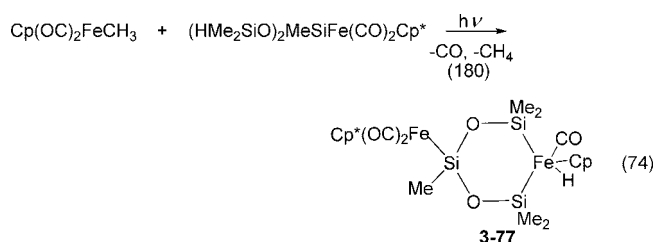
Scheme 7



The replacement of CO by solvent to give an isolable complex is not necessary to initiate the loss of methane, and CpW(CO)₃Me has been utilized to form a variety of base-stabilized silylene complexes as well as a novel hydride-bridged silylene as demonstrated in eq 71. The 1,2-rearrangement shown in eq 72 is similar to that illustrated in Scheme 6. In this case, it is a silyl group from the disilane HSiMe₂SiMeR₂ that migrates to the tungsten center. When the R group in the disilane is small, the silylene dimerizes to provide a “base-stabilized” system through coordination of the oxygen of a carbonyl group (3-46). When R is large, the initially formed silylene undergoes a 1,3-shift to generate a new silylene that is sterically protected and donor free (3-39).¹⁵⁶ A similar reaction but with aryl group migration is shown in eq 73, and in this case, the silylene exhibits intramolecular stabilization by an amine group. The iron analogue of 3-39, Cp*(OC)(Me₃Si)Fe=SiMe₂ (3-69), has been isolated using a reaction strategy similar to that shown in eq 72.^{22b,175a}

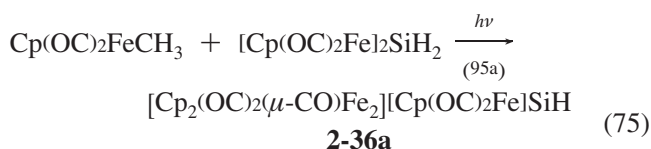


Replacement of Me in Fe–Me and W–Me with a silyl group occurred with loss of methane to give a complex with the same remaining ligand set at the metal in the formation

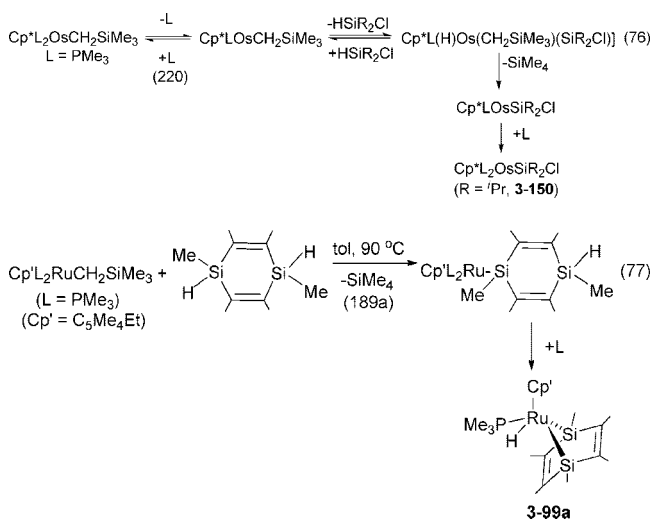


of Cp*(OC)₂FeSi(CHPh₂)H₂ (1-33b),^{42b} Cp*(OC)₂FeSiMe₂-NPh₂ (3-68b),^{174b} and Cp(OC)₃W–SiH₂[C(SiMe₃)₃] (1-28).^{38a} Both Cp(CO)₃WMe and Cp(CO)₂FeMe have been

utilized for the formation of bimetallic complexes such as **2-28**^{42b} (eq 33) and **3-77**¹⁸⁰ (eq 74). The first tris-metalated silane was also prepared from Cp(CO)₂FeMe as shown in eq 75.

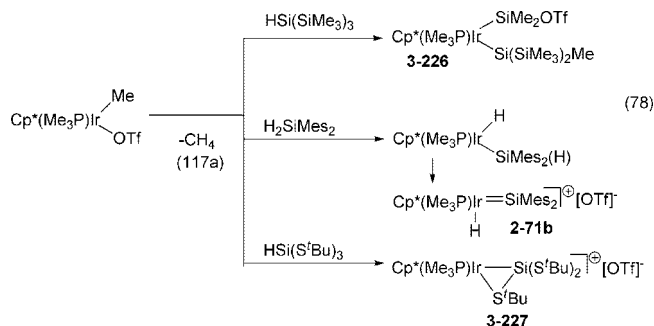


There are phosphine analogues related to the metal carbonyl derivatives described earlier in this section. Particularly useful have been derivatives of the type Cp'(PR)₃M–R where M = Ru, Os, L is a phosphine (usually PMe₃), and R is Me or CH₂SiMe₃. These complexes are used as precursors for exchange of R with a silyl group. For instance, CpL₂RuSiCl₃ (**3-82**; L = PMePh₂) was formed from the thermal reaction of CpL₂RuMe with HSiCl₃.¹⁸ Other examples include Cp*L₂RuSiCl₃ (**3-83**, L = PMe₃),⁴⁷ Cp*L₂RuSiⁱPr₂Cl (**3-84**, L = PMe₃),¹⁸³ Cp*L₂OsSiⁱPr₂Cl (**3-150**, L = PMe₃),²²⁰ and [Cp*LL'RhSiPh₃][BAR'₄] (**3-180**, L = PMe₃, L' = CH₃CN).²³⁸ It is likely that the sequence proposed for the formation of **3-150** and shown in eq 76 is similar for all these cases. Complexes such as **3-150** contain a functional group on silicon, thus allowing access to new derivatives. The SiCl bond in **3-150** can be converted to SiOTf on reaction with Me₃SiOTf. The covalent form of the complex, Cp*L₂OsSiⁱPr₂OTf, appears to be a source of the silylene complex, [Cp*L₂Os=SiⁱPr₂]OTf, when dissolved in CD₂Cl₂ as indicated by the ²⁹Si NMR resonance that was downshifted to 223 ppm relative to a value of 100 ppm when the complex was dissolved in C₆D₆. Another example of the use of a functional group at silicon is provided in the sequence that led to the disilabenzene complex of ruthenium, as shown in eq 77.



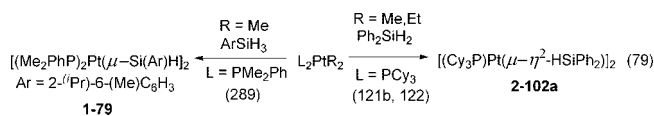
A potential anionic leaving group at the metal has been useful in developing novel silyl–osmium complexes from the 18-electron complex, Cp*(Me₃P)(OTf)IrMe. Examples are shown in eq 78, where loss of methane occurs in solution at room temperature.^{117a} It is clear from the nature of the reaction products that migration of groups from Si to Ir occurred.

The precursor complexes of electron-rich metals in this section tend to contain only phosphine ligands in addition



to the organic substituents, and reactions of these phosphine complexes with silanes generally require heating. There was reported an interesting contrast in products from (Me₃P)₄RuMe₂ and HSiMe₃ as a function of temperature. At 25 °C, elimination of methane provided (Me₃P)₄Ru(Me)SiMe₃ (**3-116**, ~13%), whereas at 65 °C with excess HSiMe₃, the product was (Me₃P)₄Ru(H)SiMe₃ (**3-117**, 89%), indicating that there are separate reductive elimination steps.⁹⁷ There are several reports of the reactions of various types of silanes with L₂PtR₂ or LL'MR₂ (M = Pt or Pd). When *cis*-(Me₃P)₂PtEt₂ was treated with H₂SiPh₂ at room temperature, *trans*-(Me₃P)₂Pt(SiHPh₂)₂ (**2-87**) was isolated, but when **2-87** was redissolved, a mixture of *cis*- and *trans*-**2-87** was observed whose ratio depended on the solvent.¹²⁵ When a solution of *cis*-**2-87** was heated in toluene to 100 °C, the trinuclear complex **3-298a** formed (see eq 32).^{298b} The reaction of the Pd analogue, (Me₃P)₂PdEt₂, with H₂SiPh₂ at 55 °C, however, gave two dimeric Pd complexes, [(Me₃P)Pd](μ-η²-H–SiPh₂)₂[Pd(PMe₃)₂] (**2-79a**) and [(Me₃P)Pd]₂(μ-η²-H–SiPh₂)₂ (**2-81**) in 63% and 3% yields, respectively.^{121ab}

Temperature, the cone angle of the phosphine, and the size of the substituents at silicon most likely will influence the nature of the silyl–metal complex that forms, although no systematic study of any of these factors has been reported except in calculations (section 7.3.7). As an example of the subtle aspects in Pt dimer formation, see the products summarized in eq 79. In **2-102a**^{121b,122} there are bridging hydrides and only one phosphine coordinated to a Pt center, whereas in **1-79**⁷⁰ there are no bridging hydrides and two phosphines per Pt center.

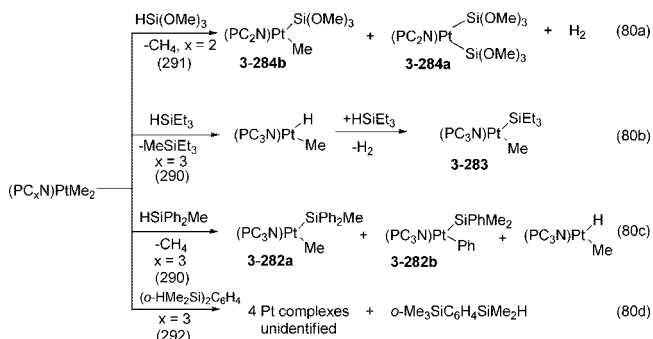


Schubert and coworkers have developed the chemistry of ligands that contain hemilabile chelates including Ph₂P(CH₂)_xNMe₂ (x = 1, 2, 3) and *o*-Ph₂PC₆H₄NMe₂. The reactivity of the (P∩N)PtMe₂ (∩ indicates a linker between P and N) appears to be a function of the P∩N ligand and how easily the amino group is decoordinated from the metal center during reaction with the silane or to the differential activation of Pt–Me by the chelate.^{290,291} The reactions of (P∩N)PtMe₂ (P∩N = Ph₂P(CH₂)_xNMe₂, PC_xN, x = 2, 3) with a variety of silanes are illustrated in eq 80. The PtMe and PtPh groups shown in eq 80a,b,c are located *trans* to the phosphorous of the chelate. Analogues **3-282ab**, **3-283**, and **3-284ab** prepared from Ph₂P(CH₂)₂NMe₂ and silanes will

Chart 5. Selected Examples of Metal Hydride Complexes that Lose Hydrogen during the Oxidative Addition of a Hydrosilanes (from Tables 1, 2, and 3) [Cp' Represents Both C₅H₅ and Substituted Cp Derivatives; L_x (x = 2, 3, 4) Represents Monodentate Ligands and LL Represents a Chelate]

Cp'^{*}MH_y: **1-12** (Ti); **3-12ab**, **3-14**, **3-16** (Nb); **1-23**, **2-9**, **3-31** (Mo); **3-38** (W).
 Cp'^{*}M(μ-H)_yMCp': **1-82** (Sm), **1-83** (Lu); **2-34**, **2-35** (Fe); **2-41**, **3-135a,b**, **3-136**, **3-137a,b**, **3-138** (Ru).
 Cp'^{*}LMH_x: **3-86**, **3-88**, **3-89ab**, **3-90**, **3-91ab**
 L_xMH_y: **3-64**, **3-65** (Re); **2-38a**, **2-39** (Ru); **3-160** (Os).
 LL'_xMH_y: **3-109**
 (LL)MH_y: **1-26**, **1-27**, **2-15** (Mo).
 [(LL)M]₂(μ-H): **2-67**, **2-68**, **2-69** (Rh)
 Miscellaneous: **1-38a** (Fe); **1-42**, **3-108**, **3-122**, **3-125c** (Ru); **3-154**, **3-160** (Os); **3-300**, **3-301ab** (Pt).

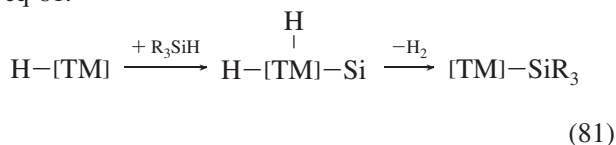
be found in Table 3. Calculations using SiH₄ supported the role of 6-coordinate Pt(IV) intermediates in the oxidative addition adduct (P(N)PtMe₂(SiH₃)(H) that then eliminated MeSiH₃ to give (P(N)Pt(H)Me followed by oxidative addition of SiH₄ to provide a second Pt(IV) intermediate that would eliminate H₂ to give (P(N)Pt(SiH₃)Me.²⁹⁵ Note that only in the case of “activated” silanes such as HSi(OMe)₃ was a disilyl–platinum complex observed. Although Pt(IV) complexes have not often been used as precursors to Pt–Si complexes, there was one report of the thermal reaction of Tp'PtMe₂H (Tp' = hydridotris(3,5-dimethylpyrazolyl)borate) with Et₃SiH where Tp'Pt(SiEt₃)(H)₂ (**3-289**) was produced.²⁹⁵ The facile reaction of **3-289** with MeOH was shown to provide the stable platinum(IV) trihydride, Tp'PtH₃.²⁹⁵



Although this section included reactions of phosphine complexes of the Ni triad in the +2 oxidation state, these are not the only precursors to silicon complexes of this triad, and reactions starting with M(0) derivatives will be discussed in section 3.6.

3.3.2. TM–H Precursors

In this section, the reactions of a complex may (or may not) proceed by loss of a neutral ligand followed by oxidative addition of the silane, and, in addition, elimination of H₂ also occurs, effectively replacing [TM]–H with [TM]–SiR₃; thus, the oxidation state of the metal does not change. A possible sequence for the reaction is shown in a general form in eq 81.

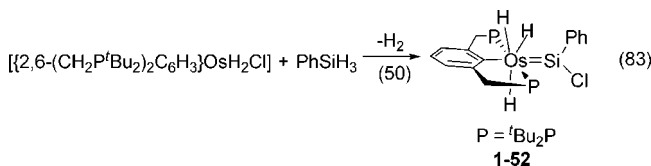
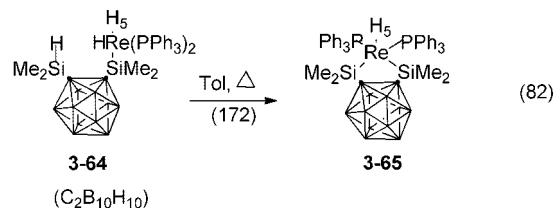


The hydride precursors that undergo this type of transformation are not easily classified. The derivatives tend to contain Cp' ligands or primarily phosphine ligands and may be mononuclear with regard to the metal or may be metal dimers with bridging hydrides. Chart 5 summarizes selected

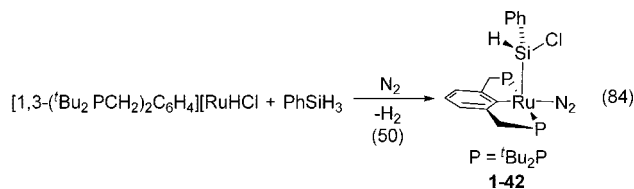
cases from Tables 1, 2, and 3.

When a mononuclear metal hydride interacts with a silane, direct replacement of the MH with MSiR₃ may occur. Reaction of Cp₂MH₂ with primary, secondary, or tertiary silanes has provided several examples of formation of derivatives of Cp₂(H)MSiR₃ including R = Et (M = Mo, **3-31**) and R = Cl (M = W, **3-38**).³⁵ Niobium hydrides have also been used as precursors to silyl–niobium complexes. When Cp₂NbH₃ was reacted with HSiMe₂Cl in toluene at 50–60 °C, a mixture of two isomers of Cp₂(H)₂NbSiMe₂Cl (**3-12ab**) formed, but at 95 °C, the product was the symmetrical isomer of Cp₂Nb(SiMe₂Cl)₂H (**3-16**).¹⁴²¹⁴⁴¹⁴⁵ Analogues of **3-12a**, **3-13**, and **3-14**, were similarly prepared from HSi(ⁱPr)₂Cl¹⁴³ and HSiMe₂OEt.¹⁴⁴ The equivalent of one of the three hydrides in Cp*(L)Ru(H)₃ was replaced in the thermally induced reaction with HSiMe₂Ph to give Cp*(L)(H)₂RuSiMe₂Ph (L = (pyl)₃P; **3-86**).¹⁸⁴ It is probable that, under thermal conditions, H₂ was eliminated followed by OA of the silane.

Phosphine complexes of metal hydrides will also exhibit simple replacement of MH with MSi, although more complicated reactions also occur. Reaction of L₄RuH₂ with secondary silanes provided L₄(H)RuSiR₂H (L = PMe₃, R = Ph, **2-38a**, and R = Me, **2-39**).⁹⁶⁹⁷ The complex ReH₇(PPh₃)₂ reacted with 1,2-(HMe₂Si)₂C₂B₁₀H₁₀ at 0 °C to form the kinetic intermediate (PPh₃)₂ReH₆[η¹-SiMe₂C₂B₁₀H₁₀(SiMe₂H)-Si] (**3-64**).¹⁷² On heating, **3-64** converted to the chelated complex, **3-65**, shown in eq 82. The osmium hydride (Ph₃P)₃OsH₄ reacted with the silatrane, N{OCH₂CH₂}₃SiH, to replace one of the hydride ligands to give the 7-coordinate complex [N{OCH₂CH₂}₃Si](Ph₃P)₃OsH₃ (**3-160**).²²¹ The silane, HSi(Me)(CH₂CH₂CH₂PPh₂)₂, (biPSiH) reacted as a “tridentate” with *mer*-RuH(PPh₃)₃(CO)Cl to give the “exchange” product, (biPSi)(OC)ClRu (**3-115**).²⁰⁴

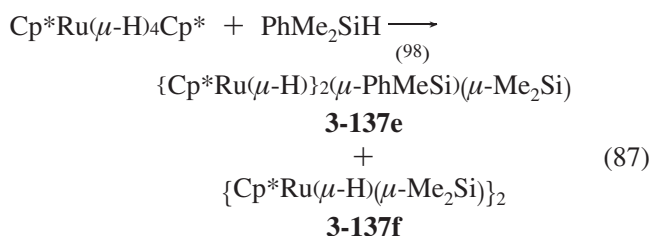
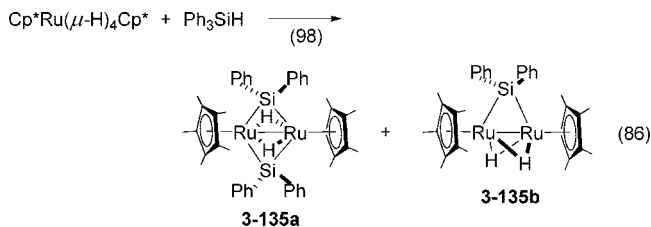
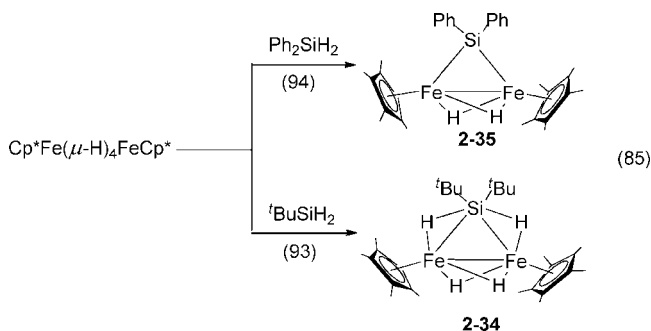


As with cases described in earlier sections, reactions with metal hydrides can result in formation of H₂, but additional subsequent reactions may also result. Hydrogen evolution



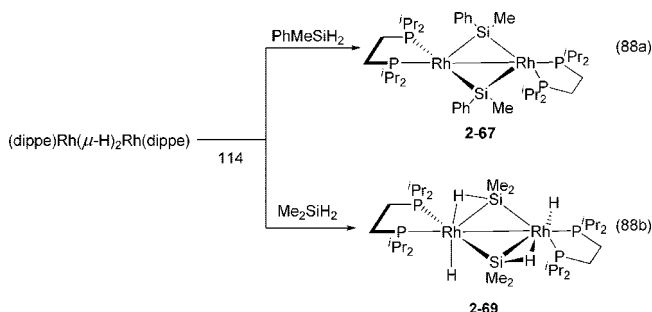
occurred on addition of HSiCl_3 to $(\text{C}_3\text{P})_2(\text{OC})(\text{Cl})\text{RuH}$ to generate the intermediate $(\text{C}_3\text{P})_2(\text{OC})(\text{Cl})\text{RuSiCl}_3$, which reacted further to give the isolated salt, $[\text{C}_3\text{PH}][(\text{C}_3\text{P})(\text{OC})(\text{Cl})\text{Ru}(\text{SiCl}_3)_2]$ (**3-114**).²⁰³ In an interesting contrast in Ru and Os chemistry, elimination of H_2 occurred on addition of PhSiH_3 to the “pincer” complex, $\{2,6-(\text{CH}_2\text{P}^t\text{Bu}_2)_2\text{C}_6\text{H}_3\}\text{OsH}_2\text{Cl}$, which was accompanied by rearrangement of a chloride from Os to Si to give the osmium–silylene complex **1-52** as two rotamers in solution (eq 83).⁵⁰ The closely related Ru analogue, $\{1,3-(\text{CH}_2\text{P}^t\text{Bu}_2)_2\text{C}_6\text{H}_3\}[\text{RuHCl}]$, which contained an agostic interaction between the central C–H unit and the Ru center, also exhibited a rearrangement of a RuCl to SiCl , but the resultant complex was captured by N_2 to give the product shown in eq 84.⁵⁰

Hydride-bridged dimers with Cp^*_2M ($\text{M} = \text{Sm}, \text{Lu}$) or Cp^*M ($\text{M} = \text{Fe}, \text{Ru}$) units react with retention of the dimer unit or with the formation of a monomeric silyl unit. Tilley and coworkers developed reactions of the silane 1,2- $\text{H}_3\text{SiC}_6\text{H}_4\text{OMe}$ with dimers of Sm and Lu, where the monomer product was stabilized by coordination of ArOMe as shown for Sm earlier in eq 24.⁷³ However, the hydride-bridged dimers of Fe and Ru are converted to silyl-bridged dimers as shown in eqs 85–87. In the last two cases, redistribution of the starting tertiary silane probably occurred to form the products shown.



The hydride-bridged phosphine rhodium dimer also reacted with secondary silanes in a fashion somewhat similar to the

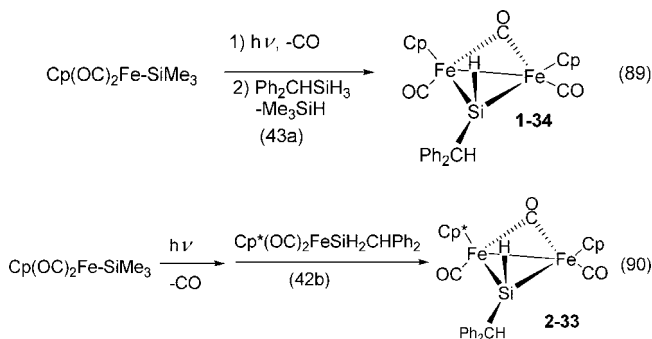
Cp^* counterparts. When PhMeSiH_2 was added to the rhodium dimer $[(\text{dippe})\text{Rh}]_2(\mu\text{-H})_2$, the bridging hydrides were replaced by PhMeSi groups (eq 88a) to give two isomers with *cis*- or *trans*-Ph groups. However, with Me_2SiH_2 , a different dimer was produced that contained nonclassical hydrides bridging a $\text{Rh}\text{--Si}$ bond (eq 88b).¹¹⁴ Direct replacement of a terminal PtH in $[\text{Pt}_3\text{H}(\mu\text{-PPh}_2)_3(\text{PEt}_3)_3]$ by HSiPh_3 occurred to give $[\text{Pt}_3(\text{SiPh}_3)(\mu\text{-PPh}_2)_3(\text{PEt}_3)_3]$ (**3-300**).¹³⁵



3.3.3. TM–Si Precursors

The reaction of $\text{TM}\text{--SiR}'_3$ with HSiR'_3 to give $[\text{TM}]\text{--SiR}'_3$ constitutes an exchange reaction. Examples of complexes produced by this approach are summarized in Chart 6. As can be seen from Chart 6, the exchange route has been exploited primarily in the iron triad and for Pt complexes.

It is likely that the steps for silyl exchange parallel those that occur in the loss of an organic group from $[\text{TM}]\text{R}$ on addition of HSiR'_3 as illustrated earlier in section 3.3.1. Examples of related silyl exchanges are shown in eqs 89 and 90.



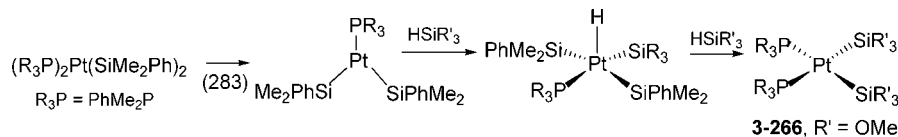
The exchange of silyl groups in *trans*- $[(\text{Et}_3\text{P})_2(\text{I})\text{PtSiMe}_3]$ on addition of MePhSiH_2 was proposed to occur by oxidative addition to give $[(\text{Et}_3\text{P})_2(\text{H})(\text{I})\text{Pt}(\text{SiMe}_3)(\text{SiHPhMe})]$ followed by reductive elimination of Me_3SiH to provide $[(\text{Et}_3\text{P})_2(\text{I})\text{PtSiMePhH}]$ (**2-97a**) in 100% yield.¹³⁰

However, in the case where a silyl–metal hydride, $\text{R}_3\text{Si}[\text{TM}]\text{H}$, is reacted with a new silane, reductive elimination of R_3SiH is generally speculated to occur prior to the oxidative addition of the new silane $\text{R}'_3\text{SiH}$. Generally, but not in all examples, the reacting silane is smaller than the silyl group originally bound to the metal center in the electron-rich metals (eq 91 is an exception). When the displaced silane is Me_3SiH , removal of this volatile silane can drive the reaction with a “larger” incoming silane to provide the new silyl–metal complex (eqs 92 and 93). The 7-coordinate ruthenium complex shown in eq 93 has been used to form bis-silyl complexes including those with a chelating bis-silyl group. It is likely that exchange in 7-coordinate $[(\text{Ph}_3\text{P})_2(\text{OC})(\text{H})_3\text{OsSiMe}_3]$ (**3-153**) in the pres-

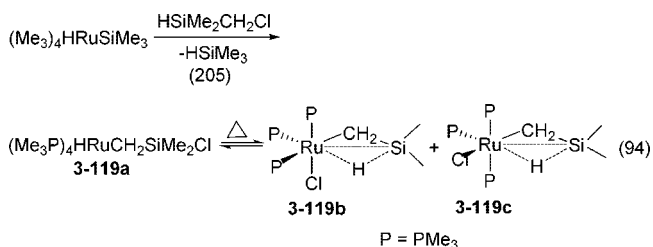
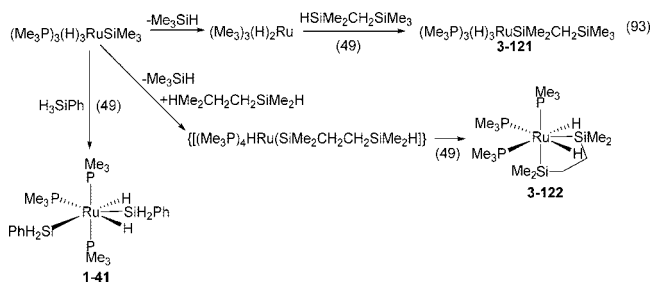
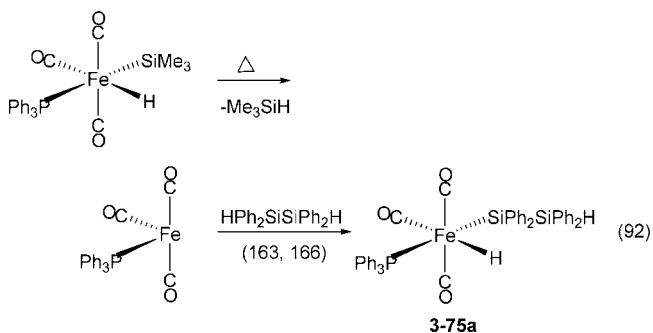
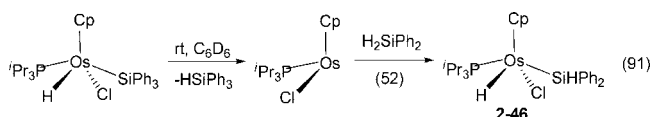
Chart 6. Complexes Formed from Reaction of [TM]SiR₃ and HSiR'₃

Sc through Mn Triads: **1-15** (Zr); **3-11b** (V); **1-20ab** (Ta); **3-11b** (V); **1-25c** (Mo), **1-32** (Re)
 Fe Triad: **1-34**, **1-38bcd**, **2-33**, **3-75a** (Fe); **1-41**, **2-40**, **2-43ab**, **3-121**, **3-122** (Ru); **2-46**, **3-153** (Os).
 Co and Ni Triads: **3-216** (Rh); **2-90**, **2-96cde**, **2-97a**, **3-262**, **3-263**, **3-265**, **3-266**, **3-273** (Pt).

Scheme 8



ence of HSiEt₃ to give [(Ph₃P)₂(OC)(H)₃OsSiEt₃] (**3-153**) also occurred by reductive elimination of Me₃SiH prior to addition of the Et₃SiH.²²² The exchange of a silyl group may take a decidedly unique pathway, as was the case in the reaction of (Me₃P)₄HRuSiMe₃ with HSiMe₂CH₂Cl.²⁰⁵ In this case, at least two rearrangements took place to give a final product with a Ru—CH₂Si sequence and a nonclassical Ru···H···Si interaction (eq 94).



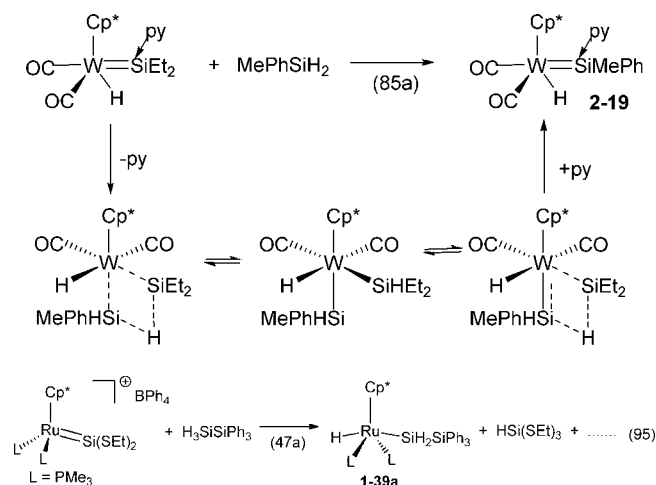
Factors that influence silyl group exchange at Pt(II) centers have been studied by Schubert and co-workers,^{128,283} Tanaka and co-workers,^{130a} and Ozawa and Kamite.²⁸¹ Schubert and co-workers showed that *cis*-(PhMe₂P)₂Pt(SiMe₂Ph)₂ exchanged with an excess of HSi(OMe)₃ (in benzene solvent) to give *cis*-(PhMe₂P)₂Pt{Si(OMe)₃}₂ but that the *trans*-

isomer exhibited no exchange with either HSi(OMe)₃ or HSiMe₂SiPh₃.^{128,283} The rate of disappearance of *cis*-(PhMe₂P)₂Pt(SiMe₂Ph)₂ on addition of a series of hydrosilanes followed the order H₂SiPh₂ (~1 h) > HPh₂SiSiMe₃ (~3 h) > HSi₃Ph₇ (~1 day) > HSiPh₃ (~4 days). The rate of exchange of the second silyl group was even slower and, in the case of HSiPh₃, required 10 d at 60 °C in the more coordinating solvent THF.¹²⁸ The phosphine (PPh₂Me, PEt₃, PPhMe₂) also influenced the exchange rate with (MeO)₃SiH and correlated with the cone angle (136°, 132°, and 122°, respectively). A smaller cone angle in the entering silane as well as electronegative substituents at silicon promoted the exchange reaction. For example, the addition of HSiMe₂Ph to *cis*-(PhMe₂P)₂Pt(SiPh₃)₂ gives *cis*-(PhMe₂P)₂Pt(SiPh₃)(SiMe₂Ph) in benzene within 10 min at rt.²⁸¹ Chelating phosphine complexes, [(R₂PCH₂CH₂PR₂)Pt(SiMe₂Ph)₂] (R = Ph, Me, Cy), react much more slowly with HSi(OMe)₃. The reactivity of the phosphine complexes followed the order 2PR₃ >>> dppe > dmpe >> dcpe.²⁸³ Schubert and co-workers determined that the dissociation of the phosphine ligand was the rate-determining step in silyl group exchange (even with chelating phosphines). The sequence shown in Scheme 8 was proposed for silyl group exchange at Pt(II) centers. Pt(II) complexes with only one silyl substituent also exchange with silanes. After 30 min at 90 °C, *trans*-(Et₃P)₂Pt(Br)SiMe₃ reacted with PhMe₂SiH to give *trans*-(Et₃P)₂Pt(Br)SiMe₂Ph (**3-262**) (95% conversion of starting complex).¹³⁰ The reaction of the corresponding iodide complex, *trans*-(Et₃P)₂Pt(I)SiMe₃, with the secondary silane MePhSiH₂ gave quantitative yields of [(Et₃P)₂Pt(I)SiHMePh] (**2-97a**) after 4 h at rt.¹³⁰ In contrast, there are probably two oxidative addition/reductive elimination steps when *cis*-(PhMe₂P)₂PtMe(SiPh₃) reacted with excess HSiPh₂F (60°, 12 h, C₆H₆) to give *cis*-(PhMe₂P)₂Pt(SiFPh₂)₂ (**3-265**).²⁸¹ Thus, these four studies indicated both an electronic and a steric influence on the exchange of silyl groups at Pt(II) centers.²⁸³

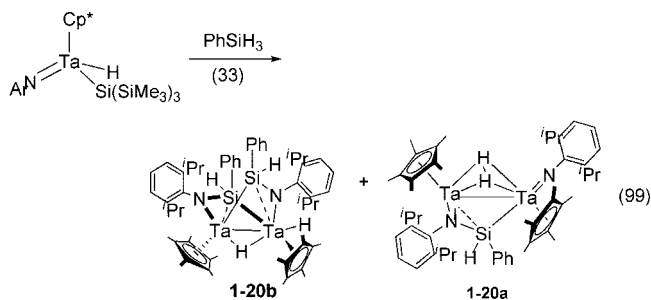
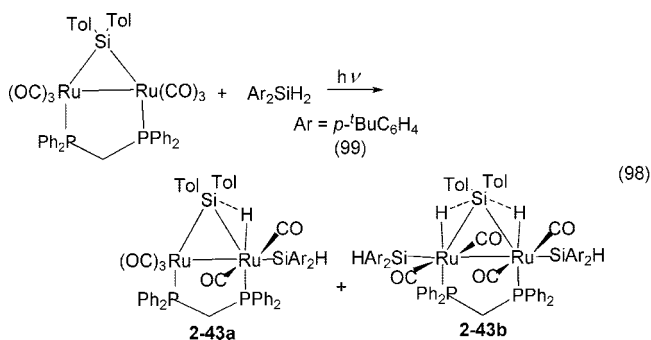
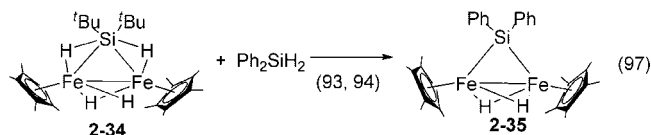
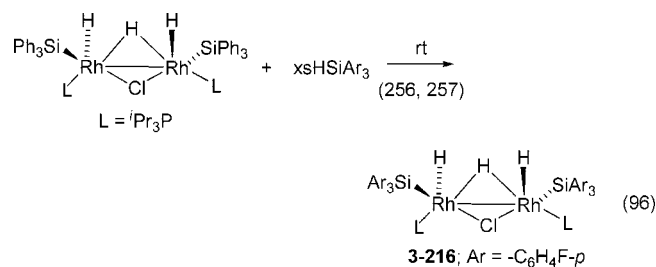
Although the previous examples described exchange of TM—silyl complexes, *silylene* exchange has also been observed. The proposed mechanism is shown in Scheme 9 and involved HSi addition to the TM=Si bond to give HSi[TM]SiH followed by elimination of H₂SiR₂ through a 4-centered transition state. With MePhSiD₂ as a reactant, only Et₂SiD₂ was detected as the silyl exchange product; thus, the W—H bond in the starting complex was not involved in the silylene exchange reaction. Another [TM]=Si reaction with a “primary” silane was reported but took an obviously different pathway as shown in eq 95.^{49a}

Silyl group exchange reactions also can occur in bimetallic complexes, although the sequence from starting to final complex is certainly unknown. Four examples are shown in eqs 96–99. The Ru complex in eq 98 appears to react

Scheme 9



stepwise to give **2-43a** then **2-43b** where the bridging silylene remains intact. At room temperature, after a day, complexes with Ar_2Si bridges were tentatively identified.⁹⁹



The replacement of the bulky $\text{Si}(\text{SiMe}_3)_3$ group in $\text{Cp}^*(\text{ArN}=\text{CH})\text{TaSi}(\text{SiMe}_3)_3$ ($\text{Ar} = 2,6\text{-}i\text{Pr}_2\text{C}_6\text{H}_3$) by the primary silane PhSiH_3 takes an unusual pathway, most likely as a result of the presence of additional hydrides on silicon. There

were two silicon-containing dinuclear complexes produced, diamagnetic **1-20b** and paramagnetic **1-20a**, as shown in eq 99.³³ Transition metal complexes can cause disproportionation of phenylsilanes. When the complexes $(\text{DippN}=\text{CH})_3\text{ReSiMe}_3$ or $(\text{DippN}=\text{CH})_3\text{ReSiHPh}_2$ ($\text{Dipp} = 2,6\text{-}i\text{Pr}_2\text{C}_6\text{H}_3$) were treated with PhSiH_3 , reaction mixtures were produced that contained $(\text{DippN}=\text{CH})_3\text{ReSiH}_2\text{Ph}$ (prepared by an independent route) in addition to Ph_2SiH_2 , SiH_4 , and C_6H_6 , the last of which indicated that some type of Si–C bond activation process occurred.⁴¹

3.4. Addition of Silanes to Metals and to Low-Valent Metal Complexes

In the previous sections, the oxidative addition of hydrosilanes to metal centers (in complexes) featured the loss of a neutral ligand (section 3.2) or of an anionic ligand (section 3.3) from the metal center in conjunction with the addition of the hydrosilane. In general, 18e silyl–metal complexes were produced. In section 3.4, reactions of metals and coordinatively unsaturated, low-valent metals are featured. There is some overlap with sections 3.2 and 3.3, but the retention of the original ligand set of the reactant in the product produced is a feature of the examples described in section 3.4. Also included are reactions where the H–Si bond functioned as a σ -donor and essentially replaced a σ -donor in the original complex. In this case, there is no change in oxidation state for the central metal upon reaction with the silane.

Oxidative addition of a hydrosilane to a metal in the zero oxidation state will lead, at least initially, to a $\text{H}[\text{TM}]\text{SiR}_3$ fragment. There are a few cases that involve metals as reactants, and these include Ti, Fe, Ni, Zn, and Au_s . When gaseous Ni^{23} and Zn^{25} metal atoms were reacted with SiH_4 and the products were condensed in an argon matrix, H-Ni-SiH_3 (**1-5**)²³ and H-Zn-SiH_3 (**1-7**)²⁵ were identified as the products. The H–Ni–Si angle is less than 90° , suggesting an interaction of the Ni–H with the Si center somewhat like an arrested addition of the nickel atom into an Si–H bond. In the case of Ti, the trapped TiSiH_4 species contained hydride bridges between Ti and Si and were assigned the structures $\text{HTi}(\mu\text{-H})_2\text{SiH}$ (**1-2a**) and $\text{HTi}(\mu\text{-H})_3\text{Si}$ (**1-2b**).^{20a} In a metal atom reactor, Fe atoms were interacted with toluene and HSiMeCl_2 to form the intermediate $(\text{C}_6\text{H}_5\text{CH}_3)_2\text{Fe}$, which reacted with the silane to give the Fe(IV) derivative, $(\text{C}_6\text{H}_5\text{CH}_3)(\text{H})_2\text{Fe}(\text{SiMeCl}_2)_2$ (**3-70**).⁹² It is unlikely that any of these complexes would be observed on reaction of the silane with bulk metal. However, when a solid gold metal surface was treated with HexSiH_3 , 95% coverage of the surface by a monolayer of HexSi (**1-80**) was observed.^{71a} A similar reaction of the silsesquioxane, $\text{H}_8\text{Si}_8\text{O}_{12}$, generated SiO on a gold surface (**3-302**).³⁰¹

A more practical solution to reactions of $\text{M}(0)$ would be to convert the metal into a suitable soluble form that would then react with the silane in a solvent. This could be accomplished by using neutral, ancillary ligands such as carbonyls and/or phosphines to produce organic soluble $\text{M}_x(\text{CO})_y$ or $\text{M}(\text{PR}_3)_x$ derivatives or in complexes that contain a mixture of these two ligands, $\text{M}(\text{L})_x(\text{CO})_y$ ($\text{L} = \text{phosphine}$). Most of these metal complexes are included in sections 3.2.1 and 3.2.2, where loss of a phosphine or of a carbonyl from the metal center prior to oxidative addition of the silane was summarized. The carbonyl precursors listed in section 3.2.2 (Chart 2) are generally commercially available and include the following: $\text{M}(\text{CO})_6$, ($\text{M} = \text{Cr}, \text{Mo}, \text{W}$); $\text{Fe}(\text{CO})_5$;

$\text{Ru}_3(\text{CO})_{12}$; and $\text{Co}_2(\text{CO})_8$. Of these, $\text{Co}_2(\text{CO})_8$ or $\text{Ru}_3(\text{CO})_{12}$ can either deliver a $\text{M}(\text{CO})_x$ unit or the metal framework can remain intact. In the case of $\text{Ru}_3(\text{CO})_{12}$, a Ru_2 complex may also be generated. The examples where multinuclear products are formed from polynuclear metal reactants are included primarily in section 3.5.

In section 3.2, the loss of a neutral ligand from the metal center followed by oxidative addition of a hydrosilane was discussed for ligands such as carbonyls, phosphines, olefins (and acetylenes), dihydrogen, and coordinated solvents. In general, the ligand that was lost does not re-enter the coordination sphere of the metal in the examples in section 3.2. The most common examples will be found in Charts 1 (section 3.2.1), 2 (section 3.2.2), and 3 (section 3.2.3). In section 3.4, reactions of low-valent metal complexes will be discussed with the following focus: (a) replacement of a ligand at the metal center by the silicon unit *without* a change in oxidation state of the metal center and (b) addition of a hydrosilane to a $\text{M}(0)$ or low-valent M complex without loss of a ligand from the original coordinatively unsaturated complex.

A CO may be replaced at the metal center with a “neutral” silicon fragment that functions as a σ -donor through the H–Si bond. Examples have been reported for $\text{M}(\text{CO})_6$ ($\text{M} = \text{Cr}, \text{Mo}, \text{W}$), but the products will depend on the type of hydrosilane used. An R_2Si unit (a silylene) can be introduced into the coordination sphere of the metal through the reaction of a secondary silane as illustrated in the formation of **2-7** (Cr ; eq 47; structure later retracted^{80a}), **2-25**,^{87ab} and **2-26c**,^{87b,88} (W ; eq 44). However, when a tertiary silane was used, a σ -complex was obtained from $\text{Cr}(\text{CO})_6$, $\text{Mo}(\text{CO})_6$, and $\text{W}(\text{CO})_6$ as illustrated in eq 100 for formation of **3-29**,^{81,83a} **3-36**,^{81,83a} and **3-49**,^{81,83a} respectively. In one study,^{83a} the nature of the product was deduced from femtosecond infrared studies, whereas in a second study, the complexes were generated in solution and characterized by NMR methods (but not isolated).⁸¹ A related study of the photolysis of $\text{CpV}(\text{CO})_4$ in the presence of HSiEt_3 produced a product assigned the structure $\text{Cp}(\text{OC})_3\text{V}(\eta^2\text{-H-SiEt}_3)$ (not isolated; eq 43).¹⁴¹ Photolysis of $\text{Cp}'\text{Mn}(\text{CO})_3$ or $\text{Cp}'\text{Mn}(\text{CO})_2(\text{PMe}_3)$ in the presence of tertiary silanes gave isolable products where $\eta^2\text{-H-Si}\equiv$ replaced a CO (see **3-54**¹⁶⁶ (eq 45), **3-55**,¹⁶⁷ and **3-56**¹⁶⁶). When a tertiary silane is tethered to a ligand coordinated to a metal carbonyl complex, photolysis results in loss of CO and the H–Si unit became a σ -donor (**3-51**,¹⁶³ eq 44; **3-52a**,¹⁶⁴ eq 51).



Displacement of ligands other than CO are less common. Although possibly unique to group 6 chemistry, replacement of a σ -donor N_2 ligand in $[\text{Mo}(\text{CO})(\text{depe})_2]_2(\mu\text{-N}_2)$ by H_2SiPh_2 gave $(\text{OC})(\text{depe})_2\text{Mo}(\eta^2\text{-H-SiPh}_2\text{H})$, **2-13**,^{21b} and from SiH_4 , $(\text{OC})(\text{depe})_2\text{Mo}(\eta^2\text{-H-SiH}_4)$, **1-3d**, was isolated.^{21b} In these two cases, N_2 is lost and the metal retained a 0 oxidation state.

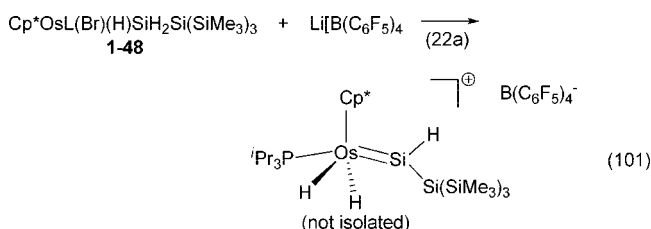
If the metal complex is electronically unsaturated, a silane σ -donor can add to the coordination sphere to increase the electron count of the metal. This was the case in the reaction of $\text{Mo}(\text{CO})(^i\text{Bu}_2\text{PCH}_2\text{CH}_2\text{P}^i\text{Bu}_2)_2$ (a 16e complex) with H_2SiPh_2 , which gave $(\text{OC})(^i\text{Bu}_2\text{PCH}_2\text{CH}_2\text{P}^i\text{Bu}_2)_2\text{Mo}(\eta^2\text{-H-SiPh}_2\text{H})$ (**2-14**).^{21b} Another example involves addition of HSiMe_2Cl to the unsaturated complex $\text{Cp}^*(^i\text{Pr}_3\text{P})\text{RuCl}$ to give $\text{Cp}^*(^i\text{Pr}_3\text{P})\text{ClRu}(\eta^2\text{-H-SiMe}_2\text{Cl})$ (**3-92**), which is an Si–H σ -complex that also contains a $\text{RuCl}\cdots\text{SiCl}$ interligand interaction.¹⁸⁷ Reactions of other silanes (HSiCl_2Me , HSiCl_3 (**3-93**),¹⁸⁶ H_3SiPh , $\text{H}_2\text{PhSiSiPhH}_2$) apparently form classical oxidative addition products, and secondary silanes do not provide stable adducts.

Examples of phosphine replacement by an $\eta^2\text{-HSi}$ ligand are rare, although one PMe_3 is displaced by an $\eta^2\text{-H-SiMeCl}_2$ in the reaction of $\text{Cp}_2\text{Ti}(\text{PMe}_3)_2$ with HSiMeCl_2 (forming **3-1**).^{20b} Coordinated solvent can be replaced by $\eta^2\text{-H-SiR}_3$ as illustrated previously in eq 64 as well as the displacement of coordinated THF by the “tethered” H–Si group in the $\text{HMe}_2\text{SiC}\equiv\text{CR}$ complex of “ $\text{Cp}_2\text{Zr}(\text{THF})$ ” to give **3-8**.¹³⁹ A coordinated ClCH_2Cl in $[(\text{OC})_3\text{L}_2\text{M}(\text{ClCH}_2\text{Cl})]^+$ ($\text{L} = \text{P}(\text{OCH}_2)_3\text{CMe}_2$; $\text{M} = \text{Mn}, \text{Re}$) and in $[(\text{OC})_4\text{L}_2\text{Re}(\text{ClCH}_2\text{Cl})]^+$ was replaced by $\eta^2\text{-H-SiEt}_3$ in the formation of **3-57**, **3-62**, and **3-63**.^{168,171}

In the remaining examples in this section, addition of hydrosilane resulted in an increase in the electron count of an electronically and coordinatively unsaturated metal complex. The original ligand set was retained in the product, and this distinguishes these examples from those discussed in section 3.2 and earlier in the current section. The complexes that contain electron-rich metals generally contain phosphines, but the metal can be either in a zero or a positive oxidation state. Examples of addition to a $\text{M}(0)$ complex involve the 14e complex, L_2Pt , ($\text{L} = \text{P}(\text{Cy})_3$). The reaction of secondary silanes with L_2Pt gave *cis*- $\text{L}_2\text{Pt}(\text{H})\text{SiHAr}_2$ ($\text{Ar} = \text{Mes}$, **2-95**,^{11,12,129} Ph , **2-94**,¹²⁹), and the related *cis*-complex (**3-278a**) was formed from the tertiary silane HSiPh_3 .¹²⁹ However, addition of HSiCl_2Me to L_2Pt gave *trans*- $\text{L}_2\text{Pt}(\text{H})(\text{SiCl}_2\text{Me})$ (**3-277**).¹²⁹ A rather unusual case involved addition of HSiEt_3 to the novel 16e complex, $(\text{Cp}^*\text{Al})_3\text{Ni}$, to give $(\text{Cp}^*\text{Al})_3(\text{H})\text{NiSiEt}_3$ (**3-253**).²⁷³ The remaining $\text{M}(0)$ complex, $(\text{OC})_3(\text{R}_3\text{P})\text{W}$ ($\text{R} = \text{C}_6\text{H}_{11}$, ^iPr), formed the complex $(\text{OC})_3(\text{R}_3\text{P})_2\text{HWSiPhH}_2$ (**1-31**) with H_3SiPh , although the corresponding Cr precursor complex exhibited no reactivity towards the same silane.⁴⁰

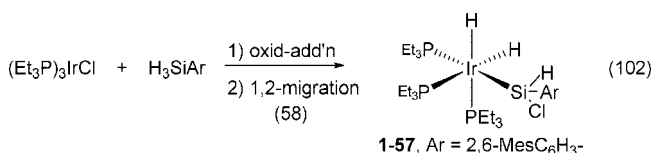
Metal complexes where the metal has an oxidation state > 0 must contain anionic ligands (or anionic counterions) as well as neutral ligands. The majority are 16e complexes, although there are two examples of 14e complexes of rhodium that add tertiary silanes: $(\text{Me}_3\text{P})_2\text{RhSiMe}_2(\text{CH}_2)_2\text{PPh}_2$ and HSiMe_2Ph gave **3-199a**,^{246,242} and $(^i\text{Pr}_3\text{P})_2\text{RhCl}$ with $\text{HSi}(\text{CH}_2\text{CH}_2\text{Ph})_3$ gave **3-201**.²⁴⁹ The majority of the 16e complexes contain phosphine ligands, particularly those of Os, Rh, and Ir. Glaser and Tilley have developed a 16-electron Os(II) complex for the activation of SiH bonds.⁵³ The reaction of $\text{Cp}^*\text{OsBr}(\text{P}^i\text{Pr}_3)$ with SiH_4 , ArSiH_3 (five examples), HexSiH_3 , $\text{H}_3\text{SiSi}(\text{SiMe}_3)_3$, $\text{H}_3\text{SiSiPh}_3$, Me_2SiH_2 , and Ph_2SiH_2 produced 18-electron, Os(IV) complexes of the type $\text{Cp}^*\text{Os}(\text{P}^i\text{Pr}_3)(\text{X})(\text{H})(\text{SiHRR}')$ ($\text{X} = \text{Br}$; R and R' are determined by the primary or secondary silane employed).^{22a,52} The oxidative addition of the hydrosilane to $\text{Cp}^*\text{OsBr}(\text{P}^i\text{Pr}_3)$ appeared to be complete based on a $^2J_{\text{SiH}}$ coupling < 20 Hz (see section 5.2). One of the objectives in these preparations was the generation of silylene complexes as depicted in eq 101.^{22a} The ^{29}Si NMR resonance in the silylene complex shown in eq 101 was shifted about 500 ppm downfield from that of the starting complex, **1-48**, but the silylene was not isolated. Additional

examples of silylene–metal complexes will be described in section 3.6.2.



The majority of the cases in this category involve Rh(I), particularly complexes of the type L_3RhX ($\text{X} = \text{SAr}, \text{Cl}$), which, on reaction with HSiR_3 , gave $\text{L}_3\text{XRh}(\text{H})(\text{SiR}_3)$. Examples include **2-61**,¹⁰⁹ **2-62**,¹¹⁰ **3-192** to **3-194**¹⁰⁹ ($\text{X} = \text{SAr}$), and **3-185**,²⁴² **3-186**,²⁴³ **3-189a**,²⁴³ ($\text{X} = \text{Cl}$). The initially formed 5-coordinate complex, **3-201**,²⁴⁹ from $(\text{iPr}_3\text{P})_2\text{RhCl}$ and HSiR_3 ($\text{R} = \text{CH}_2\text{CH}_2\text{Ph}$), was detected spectroscopically but reacted further to form a Rh dimer with bridging silylene units. When the reacting silane contained a substituent with a phosphine tether, then displacement of one of the PMe_3 ligands in $(\text{Me}_3\text{P})_3\text{RhCl}$ by the PPh_2 tether occurred when $\text{Ph}_2\text{PCH}_2\text{CH}_2\text{SiMe}_2\text{H}$ was added. A 6-coordinate rhodium center was produced in which the three phosphorous centers occupy positions that correspond to a *mer*-isomer as shown in eq 21 (formation of **3-197**).^{242,246} Four-coordinate $(\text{Me}_3\text{P})_2\text{RhSiMe}_2\text{CH}_2\text{CH}_2\text{PPh}_2$ in the presence of excess HSiMe_2Ph gave 6-coordinate **3-199a**, which was not isolated due to its thermal instability.²⁴⁶ Another ligand that contained a phosphine tether was $\text{PhP}(\text{CH}_2\text{CH}_2\text{CH}_2\text{P}^i\text{Pr}_2)_2$, PP_2 . When $(\text{PP}_2)\text{RhH}$ was reacted with $\text{HSi}(\text{SEt})_3$, oxidative addition occurred to give a 6-coordinate complex, **3-196**,²⁴⁵ in which the two hydrides were *cis* and the tridentate phosphine occupied *mer*-sites.²⁴⁵ In contrast, when $(\text{PP}_2)\text{RhMe}$ reacted with $\text{HSi}(\text{SEt})_3$, methane was eliminated to give 4-coordinate $(\text{PP}_2)\text{RhSi}(\text{SEt})_3$ (**3-195**), although $(\text{PP}_2)\text{IrMe}$, the iridium analogue, simply added the hydrosilane to give 6-coordinate **3-239** (*fac*-isomer).²⁴⁵ The phosphine can influence the course of the reaction as illustrated in the reaction of $(\text{Et}_3\text{P})_3\text{IrCl}$ and $(\text{Et}_2\text{PhP})_3\text{IrCl}$ with the primary silane, H_3SiAr ($\text{Ar} = \text{C}_6\text{H}_3\text{—Mes}_2\text{, 2,6}$) as shown in eq 102 for formation of **1-57**, although Cl migration from Ir to Si in this case must also occur.⁵⁸ Just changing one of the ethyl groups in the phosphine for a phenyl group resulted in cyclometallation (at Ir) of an *ortho*-mesityl CH bond, to give $(\text{Et}_2\text{PhP})_3(\text{H})_2\text{Ir}[\text{Si}(\text{Cl})\text{—CH}_2(\text{C}_6\text{H}_2\text{—Me}_2\text{, 2,4})(\text{C}_6\text{H}_3)(\text{Mes})]$, **1-58**.⁵⁹ The difference in reactivity was attributed to the more sterically hindered silane. When **1-57** was reacted with $\text{Li}[\text{B}(\text{C}_6\text{F}_5)_4]$, the hydride-substituted silylene, $[(\text{Et}_3\text{P})_3(\text{H})_2\text{Ir}=\text{Si}(\text{H})(\text{C}_6\text{H}_3\text{—Mes}_2\text{, 2,6})][\text{B}(\text{C}_6\text{F}_5)_4]$, formed in almost quantitative yield but was not isolated.⁵⁸ The ^1H NMR chemical shift of the SiH (dt) in the silylene complex appears at 10.5 ppm, shifted about 4 ppm relative to that in **1-57**, and the ^{29}Si NMR resonance was shifted downfield by about 250 ppm relative to the starting complex. Both pieces of data suggest that the product contained a silylene unit.⁵⁸ When $[\text{Ir}(1,2,5,6\text{-}\eta\text{-C}_8\text{H}_{12})(\text{NCCH}_3)(\text{PMe}_3)]\text{BF}_4$ was reacted with $\text{HSi}(\text{OMe})_3$, neither the olefin nor the solvent (CH_3CN) nor the phosphine was displaced from the Ir center, and the complex, $[(\text{Me}_3\text{P})(\text{cod})\text{—}(\text{CH}_3\text{CN})(\text{H})\text{Ir}\{\text{Si}(\text{OMe})_3\}][\text{BF}_4]$ (**3-241**), formed.²⁶³ The product (**3-241**) disproportionates into the starting complex, $[(\text{Me}_3\text{P})(\text{cod})(\text{CH}_3\text{CN})(\text{H})_2\text{Ir}]\text{BF}_4$, and $(\text{MeO})_3\text{SiSi}(\text{OMe})_3$,²⁶³ and similar reactions were observed when HSiEt_3 was employed. The 4-coordinate, 16e cationic complex, $[(\text{NN})\text{Pt}$

$\text{Me}]^+$ [NN = 1,4-bis(methoxypropyl)-2,3-dimethyl-1,4-diazabutadiene] adds HSiEt_3 to give the 6-coordinate, 18e **3-290a**, paralleling the Rh(I) chemistry.²⁷⁸



Although this is not a clear-cut example, the niobium precursors Cp_2NbH_3 and Cp_2NbBH_4 (usually in the presence of NEt_3) react with tertiary silanes. It is speculated that these two niobium precursors actually eliminate H_2 and H_3BNEt_3 , respectively, to give Cp_2NbH prior to reaction with the hydrosilane. Thus, addition of HSiR_3 would occur with retention of the original substituents at Nb(III). Examples include the following silanes: HSiMe_2Cl (**3-12a**),¹⁴² $\text{HSiCl}^i\text{Pr}_2$ (**3-13**),¹⁴³ HSiMe_2OEt (**3-14**),¹⁴⁴ and $\text{HSi}(\text{OEt})_3$ (**3-15**).¹⁴²

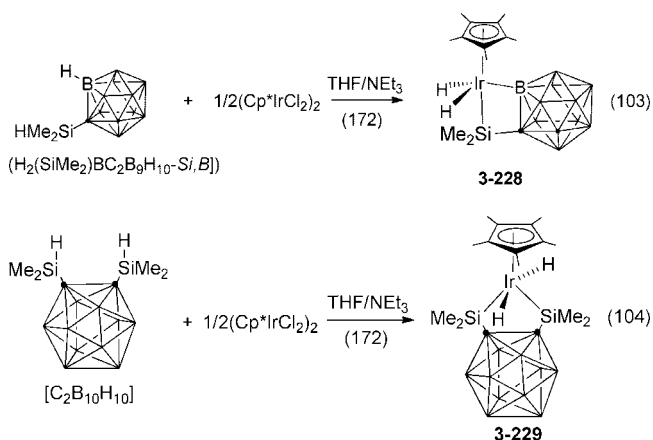
3.5. Reactions of Polynuclear Metal Complexes with Silanes

In the previous sections (sections 3.1–3.4), the focus has been on the reactions of silanes with primarily mononuclear metal complexes and illustrating the types of processes that occur. Polynuclear metal complexes have also been used as reactants, and this section will describe first the delivery of a monometallic fragment from M_x ($x > 1$) and then the reactions that essentially leave the M_x intact or that give M_{x-1} ($x \geq 2$) species.

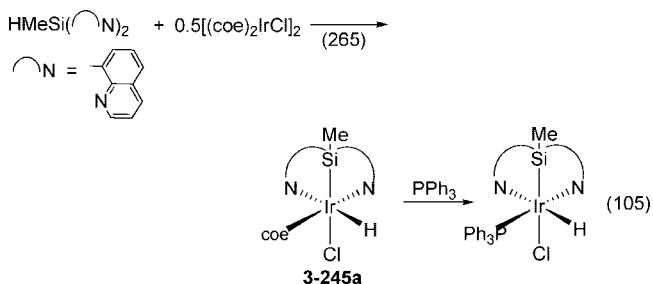
Metal dimers can be used to deliver monomeric metal units. Such dimers include carbonyl complexes as well as hydride- and chloride-bridged complexes. The dinuclear $\text{Fe}_2(\text{CO})_9$ provided a $\text{Fe}(\text{CO})_4$ unit when reacted with the chelate, 1,6- $(\text{HMe}_2\text{SiC}_6\text{H}_3\text{Br})_2$, to provide $(\text{OC})_4\text{Fe}[8\text{-Br-1,6-}(\text{Me}_2\text{Si})_2\text{C}_6\text{H}_3]$, **3-72c**,^{177c} but did not react with Xantsil to give **3-72b**^{177b} (produced instead from $\text{Fe}(\text{CO})_5$). Dinuclear $\text{Co}_2(\text{CO})_8$ supplies a $\text{Co}(\text{CO})_4$ unit in the formation of the silylcobalt carbonyl derivatives **3-166** to **3-168a**, **3-169**, **3-170**,^{229,230a,231,232} **3-174**²³⁴ (a functionalized dendrimer), and **3-175**²³⁵ (a functionalized octasilsequioxane), whereas trinuclear $\text{Ru}_3(\text{CO})_{12}$ provided a $\text{Ru}(\text{CO})_4$ group to the Xantsil ligand in formation of **3-104**,^{177b,192} and similar chemistry was observed with $\text{Os}_3(\text{CO})_{12}$.^{177b} An additional example where $\text{Ru}_3(\text{CO})_{12}$ delivered the equivalent of $\text{Ru}(\text{CO})_4$ includes $[(\text{OC})_4\text{Ru}\{\mu\text{-Me}_2\text{SiTTf}\mu\text{-Me}_2\text{Si}\}\text{Ru}(\text{CO})_4]$ (**3-134d**).^{213c} The reaction of $\text{Ru}_3(\text{CO})_{12}$ with the silane, $\text{HSiMe}(\text{CH}_2\text{CH}_2\text{CH}_2\text{—PPh}_2)_2$, also provided a single Ru unit in which the silyl group was incorporated into a 6-coordinate complex where the tethered phosphino groups are also coordinated to the metal center, $(\text{OC})_2\text{HRuSiMe}(\text{CH}_2\text{CH}_2\text{CH}_2\text{PPh}_2)_2$, **3-106**.¹⁹⁴ Complexes in which N_2 bridges two metal units are also good sources of mononuclear complexes as demonstrated in the reactions described previously for $[\text{Mo}(\text{CO})(\text{depe})_2]_2(\mu\text{-N}_2)$ with SiH_4 and Ph_2SiH_2 to form **1-3d**^{21b} and **2-14**,^{21b} respectively. The related ruthenium complex $[(\text{Me}_3\text{P})_3\text{HRu}(\text{SiMe}_3)_2(\text{N}_2)]$ provided $(\text{Me}_3\text{P})_3\text{H}_2\text{Ru}(\text{SiMe}_3)_2$, **3-123**, on reaction with excess Me_3SiH .⁴⁹

Hydride- and chloride-bridged dimers have been employed as reactants with silanes. The complexes with hydride bridges between two metals tend to give mononuclear silyl complexes. For instance, $[\text{Cp}^*_2\text{M}(\mu\text{-H})_2]$ ($\text{M} = \text{Sm}, \text{Lu}$) reacted with ArSiH_3 (the aryl group bears a methoxy tether) to give $\text{Cp}^*_2\text{M}(\text{SiArH}_2)$ ($\text{M} = \text{Sm}$ (**1-82**), Lu (**1-83**)) in which the

tether coordinates to the metal center.^{73,74} The reaction of $[(OC)_4(R_3P)Re]_2(\mu-H)^+[BAR_F]^-$ provided a novel σ -complex, $[(OC)_4(R_3P)Re(\eta^2-H-SiEt_3)]^+[BAR_F]^-$, **3-61**.^{165a,170} Chloride-bridged M_2 units also can provide mononuclear complexes, especially when chelating silanes or silanes with chelating tether groups are involved. For instance, mono(silyl)- and bis(silyl)-*o*-carboranes react with 0.5 equiv of $(Cp^*IrCl_2)_2$ to give cyclometalates through Si-H and B-H activation of the carborane as shown in eqs 103 and 104 (formation of **3-228** and **3-229**, respectively).¹⁷² In a related reaction of excess *o*-(HMe₂Si)C₆H₄ with $(1/2)[Cp^*IrCl_2]_2$, the complexes *trans*-Cp^{*}(Cl)(H)Ir-[SiMe₂C₆H₄SiMe₂] (**3-230**) and *trans*-Cp^{*}(H)₂Ir-[SiMe₂C₆H₄SiMe₂] (**3-231**) were isolated in about a 1.5:1 ratio.¹⁷² The Ru(II) dimer, $[(p\text{-cymene})RuCl_2]_2$, reacted with HSiPh₃ to give the equivalent of oxidative addition to provide monometallic **3-102**.¹⁹¹

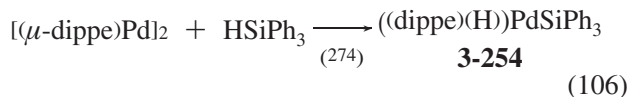


Hydrosilanes that contain two base tethers may function as a “tridentate”. Two such silanes that have been developed are the previously mentioned HSiMe[(CH₂)_xPPh₂]₂ (*x* = 2, 3; biPSi) as well as bis(8-quinolyl)methylsilane (NSiN). The reaction of (biPSi) with $[Ir(cod)Cl]_2$ to give a pentacoordinate Ir(III) complex (**3-243**) was depicted in section 3.1, eq 22.¹⁹⁴ The reaction of the “NSiN” ligand with 0.5 equiv of $[(coe)_2IrCl]_2$ is shown in eq 105. In this case, a 6-coordinate Ir(III) complex (**3-245a**)²⁶⁵ forms in which one *coe* ligand is coordinated to Ir(III); however, it can be displaced by added PPh₃. The $[(coe)_2IrCl]_2$ precursor was also used with K[PyInd] (a chelate) and R₃SiH to give 6-coordinate $\{[PyInd](H)_2Ir(SiR_3)_2\}$, **3-244**.²⁵⁵

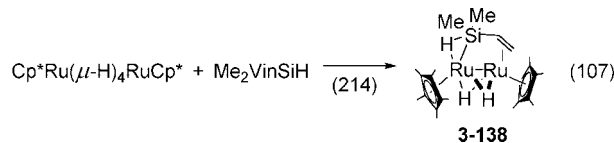


The first stable mononuclear silyl-palladium hydride (such as **3-254**) was prepared from the symmetrical Pd(0) dimer, $[(\mu\text{-dippe})Pd]_2$, with tertiary silanes as shown for one example in eq 106.²⁷⁴ The more phenyl groups on the reacting silane, the more stable was the silyl-palladium hydride produced.²⁷⁴ A related example, **3-255**, was also prepared from $[(\mu\text{-dcpe})Pd]_2$. The Pd₂ species, Pd₂dba₃ reacted with the chelate, (phosphino-*o*-carboranyl)dimeth-

ylsilane, to give square-planar complexes, *cis*- and *trans*-(Cab^{P,Si})₂Pd (Cab^{P,Si} = $\eta^2\text{-(PR}_2\text{)(SiMe}_2\text{)C}_2\text{B}_{10}\text{H}_{10}\text{-P,Si}$), **3-256a** and **3-257a**.^{275,276a}



Complexes with multiple hydride bridges between two iron centers or two ruthenium centers, Cp^{*}M(μ -H)₄MCp^{*}, have been reacted with both secondary and tertiary silanes. In general, a silylene replaces 2 bridging hydrides, although the products seem to differ depending on whether an alkylsilane or an arylsilane is used. This is exemplified in the sequence shown for reaction of Bu_2SiH_2 and Cp^{*}Fe(μ -H)₄FeCp^{*} in eqs 85 and 97 (forming **2-34** and **2-35**, respectively).^{93,94} The bridging dialkylsilylene unit will exchange with Ph₂SiH₂, although the nonclassical Fe-H-Si interactions are lost in formation of **2-35**. The Ru analogue, Cp^{*}Ru(μ -H)₄RuCp^{*}, has been reacted with the series of tertiary silanes, Ph_{3-n}Me_nSiH. When *n* = 0, a phenyl group was cleaved to give a complex with two SiPh₂ bridges (**3-135b**) and one with a single SiPh₂ bridge (**3-135a**), both resulting from cleavage of a phenyl group in the starting silane (shown earlier in eq 86).⁹⁸ When *n* = 1 (**3-136**), a complex analogous to **3-135b** was formed in which there were two PhMeSi bridging groups produced as two diastereomers. When *n* = 2, two complexes, Cp^{*}Ru(μ -SiRMe)(μ -SiMe₂)(μ -H)₂RuCp^{*} (R = Ph, **3-137e**; Me, **3-137f**) formed whose ratio, (R = Ph)/(R = Me), of 16:1 suggests the preference for phenyl cleavage over alkyl cleavage.⁹⁸ When the secondary silane Me(Vin)SiH₂ was employed, another variation occurred in which the vinyl group was reduced to an ethyl group and the dimer, **2-41** (analogous to **3-135a**, eq 86), was obtained.⁹⁸ However, use of the tertiary vinylsilane, Me₂(Vin)SiH, gave rise to a third structural variation with a bridging Ru-H-Si interaction as shown in eq 107 (formation of **3-138**).²¹⁴ Complex **3-138** also exhibits a $>C=C<$ π -interaction to a second Ru center. When the hydride-bridged rhodium dimer, (dippe)Rh(μ -H)₂Rh(dippe), was reacted with secondary silanes, the hydride bridges were replaced with a silylene unit, although the nature of the dimer differed when an aryl group was present on silicon as shown earlier [see formation of **2-67** in eq 88a (and the related **2-68**) as well as **2-69** in eq 88b]. Thus, although a single hydride-bridged M_2 species provided mononuclear complexes, the $M(\mu\text{-H})_xM$ (*x* > 1) precursors appear to retain a dimetallic framework in the product.

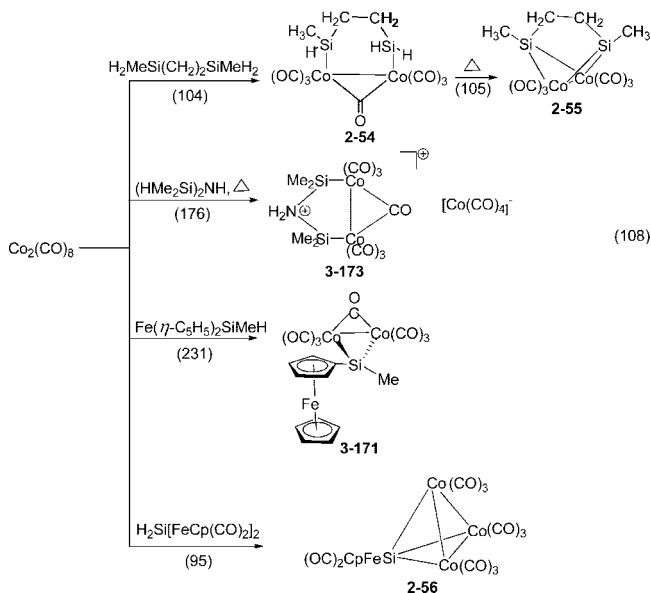


Although not, strictly speaking, a bridging hydride complex, the novel silane-bridged ruthenium dimer, L₂(H)₂Ru(SiH₄)Ru(H)₂L₂ (L = PCy₃; **2-45**), reacted with excess HSi(OMe)₃ with disproportionation of the alkoxysilane to give H₂Si(OMe)₂. This then formed an unusual diruthenium complex with three bridging H₂Si(OMe)₂ molecules, (Cy₃P)(H)Ru(μ - η^2 - η^2 -H₂Si(OMe)₂)₃Ru(H)(PCy₃) (**3-144a**).¹⁰¹ The nature of the eight hydrogens (RuH and SiH) could not be determined from X-ray data, but DFT calculations supported a dihydride formulation with three bridging

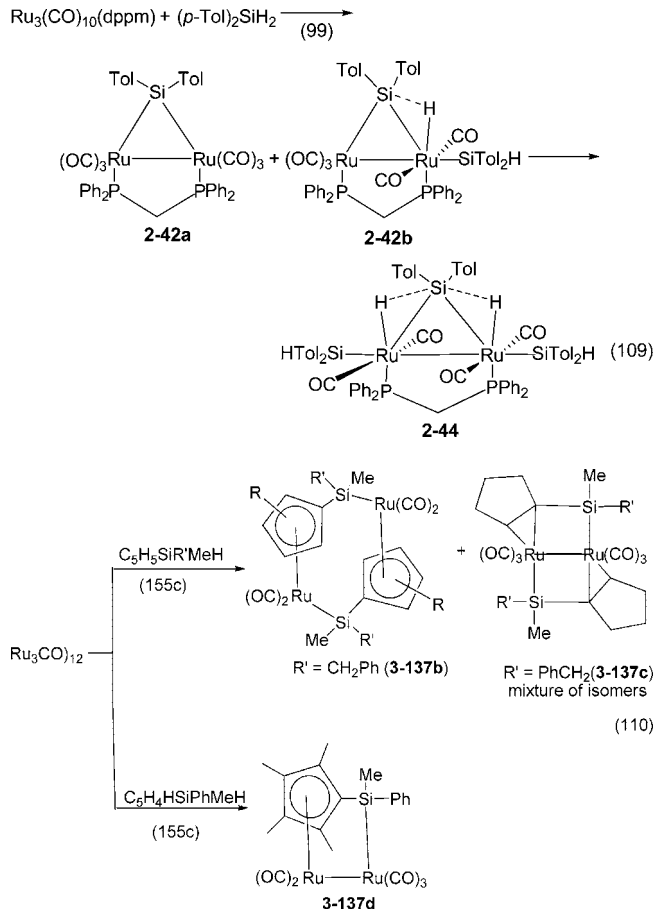
$\text{H}_2\text{Si}(\text{OMe})_3$ ligands that are coordinated to the two ruthenium centers through $\sigma\text{-H-Si}$ bonds.

In a last variation, when the mixed bridge system, $\text{L}(\text{H})(\text{SiPh}_3)\text{Rh}(\mu\text{-H})(\mu\text{-Cl})\text{RhH}-(\text{SiPh}_3)\text{L}$ ($\text{L} = \text{P}^i\text{Pr}_3$), reacted with $\text{HSiPh}_n\text{Ar}_{3-n}$, neither the terminal nor the bridging hydride were replaced but the Ph_3Si group at each Rh center became a $\text{SiPh}_n\text{Ar}_{3-n}$ substituent ($\text{Ar} = \text{C}_6\text{H}_4\text{-F}$, $n = 0, 1, 2$; $\text{C}_6\text{H}_4\text{CF}_3$, $n = 0$ (**3-216**)) where both bridging atoms were retained.²⁵⁶

Carbonyl derivatives such as $\text{Co}_2(\text{CO})_8$ lose CO on photolysis, and the resultant $\text{Co}_2(\text{CO})_7$ fragment can react, essentially intact, as shown for selected examples in eq 108. Trinuclear $\text{Ru}_3(\text{CO})_{12}$ tends to provide a dinuclear metal unit. In the simplest case, $\text{Ru}_3(\text{CO})_{12}$ reacted with PhMe_2SiH to give $[\text{PhMe}_2\text{SiRu}(\text{CO})_4]_2$, **3-140**, and with $p\text{-HMe}_2\text{SiC}_6\text{H}_4\text{SiMe}_2\text{H}$ to give the polymer $-\text{[Me}_2\text{SiRu}(\text{CO})_4\text{Ru}(\text{CO})_4\text{SiMe}_2]_n-$, **3-141**.²¹⁶ A more complicated sequence occurred when $\text{Ru}_3(\text{CO})_{10}(\text{dppm})$ (which contains a triangular Ru_3 core with dppm displacing a CO ligand at each of two Ru centers) reacted with the secondary silane, $(p\text{-Tol})_2\text{SiH}_2$.⁹⁹ In the first step (reaction conducted at 40 °C), $(p\text{-Tol})_2\text{Si}$ displaces the $\text{Ru}(\text{CO})_4$ unit, giving **2-42a**. A second molecule of $(p\text{-Tol})_2\text{SiH}_2$ oxidatively adds to one of the $\text{Ru}(\text{CO})_3$ groups (after loss of CO) to give **2-42b**. Irradiation of a mixture of **2-42a/2-42b** using a high-pressure mercury lamp provided the product of oxidative addition of another molecule of $(p\text{-Tol})_2\text{SiH}_2$ to give **2-44**. The sequence is shown in eq 109. The reaction of $\text{Ru}_3(\text{CO})_{12}$ with various $\text{Cp}'\text{SiR}'\text{MeH}$ provided three different types of products, two of which contained a $\text{Ru}_2(\text{CO})_n$ ($n = 6, 5$) unit as shown in eq 110.



Metal-metal bonded dimers are formed when each of the carbonyls, $\text{FvRe}_2(\text{CO})_6$ and $\text{H}_2\text{Si}[\text{FeCp}(\text{OC})_2]_2$, are photolyzed in the presence of secondary silanes to give **2-31**⁹¹ (with loss of CO from each Re center) and **2-36a**,^{95a} a tris(metallo)silane, respectively. In a ruthenium “trimer” complex where a $\text{Ru}_3(\text{CO})_7$ unit is coordinated to a μ_3 -acenaphthylene ligand or a μ_3 -azulene ligand, reaction with a tertiary silane resulted in displacement of the bridging CO and formation of an intact Ru_3 unit with a terminal SiR_3 substituent and a bridging hydride, **3-145**²¹⁸ and **3-146**,²¹⁵ respectively. The basic trinuclear core in the unsaturated clusters, $\text{H}_2\text{Os}_3(\text{CO})_{10}$ and $\text{Os}_3(\mu\text{-H})\{\mu_3\text{-Ph}_2\text{PCH}_2\text{PPh}(\text{C}_6\text{H}_4)\}(\text{CO})_8$, was also retained on reaction with tertiary silanes. The former complex



gave $\text{H}_3\text{Os}_3(\text{CO})_{10}\text{SiEt}_3$ (as a mixture of three isomers), and upon longer reaction times, up to three Et_3Si groups were incorporated (see **3-161**).²²⁶ The latter complex gave both an unsaturated cluster $\text{Os}_3(\mu\text{-H})_2(\mu\text{-SiPh}_3)\{\mu_3\text{-Ph}_2\text{PCH}_2\text{PPh}(\text{C}_6\text{H}_4)\}(\text{CO})_7$ (**3-162b**) and a saturated cluster, $\text{Os}_3(\mu\text{-H})(\mu\text{-SiPh}_3)(\text{CO})_9(\mu\text{-dppm})$ (**3-162a**).²²⁷ The PhPt in $[\text{Pt}_3\text{Ph}][(\mu\text{-PPh}_2)_3(\text{PPh}_3)_2]$ was replaced with $\text{PtSi}(\text{OSiMe}_3)_3$ on reaction with $\text{HSi}(\text{OSiMe}_3)_3$, leaving the triangular Pt_3 unit intact and giving **3-299**.²⁹⁹

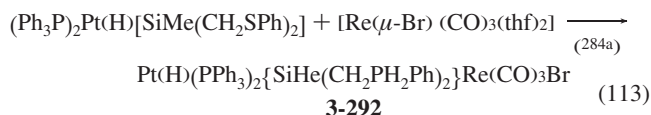
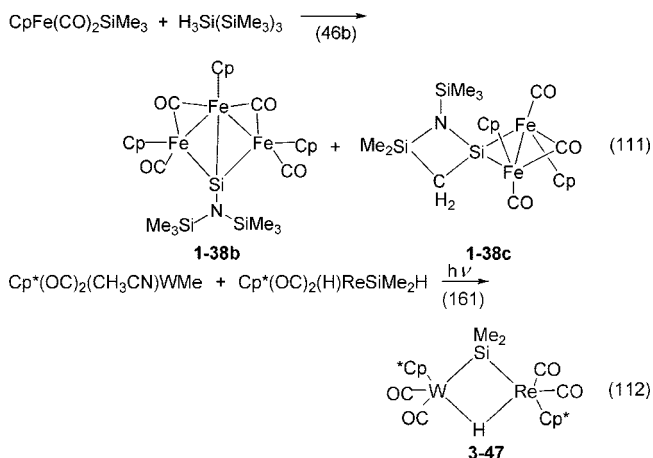
3.6. Miscellaneous Methods

Each of the previous sections discussed a particular feature of the formation of silyl-metal complexes. Obviously, not all of the complexes listed in Tables 1, 2, and 3 fit into a convenient pattern. A discussion of three groups of complexes will be presented in the indicated order. The reactions of polynuclear metal complexes with silanes were discussed in section 3.5. However, there were also several examples where mononuclear complexes produced dinuclear (or polynuclear) products incorporating silyl substituents, and although some of these cases appear in previous sections, they will be mentioned in section 3.6.1 as well. Silylene complexes have also been prepared by various routes starting from hydrosilanes, and these will also be reported in section 3.6.2. Although the focus of this review involves reactions of silanes and metal complexes that lead to TM-Si bonds, there are cases where the silane reacts preferentially with a ligand at the metal, and this was particularly true for complexes that contained a multiple TM=X bond (section 3.6.3). In some cases where a Si-TM bond was formed, a rearrangement of a group between the Si and TM centers occurred, and these cases are described in section 3.6.4. Since

silanes are also reducing agents, a hydride can be transferred to the metal without involving the isolation of a complex with a TM–Si bond. Such cases appear in Table 4 and will be discussed in section 3.7.

3.6.1. Reactions Providing Polynuclear Metal Complexes from Mononuclear Systems

The majority of the cases where mononuclear metal precursors form dinuclear (or higher nuclearity) complexes occurred with either carbonyl derivatives (particularly with Fe) or with M(0) complexes of the nickel triad containing phosphine ligands. Examples of FeFe dimers from Cp'Fe(CO)₂X precursors were previously described in eqs 89 (**1-34**^{43a}), 90 (**2-33**^{42b}), and 75 (**2-36a**).^{95a} When Cp(CO)₂FeSiMe₃ reacted with primary silanes, both dinuclear and trinuclear complexes (**1-38b** and **1-38c**) were produced, two of which are shown in eq 111.^{46b} The complex **1-38d**, produced on reaction with H₃SiN(SiMe₃)₂, was a more complicated trinuclear structure.^{46b} Two different binuclear complexes have been reported in the photolytic reaction of W(CO)₆ with Ph₂SiH₂. In one case, the product contained a triangular SiW₂ core (**2-25**),^{87a,b} and the other contained a four-membered Si₂W₂ ring (two silylenes bridge the two tungsten centers (**2-26c**,⁸⁸ eq 44). Another variation of the reaction of Ph₂SiH₂ with the W(0) complex, W(CO)₃(PⁱPr₃)₂, produced a dimer with a four-membered ring in which two opposite sides contained a W···H···Si bridge (**2-27**, eq 39).⁴⁰ Heterobinuclear complexes can also be prepared from a similar approach as was illustrated earlier for **2-28**^{42b} in eq 33, and an additional example is given in eq 112 (formation of **3-47**).¹⁶¹ The formation of **2-28** requires loss of a CO from W as described in section 3.2.2, whereas formation of **3-47** required loss of a solvent molecule coordinated to W (see section 3.2.4); in both cases, loss of methane occurred (section 3.3.1). Another example of loss of solvent in the formation of a heterodinuclear complex is shown in eq 113.^{284a} The advantage of a silyl–metal complex with a functional group at silicon would be to provide the opportunity to build heteronuclear complexes as illustrated in the formation of **2-28** (eq 33), **3-47** (eq 112), and **3-292** (eq 113).



Secondary silanes have two SiH bonds that may react with a single metal center to produce a silylene or produce a functional metal complex with a SiR₂H group or can react with two metal complexes to produce a TM(SiR₂)TM sequence. Another type of silane that can react with one or two metal centers is a 1,2-dihydrodisilane or a suitable disilyl-substituted reagent such as HR₂Si–X–SiR₂H. Tetramethyldisilane reacted with Cp'Mn(CO)₃ to provide unstable Cp'(OC)₂Mn(η²-H–SiMe₂SiMe₂H) and the disubstituted derivative, Cp'(OC)₂Mn(η²-H–SiMe₂SiMe₂–H–η²)Mn(CO)₂Cp' (eq 25), which was characterized only in solution.¹⁶⁶ In contrast, HPh₂SiSiPh₂H reacted with Cp'Mn(CO)₃ to give the stable complex **3-54** (Cp' = C₅H₄Me) incorporating one Cp'Mn(CO)₂ unit, but Cp'(OC)₂Mn(η²-H–SiPh₂SiPh₂H–η²)Mn(CO)₂Cp' decomposed on workup. However, the analogue Cp'(OC)₂Mn(η²-H–SiPhMeSiPhMeH–η²)Mn(CO)₂Cp', **3-56**, was isolated.¹⁶⁶ A related reaction of CpRe(CO)₂(THF) with HSiMe₂SiMe₂H produced [(OC)₂(H)CpReSiMe₂–]₂ (Table 3, footnote 67; eq 26), and with HPh₂SiSiPh₂H, monosubstituted **3-59** was produced. A related disubstituted product (Table 3, footnote 82; not isolated) was obtained from 6-coordinate *mer*-(OC)₃(Ph₃P)-(H)FeSiMe₃ and HMe₂SiSiMe₂H, although, again, HPh₂SiSiPh₂H gave monosubstituted **3-75a**.^{163,166} The reaction of CpMn(CO)₂L (L = PMe₃, CO) with HMe₂Si–X–SiMe₂H (X = 1,2-C₆H₄, C₂H₄, O) also gave products incorporating either one or two manganese units (see **3-55** for an example).¹⁶⁷

Phosphine metal(0) complexes were common precursors to metal dimers of the structural types that are shown in Table 4. Several of these complexes have been described in equations given in earlier sections, and these complexes are also indicated in Table 4. Osakada and Tanabe have reviewed Pt–Si and Pd–Si complexes, and the review contains a major section on dimer products that have been published from investigations of his group.^{160b} A number of M(0) as well as M(II) complexes give rise to dimers, the majority of which seem to contain M–H–Si bridges. The three structural types differ in the number of phosphines per M as well as in the presence of M–H–Si bridges (types A, B, and C, Table 4) or the absence of such interactions (type D). The complex L₂Pt(SiHAr₂)₂ has been utilized for the formation of heterodinuclear complexes as shown in eq 35 for the formation of **3-218** from (Me₃P)₃RhMe and (Me₃P)₂Pt[SiH(C₆H₄F-*p*)₂].²⁵⁸ The related derivative, **3-219**, was formed from (Me₃P)₃RhCl and (Me₃P)₂Pt[SiH(C₆H₄F-*p*)₂], but in this case a Cl[–] migrated from Rh to Si in the terminal Pt–silyl group.^{244,258} Additional heterodinuclear complexes are shown in eqs 114 and 115.

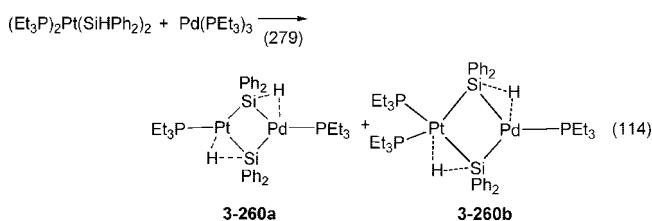
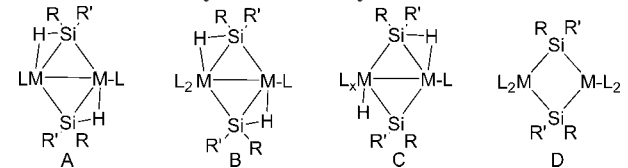
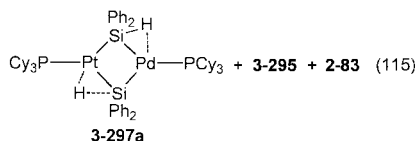
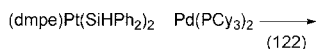


Table 4. Basic Dimer Structures Produced from Primary and Secondary Silanes in Reaction with Nickel Triad Complexes

Table 1. Basic Dimer Structures Produced From Primary and Secondary Silanes in Reaction With Nickel Complexes					
					
metal complex	silane	A	B	C	D
(Cy ₃ P) ₂ Pd	H ₂ SiPh ₂	2-83 ^{122,1}			
(Cy ₃ P) ₂ Pd	(HPh ₂ Si) ₂ Pt(PEt ₃) ₂	3-297a ^{122,2}			
(Et ₃ P) ₃ Pd	(HPh ₂ Si) ₂ Pt(PEt ₃)	2-260a ^{279,3}	3-260b ^{279,3}		
(Me ₃ P) ₂ PdEt ₂	H ₂ SiPh ₂	2-81 ^{121ab}	2-79a ^{121ab}		
	H ₂ SiPhMe	2-80 ^{121b}			
(Et ₃ P) ₂ PdEt ₂	H ₂ SiPh ₂	2-82 ^{121b}			
(Cy ₃ P) ₂ PdMe ₂	H ₂ SiPh ₂	2-102a ^{122,4}			
(dmpe) ₂ PdMe ₂	(HAr ₂ Si) ₂ Pt-(Me ₃ P) ₂				3-296 ²⁴⁴
—	(HPh ₂ Si) ₂ Pd-(dmpe) + Δ				3-260c ^{120b}
(Et ₃ P) ₃ Pt	H ₃ SiHex			1-72 ^{69,5}	1-70 ⁶⁹
(Pr ₃ P) ₃ Pt	H ₃ SiHex	Table 1, footnote 84 ⁶⁹			1-71 ⁶⁹
(Cy ₃ P) ₂ Pt	H ₂ SiEt ₂	2-96b ^{127a}			
	H ₂ Si(Hex) ₂	Table 2, footnote 127 ^{127a}			
(Cy ₃ P) ₂ Pt	(HPh ₂ Si) ₂ Pd-(dmpe)				3-295 ^{122,6}
(Ph ₃ P) ₄ Pt	H ₃ SiAr ⁷	1-78 ^{68b}			
(Ph ₃ P) ₂ Pt(C ₂ H ₄)	H ₂ SiMe ₂	Table 3, footnote 317 ^{284c, 8}			
	H ₃ SiAr	1-73 ^{68a,9}			
		1-77 ^{68a} (e) ¹⁰			
		Table 1, footnote 85 ^{68a, 11}			
	H ₂ SiPh ₂	2-98 ^{127c}			
	HSiPh ₂ SiPh ₂ H	Table 3, footnote 317 ^{284c, 12}			
	H ₂ SiC ₂₀ H ₂₄ ¹³			2-103 ^{132,127c, 14}	
	2-103 + Δ	2-99 ^{127c,15}			
	H ₂ SiC ₁₃ H ₉ Br ₂ N			2-104 ^{131,16}	
	H ₂ SiC ₁₂ H ₈ O	2-100 ^{131,17}			
	H ₂ SiC ₁₃ H ₁₁ N	2-101 ^{131,18}			
(Me ₃ P) ₂ PtMe ₂	H ₃ SiAr ¹⁹				Table 1, footnote 90
(MePh ₂ P) ₂ PtMe ₂	H ₃ SiAr ¹⁹				Table 1, footnote 90
(Me ₂ PhP) ₂ PtMe ₂	H ₃ SiAr ¹⁹				1-79 ⁷⁰
(Cy ₃ P) ₂ PtMe ₂	H ₂ SiPh ₂	2-102a ^{121b}			
[Cy ₃ P]Pt(μ-η ² -HSiEt ₂) ₂	H ₂ SiPhMe	2-96c ^{127a, 20}			
[Cy ₃ P]Pt(μ-η ² -HSiEt ₂) ₂	H ₂ SiPh ₂	2-96d ^{127a,21}			
	xs H ₂ SiPh ₂	2-96e ^{127b}			
		Table 2, footnote 109 ^{127a, 22}			
	<i>cis</i> -(Ph ₃ P) ₂ Pt-(SiMe ₂ H)			3-297b ^{284c,23}	
	[(Cy ₃ P)Pt(μ-η ² -HSiPh ₂) ₂] + dmpe				2-102b ^{127a}
	[(Cy ₃ P)Pt(μ-η ² -HSiPh ₂) ₂] + dppe				Table 2, footnote 116 ^{127a, 24}
	[(Ph ₃ P) ₂ Pt(H)(μ-SiMe ₂) (μ-SiHMe ₂)Pt(PPh ₃)] ²⁵	Table 3, footnote 317 ^{284c}			

¹ Also prepared as one of the products from reaction of (dmpe)Pt(SiPh₂H)₂ + Pd(PCy₃)₂.^{122, 2} PtPd dimer. Additional product observed, [(Cy₃P)Pd(μ-η²-H-SiPh₂)₂]₂.^{122, 3} PtPd dimer.^{279, 4} Also reported as one of the products from Pt(Cy₃)₂ + (dmpe)Pd(SiPh₂H)₂.^{279, 5} One hydride is terminal on the PtL₂ center.^{69, 6} Additional product observed, [(Cy₃P)Pd(μ-η²-H-SiPh₂)₂]₂ (**2-83**) (see Table 2). The major product of the reaction was **3-297a** in addition to **3-295**.^{122, 7} Ar = 2'-Pr-6-Me-C₆H₂.⁸ Product is [(Ph₃P)Pt(μ-SiHMe₂)₂]₂.^{284c, 9} Ar = 2,4,6-(MeO)₃C₆H₂.¹⁰ Ar = 2,3,4,5,6-(Ph)₅C₆.¹¹ Ar = 2,4,6-tris(trifluoromethyl)phenyl(trans only).¹² [(Ph₃P)Pt(μ-SiHPh₂)₂]₂.^{284c, 13} H₂SiC₂₀H₂₄ = 3,7-di-*tert*-butylsilafuorene.¹⁴ (Ph₃P)₂(H)Pt(μ-SiAr₂)(μ-η²-HSiAr₂)Pt(PPh₃).^{127c, 132} Additional derivative prepared from (Ph₃P)₂Pt(η²-C₂H₄) + H₂SiC₁₂H₈O. X-ray structure of **2-103** was of poor quality but sufficient to determine the connectivity.^{127c, 15} Additional derivative prepared from C₁₂H₈SiH₂ and (Ph₃P)₂Pt(η²-C₂H₄).^{127c, 132, 134, 16} **2-104** = (Ph₃P)₂(H)Pt(μ-SiAr₂)(μ-η²-HSiAr₂)Pt(PPh₃). H₂SiC₁₃H₉Br₂N = 2,8-dibromo-5-methyl-10,10-dihydrophenazasiline. Related derivatives reported, 5-methyl-10,10-dihydrophenazasiline, 2,5,8-trimethyl-10,10-dihydrophenazasiline, 2,8-dimethyl-10,10-phenoxasilin.^{131, 17} H₂C₁₂H₈O = 10,10-dihydrophenoxasilin.^{131, 18} H₂SiC₁₃H₁₁N = 5-methyl-10,10-dihydrophenazasiline.^{131, 19} Ar = 2,4,6-(F₃C)₃C₆H₂.²⁰ Similar reaction of [(Cy₃P)Pt(μ-η²-HSiEt₂)₂] and of **2-96c** (mixture) with H₂SiPh₂ gave [(Cy₃P)Pt(μ-η²-HSiPh₂)₂]₂.^{127a, 21} Dimer has one η²-HSiEt₂ bridge and one η²-HSiPh₂ bridge. A second complex, **2-96e** with one (μ-η²:η²-H₂SiEt₂) bridge and one μ-SiPh₂ bridge also formed.²² (Cy₃P)Pt(μ-η²-HSiPh₂)₂.^{127a, 23} If **3-297b** is left in solution for a few days at rt, colorless crystals of [(Ph₃P)Pt(μ-SiHMe₂)₂] form (X-ray). [(Ph₃P)Pt(μ-SiHMe₂)₂] was also formed from (Ph₃P)₂Pt(η²-C₂H₄) and H₂SiMe₂. The related complex, [(Ph₃P)Pt(μ-SiHPh₂)₂]₂, was formed from (Ph₃P)₂Pt(η²-C₂H₄) and HSiPh₂SiPh₂H at rt.^{284c, 24} [(Pt(dppe))₂(μ-SiPh₂)₂].^{127a, 25} Forms [(Ph₃P)Pt(μ-SiHMe₂)₂]₂.^{284c}



Two of the metal precursors shown in Table 4 have also been used to generate trimers. Thermolysis of (Me₃P)₂Pt-(SiPh₂H)₂ provided the trimer, {[(Me₃P)Pt][μ-SiPh₂]}₃ (**3-298a**), as was illustrated in eq 32.^{298b} The reaction of

(Ph₃P)₂Pt(CH₂=CH₂) with 9-silafuorene at room temperature provided the trimer, {[(Ph₃P)Pt][μ-SiC₁₂H₈]}₃ (**2-106**).^{132, 134} Both of these trimers have a triangular Pt₃ core with the sides bridged by silylene units. A third type of M₃ trimer is illustrated in the thermolysis of (depe)Pd[*o*-(H₂Si)₂C₆H₄], which gave Pd₃[*o*-(HSi)(H₂Si)-C₆H₄]₂[*o*-(HSi)₂C₆H₄](depe)₂ (**2-84**), although the metals do not form a triangular unit.¹²³

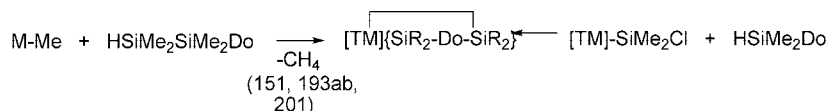
Dimers are also formed in the reaction of L₂RhCl (L = P'Pr₃) with [Ph(CH₂)_x]₃SiH (x = 1, 2). Since (PhCH₂CH₂)₄Si and (PhCH₂CH₂)₃SiCl were observed in the reaction of (PhCH₂CH₂)₃SiH, it is likely that the rhodium complex

Chart 7. Silylene Complexes Prepared from Hydrosilanes As Listed in Tables 1–3^a

Ti triad: - [Table 6, Footnote 9: Hf^{351d}]
V triad: **3-24b**¹⁵⁰ (Ta).
Cr triad: **2-7**,^{80a} **3-27**¹⁵¹ (Cr). **1-24**,³⁶ **2-10(4)**,^{36a} **2-11**,⁸² **3-32(1)**,¹⁵¹ **3-33**¹⁵³ (Mo). **1-29ab(1)**,^{38a} **1-30(4)**,³⁹ **2-19**,^{85a} **2-20(2)**,^{85a} **2-21(2)**,^{86,39} **3-9**,¹⁵⁶ **3-40a**,¹⁵⁷ **3-41(1)**,¹⁵⁸ **3-43**,¹⁶⁰ **3-46(1)**¹⁵⁶ (W). [Table 6, Footnote 25: Cr(4),^{90(2),363(2)} Mo(4),^{82,363(2),365a} W(4)^{363,368bc,369a}]
Mn triad: **2-30**,⁹⁰ (Mn).
Fe Triad: **1-37**,⁴⁵ **1-39b(1)**,^{47b} **3-69a**,^{175,22b} **3-73**,^{177b} **3-74**,^{178a} (Fe). **3-105(1)**,^{193ab} **3-111**,²⁰¹ **3-112**,²⁰¹ **3-143**²⁰¹ (Ru). **1-50(1)**,⁵⁵ **1-51**,⁵⁰ **1-52**,⁵⁰ **2-36d(1)**,^{47b} **3-134**,²¹³ **3-158**,²⁰¹ **3-159**²⁰¹ (Os). [Table 6, Footnote 56: Fe(9),^{47b,193b(2),201,363,393a,393b,394} Os(2),²²⁰ Ru(9),^{47b,193b(2),201,363,393a,393b,394} Os(2),²²⁰]
Co Triad: **1-54ab**,^{57ab} (Co). **1-59a(1)**,^{60ab} **2-53a**,^{57ab} **2-71b**,^{116,117} **2-74(3 in soln)**^{60,61} (Ir). [Table 6, Footnote 92: Rh(2)^{340,349}]
Ni Triad: [Table 6, Footnote 121: Ni(5),^{415a,339,421(2)} Pd(4),^{14(2),339,421d} Pt(4),^{11,339,415a(2)}]
Cu Triad: [Table 6, Footnote 124: Cu³³⁹]
Ln: [Table 6, Footnote 126: Y,^{443a} Sm⁴⁴²]

^a The number of related examples listed in the footnotes in Tables 1–3 is given in parentheses. Silylenes prepared by other routes and also crystallographically characterized are identified from the footnotes to Table 6 when structures were determined.

Scheme 10



initiated a disproportionation of the tertiary silane to produce (PhCH₂CH₂)₄Si and (PhCH₂CH₂)₂SiH₂. The observation of (PhCH₂CH₂)₃SiCl also suggests an exchange between RhCl and SiH. The secondary silane appears to react preferentially with L₂RhX (X = H or Cl) to give the dimer [(ⁱPr₃P)(H)₂Rh]₂(μ-SiR₂)₂ (R = CH₂CH₂Ph; **3-214**).²⁴⁹ In contrast, (PhCH₂)₃SiH and L₂RhCl afforded, as one of the products, the dimer, [L(H)RhSiAr₃]₂(μ-Cl)₂, **3-217**.²⁴⁹ In the case of these dimers, the hydride ligands are all terminal and there were no bridging Rh–H–Si linkages reported.

3.6.2. Formation of Silylene Complexes

The term “silylene” is used in two contexts: (i) to describe systems that contain (or are assumed to contain) the unit [TM]=Si<; and (ii) to describe systems that contain a SiR₂ that bridges two metal centers. It is the first of these that will be described in this section, and a few examples of the second were included in 3.6.1.

The formation of silylene complexes has been demonstrated in previous sections, but the purpose here is to summarize reactions that lead to [TM]=Si directly from a metal precursor and a hydrosilane. There are certainly other routes to metal silylenes, but these often involve manipulation of a silicon functional group in [TM]–SiR₂X. Ogino has summarized the synthesis of silylene and silyl(silylene)metal complexes, and a section on mono- and bimetallic silylene complexes is included in Braunstein and co-workers’ review.^{337a,b}

One of the possible reactions of a secondary silane or a primary silane is the formation of a metal silylene [TM]=SiR₂ or a silicon-functional silylene, [TM]=SiHR], respectively. If a tertiary silane is employed, migration of a substituent from silicon to the metal center would be required to produce [TM]=Si<. There are 44 examples listed in Tables 1–3 plus 23 related examples in the footnotes to these tables illustrating this type of reaction. In addition, there are 61 cases in the footnotes to Table 6 (complexes prepared by other routes and characterized crystallographically are included later in Table 7, section 4). The examples from hydrosilanes are summarized in Chart 7 (listing includes

base-free and base-coordinated examples, some of which result from an intramolecular interaction). There are also metal–silyl complexes listed in the tables that are precursors to metal silylenes through some subsequent reaction, and a few of the examples will be discussed later for illustrative purposes.

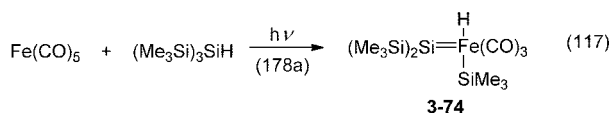
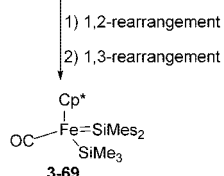
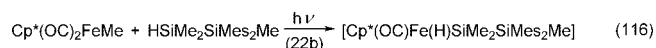
The basic reaction processes that provide silylene complexes are similar to those discussed in sections 3.2–3.4. Several cases involve loss of CH₄, RH, or H₂ from a [TM]–R precursor (see section 3.3.1) or a [TM]–H precursor (section 3.3.2). Examples accompanied by loss of CH₄ include **3-27** (Cr); **3-32** and **3-33** (Mo); **1-29a** (eq 71), **2-20** (Scheme 6), **2-21**, **3-39** (eqs 27, 72), **3-40a** (eq 73), **3-41**, and **3-46** (eq 72) (W); **3-69** (Fe); and **2-71b** (Ir). Another smaller grouping of precursors involves the loss of an unsaturated, allyl-type ligand (section 3.2.3): **1-24**, **2-10**, **2-11** (Mo, loss of η³-CH₂C₆H₅); **2-74** (Ir, loss of η³-C₈H₁₅). Loss of tucked-in Cp was observed in the formation of **1-30** and **2-21**. Photolysis of carbonyl complexes (producing loss of CO; see section 3.2.2) and reaction with hydrosilanes produced silylene complexes **2-30** (Mn) and **3-74** (Fe).

Half of the examples listed above from Tables 1–3 involve a Cp[TM] derivative (or substituted Cp such as Cp*), and nearly half of the examples involve the Cr triad mostly for molybdenum or tungsten centers. There are about a dozen cases of intramolecularly stabilized silylenes of the type [TM]{SiR₂–Do–SiR₂} [Do = OR, NR₂; TM = Cr, Mo, W, Ru, Os] that are generally prepared by one of the two processes shown in Scheme 10, one of which requires cleavage of the Si–Si bond in a disilane as demonstrated earlier in eqs 29, 30, and 31 for the formation of **3-27**, **3-32**, **3-105**, and **3-143**.^{151,193ab,201}

To form a silylene complex from reaction of a tertiary silane requires rearrangement of a group from the metal-bound silicon to the metal center. The most common cases involve migration of an aryl group or of a silyl group. A unique case involved the photolytic reaction of *o*-Me₂NC₆H₄SiMe₂H with Cp*(OC)₃WMe, which provided an initial oxidative addition product (with loss of CH₄), Cp*(OC)₂WSiMe₂C₆H₄NMe₂-*o*. An aryl migration from this

initial product provided $\text{Cp}^*(\text{OC})_2(\text{Ar})\text{W}=\text{SiMe}_2$ in which the NMe_2 substituent of the aryl group then coordinated to the silicon center to produce a base-stabilized silylene derivative (eq 73).^{157a} The results of the photolysis of $\text{Cp}^*(\text{OC})_3\text{WMe}$ with the monofunctional disilane $\text{HSiMe}_2\text{-SiR}_2\text{Me}$ depended on the nature of the R group (eq 72). The initial oxidative addition product, $\text{Cp}^*(\text{OC})_2\text{WSiMe}_2\text{-SiR}_2\text{Me}$, subsequently underwent a 1,2-rearrangement of the SiR_2Me group (typical of metal–disilane complexes),¹⁵⁶ followed by a 1,3-methyl migration from the initially formed $\text{W}(\text{SiR}_2\text{Me})=\text{SiMe}_2$, to produce the stable silylene complex when R is a sterically bulky group such as mesityl (see **3-39**, eqs 27 and 72). When R was a small group such as Me, the silylene that formed after the 1,2-rearrangement dimerized to the novel complex **3-46** with a transannular coordination of CO to the silicon center.¹⁵⁶ A similar tactic has been employed to form $\text{Me}_3\text{Si}[\text{TM}]=\text{SiRR}'$ (TM = Fe (**3-69**)^{22b} and **3-74**^{178a})). When the solid-state structures of such complexes are determined, a comparison of TM–Si and TM=Si distances in the same molecule is possible.

Photolysis of carbonyl derivatives can result in loss of CO and formation of a coordinatively unsaturated metal center. The reaction of $\text{H}_2\text{Si}(o\text{-Me}_2\text{NCH}_2\text{C}_6\text{H}_4)(\text{Vin})$ with the photolysis product from $\text{Cr}(\text{CO})_6$ was originally claimed to produce the complex **2-7**, although the formation of **2-7** by this route was later retracted.^{80a} Successful preparation of **2-7** was reported from reaction of $\text{K}_2\text{Cr}(\text{CO})_5$ with $\text{Cl}_2\text{Si}(o\text{-Me}_2\text{NCH}_2\text{C}_6\text{H}_4)(\text{Vin})$ as well as another route that involved reaction of a preformed silylene complex, as will be discussed later in this section.⁹⁰ A related reaction of $\text{H}_2\text{Si}(o\text{-Me}_2\text{NCH}_2\text{C}_6\text{H}_4)\text{Me}$ and $\text{CpMn}(\text{CO})_3$ provided the silylene complex, **2-30**.⁹⁰ The iron analogue (**3-69**) of the previously described tungsten complex **3-39** was formed from the reaction of $\text{Cp}^*\text{Fe}(\text{CO})_2\text{Me}$ and $\text{HSiMe}_2\text{SiMes}_2\text{Me}$, as shown in eq 116, and **3-74** was formed from $\text{Fe}(\text{CO})_5$ and the tertiary silane $(\text{Me}_3\text{Si})_3\text{SiH}$, as illustrated in eq 117. Both of these reactions involve a 1,2-rearrangement, and in the case of **3-69**,^{22b} an additional 1,3-rearrangement is required to produce the product just as in the case of the tungsten complex. The corresponding reaction of $\text{CpFe}(\text{CO})_2\text{Me}$ provided the analogue of **3-69**, but the complex was too unstable to isolate.^{22b}



Using the ligand $[\{\text{Bu}_2\text{PCH}_2\text{SiMe}_2\}_2\text{N}]^-$, a 3-coordinate Co(I) 14e-complex has been prepared that exhibits an unusual reaction sequence leading to both Co(V) and Co(III) silylene complexes. The overall reaction is shown in eq 118. The Co(I) complex reacts with 4 equiv of PhSiH_3 to give 1 equiv of Ph_2SiH_2 and incorporates the other 3 equiv of PhSiH_3 to provide two ligated SiH_2Ph groups, and the last equivalent forms the silylene. This last transformation also involves

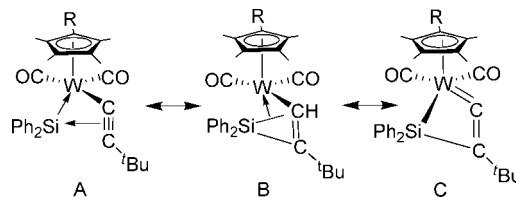
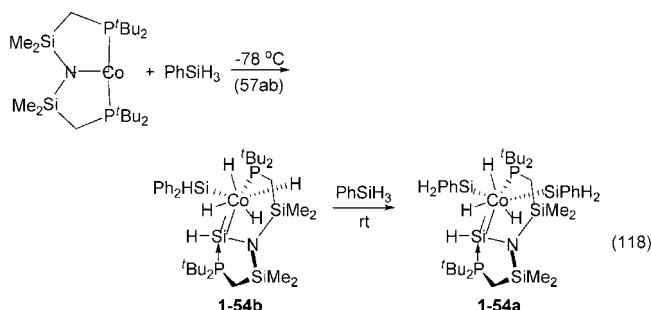


Figure 3. Contributing resonance structures proposed for $(\text{C}_5\text{Me}_4\text{Et})(\text{OC})_2\text{W}(\mu\text{-}\eta^1\text{:}\eta^3\text{-C}\equiv\text{C}'\text{Bu})(\text{SiPh}_2)$.^{160a}

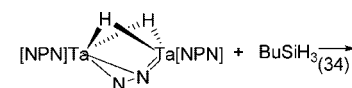
migration of N from the coordinating ligand to the Si center and coordination of one of the P tethers to the silylene silicon.^{57a,b} The complex **1-54b** is an analogue of **1-54a**, but a phenyl group from the silylene silicon has migrated from Co to Si, forming $\text{Si}(\text{H})\text{Ph}_2$. Addition of PhSiH_3 to **1-54b** leads to **1-54a** quantitatively and produces a stoichiometric quantity of Ph_2SiH_2 .^{57a,b} Reaction of the acetonitrile solvate of $\text{Cp}^*(\text{OC})_2\text{WMe}$ with $\text{HPh}_2\text{SiC}\equiv\text{C}'\text{Bu}$ gave rise to a complex that appears to exhibit characteristics intermediate between a triple bond coordinated to the silylene center and coordination of the C–Si bond of a silacyclopentene ring to the W center. The contributing resonance structures that were suggested are shown in Figure 3 and includes complexation of the acetylene to the Si center of the silylene (A), coordination of an α -agostic Si–C bond of silacyclopentene (B), and a tungstaallene structure (C).^{160a} A computational study concluded that the silylene group interacted both with the W center and the acetylide group.^{338a}



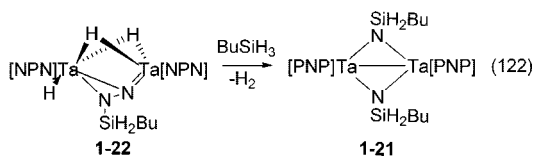
Exchange of a silicon center in a preformed silylene complex has also been reported, and the sequence of possible steps leading to this exchange between $\text{Cp}^*(\text{OC})_2\text{W}=\text{SiEt}_2\text{py-d}_5$ and H_2SiPh_2 was outlined in Scheme 9 (examples of silyl exchange reactions were discussed in section 3.3.3).^{85a} This is possibly a general approach to make new silylene complexes from more easily prepared versions, but more examples need to be developed. Another potential method for the preparation of new silylene complexes is to exploit the reactivity of silicon-functional $[\text{TM}]=\text{Si}$ derivatives. If primary silanes are used in the formation of a silylene complex, there is a SiH functional group in place at the silylene silicon center. Since transition metal complexes also promote hydrosilylation reactions, this could provide an entry into silylenes with mixed substituents, $[\text{TM}]=\text{SiRR}'$. In fact, there is an example of this sequence in the formation of **1-59a**^{60a,b} as shown in eq 119. In this case, oxidative addition of ArSiH_3 resulted in reductive elimination of cyclooctene and the formation of an iridium silylene bearing a SiH group. Hydrosilylation of COE released in the initial reaction of the silane with the metal complex and the silylene SiH that was produced resulted in the formation of the mixed substituted silylene, $\text{Ir}=\text{SiAr}(\text{C}_8\text{H}_{15})$.^{60b} Note that the formation of the intermediate $[\text{PhBP}_3](\text{H})_2\text{Ir}=\text{Si}(\text{Ar})(\text{H})$ required migration of a hydride from silicon to iridium presumably

3.6.3. Reactions of Silanes and Other Substrates with [TM]=X

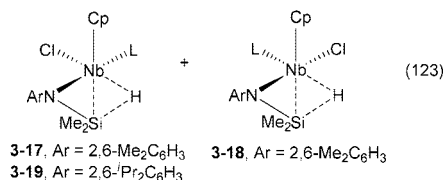
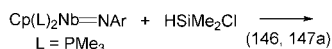
Although the purpose of this review is to survey the reactions of hydrosilanes with metal complexes that give rise to [TM]–Si bonds, there are examples where reaction of the silane takes place preferentially at a ligand. Such is particularly the case for imine complexes of Ta and Nb. The imido–amido chelate complex of Ta, $\text{Cp}^*(\text{Me})\text{Ta}[\text{N}(\text{C}_6\text{H}_3\text{Me})_2\text{NSiMe}_3]$, adds PhSiH_3 across the imine bond to form $\text{Cp}^*(\text{Me})\text{HTa}[\text{PhSiH}_2\text{N}(\text{C}_6\text{H}_3\text{Me})_2\text{NSiMe}_3]$ (**1-17c**).^{32b} Starting with the related complex, $\text{Cp}^*(\text{Cl})\text{Ta}[\text{N}(\text{C}_6\text{H}_3\text{Me})_2\text{NSiMe}_3]$, reaction with PhSiH_3 in CH_2Cl_2 produced $\text{Cp}^*(\text{Cl})\text{HTa}[\text{PhSiH}_2\text{N}(\text{C}_6\text{H}_3\text{Me})_2\text{NSiMe}_3]$ (**1-18**) as well as $\text{Cp}^*(\text{Cl})_2\text{Ta}[\text{PhSiH}_2\text{N}(\text{C}_6\text{H}_3\text{Me})_2\text{NSiMe}_3]$ and $\text{Cp}^*(\text{Cl})\text{HTa}[\text{PhSiH}_2\text{N}(\text{C}_6\text{H}_3\text{Me})_2\text{NSiPhHCl}]$ (**1-19**).^{32b} Ditantalum hydride complexes are formed when PhSiH_3 adds to the mononuclear imine complex, $\text{Cp}^*(\text{ArN}=\text{H})\text{TaSi}(\text{SiMe}_3)_3$, with elimination of $\text{HSi}(\text{SiMe}_3)_3$.³³ Two dimers are produced, from addition of 1 or 2 equiv of PhSiH_3 . The products, **1-20a** and **1-20b** (major), are shown in eq 99. The core structures in both contain a TaTaSiN cycle, although both Ta...Si distances are similar. One or two silanes also add to N in the dinuclear complex ($[\text{NPN}]\text{Ta}_2(\mu\text{-H})_2(\mu\text{-}\eta^1\text{:}\eta^2\text{-N}_2)$ ($\text{NPN} = \{\text{PhP}(\text{CH}_2\text{SiMe}_2\text{NPh})_2\}^{2-}$) as illustrated in eq 122.



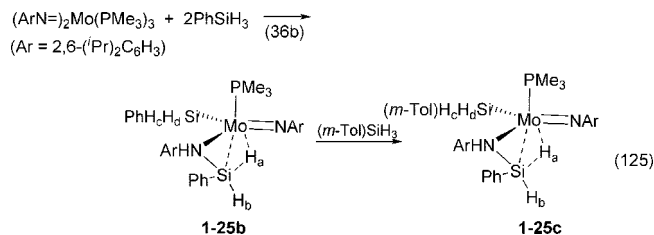
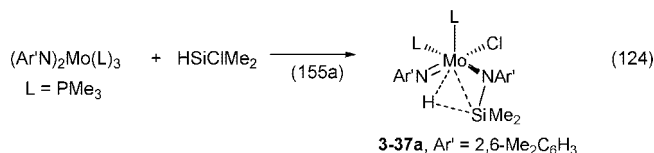
$\text{NPN} = (\text{PhNSiMe}_2\text{CH}_2)_2\text{PPh}$



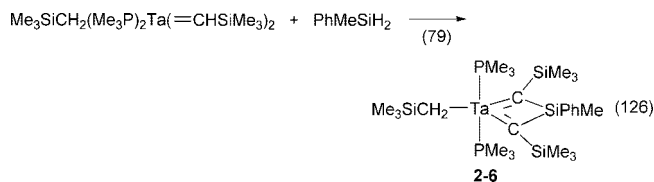
A series of complexes have been formed from reaction of $\text{CpL}_2\text{M}=\text{NAr}$ ($\text{M} = \text{Nb}, \text{Ta}$; $\text{Ar} = 2,6\text{-Me}_2\text{C}_6\text{H}_3$, $2,6\text{-}^i\text{Pr}_2\text{C}_6\text{H}_3$) with HSiMe_2Cl . The products from Nb (**3-17–3-19**) are shown in eq 123 and appear to be consistent with a “stretched” β -agostic interaction.^{146,147a} In contrast to the Nb system, $\text{Cp}(\text{Me}_3\text{P})_2\text{Ta}=\text{NAr}$ reacted with both HSiMe_2Cl and HSiMeCl_2 to give complexes **3-25a**^{146,147a} and **3-26a**^{78a} in which Si was bound to Ta and which were described as IHI complexes. Another example of a reaction in which a silane became bound to the N of an imine group was reported from the molybdenum complex $(\text{Ar}'\text{N})_2\text{Mo}(\text{PMe}_3)_3$ and HSiClMe_2 shown in eq 124.^{155a} A β -agostic interaction was proposed for **3-37a**, which is thus an analogue of the niobium complex, **3-17**. An additional example produced from PhSiH_3 (eq 125) contains both a classical SiH_2Ph substituent as well as SiH_2Ph group that exhibits a β -agostic interaction.



Studies of other multiply bonded metal complexes were rare. Tantalum alkylidene complexes reacted with silanes to give C–Si bonds as illustrated in eq 126.

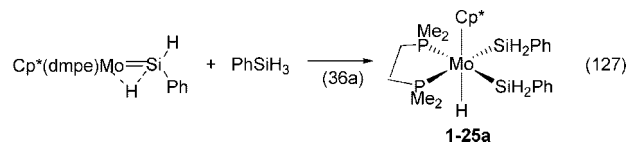


A similar reaction of $(\text{Me}_3\text{SiCH}_2)_3(\text{PMe}_3)_2\text{Ta}(=\text{CHSiMe}_3)$ with H_2SiMePh gave $(\text{Me}_3\text{SiCH}_2)_3\text{Ta}=\text{C}(\text{SiMePhH})\text{SiMe}_3$ (**2-5**).⁷⁹ The sequence leading to the product was proposed to occur through (a) loss of phosphine, (b) addition of HSi across $\text{Ta}=\text{C}$ to give $\text{Ta}(\text{H})\text{C}(\text{H})(\text{SiPhMeH})\text{SiMe}_3$, (c) loss of H_2 and addition of a second H_2SiPhMe to give $\text{Ta}(\text{SiHPhMe})\text{C}(\text{H})(\text{SiPhMeH})(\text{SiMe}_3)$, and (d) elimination of PhMeSiH_2 to give the observed product, **2-5**.⁷⁹



The reactivity of metal silylenes has been recently reviewed.³⁴¹ The sections of this review are grouped in terms of (a) nucleophilic attack on the silylene silicon center, (b) reactions with polar unsaturated compounds, (c) reactions with HX ($\text{X} = \text{Cl}, \text{H}, \text{SiR}_3$), (d) dissociation of silylene fragments from the metal center, (e) C–H bond activation by the metal–silylene, (f) reaction with chloroalkanes, and (g) rearrangement of substituents on silyl(silylene) complexes. Only a few representative examples will be described here.

One interesting result was the reaction of the silylene complex, $\text{Cp}^*(\text{dmpe})(\text{H})\text{Mo}=\text{SiHPh}$, with a silane, which resulted in the formation of a disilyl complex (**1-25a**) as shown in eq 127.^{36a} When the reaction was conducted with PhSiD_3 , the deuterium label was found in the Mo-H position as well as in one of the silyl groups.^{36a} It will be interesting to determine whether the direction of addition of HSi to $[\text{TM}]=\text{Si}$ as shown in eq 127 is the exception or the rule.



The cationic osmium–silylene complex, $[\text{Cp}^*(\text{Me}_3\text{P})_2\text{Os}=\text{SiMe}_2]^+[\text{B}(\text{C}_6\text{F}_5)_4]^-$, was prepared by abstraction of SiCl in $\text{Cp}^*(\text{Me}_3)_2\text{OsSiMe}_2\text{Cl}$ with $\text{Li}(\text{OEt})_2[\text{B}(\text{C}_6\text{F}_5)_4]$.³⁴² Addition of CH_2Cl_2 (or $\text{C}_6\text{H}_5\text{CH}_2\text{Cl}$) to the cationic silylene complex resulted in both abstraction of chloride by the silicon center and oxidation of the $\text{Os}(\text{II})$ to $\text{Os}(\text{III})$. The organic radical was detected at low temperature through electron paramagnetic resonance (EPR) measurements of freshly prepared reaction mixtures. The reaction is considered a model for a step in the Direct Process reaction, which may occur through

a metal–silylene species.³⁴² The tactic of abstracting a silyl-functional group in the complex $\text{Cp}^*(\text{Me}_3\text{P})\text{MeIrSiMe}_2\text{OTf}$ with $\text{LiB}(\text{C}_6\text{F}_4)_4(\text{OEt})_2$ provided a mixture of a cationic silene complex $[\text{Cp}^*(\text{Me}_3\text{P})(\text{H})\text{Ir}(\eta^2\text{-CH}_2\text{SiMe}_2)]^+$ and the base-stabilized, cationic, silylene, $[\text{Cp}^*(\text{Me}_3\text{P})(\text{Me})\text{Ir}=\text{SiMe}_2(\text{OEt}_2)]^+$.³⁴³

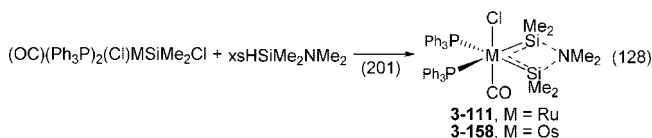
Base-stabilized silylene complexes appear to be reluctant to generate silylene photochemically as photochemical irradiation of $\text{CpFe}(\text{CO})_2\text{SiMe}_2\text{SiMe}_2\text{O}^t\text{Bu}$ in the presence of the silylene trap $(\text{Me}_3\text{Si})_3\text{SiH}$ leads to formation of the intramolecularly base-stabilized complex, $\text{Cp}(\text{OC})\text{Fe}(\eta^2\text{-SiMe}_2\text{-O}^t\text{Bu-SiMe}_2)$, and not to the silylene insertion product, $(\text{Me}_3\text{Si})_3\text{SiSiMe}_2\text{H}$.³⁴⁴ However, heating a solution of this “base-stabilized” silylene complex generates an equilibrium mixture of the base-coordinated complex as well as the base-free complex, $\text{Cp}(\text{OC})[(^t\text{BuO})\text{Me}_2\text{Si}]\text{Fe}=\text{SiMe}_2$, and the base-free component reacted with $(\text{Me}_3\text{Si})_3\text{EH}$ to give $(\text{Me}_3\text{Si})_3\text{ESiMe}_2\text{H}$ ($\text{E} = \text{Si}, \text{Ge}$). However, attempts to trap SiMe_2 with other tertiary silanes such as Ph_2MeSiH or Et_3SiH failed. This suggests that the sequence leading to the observed products probably involved addition of SiH to the silylene, $\text{Fe}=\text{SiMe}_2$, to give $\text{Fe}(\text{SiMe}_2\text{H})(\text{SiMe}_2\text{O}^t\text{Bu})[\text{E}(\text{SiMe}_3)_3]$ followed by reductive elimination of $(\text{Me}_3\text{Si})_3\text{ESiMe}_2\text{H}$ to give $\text{Cp}(\text{OC})_2\text{FeSiMe}_2\text{O}^t\text{Bu}$. Attempts to use another standard silylene trap, Bu_3SnH , resulted in the formation of $\text{Cp}(\text{OC})\text{Fe}(\text{SnBu}_3)_2\text{H}$ and $\text{HSiMe}_2\text{SiMe}_2\text{O}^t\text{Bu}$.

Reaction of a hydrosilane with $\text{Ru}=\text{Si}(\text{SEt})_2^+$ resulted in displacement of the silylene to give a silyl–metal complex (formation of **1-39a**^{47a}) and, in another case, exchange of one silylene for another silylene at a W center (formation of **2-19**^{85a}) as described previously in this section.

3.6.4. Reactions at Silyl Substituents

Reactions of functional groups on a silicon leading to silylene and silenes that are coordinated to a metal center were briefly described in section 3.6.3, for example, the formation of $[\text{TM}]=\text{SiR}_2$ by abstraction of chloride from $[\text{TM}]-\text{SiR}_2\text{X}$. Chlorosilanes are common building blocks to other silicon compounds, and this role can also be played by $[\text{TM}]\text{SiR}_2\text{Cl}$ complexes. A common reaction of chlorosilanes is substitution of chloride using protic reagents such as alcohols and primary or secondary amines. This approach has been used, particularly with complexes that contain the sequence $\text{Cl}[\text{TM}]\text{SiR}_2\text{Cl}$ to form internally coordinated silylene complexes. An interesting set of examples has been generated from 5-coordinate $(\text{OC})(\text{Ph}_3\text{P})_2(\text{Cl})\text{MSiMe}_2\text{Cl}$ ($\text{M} = \text{Ru}, \text{Os}$) in the presence of excess $\text{HSiMe}_2\text{NMe}_2$ as a mixture **3-111** and **3-158** (as shown in eq 128) and the corresponding hydrides, **3-112** and **3-159** (products are a function of time).²⁰¹ The sequence leading to the products is not clear but may involve OA of the hydrosilane and elimination of HCl with the amine acting as an acid sponge. If HCl was eliminated from the metal center, then chloride migration from silicon to the metal center would be required or, alternatively, the chloride could be eliminated from the silicon center and either reaction would produce a silylene. Finally, coordination of the amino group from $[\text{TM}]-\text{SiMe}_2\text{NMe}_2$ to the silylene would produce the indicated product. When the reaction is conducted at a higher temperature, the chloride ligand was replaced by hydride (**3-112** and **3-159**), a type of reaction that will be described in section 3.7, and in the ruthenium case, a binuclear complex, **3-143**,²⁰¹ was also produced in which one of the ruthenium centers contained the same SiNSiRu sequence as present in

3-111. The reaction of $\text{Cp}_2\text{Nb}(\text{SiMe}_2\text{I})_2\text{H}$ with a 10-fold excess of $\text{H}_2\text{N}^t\text{Bu}$ took another pathway, forming an imido-bridged silaniobocyclobutane, $[\text{Cp}_2\text{Nb}(\text{H})\{\mu\text{-SiMe}_2\}_2\text{N}^t\text{Bu}]$. Remarkably, the related reaction of $\text{Cp}_2\text{Nb}(\text{SiMe}_2\text{I})_2\text{H}$ with HNEt_2 formed a similar complex that required the cleavage of a $\text{N}-\text{C}$ bond. The crystal structure of the complex formed from $^t\text{BuNH}_2$ exhibited a short $\text{Si}\cdots\text{Si}$ distance and a long $\text{Nb}-\text{Si}$ distance, suggesting the possibility of a stretched $\text{Si}-\text{Si}$ σ -complex.³⁵⁸



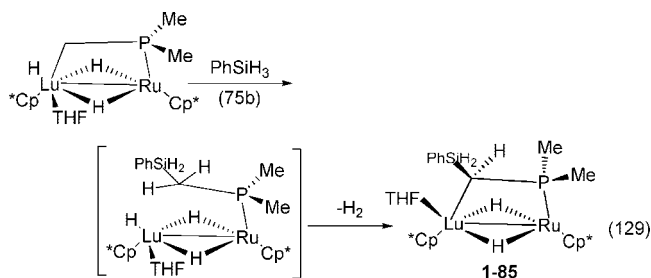
Exchange between a group on silicon and a group on the metal has been described previously. The most common of these were $\text{Cl}-[\text{TM}]-\text{SiH}$ to $\text{H}-[\text{TM}]-\text{SiCl}$, and examples included Ru (**1-42**, **1-43**),^{50,51a} Os (**1-51**, **1-52**);⁵⁰ and Ir (**1-57**, **1-58**).^{58,59} The reverse migration has also been observed, i.e., a hydride was transferred from the metal to silicon and chloride from silicon to the metal in the formation of the niobium complex **3-22**¹⁴⁹ and the molybdenum complex **3-37a**.^{155a} When $\text{Cp}^*(\text{Me}_3\text{P})\text{IrMe}_2$ was treated with $[\text{Cp}_2\text{Fe}][\text{PF}_6]$ and Ph_3SiH , the final product was $\text{Cp}^*\text{Ph}(\text{Me}_3\text{P})\text{IrSiPh}_2\text{F}$ (**3-222**). The Cp_2Fe^+ initiates a one-electron oxidation of the iridium complex, which then loses a methyl radical to produce a cationic Ir complex. Phenyl migration from Si to Ir and trapping with F^- provided **3-222**.²⁵⁹

Although there are examples where a triflate ligand originally coordinated to a transition metal appears on the silicon in the product (see, for example, **3-223** and **3-226**),^{117a} there are at least two sequences that have been proposed that both involve displacement of the triflate anion from the metal center producing the silylene intermediates $[\text{Cp}(\text{Me}_3\text{P})(\text{H})\text{Ir}=\text{Si}(\text{OEt})_2]^+$ and $\{\text{Cp}^*(\text{Me}_3\text{P})[\text{Me}(\text{Me}_3\text{-Si})_2\text{Si}]\text{Ir}=\text{SiMe}_2\}^+$, respectively, followed by attack of the triflate anion at the silicon of the silylene center to produce the observed products.^{117a} Alternatively, disproportionation of the starting silane, $\text{HSi}(\text{OEt})_3$, used to generate **3-223** occurred to give $\text{H}_2\text{Si}(\text{OEt})_2$ and $\text{Si}(\text{OEt})_4$ and subsequent reactions of $\text{H}_2\text{Si}(\text{OEt})_2$, also involving formation of a silylene, that could produce the observed product.^{117a} It is the disproportionation of the starting silane that sometimes gives silyl–metal products that do not include what would be expected from OA of the starting silane. A dramatic example of this was the product isolated from the reaction of $(\text{Cy}_3\text{P})_2(\text{H}_2)_2\text{RuH}_2$ with the secondary silane, H_2SiMePh .^{100,101} The complex that formed, **2-45**, contained two $(\text{Cy}_3\text{P})_2(\text{H}_2)_2\text{Ru}$ units bound to SiH_4 (all four $\text{Si}-\text{H}$ bonds participate in a σ -interaction with a Ru center).^{100,101} Addition of $\text{HSi}(\text{OMe})_3$ to **2-45** also produced $\text{H}_2\text{Si}(\text{OMe})_2$, and $\text{Si}(\text{OMe})_4$ and the $\text{H}_2\text{Si}(\text{OMe})_2$ reacted to form complex **3-144**, $(\text{Cy}_3\text{P})(\text{H})\text{Ru}\{\text{H}_2\text{Si}(\text{OMe})_2\}_3\text{Ru}(\text{H})(\text{PCy}_3)$.¹⁰¹

When the lanthanide complex, $[\text{Cp}^*_2\text{Sm}(\mu\text{-H})_2]$, was reacted in pentane with excess PhSiH_3 , the cluster, $[\text{Cp}^*_2\text{SmSiH}_3]_3$ (**1-81**), formed as the first reported example of a f-element complex with a SiH_3 substituent.⁷² In addition, Ph_2SiH_2 and SiH_4 (products of disproportionation) and C_6H_6 suggests that the cleavage of the $\text{Si}-\text{Ph}$ bond also occurred. To verify the $\text{Si}-\text{C}$ bond cleavage, the reaction of $\text{Cp}^*_2\text{SmCH}(\text{SiMe}_3)_2$ and excess PhSiH_3 was conducted in $c\text{-C}_6\text{D}_{12}$. In this case, $\text{CH}_2(\text{SiMe}_3)_2$ and H_2 formed as well

as C_6H_6 (product of Si–C cleavage), Ph_2SiH_2 , and SiH_4 (disproportionation products), as was $H(PhSiH)_2H$ and silane oligomers (dehydrocoupling products).⁷² Silyl complexes of Eu (**1-84**), Sm, and Yb of the composition, $Cp^*Ln(SiH_3)(THF)Cp^*K(THF)_n$, formed when $Cp^*Ln(THF)_2$ was treated with KH and $PhSiH_3$. However, in this case, the mixture of KH and $PhSiH_3$ was thought to contain $KSiH_3$ and $KSiH_2Ph$, which could account for the observed silyl complexes.^{75a}

In a rather unique reaction of a primary silane with a heterobimetallic complex of Lu and Ru, the overall equivalent of cleavage of a Lu–C bond occurred with the silyl group incorporated at the carbon center. The sequence is shown in eq 129.



3.7. Transfer of Hydride from Si to TM

In some cases, reaction of the hydrosilane with a transition metal complex resulted in the equivalent of transfer of hydride from silicon to the metal center. This could possibly occur by a σ -bond metathesis process or by oxidative addition followed by reductive elimination of the silyl group, although the mechanism for the transformation to $[TM]H$ is not often addressed. The cases reported during the period covered by the review are summarized in Table 5. Nearly half of the complexes in Table 5 contain electrophilic metals from the scandium and titanium triads or the lanthanoids.

Four examples in Table 5 involve transfer of a $-NMe_2$ group from Ti, Zr, Hf, or Ta in $Cp_2M(NMe_2)_2$ [$M = Ti$ (**5-2**), Zr (**5-2**),³⁰⁴ or $M(NMe_2)_x$ ($x = 4$, $M = Zr$ (**5-4**),^{305,306} Hf,³⁰⁶ $x = 5$, $M = Ta$ (**5-7a**)^{308a})] to the silicon center. In the case of $Ti(NMe_2)_4$ and hydrosilanes, almost 95% of the NMe_2 groups were transferred to the silicon to give aminosilanes and black solids. However, with $M(NMe_2)_4$ ($M = Zr, Hf$), only about 45% of the amide groups were transferred, and novel trinuclear complexes containing both terminal and bridging amide groups as well as hydride bridges were isolated (**5-4** and **5-5**).^{305,306} The ab initio MO calculations for the σ -bond metathesis reaction of $Ti(NH_2)_4$ and SiH_4 showed that the lowest-energy pathway involved the formation of $M-H$ and H_3SiNH_2 or path 1 in Scheme 11. Calculations also showed that $HTi(NH_2)_3$ reacted further with SiH_4 to give $H_2Ti(NH_2)_2$.^{305,306} The transfer of a NMe_2 from $Cp_2M(NMe_2)_2$ ($M = Ti, Zr$) to primary, secondary, and tertiary silanes also has been reported and most likely involves a σ -bond metathesis reaction similar to that shown in path 1 in Scheme 11,³⁰⁴ and the product silylamines were identified in reaction mixtures. Although a more complex tantalum dimer product was ultimately produced from $Ta(NMe_2)_5$ and H_2SiRPh , transfer of a NMe_2 group to silicon in the first step was proposed through a metathesis intermediate similar to that shown in Scheme 11, which produced $PhRSiH(NMe_2)$.^{308a} There was one additional example of a TM– NR_2 exchange with HSi in Table 5, and that involved the nickel complex $Cp^*Ni(PEt_3)NHTol$ and Me_3SiH (see

entry **5-18**).³¹⁴ This reaction could occur by a metathesis process (not well established for electron-rich metals) or an oxidative addition/reductive elimination reaction, although reductive elimination of Si–N is not common.

Other X-groups in Cp_2MX_2 such as $X = F$ or OPh will exchange with hydrosilanes, although the identity of the metal hydride species could generally not be established. However, the formation of $FSiR_3$ and $PhOSiR_3$ in the product mixtures was determined.³⁰⁴ Organic groups may also be transferred to silicon, as was demonstrated in the stoichiometric reaction of the cationic species $[Cp_2ZrMe(CIC_6D_5)]^+$ (Table 5, **5-3b**) with $PhSiH_3$.^{31a} A series of silanes, $Ph_xMe_{3-x}SiH$ ($x = 1, 2, 3$), $Ph_xMe_{2-x}SiH_2$ ($x = 1, 2$), and Ph_xSiMe_{4-x} ($x = 1, 2, 3, 4$) were identified in the reaction solutions.^{31a} The transfer of a Me group from the Zr center to Si most likely occurred by a σ -bond metathesis process. The observation of silanes with more than one Ph substituent implies a redistribution of Si–Ph groups. The oil formed from the reaction of $[Cp_2ZrMe(CIC_6D_5)]^+$ and $PhSiH_3$ when dissolved in $THF-d_8$ showed the presence of $Cp_2ZrPh(THF-d_8)^+$, indicating that a Ph group was transferred from Si to Zr.^{31a} In the case of the cationic hafnium complex, $[CpCp^*HfMe][\mu-MeB(C_6F_5)_3]$, reaction with $PhSiH_3$ led to the cationic hydride complex, $[CpCp^*HfH][\mu-HB(C_6F_5)_3]$ (**5-6**) and $PhMe_2SiH$.^{307ab} It is probable that the zwitterionic starting complex provided the electrophilic cation $[CpCp^*HfMe]^+$, which is more reactive in a σ -bond metathesis reaction with a hydrosilane than would be the neutral precursor $CpCp^*HfMe_2$.^{307abc}

Complexes that contain $Ln-R$ ($Ln = Sm, Lu, Yb, Y$) also “transfer” a R group to $PhSiH_3$ to give $PhRSiH_2$ and produce $Ln-H$ dimers and, in some cases, more complex clusters. The R group was usually $-CH_2SiMe_3$, $-CH(SiMe_3)_2$, or Me. Examples in Table 5 include **5-30–5-34**.^{75a,328–332a}

The remainder of the entries in Table 5 involve an assortment of transition metal complexes from the iron through zinc triads. In most cases, there were no speculations concerning the stepwise path by which a hydride is transferred from silicon to the metal center and a group on the metal is transferred to silicon. It is probable that oxidative addition of the SiH bond becomes involved with the more electron-rich metals. The possible reductive elimination processes for a hypothetical, general complex are outlined in Scheme 12. The balance of factors leading to a particular elimination is unknown, but three cases where authors have speculated on a sequence of reactions leading to elimination of Si–Si and Si–C will be discussed in the following paragraphs.

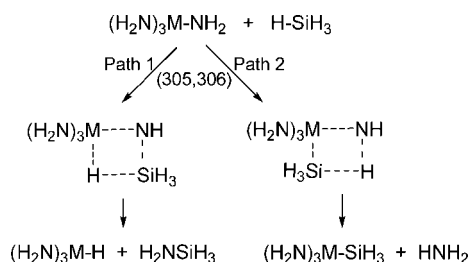
In the reaction of the square-planar rhodium(I) complex $Rh[(\kappa^2-Si,P)-Me_2SiCH_2CH_2PPh_2](PMe_3)_2$ with $HSiMe_2Ph$, two successive steps were proposed, each involving loss of PMe_3 followed by oxidative addition (Scheme 13).²⁴² The initial oxidative addition to $Rh[(\kappa^2-Si,P)-Me_2SiCH_2CH_2PPh_2](PMe_3)_2$ gives a 6-coordinate complex where one of the PMe_3 ligands is *trans* to a silyl ligand (the Si of the chelate). The strong *trans*-effect of the silyl ligand results in loss of that phosphine, and a second silane oxidatively adds to give a 7-coordinate $Rh(V)$ intermediate that then reductively eliminates disilane to give the 6-coordinate RhH_2 complex that was observed as the final metal complex. This room-temperature reaction thus provides mild coupling conditions for tertiary silanes but, unfortunately, not on a catalytic basis.^{242,246}

Table 5. Reactions of Hydrosilanes with Metal Complexes Leading to Metal Hydrides[†]

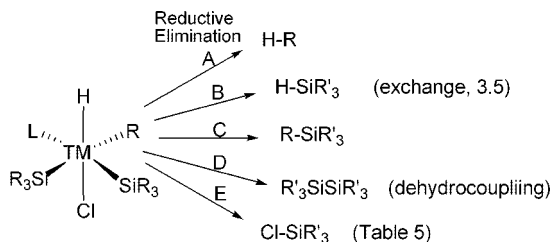
product	starting complex	silane	ref
Ti and V triads			
5-1 "Cp ₂ MH _x " (M = Ti, Zr, Hf; x = 1, 2) + Ph ₂ MeSiF	Cp ₂ MF ₂	HSiMePh ₂ ²	304
5-2 "Cp ₂ MH _x " (M = Ti, Zr; x = 1, 2) + Ph ₂ MeSiNMe ₂	Cp ₂ M(NMe ₂) ₂	HSiMePh ₂	304
5-3a [{Cp ₂ (μ-Cl)] ₂][B(C ₆ F ₅) ₄] + 5-3b [{Cp ₂ (μ-H)] ₂][B(C ₆ F ₅) ₄] 4-3a/4-3b ≈ 1/3	Cp ₂ Zr(Me)(ClC ₆ D ₅) ⁺ B(C ₆ F ₅) ₄ ⁻³	H ₃ SiPh	31a
5-4 * [(Me ₂ N) ₃ Zr(μ-H)(μ-NMe ₂) ₂] ₂ Zr	Zr(NMe ₂) ₄	H ₃ SiPh (0.67 equiv) ^d	305, 306
5-5 [(Me ₂ N) ₃ Hf(μ-H)(μ-NMe ₂) ₂] ₂ Hf	Hf(NMe ₂) ₄	H ₂ SiPh ₂ ⁵	306
5-6 CpCp*HfH(μ-H)B(C ₆ F ₅) ₃	CpCp*HfMe(μ-Me)B(C ₆ F ₅) ₃	H ₃ SiPh	307a,b,c
5-7a (Me ₂ N) ₃ Ta(μ-H) ₂ (μ-N,C-CH ₂ NMe)Ta(NMe ₂) ₃	Ta(NMe ₂) ₅	H ₂ SiPhR R = Me, Ph	308a
Mn triad			
5-7b Re(O)Cl ₂ (H)(PPh ₃) ₂	Re(O)Cl ₃ (PPh ₃) ₂	xs HSiEt ₃	308b
Fe triad			
5-8 (Ph ₃ P) ₂ (OC) ₂ Fe(H) ₂	(Ph ₃ P)(OC) ₄ Fe	HMe ₂ SiSiMe ₂ H	163, 166
5-9 [L ^{Me} Fe(μ-H)] ₂	[L ^{Me} Fe(μ-F)] ₂ ⁷	Et ₃ SiH	309
5-10 Tp(Ph ₃ P)HRu(NCCH ₃) [*] ⁸	Tp(Ph ₃ P)ClRu(NCCH ₃)	H ₂ SiPh ₂	48a
5-11 (Me ₃ P) ₂ H ₂ RuSiMe ₂ CH ₂ CH ₂ PPh ₂	(PMe ₃) ₂ RhSiMe ₂ CH ₂ CH ₂ PPh ₂	xs HSiMe ₂ Ph	242
5-12 Cp(OC)Ru(μ-dppm)MoCp(CO) ₂	[Cp(OC)Ru(μ-dppm)(μ-H) MoCp(CO) ₂] ⁺	HSiEt ₃	310
Co triad			
5-13 (PEt ₃) ₃ RhH ⁹	(PEt ₃) ₃ RhF	xs HSiPh ₃	241
5-14 (PPh ₃) ₃ RhH ¹⁰	(PPh ₃) ₃ RhCl	HSiEt ₃ (2 equiv)	311
5-15 * [(μ ₄ -H)Rh ₄ (PNNP) ₂ (CO) ₄](BF ₄)	[Rh ₂ (PNNP)(CO) ₂]	HSiEt ₃ ¹¹	312
5-16 "R ₃ SiIrH" ¹²	[(C ₈ H ₁₂)IrCl] ₂	HSiR ₃ ¹³	313
5-17a [Ir(H) ₂ {η ² -Me ₂ Si(CH ₂) ₂ PPh ₂ }(PMe ₃) ₂] + HexMeSiH ₂	[Ir(Me)(H){η ² -Me ₂ Si(CH ₂) ₂ PPh ₂ }(PMe ₃) ₂]	H ₃ SiHex ¹⁴	262
5-17b [Cp' IrI] ₂ (μ-H)(μ-I)	[η ⁵ -Cp' IrI] ₂ (Cp' = C ₅ H ₄ CH ₂ CH ₂ OMe)	HSiEt ₃ (~2 equiv/Ir)	260
Ni triad			
5-18 Cp*Ni(PEt ₃)(H)	Cp*Ni(PEt ₃)NHTol	HSiMe ₃	314
5-19 Pd nanoparticles	PdX ₂ (X = Cl ⁻ , OAc ⁻)	HSiMe ₂ Bu	315, 316
5-20 [Pd] _n (polysiloxane)	Pd(OAc) ₂	Me ₃ SiO(MeSiH-O) _n -SiMe ₃	317a,b
5-21 Pt(η ² -Ph-C≡CPh) ₂	PtCl ₂ (PhCH=CH ₂) ₂ + PhC≡CPh (10 equiv)	Ph ₃ SiH (2 equiv)	318
5-22 trans-(Ph ₃ P) ₂ IPtH	trans-(Ph ₃ P) ₂ PtI ₂	HSiEt ₃	319
5-23 * trans-(DIPPIDH)(DIPPID)PtH	cis-(DIPPIDH)(DIPPID)PtMe	HSiR ₃ ¹⁵	320
Cu and Zn triads			
5-24 "CuH" ¹⁶	CuF(PPh ₃) ₃ or CuCl or CuX	HSiPhMe ₂	321, 322, 323
5-25 [LCuH] ₂ ¹⁷	^t BuOCuL	HSi(OEt) ₃	324
5-26 NHCCuH ¹⁸	NHCCuO ^t Bu	HSiEt ₃	325
5-27 * [{HC(CMeNAr) ₂ }Zn(μ-H)] ₂ Ar = 2,6-Me ₂ C ₆ H ₃	[{HC(CMeNAr) ₂ }Zn(μ-F)] ₂	HSiEt ₃	326
5-28 "EtZnH" + (EtO) ₃ SiOCH ₂ CH ₂ NMe ₂	[EtZn(OCH ₂ CH ₂ NMe ₂) ₂]	HSi(OEt) ₃	327
5-29 "ZnH ₂ " + (EtO) ₃ SiOCH ₂ CH ₂ NMe ₂ or (EtO) ₃ SiNMeCH ₂ CH ₂ NMe ₂	[HZn(OCH ₂ CH ₂ NMe ₂) ₂] or [HZn(NMeCH ₂ CH ₂ NMe ₂) ₂]	HSi(OEt) ₃	327
Sc, lanthanides, actinides			
5-30 * [(C ₅ Me ₅)Sm(μ-H) ₂] ₆ [(μ-H)K(THF) ₂] ₃ ¹⁹	[(C ₅ Me ₅)Sm(CH(SiMe ₃) ₂)-(C ₅ Me ₅)K(THF) ₂] _n	H ₃ SiPh (5 equiv)	75a, 328
5-31 * [Ln(η ⁵ :η ¹ -C ₅ Me ₄ SiMe ₂ NCMe ₂ R)(L)(μ-H)] ₂ Ln = Lu, Yb, Y; R = Me, Et; L = THF	[Ln(η ⁵ :η ¹ -C ₅ Me ₄ SiMe ₂ NCMe ₂ R)(CH ₂ SiMe ₃)(THF)]	H ₃ SiPh	329
5-32 [(C ₅ Me ₄ SiMe ₃)Lu(CH ₂ SiMe ₃)(μ-H)(THF)] ₂	(C ₅ Me ₄ SiMe ₃)Lu(CH ₂ SiMe ₃) ₂ (THF)	H ₃ SiPh	330
5-33 [(C ₅ Me ₄ SiMe ₃)Lu(μ-H)] ₂ ⁴	[(C ₅ Me ₄ SiMe ₃)Lu(CH ₂ SiMe ₃)(μ-H)(THF)] ₂	H ₃ SiPh	330
5-34 [{DADMB}YH(THF)] ₂ ²⁰	[DADMB]YMe(THF) ₂	H ₃ SiPh	331a,332a
5-35 (Me ₂ SiCp ₂ UH) ₂ O	(Me ₂ SiCp ₂ UBu) ₂ O	H ₃ SiPh (xs)	331b

[†] Cp = C₅H₅; Cp* = C₅Me₅; PNNP = 3,5-bis(diphenylphosphinomethyl)pyrazolate; Hex = C₆H₁₃; DIPPIDH = α²-(diisopropylphosphino)isodurene; DADMB = 2,2'-bis(*tert*-butyldimethylsilylamido)-6,6'-dimethylbiphenyl. ¹ Complex not isolated, but formation was inferred from exchange of the hydrosilane with Cp₂MF₂ or Cp₂M(NMe₂)₂ to form the fluorosilane or the aminosilane.³⁰⁴ ² Other silanes (PhMeSiH₂, PhSiH₃) also exhibited exchange with Cp₂MF₂.³⁰⁴ ³ Generated from Cp₂ZrMe₂ and Ph₃C⁺B(C₆F₅)₄⁻ in ClC₆D₅ (ambient light). Also identified (by GC-MS) were PhSiMeH₂, PhSiMe₂H, PhSiMe₃, Ph₂SiH₂, Ph₂SiMeH, Ph₂SiMe₂, Ph₃SiH, Ph₃SiMe, Ph₄Si, and C₆D₆-C₆D₆. In the dark, no **5-3a** was observed and **5-3b** was obtained in >90% yield. Analogous compounds were obtained from the precursor (C₅H₄Me)₂ZrMe₂.^{31a} ⁴ Decomposition of **5-4** occurs in the presence of excess silane. Other silanes could be used including H₂SiMePh and HSi(NMe₂)Ph₂. Deuterium analogue prepared from D₂SiPh₂.^{305,306} ⁵ Other silanes could be used including H₃SiPh, H₂SiMePh, and HSi(NMe₂)Ph₂. Deuterium analogue prepared from D₂SiPh₂.³⁰⁶ ⁶ Analogue with bridging TaDTa made from PhRSiD₂ (R = Me, Ph).^{308a} ⁷ L^{Me} = [ArNCMeCHCMeNAr]⁻ (Ar = 2,6-ⁱPr₂C₆H₃).³⁰⁹ ⁸ Final product is Tp(Ph₃P)(H)Ru(η-HSiPh₂H).^{48a} ⁹ Additional product formed in 5–10% yield was (Et₃P)₃(H)₂RhSiPh₃.²⁴¹ ¹⁰ Assignment based on a broad hydride peak at -7.90 ppm.³¹¹ ¹¹ Other silanes such as HSiMe₂Ph and H₂SiPh₂ gave the same results.³¹² ¹² The silyliridium hydride was tentatively assigned on the basis of a ¹H resonance at -8.51 ppm (CD₃CN).³¹³ ¹³ Hydrosilanes used in this study: Et₃SiH, (^tBu)₃SiH, CH₃(CH₂)₁₇SiMe₂H, PhMe₂SiH, Ph₂MeSiH, Ph₂SiH, Ph₂SiH₂, 4-MeOC₆H₄SiMe₂H,¹⁸ BuC₆H₄SiMe₂H, 4-MeC₆H₄CH₂SiMe₂H.³¹³ ¹⁴ Other silanes such as *n*-BuSiH₃ and *n*-PentylSiH₃ gave similar results. An iridium-silylene complex was proposed as the intermediate.²⁶² ¹⁵ SiR₃ = Et₃, EtMe₂, Me₂Ph.³²⁰ ¹⁶ Used for the reduction of α,β-unsaturated ketones.^{321–323} ¹⁷ L = 1,3-bis(2,6-diisopropylphenyl)imidazol-2-ylidene.³²⁴ ¹⁸ NHC = *N*-heterocyclic carbene. **5-26** is an intermediate in the reduction of carbonyl compounds.³²⁵ ¹⁹ Full paper includes Sm, Eu, and Yb examples.^{75a,328} ²⁰ Generated in situ.^{331a,332}

Scheme 11



Scheme 12



Ogino and coworkers also studied the reaction of primary silanes with the related iridium complex, $[\text{IrMe}(\text{H})\{\eta^2\text{-Me}_2\text{Si}(\text{CH}_2)_2\text{PPh}_2\}(\text{PMe}_3)_2]$.²⁶² In this case, RMeSiH_2 formed (for an example, see **5-17a**). The possibility of oxidative addition of the silane followed by elimination of Si—C from a 7-coordinate intermediate was considered, but the sequence shown in Scheme 14 was favored since SiC elimination was inhibited by the presence of excess PMe_3 and ArSiMe_3 and was not observed when the tertiary silane ArSiMe_2H was utilized as a substrate. The sequence for Ir(III) requires loss of PMe_3 followed by an oxidative addition. Elimination of H_2 with formation of a silylene followed by a 1,2-shift of a Me group from the metal center to the silicon is the key Si—C bond-forming step and not a Si—C reductive elimination.²⁶²

However, SiC elimination was observed from the platinum(II) alkyl complex *cis*-(DIPPIDH)(DIPPID)PtMe (DIPPIDH = α^2 -(diisopropylphosphino)isodurene), which was reacted with R_3SiH to give R_3SiMe (**5-23**).³²⁰ The preference for Si—C elimination over C—H elimination appears to support a kinetically controlled reaction governed by electronic factors including a strong *trans*-influence of a benzyl-type ligand.³²⁰

Reduction of Pd(II) and Pt(II) complexes to M(0) with hydrosilanes has also been reported. When PdX_2 ($\text{X} = \text{Cl}^-$, OAc^-) was treated with HSiMe_2Bu , Pd nanoparticles were produced (see entry **5-19**).^{315,316} The size of the particles formed appeared to be related to the counterion and the temperature, with the smaller particles being produced from PdCl_2 .^{315,316} In a related reaction, polymethylhydrosiloxane (PMHS) was used to reduce a solution of $\text{Pd}(\text{OAc})_2/\text{HOAc}$ in benzene, forming Pd colloids that were stabilized by the siloxane polymer network.^{317ab} The particles were ~40–50 nm in size and could be utilized as catalysts to convert Si—H bonds to silyl esters. In these two cases, it is likely that there is an exchange of Pd—Cl (or Pd—OAc) with SiH to give Pd—H, which then undergoes elimination of H_2 to form Pd(0). The silicon byproduct, ClSiMe_2Bu , however, was not described.^{315,316} In the Pd colloid stabilized by the siloxane network, units containing Si—H, Si—OCOR, and Si—OH could be identified in the ^{29}Si NMR spectrum. Under certain conditions, a monomolecular Pd(0) complex may be trapped. For instance, when $\text{Pt}(\text{II})\text{Cl}_2$ was dissolved in styrene that

contained $\text{PhC}\equiv\text{CPh}$ and then Ph_3SiH was added, the solid complex, $\text{Pt}(\text{PhC}\equiv\text{CPh})_2$, could be isolated (the silicon product was not identified; see example **5-21**).³¹⁸

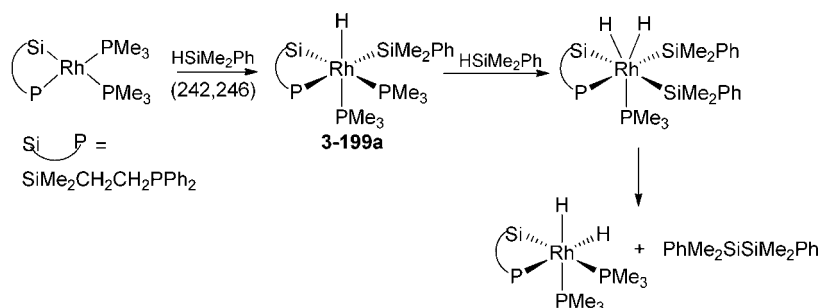
There are other “exchange” cases where a silane transfers a hydride to a metal halide to generate a metal hydride in situ, which was then used as a reducing agent for an organic substrate (particularly ketone functionalities). For instance, $\text{CuF}(\text{PPh}_3)_3$ ³²¹ (or CuCl ³²³ or CuOAc ³²³) reacted with HSiMe_2Ph to give CuH, although the solvent can be critical for the success of this process.³²² In the case of $[\{\text{HC}(\text{CMeAr})_2\}\text{Zn}(\mu\text{-F})]_2$ ($\text{Ar} = 2,6\text{-Me}_2\text{C}_6\text{H}_3$), reaction with Et_3SiH provided Et_3SiF and the first example of a hydrido zinc dimer $[\{\text{HC}(\text{CMeAr})_2\}\text{Zn}(\mu\text{-H})]_2$ (**5-27**) that was crystallographically characterized.³²⁶ The enantioselective reduction of ketones by PMHS in the presence of zinc catalysts activated by chiral diamines or diimines was also reported.³²⁷ Reduction of the Zn alkoxides, $[\text{RZn}(\text{OCH}_2\text{CH}_2\text{NMe}_2)]_2$ ($\text{R} = \text{Et}, \text{H}$), gave RZnH .³²⁷ Both the Zn—F and Zn—OR exchange reactions are similar to those described earlier for $\text{Cp}_2\text{Ti}(\text{OPh})_2$.

3.8. Summary

In section 3, the products of the reaction of hydrosilanes with transition metal complexes has been described in terms of products that incorporate the silicon unit (sections 3.2–3.6.1) and those that result in transfer of the hydride from the hydrosilane to the transition metal center (section 3.7). When the silyl group becomes bound to the transition metal, other events also take place that were categorized in terms of the loss of neutral ligands (section 3.2) and ligands that are assigned a negative charge (section 3.3). The reactions are believed to occur by either oxidative addition or by a metathesis process. In the case of oxidative addition of H—Si, if the transition metal complex has less than an 18-electron count, retention of the original ligand set can be preserved (section 3.4). The chemistry of polynuclear complexes can be more complex, resulting in the retention of the nuclearity of the $(\text{TM})_x$ unit or a lowering of the nuclearity, and both these cases are covered in section 3.5. The other side of this process is the formation of polynuclear complexes from a mononuclear complex upon reaction with the hydrosilane (section 3.6.1), and in these cases, the silyl group is commonly found bridging two metals. Although the review focuses on those processes that lead to the formation of silyl—metal complexes, a few specific reactions of stable silyl—metal derivatives were covered in sections 3.6.2–3.6.4 in order to illustrate some of the motivation for studying the reactions of silanes and transition metals originally.

Tables 1, 2, 3, and 9 (section 5) provide listings of representative examples of compounds that were reported during the review period as well as the characterization obtained for the compounds. When more than one example of a type was reported, the additional compounds are listed in the appropriate footnotes. Selected details of the solid-state structures for all silyl—metal complexes for the indicated tables and their respective footnotes are detailed in section 4 in Table 6. As can be seen by the lengths of Tables 1, 2, and 3, the reactions of tertiary silanes dominate this subclass of silicon chemistry. However, the variations in the products produced from both primary and secondary silanes are often more interesting as well as challenging to characterize, especially for those that exhibit nonclassical interactions (section 5). Many of the silyl—metal complexes

Scheme 13



Scheme 14

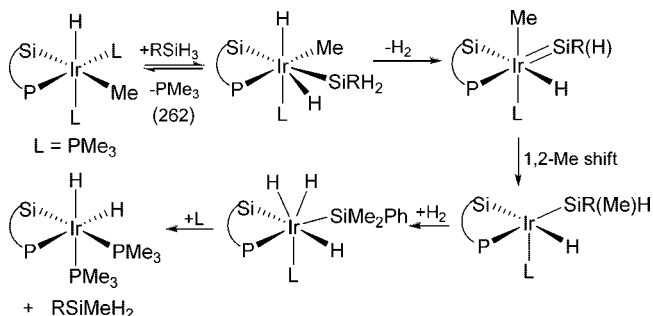


exhibit fluxional properties in solution, particularly those that contain hydrides at the metal and/or the silicon center, and the variations will be discussed in section 6. Tables 1, 2, and 3 also indicate the complexes for which calculations were performed. These may also be viewed as a characterization method and are summarized primarily in section 7.

4. Solid-State Structures

Structural data reported for silyl–transition metal complexes prepared from hydrosilanes that include both “classical” $\text{M}–\text{Si}$, $\text{M}–\text{H}$, and/or $\text{Si}–\text{H}$ bonds and “nonclassical” $\text{M}\cdots\text{H}\cdots\text{Si}$ interactions as well as silylene complexes (formed from hydrosilanes) are summarized in Table 6 and includes entries from Tables 1, 2, and 3 as well as additional complexes listed in the footnotes to these tables. Data for $\text{Si}–\text{TM}$ bond distances reported for silyl–metal complexes prepared by routes that did not involve hydrosilanes and that have been reported in the Cambridge Data Base through Mar 2009 (version 5.30) are recorded in the footnotes to Table 6.^{333–443}

Several reviews that feature or include solid-state structures of silyl–transition metal complexes have been published. The general review on silyl–metal compounds by Eisen contains tabulated information on $\text{Si}–[\text{TM}]$ distances for groups 4–10.^{1b} Lukevics, Arsenyan, and Pudova have published four reviews of the molecular structures of organosilyl complexes as a function of the metal, and these include (Ru, Rh, and Pd),⁴⁴⁴ (Os, Ir and Pt),⁴⁴⁵ (Co and Ni),⁴⁴⁶ and (Ti, Zr, Hf).⁴⁴⁷ Additional reviews tend to focus on a class of compounds. For example, Gossage has summarized the structurally characterized silyls (i.e., $–\text{SiH}_3$), which included a section on silyl–transition metal complexes, most of which have been reported earlier than the period covered by the current review.^{448a} Bridged silylene complexes have also been summarized up to 1998.⁴⁷⁸

Of the 30 metals in groups 3–12, only Tc does not have silyl complexes characterized by diffraction methods (although not all of the structurally characterized complexes

have been formed from hydrosilanes). The La (and Y) complexes that contain Si in the β -position for which solid-state data have been reported are described later in section 8.1. The range of silicon–transition metal bond lengths that include both 2c–2e, 3c–2e, and $\text{TM}=\text{Si}$ interactions for the remaining metals are summarized in Table 7, which also includes the number of independent $\text{TM}–\text{Si}$ distances for each element (including those from the previous review and the footnotes from Table 6). For six of the metals in the “d” block, the difference between the largest and smallest reported distances falls between 0.07 and 0.2 Å (Sc, Nb, Cr, Re, Au, Zn, Hg; there are too few distances determined for Cd–Si). For the remaining 16 metals (exclusive of Y, La, V, Ag, for which there are too few examples), the difference falls between 0.24 Å [observed for Ta (32 values), Ir (82 values), and Ni (46 values)] to 0.79 Å [Fe (317 values)]. Table 7 illustrates that the ranges within each member of a triad significantly overlap and that the values for the $[\text{TM}]–\text{Si}$ distances decrease overall in progressing from group 3 to group 12. It also demonstrates that the ranges for the elements has expanded in all cases (indicated by the italicized values). Supporting Information Table 7a provides the breakdown summary of the origin of the ranges. There have been no systematic studies to determine experimentally the effect that substituents at either the metal or the silicon center exert on the $[\text{TM}]–\text{Si}$ bond distance, although there have been density functional calculations that address the energetics and distances in 33 variations of the model complex, $(\text{dhpe})\text{M}(\text{H})\text{SiR}^1\text{R}^2\text{R}^3$ ($\text{M} = \text{Pd}, \text{Pt}$; $\text{R} = \text{H}, \text{Me}, \text{Ph}, \text{F}, \text{Cl}$)⁴⁴⁹ (see section 7.3.7).

The shortest $\text{Si}–\text{TM}$ distances might be expected to be associated with silylene complexes $\text{Si}=[\text{TM}]$, especially those that are not base-stabilized; however, not all silylene complexes have been characterized crystallographically. The silylene complexes that have been reported from hydrosilanes during this review period are listed in Chart 7 (section 3.6.2), and those that have been characterized by X-ray crystallography including those in the footnotes to Tables 1–3 are summarized in Table 8, which also includes silylene complexes reported prior to 1998. In order to define the range of bond lengths obtained for silylene complexes, the complexes reported from other routes that appear in footnotes to Table 6 have been included.

Silylene complexes characterized by X-ray diffraction are known for Y, Hf, Ta, Cr, Mo, W, Mn Fe, Ru, Os, Co, Rh, Ir, Ni, Pd, Pt, Cu, Sm, and Yb and can be grouped into three categories: (a) base-free; (b) with intramolecular base stabilization; and (c) with intermolecular stabilization. A number of base-free complexes have been generated by reacting a suitable transition metal complex with stable silylenes, especially the *N*-heterocyclic silylenes. Most of the remainder are formed by a reaction of a suitable $\text{TM}–\text{SiR}_2\text{X}$

Table 6. Structural Data for Silyl Metal Complexes¹

complex	temp. (K)	M–H ^{2,3}	SiH ^{2,3}	M–Si ²	ref
Sc triad ⁴					
Cp* ₂ ScSiH ₂ SiPh ₃ (1-9)	135		1.39(3) 1.47(3)	2.797(1)	26b
Cp* ₂ ScSiH(SiMe ₃) ₂ (2-1) other derivatives ⁶	132			2.849, 2.804 ⁵	26b
Ti triad					
Cp ₂ (PMe ₃)Ti(SiH ₃)(PMe ₃) (1-1)	220		1.53(7) ⁷	2.594(2)	19
Cp ₂ TiSiHPh ₂ (py)(0.25 py) (2-2)	220			2.678(3)	27, 77
Cp ₂ (Me ₃ P)Ti(η ² -HSiMeCl ₂) (IHI complex) (3-1)	150	1.733(18)	1.749(17)	2.5167(7)	20b
Cp ₂ (Me ₃ P)Ti(η ² -HSiMePhCl) ⁸ (IHI complex)	150			2.545(2)	20b
Cp ₂ (Me ₃ P)Ti(η ² -HSiCl ₃) ⁸ (IHI complex)	150	1.72(2)	1.75(3)	2.491(1)	20b
Cp ₂ Ti[2-SiMe ₂ (C ₅ H ₄ N)] (3-2) (dmpe) ₂ Ti(Si ₄ H ₆ Ph ₄) (*1-14c)	220 198			2.651(2) 2.539(2) 2.519(2)	138 29b
			1.83(2) 1.83(2) (Si–H _{br}) 1.54(3) 1.54(3) 1.46(4) 1.45(3) (Si–H _{term})		
Cp ₂ Zr(η ² -HMe ₂ SiC ₂ SiMeH) (3-9) (β-complex) [[η ² -C ₅ H ₄ (SiMe ₂ H)]ZrCl ₃] ₂ (3-10*) (linear Si–H–Zr) other derivatives ⁹	200 r.t.	Zr···H, 2.042(4) 2.28(3)	Si···H, 1.634(4) 1.47(2)	2.758(1)	139 140
V triad					
Cp(dmpe)VSiH ₂ Mes (1-17a)			1.41(4) 1.38(4) 1.50(5) 1.43(5) 1.46(3)	2.2576(3) 2.577(2)	31b
Cp(dmpe)VSiHPh ₂ (2-3a) Cp ₂ (H)Nb(SiMe ₂ Ph) ₂ ¹⁰	173	not supplied		2.5629(8) 2.654(1)	31b 142
Cp ₂ (H)Nb(η ² -H-SiMe ₂ Cl) (3-12b*) (IHI)	190	(get from CBD)	1.860	2.579(2)	142
Cp ₂ (H)(H)NbSiCl ⁱ Pr ₂ (3-13)	120	1.65(3)		2.6496(7)	143
Cp ₂ (H)Nb(SiMe ₂ Cl) ₂ (3-16) (IHI)	X-ray: 190 X-ray: 173 ND: 100	1.74(7) ¹² 1.816(8) ¹¹	2.056 ¹² 2.076(3) ¹¹	2.597(1) ¹² 2.612(4) ¹¹	142, 144, 145a
Cp(ArN=)Nb(PMe ₃)(H)(SiPhH ₂) Ar = 2,6- ⁱ Pr ₂ C ₆ H ₃ (1-17b)	150	1.74(3)	1.34(5) 1.54(4)	2.5908(10)	32a
[CpNb{η ³ -N(Ar)SiMe ₂ H}Cl(PMe ₃)] (3-17*) Ar = 2,6-C ₆ H ₃ ⁱ Pr ₂	150	1.91(5)	1.52(5)	2.646(1)	146, 147a
[CpNb{η ³ -N(Ar')SiMe ₂ H}-Cl(PMe ₃)] (3-19*) ¹³ Ar' = 2,6-C ₆ H ₃ Me ₂	150			¹³	146, 147a 32a
β-complex [CpNb{η ³ -N(Ar')SiMe ₂ H}Cl(PPhMe ₂)]	150			2.6794(12)	32a
CpNb(=NAr)(PMe ₃)(H)SiPh ₂ Cl ¹⁴	150			2.587(2)	149
Ar = 2,6-C ₆ H ₃ ⁱ Pr ₂ (3-21) CpNb(=NAr)(PMe ₃)(H)SiCl ₃	150	1.91(4)	2.32	2.577(2) 2.541(4)	32a
Ar = 2,6-C ₆ H ₃ ⁱ Pr ₂ Cp ₂ Ta(H)(SiMe ₂ H) ₂ (classical)	298	1.785(15) (ND)	2.189(18) 2.190(17) (ND)	2.644(14) 2.631(12) (ND)	343b
Cp ₂ Ta{SiMe ₂ ···OMe···SiMe ₂ } (3-24b)	150			2.605(1) 2.597(1)	150
[Cp(Me ₃ P)(ArN)HTa(SiMe ₂ Cl)] (3-25a*) Ar = 2,6-C ₆ H ₃ ⁱ Pr ₂ (IHI complex)	150	1.6(1)	2.3(1)	2.574(1)	146, 147a
[Cp(Me ₃ P)(ArN)Ta(H)(SiMeCl ₂)] Ar = 2,6-C ₆ H ₃ ⁱ Pr ₂ (3-26a) (IHI complex)		1.95(7)	2.15(7) Ta–H···Si	2.569(2)	78
Cp(Ar'N=)Ta(PMe ₃)(ClSiMeCl···H) (Ar' = 2,6-Me ₂ C ₆ H ₃) (3-26b)				2.570(6)	147b
Cp*Ta[PhSiH ₂ N(C ₆ H ₃ Me) ₂ N-SiPhHCl](H)(Cl) (1-19*) (no direct Si–Ta; proposed TaH to Si transfer)	163	1.83(4)	1.36(5) SiHPhCl 1.86(4) TaH···Si		32b
Cp* ₂ (ArN=)Ta ₂ H ₂ (μ-ArNSiHPh) (1-20a) Ar = 2,6- ⁱ Pr ₂ C ₆ H ₃	123	1.72(5) 1.79(5) 1.95(5) 2.17(5) ¹⁵	1.42(5)	2.648(1) 2.709(1)	33
Cp* ₂ Ta ₂ H ₂ (μ-ArNSiHPh) ₂ (1-20b*) Ar = 2,6- ⁱ Pr ₂ C ₆ H ₃	161		1.553, 1.429 ¹⁶	2.695(3) 2.614(3)	33
{Cp*Ta[N(ⁱ Pr)C(Me)N(ⁱ Pr)-SiH ₂ Ph]} ₂ (η ¹ , η ¹ -μ-N ₂) {Cp*Ta-[N(ⁱ Pr)C(Me)N(ⁱ Pr)H]} (1-20c)	220	1.69(5)	1.3862,	2.632	34b

Table 6a. Continued

complex	temp (K)	M–H ^{2,3}	SiH ^{2,3}	M–Si ²	ref
{Cp*Ta[N(ⁱ Pr)C(Me)N(ⁱ Pr)(=NSiH ₂ Ph)](μ -N) (Cp*Ta(ⁱ PrNC(Me)-N ⁱ Pr)H) (1-20d)	220	1.75(5)	1.361 1.4357, 1.4357		34b
[NPN]Ta(μ -NSiH ₂ Bu) ₂ (1-21)	198			no direct TaSi bond	34b
[NPN]HTa(μ -H) ₂ (μ - η^1 : η^2 -BuH ₂ SiNN)Ta[NPN] (1-22) other derivatives ¹⁷	198			no direct TaSi bond	34a
Cr triad					
Cp(OC) ₂ Cr{(SiMe ₂) \cdots OMe \cdots (SiMe ₂)} (3-27)*	293			2.355(2)	151
Cp(OC) ₂ Mo{(SiMe ₂) \cdots OMe \cdots (SiMe ₂)} (3-32)	293			2.4804(9) 2.4795(9)	151
Cp(OC) ₂ Mo{(SiMe ₂) \cdots NEt ₂ \cdots (SiMe ₂)} ¹⁸	293			2.4996(9) 2.5008(9)	151
Cp ₂ Mo[SiH ₂ C ₃ Me ₄ H]H (1-23)	163	1.58(6)	1.39 (5) 1.47(4)	2.516(2)	17, 35
Cp ₂ Mo[SiH ₂ C ₃ Me ₅]H ¹⁹	173	(not located)	1.44(4)	2.5211(12)	17, 35
Cp ₂ Mo(H)SiH(C ₃ Me ₄ H) ₂ (2-9)	173	1.65(5), 1.83(4)	1.35(4), 1.51(4)	2.5683(12), 2.5637(11)	17, 35
Cp*(dmpe)(H)Mo=Si(H)Ph (1-24)	143		1.43(4)	2.317(1)	36
Cp*(OC) ₂ (Me ₃ Si)Mo=SiMes ₂ (3-33)	113			2.6391(7) (SiMe ₃) 2.3872(7) (SiMes ₂) 2.504(3)	153
Cp*(dmpe)(H)Mo(SiH ₂ Ph) ₂ (1-25a)	116			2.348(7)	36a
Cp*(dmpe)(H)Mo=SiEt ₂ (2-10)	144 (X-ray) 20 (ND)	1.809 (CDB) 1.847(12)	1.738 (CDB) 1.683(13)	2.343(10) 2.315(2)	36a
Cp*(dmpe)(H)Mo=SiMe ₂ ²⁰	171			2.288(2)	82
Cp*(dmpe)(H)Mo=Si(Cl)Mes (2-11)	CCDC 194 946				
(ArN)(PMe ₃)(PhH ₂ Si)Mo(η^3 -NAr-SiHPh-H) Ar = 2,6- ⁱ Pr ₂ C ₆ H ₃ (*1-25b)	153			2.634(1) (Mo–Si _{agostic}) 2.634(1) (Mo–Si _{term}) 2.668(1)	36b
(Me ₃ P) ₂ (ArN=)ClMo[N(SiMe ₂ H)Ar'] (3-37a) Ar' = 2,6-Me ₂ C ₆ H ₃ (β -agostic)	CCDC	1.92(4)	1.54(4)		155a
(Me ₃ P) ₂ (ArN=)ClMo[N(SiMeClH)-Ar'] ²¹ Ar' = 2,6-Me ₂ C ₆ H ₃		1.9(4)	1.51(3)	2.657(1)	155a
(OC)(depe) ₂ Mo(η^2 -HSiHPh ₂) (2-13)	203	2.04(2)	1.54(6) (SiH _{Si}) 1.66(6) (SiH _{Mo})	2.563(3)	21b
[H ₃ Mo{[Ph ₂ PCH ₂ CH ₂ P(Ph)-C ₆ H ₄ -o]- (Ph)(Ph)Si- <i>P,P,P,P,Si</i> } (2-15)	296	1.70(6) 1.76(6) 1.72(6)		2.541(2)	37a,b
[MoH ₂ (Ar){[Ph ₂ PCH ₂ CH ₂ P(Ar)C ₆ H ₄ -o] ₂ - (Ar)Si- <i>P,P,P,P,Si</i> }] ²² (1-27)	295			2.620(2)	37b
<i>trans</i> -[(R'MeSi)(η^5 -RC ₅ H ₅)Mo(CO) ₃] ₂ R' = CH ₂ Ph, R = 'Bu (3-37b)	294			2.559(2) 2.6294(8)	155c
[{Mo(μ - η^2 -H-SiEt ₂)(CO) ₄ }] ₂ (2-16)	100	1.786(5)	1.615(3)	2.6152(6) 2.7093(6)	84
Cp'(OC) ₂ (H)W=Si(H){C(SiMe ₃) ₃ } (1-29a)	150	1.82(7)	1.71(6) 1.54(7)	2.3703(11)	38a
<i>trans</i> -Cp*(py)(OC) ₂ WSiHPh ₂ (2-17)	286			2.570(4), 2.482(4)	85a
Cp*(OC) ₂ (H)W=SiR ₂ ·py R = Ph (2-20)	286	²³		2.445(2)	85a
[Cp*(dmpe)(H) ₂ W=SiMe ₂] ⁺ [B(C ₆ F ₅) ₄] [–] (2-21)	155			2.358(2). 2.354(3)	39, 86
Cp*(OC) ₂ W(=SiMe ₂)SiMe ₃ (3-39)	150			2.3850(12) (=Si) 2.6456(13)	156
Cp*(OC) ₂ W{(κ^2 -Si,C)-SiMe ₂ NMe ₂ (<i>o</i> -C ₆ H ₄)} (3-40a)	150			2.487(3)	157a
Cp*(OC) ₂ PhW=SiMe ₂ *DMAP (3-41)	150			2.511(5)	158
Cp*(OC) ₂ W(η^3 -Me ₂ SiCHCMe ₂) (3-42)				2.571	159a
(C ₅ Me ₄ Et)(OC) ₂ W(μ - η^1 : η^3 -C'CBu')(SiPh ₂) (3-43)	173			2.5672(19)	160
Cp*(OC) ₂ HW{ κ^2 (Si,Si)-Xantsil} (3-44)	150			24	154
Cp*(OC) ₂ HW{ κ^2 (Si,Si, <i>O</i>)-Xantsil} (3-45)	150			2.553(3) 2.582(3)	154
[Cp'W(CO) ₂ (=SiMe ₂)(SiMe ₃) ₂] (3-46)	150			2.489(2) (W=Si) 2.609(2)	156
Cp'(OC) ₂ (H)W=Si(H){C(SiMe ₃) ₃ } (Cp' = C ₃ Me ₄ Et) (1-29*)	150	1.82(7)	1.71(6) 1.54(7)	2.3703(11)	38a
(μ -SiPh ₂)[W ₂ (CO) ₁₀] (2-25)	100			2.577(2)	87a

Table 6b. Continued

complex	temp (K)	M–H ^{2,3}	SiH ^{2,3}	M–Si ²	ref
[{W(μ - η^2 -H-SiEt ₂)(CO) ₄] ₂ (2-26b)	100			2.591(2) 2.695(1) 2.712(1)	87c
(OC) ₃ (ⁱ Pr ₃ P)W(μ -HSiPh ₂) ₂ W(P ⁱ Pr ₃)(CO) ₃ (2-27)* (σ -complex)	193	¹⁵		2.523(3), 2.708(3)	40
<i>trans</i> -[(R' ⁺ MeSi)(η^5 -RC ₅ H ₃)W(CO) ₃] ₂ (R' = CH ₂ Ph, R = ^t Bu) (3-52c)	294			2.6235(16)	155c
<i>trans</i> -[(R' ⁺ MeSi)(η^5 -RC ₅ H ₃)W(CO) ₃] ₂ (R' = CH ₂ Ph, R = H) (Table 3, footnote 60)	294			2.6252(12)	155c
Cp*(OC)Fe(μ -CO)(μ -SiHCHPh ₂)-WCp(CO) ₂ (2-28)*	298			WSi, 2.519(2) FeSi 2.259(2)	42b
other derivatives ²⁵					
Mn triad					
(η^5 -C ₅ H ₄ Me)(OC) ₂ Mn(η^2 -HSiHPh ₂) (2-29)	120	1.575(14) ²⁶	1.806(14) ²⁶	2.391(12) ²⁶	89a,d
(η^5 -C ₅ H ₄ Me)(OC) ₂ Mn(η^2 -HSiFPh ₂) ²⁷	120	1.570 ²⁸ [1.569(4), ND]	1.806 ²⁸ [1.802(5), ND]	2.3509(2) [2.352(4), ND]	89a,b
(OC) ₅ MnSiPh ₃ ²⁹	295			2.509(2) 2.498(2)	371a
(OC) ₂ Re(μ -C ₅ H ₄ -C ₅ H ₄)(μ -SiPh ₂)Re(CO) ₂ (2-31)*	143	³⁰		2.446(3) 2.455(3)	91
(Ph ₃ P) ₂ H ₆ Re[η^1 -(SiMe ₂ C ₂ B ₁₀ H ₁₀ (SiMe ₂ H))-Si] (3-64)	293	³¹		2.449(5)	172
(PPh ₃) ₂ H ₅ Re[η^1 -(SiMe ₂) ₂ C ₂ B ₁₀ H ₁₀ -Si] (3-65)	293	³²		2.475(3) 2.477(3)	172
(OC) ₃ ReSiPh ₃ (3-66a)	296			2.617(4)	173
(OC) ₆ Re ₂ (μ - η^7 -SiPh ₃)(μ -H) (3-66b)	296	1.894(10) 1.897(10)		2.5175(11)	173
(OC) ₈ Re ₂ (μ -SiPh ₂)(SiPh ₃)(μ -H) (3-66c)	296	1.67(4)	1.73(4)	2.5792(9) (Si _{br}) 2.5041(10) (Si _{br}) 2.5901(9)	173
(OC) ₈ Re ₂ (μ -SiPh ₂) ₂ (3-67)	296			2.5633(8)	173
other derivatives ³³					
Fe triad					
Cp(ⁱ Pr ₂ MeP)FeH ₂ SiMeCl ₂ (3-68a)	?	1.37(2) 1.42(2)	1.90(2) 1.91(2) Si...H _{br}	2.1948(6)	42a
Cp(ⁱ Pr ₂ MeP)FeH ₂ SiMeCl ₂ ³⁴	?	1.35(3)	1.88(3)	2.168(1)	42a
Cp*(OC) ₂ FeSiMe ₂ NPh ₂ (3-68b)	150			2.3355(7)	174b
[Cp*Ru(κ -P,N-2-Me ₂ N-3-P ⁱ Pr ₂ -indene)(H) ₂ Ru=SiPh ₂] ⁺ X ⁻ X ⁻ = O ₃ SCF ₃ ⁻ (Table 2, footnote 42)	?	1.59(4) 1.54(3)		2.2811(9)	47b
(η^6 -C ₆ H ₅ Me)Fe(H) ₂ (SiHCl ₂) ₂ (2-32)	113	1.1(1), 1.31(8)	1.538(8), 1.51(1)	2.219(4), 2.222(4)	92
Cp*(OC)(Me ₃ Si)Fe=SiMe ₂ (3-69a)	150			2.154(1) (Fe=Si) 2.343(1) (Fe–Si)	22b, 175a
<i>cis</i> -[(OC) ₄ Fe(Xantsil)] (3-72b)	rt			2.497(3) 2.489(3)	177b
(OC) ₄ Fe[8-Br-1,6-(Me ₂ Si) ₂ C ₆ H ₃] (3-72c)	173			2.418(6) 2.399(2)	177c
(ⁱ PrPDI)Fe(η^2 -H–SiH ₂ Ph) ₂ (1-36)	173	1.45(3), 1.51(3)	1.59(2) 1.82(3) 1.41(2) 1.39(3) 1.33(2) 1.38(2)	2.4733(7) 2.3266(8)	44b
[PhBCH ₂ P ⁱ Pr ₃](Fe(H)(η^3 -H ₂ SiPhMe)] (1-37)	293	1.553(1) H ¹ 1.482(1) H ² 1.566(1) H ³	1.464(1) H ¹ 2.001(2) H ² 1.552(2) H ³	2.1280(7)	45
[(SiPPh ₃)FeMes] (3-75b)	100			2.198 2.199	178c
[(SiPPh ₃)FeCl] (Table 3, footnote 83)	100			2.306	178c
[(SiPPh ₃)Fe(N ₂)] (Table 3, footnote 83)	100			2.268	178c
[(Si ⁱ Pr ₃)FeCl] (3-75c)	100			2.305	178c
[(Si ⁱ Pr ₃)Fe(N ₂)] (Table 3, footnote 84)	100			2.290	178c
(ⁱ PrPNP)FeH(SiH ₂ Ph)N ₂ (1-38a)	173			2.718(6)	46a
Cp ₂ (CO) ₂ Fe ₂ (μ -CO)(μ -Si(H)CHPh ₂) (1-34)*	298		³⁵	2.257(1), 2.267(1)	43a
[Cp(OC)HFe] ₂ [μ_2 -SiMe ₂ OSi(<i>p</i> -Tol) ₂] ₂ (3-76)	223	1.4644(5)		2.339(1) 2.311(1)	179
Cp*(OC)Fe(μ -CO){ μ -SiH(CHPh ₂)} FeCp(CO) (2-33)*	298		³⁶	2.253(1), 2.266(1)	42b
(Cp*Fe) ₂ (μ -H) ₂ (μ - η^2 : η^2 -H ₂ Si ^t Bu ₂) (2-34)*	233	Fe–H ₁ –Fe ³⁷	Si–H ₃ –Fe	2.3830(12),	93

Table 6c. Continued

complex	temp (K)	M–H ^{2,3}	SiH ^{2,3}	M–Si ²	ref
		1.638 1.618 Fe–H ₂ –Fe ³⁷ 1.613 1.602 Fe–H ₃ –Si ³⁷ 1.518 Fe–H ₄ –Si ³⁷ 1.505	1.604 Si–H ₄ –Fe 1.637	2.3692(13)	
(Cp*Fe) ₂ (μ-H) ₂ (μ-SiPh ₂) (2-35)	223	1.66(3), 1.62(3), 1.66(3), 1.63(3)		2.2582(8)	93, 94
Cp ₂ Fe ₂ (CO) ₂ (μ-CO)(μ-SiN(SiMe ₃) ₂ SiMe ₂ CH ₂) (1-38c)	133			2.2549(8) 2.919(5) 2.2771(5)	46b
Fe ₂ (μ-H)(edt)(SiPh ₂ H)(CO) ₃ (dppbz) (2-36b)	?	1.6416 (381) 1.7094 (375)		2.3025(12)	95b
Fe ₂ (η-H ₂ SiPh ₂)(edt)(CO) ₂ (dppv) (2-36c)	?	1.512(10) 1.511(10)	1.625(19) 1.626(19)	2.308(4) 2.355(4)	95b
Cp ₃ Fe ₃ (CO) ₄ N(SiMe ₃) ₂ (1-38b)	113			2.3544(6) 2.2741(6) 2.2810(6) 2.2830(6)	46b
Cp ₃ Fe ₃ {μ ₂ -SiHN(SiMe ₃) ₂ }-[μ ₃ -COSiH ₂ N(SiMe ₃) ₂] {μ ₃ -η ² -C ₂ P ₂ -SiHN(SiMe ₃) ₂ } (* 1-38d)	133			2.2889(6)	
Cp*(OC) ₂ Ru[SiH ₂ C{SiMe ₃ } ₃] (1-38e)	150			2.438	393a
Cp*(OC)(py)RuSiH ₂ [SiH ₂ C{SiMe ₃ } ₃] (1-38f)	150			2.404	393a
[Cp*Ru(κ-P,N-2-Me ₂ N-3-P ⁱ Pr ₂ -indene)(H) ₂ Ru=SiHPh] ⁺ X ⁻ X ⁻ = SO ₃ CF ₃ ⁻ (* 1-39b)		1.60(5) 1.52(5)	1.52(5)	2.262(2)	47b
[C ₃₃ H ₄₉ PNSiRu][SO ₃ CF ₃] (1-39d) (see structure in Table 1)		1.525 1.565		2.291(2)	47b
[Cp*Ru(κ-P,N-2-Me ₂ N-3-P ⁱ Pr ₂ -indene)(H) ₂ - Ru=SiPh ₂] ⁺ SO ₃ CF ₃ ⁻ (2-36d)		1.59(4)	1.54(3)	2.2811(9)	47b
* 2-36e C ₃₇ H ₄₃ OPSiRu (see structure 2-36e in Table 2)	193	CCDC 654 072	~2.12, 2.14 (Ru–H···Si)	2.3102(6)	47c
* 2-36f C ₃₉ H ₅₀ NSiRu (see structure 2-36f in Table 2)	173	1.48(9)	1.90(8)	2.391(2)	47d
[Cp*Ru(η ⁶ -C ₆ H ₅ SiPh ₂ OCH ₃) ⁺ [BPh ₄] ⁻ (3-79)				no Si–Ru	181a
[Cp(Me ₃ P) ₂ Ru(η ² -H-SiCl ₃)] ⁺ [BARF ₄] ⁻ (3-80*)	203	1.60(5)	1.77(5)	2.329(1)	182
[Cp(ⁱ Pr ₃ P)(H) ₂ RuSiMe ₂ Cl] (3-81b)	123	1.51(3) 1.50(3)	2.02(3) 2.09(4)	2.377(7)	181c
[Cp(Ph ₃ P)(H) ₂ RuSiMe ₂ Cl] (Table 3, footnote 91)	123	1.51(2) 1.54(2)	2.11(5) 2.04(7)	2.3544(4)	181c
[Cp(ⁱ Pr ₂ PhP)(H) ₂ RuSiMe ₂ Cl] (Table 3, footnote 91)	123	1.56(4) 1.48(2)	2.11(4) 2.20(4)	2.3286(8)	181c
Cp*[(pyl) ₃ P](H) ₂ RuSiMe ₂ Ph (3-86)	160	1.43(3) 1.56(3)	1.95(3) 2.03(3)	2.4213(7)	184
Cp*(Ph ₃ P)(H) ₂ RuSiMe ₂ Cl (3-87) (IHI)	173	1.49(2), 1.50(2)		2.364(2)	185
Cp*(ⁱ Pr ₃ P)H ₂ RuSiMe ₂ Cl (3-88)	123	1.51(4)(br) 1.53(4)	2.03(4) 2.04(4)	2.332(1)	186
Cp*(Me ⁱ Pr ₂ P)(H) ₂ RuSiMe ₂ Cl ³⁸	120	1.53(6)(br) 1.63(6)	2.17(6)(br) 2.03(6)	2.3352(8)	186
Cp*(Me ₂ ⁱ PrP)(H) ₂ RuSiMeCl ₂ (3-89b)	120	1.49(5) 1.68(8)	2.07 1.99	2.3099(9)	186
Cp*(ⁱ Pr ₃ P)H ₂ RuSiMeCl ₂ (3-90)	123	1.56(3) 1.64(3)	2.11 2.15	2.2950(5)	186
Cp*(Me ⁱ Pr ₂ P)(H)ClRuSiCl ₃ ³⁹	123	1.36(2)		2.3152(8)	186
Cp*(Me ₂ ⁱ PrP)(H)ClRuSiCl ₃ ³⁹	123	1.49(3)		2.3111(5)	186
Cp*(Me ₂ PhP)(H)ClRuSiCl ₃ ³⁹	120	1.62(3)		2.3107(7)	186
Cp*(ⁱ Pr ₃ P)ClRu(η ² -H–SiMe ₂ Cl) (3-92) IHI		1.53(3)	2.05(3)	2.3982(7)	187
Cp*(OC)(Py)RuSiMe ₂ NPh ₂ (3-96a)	150			2.3330(4)	188
Cp*(OC)HRu{κ ² (Si, C)-SiMe ₂ N-(<i>o</i> -C ₆ H ₃ (4-Me)(<i>p</i> -Tol)} ⁴⁰	150			2.4353(17)	188
Cp'(Me ₃ P)(H)Ru(η ² -1,4-Si ₂ C ₄ Me ₆) (3-99*)	167	⁴¹		2.430(1), 2.430(2)	189a
[(η ⁵ -indenyl)(Ph ₃ P)(HCy ₂ P)Ru–SiEt ₃] (3-99b)	193	1.552 1.549		2.4108(8)	189b
(C ₆ H ₆)(Ph ₃ P)Ru(SiCl ₃) ₂ (3-100)	295			2.3273(8)	190
(OC) ₄ Ru(Xantsil) (3-104*)	293			2.562(2), 2.564(2)	177b, 192
(Xantsil)(H)(CO)Ru{SiMe ₂ ···O ^t Bu···SiMe ₂ } (3-105)	150			silylene:	193a,b

complex	temp (K)	M–H ^{2,3}	SiH ^{2,3}	M–Si ²	ref
(Xantsil)(H)(CO)Ru{ SiMe ₂ •••OMe•••SiMe ₂ }	150			2.395(4) 2.402(4) 2.407(4) 2.394(4) Xantsil: 2.443(3) 2.424(4) 2.439(3) 2.425(3) silylene: 2.4108(6) 2.4191(7) Xantsil: 2.4970(6) 2.4970(7) 2.457(7) 2.3702(6)	193b
(OC) ₂ HRu{ SiMe[(CH ₂) ₃ PPh ₂] } (3-106)	291	⁴²			194
(OC)(Ph ₃ P) ₂ (H)Ru{ SiMe ₂ •••NMe ₂ •••SiMe ₂ } (3-112)	150	1.62(2)		2.3702(6)	201
(OC)(Ph ₃ P) ₂ (κ ² -S ₂ CNMe ₂)RuSiClPh ₂ (3-113)	150			2.3821(6) 2.4089(7)	202
[(OC)(PCy ₃)(Cl)Ru(SiCl ₃) ₂] [−] [Cy ₃ PH] ⁺ (3-114)	173			basal: 2.316(2) apical: 2.249(2)	203
(OC)(biPSi)RuCl (3-115)*	293			2.339(5)	204
(PMe ₃) ₄ (Me)RuSiMe ₃ (3-116)	200	1.61(4)		2.4796(9)	97
(PMe ₃) ₄ (H)RuSiMe ₃ (3-117)	210	1.59(4)		2.4630(9)	97
(PMe ₃) ₄ (H)RuSiMe ₂ H (2-39)	227	1.524(58)	1.523(79)	2.426(1)	97
cis-(Me ₃ P) ₄ Ru(H)(CH ₂ SiMe ₂ Cl) (3-119a)	CCDC-166038		Si•••H 3.34 (Ru•••Si)	3.617 2.526(2)	205
fac-(Me ₃ P) ₃ (Cl)Ru(CH ₂ SiMe ₂ H-μ) (3-119b) (β-complex)	200	1.550	1.664	2.526(2)	205
mer-(Me ₃ P) ₃ (Cl)Ru(CH ₂ SiMe ₂ H-μ) (3-119c) (β-complex)	200	1.732	1.557	2.468(2)	205
(PMe ₃) ₃ (H) ₃ Ru(SiMe ₃) (3-120)	296	1.488(43) 1.637(66) 1.431(45)	Si•••H 2.228(42) 2.179(48) 2.128(48)	2.376(1)	97
(Me ₃ P) ₃ (H) ₃ Ru(SiMe ₂ CH ₂ SiMe ₃) (3-121)	200	1.60(4) 1.61(3) 1.58(5)	2.00(4) 2.09(4)	2.3774(8)	49
(Me ₃ P) ₃ (H) ₂ Ru[Me ₂ SiCH ₂ CH ₂ SiMe ₂] (3-122)	210	1.56(4), 1.50(4)	H•••H 2.33(5) 2.36(6) 1.81(4)	2.4682(9) 2.4524(9)	49
(PPh ₃) ₃ H ₃ RuSiCl ₂ Me (3-124)*	183	1.68(3), 1.54(2), 1.59(2)	1.94(3), 1.86(2), 1.94(2)	2.2760(4)	206
(Me ₃ P) ₃ (H) ₂ Ru(SiPhH ₂) ₂ (1-41)	ambient			2.390(2) 2.437(2)	49
(PCy ₃)[(η ² -C ₆ H ₈)PCy ₂](H)- Ru(η ² -H–SiMe ₂ Cl) (3-126a)	180	1.57(2)	1.91(2)	2.3534(11)	207a
(Cy ₃ P) ₂ (η ² -H ₂)(Cl)Ru(SiMeCl ₂) (3-126b)	100	1.62(3) Ru–H 1.59(2) 1.62(2) H ¹ –H ² 1.05(3)	1.99(2) Si•••H 2.25(2)	2.2727(5)	207b
[(Cy ₃ P) ₂ H ₂ Ru{(η ² -HSiMe ₂) ₂ X}]	180	Ru–Hb1: 1.60(3)	Si–Hb1: 1.84(2), 1.84(2)	2.4162(5)	208, 209
X = C ₆ H ₄ (3-127)* ⁴³		1.59(3) Ru–H1 1.59(2) 1.54(2)	Si•••H1: 2.22(2), 2.21(2) Si•••H2: 2.18(2), 2.12(2)	2.4280(5)	
[(Cy ₃ P) ₂ H ₂ Ru{(η ² -HSiMe ₂) ₂ X}] X = –CH ₂ CH ₂ – ⁴⁴ (σ-complex)	160	Ru–Hb1, 1.55(3) Ru–Hb2, 1.54(3) Ru–H1, 1.53(3) Ru–H2, 1.60(3)	1.73(3) 1.78(3)	2.4282(6) 2.4109(7)	208
[(Cy ₃ P) ₂ H ₂ Ru{(η ² -HSiMe ₂) ₂ X}] X = –OSiMe ₂ O– ⁴⁴ (σ-complex)	180	Ru–Hb1 1.62(4) Ru–Hb2 1.58(4) Ru-H1,	Si1–Hb1, 1.77(4) Si2–Hb2, 1.81(3) Si1•••H1, 2.25(3)	2.4841(7) 2.4336(7)	208

Table 6e. Continued

complex	temp (K)	M–H ^{2,3}	SiH ^{2,3}	M–Si ²	ref
(Cy ₃ P) ₂ H ₂ Ru(η^2 -H ₂)(η^2 -HSiPh ₃) (3-129)* ⁴⁵	160	1.55(4) Ru–H ₂ , 1.51(3) RuH ₁ , 1.66(2) RuH ₂ , 1.64(3)	Si2···H ₂ , 2.04(3) Si1···H ₂ , 2.43(3) Si2···H ₁ , 2.32(3) Si···H ₃ , 2.40(4) Si···H ₄ , 2.071; H ₁ –H ₂ , 0.82(2) 1.59(8)	2.3846(18)	210, 101
[(Cy ₃ P) ₂ H ₂ Ru(η^4 -HSiMe ₂ (CH=CHMe))] (3-130a)* (β -complex) Ru(PPh ₂ CH ₂ OSiMe ₂ H) ₃ (3-130b)	140	1.61(7) 1.64(9) 1.74(7) 1.60(3) Ru–Hy1 1.61(3) Ru–Hy2 Ru–Hb1 1.63(3) Ru–Hb2 1.59(3) Ru–H1, 1.54(3) Ru–H ₂ , 1.59(3)	2.28(3) Si–Hy1 1.75(3) Si–Hy2 Si1–Hb1 1.93(3) Si2–Hb2 1.87(3)	2.498(2) 2.4240(11) 2.4647(11)	211a, 212 211a, 212
[(Ph ₃ P) ₂ H ₂ Ru(η^2 -HSiMe ₂) ₂ X]] X = –CH ₂ CH ₂ – ⁴⁶	150	1.61(3) Ru–Hb1 1.63(3) Ru–Hb2 1.59(3) Ru–H1, 1.54(3) Ru–H ₂ , 1.59(3)	1.75(3) Si–Hy2 Si1–Hb1 1.93(3) Si2–Hb2 1.87(3)	2.4481(7) 2.4326(7)	208
[(Cy ₃ P) ₂ H ₂ Ru(η^2 -HSiMe ₂) ₂ NH]] (3-132)	180	1.456 ⁴⁷ 1.468 Ru–H _{term} 1.582 1.648 Ru–H _{br} –Si	Si ₁ –H _{1(br)} 1.93(5) Si ₂ –H _{2(br)} 1.91(5) Si ₁ ···H _{2(br)} 3.53(4) Si ₂ ···H _{1(br)} 2.35(6) Si ₁ ···H _{1(term)} 2.25(6) Si ₁ ···H _{2(term)} 2.39(5) Si ₂ ···H _{2(term)} 3.68(5) Si ₂ ···H _{1(term)} 2.09(6)	2.395(2) 2.434(2)	212
[{1,3-(CH ₂ P ^t Bu ₂) ₂ C ₆ H ₃ }(N ₂)Ru(SiClPhH)] (1-42) <i>fac</i> -[PSiP](Ph ₃ P)RuCl (3-134a) Ru(η^2 -HSiMe ₂ CH(C ₆ H ₄)PPh ₂) ₂ (3-134c)	193 ? ?	1.71(4) 1.68(4)	1.76(4) 1.65(3)	2.281(7) 2.3361(6) 2.4587(13) 2.4367(13)	50 213a 213c
[N ₃]Ru(H)(Cl){Si(NN)} (3-134e) {Cp [*] Ru(μ -H)} ₂ (μ -SiMeEt) (2-41)	143 298			2.304(1) 2.356(2) 2.361(2)	213b 98
{Cp [*] Ru(μ -H)} ₂ (μ -SiPh ₂) (3-135a)	296	1.86(5) 1.80(7) 1.83(5) 1.83(5)		2.3498(12) 2.3436(11)	98
<i>trans</i> -[(R [′] MeSi)(η^5 -RC ₅ H ₃)Ru(CO) ₂] ₂ R [′] = Ph, R = H (3-137a) [(η^2 -C ₅ H ₇)SiMeR [′] Ru(CO) ₃] ₂ R [′] = CH ₂ Ph (3-137c) [PhMeSi)(η^5 -C ₅ Me ₄)]Ru ₂ (CO) ₆ (3-137d) {Cp [*] Ru(μ -H)} ₂ (μ -SiPhMe)(μ -SiMe ₂) (3-137e)	294 294 294 296	1.7744(7) 1.8811(6) 1.9146(6) 1.7367(7) 1.7717(6) 1.8437(7) 1.7778(7) 1.8297(6)		2.4001(11) 2.4178(18) 2.4195(17) 2.4834(11) 2.355(2) 2.364(2) 2.353(2) 2.3528(19) 2.360(2) 2.363(2) 2.345(2) 2.3568(19) 2.328(2), 2.332(2),	155c 155c 155c 98
[(Cp [*] Ru) ₂ (H)(μ -H)(μ , η^2 -HSiHexCl)(μ -ClSi(^t BuNCH=CHN ^t Bu))] (1-43)*	136	⁴⁸		2.394(2) 2.386(2)	51a
{Cp [*] Ru(μ -H)} ₂ { μ - η^2 : η^2 -HSiMe ₂ (CH=CH ₂)} (3-138)*	296	1.67(5), 1.61(6), 1.56(4), 1.85(5), 1.96(6)	1.66(4)		214
(μ_3 , η^5 : η^5 -4,6,8-trimethyl-4,5-dihydroazulene)Ru ₂ -(CO) ₄ (SiMe ₂ Ph) ₂ (3-139)	293			2.442(3)	215
[(CO) ₄ RuSiMe ₂ Ph] ₂ (3-140) [Ru ₂ (CO) ₆ (μ -dppm)(μ -Si(Tol) ₂)] (2-42a)	150			2.404(3) 2.425,	216 99

Table 6f. Continued

complex	temp (K)	M–H ^{2,3}	SiH ^{2,3}	M–Si ²	ref
{Ru(CO) ₂ (SiTol ₂ H) ₂ }(μ-dppm)(μ-η ² :η ² -H ₂ SiTol ₂) (2-44)	150	1.58(9) 1.61(9)	1.56(9) 1.57(10) (term) 1.86(9), 1.88(12) (br)	2.2427 2.422(2) 2.427(2) (term) 2.432(2) (br)	99
[Ru ₂ (μ-Cl)(μ-H)(SiEt ₃) ₂ (CO) ₂ (P ⁱ Pr ₃) ₂] (3-142)	100	1.91(4) 1.80(4)		2.364(2) 2.3685(19)	217
[{SiMe ₂ ···NMe ₂ ···SiMe ₂ }Ru(CO)-(μ-{SiMe ₂ }) ₂ (μ-Cl)RuH ₂ (CO)(PPh ₃) ₂] (3-143)*	150	1.66(2) 1.69(2)	1.67(2) 1.56(2)	Ru ₁ –Si ₂ = 2.5624(6) Ru ₁ –Si ₁ = 2.5678(6) Ru ₂ –Si ₂ = 2.3781(6) Ru ₂ –Si ₄ = 2.3790(6) Ru ₂ –Si ₃ = 2.3791(6) Ru ₂ Si ₂ = 2.3822(6)	201
(ⁱ Pr ₃ P) ₂ (H) ₂ Ru(SiH ₄)Ru(H) ₂ –(P ⁱ Pr ₃) ₂ * ⁴⁹	160	1.49(2) 1.52(3) (Ru–H _{term}) 1.62(3) 1.62(3) (Ru–H _{br})	1.69(3) 1.73(4)	2.1875(4)	100
Ru ₂ H ₂ (μ-η ² :η ² -H ₂ Si(OMe) ₂) ₃ (PCy ₃) ₂ (3-144a)*	see CCDC 208 493	⁵⁰		2.456(3) 2.408(3) 2.355(3) 2.364(3) 2.419(3) 2.408(3)	101
[(OC) ₁₀ Ru ₃ (Xantsil)(μ-H) ₂] 3-144b ⁵¹	150			2.4854(8) 2.4479(9)	177b
(OC) ₆ (H)Ru ₃ (μ ₃ :η ⁵ :η ⁵ -4,6,8-trimethyl-4,5-dihydroazulene)(SiMe ₂ Ph) (3-146)	293			2.392(2)	215
[Ru ₄ (μ-Cl) ₂ (μ-H) ₂ (μ-SiEt ₂) ₂ (CO) ₄ –(P ⁱ Pr ₃) ₄] (3-147)*	173	2.00, 2.09, 2.19, 1.94 1.62, 1.66 1.87(7) 1.86(8) (not supplied)		2.361(3) 2.377(3) (4 values)	217
Ru ₅ (CO) ₁₄ (SiEt ₃)(μ ₅ -C)(μ-H) (3-148a)	293			2.454(2)	219
Ru ₅ (CO) ₁₅ (SiEt ₃)(μ ₅ -C)(μ-H) (3-148b)	293			2.539(2)	219
Cp*(Me ₃ P) ₂ OsSi ⁱ Pr ₂ Cl (3-150)	121			2.404(3) ⁵²	220
Cp*(ⁱ Pr ₃ P)Br(H)OsSiH ₂ Ph (1-45)	161			2.3983(3)	22a
Cp*(ⁱ Pr ₃ P)Br(H)Os[Si(C ₆ F ₅)H ₂] (1-46)	164			2.389(2)	22a
Cp*(ⁱ Pr ₃ P)Br(H)OsSiH ₂ SiPh ₃ ·C ₆ H ₆ ⁵³	154			2.406(3)	22a
Cp(ⁱ Pr ₃ P)Cl(H)OsSiHPh ₂ (2-46)	190	1.69(8)	1.32(8)	2.406(2)	52
Cp*(ⁱ Pr ₃ P)(Br)HOsSiMe ₂ H·(C ₆ H ₅ F) _{0.5} (2-47)	171			2.431(6)	22a
Cp*(ⁱ Pr ₃ P)(Br)HOsSiPh ₂ H–(C ₃ H ₁₂) ₂ (2-48)	160			2.414(2) 2.412(2)	22a
Cp*(ⁱ Pr ₃ P)(H)Os=SiH(trip) (1-50)	135	1.871(5)	1.4775(5)	2.219(2)	55
cis-(OC) ₄ Os(Xantsil) (3-151a)	150			2.5750(18) 2.5689(18)	177b
(OC)(Ph ₃ P) ₂ H ₃ OsSiMe ₃ (3-152)	203	1.58(9) 1.55(9) 1.45(10)	1.980 ⁵⁴ 2.062 2.211 Si···H–Os	2.4533(8)	222
(OC)(Ph ₃ P) ₂ (Me ₂ NCS ₂)OsSiCl ₃ (3-154)	150			2.3449(12)	223
(OC)(Ph ₃ P) ₂ (Me ₂ NCS ₂)OsSiMeCl ₃ ⁵⁵	203			2.3672(10)	223
(OC)(Ph ₃ P) ₂ (Cl)OsSi(OEt) ₃ (3-155)	200			2.3311(18), 2.317(2) 2.3166(18) 2.312(2)	224
(OC)(Ph ₃ P) ₂ ClOsSi{OCH ₂ CH ₂ } ₃ N (3-156)	203			2.326(2)	225
(OC)(Ph ₃ P) ₂ (Cl)Os{SiMe ₂ ···NMe ₂ ···SiMe ₂ } (3-158)	150			2.393(4) 2.432(4)	201
(OC)(Ph ₃ P) ₂ (H)Os{SiMe ₂ ···NMe ₂ ···SiMe ₂ } (3-159)	150			2.3929 (7) 2.4024(6)	201
H ₃ (PPh ₃ P) ₃ OsSi{OCH ₂ CH ₂ } ₃ N (3-160)	203	1.52(3), 1.66(3) 1.57(3)		2.3442(8)	221
[^t Bu ₂ PC ₂ H ₄ CHC ₂ H ₄ P ⁱ Bu ₂][H ₃ Os(=SiH ₂)SiClPh ₂] (1-51)	?			2.3739(8) (OsSiPh ₂ Cl) 2.3857(8) (OsSiH ₂ ···P)	50
(1,3-CH ₂ P ⁱ Bu ₂ C ₆ H ₃)H ₃ Os=SiPhCl (1-52)	chk CDB (see paper)	1.670 1.641 1.651		2.281	50
Os ₃ (μ-H)(μ-SiPh ₃)(CO) ₉ (μ-dppm) (3-162a) other derivatives ⁵⁶	150			2.4503(9)	227
Co triad (η ⁵ -C ₅ H ₄ CH ₂ CH ₂ P(^t Bu) ₂)(H)CoSiHMePh (2-50)				2.246(3)	56
(η ⁵ -C ₅ H ₄ P(^t Bu) ₂)(H)CoSiHPh ₂ ⁵⁷ (2-51)	300	1.51(3)	1.48(2)	2.236(2)	56
Cp*(H) ₂ Co(SiPh ₂ H) ₂ 58 (2-52a)	163	⁵⁹	⁵⁹	2.256–2.261 ⁶⁰ (4 values) 2.243–2.247 ⁶⁰ (4 values)	103
(OC) ₄ CoSiPh ₃ (3-167)	203			2.3810(7)	229
[tripod (H) ₂ CoSiPh ₃] 3-168b	200	1.34(3)	1.98(4)	2.278(1)	230b

Table 6g. Continued

complex	temp (K)	M–H ^{2,3}	SiH ^{2,3}	M–Si ²	ref
		Co–H(1) 1.32(3) Co–H(2) 1.83(6) H(1)···H(2)	Co–H(1)···Si 1.89(4) Co–H(2)···Si		
(OC) ₄ Co[Si(Me)Fe(η^5 -C ₅ H ₅) ₂] (3-169)	150			2.3672(5)	231
{ κ^2 -Bu ₂ PCH ₂ Me ₂ SiNSiMe ₂ CH ₂ 'Bu ₂ P(H)Si=}Co(H) ₃ (SiH ₂ Ph) ₂ (1-54a)	130			2.1848(8) (silylene) 2.2622(9) 2.2477(8)	57a
[(OC) ₃ Co] ₂ [μ -SiMe(CH ₂) ₂ SiMe] (2-55)	163			2.284(1) 2.278(2) 2.281(1) 2.275(2)	104, 105
[(OC) ₃ Co] ₂ [μ -SiPh(CH ₂) ₂ SiPh] ^{6l}	165			2.292(2) 2.295(2) 2.289(2) 2.286(2)	105
[(OC) ₃ Co] ₂ [μ -SiPh(CH ₂) ₃ SiPh] ^{6l}	165			2.268(2) 2.290(2) 2.310(2) 2.302(2)	105
[(OC) ₃ Co] ₂ [μ -SiMe(X)SiMe] X = C ₆ H ₄ -o ^{6l}	165			2.288(1) 2.281(1) 2.290(1) 2.293(1)	105
[(OC) ₇ Co ₂]Si(Me)(η^5 -C ₅ H ₅)Fe(η^5 -C ₅ H ₅) ⁶² (3-171)	100			2.2842(17) 2.3208(18) 2.2813(18) 2.3112(18)	231
(OC) ₃ Co(μ -SiMe ₂) ₂ Co(CO) ₃ (3-172)	100			2.2852(13) ⁶³ 2.2841(12) 2.2839(13) 2.2841(12)	233
[(OC) ₄ Co] ₈ Si ₈ O ₈ (3-175)	190			2.282(3)–2.293(3) (8 values)	235
Cp(Ph ₃ P)(H)RhSi(ⁱ Pr) ₃ (3-177)	220	1.50(9)		2.386(2)	237
Cp(Me ₃ P)(H)RhSi(ⁱ Pr) ₃ (3-178)		1.508(17)	2.278(18) (Si···H)	2.3617(3)	106
<i>mer</i> -(Me ₃ P) ₃ (Cl)(H)Rh[Si(C ₆ H ₄ X- <i>p</i>) ₂ H] (2-59) X = H	⁶⁴	⁶⁵	⁶⁵	2.313(4)	108
<i>mer</i> -(Me ₃ P) ₃ (Cl)(H)Rh-(Si(C ₆ H ₄ X) ₂ H) X = OMe ⁶⁶	⁶⁴	⁶⁵	⁶⁵	2.319(2)	108
<i>mer</i> -(Me ₃ P) ₃ (Cl)(H)Rh-(Si(C ₆ H ₄ X) ₂ H) X = F ⁶⁶	⁶⁴	⁶⁵	⁶⁵	2.311(2)	108
<i>mer</i> -(Me ₃ P) ₃ (Cl)(H)Rh-(Si(C ₆ H ₄ X) ₂ H) X = CF ₃ ⁶⁶	⁶⁴	⁶⁵	⁶⁵	2.312(2)	108
<i>cis-fac</i> -(Et ₃ P) ₃ (H) ₂ RhSiPh ₃ (3-184) ⁶⁷	104	1.52(4) 1.51(5) 1.48(3) 1.47(4) 1.54(3) 1.48(4)		2.3571(10) 2.3548(9) 2.37189(9)	241
<i>mer</i> -(Me ₃ P) ₃ ClHRhSiPh ₃ ⁶⁸ (3-186)	⁶⁴	⁶⁹		2.346(2)	243
<i>mer</i> -(Me ₃ P) ₃ ClHRhSiAr ₃ Ar = C ₆ H ₄ -4-CF ₃ 70 (3-189a)	⁶⁴	⁵⁹		2.377(8)	243
<i>fac</i> -(Me ₃ P) ₃ (H) ₂ RhSiAr ₃ Ar = C ₆ H ₄ -4-CF ₃ ⁷¹ (3-189b)	⁶⁴	72		2.338(4)	243
<i>mer</i> -(Me ₃ P) ₃ (ArS)HRhSiPh ₃ ⁷³ Ar = C ₆ H ₅ (3-192)	⁶⁴	1.82		2.383(2)	109
<i>mer</i> -(Me ₃ P) ₃ (ArS)(H)RhSiPh ₃ Ar = C ₆ H ₄ -4-CH ₃ ⁷⁴	⁶⁴	1.58		2.379(2)	109
<i>mer</i> -(Me ₃ P) ₃ (ArS)(H)RhSi(OMe) ₃ Ar = Ph (3-194)		⁵⁹		2.229(3) 2.293(3)	109
(PP ₂)RhSi(SET) ₃ (3-195)	120			2.3747(14)	245
<i>fac</i> -(Me ₃ P) ₃ (H)Rh[Si(H) (Mes)C ₆ H ₂ Me ₂ CH ₂] (2-60)	161	1.514(3)	1.456(3)	2.365(1)	107
(Me ₃ P) ₂ (Cl)HRh[SiMe ₂ (CH ₂) ₂ PPh ₂] (3-197)	150	1.71(8)		2.331(1)	242, 246
[(Ph ₃ P) ₂ (H)Rh(SiMe ₂ C ₆ H ₄ SiMe ₂)] (3-199c)	123			2.308(2) 2.2918(13)	247b
[(Ph ₃ P)Rh(SiMe ₂ C ₆ H ₄ SiMe ₂)- (η^1 HSiMe ₂ C ₆ H ₄ SiMe ₂) (3-199d)	123		1.41(10)	2.273(2) (apical) 2.356(2) 2.345 Rh···H _{agostic} Si 3.082	247b
(Ph ₃ P) ₂ (Cl)HRhSi(OEt) ₃ (3-205)	⁶⁴	⁷⁵		2.251 (2)	252
(Ph ₃ P) ₂ (I)HRhSi(OEt) ₃ (3-206)	⁶⁴	⁷⁵		2.251 (2)	252
(Ph ₃ P) ₂ (I)HRh(SiMe ₂ OSiMe ₃) (3-207)	⁶⁴	⁷⁵		2.291 (2)	252

Table 6h. Continued

complex	temp (K)	M–H ^{2,3}	SiH ^{2,3}	M–Si ²	ref
[CyPSiP]RhHCl (3-212b)	?	1.51(3)		2.282(2)	254b
(PNP)(H)Rh(SiClMe ₂) (3-212c)	120	1.50(2)	1.93(2)	2.2616(7)	254c
PhB(CH ₂ PiPr ₂) ₂ (H) ₂ PMc ₃ RhSiHPh ₂ (2-63)	174			2.600(5)	111
<i>trans</i> -[(dippe)Rh] ₂ (μ-SiMePh) ₂ (2-67)	294			2.356(2)	114
				2.345(1)	
				2.3531(8)	
[(dippe)Rh] ₂ (μ-SiPh ₂) ₂ ⁷⁶	294			2.357(2)	114
				2.054(5)	
[(dippe)HRh] ₂ (μ-η ² -H–SiMe ₂) ₂ (σ-complex) (2-69)	294	1.69(4)	1.67(5)	2.526(1)	114
		1.52(5)	1.72(4)	2.337(1)	
		1.52(4)		2.324(1)	
		1.70(4)		2.474(1)	
[(ⁱ Pr ₃ P)(H) ₂ Rh] ₂ (μ-SiR ₂) ₂ R = CH ₂ CH ₂ Ph (3-214)	64	⁵⁹		2.65(3)	249
				2.367(3)	
[L(H)RhSiAr ₃] ₂ (μ-H)(μ-Cl)	298	1.59(2) (br)		2.289(2)	256
L = ⁱ Pr ₃ P; Ar = C ₆ H ₅ ⁷⁷		1.37(5) (term)			
[L(H)RhSiAr ₃] ₂ (μ-H)(μ-Cl)	298	1.55 (Rh–H bridg.)		2.293	256, 257
L = ⁱ Pr ₃ P; Ar = <i>p</i> -FC ₆ H ₄		1.30 (Rh–H term)			
(3-216)					
[L(H)RhSiAr ₃] ₂ (μ-Cl) ₂	64	⁵⁹		2.315(5)	249
L = P(ⁱ Pr) ₃ ; Ar = CH ₂ Ph ⁷³				2.301(5)	
(3-217)					
[(Me ₃ P)(Ar ₂ HSi)Pt](μ-H)(μ-η ² -HSiAr ₂)[Rh(PMe ₃) ₃]	64	1.66 (Pt–H bridg.)	2.28 (Si–H bridg.)	2.319(5) (Pt–Si term.)	258, 244
Ar = C ₆ H ₄ -4-F		2.24 (Rh–H bridg.)	⁷⁸	2.323(5) (Pt–Si bridg.)	
(3-218)		1.63 (Rh–H–Si bridg.)		2.368(5) (Rh–Si bridg.)	
[(Me ₃ P)(ClAr ₂ Si)Pt](μ-H)(μ-η ² -HSiAr ₂)[Rh(PMe ₃) ₃]	296	¹⁵		Pt–Si	244
Ar = C ₆ H ₅ ⁷⁹				2.300(3)	
				2.313(2)	
				Rh–Si	
				2.382(3)	
[(Me ₃ P)(ClAr ₂ Si)Pt](μ-H)(μ-η ² -HSiAr ₂)[Rh(PMe ₃) ₃]	64	⁵⁹	⁶⁴	2.378(8) (Si–Rh bridg.)	258, 244
Ar = C ₆ H ₄ - <i>p</i> ⁸⁰				2.289(8) (Si–Pt term.)	
(3-219)				2.324(8) (Si–Pt bridg.)	
(tmp)RhSiPh ₂ Me (3-220)	293			2.329(3)	62
(tmp)RhSiPhMe ₂ ⁸¹	293			2.438(5)	62
Cp*(L)PhIrSiPh ₂ F (3-222)	293			2.318(7)	259
L = PMe ₃					
[Cp*(Me ₃ P)(H)Ir[SiPh ₂ C ₆ H ₄]][BAr ₄]	156	¹⁵		2.479(2)	116, 117
Ar = C ₆ F ₅ (3-224)					
Cp*(Me ₃ P)(Ph)Ir[SiPh ₂ OTf] ⁸²	170			2.317(2)	117
Cp*(Me ₃ P)Ir[SiMe ₂ OTf][SiMe(SiMe ₃) ₂] (3-226)	166			2.2987(18)	117
				(IrSiMe ₂ OTf)	
				2.446(2)	
				(IrSiMe(SiMe ₃) ₂)	
<i>trans</i> -(Me ₃ P) ₂ Cl(H)Ir{η ² -SiMesH(CH ₂) ₂ PPh ₂ } ⁸³ (2-73)	293	⁵⁹	⁵⁹	2.352(5)	118
(Et ₃ P) ₃ (H) ₂ Ir[Si(C ₆ H ₃ Mes-2,6)(Cl)H] (1-57)	64	1.80(10)	1.52(8)	2.341(2)	58
		1.69(11)			
(Et ₂ PhP) ₃ (H) ₂ Ir[Si(Cl)CH ₂ (C ₆ H ₂ Me ₂ -2,4)(C ₆ H ₃)(Mes)] (1-58)	100	1.68 ⁸⁴		2.358(2)	59
[PhB(CH ₂ PPh ₂) ₃](H) ₂ Ir=Si(Mes)(c-C ₈ H ₁₅) ⁸⁵ (1-59a)	154	⁸⁶		2.250(3)	60a,b
[PhB(CH ₂ PPh ₂) ₃](H) ₂ Ir=SiR ₂	167	⁶⁴		2.260(3)	60a,b
R = Mes ⁸⁷ (2-74)					
[PhB(CH ₂ PPh ₂) ₃](H) ₂ Ir(SiHEt ₂) (2-75a)	124			2.413(3)	111
{Cp*(Me ₃ P)Ir[κ ² -Si(S'Bu) ₂ S'Bu]} ⁺ [OTf] [–] (3-227)	160			2.3044(16)	117a
Cp*(H) ₂ Ir[η ¹ :η ¹ -(SiMe ₂)BC ₂ B ₉ H ₁₀ -Si,B] (3-228)	64	88	88	2.380(2)	172
<i>trans</i> -Cp*(Cl)(H)Ir[SiMe ₂ C ₆ H ₄ SiMe ₂] (3-230)	293 ⁸⁹			2.378(6)	172
				2.388(6)	
<i>trans</i> -Cp*(H) ₂ Ir[SiMe ₂ C ₆ H ₄ SiMe ₂] (3-231)	298	⁹⁰	⁹⁰	2.359(1)	172
				2.355(1)	
(OC)(Ph ₃ P)ClIr{κ ² -(Si,P)-Me ₂ SiCH ₂ PPh ₂ } (3-236a)					261a
(Me ₃ P) ₃ (H)(Cl)IrSiMe ₂ (CH=CMe–CMe=CH ₂) (<i>fac</i> -E)	100	1.71(4)		2.4061(11)	261c
(Table 3, footnote 254)					
<i>fac</i> -(Me ₃ P) ₃ (H)(ClMe ₂ Si)IrCH=CMe–CMe=CH ₂ (Table 3, footnote 254)	100			2.3698(16)	261c
(Me ₃ P) ₃ (H)IrSiMe ₂ (CH=CMe ₂) (3-237b)	100	1.55(3)		2.4166(6)	261b
(Me ₃ P) ₃ (H)(Me)IrSiMe ₂ (CH=CMe–CMe=CH ₂) (<i>fac</i> -E) (3-237e)	100	1.55(3)		2.4166(6)	261c
(κ ¹ -NSiN)Ir(H)(Me)(PMe ₃) ₃ (3-237f)	155			2.388	57d
[PhB(CH ₂ PPh ₂) ₃](H) ₂ IrSiMe ₃ (3-238a)	64	⁹¹		2.437(3)	60b
[(η ² -SNC ₃ H ₄)(PPh ₃) ₂](H)IrSiMePh ₂] (3-240b)	90			2.3810(9)	248b
(TpMe ₂)(H) ₃ IrSiEt ₃ (3-242a)	298	1.89(4)		2.405(11)	264a
		1.87(4)			
<i>mer</i> -(H)(C ₆ F ₅)(ArNC) ₃ IrSiPh ₃	173			2.3963(10)	264b
(S and Si <i>trans</i>) (3-242b)					
Cl(H)Ir(biPSi) (3-243)	295	⁶⁴		2.287(3)	194
[PyInd](H) ₂ Ir(SiR ₃) ₂	161	1.61(2)		2.326(1)	255
R ₃ = Ph ₂ Me (3-244)		1.60(2)		2.338(1)	
(coe)Cl(H)Ir(NSiN) (3-245a)	164	⁶⁴		2.275(3)	265
[NSiN]PhIr(SiPh ₂ OTf)] (3-245b)	115			2.289(2)	57d
[NSiN]Ir(SiPh ₃)(NCMe ₂) ⁺ [OTf] [–] (3-245c)	159			2.369(1)	57d
(ttp)Ir[Si(OEt) ₃] (3-245d)	?			2.2277(3)	62b
(ttp)Ir[SiBnMe ₂]				2.328(5)	62b

Table 6i. Continued

complex	temp (K)	M–H ^{2,3}	SiH ^{2,3}	M–Si ²	ref
(Table 3, footnote 263) [(POCOP)Ir(H)(η^1 -HSiEt ₃)] ⁺ [B(C ₆ F ₅) ₄] [–] (3-245e)		1.94(3) Ir–H _{br} –Si 1.425(18) Ir–H _{term} 1.55	1.48(3) Si–H _{br}	3.346(1)	266a
[CyPSiP]IrHCl (3-246a)				2.274(1)	254b
[PNP](Cl)Rh(SiMe ₂ Cl) (18-26d)	120			2.2777(9)	254c
[C \cap N]Cl(H)(CH ₃ CN)IrSiMe ₂ Ph ⁺ MeOH (3-247) additional derivatives ⁹²	293				267
Ni triad (Et ₃ P) ₂ Ni[SiMe ₂ (C ₂ B ₁₀ H ₁₀)SiMe ₂] (3-248)	153			2.2371(9) 2.2477(9)	268, 269
(dmpe)Ni[(SiH ₂) ₂ C ₆ H ₄] ₂ ⁹³ (1-60)	296	⁶⁴	⁶⁴	2.2522(7) 2.2900(9)	63
{(dmpe)Ni[(H ₂ Si) ₂ C ₆ H ₄] ₂ } ₂ (μ -dmpe) (1-61)	296	⁶⁴	⁶⁴	2.247(3) 2.255(3)	63
[{1,2-C ₆ H ₄ (SiH ₂)(SiH)} ₂ Ni ₂ (dmpe) ₂] (1-62)				2.210(1)–2.304(1) (6 values)	64
[{1,2-C ₆ H ₄ (SiH ₂)(SiH)} ₂ Ni ₂ (depe) ₂] (1-63)	⁶⁴			2.2098(6)–2.2976(6) (6 values)	64
(depe)Ni[η^2 -HSiH(C ₆ H ₄ SiH ₂) ₂] (1-64)	113	1.47(3)	1.75(3)	2.2552(6) 2.3480(8) 2.2445(6)	65
[(dmpe)Ni(SiH ₂ C ₆ H ₄)](μ -SiC ₆ H ₄ SiH ₂)[Ni(dmpe)](2-76) ⁹³	⁶⁴		⁶⁴	2.210(1)–2.304(1)	64
(dtbpe)Ni(H)SiHAr ₂ (Ar = 2,4,5-Me ₃ C ₆ H ₂) (2-77)	103	1.41(2), br	1.42(4) 1.92(4), br	2.245(2)	119
{(dmpe)Ni[SiH(SiMe ₂ C ₆ H ₄)] ₂ } ₂ (μ -dmpe) (3-250)	⁶⁴		⁶⁴	2.263(2) 2.257(2)	64
(Cp [*] Al) ₃ (H)NiSiEt ₃ (3-253)	213	1.424(5)		2.239(8)	273
(dcpe)(H)PdSiPh ₃ ⁹⁴ (3-255)	120	⁹⁴		2.335(2) 2.330(2)	274
(Cab ^{SiP}) ₂ Pd (3-257a)	293			2.358(2) 2.361(2)	276a
<i>cis</i> -(κ -NSiN) ₂ Pd (3-256b) [R ₂ P(CH ₂) ₂ PR ₂][Pd[SiH(C ₆ H ₄ - <i>o</i> -SiH ₂ SiH(C ₆ H ₄))] R = Cy (1-65) (PN)Pd(SiCl ₃) ₂ PN = dichloro{1-[(Ph)-1-[(<i>S</i>)-2-(diphenylphosphino- κ P)ferrocenyl]- ethyl]-3-phenyl-5-methyl-1 <i>H</i> -pyrazole- κ N]} (3-258) (PN')Pd(SiCl ₃) ₂ ⁹⁵ (PN' = {1-[(Mes)-1-[(<i>S</i>)-2-(diphenylphosphino- κ P)ferrocenyl]ethyl]-3-(2,4,6- trimethylphenyl)-1 <i>H</i> -pyrazole- κ N]}	⁶⁴		⁶⁴	2.276(2) 2.348(3) 2.356(3)	276b 66a
	298			2.3243(17) (trans to P) 2.2594(17) (Si trans to N)	277
	298			2.309(2) (trans to P)	277
[(Me ₃ P)Pd](μ - η^2 -H-SiPh ₂) ₂ [Pd(PMe ₃) ₂] (2-79a)	298	1.75 1.89	1.56 1.68	2.261(2) (trans to N) 2.351(2) 2.318(2) 2.341(2) 2.411(2)	121a,b
[{1,2-C ₆ H ₄ (SiMe ₂)(SiH)}Pd(dmpe)] ₂ (2-79b)	153			<i>meso</i> -279b 2.3634(10) 2.3409(9) (PdSi) 2.3720(13) (Si–Si) <i>dl</i> -279b 2.3717(16) 2.3626(16) 2.3632(17) 2.3613(15) (PdSi) 2.3552(2) (Si–Si)	66b
[(R ₃ P)Pd] ₂ (μ - η^2 -H-SiMePh) ₂ R = Me (σ -complex) (2-80)	298	1.85	1.60	2.387(1) 2.333(2)	121b
[(Me ₃ P)Pd] ₂ (μ - η^2 -H-SiPh ₂) ₂ ⁹⁶ (2-81)	298	1.91	1.75	2.328(2) 2.386(2)	121a,b
[(Et ₃ P)Pd] ₂ (μ - η^2 -H-SiPh ₂) ₂ (2-82)	298	2.04	1.60	2.332(2) 2.396(2)	121b
[(Cy ₃ P)Pd] ₂ (μ - η^2 -HSiPh ₂) ₂ (2-83)		1.61	1.63	2.326(2) 2.384(2)	122
{[R ₂ P(CH ₂) ₂ PR ₂][Pd] ₂ [Si(C ₆ H ₄ - <i>o</i> -SiH ₂) ₂]} (1-66a) C ₃₆ H ₆₄ P ₄ Pd ₃ Si ₆ (2-79c)	⁶⁴ 153			2.3818(8) 2.334(1) 2.2903(8) 2.3464(11) 2.3526(11) 2.3832(9) 2.3885(8) 2.4015(8) 2.4033(11) 2.5273(10)	66a 66b
Pd ₃ [<i>o</i> -(HSi)(H ₂ Si)C ₆ H ₄] ₂ [<i>o</i> -(HSi) ₂ C ₆ H ₄](dmpe) ₂ ⁹⁷	173		⁹⁸	2.348(3)	123

Table 6k. Continued

complex	temp (K)	M–H ^{2,3}	SiH ^{2,3}	M–Si ²	ref
<i>trans</i> -(Cab ^{Si,P}) ₂ Pt R = Me (3-287)	293			2.304(2) (Si trans to N) 2.408(1)	275, 276
<i>trans</i> -(Cab ^{Si,P}) ₂ Pt (3-288) R = Ph	293			2.408(1) 2.362(1)	276
TP'(H) ₂ PtSiEt ₃ (3-289)	173			2.361(1) 2.325(3)	295
ClPt(NSiN) (3-290b)	(?)			2.225(2)	276b
(NSiN)Pt(Me) ₂ OTf (3-290e)	(?)			2.244(2)	276b
(cod)Pt(SiMeCl ₂) ₂ (3-291)	153			2.3090(1)	296
[(dmpe)Pt(μ-SiAr ₂)] ₂ (Ar = C ₆ H ₄ F-p) (3-296)	296			2.390(3)	244
[[C(Cy ₃ P)Pt](μ-η ² -H-SiPh ₂)] [Pd(PCy ₃)] (3-297a) ¹¹¹	93			2.377(3) 2.328(4)	122
[(C ₃ P)Pt(μ-η ² -HSiEt ₂)] ₂ (2-96b)	113	1.91(7) (Pt–H) 2.7011(3) Pt···Pt	2.07(5)	2.323(2) 2.423(2)	127a
<i>trans</i> -[(C ₃ P)Pt(μ-η ² -HSi(Hex) ₂)] ₂ (Table 2, footnote 107)	113	1.92(9) (Pt–H) 2.6988(6) Pt···Pt	2.0(1)	2.317(2) 2.413(3)	127a
<i>trans</i> -[(C ₃ P)Pt(μ-η ² -HSiPhMe)] ₂ (2-96c)	113	1.83(1)	1.99(1)	2.324(2) 2.409(2)	127a
[(C ₃ P)Pt(μ-η ² -HSiPh ₂)] ₂ (Table 2, footnote 109)	113	Pt···Pt 2.6982(3) 1.94(8) (Pt–H) 2.6985(3) (Pt···Pt)	1.88(7)	2.326(2) 2.385(2)	127a
[Pt(PCy ₃)] ₂ (μ-η ² -HSiPh ₂)(μ-η ² -HSiEt ₂) (2-96d)	133			2.402(4) 2.318(3)	127b
[Pt(PCy ₃)] ₂ (μ-η ² :η ² -H ₂ SiEt ₂)(μ-SiPh ₂) (2-96e)	133	2.6591(7) Pt···Pt		2.306(4) 2.388(3) 2.375(8) 2.39(1) Pt–SiEt ₂ –Pt 2.314(8) 2.304(7)	127b
[(Ph ₃ P) ₂ Pt(H)(μ-SiMe ₂)(μ-SiHMe ₂)Pt(PPh ₃)] (3-297b)	120	2.708(1) Pt···Pt 1.57(5) Pt(1)–H(1)	1.79(5) Si(1)–H(1)	2.4602(2) Pt(1)–Si(1) 2.3609(13) Pt(1)–Si(2) 2.3464(12) Pt(2)–Si(1) 2.4241(12) Pt(2)–Si(2) 2.4273(16)	284c
[(Ph ₃ P)Pt(μ-SiHMe ₂)] ₂ (Table 3, footnote 317)	120	Pt(2)–Si(2) 1.63(5) Pt(1)–H(1)	Si(2)–H(2) 1.95(5)	Pt(1)–Si(1) 2.3304(16) Pt(1)–Si(1)* 2.4228(10) 2.3110(10)	284c
[(Ph ₃ P)Pt(μ-η ² -HSiPh ₂)] ₂ (2-98)	170	1.80(5) (Pt–H) 2.6832(3) (Pt···Pt)	1.72(5)		127c
{(Et ₃ P)Pt(μ-η ² -H-Si(Hex)[Pt(H)(PEt ₃) ₂]} ₂ (σ-complex) (1-72)	147	¹¹²	¹¹²	terminal Si–Pt: 2.375(4) 2.377(4) ring Pt–Si: 2.431(4) 2.347(3) 2.353(3) 2.441(4)	69
[(dmpe)(H)Pt ^{IV} {1,2-C ₆ H ₄ (SiMe ₂)(μ-SiH)} ₂] (1-74b) ¹¹³	153			2.3888(9) 2.3862(9) 2.4124(9)	66c
[(depe)(H)Pt ^{IV} {1,2-C ₆ H ₄ (SiMe ₂)(μ-SiH)} ₂] ¹¹⁴	223			2.394(1) 2.391(1) 2.433(1)	66c
{[1,2-C ₆ H ₄ (SiMe ₂ H)(SiH ₂)](1,2-C ₆ H ₄ (SiMe ₂)- (SiH ₂))(H)Pt ^{IV} (dmpe)] (1-75a)	153			2.388(1)	66c
{[1,2-C ₆ H ₄ (SiMe ₂ H)(SiH ₂)](1,2-C ₆ H ₄ (SiMe ₂)(SiH ₂))(H)Pt ^{IV} (dmpe)] (1-75b)	153			2.393(1) 2.371(1) 2.388(1) 2.393(1) 2.371(1)	66c
{[1,2-C ₆ H ₄ (SiMe ₂)(SiH ₂) ₂ Pt ^{IV} (dmpe)] ¹¹⁵ (1-76a)	153			2.406(2) 2.394(2) 2.404(2) 2.401(2) 2.406(1) 2.394(2) 2.402(2)	66c

Table 6l. Continued

complex	temp (K)	M–H ^{2,3}	SiH ^{2,3}	M–Si ²	ref
[[1,2-C ₆ H ₄ (SiMe ₂)(SiH ₂) ₂ Pt ^{IV} (dmpe)] (1-76b)	153			2.413(1) 2.404(1) 2.368(1) 2.451(1)	66c
{(Ph ₃ P)Pt[μ-η ² -H-Si(Ar)H]} ₂ Ar = 2,3,4,5,6-penta(phenyl)phenyl (1-77)	223	1.74	1.64 (br) ¹¹⁶	2.321(2) 2.428(2)	68a
{(Ph ₃ P)Pt[μ-η ² -H-Si(Ar)H]} ₂ Ar = 2- ⁴ Pr-6-Me-C ₆ H ₂ (cis/trans = 1/3) (1-78)	223	1.799	1.593 (term) 1.669 (br)	2.3248(9) 2.4280(9)	68b
{(Ph ₃ P)Pt[μ-η ² -H-SiH(Ar)]} ₂ ¹¹⁷ Ar = 2,4,6-tris(trifluoromethyl)phenyl (σ-complex)	223	⁵⁹	1.445 (terminal)	2.2998(11) 2.4051(11)	68a
[(Me ₃ P) ₂ Pt(μ-SiHAr)] ₂ Ar = 2-isopropyl-6-methylphenyl ¹¹⁸	293		¹¹⁹	2.4054(12) 2.4087(12)	70
[(Ph ₂ MeP) ₂ Pt(μ-SiHAr)] ₂ Ar = 2-isopropyl-6-methylphenyl ¹¹⁸	223		¹¹⁹	2.4070(8) 2.4089(9)	70
[(Me ₂ PhP) ₂ Pt(μ-Si(Ar)H)] ₂ Ar = 2-(⁴ Pr)-6-(CH ₃)C ₆ H ₃ (1-79)	223		1.48(5)	2.4039(8) 2.4006(10)	70
[[Pt(dmpe)] ₂ (μ-SiPh ₂) ₂] (2-102b)	113			2.385(1) 2.3847(9)	127a
		3.9193(2) Pt···Pt		2.718(2) Si···Si	
[[Pt(dppe)] ₂ (μ-SiPh ₂) ₂] (Table 2, footnote 116)	113			2.374(1) 2.391(1) 2.389(1) 2.395(1)	127a
		3.9723(2) Pt···Pt		2.646(2) Si···Si	
[(Ph ₃ P)Pt(μ-η ² -HSiAr ₂)] ₂ Ar ₂ = C ₂₀ H ₂₄ (2-99)	150			2.327 2.371	127c
[(Ph ₃ P)Pt(μ-η ² -HSiAr ₂)] ₂ Ar ₂ = SiC ₁₃ H ₁₁ N (σ-complex) (2-101)	160	1.54	1.64	2.411(2) 2.322(3)	131
(Ph ₃ P) ₂ (H)Pt(μ-SiC ₂₀ H ₂₄)(μ-η ² -HSiC ₂₀ H ₂₄)Pt(PPh ₃) (σ-complex) (2-103)	150	1.50, 1.63 Pt ₁ –H _{br}	1.96, 1.71 Si–H _{br}	2.3365(9) 2.3626(9) 2.3035(10) 2.4875(9)	127c, 132
(Ph ₃ P) ₂ (H)Pt(μ-SiAr ₂)(μ-η ² -HSiAr ₂)Pt(PPh ₃) Ar ₂ = C ₁₃ H ₉ Br ₂ N (σ-complex) (2-104)	150	1.55 (Pt ^I H) 1.79 (Pt ² ···H···Si ²)	1.73(SiH ^I) 1.89(Si ² ···H ² ···Pt ²)	2.4984(13) 2.3409(13) 2.3151(13) 2.3931(13)	131
[(dmpe)Pt(Me ₂ SiC ₆ H ₄ SiH-μ) ₂ Pt(dmpe)] (2-105)	153			2.3676(9) 2.3757(10) 2.3486(9) 2.3777(9) 2.3370(9)	133
				2.4095(9)	
{[(Ph ₃ P)Pt][μ-SiC ₁₂ H ₈]} ₃ (2-106)	223			2.374(6) 2.388(6) 2.348(6) 2.346(6) 2.344(6)	132, 134
				2.355(6)	
{[(Ph ₃ P)Pt][μ-SiC ₁₄ H ₁₂ O]} ₃ (2-108)	165			2.379(3) 2.373(3) 2.336(3) 2.360(3)	131
				2.356(3) 2.332(3)	
{[(Me ₃ P)Pt][μ-SiPh ₂]} ₃ (3-298a)	⁶⁴			2.364(5) 2.357(5) 2.355(5) 2.345(5) 2.343(5) 2.337(5)	298b
				2.313(1)	135
[Pt ₃ (SiHPh ₂)(μ-PPh ₂) ₃ (PEt ₃) ₂] (2-109)	180			2.27(1)	299
[Pt ₃ {Si(OSiMe ₃) ₃ }(μ-PPh ₂) ₃ (PPh ₃) ₂] (3-299)	297				
[Pt ₃ (SiPh ₃)(μ-PPh ₂) ₃ (PEt ₃) ₂] (3-300)	293			2.314(2)	135
[Pt ₃ (SiMe ₂ C ₆ H ₄ SiMe ₂ H)(PEt ₃) ₂ (μ-PPh ₂) ₃] (3-301a)	113			2.322(2)	300
[(Et ₃ P) ₂ (μ-PPh ₂) ₂ Pt ₃ (SiMe ₂ C ₆ H ₄ SiMe ₂)Pt ₃ (PEt ₃) ₂ (μ-PPh ₂) ₃] (3-301b) ¹²⁰ additional derivatives ¹²¹	113			2.33(1)	300
Cu and Zn triads					
(Me ₃ SiMe ₂ Si) ₃ SiHgHgSi(SiMe ₂ SiMe ₃) ₃ (3-305)	173			2.485(2)	303
[^t Bu)Hg(ⁱ Pr ₃ Si) ₂ SiHg(ⁱ Pr ₃ Si) ₂ SiHg(ⁱ Bu)] (2-110)	230			2.47(3) 2.43(3)	137
[ⁱ Bu)Hg(ⁱ Bu ₂ Me) ₂ SiHg(ⁱ Bu ₂ MeSi) ₂ SiHg(ⁱ Bu)] ¹²²	295			2.49(3) 2.49(3) 2.46(4)	137
				2.55(10) 2.50(10) 2.51(11) 2.54(11) 2.50(10)	137
[[ⁱ Pr ₃) ₂ SiHg] ₄ ¹²³	210				
additional derivatives ¹²⁴					
Ln and Ac Cp [*] ₂ LuSiH ₂ (<i>o</i> -MeOC ₆ H ₄) (1-83)	156			2.823(5)	74

Table 6m. Continued

complex	temp (K)	M–H ^{2,3}	SiH ^{2,3}	M–Si ²	ref
Cp*Eu(SiH ₃)(THF)Cp*K(THF) ₂ (1-84)	293			3.239(3)	75a
Cp*Yb(SiH ₃)(THF)Cp*K(THF) ₂	293			3.091(3)	75a
additional derivatives ¹²⁶					

¹ Only compounds with direct metal–silicon bonds or related agostic interactions are included in the table. Compound numbers are the same as those in Tables 1, 2, and 3. If a compound number is absent, a footnote to a table will be indicated. ² Values are given in Angstroms. ³ Hydrogens located on metal and silicon and refined unless noted otherwise. ⁴ Sc triad: Only complexes with direct metal–silicon bonds are included. ⁵ The silicon was disordered over two locations relative to the metallocene wedge.^{26b} ⁶ Values for Si directly bonded to Sc, Y, and La: Sc–Si, 3.038(2)³³³; Y, 3.038(2)⁴⁴³. Values for α-agostic interactions will be summarized in Table 7a: Y–Si, 3.0505(8);^{345b} 3.0521(7);^{345c} 3.0569(7);^{345c} 3.0929(7);^{345c} 3.1012(7);^{345c} 3.1213(6);^{345b} 3.1375(7);^{345c} 3.1620(7);^{345c} 3.1990(7);^{345c} 3.228;^{26c} 3.2887(5);^{345b} 3.5365(7);^{345b} La–Si, 3.193(2);^{345b} 3.261(2);^{345b} 3.472(2);^{345b} 3.889(3). ⁷ Average value. ⁸ Table 3, footnote 6. ⁹ **Ti–Si**: 2.635(2);^{347a} **Zr–Si**: 2.74(2);^{348a} 2.7429(16);^{349a} 2.7563(16);^{349a} 2.76(2);^{348a} 2.7611(6);^{348b} 2.784(4);³³⁵ 2.7849(8);^{349a} 2.7959(4);^{349b} 2.7964(8);^{349a} 2.803(2);^{347a} 2.818(5);^{347b} 2.8214(4);^{348b} 2.8264(19);^{349c} 2.843(3);³⁵⁰ 2.8497(19);^{349c} 2.853(2);^{349d} 2.860;^{347a} 2.875(2);^{349a} 2.8771(10);^{349d} 2.8862;³³⁹ 2.8927;^{351a} 2.9064;^{351a} 2.9079;^{351a} 2.9331(13);^{351a} 2.9331(14);^{351a} 2.9331(4);^{351b} 2.9507(7);^{351c} 2.9507(7);^{351c} 2.9843(3) (multicentered bond);^{352a} 2.9907(3) (multicentered bond);^{352a} 3.0036(3) (multicentered bond);^{352a} **Hf–Si**: 2.6515(9);^{351d} 2.7825(13);^{351d} 2.791(14);^{349c} 2.802(6);^{349c} 2.807(4);³⁴⁷ 2.8106(16);^{351e} 2.823(15);^{349c} 2.8309(6);³⁵³ 2.8332(5);³⁵³ 2.835(2);^{307c} 2.846(2);^{351a} 2.85;³⁵⁴ 2.850;^{349d} 2.851(3);³⁰⁷ 2.863(2);^{351a} 2.87;³⁵⁴ 2.896(7);^{351a} 2.918(7);^{351a} 2.9631(5) (multicentered bond);³⁵² 2.9709(5) (multicentered bond);³⁵² 3.0200(4) (multicentered bond);³⁵². ¹⁰ Table 3, footnote 28. ¹⁴¹ Values obtained from neutron diffraction study.¹⁴⁵ ¹² Values obtained from X-ray diffraction study.¹⁴² ¹³ X-ray data was only of sufficient quality to establish overall geometry.^{147a} ¹⁴ Two independent molecules in the unit cell.¹⁴⁹ ¹⁵ Hydride ligands were not located.³³ ¹⁶ Hydrogen atoms were included in calculated idealized positions but not refined.³³ ¹⁷ **Nb–Si**: 2.5597(5);¹⁴³ 2.5776(5);¹⁴³ 2.5782(8);^{356b} 2.5817(7);^{356b} 2.586(2);^{356b} 2.5837(9);^{356b} 2.585;^{356a} 2.586(2);^{356b} 2.5908(10);^{32a} 2.594(1);^{356b} 2.595(3);¹⁴⁴ 2.5961(5);^{356a} 2.5969(6);^{356b} 2.5986(4);^{356b} 2.5986(4);^{356b} 2.6038(8);^{356b} 2.604(2);¹⁴² 2.6045(8);^{356b} 2.6045(8);^{356b} 2.605(8);^{356b} 2.6148(9);^{356b} 2.6167(8);^{356b} 2.618(1);¹⁴² 2.6206(8);^{356b} 2.622;¹⁴² 2.6240(9);¹⁴⁴ 2.625(1);^{356b} 2.6285(9);¹⁴⁴ 2.6411(8);^{356b} 2.6426(2);^{356b} 2.649;^{356a} 2.649(2);^{356b} 2.6491(4);¹⁴⁴ 2.6522(6);^{356a} 2.6528(5);^{356a} 2.6645(6);^{356b} 2.670(3);³⁵⁷ 2.680(2);³⁵⁸ 2.685(1);³⁵⁸ **Ta–Si**: 2.631;³⁵⁵ 2.645;³⁵⁵ 2.666(3);³⁵⁹ 2.689(1);³⁶⁰ 2.710(4);^{351b} 2.7167(8);³⁶¹ 2.722(3);³⁶⁰ 2.726(4);³⁶¹ 2.754(3);³⁶¹ 2.809(2);³⁶². ¹⁸ Table 3, footnote 45. ¹⁵¹ Table 1, footnote 20. ³⁵ Table 2, Footnote 16. ³⁶ Table 3, footnote 46. ^{155a} ²² Non-hydrogen atoms were refined anisotropically. Hydrogen atoms were included but not refined.^{37b} ²³ Hydrogen bound to tungsten could not be located in a reasonable position.^{85a} ²⁴ Poor quality crystal showed a piano-stool structure with mutually cis arrangements of the 2 COs and 2 Si– groups.¹⁵⁴ ²⁵ **Co–Si**: 2.326;³⁶³ 2.329;³⁶³ 2.335(2);⁹⁰ 2.355(2);¹⁵¹ 2.406(1);⁹⁰ 2.4864(13). **Mo–Si**: 2.219(2);⁸² 2.4125(13);^{365a} 2.4439(14);⁸³ 2.4472(6);^{365b} 2.459(3);¹⁷ 2.4636(8);¹⁷ 2.471;^{365b} 2.4795(9);¹⁵¹ 2.480;³⁶³ 2.4804(9);¹⁵¹ 2.4919(12);¹⁶³ 2.4996(9);¹⁵¹ 2.5008(9);¹⁵¹ 2.5188(9);^{366a} 2.519(3);^{366a} 2.520(3);³⁶⁷ 2.528(1);^{368c} 2.538(2);^{365a} 2.5554(5);^{37a} 2.5593(9);^{366a} 2.595(1);^{368c} 2.603(14);¹⁵³ 2.6315(10);^{366b} 2.651(2);¹⁵⁴ 2.666(1);^{368a} **W–Si**: 2.470;³⁶³ 2.471;³⁶³ 2.481(3);^{369a} 2.485(2);^{368b} 2.485(2);^{368b} 2.4866(4);^{547a} 2.4902(9);^{368d} 2.528(1);^{368c} 2.4915(4);^{547a} 2.549(2);^{368b} 2.553(3);^{369a} 2.5604(9);^{85b} 2.567(3);^{368d} 2.576(3);³⁹ 2.576(4);^{368d} 2.595(1);^{368c} 2.617(3);^{369b} 2.617(3);¹⁵⁸ 2.620(3);^{369b} 2.651(2);¹⁵⁴ 2.6851(13);^{369c} 2.670(2);^{370a}. ²⁶ From a preliminary neutron diffraction study.^{89a,b} ²⁷ Complex prepared from MeC₅H₄(OC₂H₅)Mn(H)SiPh₂ and [Ph₃C][BF₄]. ^{89a} ²⁸ The H atom positions and their anisotropic thermal parameters were fixed at the values obtained from the earlier neutron diffraction study.^{89a} ²⁹ Publication provides only the X-ray structure. Two molecules in the asymmetric unit.^{371,216} ³⁰ Hydrogens were included in the model at geometrically calculated positions but were not refined.⁹¹ ³¹ Precise location of the 6 H's could not be confirmed; they were presumed to be in axial positions of a tricapped trigonal prism.¹⁷² ³² Proposed structure is a dodecahedral conformation with a transoid disposition of silyls and hydrides.¹⁷² ³³ **Mn–Si**: 2.642(6);^{370b} 2.642(3);^{370b} 2.643(4);^{370b} 2.662(6);^{370b} **Re–Si**: 2.5633(8);¹⁷³. ³⁴ Table 3, footnote 74. ^{42a} ³⁵ All hydrogen atoms were placed isotropically at calculated positions and fixed in the calculation.⁴³ ³⁶ Hydrogen atoms were placed isotropically at calculated positions and fixed in the calculation.⁴² ³⁷ Data taken from the supplemental information.⁹³ ³⁸ Table 3, footnote 95.¹⁸⁶ ³⁹ Table 3, footnote 98.¹⁸⁶ ⁴⁰ Table 3, footnote 109.¹⁸⁸ ⁴¹ PMe₃ disordered over 2 positions, and the disorder prevented location of the hydride ligand.¹⁸⁹ ⁴² Only non-hydrogen atoms were refined.¹⁹⁴ ⁴³ Structure reported previously was obtained at room temperature.²⁰⁸ ⁴⁴ Table 3, footnote 141.²⁰⁸ ⁴⁵ Two molecules in the asymmetric unit, but parameters for only 1 are given.^{210a} ⁴⁶ Table 3, footnote 147.²⁰⁸ ⁴⁷ Ru–H distances obtained from the Cambridge Data Base. ⁴⁸ Could not locate MH or SiH as there is disorder in the solvent of crystallization and the hexyl group.⁵¹ ⁴⁹ Table 2, footnote 52.¹⁰⁰ ⁵⁰ Hydrogen atoms were located on a difference Fourier map but introduced in idealized positions.¹⁰¹ ⁵¹ Cocrystal with 1-304. Parameters given only for 3-144b.^{177b} ⁵² The SiCl bond in 3-150 is unusually long at 2.209(4).²²⁰ ⁵³ Table 1, footnote 54. ⁵⁴ SiH data taken from ref 206. ⁵⁵ Table 3, footnote 169.²²³ ⁵⁶ **Fe–Si**: 2.196;³⁷² 2.199(2);^{373a} 2.204(3);^{373a} 2.204(3);^{373a} 2.206(3);^{373a} 2.2064(9);^{373a} 2.2099;^{373b} 2.2225(9);^{373a} 2.2227(13);³⁷⁴ 2.2239(7);^{375a} 2.2318;^{376a} 2.2320(1);^{377a} 2.243(4);^{376c} 2.2466;^{376a} 2.249(4);^{376c} 2.261(4);^{375b} 2.262(1);^{43a} 2.263(1);^{43a} 2.263(2);^{375d} 2.263(2);^{375b} 2.2640(10);^{375c} 2.265(1);⁹⁰ 7(4);^{378a} 2.2689(5);⁴⁶ 2.2698(2);^{379a} 2.2722(9);^{379b} 2.272(7);^{377a} 2.272(4);^{375b} 2.274(2);^{375b} 2.274(2);^{375b} 2.275(2);^{375c} 2.280(1);⁹⁰ 2.2811(11);³⁸⁰ 2.285(3);^{377a} 2.285(2);³⁸⁵ 2.289(2);^{377a} 2.290(10);^{375b} 2.290(2);^{382a} 2.291(4);^{375b} 2.2914(13);^{382b} 2.292(1);^{378a} 2.2924(4);^{378b} 2.293(3);^{379a} 2.294(2);³⁸⁰ 2.2944(8);^{383c} 2.2947(5);^{382c} 2.2955(4);^{378a} 2.296(1);^{377a} 2.296(1);^{377a} 2.296(2);^{379a} 2.298(2);^{383b} 2.2980(9);^{375a} 2.2982(8);^{383c} 2.2990;^{375c} 2.2992(16);^{382c} 2.3010(6);^{383c} 2.3021(19);^{378b} 2.3021(19);^{377b} 2.303(1);^{377b} 2.303(2);^{377a} 2.303(5) (disorder);^{382d} 2.304;³⁸⁴ 2.3048(3);^{382b} 2.3048(3);^{382b} 2.305(2);³⁸⁵ 2.306(2);^{377a} 2.307(2);^{386a} 2.308;^{386b} 2.308;^{386f} 2.309(10);^{385b} 2.3091(5);^{386c} 2.3093(8);³⁸⁵ 2.3093(10);^{385b} 2.31019(9);³⁸⁰ 2.311;^{386b} 2.311(1);¹⁷⁹ 2.311(2);^{383a} 2.312(2);^{387a} 2.313(2);³⁸⁵ 2.313(2);¹⁷⁹ 2.316(2);^{387b} 2.3169(9);^{382c} 2.317;^{386d} 2.317;^{382a} 2.317(1);^{386c} 2.317(1);^{377a} 2.317(1);^{386a} 2.319(1);^{387a} 2.319(2);¹⁷⁹ 2.3196(12);^{386f} 2.3196(12);^{382c} 2.320(1);^{377a} 2.3200(9);^{385b} 2.321;¹⁷⁸ 2.3212(17);^{382c} 2.3222(10);^{387d} 2.322(10);^{387d} 2.3229(16);^{386c} 2.323;¹⁷⁸ 2.3244(14);^{387c} 2.3256(8);^{387f} 2.326(2);^{387b} 2.329(3);^{387g} 2.329(1);^{386f} 2.329(3);^{387b} 2.333;^{377b} 2.3330(4);^{387c} 2.331(6);^{387c} 2.331(2);^{388ab} 2.333;^{377b} 2.3341(9);^{388c} 2.349;^{289c} 2.3353(5);^{377c} 2.3359(6);^{388b} 2.3372(7);^{388b} 2.3374(6);^{388b} 2.339(9);^{377a} 2.339(1);¹⁷⁹ 2.3393(12);⁹⁵ 2.3409(7);^{388b} 2.342(1);^{375b} 2.343(3);^{385a} 2.3435(12);⁹⁵ 2.344;^{389c} 2.346(1);^{389a} 2.346(3);^{387c} 2.349(3);^{389a} 2.3494(6);^{388b} 2.351(1);^{375b} 2.3520(7);^{388b} 2.3588(19);^{376a} 2.362(2);^{387b} 2.3631(19);^{376a} 2.364;^{376b} 2.383;³⁹⁰ 2.400(3);^{376a} 2.402(3);^{376a} 2.405;^{376b} 2.41(av);³⁹¹ 2.4107(7);^{22a} 2.412(3);^{376b} 2.414(3);^{376b} 2.424(17) (disorder);^{382d} 2.4269(7);¹⁰ 2.4447(5);¹⁰ 2.4853(6);^{389c} 2.489(3);^{177b} 2.497(3);^{177b} 2.4976(6);^{389c} 2.5050(6);^{389c} 2.5130(6);^{389c} 2.4682(8);^{389d} 2.4691(9);^{289d} 2.4682(8);^{389d} 2.4691(9);^{389d} 2.862;^{392a} 2.865;^{392a} **Ru–Si**: 2.177(1);^{392b} 2.220(2);^{393a} 2.2264(11);³⁹³ 2.2293(12);³⁹³ 2.238(3);⁴⁷ 2.2635(5);^{47b} 2.2635(5);^{47b} 2.265(2);⁴⁷ 2.267(4);³⁹⁴ 2.2811(11);³⁸⁰ 2.285(2);³²⁵ 2.291(2);³⁹⁴ 2.294(2);³⁸⁰ 2.31019(9);³⁸⁰ 2.3107(17);³⁹⁵ 2.311;³⁹⁶ 2.3116(7);³⁹⁵ 2.316(3);³⁹⁶ 2.328;³⁶³ 2.329;³⁶³ 2.3341(6);¹⁸⁶ 2.335(3);²¹⁴ 2.336;³⁶³ 2.337(3);²¹⁴ 2.338;³⁶³ 2.338(3);^{397a} 2.338(5);^{397a} 2.3389(8);¹⁹⁶ 2.3395(10);³⁹⁵ 2.3400(7);²⁰² 2.342(3);^{397a} 2.344(1);^{397a} 2.3454(5);¹⁹⁶ 2.3486(16);¹⁹⁶ 2.3487(4);²⁰² 2.349(4);^{397a} 2.349(3);^{389a} 2.3499(13);²⁰² 2.350(1);³⁹⁴ 2.3539(15);³⁹⁸ 2.357(2);^{397a} 2.358(2);⁹⁸ 2.358(2);^{397b} 2.359(1);²¹⁴ 2.362(3);³⁹⁹ 2.365(3);⁹⁸ 2.365(2);^{397b} 2.369(1);²¹⁴ 2.3732(6);²⁰¹ 2.376(1);⁹⁷ 2.3768(11);^{399b} 2.3768(10);^{399b} 2.381(2);⁴⁷ 2.382(3);^{397b} 2.382(3);⁹⁸ 2.382(4);⁹⁸ 2.385(4);⁹⁸ 2.3883(6);²⁰¹ 2.389(2);⁹⁸ 2.391(3);^{397b} 2.391(3);⁹⁸ 2.395(4);^{193a} 2.396(2);⁴⁰⁰ 2.399(5);^{397a} 2.401(4);^{397a} 2.402(4);^{193a} 2.402(4);⁹⁸ 2.406(2);⁴⁰¹ 2.4063(5);^{397a} 2.41(1)av;³⁹¹ 2.4108(6);^{193b} 2.4120(10);³⁹⁵ 2.413(5);^{397a} 2.413(4);⁴⁰⁰ 2.4139(9);^{401b} 2.414(1);^{397a} 2.417(7);²⁰⁴ 2.418(2);^{397c} 2.4191(7);^{193b} 2.420(4);^{397a} 2.420(2);^{177b} 2.421(1);¹⁹² 2.421(2);¹⁹² 2.4214(7);²⁰⁸ 2.422(2);^{711b} 2.4223(11);³⁹⁵ 2.424(1);⁴⁰² 2.424(4);^{193ab} 2.4348(9);⁴⁰³ 2.4352(10);¹⁹⁰ 2.4377(11);¹⁹⁰ 2.439(1);⁴⁰³ 2.443(14);^{193a} 2.4476(15);⁴⁰⁴ 2.4623(7);²⁰⁸ 2.4942(10);³⁹⁵ 2.497(1);⁴⁰³ 2.4970(6);^{193b} 2.4970(7);^{193b} 2.517(1);⁴⁰³ 2.5235(8);⁴⁰⁵ 2.5277(8);⁴⁰⁵ 2.5366(9);⁴⁰⁵ 2.5563(7);^{393a} 2.569(1);^{392b} 2.5730(9);⁴⁰⁵ 2.610(1);^{392b} **Os–Si**: 2.257(7) (multiple);²²⁰ 2.263(1) (multiple);²²⁰ 2.297(2);^{406a} 2.3121(12);¹⁹⁶ 2.3196(11);¹⁹⁶ 2.3218(9);²²⁴ 2.3258(9);²²⁴ 2.326(2);^{406a} 2.355(2);^{22a} 2.3613(11);^{406b} 2.3654(19);^{406b} 2.368(2);²²⁰ 2.3761(6);^{406b} 2.3783(17);²²⁰ 2.4021(11);^{406b} 2.412(2);^{22a} 2.414(2);^{22a} 2.4294(7);^{406b} 2.4334(5);^{406b} 2.4533(8);⁴⁰⁸ 2.4716(13);^{406c} 2.4804;²²⁴ 2.4901(8);¹⁹⁶ 2.4906(10);²²⁴ 2.5100(8);^{406c} 2.5166(7);^{406c}. ⁵⁷ X-ray structural analysis performed on one enantiomer. The second enantiomer of 2-51 was reported in the supplemental information, Co–Si = 2.32352(9).⁵⁶ ⁵⁸ Contains 4 independent molecules in cell.¹⁰³

Table 6n. Continued

⁵⁹ Hydride not located.^{103,243,249,116a, 118,109,60,194,265,284,289} ⁶⁰ Averaged value for the four molecules in the unit cell.¹⁰³ ⁶¹ See Table 2, entry 2-55, footnote 63.¹⁰⁵ ⁶² Contains two independent molecules in the unit cell and 1 molecule of hexane per 4 molecules of complex.²³¹ ⁶³ There were two independent molecules in the unit cell, but data were given for only one of the molecules.²³³ ⁶⁴ Information not provided.¹⁰⁸ ⁶⁵ Positions of Rh–H and Si–H were determined by difference Fourier map and not refined further.¹⁰⁸ ⁶⁶ See Table 2, entry 2-59, footnote 68.¹⁰⁸ ⁶⁷ Three independent molecules in the unit cell.²⁴¹ ⁶⁸ Contains toluene solvate.²⁴³ ⁶⁹ Position of hydride was determined with difference Fourier technique and included in calculations with isotropic thermal factors.²⁴³ ⁷⁰ Contains hexane solvate.²⁴³ ⁷¹ Contains 1/2 molecule of hexane solvate.²⁴³ ⁷² Position of hydride determined with difference Fourier technique without further refinement of parameters.²⁴³ ⁷³ Contains benzene solvate.^{109,249} ⁷⁴ See Table 3, entry 3-192, footnote 206.¹⁰⁹ ⁷⁵ Hydrogen atoms located by assuming ideal geometry and included in structure calculation without further refinement of parameters.²⁵² ⁷⁶ See Table 2, footnote 77.¹¹⁴ ⁷⁷ See Table 3, footnote 229.²⁵⁶ ⁷⁸ Distance for term. H not listed.²⁵⁸ ⁷⁹ Table 3, footnote 232.²⁴⁴ ⁸⁰ Contains THF solvate.²⁵⁸ ⁸¹ See Table 3, footnote 234.⁶² ⁸² See Table 3, footnote 238.¹¹⁷ ⁸³ Trans isomer formed from photolysis of cis isomer (see Table 2). X-ray structural determination reported for trans isomer only.¹¹⁸ ⁸⁴ Hydrides located from the difference map and refined using the DFIX restraint (1.68 Å).⁵⁹ ⁸⁵ The cyclooctenyl ring bound to silicon was highly disordered.^{60b} ⁸⁶ Hydrogen atom positions were calculated but not refined.^{60b} ⁸⁷ Unit cell parameters calculated with one molecule of toluene and one tetrahydrofuran per two molecules of complex.^{60ab} ⁸⁸ Positions of hydrides were determined from difference maps but were not refined.¹⁷² ⁸⁹ Crystals were of too poor a quality but verified that the basic structure was a four-legged piano stool.¹⁷² ⁹⁰ The positions of the hydrides were determined from difference maps.¹⁷² ⁹¹ All hydrogen positions were calculated but not refined.^{61b} ⁹² **Co–Si**: 2.238(2);⁴⁰⁹ 2.27;^{448b} 2.2731(10);⁴⁰⁹ 2.2775(12);²³³ 2.281;²⁵⁴ 2.2841(8);^{410a} 2.3039(7);^{410b} 2.3087(7);^{410b} 2.314(2)_{av};^{410c} 2.319(3)_{av};^{410c} 2.3208(7);^{410b} 2.322(1);^{410d} 2.3284(7);^{410b} 2.341(2);^{307a} 2.354(2);^{379a} 2.3862(7);^{406d} 2.3935(7);^{410c} 2.3940(9);^{410c} 2.3945(9);^{410c} 2.3990(7);^{406d} 2.4054(7);^{410c} 2.4082(7);^{410c} 2.4110(10);^{410c} 2.4225(7);^{410c} 2.4352(9);^{410c} **Rh–Si**: 2.119;²⁵⁴ 2.237;²⁵⁴ 2.250(3);²⁵⁷ 2.269;²⁵⁴ 2.289(2);²⁵⁶ 2.289(2);³⁴⁰ 2.290(3);²⁵⁷ 2.2922(8);³⁴⁰ 2.2988(8);³⁴⁰ 2.302(1);²⁴⁴ 2.305(2);⁴¹¹ 2.3104(8);³⁴⁰ 2.314(2);¹⁰⁸ 2.316(2);³⁴⁰ 2.336(1);¹¹⁰ 2.365(7);¹⁰⁷ 2.3681(15);⁴¹² 2.3804(10);²⁴⁰ 2.3937(8);^{242,246} 2.405(1);²⁴⁶ 2.444(4);²⁵⁷ 2.487(3);²⁵⁷ 2.8472(2) (nonbonded distance)⁴¹³. **Ir–Si**: 2.262(2)²¹²; 2.268(2)²¹²; 2.278(2)²¹²; 2.316(2); 2.352(5)⁹⁹; 2.3767(6);^{261c} 2.4006(8);^{251c} 2.405(11);³⁴⁴ 2.408(4);⁵⁵ 2.411(2);¹⁴⁴ 2.416(2); 2.42(2)¹⁵¹; 2.439(8);³⁴⁵ ⁹³ Benzene solvate.^{63,64} ⁹⁴ Two independent molecules in unit cell. Pd–H location not determined.²⁷⁴ ⁹⁵ Contains two disordered Cl atoms. See Table 3, footnote 272.²⁷⁷ ⁹⁶ Contains two crystallographically independent molecules in unit cell.^{121a} Values are similar. ⁹⁷ See Table 2, footnote 95.¹²³ ⁹⁸ Hydrides located by difference Fourier map and included in structure calculations but not refined.¹²³ ⁹⁹ Average value for Pd1–SiH₂.¹²³ ¹⁰⁰ Average value for Pd2–SiH and Pd3–SiH.¹²³ ¹⁰¹ Average value for Pd1–SiH.¹²³ ¹⁰² Structure has C₂ symmetry, which imposes disorder of Pd/Pt positions.²⁷⁹ ¹⁰³ Prepared from (dmpe)Pt(SiHPh₂)₂ + ZC≡CZ.¹²⁴ ¹⁰⁴ See Table 3, footnote 279.²⁸⁰ ¹⁰⁵ See Table 2, footnote 102.¹²⁵ ¹⁰⁶ Cocrystallizes with Pr₃PO.⁶⁷ ¹⁰⁷ The hydrides bound to Pt and Si were located in the difference map but not refined at distances of 1.5 Å (Pt–H) and 1.4 Å (Si–H).⁶⁷ ¹⁰⁸ Table 3, footnote 291.²⁸⁸ ¹⁰⁹ See Table 2, footnote 96.¹²⁴ ¹¹⁰ Contains acetone solvate.²⁹² ¹¹¹ Contains disordered metal sites; 0.5 occupancy. M–Si distance is average of Pt–Si and Pd–Si distances. Si–H not located.¹²² ¹¹² Agostic and terminal hydrides were not refined.⁶⁹ ¹¹³ Additional parameters for 1-74b: Si...Si, 2.832(1), and Pt...Pt, 3.8442(2).^{66b} ¹¹⁴ Footnote 86, Table 1.^{66c} ¹¹⁵ Two molecules in the independent unit.^{66b} ¹¹⁶ Terminal Si–H not located.^{68a} ¹¹⁷ Contains 1 disordered CF₃ group and 1.5 benzene solvate. See Table 1, footnote 85.^{68a} ¹¹⁸ See Table 1, footnote 90.⁷⁰ ¹¹⁹ SiH located and refined.⁷⁰ ¹²⁰ Contains an equimolar amount of [PtH₂(PEt₃)₂(γ-PPh₂)₄].³⁰⁰ ¹²¹ **Ni–Si**: 2.110(2);³³⁹ 2.119(2);³³⁹ 2.1428(12);⁴²¹ 2.1443(8);⁴²¹ 2.1536(13);⁴²¹ 2.1537(8);⁴²¹ 2.1580(13);⁴²¹ 1.65(2);^{415a} 2.196(2);³³⁹ 2.2023(13);^{415b} 2.215(2);³³⁹ 2.2458(3);^{421b} 2.2722(12);^{421b} **Pd–Si**: 2.260(1);^{421d} 2.261(2);²⁷⁷ 2.263(1);^{421d} 2.268(6);⁴¹⁶ 2.269(2);³³⁹ 2.309(2);²⁷⁷ 2.324(1);^{421d} 2.341(2);⁴¹⁷ 2.346(3);⁴¹⁸ 2.349(3);⁴¹⁸ 2.350(6);⁴¹⁸ 2.3610(9);⁴¹⁹ 2.364(3);⁴¹⁸ 2.3762(5);¹⁴ 2.3943(6);¹⁴ 2.399(6);⁴¹⁸ 2.3996(3);¹³ 2.401(7);⁴¹⁸ 2.4154(4);¹³ 2.4168(8);⁴¹⁹ 2.4264(8);⁴²⁰ 2.4287(10);⁴²⁰ 2.4335(5);¹⁴ 2.4340(11);⁴²⁰ 2.4411(11);⁴²⁰ 2.4543(5);¹⁴ 2.4581(9);⁴²⁰ 2.4597(8);⁴²⁰ 2.4603(8);⁴¹⁸ 2.6432(10);⁴²⁰ **Pt–Si**: 2.165(2);³³⁹ 2.210(2);¹¹ 2.261(3);³³⁹ 2.266(1);¹⁶ 2.298(3);⁴²² 2.3041(4);^{410c} 2.309(6);⁴²³ 2.313(2);⁴²³ 2.314(6);⁴²³ 2.319(2);^{388a} 2.321(2);⁹ 2.322(2);³⁰⁰ 2.329(1);^{386f} 2.33(1);³⁰⁰ 2.333(2);^{388a} 2.333(6);²⁷⁹ 2.3364(18);¹³³ 2.343(4);^{66b} 2.3492(2);^{275,276} 2.350(3);¹²² 2.351(3);⁴²⁴ 2.3530(2);²⁷⁵ 2.3532(2);^{275,276} 2.354(2);⁴²⁴ 2.355(4);^{388a} 2.355(3);¹²⁵ 2.357(5);²⁷⁹ 2.357(5);^{66b} 2.359(2);²⁸² 2.359(1);²⁴⁴ 2.360(2);^{426a} 2.361(2);²⁷⁶ 2.362(2);⁴²⁴ 2.362(2);^{426c} 2.362(1);²⁷⁶ 2.362(2);^{425b} 2.364(2);^{388a} 2.365(3);¹²² 2.366(4);¹²² 2.367(2);⁴²⁷ 2.367(2);¹²⁵ 2.368(1);⁴²⁸ 2.369(3);¹²⁵ 2.370(1);²⁸¹ 2.370(2);¹²⁴ 2.371(2);⁴²⁹ 2.373(3);²⁸¹ 2.373(2);^{426c} 2.374(3);²⁸¹ 2.374(1);⁴³⁰ 2.374(1);⁴²⁸ 2.375(4);²⁷⁹ 2.377(3);¹²² 2.3772(15);¹³³ 2.378(2);¹²⁴ 2.378(2);^{426b} 2.380(3);⁴²⁴ 2.384(5);^{66b} 2.385(3);²⁷⁹ 2.388(3);⁴³¹ 2.3881(8);⁴³² 2.389(2);²⁸¹ 2.389(5);^{66b} 2.3900(6);⁴³² 2.3910(17);⁴²³ 2.394(2);^{426c} 2.408(4);⁶¹ 2.4184(4);⁴³³ 2.4229(13);⁴³⁴ 2.426(1);¹⁶ 2.4317(8);⁹ 2.4374(7);⁴³³ ¹²² Table 2, footnote 124.^{136,137} ¹²³ Table 2, footnote 125.¹³⁷ ¹²⁴ **Cu–Si**: 2.2259(2);^{435a} 2.230(2);^{435a} 2.2727(11);^{435b} 2.2728(8);^{435d} 2.2809(14);^{435a} 2.2863(14);^{435a} 2.289(4);³³⁹ 2.2988(13);^{435a} 2.3001(13);^{435a} 2.3033(13);^{435c} 2.313(3);^{435c} 2.315(3);^{435a} 2.3298(12);^{435d} 2.347(11);^{435a} 2.3493(11);^{435b} 2.3551(12);^{435c} 2.3586(10);^{435b} 2.3737(10);^{435a} 2.3817(13);^{435c} 2.384(3);^{435c} 2.390(3);^{435c} 2.4168(12);^{435c} 2.4649(10);^{435c} 2.4774(10);^{435b} 2.4827(13);^{435d} 2.4833(13);^{435d} 2.4920(10);^{435b} **Ag–Si**: 2.4827(13);^{435d} 2.4883(13);^{435d} **Au–Si**: 2.362;³⁶⁷ 2.3629(16);^{367b}; 2.4044(17);^{435d} 2.4072(17);^{435d} **Zn–Si**: 2.353;^{437a} 2.3537(9);^{437b} 2.3652(12);^{437b} 2.3846(12);^{351c} 2.3855(13);^{351c} 2.425(2);^{438a} 2.425(2);^{438a} 2.428(2);^{438a} 2.449(2);^{438a} 2.425(2);^{438a} 2.449(2);^{438a} 2.504(2);^{438b} 2.518(3);^{438b} 2.519(2);^{438b} 2.531;^{438b} 2.748(1)_{av} [2.698(1), 2.723(1), 2.746(1), 2.751(1), 2.825(1)]⁴³⁹. **Cd–Si**: 2.599(3);^{438a} 2.609(2);^{438a} **Hg–Si**: 2.417(4);^{136a} 2.477(4);^{136a} 2.4795(13);¹³⁶ 2.485;^{440a} 2.485(2);^{440b} 2.4913(18);⁴⁴¹ 2.561(2);^{438a} 2.563(2);^{438a} 2.618;¹³⁷ ¹²⁵ See footnote 95, Table 1, 1-84.⁷⁵ ¹²⁶ Ln and Ac directly bonded to Si: 2.984(2)(Yb);^{443a} 3.091(3)(Yb);⁷⁵ 3.1903(10)(Sm);⁴⁴² 3.091(3)(U).^{443b} Data for β-agostic interactions will be found in Table 16 (section 8.1.3).

complex, often formed from a hydrosilane, where the X-substituent is a functional group that may be removed in an abstraction reaction. The intramolecular base stabilization results either from a substituent on the silylene center that has a base tether, or is formed from OA of HSiMe₂SiMe₂X (X = OMe, NR₂) to a transition metal complex followed by migration of SiMe₂X to the metal and coordination of X to the silylene center. A number of bases will react with a base-free silylene center and a common one, especially in earlier work was HMPA, which continues to be employed.

Of the examples in Chart 7, which also includes those from the footnotes to Tables 1–3, approximately 50% have been characterized by X-ray crystallography. The structures of more than 100 silylene complexes have now been determined, generating about 160 independent Si=TM distances. These distances are summarized in Table 8 for the three groups of silylene complexes. A more detailed listing of the individual complexes is provided in Tables 8a and 8b in the Supporting Information.

The bond distances listed in Table 8 contain either the shortest Si=TM distances within the respective bond ranges

(Hf, Cr, Mo, W, Fe, Os, Ir, Ni, and Pt) or nearly the shortest (Ta, Ru, Rh, Ir, Pd). Although there are not many examples as yet for each of the elements, the general trend in the Si to TM distance for silylenes overall appears to be base free silylene complex < base-stabilized complex. In four of the cases in Table 8 (formed from hydrosilanes), the complex contains both a silylene coordinated to the metal as well as a silyl group. The difference between the Si–TM and the shorter Si=TM distances is 0.26 Å (W), 0.25 Å (Mo), 0.12 Å (W), and 0.19 (Fe) for the derivatives 3-39 (W), 3-33 (Mo), 3-46 (W), and 3-69 (Fe), respectively. However, 3-46 is a dimer in which the oxygen of the CO substituent coordinates to the Si of W=Si of the second unit, thus producing a variation of a base-stabilized silylene. Thus, the Si=W would be elongated in 3-46 (relative to the distance in 3-39) and the difference between the single and the double bond would be smaller, as is observed. In the Pt complex formed from the stable silylene [Si(NN)], the product also contained not only a coordinated silylene (Pt = Si, 2.266(1) Å) but a silyl group as well (Pt–Si = 2.426(1) Å) with a difference of 0.16 Å.¹⁶ Three of the complexes (3-39, 3-46, 3-69) have

Table 7. TM–Si Bond Distance Ranges for 2c/2e, Multicenter, and Silylene Complexes

element	new range ^a	difference ^a
Sc triad		
Sc	2.797–2.863(4)	0.07
Y	3.038 ^b	
La	^b	
Ti triad		
Ti	2.491–2.765(19)	0.27
Zr	2.670–3.0036(42) ^c	0.33
Hf	2.6515–3.0200(26) ^c	0.37
V triad		
V	2.2576–2.577(3)	0.32
Nb	2.541–2.685(53)	0.14
Ta	2.569–2.809(32)	0.24
Cr triad		
Cr	2.326–2.4864(18)	0.16
Mo	2.219–2.7093(63)	0.49
W	2.354–2.712(69) ^d	0.36
Mn triad		
Mn	2.319–2.662(16)	0.34
Tc		
Re	2.434–2.617(27)	0.18
Fe triad		
Fe	2.1280–2.919(317) ^e	0.79
Ru	2.177–2.610(294)	0.43
Os	2.219–2.5750(98)	0.36
Co triad		
Co	2.1848–2.4352(123)	0.25
Rh	2.054–2.65(119) ^f	0.60
Ir	2.235–2.479(82)	0.24
Ni triad		
Ni	2.1102–2.348(46)	0.24
Pd	2.2594–2.6432(99)	0.38
Pt	2.165–2.4984(322) ^{g,h}	0.33
Cu triad		
Cu	2.2259–2.4920(33)	0.27
Ag	2.4827–2.4883(2)	<0.01
Au	2.291–2.4072(10)	0.12
Zn triad		
Zn	2.342–2.531(23) ⁱ	0.19
Cd	2.599–2.609(2)	0.01
Hg	2.417–2.618(25)	0.20

^a Includes complexes from the 1999 review and those from the current review. The number of independent distances is given in parentheses. Differences between the highest and lowest values have been rounded to the nearest hundredth. ^b Values recorded for Y and La are for Si···M distances where Si is in the β -position and are presented in Table 18. ^c Longest distance involves multicenter bonding. ^d Includes a value from heterobimetallic complex of W with Fe. ^e Two reported values are outside of the range and are nonbonded distances: 2.862 and 2.865 Å.^{392a} ^f One Rh distance (2.8472(2) Å) was outside this range and was considered a nonbonded distance.⁴¹³ ^g Three values for γ -agostic interactions are ≥ 3.5 Å and are not included in the range. ^h The range given includes six values from heterobimetallic complexes of Pt with Rh. ⁱ Questionable Si···Zn interactions were assigned to values from 2.698 to 2.825.⁴³⁹

essentially the same types of substituents. Although not as closely related, the Si=Mo in Cp*(dmpe)(H)Mo=SiHPh, **1-24**, and the Si–Mo in **1-25**, Cp*(dmpe)(H)Mo(SiH₂Ph)₂, exhibit a bond distance difference of 0.19 Å, again highlighting the expectation that the multiple bonds would be shorter than the single bonds.

The molybdenum complexes in Table 8, Cp*(dmpe)(H)Mo=SiRR' (R = R' = Me, Et; R = H, R' = Ph), are unique in that the metal hydride bridges the Mo=Si bond.^{36a} This was verified for the (H)Mo=SiEt₂ complex by a neutron diffraction study. In this derivative, the Mo···H distance was 1.847(12) Å and the Si···H distance was 1.683(13) Å. The

remaining four related derivatives reported in the study were assumed to also have bridging hydrides. A “triple” bond between molybdenum and silicon has also been reported from the reaction of Cp*(dmpe)(H)Mo=Si(Cl)Mes with Li(Et₂O)₃B(C₆F₅)₄.⁸² The Mo to Si distance was 2.219 Å, and the hydride in [Cp*(dmpe)(H)Mo=SiMes]⁺[B(C₆F₅)₄][–] was also proposed to have some interaction with the silicon center. The Mo to Si distance was significantly shorter than the Mo to Si distances in the corresponding silylene complexes also listed in Table 8.

Reactions of hydrosilanes often provide complexes with [TM]–H bonds. However, even when such complexes are characterized by X-ray diffraction, the hydrogens may or may not be located. Even when located, interpretation of the metal–hydrogen distances requires some caution. More accurate distances have been obtained by neutron diffraction, although the number of organometallic complexes containing [TM]–H bonds that have been characterized by this method are somewhat limited. In 1997, Bau reviewed and tabulated the average M–H terminal and μ_2 -H bridging distances.⁴⁵¹ The general trends show that terminal hydride distances are shorter than bridging distances (also observed from X-ray diffraction data), and although the distances have been determined for only about one-half of the transition metals, the trend is a decreasing [TM]–H distance from left to right in the series. An overview of Table 6 shows that many [TM]–H distances are missing as the hydrides were not located or refined and only four complexes have been characterized by neutron diffraction: Cp₂Ta(H)(SiMe₂H)₂ (reported in 1991 by Berry and coworkers from a reaction involving H₂SiMe₂),^{343b} Cp₂Nb(H)(SiMe₂Cl)₂ (**3-16**),^{142,144,145} Cp*(dmpe)Mo(H)Mo=SiEt₂ (**2-10**),^{36a} and Cp'(OC)₂Mn(η^2 -HSiHPh₂)^{89a,d} (for preparation, see ref 4). In the complex Cp₂(H)Nb(SiMe₂Cl)₂ (**3-16**), the Nb–H bond distance as measured by X-ray diffraction (data collected at 190 K) was 1.74(7) Å but was 1.816(8) by neutron diffraction (100 K), whereas the SiH distances were 2.056 Å (X-ray) and 2.076(3) (ND).^{142,145a} In the other complex, Cp*(dmpe)(H)Mo=SiEt₂ (**2-10**), the MH bond was located in both the X-ray structure and the neutron diffraction structure.^{36a}

Values for M–H distances tend to be shorter when measured by X-ray diffraction relative to those measured by neutron diffraction.^{451a,b} An M–H determined by neutron diffraction can have a relative precision of 1% or better.^{451b} Since H atoms are difficult to locate by X-ray crystallography, the distances involving H are relatively imprecise. Lachaize and Sabo-Etienne argue that X-ray data are now more reliable for hydrogen location when high-quality measurements are made at low temperatures and especially when complemented by DFT calculations.⁴⁵² However, the level of the calculation can be important, as was demonstrated for the complex [RuH₂{(η^2 -HSiMe₂)₂NH}(PCy₃)₂]₂ (**3-132**), which will be discussed further in section 5.4.^{212,452}

For most types of complexes, there are still insufficient numbers of metal–silicon distances in closely related structures to attempt a correlation. In general, more electronegative substituents at silicon tend to cause a decrease in the metal–silicon bond length, although the change may not be very dramatic. Only cases where the substituents on the metal fragment are held constant can a comparison of [TM]–Si distances be made. An example is the Mn–Si distance in (OC)₅MnSiPh₃^{371a} vs (OC)₅MnSi(SiMe₃)₃^{371b} which are 2.509(2) and 2.498(2) Å for the former and 2.564(2) Å for the latter. The shorter bond distance in the

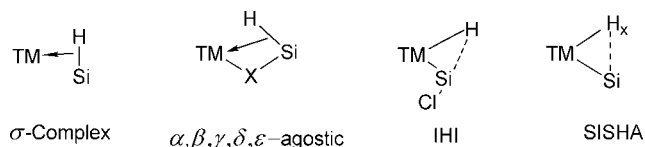
Table 8. Bond Ranges for Silylene Complexes Compared to the Range of Crystallographically Characterized Complexes

metal	bond range ^a	base-free silylene ^a [previously reported range] ^b	intramolecular stabilization ^a [previously reported range] ^b	intermolecular stabilization ^a [previously reported range] ^b
Y	2.797–652.863	3.038(1)		
Hf	2.652–3.020(26)	2.652(1)		
Ta	2.569–2.809(32)		2.597–2.605(2)	
Cr	2.326–2.486(18)	2.326–2.329(2)	2.250–2.406(4)	2.343–2.431(3)
		[2.3610(1)]	[2.408–2.414(3)]	[2.342–2.527(5)]
Mo	2.219–2.709(63)	2.219–2.480(9)	2.444–2.501(5)	
W	2.354–2.712(69)	2.354–2.470(6)	2.487–2.5672(3)	2.445–2.511(5)
			[2.490–2.502(3)]	
Mn	2.319–2.662(16)		[2.336–2.344(2)]	
Fe	2.128–2.919(317)	2.128–2.196(3)	2.199–2.296(8)	2.272–2.292(4)
			[2.207–2.659(6)]	[2.214–2.341(11)]
Ru	2.177–2.610(294)	2.226–2.338(9)	2.291–2.4191(19)	
		[2.238–2.286(2)]	[2.333(2)]	[2.269 ^c –2.328(3)]
Os	2.219–2.575(98)	2.219–2.281(4)	2.386–2.432(5)	2.325(1) ^d
		[2.419(1)]		
Co	2.185–2.435(123)		2.1848(1)	
Rh	2.054–2.65(119)	2.292–2.316(5)		
Ir	2.235–2.479(82)	2.250–2.260(2)		[2.337(1)]
Ni	2.110–2.348(46)	2.110–2.215(12)		
		[2.207–2.216(2)]		
Pd	2.259–2.643(99)	2.260–2.454(7)		
Pt	2.165–2.498(322)	2.210–2.266(4)		
		[2.270(1)]		
Cu	2.226–2.492(33)	2.289(1)		
Ln		3.1903 (Sm)		
		2.984 (Yb)		

^a Values are rounded to the nearest thousandth. Number in parentheses denotes the number of independent bond distances. Data collected during the current review period. Individual examples are listed in Supporting Information Table 8a. ^b Range in brackets is for systems reported prior to 1998 and summarized in refs 1b and 450a,b. Individual examples are listed in Supporting Information Table 8b. ^c Considered a Ru≡Si complex. ^d Woo, L. K.; Smith, D. A.; Young, V. G., Jr. *Organometallics* **1991**, 10, 3977–3982.

Ph₃Si derivative was taken as support for π -backbonding resulting from the more electronegative Ph substituents at silicon.^{371a} In the case of *cis*-Pt(PMe₂Ph)₂(SiMe_nPh_{3-n})₂, the Pt–Si distance increases from *n* = 2 to *n* = 0.²⁸¹ Several examples from Table 6 illustrate this point, and the following TM–SiRCl₂ complexes have distances that fall in the bottom half of the respective Si–[TM] range: **2-32** (η^6 -C₆H₅Me)-(H)₂Fe(SiCl₂H)₂),⁹² **3-100** [(C₆H₆)(Ph₃P)Ru(SiCl₃)₂]¹⁹⁰ and **3-114** {[C₃PH][(OC)(PCy₃)ClRu(SiCl₃)₂]}₂,²⁰³ **3-124** [(Ph₃P)₃H₃RuSiMeCl₂],²⁰⁶ and **3-258** [(PN)Pd(SiCl₃)₂]²⁷⁷ and **3-291** [(cod)Pt(SiMeCl₂)₂].²⁹⁶ Two examples illustrated here show how the effect of changing the number of Cl substituents at Si does not cause dramatic changes. For the complex, Cp(Me₃P)(ArN)HTa–SiMe_xCl_{3-x}, the difference for the Ta–Si bond distance for *x* = 1 (**3-26a**) and *x* = 2 (**3-25a**) is only 0.005 Å,^{78a,146,147a,b} and for (OC)(Ph₃P)(Me₂NCS₂)OsSiMe_xCl_{3-x} [*x* = 0 (**3-154**) and *x* = 1 (Table 3, footnote 169)] the difference is 0.022 Å.²²³ Ligands at the metal may not influence the TM–Si bond distance significantly, as is illustrated in the two Rh complexes (Ph₃P)₂(X)HRhSi(OEt)₃ (**3-205**, X = Cl, and **3-206**, X = I) that have identical Rh–Si distances.²⁵² In a series of derivatives of (Me₃P)₃(Cl)(H)Rh[Si(C₆H₄-X-*p*)₂H] (X = H, OMe, F, CF₃), the Rh–Si distance only varied from 2.311 to 2.319 Å, which suggests that an electronic variation at a site remote from the silicon center may have little effect on the Rh–Si bond distance.¹⁰⁸ Although it is a more limited sequence, the effect of changing substituents in Cp(Me₃P)₂RuSiCl₂R (R = Cl, Me, Ph) on the Ru–Si distance has been determined and shows that replacing an electronegative chloride substituent in RuSiCl₃ with the more electropositive R groups Me and Ph resulted in Ru–Si bond elongation and correlated with the spectroscopic properties observed for this series of complexes.³⁸⁰

The hemi-labile chelate, R₂N–X–PR'₂ where X = a linker group, has two different base centers that exhibit a difference in *trans*-influence. This is clearly shown in the complexes

**Figure 4.** Representations of nonclassical interactions.

(PN)Pd(SiCl₃)₂ (**3-258**) where the Si–Pd distance *trans* to P is 2.3243 Å, whereas the Si–Pd *trans* to N is 2.254 Å.²⁷⁷ In a related derivative (Table 3, footnote 272), the distances are 2.309 and 2.261 Å for Si *trans* to P and N, respectively.²⁷⁷ Such trends are also observed in P–[TM] distances as demonstrated in the structure of *cis*-[Ph₂P(CH₂)₄PPh₂]-Pt(H)SiPh₃, where the Pt–P *trans* to the silyl group is 2.374 Å and those *trans* to the hydride are 2.319 and 2.298 Å.⁴³⁰

5. Nonclassical Interactions

When a hydrosilane reacts with a transition metal complex, there are variations of bonding types in the products formed that could not have been anticipated 20 years ago. A full oxidative addition leads to the formation of 2c-2e bonds between the metal center and Si and the metal center and H. However, there are several stages on the way to full oxidative addition that have been identified in isolated complexes (and in calculations). These involve the formation of σ -complexes, complexes with agostic interactions of a Si–H bond in α -, β -, and more remote positions with a metal center, and interligand hypervalent interactions (IHI) between an MH bond and an electrophilic silicon center. In addition, there also appear to be interactions between a silicon center and a metal-bound hydrogen that have been identified especially in polyhydride systems (referred to by the term SISHA, or secondary interactions between a silicon and a hydrogen atom⁴⁵²). These various interactions are depicted in Figure 4.

There is no uniform agreement as to how to distinguish (or if a distinction may actually be realized) between these

Scheme 15

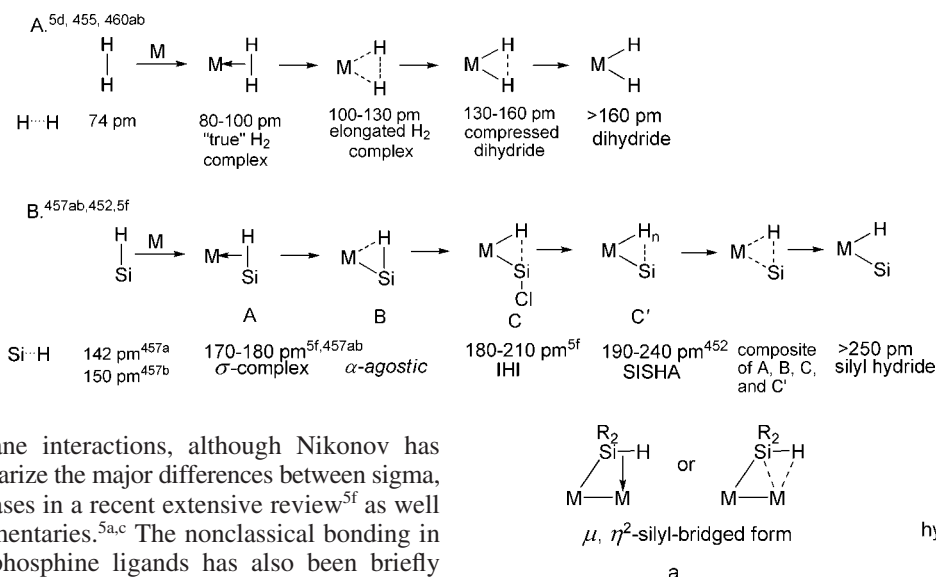


Figure 5. Alternative representations of a bridging hydridosilyl group in a dinuclear complex: (a) σ -interaction of SiH with one of the metals and (b) M–H interaction with the silylene group.⁴⁵⁶

variations for silane interactions, although Nikonov has attempted to summarize the major differences between sigma, agostic, and IHI cases in a recent extensive review^{5f} as well as in shorter commentaries.^{5a,c} The nonclassical bonding in alkyl, silyl, and phosphine ligands has also been briefly described by Braunstein and Boag.^{5b} The interrelationships between all types of σ -complexes have been thoroughly explored by Kubas in his monograph,^{5e} as well as in a short article that describes the relationship of the σ -complexes and the Dewar–Chatt–Duncanson model for metal–olefin π -bonding.^{5d} More recently, Kubas has also published a brief summary of metal-bound saturated molecules that includes H_2 , silanes, alkanes, and boranes⁴⁵⁵ and emphasizes dihydrogen complexes as prototypes for the coordination of other saturated molecules. The cases for H_2 coordination may be more clearly defined in terms of $\text{H} \cdots \text{H}$ distances as depicted in sequence A in Scheme 15.^{5d, 460a,b} Since silicon is not only more electropositive than hydrogen but also bears substituents that can influence the nature of the Si–H bond, a direct comparison of H_2 and SiH complexes may be precluded. Nonetheless, a possible correlation between HSi/TM interactions and those of H_2 is suggested in sequence B in Scheme 15.^{5f, 452, 457a,b} The main purpose is to show that both sets of complexes exhibit different ranges of distances that have been identified by some descriptor. It should be understood at the outset that interactions of Si–H with a metal center form a continuum; thus, boundaries in any classifications are blurred. Furthermore, more than one interpretation has been possible for a given data set.

The distinctions between the sigma, agostic, IHI, and SISHA groupings involve interpretation of bond distances and angles, hydride chemical shifts and coupling constants, and MH and SiH stretching frequencies with a greater weighting on the X-ray structures and NMR data. These classes are illustrated in a general fashion in Figure 4. More recently, calculations have been used to support a particular structure, although some caution must be used in terms of interpretation of results as a function of the level of the calculation. The examples of complexes with nonclassical interactions that have been reported during this review period are summarized in Table 9 and are classified in the following approximate categories: (a) σ -complexes (A in Scheme 15); (b) α , β , and more remote H–Si interactions (an Si–H interacts with the metal center; similar to B in Scheme 15B); and (c) IHI and SISHA (an M–H interacts with a silicon center; C and C' in Scheme 15). Table 9 includes one example of a specific type of silane from a publication unless other complexes of the type were crystallographically characterized. Additional, related examples appear in the

footnotes to a particular complex entered in Table 9. Added to Table 9 are nonclassical silyl–metal complexes that were formed from conversion of a classical silyl–metal complex (for an example, see **3–80**¹⁸²). Complexes that were listed in footnotes to Tables 1, 2, and 3 as well as nonclassical compounds prepared by other routes are numbered with a 9-X prefix.

As in most attempts at classifications, there are compounds that do not fit “nicely” into a single category but could be described in two (or more) ways. This is certainly the case with dimers where the silicon–metal bond is bridged by hydrogen and often carries the designation, μ, η^2 -HSiR₂. The bridging silyl group may be viewed as a Si–M bond to one metal center with the Si–H bond forming a σ -interaction with the second metal (Figure 5) or as a silylene bridge with a metal hydride interacting with a silicon center (Figure 5). A recent calculation study supports the latter view and will be discussed in section 7.⁴⁵⁶ The σ -interaction depicted in Figure 5a could also be viewed as an α -agostic interaction with the second metal center.

5.1. General Comments on X-ray Data

When the Si–H bond becomes a σ -donor to a metal center, the Si–H σ^* orbital is of appropriate symmetry to accept electron density from the metal center. The extent of back-bonding will provide variations in the weakening of the Si–H bond to the limit of cleavage of that bond and formation of $2c/2e$ Si–[TM] and M–H bonds. The average Si–H bond distance in hydrosilanes based on 451 structures was reported to be 1.425 Å^{457a} but is often set at 1.5 Å.^{457b} Thus, a Si–H distance >1.5 Å could indicate the presence of a Si–H interaction with the metal center. In his earliest review, Schubert suggested that a Si–H distance >2.0 Å should represent the shortest nonbonding Si–H contact.⁴ However, the range of complexes that involve σ -interactions has considerably expanded since then, and this criterion may need revision, as will be discussed later in this section. Substituents at silicon will influence the value of the Si–H contact, but Nikonov^{5f} argues that the range of Si–H distances measured

in complexes that are closely related such as $(\text{Cp}''\text{L}(\text{OC})\text{Mn}(\eta^2\text{-HSiR}_3))$; $\text{L} = \text{CO}$ or 2-electron donor; $\text{Cp}'' = \text{Cp}$, Cp' , or Cp^*) is too narrow to provide definitive conclusions. It has been proposed that Si–H distances in the range 1.7–1.8 Å indicate σ -coordination.^{5f,452} Longer SiH bond distances become more difficult to interpret, but values up to 2.4 Å still seem to indicate an interaction between Si and H (sum of the van der Waals radii is 3.4 Å for Si and H).⁴⁵²

Likewise, the M–H distance, established primarily by X-ray crystallography with its attendant problem in locating hydrides in the neighborhood of heavy elements, also may not be influenced significantly by substituents at the metal center as demonstrated in the range exhibited by the manganese derivatives $(\text{Cp}''\text{L}(\text{OC})\text{Mn}(\eta^2\text{-HSiR}_3))$; $\text{L} = \text{CO}$ or 2-electron donor; $\text{Cp}'' = \text{Cp}$, Cp' , or Cp^*), which was too narrow (close to three esd's) to derive reasonable conclusions. Calculations by Lin and coworkers also demonstrated that there was no significant elongation of M–H distances in the complexes $\text{Cp}(\text{OC})_2\text{M}(\eta^2\text{-HSiH}_{3-n}\text{Cl}_n)$ ($\text{M} = \text{Mn}$, Tc , and Re ; $n = 1-3$).⁴⁵⁸ A neutron diffraction study, which provides the most reliable structural data, indicated that the $\text{Mn}\cdots\text{H}$ distance in $[\text{Cp}'(\text{OC})_2\text{Mn}(\eta^2\text{-HSiFPh}_2)]$ was not elongated, is comparable to a normal Mn–H bond, and does not differ from that observed in the related complex $[\text{Cp}'(\text{OC})_2\text{Mn}(\eta^2\text{-HSiHPh}_2)]$.^{89a} Only five complexes where the metal contains both an M–H and a M–Si bond have been characterized by neutron diffraction (Table 6): $\text{Cp}_2(\text{H})\text{Nb}(\text{SiMe}_2\text{Cl})_2$ (**3-16**),^{145a} $\text{Cp}_2\text{Ta}(\text{H})(\text{SiMe}_2\text{H})_2$,³⁵⁵ $\text{Cp}^*(\text{dmpe})(\text{H})\text{Mo}=\text{SiEt}_2$ (**2-10**),^{36a} $(\eta^5\text{-C}_5\text{H}_4\text{Me})(\text{OC})_2\text{Mn}(\eta^2\text{-HSiHPh}_2)$ (**2-29**),^{89a,d} and $(\eta^5\text{-C}_5\text{H}_4\text{Me})(\text{OC})_2\text{Mn}(\eta^2\text{-HSiFPh}_2)$.⁴⁶¹ Unfortunately, the number of neutron diffraction studies of silyl–metal hydrides is too small to develop a general picture either across a number of derivatives or for the range of transition metals. Furthermore, it has not yet been possible to correlate either the SiH or the MH distances with the extent of the oxidative addition of the hydrosilane to the metal center.

The Si–TM, Si–H, and M–H distances have been used to distinguish nonclassical from classical interactions although Si–TM distances in 2c/2e bonds overlap with those in 3c/2e bonds (section 4), but the Si–TM distances are still the most reliably measured of the three.^{1a} Since hydrides are not always located in an X-ray determination, appropriate bond distance information is often not available, and even then the Si–H and M–H distances, when observed, may be shorter than those determined in the rare neutron diffraction studies of the same complex. Lachaize and Sabo-Etienne argue that X-ray data have become more reliable for hydrogen location since data are now routinely collected at low temperature with higher-quality instrumentation but that measured distances are especially reinforced when complemented by DFT calculations.⁴⁵²

5.2. General Comments for NMR and IR Data

How is an interaction of a Si–H bond with a metal center detected or inferred in solution? In a free silane, a typical value for $^1J_{\text{SiH}}$ is found between 150–200 Hz (except for HSiCl_3 , where the value is ~ 400 Hz). In a complex where a 2c/2e [TM]–SiHRR' interaction is present, the value of $^1J_{\text{SiH}}$ falls approximately 40 Hz relative to the free silane.^{1a} In examples where some type of $\text{M}\cdots\text{H}\cdots\text{Si}$ has been proposed to occur, the $^1J_{\text{SiH}}$ is reduced further. Schubert originally suggested that when the Si–H coupling constant fell in the range of ~ 40 –70 Hz a nonclassical interaction

was indicated and when the one-bond coupling constant fell below 10–20 Hz a “strong” Si–H interaction was unlikely.⁴ However, an increasing diversity in the types of interactions between SiH and [TM] has been identified, and other coupling constant ranges have been proposed. The sign on the coupling constant may also play a part, and these two features will be addressed later in this section.

Another sign of a nonclassical interaction is a shift in the infrared stretching frequency of both Si–H and M–H absorptions to lower frequency when a nonclassical interaction is observed/proposed, although IR measurements have not been routinely employed. Even in those cases where IR data were reported, an assignment of either a Si–H or a M–H stretching frequency was not always made due, in part, to overlap with other absorptions. However, a broad and intense band between 1650 and 1800 cm^{-1} is a good indication of a σ -interaction.⁴⁵² Calculations have become increasingly important but not yet routine. The systems where calculations have been reported, usually on model compounds, have been indicated in Table 9.

As discussed in section 4, each transition metal exhibits a range of distances for the Si–[TM] bond. The range for each metal generally falls between ~ 0.1 and 0.8 Å, and the bond distances overlap for metals that are adjacent to each other in the periodic table. Thus, although the Si–TM distance is the most reliably measured by X-ray diffraction of the three bonds just discussed, an individual bond length cannot be evaluated in terms of extent of the oxidative addition, especially since the distance is also influenced by substituents at silicon as well as by steric factors. A reference classical silyl system may provide a clue, but such references have yet to be identified and accepted. Thus, other independent measurements (NMR, IR) as well as computational studies are required to come to a consistent conclusion.

The markers for a nonclassical interaction should be relatively long TM–Si and TM–H bonds and “short” Si–H bonds. As the silane interacts with the metal center, the Si–H distance should increase and the other two distances should decrease. The limit of the interaction would produce a classical hydrosilane metal complex with shorter TM–Si and M–H bonds and longer Si to H distances. Related to these changes in distance are accompanying changes in $J_{(\text{SiH})}$ coupling constants in ^1H NMR spectra (also measurable in ^{29}Si NMR spectra) as well. As a silane interacts with the metal center, the coupling constant decreases relative to that observed in the free silane ($^1J_{\text{SiH}} \approx 200$ Hz). In the limit of the OA product, the $^1J_{\text{SiH}}$ coupling constant should be zero, although a small value of $^2J_{\text{SiH}}$ may be observed. For nonclassical interactions, the coupling constant values are reduced generally below 140 Hz, but the current view of a lower limit of 20 Hz for a σ -SiH has been questioned and has been proposed to be reset to ~ 65 Hz.⁴⁵² The problem is further complicated by the fact that the $J_{\text{obs}} = \{^1J_{\text{SiH}} + ^2J_{\text{SiH}}\}$ and the signs on these two coupling constants could be different. If this were the case, then a small coupling constant could be measured but a σ -interaction could still be present. This problem will be described in more detail in section 5.4.1.

5.3. Categories of Nonclassical Interactions and Selected Examples

One of the major problems in assessing nonclassical interactions is determining the role of the hydride: does the hydride on a metal interact with the silicon center of the silyl substituent and/or does a hydride on the silicon of the

silyl substituent interact with the metal center? This is particularly difficult to assess when dealing with polyhydrides (two or more hydrides in the molecule). What data are necessary to develop a particular interpretation? In the next subsections, the data will be discussed in the following order: $\text{Si-H}\cdots\text{M}$ (σ -interactions, agostic interactions) and $\text{Si}\cdots\text{H-M}$ (IHI and SISHA) with the focus on complexes with a single metal center. For each of these interactions, an example (or examples) has been selected to illustrate the features of the type (or class) and to illustrate how data are used to interpret the nature of the bonding between the hydrosilane and the transition metal. The basic question for each of the six examples that follow is how to determine the role of the hydride. Following the six examples, the features for each of the groups, $\text{Si-H}\cdots\text{M}$ (σ -interactions, agostic interactions) and $\text{Si}\cdots\text{H-M}$ (IHI and SISHA) will be summarized in sections 5.4 and 5.5, respectively.

5.3.1. Tautomeric Equilibrium between η^2 -Silane and OA.^{21b}

(Although this specific reference concerns a comparison of germanium and silicon complexes, the focus here will be on the silicon complexes.) In the reaction of $[(\text{OC})\text{-Mo}(\text{depe})_2]_2(\mu\text{-N}_2)$ with SiH_4 , the initial product isolated in 59% yield was $\text{Mo}(\text{CO})(\eta^2\text{-H-SiH}_3)(\text{depe})_2$ (**1-3d**; crystallographically characterized). This σ -complex, when dissolved in tol-d_8 , is partially converted to its seven-coordinate tautomer, the OA complex $\text{Mo}(\text{CO})(\text{H})(\text{SiH}_3)(\text{depe})_2$ (**1-3e**) (see Table 1, structure section). The $K_{\text{eq}} = 1$ at 288 K for the two forms, and there is almost no free energy difference between the σ -complex and the silyl hydride at rt. The $\eta^2\text{-SiH}_4$ tautomer exhibited 4 singlet $^{31}\text{P}\{^1\text{H}\}$ NMR resonances (δ 39–67) at room temperature and an additional 4 singlet ^{31}P resonances (δ 35–83) at -45°C due to freezing of the fluxional OA isomer (**1-3e**). The OA tautomer was studied only in solution, and the only other spectroscopic comparison that can be made for these two forms is the $^1\text{H}\{^{31}\text{P}\}$ NMR data: for **1-3d**, δ 4.56 (s, $^1J_{\text{SiH}} = 164$ Hz, SiH_3 , η^2), -8.23 (s, $^1J_{\text{SiH}} = 35$ Hz, $\text{Mo}(\eta^2\text{-SiH})$), and for **1-3e**, δ 3.48 (s, $^1J_{\text{SiH}} = 143$ Hz, SiH_3), -7.57 (s, MoH). The major difference between the two forms is the $^1J_{\text{SiH}}$ coupling constant, which highlights the importance of such data in terms of the interpretation of the interaction between the silane and the metal center. Another example of one of the complexes prepared in the same study was $\text{Mo}(\text{CO})(\eta^2\text{-H-SiHPh}_2)(\text{depe})_2$, **2-13**, which was also crystallographically characterized. This complex also exhibited 4 ^{31}P NMR resonances, each of which was a ddd (δ , 34.5–60.5) and in a similar range as observed for the $\eta^2\text{-H-SiH}_3$ form, **1-3d**. The $^1\text{H}\{^{31}\text{P}\}$ NMR spectrum exhibited a resonance at δ 6.78 (d, $^1J_{\text{SiH}} = 172$, SiH) and at -7.57 (d, $^1J_{\text{SiH}} = 50.6$, $\text{Mo}(\eta^2\text{-H-Si})$). In addition, the IR spectrum exhibited a ν_{SiH} above 2000 cm^{-1} and a $\nu_{\text{Mo-H-Si}}$ absorption shifted to lower energy (near $1700\text{--}1750\text{ cm}^{-1}$) and was consistent with the interpretation of an η^2 -interaction for **1-3d** and **2-13**. The authors also reported DFT calculations with B3LYP functional for $\text{Mo}(\text{CO})(\text{L})(\text{dhpe})_2$ as a model [dhpe = $\text{H}_2\text{PCH}_2\text{CH}_2\text{PH}_2$; L = SiH_4 and $\text{Vin}_x\text{SiH}_{4-x}$ ($x = 1, 2, 3$; Vin used as a model for the Ph group)]. Three isomers were assumed: **a** (HSi *trans* to a P center), **b** (7-coordinate OA product with H and Si abutting a P ligand), and **c** (HSi *trans* to the CO) (Figure 6). The Mo–Si and Mo–H distances were similar for isomers **a** and **b**, but longer Mo–Si and Mo–H distances were computed for **c**. Isomer **a** was

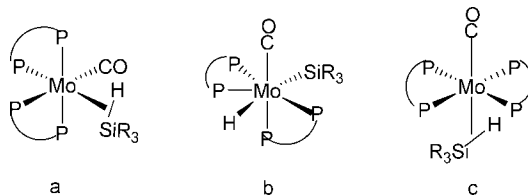


Figure 6. Models used in computational studies for **1-3d** and **2-13**.^{21b}

described as an arrested intermediate at an advanced stage of OA, and **c** was described as an arrested intermediate at an early stage of the OA path. In the family of complexes, isomer **a** appeared to be the most stable, although H_2SiVin_2 (surrogate for H_2SiPh_2) was an exception. The authors reported reactions of depe and dppe complexes with SiH_4 , primary silanes, and the secondary silane Ph_2SiH_2 , although this last silane reacted only with the depe complex, indicating possible steric hindrance to the formation of σ -complexes in this system. The study demonstrated several other points, three of which are included here. Electron-rich phosphines (alkyl vs aryl) increase back-donation to the $\eta^2\text{-H-Si}$, which results in a decrease in the value of the $^1J_{\text{SiH}}$ coupling constant (complex is further along the OA pathway). Replacing a Si–H with Si–R (a more electron-donating substituent) decreases the Si–H activation and favors the $\eta^2\text{-H-Si}$ form (suggested by the increase in the value of $^1J_{\text{SiH}}$ from $\eta^2\text{-H-SiH}_3$ to the $\eta^2\text{-H-SiPh}_2\text{H}$ complexes as described earlier). This is also reflected in the interpretation of Mo–H and Si–H distances in complexes with different silanes (successful structural characterization combined with observation of the appropriate hydrogens is necessary). A longer Mo–H distance (2.04(2) Å) was observed for $(\text{depe})_2\text{-Mo}(\text{CO})(\eta^2\text{-HSiPh}_2\text{H})$, **2-13**, signaling a less activated SiH bond consistent with a σ -ligand. The Mo–H distance in the $\eta^2\text{-HSiPh}_2\text{H}$ complex (fewer electron-donating substituents than in **2-13**) was 1.70(5) Å, which was more similar to a classical Mo–H (greater activation of the SiH bond).^{459a} The Si–H_{Mo} distance of 1.77(6) Å was longer than the uncoordinated Si–H (1.42(6) Å), also signaling a higher degree of Si–H activation in the $\eta^2\text{-HSiPh}_2\text{H}$ complex. Lastly, the ease of OA of σ -bonds in the study was found to be $\text{Ge-H} > \text{Si-H} \approx \text{H-H} \gg \text{C-H}$.^{21b} The only other case where an equilibrium between the σ -complex and the OA form has been proposed was for the dimer, $[\text{Cp}^*\text{Ru}(\text{CO})]_2(\mu\text{-}\eta^2\text{-HSi}^t\text{Bu}_2)(\text{H})$.^{459b}

5.3.2. $\text{Tp}(\text{PPh}_3)\text{Ru}''\text{H}_2\text{SiR}_3''$ [$\text{Tp} = \text{hydridotris}(\text{pyrazolyl})\text{borate}$]: $\text{Ru}(\eta^2\text{-H}_2)$ or $\text{Ru}(\eta^2\text{-H-Si})$?^{48a}

The reaction of $\text{Tp}(\text{PPh}_3)\text{RuH}(\text{CH}_3\text{CN})$ with hydrosilanes (3 tertiary silanes including **3-103**, 2 secondary silanes including **2-37**, and 1 primary silane, **1-40**) produced complexes formulated as $\text{Tp}(\text{Ph}_3\text{P})\text{Ru}''\text{H}_2\text{SiR}_3''$ that could be considered to be either an $\eta^2\text{-H}_2$ or an $\eta^2\text{-H-Si}$ complex. No X-ray structures were obtained; thus, the nature of the interaction of “ H_2SiR_3 ” had to be deduced by indirect means. All the hydride signals in the ^1H NMR spectra of the six complexes are flanked by ^{29}Si satellites, indicating an interaction of the hydrides with the Si center. The terminal SiH in the complexes derived from the secondary and primary silanes gave $J_{(\text{SiH})}$ values from 188 to 202 Hz. All the complexes are fluxional down to -100°C , and the remaining $J_{(\text{SiH})}$ values range from 23 to 53 Hz. These values, although low, suggested the presence of an η^2 -silane. Thus, an assignment of a hydrido- η^2 -silane, $\text{Tp}(\text{Ph}_3\text{P})(\text{H})\text{Ru}(\eta^2\text{-HSiR}_3)$, was favored rather than an $\eta^2\text{-H}_2$ structure, Tp-

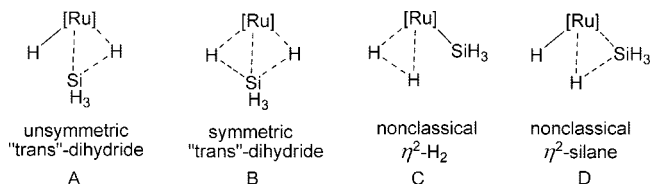


Figure 7. Isomeric structures considered in the ab initio study of $\text{Tp}(\text{Ph}_3\text{P})\text{Ru}(\text{H})_2\text{SiR}_3$.^{48a}

$(\text{Ph}_3\text{P})\text{Ru}(\eta^2\text{-H}_2)(\text{SiR}_3)$. Since the hydride signals did not decoalesce down to -100°C , it was concluded that the fluxionality, attributed to the equilibrium $\text{Tp}(\text{Ph}_3\text{P})\text{Ru}(\text{H}_a)(\eta^2\text{-H}_b\text{SiR}_3) \rightleftharpoons \text{Tp}(\text{Ph}_3\text{P})\text{Ru}(\text{H}_b)(\eta^2\text{-H}_a\text{SiR}_3)$, contributed to the averaging of the J_{SiH} values (average of the J_{SiH} for the $\eta^2\text{-H-Si}$ unit and that of the coupling between the silicon and the hydrogen not involved in the 3-centered bond) and giving rise to the lower numbers that were measured (the influence of fluxional processes on J_{SiH} values will be discussed further in section 6). The IR measurements showed weak $\nu_{\text{SiH}(\text{term})}$ bands from 2136 to 2194 cm^{-1} (3 peaks), whereas the weak ν_{RuH} values fell between 2029 and 2082 cm^{-1} (6 peaks), and these appear to be high for a nonclassical interaction and may be misassigned.

Ab initio calculations at the B3LYP level were performed on the four possible isomeric structures shown in Figure 7. The lowest energy structure was found to be the “trans-dihydride” isomer A. The two Si to H lengths in $\text{Si}\cdots\text{H-Mo}$ in the optimized structure were 2.108 and 1.823 Å, with the latter value consistent with a nonclassical η^2 -silane coordination. The Ru–H distance of 1.629 Å associated with the shorter Si to H distance in the unit $\text{Si}\cdots\text{H-Ru}$ indicated a weaker interaction than the second H–Ru with a length of 1.610 Å. The geometry optimization of C gave D with a $\text{H}\cdots\text{H}$ distance of 1.707 Å and a $\text{Si}\cdots\text{H}$ distance of 1.765 Å. The D and A forms differ by 1.9 kcal/mol, and the two are related by an $\sim 180^\circ$ rotation of the η^2 -silane ligand. This relatively simple “polyhydride” case illustrates some of the difficulty in the interpretation of the role of the hydrides, i.e., whether, in this case, the two hydrides play the same role in the complex or whether they each play a different role. This same question will appear in a later case study where there are more than two hydrides whose role needs to be determined.

T_1 measurements taken at room temperature for the six reported $\text{TpRu}(\text{PPh}_3)(\text{H}_2\text{SiR}_3)$ complexes indicated that the values for the hydride signals did not correspond to those of nonclassical η^2 -dihydrogen complexes. The use of T_1 measurements in other polyhydride complexes has also been reported. For the complex $[\text{MoH}_3\{[\text{Ph}_2\text{PCH}_2\text{CH}_2\text{P}(\text{Ph})\text{C}_6\text{H}_4\text{-}o]_2\text{Si-P,P,P,P,Si}\}]$ (**1-26**), the hydrides were observed in the ^1H NMR spectrum but were not located in the X-ray structure. T_1 measurements at rt were consistent with a classical polyhydride.^{37b} The fluxional hydride positions in the unusual pentahydridoosmiumsilylene complex, **1-51**, prompted acquisition of T_1 measurements that showed that the $T_{1(\text{min})}$ values were typical of polyhydrides with no short $\text{H}\cdots\text{H}$ contacts.⁵⁰ The absence of nonclassical $\text{H}\cdots\text{H}$ interactions in the closely related series $(\text{Me}_3\text{P})_3(\text{H})_3\text{RuSiMe}_3$, **3-120**,⁹⁷ $(\text{PPh}_3)_3\text{H}_3\text{Ru}(\text{SiMeCl}_2)$, **3-124**,²⁰⁶ $(\text{Ph}_3\text{P})_2\text{H}_3\text{Os}(\text{SiMe}_3)(\text{CO})$, **3-152**,²²² $(\text{Ph}_3\text{P})_3\text{H}_3\text{Os}(\text{Si}\{\text{OCH}_2\text{CH}_2\}_3\text{N})$, **3-160**,²²¹ and $(\text{Tp}^{\text{Me}_2})\text{H}_3\text{IrSiEt}_3$, **3-242a**,^{264a} was also supported by T_1 measurements. Only in the case of $\text{RuH}_2(\eta^2\text{-H}_2)(\eta^2\text{-H-SiMe}_2\text{Cl})(\text{PCy}_3)_2$, **3-125a**,^{207a} where all five hydrides are fluxional down to 193 K was the measured T_1 value small.

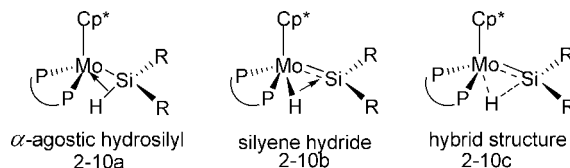


Figure 8. Three of the five proposed representations of complex **2-10**.^{36a}

5.3.3. $[\text{Cp}(\text{Me}_3\text{P})_2\text{Ru}(\eta^2\text{-H-SiCl}_3)]^+[\text{BAR}^f_4]$, Ru–H, or $\eta^2\text{-H-Si}$ and the Role of the $^2J_{(\text{SiH})}$ Coupling Constant¹⁸²

When the complex $[\text{Cp}(\text{Me}_3\text{P})_2\text{Ru}(\text{SiCl}_3)]$ was protonated with $[\text{H}(\text{OEt}_2)_2]\text{BAR}^f_4$, a complex formulated as $[\text{Cp}(\text{Me}_3\text{P})_2\text{Ru}(\eta^2\text{-H-SiCl}_3)]\text{BAR}^f_4$ (**3-80**) was isolated and characterized by X-ray crystallography and multinuclear NMR spectroscopy.¹⁸² The hydride was located with $\text{Ru-H} = 1.60(5)$ Å (similar to distances observed in terminal Ru–H bonds) and the $\text{Si-H} = 1.77(5)$ Å. The key spectroscopic parameter was the Ru–H resonance at -9.87 ppm (t) which was assigned to $\text{Ru-H}\cdots\text{Si}$, with a $^2J_{(\text{SiH})} = 48$ Hz. Another feature of **3-80** was an elongated Ru–Si bond (2.329(1) Å) relative to Ru–Si (2.265(2) Å)⁴⁶² in the starting neutral complex, $\text{Cp}(\text{Me}_3\text{P})_2\text{RuSiCl}_3$, in addition to average Si–Cl distances shorter than those in the starting material. No IR data, calculations, or ^{29}Si NMR data were reported. However, the bonding was described in terms of a lowest unoccupied molecular orbital (LUMO) of the $\text{Cp}(\text{Me}_3\text{P})_2\text{Ru}^+$ fragment (primarily a Ru d_{z^2} orbital) interacting with the $\sigma(\text{Si-H})$ orbital of HSiCl_3 and a HOMO (primarily Ru d_{yz} of $\text{Cp}(\text{Me}_3\text{P})_2\text{Ru}^+$) interacting with the $\sigma^*(\text{Si-H})$ of HSiCl_3 . Both of these interactions would lead to the lengthening of the Si–H bond (observed). Protonation of $[\text{Cp}(\text{Me}_3\text{P})_2\text{Ru}(\text{SiCl}_3)]$ may be viewed as leading to a “normal” Ru–H but a long Si–H bond and forming Ru(IV). The weakening of the back-bonding from Ru(IV) to HSiCl_3 results in a shortening of the Si–Cl bonds in **3-80**. The authors concluded that the structure of **3-80** could be a model for a later stage of OA of a hydrosilane to a transition metal.

5.3.4. $\text{Cp}^*(\text{dmpe})\text{Mo}(\text{H})(\text{SiR}_2)$, ($\text{R} = \text{Et}$, **2-10**): What Is the Role of the Hydride?³⁶

When secondary silanes were added to the 18e complex, $\text{Cp}^*(\text{dmpe})\text{Mo}(\eta^3\text{-CH}_2\text{Ph})$, colorful complexes formulated as $\text{Cp}^*(\text{dmpe})\text{Mo}(\text{H})(\text{SiR}_2)$ (four examples) were produced.^{36a} The complexes with $\text{SiR}_2 = \text{SiMe}_2$ and SiEt_2 (**2-10**) were both characterized by X-ray crystallography and the SiEt_2 complex was characterized also by neutron diffraction. In addition, ^{13}C , ^{31}P , ^{29}Si NMR, and IR data were reported and ^1H NMR data were recorded at both rt and low temperature. The ^{29}Si NMR spectrum provided a key piece of data in the downfield-shifted Si resonance in the region that is associated with a silylene complex, which in turn infers that the hydride is located on Mo. The X-ray structure of the SiMe_2 derivative exhibited a short Mo–Si distance of 2.315(2) Å, but the hydride was not located. The silicon center was planar in the solid state, consistent with an sp^2 -Si center. The observed J_{SiH} values fell between 30 and 48 Hz for the four complexes and suggested a weak $\text{Mo-H}\cdots\text{Si}$ bonding interaction. Curiously, no stretching frequencies that could be assigned to Mo–H were observed in the IR spectra. Since the role of the hydride was ambiguous, five possible representations were considered for the complex. One of the five structures would be described as an α -agostic hydrosilyl complex with a “formal” Si–H bond (Figure 8, **2-10a**) (this would be

inconsistent with planarity at the silicon center), and a second structure featured a silylene hydride complex where the hydride donates electron density to the electrophilic silylene center (Figure 8, **2-10b**) (probably the most important of the structures considered). A hybrid of these two structures was also proposed (Figure 8, **2-10c**). The actual structure has mirror symmetry, which led the authors to conclude that “the hydride is disordered over bridging positions on both sides of the Mo–Si bond and that the C, P, Mo, and Si conform to the crystallographically imposed mirror symmetry”.

In the X-ray structure of Mo(H)=SiEt₂ (**2-10**), the hydride was located and refined and appeared to be consistent with the “hybrid” structure. More important, however, was a neutron diffraction study that provided the following parameters, ND (X-ray for comparison): Mo–H, 1.847(12) Å (1.809 Å); Si–H, 1.683(13) Å (1.738 Å); Mo–Si, 2.343(10) Å (2.348(7)).^{36a} In this case, there was no mirror symmetry and the structure that was observed was close to that of the composite structure **2-10c**. The values obtained from the ND study indicated a Mo–H separation that was ~15 pm longer than those observed in the structure of Cp₂MoH₂,⁴⁶³ whereas the Si–H separation was ~20 pm longer than the average value observed in hydrosilanes, leading to the conclusion that the Mo–H was interacting with the silicon center, forming a bridging hydride.

5.3.5. [RuH₂(η²-HSiMe₂)₂X](PCy₃)₂] (X = C₆H₄, **3-127**)^{208,209} and RuH₃(SiMeCl₂)(PPh₃)₃, **3-124**.²⁰⁶ Interpreting Longer-Range Ru–H···Si Interactions

Several complexes have been prepared by reaction of chelating disilyl systems, HSiMe₂XMe₂H, with RuH₂(H₂)₂(PCy₃)₂ of which X = C₆H₄ and O appear to be the earliest examples.^{208,209} The complexes, [(Cy₃P)₂(H)₂Ru{η²-HSiMe₂)₂C₆H₄}], **3-127** (crystallographically characterized), and [(Cy₃P)₂(H)₂Ru{(η²-HSiMe₂)₂O}], **3-128**, were unusual in that the bulky phosphines occupied *cis*-positions and the η²-H–Si groups of the bis-silane derivative spanned *trans*-positions (angles > 170°) in a pseudo-octahedral environment about the Ru(II) center. These were the first two complexes that contained two H–Si, η²-coordinated to a metal center. Two types of hydride signals were observed in the ¹H NMR spectrum of **3-127** at room temperature, and these signals coalesced when the sample was heated. *T*₁ measurements ruled out an (η²-H₂) ligand in **3-127**. The *J*_{SiH} was obtained from the ²⁹Si{³¹P} NMR spectrum, and the value of 63 Hz is in the range expected for an η²-SiH bond. Consistent with the η²-formulation were Si–H bond distances of 1.88(3) and 1.83(3) Å, which demonstrate activation of the Si–H bond. The four Ru–H bonds were equal within experimental error [1.60(3)–1.67(3)]. Also present in the complex were RuH_{term}···Si distances of 2.22(2), 2.21(2), 2.18(2), and 2.12(2), which were longer than any σ-interactions. The IR spectrum showed two Ru–H stretching vibrations at 2045 and 1969 cm^{−1} and an Ru–(η²-SiH) with a broad band at 1699 cm^{−1} (distinctly red-shifted). In a later report that contained many more examples of chelating bis-silyl ligands, the results were complemented by DFT studies. Three isomers of the model complex RuH₂(PH₃)₂{(η²-HSiH₂)₂C₆H₄} were calculated, and the isomer observed that was most stable exhibited C_{2v} symmetry and resembled the crystal structure of **3-127**. The X-ray data and the theoretical calculations illustrate that the “nonbonding” H···Si interactions control the *cis* geometry observed for the bulky phosphine ligands.²⁰⁸ Later, the importance of secondary

interactions between the silicon centers and all hydrogen atoms in the coordination sphere of the metal in determining the stability of the complexes was recognized, and the term SISHA (secondary interactions between silicon and hydrogen) was coined for these long Si···H contacts. This term has been used to characterize distances in the range 2.0–2.5 Å.³⁹⁸

For **3-124**, (Ph₃P)₃H₃Ru(SiMeCl₂), the up-field signals for the ruthenium hydrides were observed as a singlet with ²⁹Si satellites (averaged *J*_{SiH} = 40 Hz). The hydrides were located in the crystal structure and the Ru–H distances were 1.54(2), 1.59(2), and 1.68(3), whereas the Si···H distances were 1.86(2), 1.94(2), 1.94(3), somewhat shorter than those observed in **3-127** (and related complexes).²⁰⁶ Although the authors interpreted the data in terms of IHI interactions, the data could also be described in terms of a SISHA assignment.⁴⁵²

5.3.6. Cp₂Nb(H)(SiMe₂H)(SiMe₂Cl): IHI, Another Interpretation of Long-Range Interactions, The Role of Calculations, and Persistence of Interactions in Solution^{356a}

An additional class of compounds that exhibited a M–H···Si interaction involved primarily group V transition metal hydrides that also contain silyl groups with halide substituents. These types of complexes have been studied and identified primarily by Nikonov and coworkers and have been described in detail in recent reviews.^{5a,c,f} The key feature was the interaction of the hydridic hydrogen of Nb–H with an electrophilic Si center forming a hypervalent silyl group, leading to the descriptor, IHI or interligand hypervalent interaction.

The structure of Cp₂Nb(H)(SiMe₂H)(SiMe₂Cl) (prepared by reaction of Cp₂NbH(SiMe₂H)₂ with HCl) has been determined by combined X-ray/neutron diffraction analysis and provided more reliable TM–H and TM–H···Si distances.^{356a} In this complex, the SiMe₂H group was rotationally disordered. The niobium hydride was located symmetrically between the two silicon centers and was approximately *trans* to the Si–Cl bond. The important overall structural observations included: (i) an elongated Nb–H bond; (ii) the Nb distance to the SiMe₂H group was longer than that to the SiMe₂Cl group; (iii) the Si–Cl was 8% longer than found in noncoordinated organochlorosilanes; and (iv) the Nb–H···Si distance to the SiMe₂Cl group was shorter than that to the SiMe₂H group. These features would be present if the Nb–H bond orbital interacts with the Si–Cl* antibonding orbital. Such an interaction would result in a longer Si–X bond, a shortened M–Si bond, an elongated M–H, and a shorter Si–H contact. The X-ray structures of Cp₂Nb(H)(SiMe₂H)(SiMe₂X) (X = F, Br) were also reported (both disordered); however, a stronger interaction of the hydride with the bromosilyl group was observed. A good agreement between the calculated DFT structures and observed structures was obtained. With increasing IHI, the Nb–H bond elongates and becomes weaker as shown by a decrease in the Wiberg bond indices (WBI) and NBO bond orders (BO) down the halogen group and the XMe₂Si···H interaction becomes stronger progressing from Cl to I.

The complex Cp₂Nb(H)(SiMe₂Cl)₂, **3-16**, has also been characterized by neutron diffraction (ND) and by X-ray diffraction.^{145a} In this case, the Nb–H and NbH···Si distances determined by neutron diffraction were 1.816(8) and 2.076(3) Å compared to 1.74(7) and 2.056 Å, respectively, determined

by X-ray diffraction. Thus, the distances determined by X-ray analysis were shorter than those determined by ND. The Nb–H distance was also determined by NMR relaxation data, and the value obtained [1.78(1) Å] was in reasonable agreement with the neutron structure and with the DFT calculation [for the model complex, $\text{Cp}_2\text{Nb}(\text{H})(\text{SiH}_2\text{Cl})_2$]¹⁴² and indicated that the NbH \cdots Si interaction persisted in solution.

The cases just described in the previous paragraphs were selected to demonstrate the importance of the interplay of characterization methods in assigning a structure to nonclassical complexes. In the next subsection, 5.4, Si–H \cdots TM interactions are presented in the following order: (section 5.4.1) σ -complexes and (section 5.4.2) α -, β -, and other long-range agostic interactions. In the section following, 5.5, M–H \cdots Si interactions are described in the following order: (section 5.5.1) IHI, (section 5.5.2) SISHA, (section 5.5.3) hydrides that span M–Si multiple bonds. Finally, in section 5.6 are unclassified examples that were difficult to fit in terms of the complexes found in sections 5.4.1–5.5.3.

5.4. Complexes with Si–H \cdots TM Interactions

5.4.1. σ -Complexes

Since the first recognized σ -interaction was reported by Graham and co-workers in 1969 for the product formed when $\text{Re}_2(\text{CO})_{10}$ reacted with Ph_2SiH_2 ,⁴⁶⁴ the number of σ -complexes reported (or proposed) has increased significantly. There are ~ 75 examples (covering the current review period) shown in Table 9 when the related derivatives given in the footnotes are included. In the discussion that follows, the σ -complexes have been divided into mononuclear derivatives and dinuclear complexes. Of the total entries under σ -complexes, about one-third have been characterized by X-ray diffraction, but for 7 of the 24 complexes (3 mononuclear and the remainder dinuclear complexes), the hydrides were either not located, not refined, or placed in idealized positions, or disorder precluded their placement. For all but three examples listed under σ -complexes in Table 9, ^1H NMR data were recorded; the three exceptions (**3-29**, **3-36**, **3-49**) were from a study specifically directed at femtosecond infrared studies.^{83a} In many cases, the assignment as a σ -complex hinges on the value of the J_{SiH} coupling constant. However, in some complexes, coupling constants cannot be obtained, and this was especially true for **1-13**,²⁸ **3-62**,¹⁷¹ and **3-259**,²⁷⁸ complexes that were not isolated and decomposed in solution. For the manganese complex, **3-57**,¹⁶⁸ J_{SiH} could not be determined due to the quadrupolar nucleus of the metal.

Another aspect that clouds the determination of the value of J_{SiH} is the observation of exchange processes that provide an averaged value for J_{HSi} . Such exchange processes occur at room temperature for the mononuclear complexes **1-3d**,^{21b} **1-36**,⁴⁴ **1-40**,^{48a} **2-37**,^{48a} and **3-103**.^{48a} For **1-3**, the exchange process involved an equilibrium between the $\eta^2\text{-H-Si}$ form and the OA form. For **1-40**, **2-37**, and **3-103**, the exchange occurred between the hydride on the metal and the hydrogen engaged in the $\eta^2\text{-H-Si}$ interaction. If these 10 complexes are excluded, the $^1J_{\text{SiH}}$ values measured at room temperature and listed in Table 9 generally fall within the range of 48–66 Hz (4 values) with one value at 95 Hz. Schubert's original proposal was that a J_{SiH} value >20 Hz should indicate a direct H–Si interaction of the silane with the metal center.⁴ However, Lachaize and Sabo-Etienne have recently sug-

gested that the lower limit for a “secure criterion of a $\sigma\text{-Si-H}$ ” bond should be set at 65 Hz, although this was in the context of ruthenium complexes.⁴⁵²

Interpretation of J_{SiH} values is somewhat more of a problem. As shown in Figure 5, there is more than one view of the interaction of a Si–H with the metal. In Figure 5a, the Si–H donates to a metal center (characterized by $^1J_{\text{SiH}}$), whereas in Figure 5b, the M–H donates to the silicon center (characterized by $^2J_{\text{SiH}}$). Nikonov has recently discussed the dilemma associated with an observed J_{SiH} .^{20b} The observed coupling constant may be considered the sum of a one-bond coupling (Figure 5a) and a two-bond coupling (Figure 5b): $J_{\text{SiH}}^{\text{obs}} = ^1J_{\text{SiH}} + ^2J_{\text{SiH}}$. The signs of each of these coupling constants then will determine both the magnitude and the sign of the observed coupling constant. Since the $^1J_{\text{SiH}}$ is negative and $^2J_{\text{SiH}}$ can be either positive or negative,⁴⁶⁵ the relative values of both 1J and 2J coupling constants as well as their sign will determine the magnitude of the observed J_{SiH} . Additionally, the substituents can cause a variation in the “s” and “p” character of the hybrid orbitals and thus will potentially alter the magnitude and the sign of the coupling constant. A negative value of $^1J_{\text{SiH}}$ should be indicative of a Si–H interaction, but if $^2J_{\text{SiH}}$ is positive, the observed J_{SiH} could be small (or smaller than Schubert's proposed 20 Hz “cutoff”). The sign on the J_{SiH} coupling constant is rarely measured in silyl–metal systems where there is a proposed σ - or agostic interaction. One of the rare cases was reported for derivatives of $\text{Cp}_2\text{Ti}(\text{PMe}_3)(\text{H})\text{SiR}_3$, and of the five complexes discussed, it was possible to determine the sign of J_{SiH} for only two ($\text{R}_3 = \text{SiMeCl}_2$ and SiCl_3). The problems associated with interpretation of the observed J_{SiH} are also discussed briefly by Lachaize and Sabo-Etienne in their review of σ -silane ruthenium complexes.⁴⁵²

For dinuclear σ -complexes, a common but not exclusive structural motif contains a hydride that bridges a Si and a TM center on the longer of two (opposite) sides of an approximate parallelogram. The majority of these cases come from the Ni triad and contain one phosphine ligand per metal [Pd: **2-79a**, **2-80**, **2-81**, **2-82**, **2-83** (+5 related examples in the footnotes)]; Pt: **1-73**, **1-77**, **1-78**, **2-96bcde**, **2-98**, **2-99**, **2-100**, **2-101**, **2-102a**; PdPt: **3-260a**, or three phosphine ligands per two metal centers [Pd: **2-79a**; Pt: **1-72**, **2-103**, **2-104** (plus related examples in the footnotes)]; PtPd: **3-260b**. Complexes containing the $[\text{TM-PR}_3]_2$ unit listed in Table 9 are generally nonfluxional except for **1-78**, but those that contain the unit $[(\text{R}_3\text{P})_2\text{TMTM}(\text{PR}_3)]$ are fluxional at room temperature by a process that is believed to be initiated through dissociation of a phosphine from the $(\text{R}_3\text{P})_2\text{TM}$ center and reattachment of the phosphine at the other TM center.^{121a}

Of the 40 dinuclear, Ni triad complexes listed in Table 4 plus the additional complexes given in the footnotes, only 9 examples have values reported for J_{SiH} . The fluxional complex, **2-79a** $[(\text{Me}_3\text{P})\text{Pd}](\mu\text{-}\eta^2\text{-H-SiPh}_2)[\text{Pd}(\text{PMe}_3)_2]$, gave an averaged $^1J_{\text{SiH}}$ value at room temperature of 79 Hz compared to 84 and 86 Hz at -90°C .^{121a,b} The complex **3-260b**²⁷⁹ appears to be a unique case where the Pd–H–Si unit could be identified with a $^1J_{\text{SiH}} = 28$ Hz at room temperature but the spectrum did not exhibit a signal that corresponded to a hydrogen for Si–H–Pt; however, the deuterium analogue, **3-260b-d**₂, was consistent with the presence of both Si–D–Pd and Si–D–Pt. The broadening of the $^31\text{P}\{^1\text{H}\}$ NMR signal suggested partial dissociation or intramolecular exchange of the phosphine ligands, which

Table 9. Complexes with Nonclassical Interactions[†]

compound	NMR data, ^l MH, (J)	NMR data, ^l SiH, J	X-ray MH	X-ray SiH	calc.	IR, cm ⁻¹ 2	ref
Si-H...M							
σ -complexes (monometallic)							
Ti triad							
*1-13 Cp ₂ (Me ₃ P)Ti-(η^2 -H-SiPhH ₂) ³	-55 °C -4.02 (d) Ti(η^2 -H-Si) -80 °C -4.99 (br, s) -6.78 (br s)	-55 °C 5.70 (br s) (SiH ₂) -80 °C 5.13 (br, s) 5.11 (br, s)					28
*1-14a Cp ₂ Ti(η^2 -H-SiH ₂ Ph)-(η^2 -H-Bcat-4-'Bu)					2051, 2095 (ν SiH ₂)		29a
1-14b (dmpe) ₂ Ti(Si ₃ H ₅ Ph ₃)	Ti...HSi 4.75 (td) ² J _{HH} = 14 4.50 (dd) ² J _{HH} = 15, 14	Si-H 6.35 (d) ² J _{HH} = 14 6.25 (d) ² J _{HH} = 15 3.27 (d)				1754-1863 (ν Ti-H-Si and Ti-H-B)	29b
*1-14c (dmpe) ₂ Ti(Si ₄ H ₆ Ph ₄)	Ti...H ^{1A} -Si ¹⁴ 4.27 (dd) J _{SiH} = <40 Ti...H ^{3A} -Si ³ 4.19 (dd) J _{SiH} = <40	Si ¹ -H ^{1B} 6.57 (d) J _{SiH} = 127 Si ³ -H ^{3B} 6.31 (d) J _{SiH} = 133 Si ⁴ -H ^{4A} 4.95 (d) J _{SiH} = 186 Si ⁴ -H ^{4B} 4.50 (d) J _{SiH} = 189	Ti...H ^{1A} 1.67(2) Ti...H ^{3A} 1.68(2)	Si ¹ -H ^{1A} 1.83(2) Si ¹ -H ^{1B} 1.54(3) Si ³ -H ^{3A} 1.83(2) Si ³ -H ^{3B} 1.54(3) Si ⁴ -H ^{4A} 1.46(4) Si ⁴ -H ^{4B} 1.45(3)			29b
Cr triad							
1-3d (OC)(depe) ₂ Mo-(η^2 -SiH ₄) ⁵	-5 °C -8.23 (s) J _{SiH} = 35 (Mo-H-Si) ⁵ -7.57 (s) (Mo-H, OA) ⁵	-5 °C 4.56 (s) ¹ J _{SiH} = 164 (SiH ₃ , η^2) ⁵ 3.48 (s) ¹ J _{SiH} = 143 (SiH ₃ , OA) ⁵			Y	2047 ^a 1995 1972 (ν SiH) 1732 ^a (ν Mo-H-Si)	21b
3-28 (η^6 -C ₆ H ₆)(OC) ₂ Cr-(η^2 -H-SiEt ₃)						6	152
3-29 (OC) ₅ Cr(η^2 -H-SiEt ₃) ^{7,8}	-33 °C -13.58 J _{SiH} = 95.2					9	83, 81
2-8 (OC) ₅ Cr(η^2 -H-SiPh ₂ H)	-33 °C -11.17 J _{SiH} = 108 (Cr-H-Si)	-33 °C 6.02 J _{SiH} = 234 (Cr-Si-H)					81
2-12 (OC) ₅ Mo(η^2 -H-SiPh ₂ H) ¹⁰	-88 -6.49 J _{SiH} = 111 (Mo-H-Si)	-88 6.04 J _{SiH} = 232 (Mo-Si-H)					81
3-36 (OC) ₅ Mo(η^2 -H-SiEt ₃) ⁸	-33 °C -8.36 ¹ J _{SiH} = 96					9	81
*9-1 (OC) ₃ (η^4 -nbd)Mo(η^2 -H-SiPh ₂ H) ¹¹	-5.86 (dd) ² J _{HH} = 5.4 Mo(η^2 -H-Si)	6.12 (dd) ² J _{HH} = 5.4 SiH _{term}					82b
*9-2 (OC) ₃ (η^4 -nbd)(H)Mo-(η^2 -H-SiEt ₂) ¹¹	-9.52 ² J _{SiH} = 93 -7.90 ¹ J _{SiH} = 54						82b
2-13 (OC)(depe) ₂ Mo-(η^2 -H-SiPh ₂ H) ¹²	-7.57 (d) J _{HH} = 8.1 ¹ J _{SiH} = 50.6 Mo(η^2 -H-Si)	6.78 (d) J _{HH} = 8.2 ¹ J _{SiH} = 172 (SiH)	2.04(2)	1.54(6) (SiH _{term}) 1.66(6) (Si-H _b ...Mo)	Y	1752 (ν Ru-H-Si) ^a 2010 (ν Si-H)	21b
2-23 (OC) ₅ W(η^2 -H-SiPh ₂ H) ¹³	-88 °C -6.40 J _{SiH} = 98 (W-H-Si)	-88 °C 6.50 J _{SiH} = 236 (W-Si-H)					81
9-3 [W(μ - η^2 -H-SiEt ₂ H)-(CO) ₅] ¹⁴	-8.05 (d) ¹ J _{WH} = 38 ¹ J _{SiH} = 93	5.10 (dq) ¹ J _{SiH} = 217					87c

Table 9a. Continued

compound	NMR data, ^l MH, (J)	NMR data, ^l SiH, J	X-ray MH	X-ray SiH	calc.	IR, cm ⁻¹ 2	ref
3-49 (OC) ₅ W(η^2 -H-SiR ₃) R = Et ^{7,8}	-33 °C -8.55 <i>J</i> _{SiH} = 86 <i>J</i> _{WH} = 36					⁹	83a
3-51 (OC) ₄ W(η^2 -H-SiMe ₂ CH ₂ CH ₂ PPh ₂) ¹⁵	-8.18 (s, br) ¹⁶ ¹ <i>J</i> _{SiH} = 95 ¹ <i>J</i> _{WH} = 36 W(η^2 -H-Si)						163
2-24b (OC) _x (η^4 -nbd)(H)W- (μ -H-SiEt ₂)	-8.33 (d) ¹ <i>J</i> _{WH} = 52 ¹ <i>J</i> _{SiH} = 29.1 W...HSi -11.47 (d) ¹ <i>J</i> _{WH} = 38.1 WH _{term}						87b
Mn triad							
2-29 (η^5 -C ₅ H ₄ Me)(OC) ₂ - Mn(η^2 -HSiPh ₂ H)	-11.5 (br d) ¹ <i>J</i> _{Mn-H-Si} = 63.5	6.7 (d) ¹ <i>J</i> _{SiH} = 205	1.575(14) ¹⁷	1.806(14) ¹⁷	Y	2032(ν SiH) 1901 (ν MnH)	89a, 89b, 89c, 89d
9-4 (η^5 -C ₅ H ₄ Me)(OC) ₂ Mn- (η^2 -HSiFPh ₂) ¹⁸	-11 (d, br)		1.569(4) (ND) 1.570 (X-ray ¹⁹)	1.802(5) (ND) 1.806 (X-ray ¹⁹)	Y	²⁰ 2105 (ν SiH) ^{d22}	89a, 89b, 89c, 89d
3-54 Cp'(OC) ₂ Mn(η^2 -H-SiPh ₂ SiPh ₂ H) ²¹	-10.71 (s) <i>J</i> _{SiH} = 57 Mn(η^2 -H-Si)	5.69 (s) ¹ <i>J</i> _{SiH} = 173 SiH					166
3-57 [P ₂ (OC) ₃ Mn(η^2 -H-SiEt ₃)] P = P(OCH ₂) ₃ CMe ²³	-60 °C -16.81 (t) Mn(η^2 -H-Si) ²⁴						168
3-60 [(OC) ₅ Re(η^2 -H-SiEt ₃)] ⁺ [B(C ₆ F ₅) ₄] ⁻	-23 °C -10.73 ²⁵ <i>J</i> _{SiH} = 55						81
3-61 [(OC) ₄ (Ph ₃ P)Re(η^2 -H-SiEt ₃)] ⁺ [B(C ₆ F ₅) ₄] ⁻²⁶	-40 °C -8.89 (d) <i>J</i> _{SiH} = 60.9 Re(η^2 -H-Si)						170
3-62 [(OC) ₄ (P)Re(η^2 -H-SiEt ₃)] [BAr _F] P = P(OCH ₂) ₃ CMe ²⁷	0 °C -10.68 (brd) Re(η^2 -H-Si)						171
3-63 [<i>fac</i> -(OC) ₃ (P) ₂ Re(η^2 -H-SiEt ₃)] [BAr _F] P = P(OCH ₂) ₃ CMe	-10.43 (t) <i>J</i> _{SiH} = 66 Re(η^2 -H-Si)					1751 (ν Re-H-Si) ^d	171
Fe triad							
1-36 (¹ PDI)Fe(η^2 -H-SiPhH ₂) ₂	23 °C -6.69 (s, 1H) Fe(η^2 -H-Si) (basal) ²⁸ -40 °C -6.80 (s, 1H) ¹ <i>J</i> _{SiH} = 119 ²⁹ Fe(η^2 -H-Si) (basal) 0.05 (s, 1H) ¹ <i>J</i> _{SiH} = 54 ²⁹ Fe(η^2 -H-Si) (apical)	23 °C (SiH ₂ not assigned) -40 °C 6.11 (s) ¹ <i>J</i> _{SiH} = 220 ³⁰ (SiH ₂ , basal) 2.78 (s) ¹ <i>J</i> _{SiH} = 196 ³⁰ (SiH ₂ , apical)	1.45(3), (Fe-H _{br} -Si; apical) 1.51(3) (Fe-H _{br} -Si; basal)	1.59(2) (Si-H _{br} -Fe; η^2 -basal) 1.82(3) (Si-H _{br} -Fe; η^2 -apical) 1.41(2) 1.39(3) (SiH _{term} , basal) 1.33(2) 1.38(2) (SiH _{term} , apical)			44
1-40 Tp(Ph ₃ P)HRu(η^2 -H-SiPhH ₂)	-10.32 (d, 2H) ¹ <i>J</i> _{SiH} = 27(av) ³² RuH + Ru(η^2 -H-Si)	5.22 (d, 2H) ¹ <i>J</i> _{SiH} = 196			Y	2029 (ν RuH) ^b	48a
2-37 Tp(Ph ₃ P)(H)Ru(η^2 -H-SiEt ₂ H) ³¹	-10.93 (dd, 2H) <i>J</i> _{SiH} = 24(av) ³² (RuH)	4.60 (m, 1H) <i>J</i> _{SiH} = 188 (SiH)			Y	2163 (ν SiH) 2062 (ν Ru-H) ^b 2194 (ν SiH)	48a
3-80 Cp(Me ₃ P) ₂ Ru(η^2 -H-SiCl ₃) ³³	-9.87 (t) ² <i>J</i> _{SiH} = 48 Ru(η^2 -H-Si)		1.60(5)	1.77(5)			182

Table 9b. Continued

compound	NMR data, ^l MH, (J)	NMR data, ^l SiH, J	X-ray MH	X-ray SiH	calc.	IR, cm ⁻¹ 2	ref
3-103 Tp(Ph ₃ P)(H)Ru- (η^2 -H-SiEt ₃) ³⁴	-11.62 (d, 2H) ³⁵ $J_{\text{SiH}} = 23.3$ (RuH) ³²				Y	2044 (ν Ru-H) ^b	48a
3-130a [(Cy ₃ P) ₂ (H) ₂ Ru{ η^4 -H-SiMe ₂ (CH=CHMe)}]	-12.46 (dt, 1H) RuH		1.61(7) 1.64(9) (Ru-H _{term})	1.59(8) (Si-H _{br} -Ru)		1945 (ν Ru-H-Si) ^a	211a
	-9.46 (dt, 1H) RuH		1.74(7) (Ru-H _{br} -Si)				
	-7.74 (s, 1H) $J_{\text{SiH}} = 105$ Ru(η^2 -H-Si)						
Co triad							
1-55ab, 2-52bc, 3-164bc [Cp(L)(H) ₂ Co(SiR ₃)] ⁺³⁶	-12.34 (d, Co*H) (η^2 -HSi) $^1J_{\text{SiH(obs)}} = 29.0$ ³⁷						57c
9-5 [Cp(Me ₃ P)Rh(SiEt ₃)- (η^2 -HSiEt ₃) ⁺ [BAR' ₄] ⁻³⁸ (-60 °C)	-12.39 (dd) $^1J_{\text{RhH}} = 36$ $^1J_{\text{SiH(obs)}} = 28$ $^1J_{\text{SiH(}\eta)} = 56$						239
3-181b [Cp(Me ₃ P)(H) ₂ - Rh(SiPh ₃) ⁺ [BAR' ₄] (-40 °C) ³⁹	-10.04 (dd) $^1J_{\text{RhH}} = 26.8$ ⁴⁰						239
3-182b [Cp*(Me ₃ P)Rh- {C ₆ H ₄ (η^2 -HSiPh ₂)}] ⁺ - [BAR' ₄] ⁻⁴¹	-8.95 (dd, $J_{\text{RhH}} = 28$; $^1J_{\text{SiH}} = 84$)						239
Ni triad							
*1-64 (depe)Ni(η^2 -H-SiH(C ₆ H ₄ SiH ₂) ₂)	-80 °C -6.70 (1H) (Ni-H _{term})	20 °C 2.61 (br s, 5H) 5.67 (t, 1H) $J = 17$	1.47(3)	1.75(3)	Y	1600 (br) ^c (ν Ni...H...Si) ⁴²	65
		-80 °C 4.79 (4H)					
2-77 (dtbpe)Ni(μ -H)SiHAr ₂ Ar = 2,4,6-Me ₃ C ₆ H ₂ ⁴³	-0.17 (t)		1.41(4) Ni-H _{br}	1.92(4) ...H _{br} Si		3041 (w) 1990 (s) 1861 (m)	119
				1.42(4) SiH _{term}			
3-259 [(NN)(Me)Pd(η^2 -H-SiEt ₃)] ⁴⁴	-78 °C -9.87 (s) Pd(η^2 -H-Si)						278
σ -complexes (binuclear)							
Ti triad							
*1-16a [{Cp ₂ Zr(SiH ₂ Ph)} ₂] ²⁺ - [B(C ₆ F ₅) ₄] ₂	-3.38 (s) (Zr...H-Si)	5.80 (s) SiH _{term}				31 [Ti-1(05)]	31
*3-10 [{ η^5 -C ₅ H ₄ (SiMe ₂ H)}- ZrCl ₃] ₂		4.50 (septet)	2.28(3) ⁴⁵	1.47(2)		2066 (ν HSi) ^c	140
Cr triad							
*2-16 [{Mo(μ - η^2 -H-SiEt ₂)(CO) ₄ }] ₂	-30 °C -8.33 (s) $^1J_{\text{SiH}} = 58$ $^2J_{\text{SiH}} = 41$		1.786(5)	1.615(3)		⁴⁶	84
	-8.25 (d) $^1J_{\text{WH}} = 35$ $^1J_{\text{SiH}} = 37$						87c
2-26a [{W(μ - η^2 -H-SiPh ₂ (CO) ₄ }] ₂	-10.39 (d) $^1J_{\text{WH}} = 32$ -7.50 $^1J_{\text{WH}} = 33$ $^1J_{\text{SiH}} = 41$ W(η^2 -H-Si)						87b
2-26b [{W(μ - η^2 -H-SiEt ₂)(CO) ₄ }] ₂	-30 °C -9.31 (s) $^1J_{\text{WH}} = 40$ $^1J_{\text{SiH}} = 34$ -7.26 (m) $J_{\text{SiH}} = 52$ ⁴⁸ W(η^2 -H-Si)		1.78	1.54		(ν CO)	
2-27 (OC) ₃ (ⁱ Pr ₃ P)W(μ -H-SiPh ₂) ₂ W(P ⁱ Pr ₃)- (CO) ₃ (described as agostic)			⁴⁹			1909, 1874, 1977 ^b (unassigned)	40

Table 9c. Continued

compound	NMR data, ^l MH, (J)	NMR data, ^l SiH, J	X-ray MH	X-ray SiH	calc.	IR, cm ⁻¹ 2	ref	
Mn triad								
9-7 Cp'(OC) ₂ Mn(η^2 -H-SiMe ₂ SiMe ₂ H- η^2)Mn-(CO) ₂ Cp' ⁵⁰	−12.85 (s) Mn(η^2 -H−Si)					51	166	
*3-66c (OC) ₈ Re ₂ (μ -H-SiPh ₂)(SiPh ₃)	−9.43 (s) ¹ J _{SiH} = 44 Re(η^2 -H−Si)		1.67(4) Re−H _{br} −Si	1.73(4) Si−H _{br} −Re		52	173	
Fe triad								
2-34 (Cp*Fe) ₂ (μ -H) ₂ (μ - η^2 : η^2 -H ₂ Si ^t Bu ₂) ⁵³	−16.25 (br s, w _{1/2} = 68 Hz, 4H) (Fe−H−Fe + Fe−H−Si) −110 °C −5.28 (s) −27.12 (s) (not assigned)		1.638 ⁵⁴ 1.618 (Fe−H _{br} −Fe) 1.613 1.602 (Fe−H _{br} −Fe) 1.518 (Fe−H _{br} −Si) 1.505 (Fe−H _{br} −Si) 1.512(10) 1.511(10)	1.604 (Si−H _{br} −Fe) 1.637 ⁵⁴ (Si−H _{br} −Fe)		1736 (ν _{Si−H−Fe}) ^c 1105 (ν _{H−Si−H})	93, 94	
*2-36c Fe ₂ (η -H ₂ SiPh ₂)(edt)-(CO) ₂ (dppv)	−14.67 (t) −11.81 (s)			1.625(19) 1.626(19) ⁵⁶		(ν CO)	95c	
1-43 {[Cp*Ru) ₂ (H)(μ -H)-(μ , η^2 -H-SiHexCl)] [μ , η^2 -(ClSi(^t BuNCH=CHN ^t Bu))] } ⁵⁵	−7.17 (d, 1H) ¹ J _{SiH} = 40 Ru(η^2 -H−Si) −12.92 (s, 1H) (RuH) −13.21 (d, 1H) (μ -H) −13.45 (s, 5H) J _{SiH} = 18 RuH −100 °C −13.64 (br, 4H) Ru−H−Si −13.40 (s, 1H) (Ru−H−Ru)					2086 (unassigned) ^b 1841 (br, ν Si−H)	51a	
*9-8 {[Cp*Ru(μ - η^2 : η^2 -H ₂ SiEt ₂) ₂ -(μ -H)][BPh ₄]} ⁵⁷			1.599 Ru ₁ −H−Si ₁ 1.629 Ru ₁ −H−Si ₂ 1.548 Ru ₂ −H−Si ₂ 1.632 Ru ₂ −H−Si ₁ 1.724 Ru ₁ ⋯ H ₁ 1.799 Ru ₂ ⋯ H ₁ 1.67(5) 1.61(6) Ru ₁ −H ₁ −Ru ₂ and Ru ₁ −H ₂ −Ru ₂	1.81(4) Si ₁ −H−Ru ₁ 1.77(3) Si ₂ −H−Ru ₁ 1.78(3) Si ₂ −H−Ru ₂ 1.73(3) Si ₁ −H−Ru ₂				403
*9-9 [(Cp*Ru) ₂ (μ - η^2 -H-SiPh ₂)-{ μ - η^2 -HSiPh(OCOCF ₃)}-(μ -H)(H)] ⁵⁸	−90 °C −14.32 (s, 1H) RuH/Ru or RuH −12.86 (s, 1H) Ru−H−Si −12.46 (s, 1H) Ru−H−Si −11.40 (s, 1H) RuH/Ru or RuH −8.87 (d) J _{SiH} = 36.0 Ru(η^2 -HSi)		1.85(5) 1.96(6) Ru ₂ −H ₁ −Ru ₁ Ru ₂ −H ₂ −Ru ₁ 1.56(4) Ru−H _{br} −Si	1.66(4) Si−H _{br} −Ru		2060 (ν Ru−H) ⁵⁹	453	
*2-42b (CO) ₅ Ru ₂ [Si(<i>p</i> -Tol) ₂ H] ₂ -(μ -dppm)-[μ - η^2 -H−Si(<i>p</i> -Tol) ₂] ⁶⁰		5.91 (d) J _{SiH} = 178.5 (SiH)				1790 (br, ν Ru−H−Si) ^b 2054 (ν SiH)	99	
*2-43b {(OC) ₂ Ru [Si(<i>p</i> - ^t BuC ₆ H ₄) ₂ H]} ₂ (μ -dppm)-[μ - η^2 : η^2 -H ₂ Si(<i>p</i> -Tol) ₂]} ⁶¹	−8.44 (m) Ru(η^2 -HSi)	5.88 (m) (SiH)					99	
2-44 {(OC) ₂ Ru[Si(<i>p</i> -Tol) ₂ H] ₂ }(μ -dppm)-[μ - η^2 : η^2 -H ₂ Si(<i>p</i> -Tol) ₂]	−8.44 ⁶² J _{SiH} = 24.4 Ru(η^2 -HSi)	5.85 (m) J _{SiH} = 177	1.58(9) 1.61(9) (Ru−H _{br} −Si)	1.56(9) 1.57(10) (Si−H _{term}) 1.86(9), 1.88(12) Si−H _{br} −Ru		1863, 1817 (br, ν Ru−H−Si) ^b 2056, 2071 (ν SiH)	99	

Table 9d. Continued

compound	NMR data, ^l MH, (J)	NMR data, ^l SiH, J	X-ray MH	X-ray SiH	calc.	IR, cm ⁻¹ 2	ref
2-45 (Cy ₃ P) ₂ (H) ₂ Ru(SiH ₄)- Ru(H) ₂ (PCy ₃) ₂ ⁶³	23 °C, C ₆ D ₆ −7.89 (pt) <i>J</i> _{SiH} = 36 (av)				Y	1667 ^a (br, <i>ν</i> Ru–H–Si) 1911 (br, <i>ν</i> Ru–H)	100, 101
	20 °C, tol- <i>d</i> ₈ −7.67 (pt, 8H)						
	−80 °C, tol- <i>d</i> ₈ −6.0 (br) ⁶⁴ −8.6 (br)						
9-10 (ⁱ Pr ₃ P) ₂ (H) ₂ Ru(SiH ₄)- Ru(H) ₂ (P ^{<i>i</i>} Pr ₃) ₂ ⁶⁵	−7.75 (pt, 8H)		1.49(2) 1.52(3) (Ru–H _{term})	1.69(3) 1.73(4) (Si–H _{br} –Ru)	Y		100, 101
			1.62(3) 1.62(3) (Ru–H _{br} –Si)				
3-138 {Cp*Ru(<i>μ</i> -H)} ₂ - { <i>μ</i> - <i>η</i> ² : <i>η</i> ² -H–SiMe ₂ - (CH=CH ₂)} ⁶⁶	Tol- <i>d</i> ₈ , 23 °C −14.50 (br, <i>W</i> _{1/2} = 1275, 3H)		1.56(4), (Ru–H _{br} –Si)	1.66(4) (Si–H _{br} –Ru)		1943 (<i>ν</i> Ru–H–Si) ^b	214
	Tol- <i>d</i> ₈ /THF- <i>d</i> ₈ −70 °C −14.54 (s, 1H) (Ru–H _b –Ru) −20.22 (s, 1H) (Ru–H _c –Ru)		1.61(6), 1.67(5), 1.85(5), 1.96(6) (Ru–H _{br} –Ru)				
	−9.28 (s, 1H) <i>J</i> _{SiH} = 36.3 (Ru–H _{br} –Si)						
	THF- <i>d</i> ₈ 23 °C <i>J</i> _{SiH} = 31 (av) ⁶⁷						
	−70 °C <i>J</i> _{SiH} = 54 Ru(<i>η</i> ² -H–Si)						
3-143 [Ru(SiMe ₂ NMe ₂ - SiMe ₂)(CO)(<i>μ</i> - {SiMe ₂ }) ₂ - (<i>μ</i> -Cl)Ru–H ₂ (CO)(PPh ₃)]	−6.37 (d, 2H)		1.66(2) 1.69(2)	1.67(2) 1.56(2)			201
3-144 Ru ₂ H ₂ (<i>μ</i> - <i>η</i> ² : <i>η</i> ² - H ₂ Si(OMe) ₂) ₃ - (PCy ₃) ₂ ⁶⁸	−9.94 (d, 8H) <i>J</i> _{SiH} = 22 (av) ⁶⁹ (Ru–H)		⁷⁰		Y	1703 (br, <i>ν</i> Ru–H–Si) ^a 1899 (br, <i>ν</i> Ru–H) 2022 (br, <i>ν</i> Ru–H)	101
Co triad							
2-69 [(dippe)HRh] ₂ [<i>μ</i> - <i>η</i> ² - H–SiMe ₂] ₂	−11.59 (m, 4H)		1.52 (5) 1.52 (4) Rh–H _{term}	1.67 (5) 1.72 (4) Si–H _{br} –Rh			114
	−64 °C −10.6 (brd s) (Rh–H _{br} •••Si) −12.7 (brd s) (Ru–H _{term})		1.69 (4) 1.70 (4) Rh–H _{br} –Si				
Ni triad							
*2-79a [(Me ₃ P)Pd](<i>μ</i> - <i>η</i> ² -H- SiPh ₂) ₂ [Pd(PMe ₃) ₂]	25 °C: 0.59 (br, 2H) ¹ <i>J</i> _{SiH} = 79 (av)		1.75 1.89	1.56 1.68			121a, 121b
	−90 °C 1.24 (d, 1H) <i>J</i> _{SiH} = 84 −2.34 (t, 1H) <i>J</i> _{SiH} = 86 ⁷¹						
2-80 [(Me ₃ P)Pd] ₂ (<i>μ</i> - <i>η</i> ² -H- SiMePh) ₂ ⁷²	1.07 (br t, 2H)		1.85	1.60			121b

Table 9e. Continued

compound	NMR data, ^l MH, (J)	NMR data, ^l SiH, J	X-ray MH	X-ray SiH	calc.	IR, cm ⁻¹ 2	ref
2-81 [(Me ₃ P)Pd] ₂ (μ-η ² -H-SiPh ₂) ₂	25 °C: 1.77 (s, 2H) ¹ J _{SiH} = 77		1.91	1.75			121a, 121b
2-82 [(Et ₃ P)Pd] ₂ (μ-η ² -H-SiPh ₂) ₂ ⁷⁴	−90 °C: 1.62 (s, 2H) ¹ J _{SiH} = 80 ⁷³ Pd(η ² -H-Si) 1.76 (br d, 2H) Pd(η ² -H-Si) ¹ J _{SiH} = 78		2.04	1.60			121a, 121b
2-83 [(Cy ₃ P)Pd] ₂ (μ-η ² -H-SiPh ₂) ₂ ⁷⁵	2.07 (app t, 2H) Pd(η ² -H-Si)		1.61	1.63			122
1-72 [(Et ₃ P)Pt(μ-η ² -H-Si(Hex){Pt(H)(PEt ₃) ₂ }] ₂ (<i>trans/cis</i> ≈ 15:1) ⁷⁶	−2.29 (s) ⁷⁷ ¹ J _{PtH} = 995 (Pt- <i>H</i> _{term}) ⁷⁸	1.03–1.05 (q) ¹ J _{SiH} = 30 ⁷⁹ ¹ J _{SiPt} = 707 (Si-H-Pt)	⁸⁰	⁸⁰			69
3-297b [(Ph ₃ P) ₂ Pt(H)(μ-SiMe ₂)-(μ-SiHMe ₂)Pt(PPh ₃)]	−70 °C −7.05 (t) ¹ J _{PtH} = 553 ² J _{PtH} = 86 Pt-H		Pt-H _{br} 1.57(5) 1.63(5)	1.79(5) 1.95(5)			284c
9-11 {(Ph ₃ P)Pt[μ-η ² -H-SiMe ₂]} ₂ (Table 3, footnote 316)	0.70 (d) Pt···H-Si −70 °C 1.58 (Pt···H-Si)		1.86(8)	1.70(8)			284c
1-77 {(Ph ₃ P)Pt[μ-η ² -H-Si(Ar)H]} ₂ ⁸¹ Ar = 2,3,4,5,6-(Ph) ₅ C ₆ (<i>trans</i> only)	0.35 (d, 2H) ¹ J _{SiH} = 48 ² J _{SiH} = 25 ¹ J _{PtH} = 650 ² J _{PtH} = 112 Pt(η ² -H-Si) 2.17 ⁸⁵ Pt(η ² -H-Si) (<i>cis</i> and <i>trans</i>)	7.48 (s) ⁸² (SiHAr)	1.74	1.65 (br) ⁸³		2118 (νSi-H) ^b 1654 (νPt-H)	68a
1-78 {(Ph ₃ P)Pt[μ-η ² -H-Si(Ar)H]} ₂ Ar = 2- ⁶ⁱ Pr-6-Me-C ₆ H ₂ ⁸⁴ (<i>cis/trans</i> ≈ 1/3)	2.17 ⁸⁵ Pt(η ² -H-Si) (<i>cis</i> and <i>trans</i>)	8.42 (br s) ⁸⁶ ² J _{PtH} = 137, 78 (Si-H) (<i>cis</i>) 8.92 (br s) ¹ J _{SiH} = 216 ² J _{PtH} = 137, 72 (SiH) (<i>trans</i>)	1.799	1.669 Si···H 1.593 Si-H		2111 (νSiH) ^b 1680 (νPt-H-Si)	68a, 68b
2-98 [(Ph ₃ P)Pt(μ-η ² -H-SiPh ₂)] ₂	2.84 (s) ¹ J _{PtH} = 624 ² J _{PtH} = 111 Pt(η ² -H-Si)					1685 (νPt-H-Si) ^c	127c
2-99 [(Ph ₃ P)Pt(μ-η ² -H-SiAr ₂)] ₂ Ar ₂ = C ₂₀ H ₂₄ ⁸⁷	87 °C 3.27 (s) ¹ J _{PtH} = 696 ² J _{PtH} = 119 Pt(η ² -H-Si)		⁸⁸				127c
2-100 [(Ph ₃ P)Pt(μ-η ² -H-SiAr ₂)] ₂ ⁸⁹ Ar ₂ = SiC ₁₂ H ₈ O	3.25 (s) ¹ J _{PtH} = 691 ² J _{PtH} = 136 Pt(η ² -H-Si)					1686 (νPt-H-Si) ^c	127c
2-101 [(Ph ₃ P)Pt(μ-η ² -H-SiAr ₂)] ₂ Ar ₂ = SiC ₁₃ H ₁₁ N	2.36 (s) ⁹⁰ Pt(η ² -H-Si)		1.54	1.64		1687 (νSi-H-Pt) ^c	127c
*2-96b [(Cy ₃ P)Pt(μ-η ² -H-SiEt ₂)] ₂ ⁹¹	⁹²		1.91(7)	2.07(5)		1655 (νSi-H-Pt) ^b	127a
*2-96c <i>trans</i> -[(Cy ₃ P)Pt(μ-η ² -H-SiPhMe)] ₂ ⁹³	⁹²		1.83(1)	1.99(1)			127a
*2-96e [Pt(PCy ₃)] ₂ [(μ-η ² -H ₂ -SiEt ₂)(μ-SiPh ₂)]	^{92,94}		⁹⁵			1696 (νSi-H-Pt)	127b
2-102a [(Cy ₃ P)Pt] ₂ (μ-η ² -H-SiPh ₂) ₂	2.47 (app t, 2H) ⁹⁶ Pt(η ² -H-Si) ¹ J _{PtH} = 604.5 ² J _{PtH} = 87.5 2.71 (d) ⁹⁷ Pd(η ² -H-Si) ² J _{HPt} = 96		⁹⁸			1653 (νSi-H-Pt) ^b	122
3-260a (Et ₃ P)Pt(μ-η ² -H-SiPh ₂) ₂ Pd(PEt ₃)	2.06 (d) Pt(η ² -H-Si) ¹ J _{HPt} = 650						279

Table 9f. Continued

compound	NMR data, ^l MH, (J)	NMR data, ^l SiH, J	X-ray MH	X-ray SiH	calc.	IR, cm ⁻¹ 2	ref
3-297a [(C ₃ P) ₂ Pt](μ-η ² -H-SiPh ₂) ₂ [Pd(PCy ₃)] ⁹⁹	40 °C 2.49 (d, 1H) ¹⁰⁰ ² J _{HPt} = 73 Pd(η ² -H-Si)		¹⁰¹			1655 (νSi-H-Pt) ^b	122
2-103 (Ph ₃ P) ₂ (H)Pt(μ- Si-C ₂₀ H ₂₄)(μ-η ² -H-SiC ₂₀ H ₂₄)Pt(PPh ₃) ¹⁰²	1.70 (d, 1H) Pt(η ² -HSi) J _{HPt} = 601 -50 °C ¹⁰³ 1.93 (d) Pt(η ² -HSi)		1.50 1.63	1.96 1.71			127c, 132
2-104 (Ph ₃ P) ₂ (H)Pt(μ- Si-Ar ₂)(μ-η ² -H-SiAr ₂)Pt(PPh ₃) Ar ₂ = C ₁₃ H ₉ Br ₂ N ¹⁰⁴	-5.2 (t) (PtH) ¹ J _{PtH} = 572 ² J _{PtH} = 90 -50 °C 2.91 (d) Pt(η ² -HSi)		1.55 1.79	1.73 1.89		2276 (νPtH) 1798 (νPt-H-Si)	131
3-218 [(Me ₃ P)(Ar ₂ HSi)Pt]-(μ-H)(μ-η ² -H-SiAr ₂)[Rh(PMe ₃) ₃] Ar = C ₆ H ₄ F- <i>p</i>	-6.34 (t) ¹ J _{PtH} = 564 (PtH) rt ¹⁰⁵ -90 °C 4.47 (d) (SiH) -90 °C -12.9 (d) ¹ J _{RhH} = 148 Rh(η ² -HSi) -7.69 (d) ¹ J _{RhH} = 70 ¹ J _{PtH} = 356 (Pt-H-Rh) rt ¹⁰⁵	-90 °C 4.47 (d) (SiH) -90 °C -12.9 (d) ¹ J _{RhH} = 148 Rh(η ² -HSi) -7.69 (d) ¹ J _{RhH} = 70 ¹ J _{PtH} = 356 (Pt-H-Rh) rt ¹⁰⁵	1.66 (Pt-H _{br} -Rh) 2.24 (Rh-H _{br} -Pt) 1.63 (Rh-H _{br} -Si)	2.28 (Si-H _{br} -Rh) ¹⁰⁶			258, 244
3-219 (Me ₃ P)(ClAr ₂ Si)Pt]-(μ-H)(μ-η ² -H-SiAr ₂)-[Rh(PMe ₃) ₃] Ar = C ₆ H ₄ F- <i>p</i> ¹⁰⁷	-90 °C -13.1 (d) ¹ J _{RhH} = 143 Rh(η ² -H-Si) -7.47 (d) ¹ J _{RhH} = 63 ¹ J _{PtH} = 358 Pt-H-Rh) -90 °C ¹⁰⁹ -8.61 (t) (PtH) ¹ J _{PtH} = 550		¹⁰⁸				244, 258
3-260b (Et ₃ P) ₂ Pt(μ-η ² -H-SiPh ₂) ₂ Pd(PEt ₃)	-90 °C ¹⁰⁹ -8.61 (t) (PtH) ¹ J _{PtH} = 550	25 °C 2.03 (s, 1H) Pd(η ² -H-Si) ² J _{HPt} = 65 ¹ J _{SiH} = 28 (av) 1.28 ¹¹⁰	¹¹¹				279
α-agostic interactions							
Ti triad *9-12 Cp ₂ Hf(η ² -H-SiMe ₂)-(μ-Me)B(C ₆ F ₅) ₃ ^{112,113}		1.80 (s) ¹ J _{SiH} = 57 SiH			Y	1414 (νSiH) ^a	307c
β-agostic interactions							
Sc triad ¹¹⁴ Ti triad 3-3* Cp ₂ Ti(η ² -PhC ₂ SiMe ₂ H) ¹¹⁵	30 °C -5.96 (sept, 1H) ¹ J _{SiH} = 99 SiH					1752, 1737 (νSiH, C≡C) ^a	139
*3-4 Cp ₂ Ti(HMe ₂ SiC ₂ SiMe ₂ H) ¹¹⁶	-108 °C -8.04 ¹ J _{SiH} = 34 Ti(η ² -H-Si)	-108 °C 4.58 ¹ J _{SiH} = 186 SiH _(free)				2106 (νSiH _{free}) ^a 1771, 1759 (νSiH, C≡C)	139

Table 9g. Continued

compound	NMR data, ¹ MH, (J)	NMR data, ¹ SiH, J	X-ray MH	X-ray SiH	calc.	IR, cm ⁻¹ 2	ref
3-7 [(Me ₂ Si(η ⁵ -C ₅ H ₄) ₂)Ti-(η ² - ^t BuC≡CSiMe ₂ H)]	−6.54 (1H) ¹ J _{SiH} = 100 SiH					1753 ^a (νSiH, C≡C)	139
3-8 Cp ₂ Zr(η ² - ^t BuC≡C-SiMe ₂ H) ¹¹⁷	−3.74 (1H) ¹ J _{SiH} = 72 SiH					1689 ^a (νSiH, C≡C)	139
3-9 Cp ₂ Zr(η ² -H-Me ₂ SiC ₂ SiMe ₂ H) ¹¹⁸	−56 °C −3.69 (1H) ¹ J _{SiH} = 72 17 °C −4.35 (1H) ¹ J _{SiH} = 70	17 °C (1H) 4.98 J _{SiH} = 190 SiH _{free}	2.042(4) Zr⋯H _{br}	1.634(4) Si⋯H _{br} 1.425 Si-H _{term}			139
	−27 °C −4.40 ² J _{SiH} = 69 SiH	−27 °C 5.05 (1H) ¹ J _{SiH} = 187 SiH _{free}					
V triad							
*3-17 [Cp(Me ₃ P)ClNb{η ³ -N-(Ar)SiMe ₂ -H}] ¹¹⁹ Ar = 2,6-C ₆ H ₃ ^t Pr ₂	−5.67 (s, 1H) ¹ J _{SiH} = 97 NbH		1.91(5)	1.52(5)	Y	1620 (νNb-H) ^a	146 147a
*3-18 [Cp(Me ₃ P)ClNb{η ³ -N-(Ar)SiMe ₂ -H}] ¹¹⁹							
3-19 [Cp(Me ₃ P)ClNb{η ³ -N-(Ar')SiMe ₂ -H}] Ar' = 2,6-C ₆ H ₃ Me ₂	−3.41 (s, 1H) ¹ J _{HSi} = 116 NbH		¹²⁰		Y	1670 (νNb-H) ^a	147a, 32a
Cr triad							
*1-25b (ArN)(PMe ₃)-(PhH ₂ Si)Mo(η ³ -NAr-SiHPh-H) Ar = 2,6- ^t Pr ₂ C ₆ H ₃	4.35 (bm) ¹²¹ ¹ J _{SiH(a)} = 113 Mo⋯H _a Si	6.03 (bd) ¹ J _{SiH(b)} = 245 5.68(s), 5.97(s) ¹ J _{SiH(c,d)} = 154	1.929 (Mo⋯H _a)	1.484 (SiH _a) 1.425 (Si _{bcd})		1694 ^a (νMo⋯H-Si) 2014, 2041, 2165 (νSi-H) ^a	36b
1-25c (ArN)(PMe ₃)(<i>m</i> -Tol)-H ₂ Si)Mo-(η ³ -NAr-SiHPh-H) Ar = 2,6- ^t Pr ₂ C ₆ H ₃	4.36 (m) ¹²² (Si-H _a)	6.12 (m) (Si-H _b) 5.97 (bs) 5.64 (bs) (Si-H _c H _d)					36b
3-37a (Me ₃ P) ₂ (ArN=)ClMo-[N(SiMe ₂ H)Ar] Ar = 2,6-Me ₂ C ₆ H ₃	¹ J _{SiH} = 97		1.92(4)	1.54(4)	Y		155a
(Me ₃ P) ₂ (ArN=)ClMo-[N(SiMeClH)Ar] Ar = 2,6-Me ₂ C ₆ H ₃ Table 3, footnote 46)	¹ J _{SiH} = 129		1.93(4)	1.51(3)			155a
Fe triad							
3-119b <i>fac</i> -(Me ₃ P) ₃ (Cl)Ru-(CH ₂ SiMe ₂ -H-μ)	−7.85 (dt, 1H) J _{SiH} = 75 RuH		1.550	1.664		1615 (vw) ¹²³	205
3-119c <i>mer</i> -(Me ₃ P) ₃ (Cl)Ru-(CH ₂ SiMe ₂ -H-μ)	−6.0 (dt, 1H) J _{SiH} = 77.5 RuH		1.732	1.557			205
*3-134c Ru[η ² -H-SiMe ₂ -(CH(C ₆ H ₄)PPh ₂) ₂]	−9.77 (t) J _{SiH} = 67 η ² -SiH		1.71(4) 1.68(4)	1.76(4) 1.65(3)	Y		213c
γ-agostic interactions and beyond							
V triad							
9-13 [Cp({2,6- ⁱ Pr ₂ C ₆ H ₃ }-N=)(H)TaCH ₂ Si-(SiMe ₃) ₂ SiMe ₂ H}] ^{124,125} (γ-agostic)	9.58 (dd, 1H) TaH	2.57 (dddq, 1H) ¹ J _{SiH} = 87 SiH −70 °C ¹ J _{SiH} = 78 80 °C ¹ J _{SiH} = 101					360

Table 9h. Continued

compound	NMR data, ^l MH, (J)	NMR data, ^l SiH, J	X-ray MH	X-ray SiH	calc.	IR, cm ⁻¹ 2	ref
Fe triad							
*9-14 [(η^5 -C ₅ Me ₄ Et)(OC)- Ru[CMe=NSi(H) ₂ - {C(SiMe ₃) ₃ }]}] ¹²⁶ (γ -agostic)	−10.60 (d) ¹ J _{SiH} = 74.7, (Ru⋯SiH)	4.80 (d) ¹ J _{SiH} = 225.0, (SiH)		1.71(3) Si–H _{br}	?		393a
*3-134b H ₂ Ru{ η^2 -HSiMe ₂ - CH ₂ (<i>o</i> -C ₆ H ₄)PPh ₂] ₂ (ϵ -agostic)	−80 °C −10.4 (AA'XX') J _{SiH} = 15 RuH				Y		213c
*3-134d RuH{ η^2 -H–SiMe ₂ - CH ₂ (<i>o</i> -(C ₆ H ₄)PPh ₂)- { η^2 -H–SiMe ₂ }CH- (<i>o</i> -C ₆ H ₄)PPh ₂ } (ϵ - and β -agostic)	−5.2 (br s) J _{SiH} = 27.8 η^2 -SiH −9.36 (dd) J _{SiH} = 40 −8.00 (pt) J _{SiH} = 27 −6.04 (br s) J _{SiH} = 76				Y		213c
Co triad							
3-182b [Cp(Me ₃ P)Rh[C ₆ H ₄ - (η^2 -HSiPh ₂)] ⁺ BAR' ₄ [−] (γ -agostic)	−8.95 (dd, 1H) J _{RhH} = 27.8 J _{SiH} = 84 SiH⋯Rh						239
*3-199d (Ph ₃ P)Rh(SiMe ₂ C ₆ H ₄ SiMe ₂)- (η^1 -HSiMe ₂ C ₆ H ₄ SiMe ₂) (δ -agostic)	−0.26 (br s) J _{SiH} = 112 Rh⋯H–Si		3.082 Rh⋯Si ¹²⁷	1.41(10)		1966 (ν SiH) ^b	247b
Ni triad							
2-85 <i>cis</i> -(Me ₃ P) ₂ Pt- (CZ=CZSiPh ₂ H)(SiPh ₂ H)		5.45 (app t, 1H) J _{H-Pt} = 40 PtSiH				2098, 2070 ^b (ν Si–H)	124 454
2-86 (2-51b) <i>trans</i> -(Me ₃ P) ₂ Pt- (CZ=CZ–SiPh ₂ H)- (SiPh ₂ H) Z = COOMe		6.35 (s, 1H) ¹ J _{SiH} = 197 J _{H-Pt} = 19 CSiH 4.98 (t, 1H) J _{PtH} = 28 PtSiH	2.93 (Pt⋯HSiC)	1.37(6) 1.37(6)		2078, 2049 ^b (ν Si–H)	124 454
*9-15 (dmpe)Pt(CZ=CZ- SiPh ₂ H)(SiPh ₂ H) ¹²⁸ Z = COOMe		6.21 (s, 1H) ¹ J _{SiH} = 196 J _{PtH} = 14 CSiH 5.60 (app t, 1H) J _{H-Pt} = 36 PtHSi	2.427 Pt⋯H	1.60 CSiH 1.50 SiH		2116, 2043 ^b (ν Si–H)	124 454
M–H⋯Si							
IHI interactions							
Ti triad							
*3-1 Cp ₂ (Me ₃ P)Ti(η^2 -H- SiMeCl ₂)	−4.35 (d + dd, 1H) J _{SiH} = 22 ¹²⁹ TiH		1.733(18)	1.749(17)	Y	1524 ^a (ν TiH)	20b
9-16 Cp ₂ (Me ₃ P)Ti(η^2 -HSi- MePhCl) ¹³⁰	−4.67 (d + dd, 1H) J _{SiH} = 31 ¹³¹ TiH		¹³²			1566 ^a (ν TiH)	20b
9-17 Cp ₂ (Me ₃ P)Ti(η^2 -HSiCl ₃) ¹³⁰	−3.61 (d + dd, 1H) J _{SiH} = 34 ¹²⁹ TiH		1.72(2)	1.749(17)	Y	1524 (ν TiH)	20b

Table 9i. Continued

compound	NMR data, ^l MH, (J)	NMR data, ^l SiH, J	X-ray MH	X-ray SiH	calc.	IR, cm ⁻¹ 2	ref
V triad							
*3-12b Cp ₂ (H) ₂ Nb(η ² -H-SiMe ₂ Cl) (Si lateral)	−4.42 (s, 1H) NbH		1.766 ¹³³ 1.671 ¹³³	1.860	Y	1693.9 (νNbH) ^a	142
3-13 Cp ₂ Nb(H) ₂ (SiCl ^l Pr ₂) (Si central)	−4.61 (s, 1H) NbH −4.64 (s, 2H)		1.65(3) 1.65(3)	2.204 2.447 Nb—H⋯Si ¹³³		1736 (νNb—H) ^a	143
9-18 Cp ₂ Nb(H) ₂ (SiMe ₂ PPh ₂) ¹³⁴ (Si central)	−4.44 (s, 2H)		1.65(2) 1.70(2)	2.148 2.445 Nb—H⋯Si ¹³³		1751 (νNb—H) ^a	144
*3-16 Cp ₂ (H)Nb(SiMe ₂ Cl) ₂ ¹³⁵	−5.15 (br s, 1H) (tol- <i>d</i> ₈)		1.74(7) (X-ray)	2.056 ClSi⋯H (X-ray)	Y	1722 ^a (νNb—H)	142, 144, 145a
9-19 Cp ₂ (H)Nb(SiMe ₂ F) ₂ ¹³⁶	−4.93 (s, 1H) (CDCl ₃) −5.26 (br s, 1H)		1.816(8) (ND) 1.652	2.076(3) (ND) 1.980		1723 ^a (νNb—H)	142
9-20 Cp ₂ (H)Nb(SiMe ₂ Br) ₂ ¹³⁶	−5.16 (br s, 1H)		1.780 (CDB)	2.053 BrSi⋯H		1717 ^a (νNb—H)	142
9-21 Cp ₂ (H)Nb(SiMe ₂ I) ₂ ¹³⁶	−4.91 (s, 1H) NbH		1.881 (CDB)	2.07 ISi⋯H		1713 ^a (νNb—H)	144
9-22 Cp ₂ (H)Nb(SiMe ₂ OMe) ₂ ¹³⁷	−4.49 (s, 1H) NbH		1.88(5)	2.113, 2.192 MeOSi⋯H		1735 ^a (νNb—H)	144
9-23 Cp ₂ (H)Nb(SiMe ₂ Ph) ₂ ¹³⁸	−3.23 (br s, 1H)		1.672	2.191 Nb—H⋯Si ¹³³	Y ¹³⁹		142
9-24 Cp ₂ (H)Nb(SiCl ₃) ₂ ¹⁴⁰	−3.29 (br s)		1.79(3)	2.14(3) 2.11(3) Nb—H⋯Si		1694 ^a (νNb—H)	143
*9-25 Cp ₂ Nb(SiMe ₂ H)(H)- (SiMe ₂ Cl) ^{141, 142}	−4.58 (s, 1H) NbH	4.81 (sept, 1H) SiH	ND/X-ray 1.804(17)	ND/X-ray ClSi⋯H ¹⁴³ 2.085(17) HSi⋯H 2.126(17) Si—H 1.603(18) 2.018 2.191 FSi⋯H ^{133, 145}	Y	1720 (νNb—H) ^a 2006 (νSi—H)	356a
9-26 Cp ₂ Nb(SiMe ₂ H)(H)- (SiMe ₂ F) ¹⁴⁴	−5.22 (s, 1H)	5.02 (sept, 1H)	1.708 (CDB)		Y	1728 (νNb—H) ^a	356a
9-27 Cp ₂ Nb(SiMe ₂ H)(H)- (SiMe ₂ Br) ¹⁴⁶	−4.61 (s, 1H)	4.77 (sept, 1H)	1.711	2.074 Nb—H⋯SiBr	Y	1996 (νSi—H) 1704 ^a (νNb—H)	356a
9-28 Cp ₂ Nb(SiMe ₂ H)(H)- (SiMe ₂ I) ¹⁴⁷	−4.55 (s, 1H)	4.70 (sept, 1H)		2.165 Nb—H⋯SiH (CDB) ¹⁴⁵		2004 (νSi—H)	356b
9-29 Cp ₂ Nb(SiMe ₃)(H)- (SiMe ₂ I) ¹⁴⁸	−4.46 (s, 1H)		¹⁴⁸			1695 ^a (νNb—H)	356b
9-30 Cp ₂ Nb(SiMe ₂ Cl)(H)- (SiMe ₂ F) ¹⁴⁹	−5.24 (s, 1H)					2000 ^a (νSi—H) 1692 ^a (νNb—H)	356b
9-31 Cp ₂ Nb(SiMe ₂ Br)(H)- (SiMe ₂ F) ¹⁵⁰	−5.25 (s, 1H)					1712 ^a (νNb—H)	356b
9-32 Cp ₂ Nb(SiMe ₂ I)(H)- (SiMe ₂ F) ¹⁵¹	−4.93 (s, 1H)					1704 ^a (νNb—H)	356b
9-33 Cp ₂ Nb(SiMe ₂ Cl)(H)- (SiMe ₂ Br) ¹⁵²	−5.17 (s, 1H)					1691 ^a (νNb—H)	356b
9-34 Cp ₂ Nb(SiMe ₂ Cl)(H)- (SiMe ₂ I) ¹⁵³	−4.55 (s, 1H)					1720 ^a (νNb—H)	356b
3-21 CpNb(=NAr)(PMe ₃)- (H)SiPh ₂ Cl ¹⁵⁴ Ar = 2,6-C ₆ H ₃ Pr ₂	2.86 (d) NbH		¹⁵⁵			1616 (νNb—H)	149
3-25a [Cp(Me ₃ P)Ta(NAr)- (H)(SiMe ₂ Cl)] ¹⁵⁶	5.13 (d, 1H) TaH		1.6(1) ¹⁵⁸	2.3(1)	Y	1736 (νTa—H) ^a	146 147a

Table 9j. Continued

compound	NMR data, ¹ MH, (J)	NMR data, ¹ SiH, J	X-ray MH	X-ray SiH	calc.	IR, cm ⁻¹ 2	ref
Ar = 2,6-C ₆ H ₃ ⁱ Pr ₂ 3-25b Cp(ArN≡)Ta(PMe ₃)- (H)(ClSiMePh)	¹ J _{SiH} = 33 ¹⁵⁷ 5.78 (d) 5.34 (d)				Y		147b
Ar = 2,6-C ₆ H ₃ ⁱ Pr ₂ 3-26a [Cp(Me ₃ P)Ta(NAr)- (H)(SiMeCl ₂)] ¹⁵⁹	6.14 (d, 1H) ¹ J _{SiH} = 40		1.802	2.164	Y	1660 (νTa-H) ^a	78a
Ar = 2,6-C ₆ H ₃ ⁱ Pr ₂ 3-26b Cp(Ar'N≡)Ta(PMe ₃)- (H)(ClSiMeCl) (Ar' = 2,6-Me ₂ C ₆ H ₃) ¹⁶⁰	TaH 6.00 (d) J _{SiH} = -41		¹⁶¹			1650 (νTa-H) ^a	147b
Fe triad							
3-81b Cp(ⁱ Pr ₃ P)(H) ₂ Ru- SiMe ₂ Cl] ¹⁶²	-12.46 (d + sat) J _{SiH} = 12.2		1.51(3) 1.50(3)	2.02(3) 2.09(4)		2012 (νRu-H) ^a	181c
3-81d Cp(ⁱ Pr ₂ MeP)(SiMeCl ₂) ₂ RuH]	-10.7 (d + sat) J _{SiH} = 19.7					2017 (νRu-H) ^a	181c
3-87 Cp*(Ph ₃ P)(H) ₂ Ru- SiMe ₂ Cl	-11.6 (d, 2H)		1.49(2), 1.50(2)	2.191 2.264			185
3-88 Cp(ⁱ Pr ₃ P)(H) ₂ Ru- SiMe ₂ Cl] ¹⁶³	-12.23 (d) J _{SiH} = 11.7		1.51(4) 1.53(4)	2.03(4) 2.04(4)		1998, 2026 (νRu-H) ^a	185
9-35 Cp*(Me ⁱ Pr ₂ P)(H) ₂ Ru- SiMe ₂ Cl] ¹⁶⁴	-12.21 (d) J _{SiH} = 12.9		1.53(6) 1.63(6)	2.17(6) 1.942(3)		1952, 2026 (νRu-H) ^a	186
3-89b Cp*(Me ₂ ⁱ PrP)(H) ₂ Ru- SiMeCl ₂	-11.54 (d) J _{SiH} = 11		1.49(5) 1.68(8)	2.07 1.99			186
3-90 Cp*(ⁱ Pr ₃ P)(H) ₂ Ru- SiMeCl ₂	-11.55 (d)		1.56(3) 1.64(3)	2.11 2.15		2010, 2081 (νRu-H) ^a	186
3-92 Cp(ⁱ Pr ₃ P)ClRu- (η ² -H-SiMe ₂ Cl)	-40 °C -9.67 J _{HSi} = 33.5		1.53(3)	2.05(3)	Y	1916 (νRu-H) ^a	187
SISHA ¹⁶⁵							
Cr triad							
9-36 Cp(OC) ₂ W(H) ₂ - (SiHCl ₂) ¹⁶⁶	-60 °C -6.34 (d) ¹ J _{WH} = 55.3	-60 °C 8.11 (t) ¹ J _{SiH} = 287 ² J _{WH} = 23.6	1.67(4) 1.63(3)	1.91(3) 1.90(3)		(CO only)	368e
Fe triad							
*1-37 [PhB(CH ₂ P ⁱ Pr) ₃ - (Fe(H)(η ³ -H ₂ SiPhMe))]]	-13.45 (m) ¹ J _{SiH} = 68 ¹⁶⁷ HFe(η ³ -H ₂ SiPhMe)		1.553(1) Fe-H ¹ 1.482(1) Fe-H ² 1.566(1) Fe-H ³	1.464(1) Si-H ¹ 2.001(2) Si-H ²	Y	2034 (νFe-H)	45
9-37 [PhB(CH ₂ P ⁱ Pr) ₃ (Fe(H)- (η ³ -H ₂ SiMesMe))]] ¹⁶⁸	-13.40 (m, 3H) ¹ J _{SiH} = 70 Si/Fe-H		1.228 1.556 Fe-H	1.552(2) Si-H ³ 1.56, 1.62 1.67, 1.74 2.14, 1.97 Fe-H...Si	Y		45
*3-120 <i>fac</i> -(Me ₃ P) ₃ (H) ₃ Ru- (SiMe ₃) ¹⁶⁹	-10.18 (br m)		1.488(43) 1.637(50) 1.431(45) Ru-H _{term}	2.228(42) 2.179(48) 2.128(48) (Ru-H...Si)		1890 ^b (νRuH)	97
*3-121 (Me ₃ P) ₃ (H) ₃ Ru- (SiMe ₂ CH ₂ SiMe ₃)	-10.15 (br, m, 3H)		1.60(4) 1.61(3) 1.58(5) Ru-H	2.00(4) 2.09(4) 2.05(5) Si...HRu		1898 (νRuH)	49
3-122 (Me ₃ P) ₃ (H) ₂ Ru- (Me ₂ SiCH ₂ CH ₂ SiMe ₂)	-10.37 (s) J _{SiH} = 16		1.56(4) 1.50(4)	1.81(4) 2.15(3) Si...H		1940 (νRuH) 1740 (νRuH...Si)	49
3-124 (Ph ₃ P) ₃ H ₃ RuSiMeCl ₂	-9.76 (m, 3H) J _{SiH} = 38 RuH ₃		1.68(3), H ¹ 1.54(2), H ² 1.59(2), H ³	1.94(3), H ¹ 1.86(2), H ² 1.94(2), H ³		1961.5 (br, Ru-H-Si) ^b	206
9-38 (Ph ₃ P) ₃ H ₂ Ru{(η ² -H- SiPh ₂)O(SiHPh ₂)} ¹⁷⁰	20 °C -9.12 (m, 3H) RuH ₃	5.31 (s, SiH)					398
	-60 °C -9.15 (dt, 1H, RuH ₃) -8.75 (brt, 2H, RuH ₃)	-60 °C 5.26 (s, SiH)					
9-39 (Ph ₃ P) ₃ H ₂ Ru{(η ² -H- SiPh ₂)O[Si(OH)Ph ₂]} ¹⁷¹	20 °C -9.15 (m, 3H)		1.59(3) 1.61(5) 1.57(3)	1.97(5) 2.03(5) 2.07(5)			398

Table 9k. Continued

compound	NMR data, ^l MH, (J)	NMR data, ^l SiH, J	X-ray MH	X-ray SiH	calc.	IR, cm ⁻¹ 2	ref
*3-125a (Cy ₃ P) ₂ (H) ₂ (η ² -H ₂)- Ru(η ² -H-SiMe ₂ Cl)	15 °C -8.51 (br, 5H, RuH) ¹⁷²						207a
*3-125b (PCy ₃) ₂ (H) ₂ Ru- (η ² -H-SiMe ₂ Cl) ₂	-40 °C -10.69 (2H, AA'XX') ¹⁷³ (RuH)						207a
3-126a (PCy ₃) ₂ {(η ² -C ₆ H ₈)- PCy ₂ (H)Ru-(η ² -H- SiMe ₂ Cl)}	-7.90 (br t, 2H) Ru(η ² -H-Si) -11.98 (dd, 1H, RuH)		1.57(2) Ru-H _{br} -Si	1.91(2) Si-H _{br} -Ru			207a
	-9.06 (t, 1H) Ru(η ² -H-Si)		1.62(3) Ru-H _{br} -Si	1.99(2) Si-H _{br} -Ru			
3-127 [(Cy ₃ P) ₂ (H) ₂ Ru{(η ² -H- SiMe ₂) ₂ X}] X = C ₆ H ₄ ¹⁷⁵	$J_{\text{SiH}(1)} = 37.3$ $J_{\text{SiH}(2)} = 24.1$ ¹⁷⁴ 15 °C -7.74 (t) $J_{\text{SiH}} = 65$ Ru(η ² -H-Si) -12.03 (m) (RuH)		1.60(3) 1.59(3) Ru-H _{br} -Si	1.84(2), 1.84(2) Si-H _{br} -Ru	Y	1778 (νRu-H-Si) ^a 1969, 1985 (νRu-H)	208 209
9-40 [(Cy ₃ P) ₂ (H) ₂ Ru{(η ² -H- SiMe ₂) ₂ X}] X = -(CH ₂) ₂ - ¹⁷⁶	15 °C -12.65 RuH -8.21 $J_{\text{SiH}} = 70$ Ru(η ² -H-Si)		1.55(3) 1.54(3) Ru-H _{br} -Si	1.73(3) 1.78(3) Si-H _{br} -Ru	Y	1773 (νRu-H-Si) ^a 1981, 2012 (νRu-H)	208, 209, 398
9-41 [(Cy ₃ P)(Ph ₃ P)(H) ₂ Ru- {(η ² -HSiMe ₂) ₂ X}] X = -(CH ₂) ₂ - ¹⁷⁷	-11.10 (dd) -11.47 (dd) (RuH) -7.68 (pt) $J_{\text{SiH}} = 64$ Ru(η ² -H-Si) -10.92		1.64(3) 1.66(3) Ru-H _{br} -Si	1.80(3) 1.98(3) Si-H _{br} -Ru	Y	2008, 1989 ^a (νRu-H) 1768 (νRu-H-Si)	208c
9-42 [(Ph ₃ P) ₂ (H) ₂ Ru{(η ² -H- SiMe ₂) ₂ X}] X = -(CH ₂) ₂ - ¹⁷⁸	-7.60 $J_{\text{SiH}} = 64$		1.63(3) 1.59(3) Ru-H _{br} -Si	1.87(3) 1.93(3) Si-H _{br} -Ru	Y		208
9-43 [(Cy ₃ P) ₂ (H) ₂ Ru{η ² -H- SiMe ₂) ₂ X}] X = -OSiMe ₂ O- ¹⁷⁹	15 °C -11.20 RuH -9.14 $J_{\text{SiH}} = 82$ Ru(η ² -H-Si)		1.53(3) 1.60(3) Ru-H _{tm} 1.62(4) 1.58(4) Ru-H _{br} -Si	1.77(4) 1.81(3) Si-H _{br} -Ru	Y	1798 (νRu-H-Si) ^a 1955, 2045 (νRu-H)	208
3-129 (Cy ₃ P) ₂ (H) ₂ (η ² -H ₂)- Ru(η ² -HSiPh ₃)	-8.45 (br s) RuH		1.55(4) 1.51(3) Ru-H _{term} 1.66(2) 1.64(3) RuH (H ₂)	2.25(3) 2.04(3) 2.43(3) 2.32(3) Si...H _{term} -Ru 2.40(4) 1.83(3) Si...H _{term} -Ru	Y		210a, 210b, 101, 100
*3-130b Ru(PPh ₂ CH ₂ O- SiMe ₂ H) ₃ ¹⁸⁰	-5 °C -6.28 (dt) $J_{\text{SiH}} = 26$ RuH	-5 °C 4.07 (sept) $^1J_{\text{SiH}} = 200$ (SiH)	1.49(4) 1.47(4) Ru-H _{term} 1.54(4) Ru-H _{br} -Si	1.72(3) Si-H _{br} -Ru 0.82(2) H-H in H ₂ 2.28(3) 1.75(3)	Y		211b

Table 9I. Continued

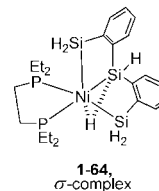
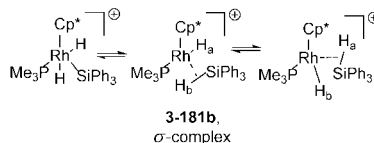
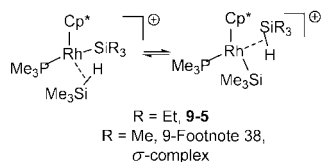
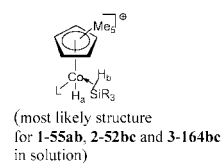
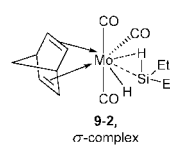
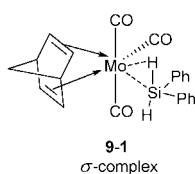
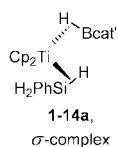
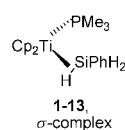
compound	NMR data, ^l MH, (J)	NMR data, ^l SiH, J	X-ray MH	X-ray SiH	calc.	IR, cm ⁻¹ 2	ref
3-131 [(pyl ₃ P) ₂ (H) ₂ Ru{(η ² -H-SiMe ₂) ₂ X}] ¹⁸¹ X = C ₆ H ₄	−8.83 (RuH) −6.47 (SiHRu) J _{SiH} = 61				Y		208
3-132 [(Cy ₃ P) ₂ (H) ₂ Ru{(η ² -H-SiMe ₂) ₂ NH}]	−9.80 (br s) 273 K −8.72 (brd s) −10.39 (brd t)		1.456 ¹⁸² 1.468 Ru—H _{term}	1.93(5) 1.91(5) Si—H _{br} —Ru	Y 2 types of DFT	2040 (νRuH) ^a 1712 (νSiH)	212
3-144a Ru ₂ H ₂ (μ-η ² :η ² -H ₂ -Si(OMe) ₂) ₃ (PCy ₃) ₂	193 (brd) −8.36, −8.62, −9.93, −10.76 −9.94 (d, 8H) J _{SiH} = 22 ¹⁸³		¹⁸⁴	1.582 1.648 Ru—H _{br} —Si 2.25(6) 3.68(5) 2.39(5) 2.09(6) Si⋯H _{term} —Ru	Y	1703 (br, ν(Ru—H—Si)) ^a 1899 (br, νRu—H) 2022 (br, νRu—H) 2054 (w) 2033 (w) 1888 (s) (νOs—H) ^a	101
*3-152 (OC)(Ph ₃ P) ₂ (H) ₃ Os-SiMe ₃	−9.03 (brd) −60 °C −8.82 (tt) ^{185 186} , −9.20 (m) −11.19 (m) ¹⁸⁸		1.58(9) 1.55(9) 1.45(10) Os—H	1.980 ¹⁸⁷ 2.062 2.211 Si⋯H—Os		2105 2059 2033 (νOs—H) ^a	222
3-160 (Ph ₃ P) ₃ H ₃ Os-Si{OCH ₂ CH ₂ } ₃ N			1.52(3) 1.57(3) 1.66(3) Os—H	1.96(3) ¹⁸⁹ 2.00(4) 2.06 Si⋯H—Os		2105 2059 2033 (νOs—H) ^a	221
Co triad							
3-168b [tripod(H) ₂ CoSiPh ₃] ¹⁹⁰	−13.1 (br s)		1.34(3) 1.32(3)	1.98(4) 1.89(2)		1928, 1616 (νCo—H)	230b
HM(multiple) Si							
Cr triad							
1-24 Cp*(dmpe)(H)Mo-Si(H)Ph ¹⁹¹	−9.96 (td, 1H) J _{SiH} = 30 MoH	9.45 (m, 1H) J _{SiH} = 130 SiH	¹⁹²	1.43(4)		1896 (νSiH) ^b	36a
2-10 Cp(dmpe)(H)Mo=(SiEt ₂)	−13.91 (t, 1H) J _{SiH} = 44 MoH −80 °C −13.9 (dd) MoH		1.847(12) (ND)	1.683(13) (ND)		¹⁹³	36a
9-44 Cp*(dmpe)(H)Mo=(SiMe ₂) ¹⁹⁴	−14.06 (t, 1H) J _{SiH} = 30 MoH −50 °C −14.04 (m, 1H) J _{SiH} = 30 MoH		X-ray			¹⁹³	36a
2-11 Cp*(dmpe)(H)Mo=Si(Cl)Mes	−12.50 (t) J _{SiH} = 38 MoH		¹⁹⁵			¹⁹³	82
9-45 [Cp*(dmpe)(H)-Mo≡SiMes] ⁺ [B(C ₆ F ₅) ₄] ^{−196}	−9.78 J _{Hsi} = 15 MoH ¹⁹⁷		1.85(5)	1.39(5)	Y	¹⁹³	82
1-29 Cp'(OC) ₂ (H)W≡Si-(H){C(SiMe ₃) ₃ } Cp' = C ₃ Me ₄ Et	−10.67 (d, 1H) ¹ J _{WH} = 65 ² J _{SiH} = 28.3 ³ J _{HH} = 1.7 MoH ¹⁹⁸	10.42 (d) ¹ J _{SiH} = 155.1 ² J _{WH} = 13.7 ³ J _{HH} = 1.7 SiH	1.82(7)	1.71(6) 1.54(7)	Y	2052 (νSiH) ^d 1589 (νWH)	38a
9-46 Cp*(OC) ₂ (H)W=Si(H)-{C(SiMe ₃) ₃ } ¹⁹⁹	−10.67 (d, 1H) ¹ J _{WH} = 65 ² J _{SiH} = 28.6 ³ J _{HH} = 1.8 WH	10.39 (d, 1H) ¹ J _{SiH} = 154.9 ² J _{WH} = 13.3 ³ J _{HH} = 1.8 SiH				2052 (νSiH) ^d 1589 (νWH)	38a

Table 9m. Continued

compound	NMR data, [†] MH, (J)	NMR data, [†] SiH, J	X-ray MH	X-ray SiH	calc.	IR, cm ⁻¹ 2	ref
unclassified							
* 1-19 Cp*(Cl)HTa- [PhSiH ₂ N(C ₆ H ₃ Me) ₂ N- SiPhHCl] ²⁰⁰	14.85 (d) ⁴ J _{HH} = 6.0 TaH	6.28 (d) ⁴ J _{HH} = 6.0 ¹ J _{SiH} = 272 SiHClPh	1.83(4)	1.36(5) (SiHPhCl)		2189, 2152 ^b (νSi-H)	32b
		5.37 (d, 1H) ² J _{HH} = 10.4 PhSiH ₂ N		1.86(4) TaH...Si		1678 (νTa-H)	
		4.54 (d, 1H) ² J _{HH} = 10.4 ¹ J _{SiH} = 208 PhSiH ₂ N					
* 2-36f C ₃₉ H ₅₀ PNSiRu (thermodynamic product) see structure	-9.40 (d) RuH		1.48(9)	1.90(8)			47d
* 1-33a Cp(ⁱ Pr ₂ MeP)FeH ₂ - SiH ₂ Ph ²⁰¹	-15.24 (d + sat) J _{SiH} = 19.8	5.39 (s + sat) J _{SiH} = 183.4			Y	2064 ^a 2025 1916 1923 ^a	42a
* 9-47 Cp(ⁱ Pr ₂ MeP)FeH ₂ - SiCl ₃	-14.6 (d, FeH)		1.35(3)	1.88(3)	Y		42a
* 3-126b (Cy ₃ P) ₂ (η ² -H ₂)(Cl)- Ru(SiMeCl ₂) ²⁰²	-12.14 (br) Ru(η ² -H ₂)		1.59(2) 1.62(2) 1.05(3) η ² -H ₂ 1.50(2)	2.25 Si...H	Y		207b
* 3-212c (PNP)(H)Rh- (SiClMe ₂) ²⁰³	-15.6 (dt) ² J _{SiH} = 31 ¹ J _{RhH} = 11			1.93(2)			254c
* 3-245e [(POCOP)Ir(H)-(η ¹ -H- SiEt ₃)] ⁺ [B(C ₆ F ₅) ₄] ⁻²⁰⁴	-70 °C -44.2 IrH		1.94(3) (Ir...H...Si)	1.48(3) (Si-H _{br})	Y		266a
	-4.9 ¹ J _{SiH} = 79 Ir...H...Si		1.425(18) (Ir-H _{term})				

†

Mononuclear σ-complexes



Bimetallic σ-Complexes

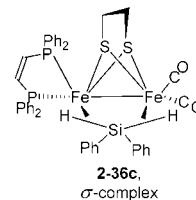
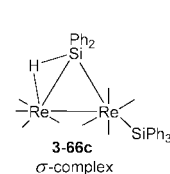
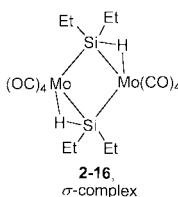
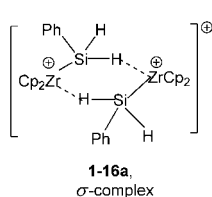
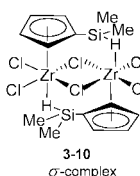
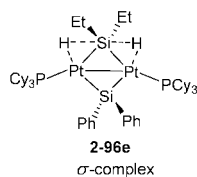
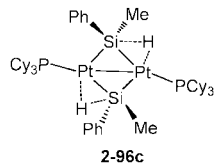
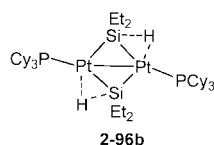
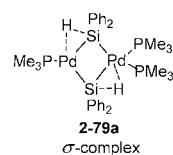
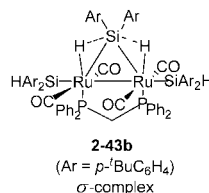
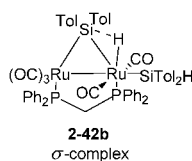
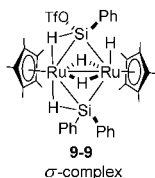
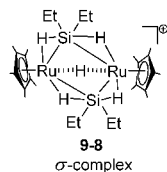
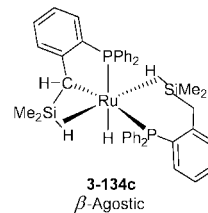
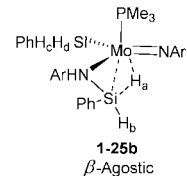
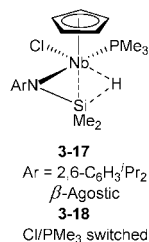
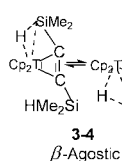
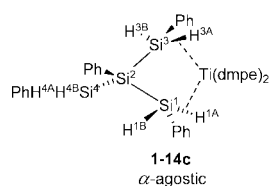
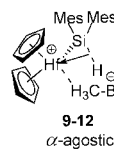
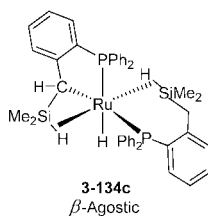
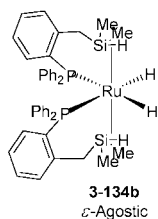
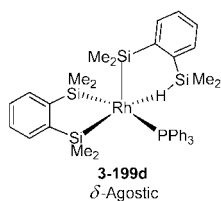
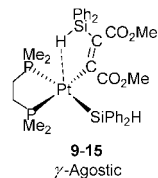
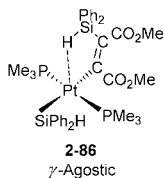
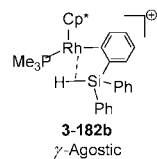
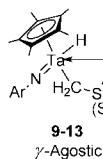
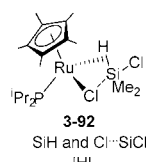
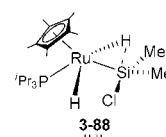
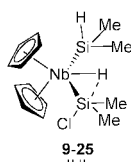
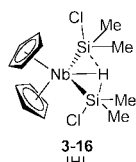
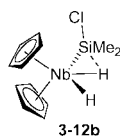
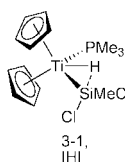


Table 9n. Continued

Bimetallic σ -Complexes α - and β -Agostic Interactions γ -Agostic and Beyond

IHI Interactions



SISHA Interactions

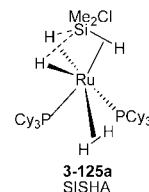
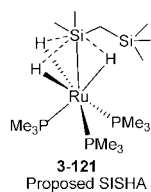
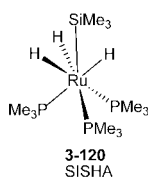
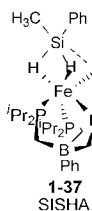
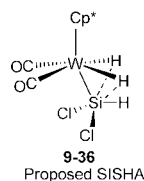
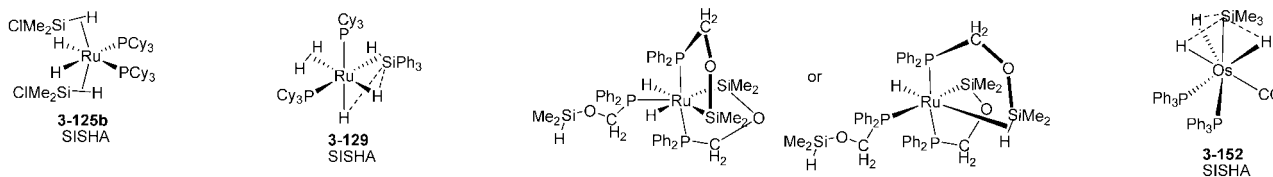
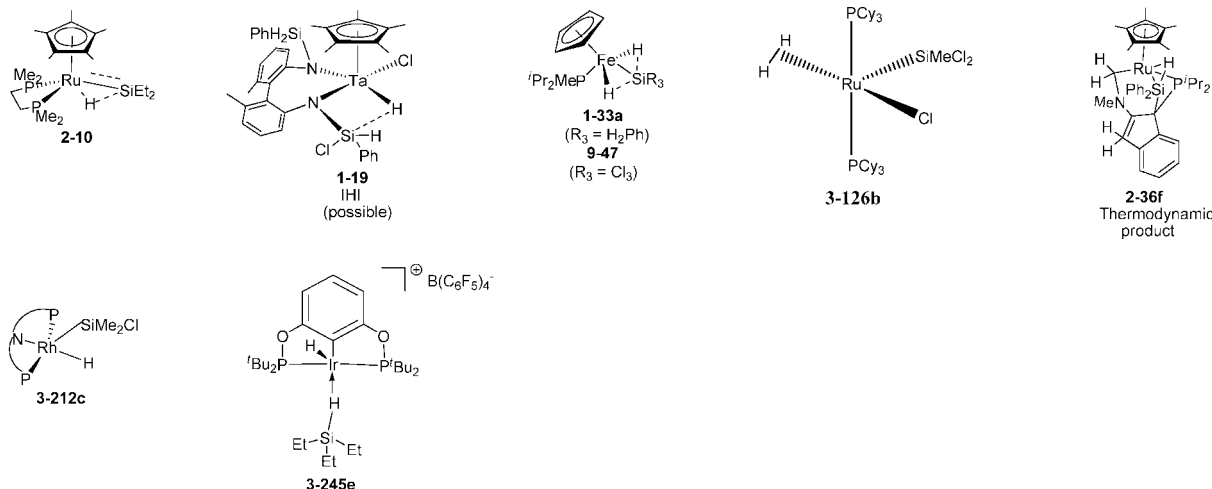


Table 9o. Continued

SiSHA Interactions

Proposed structures for **3-130b**
(OA addition vs SiSHA)H
M(multiple) Si and Unclassified Complexes

¹NMR data were collected at ambient temperature unless specified otherwise. Coupling constants are in Hz. Multiplicities are given for the indicated signals if included in the reference. ²Data collected in Nujol will be indicated by a superscript "a". Data collected as a KBr pellet will be indicated by a superscript "b". Solid IR is designated by "c", data taken in solvent is designated by "d", and if medium was not specified, "e" is used. ³Observed in solution ≤ -50 °C. ²⁸ ⁴Data from the ¹H(³¹P) NMR data in C₇D₈ at -20 °C. ^{29b} See structure section at end of table for atom labeling for **1-14c**. ⁵In solution, an equilibrium mixture of the σ -complex, **1-3d**, and the hydrosilyl tautomer of **1-3d**, MoH(SiH₃)(CO)(depe)₂ (OA product), exists. ^{21b} ⁶Only CO stretching frequencies were assigned. **3-28** exhibits a UV absorption at 281 nm. ¹⁵² ⁷Complex not isolated. ⁸³ Additional examples reported: (OC)₅Cr(η^2 -H-SiPr₃)⁸³ and (OC)₅Cr(η^2 -H-SiPh₃). ⁸¹ ⁸Characterized by IR only in ref 83. ⁹Only CO band was reported. ⁸¹ ¹⁰Complex not isolated. ^{81,83a} ¹¹Complex was observed in solution only in the photochemical reaction of [(OC)₄Mo(η^4 -nbd)] and Ph₂SiH₂ (C₆D₁₂, 283 K) and of Et₂SiH₂ (heptane, 293 K). ^{82b} ¹²Additional derivative studied only in solution: (OC)(ⁱBu₂PCH₂CH₂PⁱBu₂)₂Mo(η^2 -H-SiPh₂H). ^{21b} ¹³Complex not isolated. ^{81,83a} ¹⁴Observed as an intermediate in the reaction of W(CO)₆ with H₂SiEt₂. ^{87c} ¹⁵Additional derivatives: (OC)₄W(η^2 -H-SiMe(Tol-*p*)CH₂CH₂PPh₂) and (OC)₄W(η^2 -H-SiPh₂CH₂CH₂PPh₂). ¹⁶³ ¹⁶Temperature for the data collection was not specified. ¹⁶³ ¹⁷From a preliminary neutron diffraction study. ^{89a,b,c,d} ¹⁸Complex prepared from MeC₅H₄(OC)₂Mn(H)SiHPh₂ and [Ph₃C][BF₄]. ^{89c} ¹⁹Fixed hydrogen atom position. ^{89c} ²⁰Only CO bands were listed. ^{89d} ²¹Byproduct [Cp'(OC)₂Mn(η^2 -HSiPh₂SiPh₂H- η^2)Mn(CO)₂Cp'] decomposes during chromatographic workup. ¹⁶⁶ Additional derivatives prepared from Cp'Mn(CO)₃ and HMePhSiSiPhMeH (complex **3-56**) as well as HMe₂SiSiMe₂H, but both products decomposed on chromatographic workup. ¹⁶⁶ ²²Data taken in Et₂O. ¹⁶⁶ ²³**3-57** decomposes at room temperature. ¹⁶⁸ Additional derivative from PhSiH₃ also decomposes at room temperature. ¹⁶⁸ ²⁴*J*_{SiH} could not be measured due to Mn quadrupolar broadening. ¹⁶⁸ ²⁵Unresolved heptet. ⁸¹ ²⁶Complexes were not isolated as **3-61**, and the related complex with either a Cy₃P ligand or with the same cation as in **3-61** but with the [MeB(C₆F₅)₃] anion decomposes at room temperature. ¹⁷⁰ ²⁷**3-62** is observed only in solution, is thermally unstable, and decomposes to [cis-Re(L)(CO)₄]₂(μ -H)][BARf]. ¹⁷¹ ²⁸Broad resonance observed at room temperature may be due to paramagnetism or to ligand-exchange dynamics. ⁴⁴ ²⁹ ¹*J* value is for bound SiH. ^{44a} ³⁰ ¹*J* value is for the "free" SiH. ^{44a} ³¹Additional derivative: Tp(Ph₃P)(H)Ru(η^2 -H-SiPh₂H) (Table 2, footnote 45). ^{48a} ³²The observed *J*_{SiH} value is an average of the *J*_{SiH} value of the η^2 -SiH group and that of the coupling between the Si and the H atom not involved in the 3c-bond. H's are equivalent down to -100 °C. η^2 -HSi and SiH_{term} do not exchange up to 50 °C. ^{48a} ³³Synthetic approach involves protonation of a TM-Si bond. ¹⁸² ³⁴Additional derivatives: Tp(Ph₃P)(H)Ru(η^2 -H-SiPh₃) and Tp(Ph₃P)(H)Ru(η^2 -H-Si(OEt)₃). ^{48a} ³⁵*T*₁ = 593 ms. ^{48a} Intensity corresponds to 2H. ³⁶[Cp*(L)(H)₂Co(SiR₃)]⁺[SiR₃ = SiPh₂H] (L = P(OMe)₃ (**1-55a**), PMe₃ (**1-55b**)); Ph₂HSi (L = P(OMe)₃ (**2-52b**), PMe₃ (**2-52c**)); PhMeHSi (L = P(OMe)₃ (Table 2, footnote 60), PMe₃ (Table 2, footnote 61)); Et₃Si (L = P(OMe)₃ (**3-164b**), PMe₃ (**3-164c**)) have averaged *J*_{SiH} values between 29 and 33.5 Hz. If it is assumed that no coupling would be observed between the terminal hydrides and ²⁹Si (²*J*_{SiH} = 0), the calculated ¹*J*_{SiH} coupling constants for all the complexes would fall between 58 and 68 Hz. ^{57c} ³⁷The value given for ¹*J*_{SiH(obs)} for **1-55a** and **1-55b** represents a time-averaged value between the terminal (²*J*_{SiH}) and bridging hydrides (¹*J*_{SiH}). ^{57c} ³⁸The Me₃Si analogue was also reported. ²³⁸ ³⁹The Me₃Si and Et₃Si analogues were also reported. ²³⁹ ⁴⁰The cation is fluxional, and if the value of ¹*J*_{SiH} is 20–30 Hz, the *J*_{obs} would be ~ 10 –15 Hz and such a value would bring the satellites into the broad hydride resonance. ²³⁹ ⁴¹Not isolated. Observed in solution (> -40 °C). ²³⁹ ⁴²Data taken for the solid at room temperature. The absorption is missing in the solution spectrum. ⁶⁵ ⁴³Additional derivative prepared from [(dtbpe)Ni]₂(C₆H₆) + 2H₂SiPh₂. ¹¹⁹ ⁴⁴Not isolated. Decomposed when warmed to room temperature to give Et₃SiCl and Et₃SiOSiEt₃. Presumed (η^2 -H-Si could be Pd(IV) silyl hydride. ²⁷⁸ ⁴⁵The Si-H-Zr angle was 158°, suggesting an agostic interaction. ¹⁴⁰ ⁴⁶Only CO bands were assigned. ⁸⁴ ⁴⁷Observed as an intermediate in the reaction of W(CO)₆ with Et₂SiH₂. ^{87c} ⁴⁸Measured from the ²⁹Si NMR spectrum in THF-*d*₈ at -20 °C. The ²⁹Si signal is broad, and it is possible that the complex is still fluxional at the temperature of the measurement. The authors also concluded that M-H...Si vs M...H-Si could not be unambiguously made. ⁴⁰ ⁴⁹Hydride ligands were not located. ⁴⁰ ⁵⁰Footnote 61, Table 3. Unstable at room temperature. ¹⁶⁶ ⁵¹IR data reported in petroleum ether: ν (CO) 1978(vs); 1915(s). ¹⁶⁶ ⁵²Only ν (CO) were reported. ¹⁷³ ⁵³Additional derivative: (Cp*Fe)₂(μ -H)₂(μ - η^2 - η^2 -H₂SiPr₂). ⁹³ ⁵⁴Data taken from the supplemental information for ref 93. ⁵⁵Additional derivative: [(Cp*Ru)(H)(μ -H)(μ - η^2 -H-SiPhCl)][μ - η^2 -(ClSi(ⁱBuNCH=CHNⁱBu))]. ^{51a} ⁵⁶Could not locate MH or SiH as there is disorder in the solvent of crystallization and the hexyl group. ^{51a} ⁵⁷Prepared from protonation of [Cp*Ru(μ - η^2 -HSiEt₂)(μ -H)] with triflic acid followed by exchange of the triflate anion with BPh₄⁻. ⁴⁰³ ⁵⁸Prepared by hydrogenation of {Cp*Ru(μ -H)}₂{ μ -SiPh(OCOCF₃)}(μ -SiPh₂). ⁴⁵³ ⁵⁹ ν (Ru-H-Si) was obscured by ν (CO). ⁴⁵³

Table 9p. Continued

⁶⁰ Additional observed complex: $[(OC)_5Ru_2(\mu-dppm)[\mu-Si(p-Tol)_2], (2-42a)^{99}$ ⁶¹ Observed only in solution as a mixture of $(OC)_5Ru_2[Si(p-BuC_6H_4)_2H](\mu-dppm)-[\mu-\eta^2-H-Si(p-Tol)_2], 2-43a$. After 1 day at room temperature, **2-43a** and/or $[Ru(CO)_2[Si(p-BuC_6H_4)_2H]]_2(\mu-\eta^2-\eta^2-H_2Si(p-Tol)_2)$ were observed; ratio of **2-43a/2-43b** is 1:4.⁹⁹ ⁶² AA'XX'YY' multiplet.⁹⁹ ⁶³ Prepared from $(Cy_3P)_2(H_2)_2RuH_2$ when 2 equiv of $H_2SiPhMe$ were used, the products identified were **2-45**, $RuH_2(\eta^2-H_2)(\eta^2-HSiPh_3)(PCy_3)_2$, $HSiPh_2Me$, and $HSiMe_2Ph$ in a 1:1.3:2.2:3.4 ratio. An analogue of **2-45** was also generated from H_2SiEt_2 , although no data were provided.^{100,101} ⁶⁴ The two signals are of equal intensity, and assignments were not included.¹⁰¹ ⁶⁵ Table 2, footnote 52.¹⁰⁰ ⁶⁶ Deuterated analogues prepared from reaction of $DSiMe_2Vin$ with $Cp^*Ru(\mu-H)_4RuCp^*$ to give **3-138** with H/D (hydride region) = 47/53 and with $Cp^*Ru(\mu-D)_4RuCp^*$ to give, **3-138**, H/D (hydride region) = 86/14.²¹⁴ Additional derivative: $\{Cp^*Ru(\mu-H)_2\}(\mu-\eta^2-\eta^2-H-SiMePh(CH=CH_2))_2$ (2 diastereomers, 56:44).⁶⁷ The J_{SiH} coupling constants measured in THF- d_8 are from the ^{29}Si NMR spectrum at 23 °C and at -70 °C. The values of 31 and 54.1 Hz, respectively, indicate an average value among the J values for Si-H_a, Si-H_b, and Si-H_c at room temperature.²¹⁴ ⁶⁸ Complex **3-144** was actually prepared starting from $Ru_2H_4(\mu-\eta^2-\eta^2-\eta^2-SiH_4)(PCy_3)_4 + xs$ $HSi(OMe)_3$. Disproportionation produced $H_2Si(OMe)_2$, which displaced the SiH_4 unit in the original Ru dimer. The other product, $Si(OMe)_4$, was identified in the reaction mixture.¹⁰¹ ⁶⁹ The J_{SiH} was determined from the inept $^{29}Si-^1H\{^1H_{OMe}\}\{^31P\}$ "nonrefocused spectrum".¹⁰¹ ⁷⁰ Crystals suitable for X-ray determination were obtained, but the quality of the crystal and the data do not allow a complete analysis. Hydrogen atoms were located in the difference Fourier map but were introduced in idealized positions.¹⁰¹ ⁷¹ Resonance is assigned to the hydride that spans Si-Pd(PMe₃) edge.^{121a,b} ⁷² Additional derivative: $[(Et_3P)Pd](\mu-\eta^2-H-SiMePh)_2$, J_{SiH} was not reported.^{121b} ⁷³ Little change in the 1H NMR spectrum of **2-81** was observed from rt to -90 °C; thus, it was concluded that the complex had a similar structure both in solution and in the solid phase.^{121a} ⁷⁴ Additional derivative: $[(Ph_2MeP)Pd](\mu-\eta^2-H-SiPh_2)_2$, J_{SiH} was not reported.^{121a,b} ⁷⁵ Also prepared from reaction of $(dmpe)Pt(SiPh_2H)_2 + Pd(PCy_3)_2$ along with $\{[(Cy_3P)Pt](\mu-\eta^2-SiPh_2)_2[Pd(PCy_3)]\}$ and $[(dmpe)Pt(\mu-SiPh_2)]_2$ (see Table 3).¹²² ⁷⁶ Data are provided for the *trans*-form only. Trace amounts of the related derivative were observed when $(Pr_3P)_3Pt$ and H_2SiHex were reacted but no NMR data were reported.⁶⁹ ⁷⁷ ^{31}P decoupled 1H spectrum.⁶⁹ ⁷⁸ The agostic Si-H-Pt was not observed under the conditions of this NMR measurement.⁶⁹ ⁷⁹ Data were obtained from a 2D $^1H-^{29}Si$ gradient HMQC without ^{29}Si decoupling NMR experiment.²⁸⁵ ⁸⁰ Agostic and terminal hydrides were not refined.⁶⁹ ⁸¹ Additional derivatives: $\{(Ph_3P)Pt[\mu-\eta^2-H-Si(Ar)H]\}_2$, Ar = 2,4,6-(CF₃)₃C₆H₂ (also *trans*-form only); J_{SiH} values could not be resolved.^{68a} ⁸² The chemical shift of the terminal SiH is obscured by aromatic resonances but was located by a 2D $^1H-^{29}Si$ HMQC experiment.^{68a} ⁸³ Terminal Si-H not located.^{68a} ⁸⁴ Additional derivatives: $\{(Ph_3P)Pt[\mu-\eta^2-H-Si(Ar)H]\}_2$, Ar = 2,4,6-Me₃C₆H₂, 2,4,6-(MeO)₃C₆H₂, both as mixtures of *cis/trans* isomers. J_{SiH} values could not be resolved.^{68a} ⁸⁵ Resonances overlap with the *o*-Me protons of the aromatic ring. The presence of the $Pt(\eta^2-H-Si)$ resonance was confirmed by a 2D $^1H-^1H$ EXSY experiment. The J -values are not resolved. The complex is fluxional at rt involving exchange of bridging SiH and terminal SiH.^{68b} ⁸⁶ Complex is fluxional at room temperature involving exchange of SiH_{term} and SiH_{br} with simultaneous *cis-trans* isomerization.^{68b} ⁸⁷ The coalescence temperature was found to be 69 °C by monitoring the terminal Si-H resonances.^{68a} ⁸⁸ Reversible phosphine dissociation observed on heating **2-99**. Additional derivative prepared from $C_{12}H_{18}SiH_2$ and $(Ph_3P)_2Pt(\eta^2-C_2H_4)$.^{127c} ⁸⁹ X-ray structure confirmed the connectivity of the complex but was of poor quality.^{127c} ⁹⁰ Additional derivative, $[(Ph_3P)Pt(\mu-\eta^2-HSiAr_2)]_2$, Ar₂ = $SiC_{13}H_{11}N$.^{127c} ⁹¹ Pt satellites were not resolved in **2-101**; assignment is tentative.^{127c} ⁹² Additional derivative $\{[C_2P_2Pt(\mu-\eta^2-HSiHex_2)]_2\}$ (X-ray) also reported.^{127a} ⁹³ Pt-H-Si signals overlap with the Cy groups.^{127a} ⁹⁴ Partially deuterated complex $\{[Pt(PCy_3)]_2(\mu-\eta^2-HSiEt_2)(\mu-\eta^2-HSiPh_2)(\mu-\eta^2-HSiEt_2)]_2\}$ (X-ray) and $\{[C_2P_2Pt(\mu-\eta^2-HSiPh_2)]_2\}$ (Table 2, footnote 109) also reported.^{127a} ⁹⁵ Partially deuterated complex $\{[Pt(PCy_3)]_2(\mu-\eta^2-HSiEt_2)(\mu-\eta^2-HSiPh_2)(\mu-\eta^2-HSiEt_2)(\mu-SiPh_2)]_2\}$, gave a single signal at 1.01 ppm in the $^2H\{^1H\}$ NMR spectrum flanked by ^{195}Pt satellites ($J_{PtD} = 99$ Hz).^{127b} ⁹⁶ Hydrides were not located.^{127b} ⁹⁷ Apparent triplet is due to virtual coupling.¹²² ⁹⁸ Assignments were confirmed through preparation of $(Et_3P)Pt(\mu-\eta^2-DSiPh_2)_2Pd$ (PEt_3). There is no change in the 1H and $^{31}P\{^1H\}$ NMR spectra in the temperature range -90 to 25 °C.²⁷⁹ ⁹⁹ Structure has C_2 symmetry, which imposes disorder of Pd/Pt positions.²⁷⁹ ¹⁰⁰ Deuterium analogue of **3-297** was also prepared.¹²² ¹⁰¹ Assignment was verified by preparing $(Cy_3P)Pd(\mu-\eta^2-DSiPh_2)_2Pt(PCy_3)$ from $Pt(SiDPh_2)_2(dmpe)$ and $Pd(PCy_3)_2$.¹²² ¹⁰² SiH not observed due to disorder of the two metal centers.¹²² ¹⁰³ Additional derivative, $(Ph_3P)_2(H)Pt(\mu-SiC_{12}H_8)(\mu-\eta^2-HSiC_{12}H_8)Pt(PPh_3)$.^{127c,132} ¹⁰⁴ No hydride signals were observed at room temperature.¹³² ¹⁰⁵ Other unsymmetrical dimers were observed in reaction solutions from $(Ph_3P)_2Pt(\eta^2-C_2H_4) + H_2SiAr_2$ (Ar₂ = $C_{14}H_{12}O$, $C_{13}H_{11}N$, $C_{15}H_{15}N$).¹³¹ ¹⁰⁶ Pt-H-Rh and Si-H-Rh exchange rapidly on the NMR time scale at room temperature.²⁵⁸ ¹⁰⁷ Distance for terminal H not listed.^{244,248} ¹⁰⁸ Additional derivative prepared from Ph_2SiH_2 . Storage (freezer) of the filtrate from **3-190** produced a small amount of an isomer that precipitated, $(Me_3P)_2Pt(\mu-SiAr_2)RhH_2(SiClAr_2)(PMe_3)_2$, which was crystallographically characterized. Rh-H distances were 1.40 and 1.42, with the former depicted as bridging to the Pt at a Pt-H distance of 2.19 Å.²⁴⁴ ¹⁰⁹ Hydrides were not located.^{244,248} ¹¹⁰ At low temperature, 1H NMR data suggest that a terminal Pt-H is present. At room temperature, it appears that both hydrides are bridging; thus, a Pt-H-Si and a Pd-H-Si are present. The broadening of the room-temperature $^{31}P\{^1H\}$ NMR signal implies partial dissociation or intramolecular exchange of PEt_3 .²⁷⁹ ¹¹¹ Resonance does not exhibit Pt satellites at reasonable positions. The deuterium analogue exhibits signals at 2.15 ppm ($^2J_{PtD} = 10$ Hz) and 0.41 ($^1J_{PtD} = 106$ Hz), the latter of which shows that Si-D-Pt bonding is present. Complex **3-260b** is fluxional.²⁷⁹ ¹¹² Bridging hydrogen atoms were not located in the final difference map.²⁷⁹ ¹¹³ Unstable species generated from $Cp_2Hf(SiMe_2H)(Me)$ and $B(C_6F_5)_3$ and studied at -40 °C.^{307c} ¹¹⁴ Additional examples where an α -agostic form was considered or was calculated are found in the discussion portion of section 5.5.2. ¹¹⁵ The β -agostic interactions for Y and La are presented with the Ln complexes in section 8.1. ¹¹⁶ Additional derivatives exhibiting β -agostic interaction: $Cp_2Ti(\eta^2-Me_3SiC_2SiMe_2H)$, $Cp_2Ti(\eta^2-BuC_6SiMe_2H)$. Two other titanium complexes did not exhibit the β -agostic interaction: $[L_2Ti(\eta^2-RC_2SiMe_2H)]$ (L = Cp^* , R = 'Bu'; L = THf, R = 'Bu').¹³⁹ ¹¹⁷ Additional derivative, $Cp^*Ti(HMe_2SiC_2SiMe_2H)$, does not exhibit a β -agostic interaction.¹³⁹ ¹¹⁸ Additional derivatives: $Cp_2Zr(\eta^2-PhC\equiv CSiMe_2H)$, $Cp_2Zr(\eta^2-Me_3SiC\equiv CSiMe_2H)$.¹³⁹ ¹¹⁹ The Thf adducts of **3-8**, **3-9**, and complexes listed in the previous footnote were also reported and exhibited no β -agostic interaction.¹³⁹ ¹²⁰ As an isomeric ratio of 10:1. Data are given for the major isomer.^{146,147a} ¹²¹ Additional derivative, Ar = 2,6- $C_6H_3Me_2$.^{147a} ¹²² Reaction of $[NbCp(N'Bu)(PMe_3)_2]$ with $HSiMe_2Cl$ gave $[NbCp(\mu-N'Bu)Cl]_2$. No reaction of $[NbCp(NAr)(PMe_3)_2]$ occurs with the following silanes: $HClSiPr_2$, $ClSiMe_3$, Cl_2SiMe_2 or $HSiMe_2Ph$ under conditions comparable to those that gave **3-17**.^{147a} ¹²³ **3-18** is believed to be an isomer of **3-17** with the phosphine *trans* to Si-H and the Cl atom *cis* to Si-H.^{147a} ¹²⁴ X-ray structure was only of sufficient quality to establish overall geometry.^{32a,147a} ¹²⁵ See structure of **1-25b** (Table 9) for proton assignments.^{36b} ¹²⁶ See structure of **1-25c** (Table 9) for proton assignments.^{36b} ¹²⁷ The solvent specified in the supplementary information may be in error. ¹²⁸ IR in fluorolube; $\nu_{1615} \text{ cm}^{-1}$ was tentatively assigned to an agostic SiH.²⁰⁵ ¹²⁹ Prepared from reaction of $[Cp^*\{2,6-Pr_2C_6H_3\}N=](Cl)TaH_2$ with $(THF)_3LiSi(SiMe_3)_3$. The intermediate anion, $[Cp^*\{2,6-Pr_2C_6H_3\}N=](Cl)(H)Ta[Si(SiMe_3)_3]^-$ eliminated LiCl to form $[Cp^*\{2,6-Pr_2C_6H_3\}N=](H)TaSi(SiMe_3)_3$, which could be isolated but rearranges in solution to give $[Cp^*\{2,6-Pr_2C_6H_3\}N=](H)TaCH_2-m-Si(SiMe_3)_2H$ (not isolated because decomposition occurs on standing at room temperature).³⁶⁰ ¹³⁰ Complex $[Cp^*\{2,6-Pr_2C_6H_3\}N=](H)TaCH_2Si(SiMe_3)_2SiMe_2H$ could not be isolated.³⁶⁰ ¹³¹ Complex was prepared from the reaction of $[\eta^5-C_5Me_4Et](OC)(H)Ru=Si(H)\{C(SiMe_3)_3\}$ with CH_3CN .^{393a} Also reported were reactions of RCN and $[Cp^*(OC)(H)Ru=SiH\{C(SiMe_3)_3\}]$ to give $Cp^*(OC)(R)Ru\{CNSiH_2C(SiMe_3)_3\}$ (R = Me, Ph).¹²⁷ ¹³² The Rh...H...Si distance of 3.082 Å indicates that there is no direct Rh-Si bonding. The Rh...H...Si angle is 135°. ^{247b} ¹³³ Prepared from $(dmpe)Pt(SiHPh_2)_2$ and $EtO_2CC\equiv CCO_2Et$ (footnote 96, Table 2).¹²⁴ ¹³⁴ The sign on the coupling constant is negative.^{20b} ¹³⁵ Table 3, footnote 6. Additional derivatives are also reported.^{20b} ¹³⁶ Absolute value; sign of the coupling constant was not determined.^{20b} ¹³⁷ Hydrides were not located.^{20b} ¹³⁸ Values were calculated from the coordinates deposited in CCDC. ¹³⁹ Prepared from the reaction of $Cp_2Nb(H)_2(SiMe_2Cl)$ and Ph_3PLi_2THF .¹⁴⁴ ¹⁴⁰ Additional derivative, $Cp_2(H)Nb(SiMe_2Ph)_2$.^{142,144} ¹⁴¹ The formation of an inseparable mixture of $Cp_2Nb(SiMe_2Cl)_2H$ and $Cp_2Nb(C_2H_3Ph)SiMe_2Cl$ from reaction of Cp_2NbH_3 with $CH_2=CHPh$ followed by $HSiMe_2Cl$ at 65–70 °C in toluene was also reported. $Cp_2NbH(SiCl_3)_2$ was prepared from the reaction of Cp_2NbH_3 and $SiCl_4$.¹⁴⁴ ¹⁴² Prepared from $Cp_2NbH(SiMe_2H)_2$.¹⁴² ¹⁴³ Formed from $Cp_2NbH(SiMe_2I)_2$ on treatment with $MeOH/NEt_3$.¹⁴⁴ ¹⁴⁴ Prepared from $Cp_2Nb(C_2H_3Ph)H$ (Table 3, footnote 28).¹⁴⁴ ¹⁴⁵ Calculations were performed on model compounds, $[Cp_2NbH_3-m(SiH_nCl_{3-n})_m]$ ($m = 1, 2; n = 2, 3$).¹⁴² ¹⁴⁶ Prepared from Cp_2NbH_3 , $SiCl_4$, and NEt_3 .¹⁴³ ¹⁴⁷ Formed from $Cp_2Nb(SiMe_2H)_2H + Me_3SnCl$.^{356a} ¹⁴⁸ $Cp_2(H)Nb(SiMe_2H)(SiMe_2X)$ also prepared from $Cp_2HNB(SiMe_2H)_2$: X = F (X-ray); Br (X-ray); I.^{356a} ¹⁴⁹ Hydride is positioned symmetrically in the bisecting plane of niobocene.^{356a} ¹⁵⁰ Prepared from $Cp_2Nb(H)(SiMe_2H)_2$ and $[Ph_3C][PF_6]$. X-ray structure is disordered.^{356a}

Table 9q. Continued

¹⁴⁵ Disorder in the SiMe₂H group prevented determination of the Si–H_{term} distance.^{356a} ¹⁴⁶ Prepared from Cp₂Nb(H)(SiMe₂H)₂ and Me₃SnBr. X-ray structure is disordered.^{356a} ¹⁴⁷ Prepared from Cp₂Nb(H)(SiMe₂H)₂ and [PhNHMe₂]I. X-ray structure is reported.^{356b} ¹⁴⁸ Prepared from Cp₂Nb(SiMe₂Cl)(H)(SiMe₂H) and [PhNHMe₂]I. X-ray structure is reported.^{356b} ¹⁴⁹ Prepared from [Ph₃C][BF₄] and Cp₂Nb(SiMe₂Cl)(H)(SiMe₂H). X-ray structure is reported.^{356b} ¹⁵⁰ Prepared from F₃B·Et₂O and Cp₂Nb(SiMe₂Br)(H)(SiMe₂H). X-ray structure is reported.^{356b} ¹⁵¹ Prepared from F₃B·Et₂O and Cp₂Nb(SiMe₂I)₂(H). X-ray structure is reported.^{356b} ¹⁵² Prepared from Cp₂Nb(SiMe₂Cl)(H)(SiMe₂H) and [PhNHMe₂]Br. Disordered X-ray structure is reported.^{356b} ¹⁵³ Prepared from Cp₂Nb(SiMe₂Br)(H)(SiMe₂H) and I₂. Disordered X-ray structure is reported.^{356b} ¹⁵⁴ Two independent molecules in the unit cell.¹⁴⁹ ¹⁵⁵ Hydride not located.¹⁴⁹ ¹⁵⁶ No reaction occurs between [CpTa(NAr)(PMe₃)₂] and HSiMe₂Ph.¹⁴⁶ ¹⁵⁷ Measured from the ²⁹Si NMR spectrum.¹⁴⁶ ¹⁵⁸ Large estimated standard deviations of ~0.1 Å do not allow detailed discussion of the Si–H interaction.¹⁴⁶ ¹⁵⁹ Additional derivatives prepared from reaction of [CpTa(NAr)(PMe₃)₂] with H₂SiPhMe (Table 2) and HSiCl₃.^{78a} ¹⁶⁰ Related complexes prepared from HSiMe₂Cl and HSiPh₂Cl. The reaction with HSiPhMeCl was studied by NMR methods.^{147b} ¹⁶¹ Hydride was not located.^{147b} ¹⁶² Additional derivatives, Cp(L)(H)₂RuSiMe₂Cl (L = PPh₃ (X-ray), PPrPh₂, P(Pr)₂Ph (X-ray)).^{181c} ¹⁶³ Revised classification by Nikonov and contrasts to Tilley's 1992 report which assigned a classical structure. Campion, B.; Henyn, R. H.; Tilley, T. D. *Chem. Commun.* **1992**, 1201. ¹⁶⁴ See Table 3, footnote 95. ¹⁸⁶ ¹⁶⁵ SISHA corresponds to secondary interactions between silicon and hydrogen atoms.⁴⁵² ¹⁶⁶ Complex was formed from K[Cp*(OC)₂WH₂] and HSiCl₃. Complex may also be a case of IHI since the chlorides in the product are both *trans* to the bridging hydride.^{368e} ¹⁶⁷ Averaged coupling constant. An estimate of the coupling constant was proposed from the equation, $J_{\text{obs}} = 1/3[2 \cdot {}^1J_{\text{SiH}(\eta^2)} + {}^2J_{\text{SiH}(\text{terminal})}]$, assuming that ${}^2J_{\text{SiH}(\text{terminal})}$ is 0, which gave a value for ${}^1J_{\text{SiH}(\eta^2)}$ of 102 Hz.⁴⁵ ¹⁶⁸ Table 1, footnote 40. ⁴⁵ ¹⁶⁹ Additional derivatives prepared from reaction of (PMe₃)₃Ru(SiMe₃)H and HSiMe₂CH₂SiMe₃ and HSiEt₃.⁹⁷ ¹⁷⁰ Prepared from RuH₂{(η²-HSiPh₂O)(PCy₃)₂} and 5 equiv of PPh₃.³⁹⁸ ¹⁷¹ From partial hydrolysis of (Ph₃)₃H₂Ru{(η²-H-SiPh₂O)(SiHPh₂)}.³⁹⁸ ¹⁷² $T_{\text{1min}} = 32$ ms (**3-125a**); fast exchange from 199 to 293 K.^{207a} ²⁹Si measurement was both proton and phosphorous decoupled.^{207a} ¹⁷³ Signal coalescence at 20 °C.^{207a} ¹⁷⁴ Coupling constants were determined from the ²⁹Si{³¹P} spectrum.^{207a} ¹⁷⁵ Additional derivatives with {(η²-HSiMe₂)₂X}: X = O, –CH₂CH₂CH₂–; also [RuH₂{(η²-HSiPh₂O)(PCy₃)₂}] and [(Ph₃)₂(H)₂Ru{(η²-H-SiMe₂)₂X}] (X = C₆H₄).²⁰⁸ ¹⁷⁶ See Table 3, footnote 141. ²⁰⁸ ¹⁷⁷ From reaction of [(Cy₃)₂(H)₂Ru{(η²-HSiMe₂)₂X}], X = –(CH₂)₂– and PPh₃.²⁰⁸ ¹⁷⁸ From reaction of [(Cy₃)₂(H)₂Ru{(η²-HSiMe₂)₂X}], X = –(CH₂)₂– and a fivefold excess of PPh₃.²⁰⁸ ¹⁷⁹ From reaction of (Cy₃)₂(η²-H₂)RuH₂ and HMe₂SiOSiMe₂OSiMe₂H.²⁰⁸ ¹⁸⁰ Structure of **3-130b** can be formulated as having one SISHA interaction but is probably intermediate between the two structures shown in the structure section of Table 9. ^{211b} ¹⁸¹ Additional derivative: [(py₁)₂(H)₂Ru{(η²-H-SiMe₂)₂X}], X = –(CH₂CH₂)₂.²⁰⁸ ¹⁸² Ru–H distances obtained from the Cambridge Data Base. ¹⁸³ J_{SiH} represents an average between the ${}^2J_{\text{SiH}}$ involving the terminal hydrides and the ${}^1J_{\text{SiH}}$ for the σ-SiH.¹⁰¹ ¹⁸⁴ Hydrogen atoms were located on a difference Fourier map but introduced in idealized positions.¹⁰¹ ¹⁸⁵ Proton *trans* to CO.²²² ¹⁸⁶ The room-temperature signal resolves to a pattern expected for a AA'BXX' spin system.²²² ¹⁸⁷ Calculated from data in the CDB.²²² ¹⁸⁸ The multiplet at –11.19 ppm becomes a singlet in the ¹H{³¹P}-NMR spectrum. The signal broadens when the temperature is lowered from 298 to 233 K.²²¹ ¹⁸⁹ SiH data taken from ref 206. ¹⁹⁰ Additional derivative prepared from HSiEt₃.^{230b} Structure for **3-168b** is a tentative assignment based on the reported Si–H distances and was not proposed by the authors of the study. ¹⁹¹ Additional derivatives from primary silanes: Cp*(dmpe)(H)MoSi(H)R (R = Mes, CH₂Ph). Reaction with C₆F₅SiH₃ and SiH₄ led to decomposition products.³⁶ ¹⁹² The molybdenum hydride was not located in the final Fourier difference electron density map.^{36a} ¹⁹³ ν(M–H) not identified.³⁶⁸² ¹⁹⁴ Table 2, footnote 14. Additional derivatives: Cp*(dmpe)(H)Mo=(SiRR') (R = Me, R' = Ph; R = R' = Ph. Analogue was also prepared from D₂SiPh₂.³⁶ ¹⁹⁵ Location of the hydride ligand was not determined in the X-ray structure.⁸² ¹⁹⁶ Formed from reaction of **2-11** and Li(Et₂O)₃B(C₆F₅)₄.⁸² ¹⁹⁷ A bridging hydride structure has been calculated.⁸² ¹⁹⁸ Bridging hydride structure was supported by MO calculations.^{38a} ¹⁹⁹ Table 1, footnote 30. ^{38a} ²⁰⁰ No unique structure proposed for **1-19**. The bonding may best be described through resonance forms that involve HTaNSiHPhCl and a pentacoordinate Si center Ta⁺N(SiH₂PhCl)[–].^{32b} ²⁰¹ Additional derivatives prepared from H₂SiMePh (**2-25a**), HSiMeCl₂ (X-ray) (**3-68a**), and HSiCl₃ (**9-40**). Complexes were described in terms of adduct formation between the hypervalent anion [H₂SiR₃[–]] and [Cp(L)Fe]⁺, i.e., as Cp(L)Fe(η³-H₂SiR₃).^{42a} ²⁰² Additional derivatives prepared from HSiMe₂Cl and HSiCl₃.^{207b} In this case, the 2 hydrides become the σ-donor, H₂, which is an interesting contrast to other metal dihydride complexes.²⁰³ Two bonding descriptions were proposed for **3-212c**: either a classical silyl hydride (OA product) or a nonclassical η²-H–Si.^{254c} ²⁰⁴ This is a rare example of an η¹-H(Si). The J_{SiH} values fall in the range also observed for η²-H(Si) complexes.^{266a}

appears to be typical of dimers with [(R₃P)₂TMTM(PR₃)] units. This exchange could possibly account for the unusually low value of ${}^1J_{\text{SiH}}$ observed at room temperature for **3-260b**. A low-temperature value for J_{SiH} was not reported, but it appeared from the change in the chemical shift that the hydride associated with the Pt center converted from a bridging hydride at room temperature to a terminal hydride at low temperature.²⁷⁹ The assignment of a bridging versus a terminal hydride in the Pt dimers is not always unambiguous (see, for example, complex **2-103**).

Coupling constant data for one of the three Pd dimers, {[([L]Pd)₂(μ-η²-HSiPhR)₂} (L = PMe₃, R = Me, **2-80**, Ph, **2-81**;^{121b} L = PET₃, R = Ph, **2-82**)^{121b} have been reported both at room temperature and at –90 °C. The room-temperature J_{SiH} values were 77–79 Hz, and the values at –90 °C ranged from 80 to 86 Hz. There was essentially no change in the ¹H NMR spectrum on cooling, and the authors concluded that the complexes had the same structure in both the solid and in solution. For two related Pt complexes, **1-77**^{68a} and **1-78**^{68b} prepared from primary silanes, the ${}^1J_{\text{SiH}}$ could be determined at room temperature only for **1-77**, where ${}^1J_{\text{SiH}}$ was 48 Hz for Pt–H–Si but the coupling constant was not reported for the Si–H_{term}. In **1-78**, the ${}^1J_{\text{SiH}(\text{term})}$ was 216 Hz, a value that is indicative of an unbound SiH. Upon heating, the bridging and terminal SiH units undergo exchange.^{68b} Although there are a small number of dimers for which J_{SiH} values have been obtained, it appears that the values are generally near 80 Hz with the exception

of **1-78**, which, however, has been structurally characterized and exhibits a hydride in a bridging location.

An X-ray structure was reported for 31 of the 46 binuclear complexes listed in Table 4, and 27 of these have bridging hydrides. In 17 of 27, the bridging hydrides were located. For 6 additional examples, the hydrides were not located or refined, or the structure was disordered or of poor quality. For the Pd dimers, the Pd–H_{br} distance in Pd–H_{br}···Si ranges from 1.61 to 2.04 Å (6 values, but 5 values are ≤ 1.91 Å), while the Si–H_{br} varies from 1.56 to 1.75 Å (6 values; 5 values are ≤ 1.68). For **2-82**, which exhibited a Pd–H_{br} distance >2.00 Å as well as one of the shortest Si–H_{br} distances, the σ-interaction to Pd must be weak and may be better described as Si–H···Pd. The corresponding Pt–H_{br} distances tend to be somewhat shorter, 1.55–1.94 Å (15 values), and the related Si–H_{br} distances are longer, 1.64–2.07 Å (15 values). For both Pd and Pt, the Si–H_{br} distances overlap the range suggested for σ-interactions. However, these are distances from a heavy metal to hydrogen, which are not as reliable as [TM]–Si distances. An interesting comparison would be to Pt–H_{br}–Si and Pd–H_{br}–Si in monomeric σ-complexes, but only one Pd complex was reported with this unit (**3-259**)²⁷⁸ and it was not isolated since decomposition on warming to room temperature was observed.

Bimetallic complexes of W(1), Mn(1), Fe(2), Ru(10), and Rh(1) have also been reported, although these tend to have a variety of structures. The tungsten dimer, **2-27**, was structurally similar to the Pd₂ and Pt₂ dimers that were

described earlier.⁴⁰ Unfortunately, the bridging hydrides could not be located in the X-ray structure. Although a J_{SiH} was measured from the ^{29}Si NMR spectrum, the authors could not distinguish between the designation $\text{W}-\text{H}\cdots\text{Si}$ or $\text{W}\cdots\text{Si}-\text{H}$ and described the hydride as being a bridging agostic $\text{Si}-\text{H}$ interaction.⁴⁰ Although the Mn derivative, **3-56**,¹⁶⁶ was listed in the dinuclear category, the complex is actually a dimetalla-substituted disilane. The chemical shift, J_{SiH} , and IR data for the hydride were reported, and the complex decomposed at room temperature.¹⁶⁶

Interesting variations have been reported for the dimers formed from the Fe triad. There are three examples where a secondary silane spans a Fe–Fe bond (**2-34**^{93,94}) or a Ru–Ru bond (**2-44**,⁹⁹ **3-144a**¹⁰¹) with a bridging SiH to each metal. Both **2-34** and **3-144a** are fluxional, but decoalescence of the hydride signals was not achieved. A $J_{(\text{SiH})}$ value was reported only for **2-44** (24 Hz) and for **3-144** (22 Hz, av for 6 SiH and 2 RuH), and the low coupling constant reported for **2-44** may reflect a fluxional system, although this was not suggested by the authors. Structural data were reported for **2-34**, **2-44**, and **3-144**, although the quality of data for the last of these was insufficient to allow a complete analysis. Calculations of model compounds provided a structure consistent with three bridging ($\mu\text{-}\eta^2\text{-}\eta^2\text{-alkoxysilane}$) ligands and a hydride on each Ru. In the di-iron complex, **2-34**, the two SiH_{br} distances are 1.51 Å and the two Fe– H_{br} distances average 1.62 Å, which were relatively close to the average value of 1.664 Å for 11 complexes with Fe– H_{br} bonds that have been determined by neutron diffraction.^{451a} For the complex **2-44**, the RuH_{br} distances are 1.58 and 1.61 Å and the SiH_{br} distances are significantly longer at 1.86 and 1.88 Å. The SiH_{br} distances are actually close to those described as SISHA interactions (see section 5.5) for Ru complexes, although this example was not included in Lachaize and Sabo-Etienne's review⁴⁵² on the subject. Indeed, the authors of ref 101 (**3-144a**) depicted the bridging interaction with a solid line for Ru–H and a dotted line for $\text{Si}\cdots\text{H}_{\text{br}}$ (see Figure 4 or structure C' in Scheme 15B) as would be appropriate for a weak interaction between Si and H_{br} . Another variation of this particular structural theme was complex **2-42b**, which contained a RuSiRu triangle but only one side contained a bridging SiHRu. Unfortunately, there was no crystal structure, but the J_{SiH} value was determined to be 36 Hz. In this case, there was a terminal SiTol_2H group and the J_{SiH} for this group was 178.5 Hz. With this value for $J_{\text{SiH}(\text{term})}$, it is unlikely that there is exchange between the bridging and terminal hydrides. Another interesting Ru_2 dimer was produced when (Vin)MeRSiH was reacted with $\text{Cp}^*\text{Ru}(\mu\text{-H})_4\text{RuCp}^*$ to produce $\{\text{Cp}^*\text{Ru}(\mu\text{-H})\}_2\{\mu\text{-}\eta^2\text{-}\eta^2\text{-H-SiMeR}(\text{CH}=\text{CH}_2)\}$ (R = Me, **3-138**; Ph, Table 3, footnote 153).²¹⁴ In this case, there was one hydride bridging Ru–Si while the vinyl group coordinated to the second Ru center. The complex **3-138** was fluxional in $\text{tol-}d_8$ or $\text{tol-}d_8/\text{THF-}d_8$ mixtures down to -70°C , but in $\text{THF-}d_8$ an averaged J_{SiH} value of 31 Hz was obtained and at -70°C , $J_{\text{SiH}} = 54$. The fluxional process was assigned to exchange of the $\text{Ru}-\text{H}_{\text{br}}-\text{Si}$ hydride and both $\text{Ru}-\text{H}_{\text{br}}-\text{Ru}$ hydrides.²¹⁴

Probably one of the most interesting examples of a complex containing a $\text{Ru}-\text{H}_{\text{br}}-\text{Si}$ that does not conform to either of the two structural motifs just described (triangular or parallelogram) is the complex **2-45**, which resulted from addition of H_2SiPhMe to $\text{RuH}_2(\eta^2\text{-H}_2)(\text{L})_2$ (L = C_3P , **2-45**, and $^i\text{Pr}_3\text{P}$, Table 2, footnote 52).^{100,101} Under the conditions of the experiment, the silane undergoes disproportionation

to give SiH_4 (and other hydrosilane products), which is subsequently trapped to give $(\text{L})_2\text{H}_2\text{Ru}(\mu\text{-}\eta^2\text{-}\eta^2\text{-}\eta^2\text{-SiH}_4)\text{RuH}_2(\text{L})_2$. The structure of the L = P^iPr_3 complex showed that the sequence Ru–Si–Ru was linear with two hydride bridges spanning each Ru–Si bond and also two additional terminal hydrides on each Ru. The complex was fluxional and a J_{SiH} of 36 Hz was observed, which corresponded to a value averaged between the four bridging hydrides and the four terminal hydrides. Although decoalescence was observed at 203 K, no additional coupling constants were reported. Calculations (model, L = PH_3) provided an optimized D_{2d} structure that agreed with the X-ray structure including the rather short Ru–Si distances that are in the range of Ru=Si complexes (see Table 8, section 4).

The last two Ru dimers reported during this review period were both unique. The silylene complex, $\text{Cp}^*\{\eta^1\text{-Si}(\text{BuNHCHCHN}^+\text{Bu})\}\text{RuCl}$, was reacted with an equivalent of a primary silane in order to compare the results to those previously reported for a similar reaction with the 16e precursor, $\text{Cp}^*(^i\text{Pr}_3\text{P})\text{RuCl}$. The latter complex gave the OA product, $\text{Cp}^*(^i\text{Pr}_3\text{P})(\text{H})\text{Ru}(\text{SiH}_2\text{Ph})$.^{51b} Instead of the expected simple oxidative addition, the more complex product $[(\text{Cp}^*\text{Ru})_2(\text{H})(\mu\text{-H})(\mu\text{-}\eta^2\text{-HSiRCl})(\mu\text{-}\eta^2\text{-Cl-Si}(\text{BuNHCHCHN}^+\text{Bu}))]$ (R = Ph, *n*-Hex, **1-43**^{51a}) was obtained. The X-ray structure of the product produced from HexSiH_3 was reported, but disorder precluded the location of the positions of the three hydride ligands. Each of the three hydrides in the two complexes was identified in the room-temperature ^1H NMR spectrum, with the lowest field hydride resonance assigned to $\eta^2\text{-HSi}$ with a $J_{(\text{SiH})}$ of 40 Hz (**1-43**) and 42 Hz (R = Ph). Heating to 70°C did not result in coalescence of any of the hydride signals but did lead to decomposition. All three hydrides were derived from the starting primary silane as verified by using PhSiD_3 in place of PhSiH_3 .^{51b} A broad absorption $\sim 1850\text{ cm}^{-1}$ characteristic of a ($\mu\text{-}\eta^2\text{-HSiRCl}$) was also observed in the IR spectrum. The last remaining Ru dimer, **3-143**,²⁰¹ has a structure whose bonding can have a flexible interpretation. This dimer also has a four-membered ring core of alternating Ru and Si centers. However, in this case, there are two adjacent sides that appear to be bridged by a hydride in contrast to opposite parallel sides in the Pt_2 and Pd_2 dimers described earlier. The Ru–Si distances on the two adjacent sides that are bridged are longer (2.56 Å av) than the remaining two non-bridged sides (2.38 Å av). The two hydrides were located in the structure and both are on the same Ru center and may or may not be depicted as bridging. The Ru–H distances are 1.66(2) and 1.69(2) Å, and the corresponding Si–H distances are 1.67(2) and 1.56(2) Å. Related to **3-143** is the dimer $[(\text{Cp}^*\text{Ru}(\mu\text{-}\eta^2\text{-}\eta^2\text{-H}_2\text{SiEt}_2))_2(\mu\text{-H})][\text{BPh}_4^-]$ prepared from protonation of $[(\text{Cp}^*\text{Ru}(\mu\text{-}\eta^2\text{-HSiEt}_2))_2(\mu\text{-H})(\text{H})]$ with triflic acid followed by exchange of the triflate anion with BPh_4^- .⁴⁰³ The cation contains a Ru_2Si_2 core with a $\text{Ru}\cdots\text{H}\cdots\text{Ru}$ bridge, and with all four sides containing bridging $\text{Si}-\text{H}_{\text{br}}-\text{Ru}$, this “dimer” could be viewed as containing two bridging Et_2SiH_2 groups. There are alternating Ru–Si distances (2.438(av) and 2.507(av) Å). The four bridging Si–H distances range from 1.73(3) to 1.81(2) Å, the Ru– H_{br} to Si bridging distances ranged from 1.548 to 1.632 Å, and the hydride bridged the two Ru centers at distances of 1.724 and 1.799 Å. The molecule is fluxional and exhibited a single ^1H resonance for the hydrides at room temperature with a $^1J_{(\text{SiH})} = 18\text{ Hz}$ (for 5 protons).

Again, there is not much of a benchmark for a hydride bridging distance between Ru and another atom. The average of 3 values for a Ru–H_{br} in the review article on neutron diffraction of metal hydrides is 1.782 Å and of 7 values for a Ru–H_{term} is 1.611 Å.^{451a} It should be noted that the 4 Ru–H_{br} distances found in Table 9 for Ru₂ σ -complexes cluster around 1.56–1.62 Å (5 values). The Si–H_{br} distances in **3-143** are longer than the average Si–H distance of 1.50 Å determined by X-ray diffraction for hydrosilanes.^{457a} Unfortunately, the authors reported neither J_{SiH} coupling constants nor IR stretching modes other than those for the CO ligands. Three valence bond structures were suggested, including (a) a bridging dimethylsilylene and a terminal hydride ligand; (b) a Si–H bond that is bound to Ru in an η^2 -fashion; and (c) a composite form such as that depicted in Scheme 15B. That the two sides that may participate in a nonclassical bonding interaction are longer than the other two sides is supportive of a bridging hydride, but without additional spectroscopic data there can be no conclusion.

Only one bimetallic complex containing 2 Rh centers, **2-69**, has been included in Table 9. The X-ray structure was obtained, and the 2 bridging and 2 terminal hydrides were located. The 2 Rh–H_{term} distances are 1.52 Å, and the 2 Rh–H_{br} distances are 1.70 Å. Although **2-69** contains a 4-membered ring core, it is folded along the Rh–Rh bond with 2 opposite sides containing bridging hydrides. The bridging and nonbridging Rh–Si distances are 2.50 Å(av) and 2.33 Å(av), respectively. The complex was fluxional at room temperature, and at low temperature, two broad hydride signals could be resolved and were assigned to 2 agostic and 2 terminal hydrides. Unfortunately, neither coupling constants nor IR data were reported.¹¹⁴

In the cases covered under the umbrella of nonclassical interactions, it has been assumed that the interactions in the unit Si–H–TM observed in the solid state persist in solution. However, this is not the case for the complex $\{[\eta^5\text{-C}_5\text{H}_4(\text{SiMe}_2\text{H})]\text{ZrCl}_3\}_2$, **3-10**.¹⁴⁰ The solid-state structure of **3-10** showed that the two monomer units, $\{\eta^5\text{-C}_5\text{H}_4(\text{SiMe}_2\text{H})\}\text{ZrCl}_3$, are held together by Si–H \cdots Zr bridges with a normal Si–H distance of 1.47(2) Å, and a rather long SiH \cdots Zr distance of 2.28(3) Å. This weak interaction does not persist in solution, and the ¹H resonance for SiH appears at 4.50 ppm as a septet (coupling to the protons of the two methyl groups) and, thus, a “normal” environment for the SiMe₂H group in solution. No low-temperature NMR data were reported, although this might be an interesting experiment to determine whether a monomer \rightleftharpoons dimer equilibrium exists.

5.4.2. α -, β -, and Other Long-Range Agostic Interactions

5.4.2.1. α -Agostic Interactions. In the systems described in this section (see Figure 4), the main focus will be on the interaction of a Si–H group that is tethered to the metal center by one or two intervening atoms. In the α -agostic system, this will not be the case, as the silicon center itself functions as the “tether” and is also why it is difficult to determine how this description can be distinguished from the σ -complexes described in the previous section. In general, the agostic interaction is distinguished by a reduction of the J_{SiH} value relative to the free silane, a red-shift of the Si–H frequency in the infrared spectrum, and an elongation of the Si–H bond distance in the few examples where X-ray data are available and included hydrides that were actually located. In the discussion that follows, the focus will be on how the

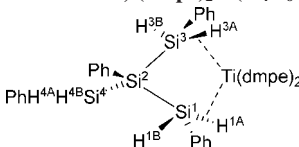
Table 10. Characterization of the α -Agostic Interaction in $\text{Cp}_2\text{Hf}(\eta^2\text{-SiHMe}_2)(\mu\text{-Me})\text{B}(\text{C}_6\text{F}_5)_3$ (9-12**)^{307c}**

spectroscopic features of the SiH unit	$\text{Cp}_2\text{Hf}(\eta^2\text{-SiHMe}_2)(\mu\text{-Me})\text{B}(\text{C}_6\text{F}_5)_3$ (A)	$\text{Cp}_2\text{Hf}(\text{SiHMe}_2)\text{Me}$ (B)	Me_2SiH_2
δ ¹ H NMR	1.80	4.98	5.29
¹ J_{SiH} (Hz)	57	145	195
²⁹ Si{ ¹ H} NMR	158	8.25	–61
ν_{SiH} (cm ^{–1})	1415	2077	2151

original investigators described their experimental results and secondarily on the results of theoretical calculations where an α -agostic interaction may be determined at a higher energy relative to the lowest energy calculated structure.

The first identified system with an α -agostic assignment, $\text{Cp}_2\text{Hf}(\eta^2\text{-SiHMe}_2)(\mu\text{-Me})\text{B}(\text{C}_6\text{F}_5)_3$ (**9-12**), was prepared from the reaction of $\text{Cp}_2\text{Hf}(\text{SiHMe}_2)\text{Me}$ with $\text{B}(\text{C}_6\text{F}_5)_3$.^{307c} The complex was unstable in solution at room temperature, but a solid complex was isolated at low temperature as a red powder. The gas-phase structure calculated for the model compound $[\text{Cp}_2\text{HfSiH}_3]^+$ as well as for $[\text{Cp}_2\text{HfSiH}(\text{2,6-C}_6\text{Me}_2\text{H}_3)_2]^+$ was also reported.^{307c} The structural features that distinguish the α -agostic interaction are highlighted by a comparison of the complex, $\text{Cp}_2\text{Hf}(\eta^2\text{-SiHMe}_2)(\mu\text{-Me})\text{B}(\text{C}_6\text{F}_5)_3$ (**A**), relative to the neutral precursor, $\text{Cp}_2\text{Hf}(\text{SiHMe}_2)\text{Me}$ (**B**), both of which are, in turn, different from the free silane Me_2SiH_2 . These features are summarized in Table 10. The values shown for the free silane are in the normal range expected. In **A**, the SiH resonance is shifted upfield relative to both the free silane and **B**, although it is not shifted as far upfield as is normally observed for the σ -SiH complexes described in section 5.4.1. However, it is shifted in a manner similar to the β -agostic complexes that will be described next in this section. The ²⁹Si resonance in **A** is shifted downfield towards the region usually identified as having silylene character. Consistent with this observation is the calculated structure that has a sum of angles about Si (ignoring the agostic hydrogen) near 360°. Lastly, the SiH stretching frequency in **A** is dramatically red-shifted relative to that in **B**. The calculated structure for the unsolvated, counterion-free models of **A** gave a final minimized geometry that contained an α -agostic interaction consistent with the proposed structure of **A**. The calculated geometry about silicon was a distorted trigonal monopyramidal environment with a bridging hydride occupying a pseudoaxial position. The relevant Hf–Si–H_{br} angle was acute at 52° for $[\text{Cp}_2\text{Hf–SiH}_3]^+$ and 50° for $[\text{Cp}_2\text{Hf–SiH}(\text{2,6-C}_6\text{Me}_2\text{H}_3)_2]^+$, which would be expected for such a bridging interaction. An interesting feature for both the calculated structures was a Hf–Si distance that was shorter than the range in crystallographically characterized complexes (see Table 7, section 4, for ranges), although there are no distances reported in Table 7 for cationic Hf–Si complexes and such distances might be expected to be shorter than those reported in both Tables 6 and 7. The Si–H_{br} is “stretched” (1.63 Å) relative to Si–H_{term} (1.49 Å), and the calculated $\nu_{\text{Si–H}}$ stretching frequency of 1475 cm^{–1} compares well to the observed value of 1415 cm^{–1}. The authors concluded that the coordinatively unsaturated complex with an electron-poor Hf center as in **A** was stabilized by the α -agostic SiH interaction.

The titanium complex, **1-14c**, $\text{Ti}(\text{Si}_4\text{H}_6)(\text{dmpe})_2$,^{29b} was described by the authors as an α -agostic complex. Titanium is certainly in the same triad as hafnium (complex just described above), but **1-14c** may or may not fit this category.

Table 11. Relevant Bond Distances, Chemical Shifts, and Coupling Constants for 1-14c, (dmpe)₂Ti(SiH₆Ph₄)^{29b}


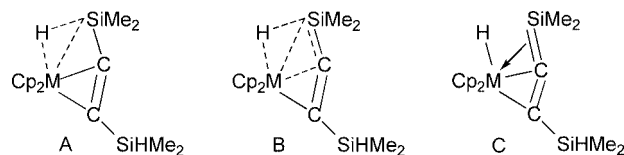
bond distances, Å	chemical shifts ¹ H δ	coupling constants ¹ J _{SiH} (Hz)
Si ¹ –H ^{1A} : 1.83(2)	4.27 (dd) ^a	<40 ^b
Si ¹ –H ^{1B} : 1.54(3)	6.57 (d) ^a	127 ^a
Ti···H ^{1A} : 1.67(2)		
Si ³ –H ^{3A} : 1.83(2)	4.19 (d) ^a	<40 ^b
Si ³ –H ^{3B} : 1.54(3)	6.31 (dd) ^a	133 ^a
Ti···H ^{3A} : 1.68(2)		
Si ⁴ –H ^{4A} : 1.46(4)	4.95 (d)	186
Si ⁴ –H ^{4B} : 1.45(3)	4.50 (d)	189
Si ¹ –Ti: 2.539(2)		
Si ² ···Ti: 3.056(2)		
Si ³ –Ti: 2.519(2)		

^a From ¹H{³¹P} NMR spectrum. ^b Number not provided.

Part of the problem is that key pieces of data are missing. Structural parameters are not available for **9-12**, but in this case, DFT calculations were used to support a structural assignment and a key piece was provided in the IR data. In addition, a comparison of parameters for a closely related silyl–hafnium complex and for the free silane was provided. However, for **1-14c**, structural data were provided but no supportive DFT calculations nor IR data were supplied. The spectroscopic and structural parameters for **1-14c** are shown in Table 11. The Si–Ti bond distances for Si¹ and Si³ for **1-14c** are within the range observed for Si–Ti bond distances (Table 7). The chemical shifts for the relevant Si–H agostic protons are shifted upfield but not to the extent observed in **9-12**, but they are separated by more than 2 ppm from the related geminal proton. The ¹J_{SiH} values are reduced from the general values observed for a free silane to ~130 Hz and are also considered consistent with the 0.1 Å elongation of these SiH bonds. The noninteracting PhSiH₂ protons on Si⁴ are observed at 4.95 and 4.50 with ¹J_{SiH} values ~187 Hz in the range observed for “free” silanes. The authors refer to the Ti···H–Si interactions as agostic α-Si–H···Ti but provide no reason for this choice over that of a σ-complex designation. However, in the σ-complex, the Si–H···M proton signal is usually shifted upfield of TMS, which was not the case for **1-14c**.

A bridging hydride has been unequivocally located in the neutron diffraction study of the complex Cp*(dmpe)Mo(H)(SiEt₂) (**2-10**), which was prepared from the reaction of Cp*(dmpe)Mo(η³-CH₂C₆H₅) with H₂SiEt₂.^{36a} This example was presented as a case study in section 5.3. The authors considered five representations (three are included in Figure 8) for the structure including the α-agostic structure shown in Figure 8, **2-10a**, but the details of the solid-state data do not support such a single representation; it was concluded that the composite structure shown in Figure 8, **2-10c**, which is a hybrid of the silylene hydride structure **2-10b** and the α-agostic form, should represent the complex. It was also concluded that the hydride ligand was disordered over the bridging positions on both sides of the Mo–Si bond.^{36a}

The calculated structure of [(dhpe)Pt(SiH₃)]⁺ showed that the more stable minimum contains an essentially planar silylene group coordinated to the Pt center and a third

**Figure 9.** Three resonance structures proposed for SiH interactions in Cp₂M(RC≡CSiMe₂H).

hydrogen that bridges the Pt–Si bond with almost equal Pt–H_{br} and Si–H_{br} distances. A second structure at a higher energy (3.1 kcal/mol) exhibited a T shape where one P of the dhpe ligand is *trans* to the empty site on Pt). In this case, the silyl group has two hydrogen atoms out of the molecular plane, while a third occupies a position in the molecular plane (Pt–Si–H angle = 93.6°) with a H-to-Pt distance in Si–H···Pt of 2.890 Å. According to the authors: “this may be indicative of, at best, a weak α-agostic Si–H bond...”⁴⁶⁶

Thus, the number of actual, isolated examples of an α-agostic Si–H bond still appears to be one (**9-12**) or two (with **1-14c**), although it is possible to use this descriptor for dimer complexes that were discussed under σ-complexes. The α-agostic Si–H bond has been found in calculated structures that can be close in energy to the minimum energy structure as described earlier in this section.

5.4.2.2. β-Agostic Interactions. For complexes in this category, a one-atom tether holds the SiH grouping in the vicinity of the metal, and this interaction is the most studied of the agostic systems. Key features in the β-agostic interaction should be a value for ¹J_{SiH} that is intermediate between those reported for σ-complexes and an uncoordinated silane, an upfield shift in the M···H–Si ¹H NMR resonance, and a red-shift of the SiH stretching frequency in the IR spectrum, although the values are different from those that were described as α-agostic. Since the coupling constant values are larger than those discussed for σ-complexes, a weaker interaction can be inferred as well as that β-agostic systems represent an earlier stage in the oxidative addition of SiH to the metal. The examples of isolated complexes assigned a β-agostic interaction during the current review period come from the Ti, V, Cr, and Fe triads.

A number of complexes of the general formula L₂M(RC≡CSiMe₂H) (L = a Cp-type ligand; M = Ti, Zr) have been reported.¹³⁹ The M···H···Si interaction depicted by the authors resembled the composite structure shown in Scheme 15B as well as A in Figure 9 (for R = SiMe₂H). In the titanium case, it could be shown that bulky Cp ligands (Cp* and THf) provided sufficient steric hindrance to prevent the formation of the β-agostic interaction. For the four isolated complexes (M = Ti, Cp ligand), the spectroscopic properties measured included SiH ¹H NMR resonances (at room temperature) that were shifted upfield (–3.7 to –6.5 ppm), ¹J_{SiH} values that ranged from 99 to 123 Hz, and ν(SiH) stretching frequencies ~1750 cm^{–1}. The solid-state ¹³C and ²⁹Si NMR spectra of Cp₂Ti(‘BuC≡CSiMe₂H) exhibited chemical shifts close to the values obtained for the low-temperature solution data; thus, the structure for the solution (low temperature) should be similar to that determined by X-ray crystallography.¹³⁹

The corresponding isolated zirconium complexes exhibited similar features, although the ¹J_{SiH} values were lower (68–86 Hz) and the ν(SiH) stretching frequencies were also more red-shifted and near ~1700 cm^{–1}. A novel feature for Cp₂M(HMe₂SiC≡CSiMe₂H) (M = Ti, **3-4**; Zr, **3-9**) was the presence of a single SiH resonance at ~360 K in tol-*d*₈,

whereas at low temperature, two different Si–H bonds are detected: at 165 K, for $M = \text{Ti}$ the $^1J_{\text{SiH(free)}} = 186 \text{ Hz}$ and the coordinated $^1J_{\text{SiH}} = 92$, and at 246 K, for $M = \text{Zr}$ the $^1J_{\text{SiH(free)}} = 187 \text{ Hz}$ and the coordinated $^1J_{\text{SiH}} = 69 \text{ Hz}$. A flip-flop coordination of the Si–H groups about the metal center was proposed to account for the temperature dependence exhibited in the ^1H NMR spectra. The crystal structure of **3-9** gave a $\text{Zr–H} = 2.042 \text{ \AA}$ and a $\text{Si–H} = 1.634(4)$ for the coordinated SiMe_2H group (and 1.425 \AA for the uncoordinated SiH). There were some unusual features revealed in the solid structure that cannot be accounted for by structure **A** in Figure 9, including an unexpectedly short distance between the alkynyl carbon and the silicon center of the group that interacted with Zr. This suggested a contribution of form **B** (Figure 9) and perhaps **C**, although the authors could not unambiguously prove OA of the Si–H from the low-temperature NMR data.¹³⁹

There are four similar complexes with a N-tether in which a β -agostic interaction was proposed: $[\text{Cp}(\text{Cl})(\text{PMe}_3)\text{Nb}\{\eta^3\text{-N}(\text{Ar})\text{SiMe}_2\text{-H}\}]$, **3-17** ($\text{Ar} = 2,6\text{-}^i\text{Pr}_2\text{C}_6\text{H}_3$), **3-19** ($\text{Ar} = 2,6\text{-Me}_2\text{C}_6\text{H}_3$),^{146,147a} and $(\text{Me}_3\text{P})_2(\text{ArN}=\text{C})\text{ClMo}[\text{N}(\text{SiMe}_2\text{RH})\text{-Ar}]$ ($\text{Ar} = 2,6\text{-Me}_2\text{C}_6\text{H}_3$), **3-37a** ($\text{R} = \text{Me}$ and $\text{R} = \text{Cl}$; Table 3, footnote 46).^{155a} The $^1J_{\text{SiH}}$ values ranged from 97 to 129 Hz and, thus, were similar to the Ti complexes just described. The X-ray structures were determined for all four complexes, although that for **3-19** was only able to establish the connectivity. The Nb–H distances were within $1.92 \pm 0.01 \text{ \AA}$ and the Si–H values ranged from 1.51 to 1.54 \AA , indicating a relatively weak Si–H interaction with the Nb center. Calculations were performed for both sets of complexes, and the results were dependent on the model used. For **3-17**, the closest comparison between the DFT and X-ray structures was obtained with the most sophisticated model that had a phenyl substituent at nitrogen and methyl substituents at both the phosphorus and silicon centers.^{147a} The data were consistent with an Si–H bond exhibiting a greater degree of OA to Nb in **3-17** than in its isomer **3-18** (phosphine and chloride exchange places, Table 3). The calculations indicated that the model compound has a d^2 , Nb(III) center and was best described with a β -agostic silylamine description. The replacement of a Si–Me in **3-37** with the more electron-withdrawing Cl substituent in **3-38** did not result in a decrease in $^1J_{\text{SiH}}$; rather, the value increased, indicating that the usual trend for such substituent changes, which generally result in a decrease in $^1J_{\text{SiH}}$ (indicating a later stage of the OA), was not observed in this system.^{155a}

In a later report by Nikonov and coworkers, the reactions of imido complexes, $[\text{Cp}(\text{ArN}=\text{M})(\text{PR}_3)_2]$ [$M = \text{V}, \text{Nb}$; $\text{Ar} = 2,6\text{-diisopropylphenyl}$; $\text{Ar}' = 2,6\text{-dimethylphenyl}$; $\text{PR}_3 =$ various phosphines (commonly PMe_3)] with the silanes H_3SiPh , H_2SiMePh , HSiR_2Cl ($\text{R} = \text{Me}, \text{Ph}, \text{Cl}$), HSiMePhCl , and HSiMeCl_2 were reported.^{32a} The products included both classical metal silyls as well as $\beta\text{-Si–H}\cdots\text{M}$ agostic complexes. The type of product obtained was controlled by the substitution at silicon and nitrogen and the steric properties of the phosphine. Donor groups at silicon in the chlorosilanes and the smaller Ar' group at nitrogen favored the formation of the $\beta\text{-Si–H}\cdots\text{M}$ agostic interaction, while electron-withdrawing groups at silicon produced metal silyl complexes. For example, HSiMeCl_2 , HSiPh_2Cl , and HSiCl_3 formed classical complexes with the $M = \text{Nb}$ precursor, whereas HSiMe_2Cl and HSiMePhCl produced a nonclassical β -agostic complex (examples are shown in Figure 10). A

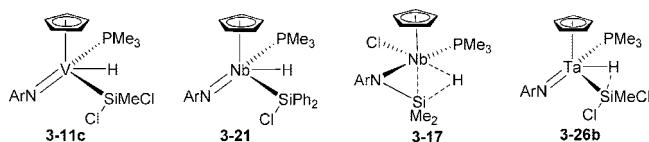
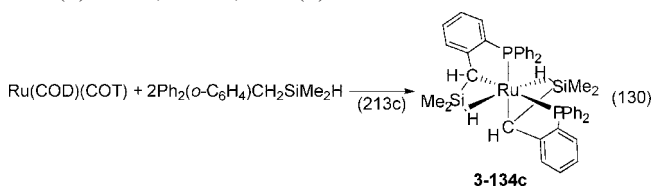


Figure 10. Comparison of classical complexes **3-11c** and **3-21**, nonclassical complexes **3-17** (β -agostic), and the IHI complex **3-26b**. $\text{Ar} = 2,6\text{-}^i\text{Pr}_2\text{C}_6\text{H}_3$ for **3-11c**, **3-21**, and **3-17**^{32a} but $2,6\text{-Me}_2\text{C}_6\text{H}_3$ for **3-26b**.^{147b}

related study was also reported with $\text{Cp}(\text{ArN}=\text{Ta})(\text{PMe}_3)_2$ and hydrosilanes.^{147b} The X-ray structure analysis, the DFT calculations, and the sign of the coupling constant J_{SiH} indicated that the complexes $\text{Cp}(\text{ArN}=\text{Ta})(\text{PMe}_3)(\text{H})\text{-(SiMe}_n\text{Cl}_{3-n})$ exhibited an IHI interaction between the Ta–H and the Si–Cl centers (Figure 10). Thus, the products that were formed were also a function of the metal, with the V and chlorosilanes producing classical complexes (but unstable). The Nb products showed a greater variation as both classical and nonclassical complexes formed and the Ta product exhibited IHI interactions. In this study, the sign of J_{SiH} was determined for several complexes and was demonstrated to be positive for the classical complex, $\text{Cp}(\text{ArN})(\text{Me}_3\text{P})(\text{H})\text{Ta}(\text{SiMePhH})$, and negative for $\text{Cp}(\text{ArN})(\text{Me}_3\text{P})(\text{H})\text{Ta}(\text{SiR}_n\text{Cl}_{3-n})$, indicating a direct Si–H interaction in the latter set of complexes supporting the IHI interaction.^{147b}

The ruthenium complex, $\text{L}_4\text{Ru}(\text{CH}_2\text{SiMe}_2\text{Cl})(\text{H})$ ($\text{L} = \text{PMe}_3$), **3-119a**, was reported by Berry and coworkers from the reaction of $\text{L}_4\text{Ru}(\text{SiMe}_3)\text{H}$ and $\text{HSiMe}_2\text{CH}_2\text{Cl}$.²⁰⁵ Thermal or photochemical treatment of **3-119a** provided *fac*- and *mer*-isomers of $(\text{Me}_3\text{P})_3(\text{Cl})\text{Ru}(\text{CH}_2\text{SiMe}_2\text{-H-}\mu)$ (**3-119b** and **3-119c**, respectively) where the spectroscopic data were consistent with a β -agostic interaction (C as a tether) and the complexes were assigned this description by the authors. The $^1J_{\text{SiH}}$ values were $\sim 76 \text{ Hz}$, which are smaller than the values observed for the other complexes described in this section. The $\text{Ru}\cdots\text{H}$ and $\text{Si}\cdots\text{H}$ distances were 1.550 and 1.664 \AA for *fac*-**3-119b** and 1.732 and 1.557 \AA for *mer*-**3-119c**, respectively. Thus, the SiH distances were also more elongated for these Ru complexes, especially in the case of the *fac*-isomer, compared to the distances described earlier.²⁰⁵ The reaction sequence to give **3-119b** and **3-119c** was the first example of the transformation of $[\text{TM}]\text{SiMe}_3$ to a β -agostic $[\text{TM}]\text{CH}_2\text{SiMe}_2\text{H}$ and was believed to occur as a result of SiH coordination to an unsaturated metal center, which would provide a greater stabilization than any similar C–H binding of the metal silyl substituent.²⁰⁵ The reaction of the chelating system, $\text{Ph}_2\text{P}(\text{o-C}_6\text{H}_4)\text{CH}_2\text{SiMe}_2\text{H}$, with $\text{Ru}(\text{COD})(\text{COT})$ provided the unusual β -agostic complex **3-134c** (eq 130). The $\eta^2\text{-SiH}$ resonance was observed at -9.77 ppm with a $J_{\text{SiH}} = 67$. A good agreement between the DFT calculations and the X-ray parameters was obtained: X-ray/DFT: $\text{Ru–Si}(1), 2.4587(13)/2.454$; $\text{Ru–Si}(2), 2.4367(13)/2.454$; $\text{Ru–H}, 1.71(4)/1.709$; $\text{Ru–H}, 1.68(4)/1.709$; $\text{Si–H}, 1.76(4)/1.709$; $\text{Si–H}, 1.65(3)/1.709$.^{213c}



Corral and coworkers have demonstrated through high-level DFT methods that the gas-phase interaction of

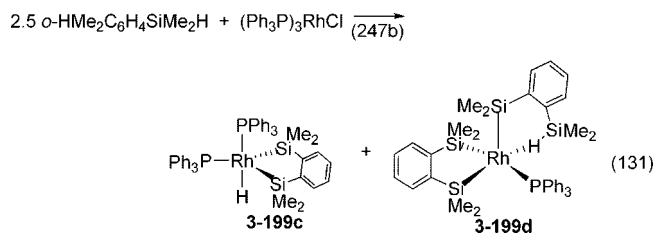
$\text{CH}_2=\text{C}(\text{H})\text{SiH}_3$ with Ni^+ led to a complex where the lowest energy structure was one in which the C_α and one of the $\text{Si}-\text{H}$ bonds coordinated to Ni^+ and thus would be classified as a β -agostic interaction.⁴⁶⁷ The most stable calculated structure for the related Cu^+ case also exhibited a similar β -agostic interaction.⁴⁶⁸ In the calculations for the related alkynyl complex of $\text{HC}\equiv\text{C}-\text{SiH}_3$ and Cu^+ , the agostic structure was only slightly higher in energy than a conventional π -complex.⁴⁶⁹ An agostic interaction with the *ortho*-carbon atom and one of the hydrogens in the $-\text{SiH}_3$ group of $\text{C}_6\text{H}_5\text{SiH}_3$ was the global minimum on the potential energy surface, but for Ni^+ , such structures are slightly less stable than the conventional π -complex.⁴⁷⁰ There are several silylamido complexes of lanthanide elements that exhibit β -agostic interactions, but these will be presented later in section 8.1.

5.4.2.3. γ -Agostic Interactions and Beyond. γ -Agostic interactions have been proposed for five complexes, but there does not appear to be a consistent pattern in the data that have been reported. Neither of the complexes $[\text{Cp}^*(\{2,6\text{-iPr}_2\text{-C}_6\text{H}_3\}\text{N}=\text{H})\text{TaCH}_2\text{Si}(\text{SiMe}_3)_2\text{SiMe}_2\text{H}]$ (**9-13**)³⁶⁰ nor $[\text{Cp}^*(\text{Me}_3\text{P})\text{Rh}[\text{C}_6\text{H}_4(\eta^2\text{-HSiPh}_2)]][\text{BAR}'_4]^-$ (**3-182b**)²³⁹ could be isolated, but three Pt complexes were isolated and two were crystallographically characterized.^{124,454} For the Ta and Rh complexes, only NMR data were reported, and the $^1J_{(\text{SiH})}$ values are close in value (87 Hz for the Ta, and 84 Hz for the Rh complex). The $\text{SiH}\cdots\text{Rh}$ resonance is shifted upfield to -8.95 ppm in **3-182b**, a shift similar to that observed in σ -complexes and also in the β -agostic complexes described in the previous subsection. In the Ir analogue of **3-182b**, the $\text{Si}-\text{H}$ undergoes full oxidative addition to the metal center.²³⁹ An upfield shift in the tantalum complex occurred to a lesser extent, although there are not enough complexes that contain a $\text{Ta}\cdots\text{HSi}$ interaction with which to compare this particular case. The ruthenium complex, **9-14**, exhibits a ^1H NMR resonance at -10.60 (d) with a $^1J_{\text{SiH}} = 75$ for the γ -agostic SiH and an additional resonance at 4.80 (d) with $^1J_{\text{SiH}} = 225$ for the terminal SiH . The agostic $\text{Si}\cdots\text{H}$ distance was $1.71(3)$ Å.^{343a}

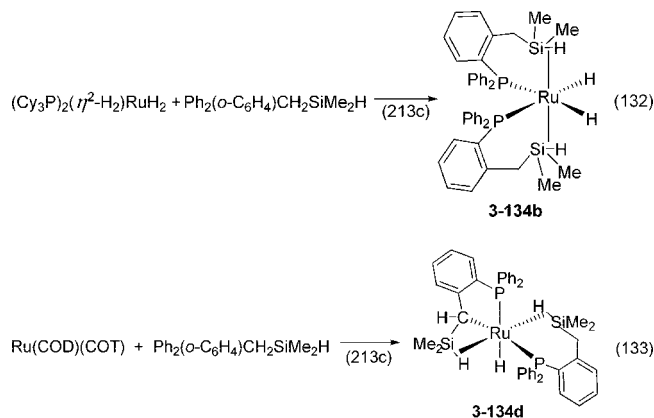
The SiH for the γ -agostic interaction in the Pt complex **2-85** exhibited a resonance somewhat downfield of that observed in the free silane, $\text{Ph}_2\text{SiH}(\text{CH}=\text{CH}_2)$, instead of the upfield shift observed in the β -agostic complexes, and the $^1J_{(\text{SiH})}$ values for both the *cis*- and *trans*-forms of **2-85** are only marginally lower than those for uncomplexed SiH , as was the case for the dmpe analogue of **2-85**.^{124,454} In the solid structure of **2-86**, the SiH bond distances for both SiPh_2H groups were the same and the value was in the range of uncomplexed silanes. The $\text{Pt}\cdots\text{HSiC}$ distance was elongated 0.10 Å over that reported for the σ -bonded PtSiPh_2H group in the same complex. For **2-86**, the γ -agostic $\text{Pt}\cdots\text{HSiC}$ distance, 2.93 Å, was shorter than that observed for the distance from platinum to the hydride of the attached silyl group (3.11 Å) but was in the range that would normally be assigned to a distance found in a silyl-metal hydride, $\text{H}[\text{TM}]\text{Si}$, complex that would be considered a full oxidative addition product. The corresponding value for the γ -agostic $\text{Pt}\cdots\text{HSiC}$ distance in $(\text{dmpe})\text{Pt}(\text{CZ}=\text{ZSiPh}_2\text{H})(\text{SiPh}_2\text{H})$ (**9-15**)^{124,454} was 2.43 Å, a value that suggested a very weak SiH interaction. In addition, the $\nu(\text{SiH})$ in the IR spectra for all three Pt complexes were barely red-shifted, which was not the case for the other α - and β -agostic complexes described in this section. The $\text{Si}-\text{H}$ coupling constants were much higher (closer to a free SiH) in the Pt complexes, in

contrast to the values obtained from **9-13** (Ta),³⁶⁰ **9-14** (Ru),^{213c} and **3-182b** (Rh).^{393a} It is possible that the weak $\text{Si}-\text{H}\cdots\text{Pt}$ interactions indicated in the solid state do not persist in solution.

Even more remote SiH sites have been demonstrated to interact with a metal center. This has occurred when a silicon-substituted ligand is part of a chelate, resulting in the SiH group functioning as a tether interacting with the metal. In a study of the reaction of the potentially chelating disilylbenzene ligand, *o*- $\text{HMe}_2\text{SiC}_6\text{H}_4\text{SiMe}_2\text{H}$, with $(\text{Ph}_3\text{P})_3\text{RhCl}$, two complexes were isolated as illustrated in eq 131.^{247b} The SiH was located in the structure of **3-199d** with a bond distance of 1.41 Å and with a $\text{Rh}\cdots\text{H}-\text{Si}$ angle of 135° . The $\text{Rh}\cdots\text{Si}$ distance was 3.082 Å, considered outside a bonding range. A ^1H resonance at -0.26 ppm ($^1J_{\text{SiH}} = 112$ Hz) was assigned to the δ -agostic hydrogen. The ν_{SiH} was observed at 1966 cm^{-1} , red-shifted from the values normally observed for a noninteracting SiH . The features somewhat resemble the $\eta^1\text{-HSiEt}_3$ complex of iridium, **3-245e**,^{266a} isolated and described by Brookhart and coworkers.



The reaction of ruthenium complexes with the chelating ligand $\text{Ph}_2\text{P}(o\text{-C}_6\text{H}_4)\text{CH}_2\text{SiMe}_2\text{H}$ produced three novel complexes, one of which, the β -agostic complex, **3-134c** (eq 130),^{213c} was described earlier in section 5.4.2.2. Two additional complexes provided complexes with an ε -HSi interaction that differed as a result of the nature of the ruthenium precursor. The complex **3-134b** (eq 132) was formed from $(\text{Cy}_3\text{P})_2(\eta^2\text{-H}_2)\text{RuH}_2$ and exhibits two novel ε -agostic interactions. At room temperature, one broad signal in the hydride region in the ^1H NMR spectrum at -7.8 ppm was observed, and at the low-temperature limit, 193 K , two resonances formed, one at -5.16 (br s, 2H , $J_{\text{SiH}} = 27.8$ Hz) assigned to the $\eta^2\text{-HSi}$ interaction and the other at -10.45 ppm (AA'XX' multiplet, $J_{\text{SiH}} = 15$ Hz) assigned to the $\text{Ru}-\text{H}_{(\text{term})}$ resonances. When $\text{Ru}(\text{COD})(\text{COT})$ was used as a precursor with $\text{Ph}_2\text{P}(o\text{-C}_6\text{H}_4)\text{CH}_2\text{SiMe}_2\text{H}$ (H_2 atmosphere), a complex, **3-134d** (mixed with **3-134b** and **3-134c**), was isolated that exhibited both ε - and β -agostic interactions as shown in eq 133. The ^1H NMR data exhibited three resonances upfield of TMS: -6.04 (br s, $J_{\text{SiH}} = 76$), -8.00 (pt, $J_{\text{SiH}} = 27$), and -9.36 (dd, $J_{\text{SiH}} = 40$). The coupling constants are in agreement with at least one agostic SiH and



a SISHA interaction (see section 5.5.1). The structure shown was consistent with the ground-state structure computed at the DFT/B3PW91 level.^{213c}

5.5. M—H...Si Interactions

In this section, the interactions of a metal–hydride with a silicon substituent will be summarized. The general classifications include (section 5.5.1) IHI (interligand hypervalent interactions);^{5f} (section 5.5.2) SISHA (secondary interactions between a silicon and a hydrogen atom⁴⁵²); and (section 5.5.3) hydrides that bridge a TM=Si or a TM≡Si linkage. There are some cases that are presented by the original investigators as having a M—H...Si interaction but that do not fit a common structural type, and these will be presented in subsection 5.6.

5.5.1. IHI Interactions

This type of M—H...Si interaction involves a hydridic hydrogen on a metal interacting with an electrophilic silicon center and was first labeled as such by Nikonov, who has also reviewed this class and their identifying properties at considerable length.^{5f} As can be seen from Table 9, the complexes generally occur with early transition metals (Ti, Nb, and Ta) but have more recently been extended to Fe (in calculations)⁴⁷¹ and experimentally to Ru.^{181b,186} A common feature of the complexes in this class is a chloride (or halide) substituent on the silicon. Incorporation of an electronegative substituent at silicon produces at least two effects: increase of “s” character in the SiH bond in a tetrahedral silane as well as producing a more electrophilic silicon center, a consequence of electronegativity differences. The alteration of “s” character of hybrid orbitals on the introduction of electronegative substituents was recognized by Bent (“s” character concentrates in orbitals to more electropositive substituents) and is generally used to account for structural changes in comparing sets of related compounds.⁴⁷² The structural features that characterize IHI complexes relative to σ -complexes include the following:^{5f}

- M—Si: bond is shorter than the bond of a σ -complex
- Si—X: longer than in averaged values found for tetrahedral silanes
- Si...H: longer contacts (in the range 1.8–2.1 Å) than those in σ -complexes (1.7–1.8 Å)
- M—H: elongated M—H bonds.

In the following discussion, the focus will be on IHI complexes that have been reported during the present review period. Earlier examples may be found in Nikonov’s review.^{5f} A series of five complexes of the general formula

$[\text{Cp}_2\text{Ti}(\text{PMe}_3)(\text{H})\text{SiClRR}']$ were prepared from reaction of $\text{Cp}_2\text{Ti}(\text{PMe}_3)_2$ and $\text{HSiClRR}'$ ($\text{R} = \text{R}' = \text{Me, Ph, Cl}$; $\text{R} = \text{Cl}$, $\text{R}' = \text{Me}$ (**3-1**), Cl (Table 3, footnote6); $\text{R} = \text{Me}$, $\text{R}' = \text{Ph}$ (Table 3, footnote 6)).^{20b} Three of the complexes were crystallographically characterized ($\text{SiClRR}' = \text{SiCl}_2\text{Me}$, SiClMePh , SiCl_3) although the hydride was located only in the SiClMePh complex. The SiClMe_2 complex was too unstable for NMR characterization, but the stability of the other complexes increased with additional chloro-substituents and spectroscopic data were obtained. The most stable complex in the grouping of five complexes was that produced from the reaction of HSiCl_3 . The Ti—H ^1H resonances ranged from -3.6 to -4.7 ppm, and the ν_{TiH} values were red-shifted to $1611\text{--}1524\text{ cm}^{-1}$. The absolute values of J_{SiH} were observed from 22 Hz (SiMeCl_2 complex (**3-1**)) to 40 Hz (SiPh_2Cl complex). The signs of J_{SiH} were determined for the SiMeCl_2 complex (**3-1**) and SiCl_3 complexes and both were negative, which supports a direct covalent interaction between the Si and H centers in these two complexes.^{20b}

A comparison of the X-ray data for isolated complexes and the DFT calculations for the model compounds $[\text{Cp}_2(\text{Me}_3\text{P})\text{Ti}(\text{H})(\text{SiMe}_{3-n}\text{Cl}_n)]$ ($n = 1, 2, 3$) is summarized in Table 12.^{20b} As the number of Cl substituents at silicon increases, the Ti—Si and Si—Cl distances decrease (both in the experimental (X-ray) and the calculated values), the Ti—H only decreases marginally, and the Si—H increases. For comparison purposes, the structure of a rotamer of $\text{Cp}_2(\text{Me}_3\text{P})\text{Ti}(\text{H})(\text{SiMeCl}_2)$ was calculated with the Me group *trans* to the hydride in an attempt to develop a model for a classical titanocene silyl hydride. In this rotamer, a Ti—Si bond and Si—H interaction were longer and weaker and a stronger Ti—H was calculated. The authors concluded that a nonclassical, but not an IHI interaction, was present and suggested that this rotamer would be best described as a stretched silane σ -complex, and presumably this could also be the case when there are no halide substituents at silicon. It was also predicted that complexes of the general formula, $[\text{Cp}_2(\text{Me}_3\text{P})(\text{H})\text{TiSiR}_3]$, would be σ -complexes for electropositive R substituents, but with at least one electronegative substituent (*trans* to the Si—H unit), an IHI structure was expected.^{20b}

The majority of the complexes that have been assigned an IHI structure are derivatives of a Cp_2Nb system. Nikonov has reported a series of complexes of the general formulas $\text{Cp}_2\text{Nb}(\text{H})_2\text{SiXR}_2$ [$\text{R} = \text{Pr}$, $\text{X} = \text{Cl}$;¹⁴³ $\text{R} = \text{Me}$, $\text{X} = \text{H}$, PPh_2 ;¹⁴⁴ $\text{R} = \text{X} = \text{OEt}$; $\text{R} = \text{Me}$, $\text{X} = \text{Ph}$; $\text{R} = \text{Me}$, $\text{X} = \text{Cl}$;^{142,147a}]; $\text{Cp}_2\text{Nb}(\text{H})(\text{SiXR}_2)_2$ [$\text{X} = \text{R} = \text{Cl}$;¹⁴³ OEt ; $\text{R} = \text{Me}$, $\text{X} = \text{Ph}$;¹⁴² H ;¹⁴² F ;⁴² Cl ;^{142,147a} Br ;^{142,144} I ;¹⁴⁴ OTf ;¹⁴⁴ SPh ;¹⁴⁴ PPh_2 ;¹⁴⁴ OMe ;¹⁴⁴ OEt ;¹⁴⁴ H ;¹⁴⁴]; $\text{Cp}_2\text{Nb}(\text{H})(\text{SiHMe}_2)(\text{SiXMe}_2)$ [$\text{X} = \text{F}$, Cl , Br , I];^{147a,356b} and $\text{Cp}_2\text{Nb}(\text{H})(\text{SiXMe}_2)(\text{SiYMe}_2)$ ^{356b} [$\text{X} = \text{F}$, $\text{Y} = \text{Cl}$, Br , I ; $\text{X} = \text{Cl}$, $\text{Y} = \text{Br}$ (disordered); $\text{X} = \text{Br}$, $\text{Y} = \text{I}$ (disordered)]. Those that have been characterized by diffraction methods are underlined, and the data are summarized in Table 13. An example from this category was discussed earlier in section 5.3 (example 6). The four signatures indicating an IHI interaction as described earlier in the present section will be described in sequence for the $\text{Cp}_2\text{Nb}(\text{H})_x(\text{SiR}_2\text{X})_{3-x}$ complexes.

The Si—Nb bond range for silyl–niobium complexes is somewhat narrow (2.54–2.68 Å for 53 measurements; Table 7). For the 20 complexes listed in Table 13, there are 12 Nb—Si distances that are ≤ 2.60 Å and 21 Nb—Si distances that fall between 2.60 and 2.65 Å, which would be considered

Table 12. Comparison of X-ray Data for $[\text{Cp}_2(\text{Me}_3\text{P})(\text{H})\text{TiSiClPhMe}]$, $[\text{Cp}_2(\text{Me}_3\text{P})(\text{H})\text{TiSiCl}_2\text{Me}]$, and $[\text{Cp}_2(\text{Me}_3\text{P})(\text{H})\text{TiSiCl}_3]$, and the DFT Calculations for Their Model Compounds, $[\text{Cp}_2(\text{Me}_3\text{P})\text{Ti}(\text{H})(\text{SiMe}_{3-n}\text{Cl}_n)]$ ($n = 1, 2, 3$, Respectively)^{20b}

X-ray →	$\text{Cp}_2(\text{Me}_3\text{P})\text{Ti}(\text{H})\text{SiPhMeCl}$	$\text{Cp}_2(\text{Me}_3\text{P})\text{Ti}(\text{H})\text{SiMeCl}_2$	$\text{Cp}_2(\text{Me}_3\text{P})\text{Ti}(\text{H})\text{SiCl}_3$
model ^a →	$[\text{Cp}_2(\text{Me}_3\text{P})\text{Ti}(\text{H})(\text{SiMe}_2\text{Cl})]$ Å	$[\text{Cp}_2(\text{Me}_3\text{P})\text{Ti}(\text{H})(\text{SiMeCl}_2)]$ Å	$[\text{Cp}_2(\text{Me}_3\text{P})\text{Ti}(\text{H})(\text{SiCl}_3)]$ Å
parameter ↓			
Ti–Si			
(exp)	2.545(2)	2.5167(7)	2.491(1)
[theory]	[2.581]	[2.535]	[2.520]
Ti–H			
(exp)		1.733(18)	1.72(2)
[theory]	[1.759]	[1.751]	[1.754]
Si–H			
(exp)	^b	1.749(17)	1.75(3)
[theory]	[1.805]	[1.822]	[1.847]
Si–Cl			
(exp)	2.223(2)	2.192(1)	2.1036(12)
[theory]	[2.292]	[2.259]	[2.225]

^a In the model calculation, a Cl is *trans* to the hydride and in the same plane. ^b The hydride was not located in the X-ray structure.

in the upper half of the range for Si–Nb bond lengths. The overall range in Table 13 is from 2.578 to 2.665 Å, which represents only a 3.4% elongation over the shortest bond. Of the complexes listed, the shortest Si–Nb bonds are associated with $\text{Cp}_2\text{Nb}(\text{H})(\text{SiMe}_2\text{X})_2$, $[\text{X} = \text{Cl}$ (**3-16**),^{142,144,145} Br (**9-20**),¹⁴² I (**9-21**)¹⁴⁴]; $\text{Cp}_2\text{Nb}(\text{H})(\text{SiCl}_3)_2$ (Table 3, footnote 28);¹⁴⁴ $\text{Cp}_2\text{Nb}(\text{H})(\text{SiMe}_2\text{H})(\text{SiMe}_2\text{X})$ [$\text{X} = \text{Cl}$ (**9-25**),^{356a} Br (**9-27**)^{356a}]; and $\text{Cp}_2\text{Nb}(\text{H})_2(\text{SiMe}_2\text{Cl})$ (**3-12a**).¹⁴² The short Si–Nb bond in $\text{Cp}_2\text{Nb}(\text{H})(\text{SiCl}_3)_2$ can be attributed to increased “s” character in the orbital used by silicon to bond to the niobium group and not to the involvement of IHI.

The increased Si–X ($\text{X} = \text{halogen}$) bonds in these complexes are relative to a distance in a model XSiR_3 compound, which was not specified by Nikonov in an earlier paper on the characteristics of IHI.¹⁴² However, the model specified later¹⁴⁴ for Si–Br was Me_3SiBr , and for Si–I, the average of five structures from the CCDC was used,^{473d} but none were specified for SiF or SiCl. In Table 13, the models used for a Si–X distance are indicated in the footnotes for selected gas-phase molecules where the bond parameters were determined by molecular weight (MW) spectroscopy or by ED. The data recorded for the complexes that are the subject of this review, are, of course, obtained for the solid state. In the $\text{Cp}_2\text{Nb}(\text{H})(\text{SiMe}_2\text{X})_2$ complexes, the elongation relative to the specified model in Table 13 was as follows: F [3.1% (av)], Cl (5.7%), Br (5.1%), I (6.2%). The elongation for the halide in the mixed derivatives, $\text{Cp}_2\text{Nb}(\text{H})(\text{SiMe}_2\text{H})(\text{SiMe}_2\text{X})$ ($\text{X} = \text{Cl}, \text{Br}$), was 6.4% for both halogens. The Si–Cl elongation in both isomers of $\text{Cp}_2\text{Nb}(\text{H})_2(\text{SiMe}_2\text{Cl})$ was also 5.7%. Using similar models (also with gas-phase parameters), an elongation of ~3% was calculated for $\text{Cp}_2\text{Nb}(\text{H})(\text{SiMe}_2\text{X})_2$ ($\text{X} = \text{OMe}, \text{Ph}$) and for $\text{Cp}_2\text{Nb}(\text{H})_2(\text{SiMe}_2\text{PPh}_2)$; however, these complexes were not assigned an IHI designation.¹⁴⁴

Another proposed characteristic of IHI was the presence of long $\text{XSi} \cdots \text{HNb}$ contacts (expected in the range from 1.8 to 2.2 Å). For all 22 of the complexes listed in Table 13, the range for this contact distance is 1.86–2.45 Å. Values that exceed 2.2 Å are found for one of the two $\text{XSi} \cdots \text{HNb}$ contacts in two symmetrical complexes of $\text{Cp}_2\text{Nb}(\text{H})_2(\text{SiR}_2\text{X})$ ($\text{X} = \text{Cl}, \text{R} = \text{Pr}$ (**3-13**); $\text{X} = \text{PPh}_2$ (**9-18**), $\text{R} = \text{Me}$ (**3-12a**)) (the Si substituent is in the central position). All of the distances listed for $\text{XSi} \cdots \text{HNb}$ contacts in Table 13 suggest some bonding interaction between the Si, Nb, and H.

The last criteria of the four chosen from those suggested by Nikonov was the presence of elongated M–H bonds in

complexes that exhibited IHI. The overall range listed for Nb–H in Table 13 is from 1.65 to 1.88 Å, which involves a 0.23 Å (14%) elongation over the shortest value given. This wide range may be due, in part, to the difficulty in placing the light hydrogen atom in the presence of a heavy metal center and, thus, is the least reliable of the four criteria based on bond distances. It is worth pointing out the values of NbH distances determined by different methods for the complex, $\text{Cp}_2\text{Nb}(\text{H})(\text{SiMe}_2\text{Cl})_2$: 1.74(7), X-ray; 1.816(8), ND; 1.78(1), NMR relaxation measurements at 210 K; and 1.811, DFT (model, $\text{Cp}_2\text{Nb}(\text{H})(\text{SiH}_2\text{Cl})_2$).^{145a} The value from the ND study is ~4% longer than the determination of Nb–H by X-ray diffraction. DFT calculations for $\text{Cp}_2\text{Nb}(\text{H})(\text{SiMe}_2\text{H})(\text{SiMe}_2\text{X})$ ($\text{X} = \text{F}, \text{Cl}, \text{Br}, \text{I}$) show only a marginal change in Nb–H from $\text{X} = \text{F}$ to $\text{X} = \text{I}$, but all are shorter than for $\text{Cp}_2\text{Nb}(\text{H})(\text{SiMe}_3)_2$ (X would be Me in this case).^{356a} Two complexes in Table 13, $\text{Cp}_2\text{Nb}(\text{H})(\text{SiMe}_2\text{H})(\text{SiMe}_2\text{Cl})$ (**9-25**) and $\text{Cp}_2\text{Nb}(\text{H})(\text{SiMe}_2\text{Cl})_2$ (**3-16**) have been studied by neutron diffraction (combined with X-ray). For $\text{Cp}_2\text{Nb}(\text{H})(\text{SiMe}_2\text{H})(\text{SiMe}_2\text{Cl})$ (**9-25**), the Nb–H value was 1.804(17), near the value previously determined by ND for **3-16**. Another interesting feature revealed by the ND study was that the hydride was located symmetrically between the two silicon centers for the $\text{X} = \text{Cl}$ complex, although the authors argue that, because the Nb–SiCl bond length was shorter than the Nb–SiH bond length, the “hydride appears to lie closer to the SiClMe_2 group than to the SiHMe_2 ligand”.^{356a,b} However, in the case of the $\text{X} = \text{Br}$ complex, a shift of the hydride ligand to the SiMe_2Br ligand is clearer as the $\text{BrSi} \cdots \text{HNb}$ contact is 2.06 Å, which contrasts to the 2.19 Å distance observed for $\text{HSi} \cdots \text{HNb}$.^{356ab} The combined structural data for $\text{Cp}_2\text{Nb}(\text{H})(\text{SiHMe}_2)(\text{SiXMe}_2)$ ($\text{X} = \text{F}, \text{Cl}, \text{Br}, \text{I}$)^{147,356b} and $\text{Cp}_2\text{Nb}(\text{H})(\text{SiXMe}_2)(\text{SiYMe}_2)$ ^{356b} ($\text{X} = \text{F}, \text{Y} = \text{Cl}, \text{Br}, \text{I}$; $\text{X} = \text{Cl}, \text{Y} = \text{Br}$ (disordered); $\text{X} = \text{Br}, \text{Y} = \text{I}$ (disordered)) indicate that the IHI interaction increases with the heavier halogens.

In order to study potential IHI interactions in other systems, $\text{CpM}(\text{NAr})(\text{L})(\text{X})_2$ ($\text{X}, \text{L} = 1\text{- and } 2\text{-electron donors}$; $\text{M} = \text{group } 5$) complexes were used as precursors in reactions with silanes of the type HSiR_2Cl ,^{146,356b} HSiRCl_2 ,^{356b} and HSiCl_3 .^{356b} With $\text{R} = \text{Me}$, and $\text{Ar} = 2,6\text{-}i\text{-Pr}_2\text{C}_6\text{H}_3$, two different complexes were formed as a function of M (Nb vs Ta). The tantalum product, $\text{Cp}(\text{PMe}_3)(\text{H})\text{Ta}(\text{NAr})(\text{SiMe}_2\text{Cl})$, **3-25a**, contained an electron-rich $\text{Ta} \cdots \text{Si}$ IHI interaction, but the corresponding Nb complex, $[\text{Cp}(\text{PMe}_3)(\text{Cl})\text{Nb}\{\eta^3\text{-N}(\text{Ar})\text{SiMe}_2\text{-H}\}]$, **3-17**, contained a β -agostic $\text{NSi} \cdots \text{H} \cdots \text{Nb}$ interaction.^{146,147b} The complex **3-25a** exhibited a Ta–Si bond

Table 13. Selected Bond Parameters (X-ray) in $\text{Cp}_2\text{Nb}(\text{H})(\text{SiMe}_2\text{X})_2$, $\text{Cp}_2\text{Nb}(\text{H})(\text{SiMe}_2\text{H})(\text{SiMe}_2\text{X})$, and $\text{Cp}_2\text{Nb}(\text{H})_2\text{SiR}_2\text{X}$ and Comparison to Uncomplexed SiX Distances in Model Compounds

complex	Nb–Si, Å X-ray [ND]	Nb–H	Si–X, Å observed (model silane)	XSi···HNb, Å	ref
	X in $\text{Cp}_2\text{Nb}(\text{H})(\text{SiMe}_2\text{X})_2$ and $\text{Cp}_2\text{Nb}(\text{H})(\text{SiCl}_3)_2$				
F (9-19)	2.618(1) 2.622(1)	1.652 ^a	1.652(3), 1.644(3) (1.597(5)) ^b	1.980	142
Cl (3-16)	2.597(1) [2.612(4)] ^c	1.74(7) [1.816(8)] ^c	2.163(1) [2.166(4)] ^c (2.052(5)) ^d	2.056(5) [2.076(3)] ^c	142,145a,b
Br (9-20)	2.604(2)	1.780 ^a	2.349(2) (2.235(2)) ^e	2.053	142
I (9-21)	2.595(3)	1.881 ^a	2.590(3) (2.437(3)) ^f	2.07	144
OMe (9-22)	2.6240(9) 2.6285(9)	1.88(5)	1.691(2) (1.640) ^g	2.113, 2.192 ^a	144
Ph (9-23)	2.654(1)	1.672 ^a	1.901 ^a (1.853(3)) ^h	2.191 ^a	142
SiCl_3 (Table 3, footnote 28)	2.5776(5)	1.79(3)	2.163(1) (2.020) ⁱ	2.11(3) 2.14(3)	144
	X in $\text{Cp}_2\text{Nb}(\text{H})(\text{SiMe}_2\text{R})(\text{SiMe}_2\text{X})$ (R = H, X = F, Cl, Br, I; R = Me, X = I)				
F (R = H) (9-26)	2.6411(8) ^j (Nb–SiF)	1.708 ^a	1.614(3) 1.581(5) (1.597(5)) ^b	2.018 ^a (FSi···HNb)	356a,b
	2.6167(8) ^j (Nb–SiH)			2.205 ^a (HSi···HNb)	
Cl (R = H) (9-25)	2.5969(6) ^k (Nb–SiCl)	1.80(2) ^k	2.1829(7) ^k (2.052(5)) ^d	2.09(2) ^k (ClSi···HNb)	356a,b
	2.649(2) ^k (NbSi–H)			2.13(2) ^k (HSi···HNb)	
Br (R = H) (9-27)	2.586(2) ^a (Nb–SiBr)	1.80(1)	2.377(2) (2.235(2)) ^e	2.06(1) (BrSi···HNb)	356a,b
	2.649(2) ^a (Nb–SiH)			2.19(1) (HSi···HNb)	
I (R = H) (9-28)	2.5782(8) (Nb–SiI)		2.6287(8) (2.437(3)) ^f		356b
	2.6426(2) (Nb–SiH)				
I (R = Me) (9-29)	2.5817(7) (Nb–SiI)		2.6413(6) (2.437(3)) ^f		356b
	2.6645(6) (Nb–SiMe)				
	$\text{Cp}_2\text{Nb}(\text{H})(\text{SiMe}_2\text{X})(\text{SiMe}_2\text{Y})$				
X = Cl, Y = F (9-30)	2.6202(8) (Nb–SiF)		1.649(2) (Si–F) (1.597(5)) ^b		356b
	2.6038(8) (Nb–SiCl)		2.180(1) (Si–Cl) (2.052(5)) ^d		
X = Br, Y = F (9-31)	2.625(1) (Nb–SiF)		1.670(4) (Si–F) (1.597(5)) ^b		356b
	2.594(1) (Nb–SiBr)		2.369(1) (Si–Br) (2.235(2)) ^e		
X = I, Y = F (9-32)	2.6148(9) (Nb–SiF)		1.647(2) (Si–F) (1.597(5)) ^b		356b
	2.5837(9) (Nb–SiI)		2.6173(9) (Si–I) (2.437(3)) ^f		
X = Br, Y = Cl ^l (9-33)	2.5986(4) ^l (Nb–SiBr)		2.272(4) ^l (Si–Cl)		356b
	2.5986(4) ^l (Nb–SiCl)		2.272(4) ^l (Si–Br)		
X = Br, Y = I ^m (9-34)	2.6045(8) ^m (Nb–SiBr)		2.4846(8) ^m (X = Br)		356b
	2.6045(8) ^m (Nb–SiBr)		2.4846(8) ^m (X = Br)		
X in $\text{Cp}_2\text{Nb}(\text{H})_2\text{SiXR}_2$ Cl (R = Me, 3-12b)	2.579(2)	1.766 ^a	2.170(2)	1.860 ^a	142

Table 13a. Continued

complex	Nb–Si, Å X-ray [ND]	Nb–H	Si–X, Å observed (model silane)	XSi···HNb, Å	ref
(Si lateral)		1.671 ^a	(2.052(5)) ^d	(ClSi···HNb)	
Cl (R = ⁱ Pr, 3-13)	2.6496(7)	1.65(3)	2.1694(9)	2.204, 2.447	143
(Si central)		1.65(3)	(2.052(5)) ^d	(ClSi···NbH)	
PPh ₂ (R = Me, 9-18)	2.6491(4)	1.65(2)	2.3065(2)	2.148 ^a	144
(Si central)		1.70(2)	(2.245(3)) ^f	2.445 ^a	
				(PSi···HNb)	

^a Calculated from data in the Cambridge Data Base. ^b In MeSiH₂F.^{473a} ^c Value from ND study. ^d In MeSiH₂Cl.^{473b} ^e In Me₃SiBr.^{473c} ^f In H₃SiI.^{473d} ^g In H₃SiOMe.^{473e} ^h In H₃SiCH=CH₂.^{473f} ⁱ In HSiCl₃.^{473g} ^j The SiFMe₂ and SiHMe₂ units are disordered in the positions of the F and H atoms. ^k Combined X-ray/neutron diffraction study.^{356a} ^l The SiClMe₂ and SiBrMe₂ units are disordered in the positions of the Cl and Br atoms. ^m The SiIme₂ and SiBrme₂ units are disordered in the positions of the I and Br atoms.

distance (2.574(1) Å) on the short end of the range of Ta–Si bond lengths (2.569–2.809, 32 values, Table 7), and the Si–Cl distance is slightly shorter than that observed in the complexes listed in Table 13.¹⁴⁶ A minor change in the NAr group to 2,6-(Me)₂C₆H₃ in the Nb precursor produced the complex **3-19**, an isomer of **3-17a** in which the phosphine and the chloride exchanged places.^{147a} However, changing the silane from HSiMe₂Cl to HSiPh₂Cl resulted in formation of the classical silylhydrido complex Cp(ArN)(Me₃P)–Nb(H)SiPh₂Cl, **3-21**,¹⁴⁹ as was the case for the SiPhMeCl, SiMeCl₂, SiCl₃ complexes, although the DFT calculations for both **3-21** and the corresponding SiCl₃ complex (Table 3, footnote 33) suggested IHI character in contrast to the X-ray data. For the complex Cp(Ar'N)Nb(PMe₃)(Cl)–(SiRR'X) (Ar' = 2,6-Me₂C₆H₃), the SiPh₂Cl complex exhibited both classical and agostic (major) forms, the SiMe₂Cl derivative is classical as is the SiCl₃ derivative, whereas the SiⁱPr₂Cl and SiPhMeCl complexes are agostic.^{32a} Thus, the substituents on silicon can play a role in the type of metal hydride that is produced. The reaction of Cp(Me₃P)₂Ta=NAr (Ar = 2,6-(ⁱPr)₂C₆H₃) with HSiMe₂Cl (forming **3-25a**), HSiMeCl₂ (forming **3-26a**), and HSiCl₃ (Table 3, footnote 38) gave the IHI complex. In the case of HSiMeCl₂, the product was characterized crystallographically and the “in-plane” SiCl (*trans* to the hydride) was elongated, as expected for an IHI interaction, by ~2.6% over the distance observed for the “out-of-plane” SiCl.^{78a}

To determine whether the presence of IHI can be claimed (or assigned) for more electronegative transition metals that are supported by Cp'/PR₃ ligands, the complex [Cp*(Ph₃P)RuH₂(SiClMe₂)], **3-87**,¹⁸⁵ was prepared and compared to the model complex [Cp*(ⁱPr₃P)RuH₂(SiClHMe)] that had been reported and structurally characterized earlier by Tilley and coworkers.⁴⁷⁴ Since the Ru–Si bond distance in **3-87** is longer and the Si–Cl is shorter than that observed in Tilley's complex, Nikonov concluded that there was no IHI interaction in **3-87** and the bonding in the complex reported by Tilley could be reinterpreted on the basis of an IHI model since electron-rich phosphines (such as ⁱPr₃P) could stabilize an IHI interaction. Thus, in a later study, the formation of Cp*(R₃P)Ru(H)₂(SiR'₃) from the reaction of Cp*(R₃P)Ru(H)₃ (R₃P = ⁱPr_{3-x}Me_xP (x = 0, 1, 2) and PhMe₂P) with the chlorosilanes HSiClMe₂, HSiCl₂Me, and HSiCl₃ was reported.¹⁸⁶ Of the 22 complexes described, 8 are characterized by X-ray diffraction (and spectroscopic data) and the remainder are characterized by spectroscopic data (at least in part). In the case of the more Lewis acidic chlorosilanes, HSiCl₂Me and HSiCl₃, the major reaction product was Cp*(R₃P)Ru(H)(Cl)(SiCl_{3-x}Me_x) (x = 1, 0). Although there may be an interligand hypervalent interaction

(Ru–H···Si–Cl) in Cp*(R'ⁱPr₂P)Ru(H)₂(SiClMe₂) (R = ⁱPr, **3-88**; Me, footnote 95, Table 3) and hypervalent interactions between both the Ru–H bonds and the silicon center in the complexes Cp*(R₃P)Ru(H)₂(SiCl₂Me) (R₃P = ⁱPr₃P, **3-90**, and ⁱPrMe₂P, **3-89b**) were also proposed,¹⁸⁶ conclusive evidence was absent. The *J*_(SiH) constants exhibited values <14 Hz in all compounds, in line with a classical description for the bonding. The authors concluded that a theoretical study was necessary to resolve the ambiguities in this system.¹⁸⁶ A study of the Ru(II) complex, Cp*(ⁱPr₃P)Ru(Cl)(η^2 -HSiClMe₂), **3-92**, showed a red-shift in ν_{RuH} , a *J*_(SiH) = 33.5, a short Si···Cl contact, and an elongated Ru–Si bond.¹⁸⁷ A RuCl···SiCl hypervalent interaction was proposed, and a DFT calculation for the model Cp(Me₃P)ClRuSiClMe₂ provided the following parameters (in Å; the X-ray distance for **3-92** is provided in brackets): Ru–H, 1.604 [1.53]; Ru–Cl, 2.451 [2.413]; Ru–Si, 2.427 [2.3980]; Si···H, 2.072 [2.054]; Si–Cl, 2.168 [2.155 (Cl is *trans* to the Cl ligand)]; Si···Cl, 3.040 [3.014].¹⁸⁷ The calculated values are all longer than the observed bond distances obtained by X-ray diffraction but were still considered in good agreement with the model used. The *J*_{calcd} was –19.5 Hz, with the negative sign indicating some direct Si–H interaction to the metal. The authors favored a description for this complex in which there was residual σ -Si–H in addition to a hypervalent Cl···Si–Cl.¹⁸⁷ As expected, the data collected for σ -complexes incorporating a –SiCl₃ substituent, Cp*(R₃P)–(H)(Cl)RuSiCl₃ (L = MeⁱPr₂P, **3-93**; Me₂ⁱPrP and Me₂PhP, Table 3 footnote 101) ruled out the presence of a σ -interaction.¹⁸⁶

5.5.2. SISHA Interactions

The type of MH···Si contacts in this section that are also a variation of hypervalent interactions were identified by Sabo-Etienne and co-workers, and the complexes involve principally M = Ru. A typical case from this category was discussed as example 5 in section 5.3. The role of secondary interactions in σ -silane ruthenium complexes has been summarized well by Lachaize and Sato-Etienne, and only the highlights will be included in the present discussion.⁴⁵² Discussed in their review are systems that include complexes of ruthenium that are formed from reactions of chelating disilanes, primary silanes, and secondary silanes. It is Sabo-Etienne who first articulated that none of the parameters *J*_{SiH}, IR bands, *d*_{Si–H} and *d*_{Ru–Si}, determined by X-ray diffraction or by DFT calculations, could be used independently to determine the extent of silane activation but that it was a combination of the parameters that was necessary to support σ -interactions. She recommended that the value of the lowest

Table 14. Ru–H_{term}, Ru–H_{br}, and Si–H_{br} Distances in Chelating Disilanes and Monosilanes Where SISHA Interactions Are Assigned

[RuH ₂ {(η ² -HSiMe ₂) ₂ X}L ₂]		Ru–H _{term} ···Si				
X	L ₂	Ru–H _{br}	Si···H _{br} Ru	Ru–H _{term}	RuH _{term} ···Si	
C ₆ H ₄ 3-127 ^{208,209}	(PCy ₃) ₂	1.60(3)	1.84(2)	1.59(2)	2.22(2)	
		1.59(3)	1.84(2)	1.54	2.21(2)	
					2.18(2)	
CH ₂ CH ₂ (Table 3, footnote 141) ²⁰⁸	(PCy ₃) ₂	1.55(3)	1.73(3)	1.53(3)	2.27(3)	
		1.54(3)	1.78(3)	1.60(3)	2.31(3)	
					2.13(3)	
CH ₂ CH ₂ ^{a208}	(PCy ₃)(PPh ₃)	1.64(3)	1.80(3)	1.65(3)	2.19 ^b	
		1.66(3)	1.98(3)	1.49(3)	2.32	
					2.09	
CH ₂ CH ₂ ^{c208}	(PPh ₃) ₂ ²⁰⁸	1.63(3)	1.93(3)	1.54(3)	2.13 ^b	
		1.59(3)	1.87(3)	1.59(3)	2.14	
					2.29	
OSiMe ₂ O (Table 3, footnote 141)	(PCy ₃) ₂ ²⁰⁸	1.62(4)	1.77(4)	1.55(4)	2.25(3)	
		1.58(4)	1.81(3)	1.51(3)	2.04(3)	
					2.43(3)	
NH ^d 3-132 ²¹²	(PCy ₃) ₂	1.456 ^b	1.93(5)	1.582	2.25(6)	
		1.468	1.91(5)	1.648	3.68(5)	
					2.39(5)	
H _y Ru(SiR ₃)L _x					2.09(6)	
H _y L _x	SiR ₃					
H ₃ (Ph ₃ P) ₃	SiMeCl ₂			1.68(3)	1.94(3)	
3-124 ²⁰⁶				1.54(2)	1.86(2)	
				1.59(2)	1.94(2)	
H ₃ (Ph ₃ P) ₃	SiPh ₂ OSi(OH)Ph ₂			1.59(3)	1.97(5)	
9-39 ³⁹⁸				1.61(5)	2.03(5)	
				1.57(3)	2.07(5)	
(H) ₃ (Me ₃ P) ₃	SiMe ₃			1.488(43)	2.228(42)	
3-120 ⁹⁷				1.637(50)	2.179(48)	
				1.431(45)	2.128(48)	
H ₃ (Me ₃ P) ₃	SiMe ₂ CH ₂ SiMe ₃			1.60(4)	2.00(4)	
3-121 ⁴⁹				1.61(3)	2.09(4)	
				1.57(3)	2.05(5)	
H ₂ (Me ₃ P) ₃	Me ₂ SiCH ₂ CH ₂ SiMe ₂			1.56(4)	1.81(4)	
3-122 ⁴⁹				1.50(4)	2.15(3)	
H ₂ (PCy ₃) ₂ {(η ² -C ₆ H ₈)PCy ₂ }	SiMe ₂ Cl			1.57(2)	1.91(2)	
3-126a ^{207,452}				1.62(3)	1.99(2)	
(H) ₃ (Cy ₃ P) ₂	SiPh ₃	1.54(4)	1.72(3)	1.49(4)	1.83(3)	
(η ² -H ₂) 3-129 ^{101,210a}				1.47(4) ^e	2.40(4)	

^a From exchange of [RuH₂{(η²-HSiMe₂)₂X}L₂] (X = CH₂CH₂; L = P(Cy)₃).²⁰⁸ ^b Obtained from the Cambridge Data Base. ^c Table 3, footnote 147. ^d *cis,cis,cis*-isomer. ^e Ru–H distances to the H₂ ligand are 1.66(2) and 1.64(3).

J(SiH) of 20 Hz often used by early investigators to support a σ-interaction should be reset to a lower limit of ~65 Hz (at least for Ru complexes), and that a broad and intense IR band in the range 1650–1800 cm^{−1} was indicative of σ-coordination. When DFT calculations supported X-ray data for a Si–H distance, a value of 1.7–1.8 Å should indicate the formation of a σ-silane complex. For Si–H distances in the range 1.9–2.4 Å, secondary interactions (such as SISHA) may be present.⁴⁵²

The earlier examples where SISHA interactions were identified occurred in complexes that were prepared by reaction of HSiMe₂XSiMe₂X [X = C₆H₄ (**3-127**), −(CH₂)₂− (**9-40**), −(CH₂)₃−, −(OSiMe₂O)− (**9-43**)] with RuH₂(H₂)₂−(PCy₃)₂ or with Ru(COD)(COT)/PPh₃ (**3-133**) or Ppy₃ (**3-131**).²⁰⁸ Also prepared by phosphine exchange were the complexes [RuH₂{(η²-HSiMe₂)₂X}(PCy₃)PR₃] (X = C₆H₄, R = Ph, pyl; X = CH₂CH₂, R = Ph, pyl). As described for the example of **3-127** in section 5.3 (example 5), these complexes were unusual in that the bulky phosphines occupied *cis*-positions and the η²-H–Si groups of the bis-

silane derivative spanned *trans*-positions (angles >170°) in a pseudo-octahedral environment about the Ru(II) center. The complexes where X = O (disiloxane, **3-128**²⁰⁸) and NH (disilazane, **3-132**²¹²) were also prepared, but these bear a *cis,cis,cis*-distribution of the two phosphines, the two MH groups, and the two η²-H–Si groups.

Three complexes [RuH₂{(η²-HSiMe₂)₂X}(PCy₃)₂] (X = C₆H₄, **3-127**; CH₂CH₂; OSiMe₂O, **9-43**) as well as those prepared from [RuH₂{(η²-HSiMe₂)₂X}(PCy₃)₂] (X = (CH₂)₂) by phosphine exchange and giving mixed phosphine derivatives, [RuH₂{(η²-HSiMe₂)₂(CH₂)₂}(PPh₃)PR₃] (R = Cy (**9-41**)), were characterized by X-ray crystallography, and selected bond-distance data are provided in Table 14. The hydrides were located in all cases, and the basic octahedral geometry was verified as was the *cis*-distribution of the phosphines in all five complexes. In the five complexes with the same isomeric distribution of ligands, the Ru–H_{br} distances spanned 1.54–1.66 Å (10 values) and the Ru–H_{term} distances ranged from 1.53 to 1.68 Å (10 values); thus, the two types of hydrides basically fall in a similar range.

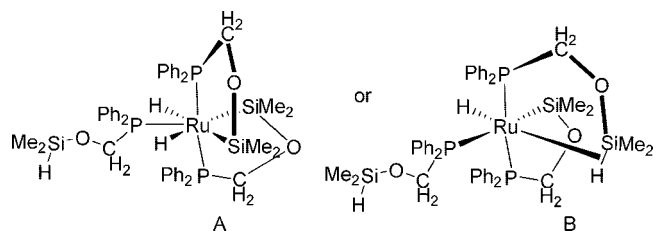


Figure 11. Proposed structures for **3-130b**.^{211b}

However, the hydride-to-silicon distances for $\text{Ru}-\text{H}_{\text{br}}\cdots\text{Si}$ and $\text{Ru}-\text{H}_{\text{term}}\cdots\text{Si}$ are distinctly different. The $\text{Si}\cdots\text{H}_{\text{br}}\text{Ru}$ distances (partnering with the $\text{Ru}-\text{H}_{\text{br}}$) fall in a range from 1.73 to 1.98 Å (10 values with only 2 values >1.90 Å (see Table 14)). The $\text{Si}\cdots\text{H}_{\text{term}}\text{Ru}$ distances are larger [2.04–2.43 Å (20 values) with 13 values ≤ 2.22 Å]. It is these longer $\text{Si}\cdots\text{H}-\text{Ru}$ distances that are described by the term SISHA. Such interactions appear to stabilize unusual structures that are observed, such as that for **3-127**, or play a role as intermediates in exchange processes (described in detail in ref 398). A feature of **3-127** and its related derivatives was the temperature-dependent ^1H NMR spectra (the two different signals in the hydride region coalesce), and the process responsible for the observed spectra was attributed to exchange between the (η^2 -Si-H) and the $\text{Ru}-\text{H}$ hydrides.²⁰⁸

In the systems just described, the silane is a potentially chelating system with the general sequence $\text{HR}_2\text{Si}-\text{X}-\text{SiR}_2\text{H}$. What would be the consequence of removing one HR_2Si group and replacing the unit with another unit that could coordinate to the metal center such as a phosphine? Sabo-Etienne and co-workers studied two such systems that differed in the length of the tether between the P and Si centers: $\text{Ph}_2\text{P}(\text{o}-\text{C}_6\text{H}_4)\text{CH}_2\text{SiMe}_2\text{H}^{213\text{c}}$ (a 3-bond tether) and $\text{Ph}_2\text{PCH}_2\text{OSiMe}_2\text{H}^{211\text{b}}$ (a 2-bond tether). Each of these systems gave unique results but not necessarily an unequivocal interpretation. The ligand, $\text{Ph}_2\text{P}(\text{o}-\text{C}_6\text{H}_4)\text{CH}_2\text{SiMe}_2\text{H}$, gave three complexes, **3-134b** (ϵ -agostic, section 5.4.2.3), **3-134c** (β -agostic, section 5.4.2.2), and **3-134d** (β - and ϵ -agostic, section 5.4.2.3). The structure of **3-134d** is shown in eq 133, and it is a complex that also contains a terminal $\text{Ru}-\text{H}$. As indicated in section 5.4.2.3, the observed coupling constants are in agreement with at least one agostic SiH and also a SISHA interaction.^{213\text{c}}} Although complex **3-134d** was isolated in the solid form, it was present in a mixture with **3-134b** and **3-134c** and was not isolated as a single component; thus, no crystal structure was reported. The ligand with the 2-bond tether formed the complex **3-130b**, $\text{Ru}(\text{PPh}_2\text{CH}_2\text{OSiMe}_2\text{H})_3$, which was characterized crystallographically as well as with a DFT calculation.^{211\text{b}}} Two interpretations of the result were presented involving the structures shown in Figure 11. Structure A would be the result of OA of two of the three SiH bonds, providing a $\text{Ru}(\text{IV})$ complex. In structure B, only one SiH has added, giving rise to a $\text{Ru}(\text{II})$ complex where the second SiH forms a δ -agostic interaction. The X-ray structure (exclusive of the “free” dangling SiH) shows an SiH distance of 1.75(3) Å, in agreement with an agostic interaction exhibited in σ -silane ruthenium complexes. The second SiH bond is 2.28(3) Å, in the range of a SISHA interaction (the RuH distance to this same hydride is 1.60 Å, which is not different from the $\text{Ru}-\text{H}_{\text{agostic}}$ distance). The dissymmetry observed for the activation of the two different Si-H bonds is reproduced in the DFT calculations. The WBI for the presumed SISHA interaction is 0.15 compared to 0.33 for the SiH distance of 1.75(3) Å associated with the agostic

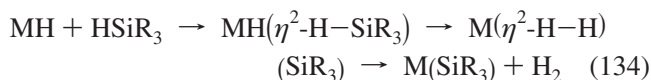
assignment. Thus, the structure is proposed to be intermediate between A and B.^{211\text{b}}}

A second grouping of complexes where there are longer-range $\text{Si}-\text{H}\cdots\text{M}$ interactions, generally ≥ 2 Å, were found in systems that were depicted as either a silyl hydride $\text{L}_3\text{H}_3\text{RuSiR}_3$ (L = phosphine, mixed phosphines, CO, or σ - H_2) or as a σ -silane $\text{L}_3\text{H}_2\text{Ru}(\eta^2\text{-H}-\text{SiR}_3)$, depending on the degree of activation of the SiH bond. The complexes that have been characterized by X-ray diffraction and where hydrides were located are also included in Table 14. For the silyl hydride representation, if all L's are identical, the *fac*-isomer is observed with the silicon “capping” the RuH_3 face. Often these complexes are fluxional. For instance, in the case of $\text{H}_3(\text{Ph}_3\text{P})_3\text{RuSiCl}_2\text{Me}$ (**3-124**, described in section 5.3, example 5), a singlet was observed in the $^1\text{H}\{^{31}\text{P}\}$ NMR spectrum with ^{29}Si satellites ($J_{\text{SiH}} = 39.7$ Hz), suggesting some type of $\text{Si}\cdots\text{H}$ interaction. The $^{31}\text{P}\{^1\text{H}\}$ spectrum also exhibited a singlet consistent with equivalent P centers on the NMR time scale. No decoalescence of either the proton or phosphorous signals was observed down to -30 °C, indicating that a fast exchange process occurred down to this temperature. The following related complexes are also fluxional: $(\text{Ph}_3\text{P})_3\text{H}_2\text{Ru}\{(\eta^2\text{-H}-\text{SiPh}_2)(\text{OSi}(\text{OH})\text{Ph}_2)\}$ (**9-39**), **3-122**,⁴⁹ **3-121**,⁴⁹ and **3-129**.^{101,210\text{a}}} However, no dynamic process on the NMR time scale was reported for **3-120**,⁹⁷ **3-124**,²⁰⁶ or **3-126a**.^{207\text{a}}} The solid-state data for $(\text{Ph}_3\text{P})_3\text{H}_2\text{Ru}\{(\eta^2\text{-H}-\text{SiPh}_2)(\text{OSi}(\text{OH})\text{Ph}_2)\}$ (**9-39**, 3 relevant protons total) were interpreted by the authors as having an elongated σ -SiH (1.97 Å) and two SISHA interactions, although the SISHA interactions were only marginally longer than the σ -SiH assignment. This case probably highlights the ambiguity in defining the roles of $\text{Si}\cdots\text{H}\cdots\text{M}$ interactions when values are at the high end of one range and the low end of another. There were no DFT calculations performed for **9-39**. However, in the related case, **3-129**, where an “elongated” σ -SiH and one SISHA interaction were proposed, there was an additional $\text{Si}-\text{H}\cdots\text{Ru}$ interaction at 2.40(4) Å. In this case, DFT/B3LYP calculations for the model $\text{RuH}_2(\eta^2\text{-HSiH}_3)(\eta^2\text{-H}_2)(\text{PH}_3)_2$, gave a ground-state structure with two SISHA interactions (2.071 and 2.116 Å) and one elongated σ -SiH (1.946 Å). For **3-126a** there was no hydride exchange at room temperature, and a 1D HMQC $^{29}\text{Si}-^1\text{H}\{^{31}\text{P}\}$ provided $J_{(\text{SiH})}$ values of 37 and 24 Hz. These values were close to those of two other complexes where SiMe_2Et and SiEt_3 replaced the SiMe_2Cl . Replacing the electronegative Cl substituent with an alkyl-donating substituent would be expected to change the Si-H bond activation, but that was apparently not the case here. Disorder in the SiMe_2Et and SiEt_3 complexes was present, and the hydrides could not be located. However, for **3-126a**, the distances in the solid state suggested one σ -SiH and one SISHA interaction. The DFT calculations gave a value of 1.891 Å (σ -SiH) and 2.076 Å (SISHA), reasonably consistent with observed $\text{H}\cdots\text{Si}$ distances.⁴⁵²

Sabo-Etienne and co-workers have studied a number of reactions of the complex $\text{RuH}_2(\text{H}_2)_2(\text{PCy}_3)_2$ with tertiary silanes, but probably the most unusual results this group obtained were in the reaction with the secondary silane, H_2SiMePh . One of the processes that can be initiated by a transition metal complex is disproportionation of a silane. In this particular case, disproportionation produced SiH_4 and the tertiary silanes HSiMe_2Ph , HSiMePh_2 , and HSiPh_3 . The silane was “trapped” as the truly novel diruthenium complex, $[\text{Ru}_2\text{H}_4(\mu\text{-}\eta^2\text{:}\eta^2\text{:}\eta^2\text{-SiH}_4)(\text{PCy}_3)_4]$, **2-45**, and the HSiPh_3

generated reacted to form $[\text{RuH}_2(\eta^2\text{-H}_2)(\eta^2\text{-HSiPh}_3)(\text{PCy}_3)_2]$, **3-129** (included in Table 14). Both of these complexes are fluxional, with **2-45** exhibiting a single resonance (nonet) in the hydride region with $J_{\text{SiH}(\text{av})} = 36$ Hz and **3-129** exhibiting a single resonance (pseudo triplet) in the hydride region at room temperature. The two complexes were described as exhibiting σ -SiH interactions (see previous sections). However, **2-45** reacted with $\text{HSi}(\text{OMe})_3$, giving two redistribution products, $\text{H}_2\text{Si}(\text{OMe})_2$ and $\text{Si}(\text{OMe})_4$. The secondary silane that was produced reacted with **2-45** to give $\text{Ru}_2\text{H}_2(\mu\text{-}\eta^2\text{:}\eta^2\text{-H}_2\text{Si}(\text{OMe})_2)_3(\text{PCy}_3)_2$, **3-144a**, which exhibited a singlet in the hydride region upon phosphorous decoupling, and the hydride signal does not change on cooling to 213 K.¹⁰¹ The $^{29}\text{Si}\text{-}^1\text{H}\{^1\text{H}_{\text{OMe}}\}$ INEPT NMR spectrum exhibited a nonet with $J_{\text{SiH}} = 22$ and, thus, was consistent with fast exchange of the eight hydrogen atoms.¹⁰¹

The reaction of $\text{RuH}_2(\text{H}_2)_2(\text{PCy}_3)_2$ with $\text{HSiMe}_{3-n}\text{Cl}_n$ resulted in the elimination of H_2 and formation of $\text{RuCl}(\text{SiMe}_{3-n}\text{Cl}_n)(\eta^2\text{-H}_2)(\text{PCy}_3)_2$, which slowly decomposes when excess chlorosilane is present.^{207b} The $\sigma\text{-H}_2$ resonates at -12.14 ppm in the ^1H NMR spectrum, and a $T_1(\text{min})$ value confirms the dihydrogen formulation. The structure of the complex with $n = 2$ (**3-126b**) with an H–H distance of $1.05(3)$ Å for the H_2 in the equatorial plane is a pseudo-octahedral environment with a vacant site *trans* to the silyl group. The H_2 formulation is reproduced in the DFT/B3PW91 calculations. The $\text{Si}_1\cdots\text{H}_1$ distance in the solid is 2.25 Å within the bounds of a SISHA interaction. The deuterated isotope, $\text{RuCl}(\text{SiMe}_{3-n}\text{Cl}_n)(\eta^2\text{-HD})(\text{PCy}_3)_2$, was generated for all 3 complexes ($n = 1\text{--}3$) and the J_{HD} values were determined, 12.0 , 17.5 (**3-126b**), and 18.9 for $n = 1\text{--}3$, respectively, providing a value for the H–D distance in **3-126b** of 1.08 ± 0.01 Å, in agreement with the value obtained for the protio complex. The interaction between Si and a H of the H_2 is related to the σ -CAM process, which allows for interconversion of σ -ligands without a change in oxidation state and with essentially no activation barrier. This sequence is shown in abbreviated form in eq 134.



The SISHA term was originally used to describe the unusual features of ruthenium complexes. However, other elements of the iron triad as well as other metals could also exhibit such interactions, and these are described in section 5.6.

5.5.3. Hydrides That Span Metal–Silicon Multiple Bonds

Complexes in this category were produced by a double activation of both secondary silanes and primary silanes.^{36a,38,39,82,86} The complex $\text{Cp}^*(\text{dmpe})\text{Mo}(\text{H})=\text{SiEt}_2$, **2-10**, was characterized by neutron diffraction^{36a} and was discussed as example 4 in section 5.3. The double activation was initiated by an appropriately designed 18e precursor complex, $\text{Cp}^*(\text{dmpe})\text{Mo}(\eta^3\text{-CH}_2\text{Ph})$, which is in equilibrium with the electron-deficient, coordinatively unsaturated 16e form $\text{Cp}^*(\text{dmpe})\text{Mo}-(\eta^1\text{-CH}_2\text{Ph})$. Upon reaction with the silane, reductive elimination of toluene and migration of a hydride from silicon to molybdenum occur. Key features of the spectroscopic data included a ^{29}Si NMR resonance downfield of TMS and in the region assigned to a sp^2 -silylene. The silylene formulation was supported by a neutron diffraction study, which indicated

a short Mo–Si bond distance [$2.343(10)$ Å; range from Table 7 for Mo–Si distances was $2.219\text{--}2.709$ Å for 63 measurements]. In addition, a hydride was located in the position bridging the Mo and Si centers, and a value of the J_{SiH} was determined (44 Hz) that did not change in the temperature range from -75 to 50 °C. The other three complexes, $\text{Cp}^*(\text{dmpe})(\text{H})\text{Mo}=\text{SiRR}'$ ($\text{R} = \text{R}' = \text{Me}, \text{Ph}$; $\text{R} = \text{Me}, \text{R}' = \text{Ph}$) had spectroscopic properties similar to those of **2-10**.^{36a}

The authors also studied the reactions of primary silanes, which afforded 3 examples related to **2-10a** (Figure 8), $\text{Cp}^*(\text{dmpe})\text{Mo}(\text{H})\text{Si}(\text{H})\text{Ar}$ ($\text{Ar} = \text{Ph}$ (**1-24**); Mes; CH_2Ph ; Table 1, footnote 21). Spectroscopic data for **1-24** supported a silylene hydride complex: $^{29}\text{Si}\{^1\text{H}\}$ at $\delta = 250$; ^1H at $\delta = 9.45(\text{m})$ for $=\text{SiHPh}$ ($J_{\text{SiH}} = 130$ Hz); a ^1H NMR signal at -9.96 (td) for Mo–H with ^{29}Si satellites ($^2J_{\text{SiH}} = 30$ Hz); and an IR stretching frequency at $\nu_{\text{SiH}} = 1896$ cm^{-1} . A crystal structure exhibited a short Mo–Si bond length of $2.317(1)$ Å, consistent with the silylene assignment. A crystallographically imposed mirror plane bisected the molecule, but the hydride on Mo was not located although the SiH was refined to a location on the mirror plane $1.43(4)$ Å from the Si center.^{36a}

In a related study, the tungsten precursor, $[(\eta^7\text{-C}_5\text{Me}_3(\text{CH}_2)_2)(\text{dmpe})\text{W}(\text{H})_2]^+[\text{B}(\text{C}_6\text{F}_5)_4]^-$, which functions as a synthon for the 14e fragment $[\text{Cp}^*(\text{dmpe})\text{W}]^+$, was used for reactions with selected secondary silanes as well as primary silanes.³⁹ Reaction of the tungsten precursor with R_2SiH_2 provided $[\text{Cp}^*(\text{dmpe})(\text{H})_2\text{W}=\text{SiR}_2][\text{B}(\text{C}_6\text{F}_5)_4]$ ($\text{R}_2 = \text{Me}_2$, **2-21**; Ph_2 ; PhMe ; Table 2, footnote 27). The complex **2-21** was crystallographically characterized, but the hydrides could not be located. The silylene ligand was planar, and the W–Si bond distances for the two independent cations ($2.358(2)$ and $2.354(3)$ Å) were on the shortest end for W–Si bond lengths in Table 7 [$2.354\text{--}2.712$ (69 measurements)]. T_1 measurements were in the range of a classical dihydride and the $^2J_{\text{SiH}}$ was only 7 Hz, suggesting little interaction between the hydride and the silylene unit.⁸⁶ The ^{29}Si resonance was observed at 314 ppm, also consistent with a metal silylene assignment. A separate theoretical study for the model $[(\eta^5\text{-C}_5\text{H}_5)(\text{PH}_3)_2\text{W}(\text{H}_2\text{SiMe}_2)]^+$ showed that the classical structure was the minimum but that the bridging hydride lay <5 kcal/mol higher in energy. The authors concluded that both the model structure and **2-21** have a fluxional $\text{W}(\text{H}_2\text{SiMe}_2)$ unit and “it was meaningless to classify the structure as classical or nonclassical”.⁴⁷⁵

The reaction with primary silanes gave mixtures of products with either PhSiH_3 or MesSiH_3 , but with DippSiH_3 , the complex $[\text{Cp}^*(\text{dmpe})(\text{H})_2\text{W}=\text{Si}(\text{H})\text{Dipp}]^+[\text{B}(\text{C}_6\text{F}_5)_4]^-$ (**1-30**) was isolated.³⁹ The Si–H ^1H NMR resonance was shifted downfield to $\delta = 10.83$ with $^1J_{\text{SiH}} = 167$ Hz. Also present was a multiplet hydride signal for MoH_2 at $\delta = -4.01$ and a ^{29}Si NMR resonance at $\delta = 286$ that was coupled to the Si–H proton ($J_{\text{SiH}} = 167$ Hz). The T_1 relaxation experiments showed that the hydrides were classical in nature. A 1D ^{29}Si HMQC BIRD filtered NMR experiment gave a value for $^2J_{\text{SiH}}$ that was less than 20 Hz for the four isolated complexes and could be interpreted with no W–H \cdots Si interaction. However, the sign of the coupling constant was not determined and the assignment could possibly be revisited as a related complex, **1-29**, described next, does have a bridging hydride.

An example related to Tilley's work, $\text{Cp}'(\text{OC})_2\text{W}(\text{H}_a)=\text{Si}(\text{H}_b)\text{C}(\text{SiMe}_3)_3$ ($\text{Cp}' = \text{C}_5\text{Me}_4\text{Et}$), **1-29a**, was reported by the Tobita group from reaction of

$\text{Cp}^*\text{W}(\text{CO})_3\text{Me}$ and $\text{H}_3\text{SiC}(\text{SiMe}_3)_3$.^{38a} In this case, a bridging $\text{W}-\text{H}_a\cdots\text{Si}$ was supported by an upfield ^1H NMR resonance at $\delta -10.67$ with a $^2J_{\text{SiH}} = 28$ Hz in addition to a downfield $\text{Si}-\text{H}_b$ resonance at $\delta 10.39$ with a $^1J_{\text{SiH}} = 155$ Hz. The hydrides were located in the X-ray structure with a $\text{W}-\text{H}_a$ of $1.82(7)$ Å and a $\text{Si}-\text{H}_b$ distance of $1.54(7)$ Å. The $\text{W}-\text{H}_a$ to Si distance was $1.71(6)$ Å, indicating an interaction of the $\text{W}-\text{H}$ and the silicon center. In this case, the IR stretching frequencies were observed for both $\text{W}-\text{H}_a$ ($\nu = 1589\text{ cm}^{-1}$) and $\text{Si}-\text{H}_b$ ($\nu = 2052\text{ cm}^{-1}$). The structural features of **1-29a** were reproduced by a DFT calculation (B3LYP level) of the model complex $[\text{Cp}(\text{OC})_2(\text{H})\text{W}=\text{Si}(\text{H})\{\text{C}(\text{SiH}_3)_3\}]$ and gave parameters in good agreement with those for X-ray structure. The NLMO/NPA bond orders were 0.511 for $\text{W}-\text{H}_a$ and 0.476 for $\text{H}_a\cdots\text{Si}$, consistent with a “normal” 3c-2e $\text{W}-\text{H}-\text{Si}$ interaction in the model complex. In the related W complex, **2-21**, $[\text{Cp}^*(\text{dmpe})(\text{H})_2\text{W}=\text{SiMe}_2]^+[\text{B}(\text{C}_6\text{F}_5)_4]^-$, T_1 measurements were in the range of a classical dihydride and the $^2J_{\text{SiH}}$ was only 7 Hz, suggesting no interaction between the hydride and the silylene unit.⁸⁶

Although not formed directly from a hydrosilane, $[\text{Cp}^*(\text{dmpe})(\text{H})\text{Mo}\equiv\text{SiMe}_3]^+[\text{B}(\text{C}_6\text{F}_5)_4]^-$ has been prepared in two steps from the reaction of $[\text{Cp}^*(\text{dmpe})\text{Mo}(\eta^1\text{-benzyl})]$ with H_2SiClMe followed by a salt metathesis reaction with $[\text{Li}(\text{OEt})_3\text{B}(\text{C}_6\text{F}_5)_4]$.^{82a} The metal silylyne was crystallographically characterized and had the shortest observed MoSi bond (see Table 7). The hydride ligand was refined and found to occupy a position between the Mo and Si centers with $\text{H}-\text{Mo}$ and $\text{H}-\text{Si}$ distances of $1.85(5)$ and $1.39(5)$ Å, respectively, and suggests that an $\text{MoH}\cdots\text{Si}$ interaction may be present, at least in the solid state. Although the silylyne complex in the solid does not exhibit mirror symmetry, there was C_s symmetry on the NMR time scale at room temperature in solution and with 4 inequivalent dmpe Me groups at lower temperature. The data suggested a rapid dynamic process that exchanged the P atoms of the dmpe ligand. A process was proposed where a hydride ligand migrated to the Si center followed by rotation about the Mo–Si bond. Albeit preliminary, computational studies gave an energy-minimized structure close to that observed in the solid state with a nonclassical Si–H interaction. The DFT energy-minimized structure resembled the X-ray structure and exhibited a hydride ligand that bridged the Mo–Si bond.^{82a}

Reaction of $\text{Cp}^*(\text{Pr}_3\text{P})\text{Ru}(\text{H})(\text{Cl})(\text{SiH}_2\text{Ph})$ with $\text{Li}[\text{B}(\text{C}_6\text{F}_5)_4]\cdot 3\text{Et}_2\text{O}$ afforded the base-stabilized silylene complex, $\text{Cp}^*(\text{Pr}_3\text{P})(\text{H})_2\text{Ru}=\text{Si}(\text{H})\text{Ph}\cdot\text{Et}_2\text{O}$, where the Et_2O was loosely bound and could be displaced in CD_2Cl_2 solvent by THF. The published spectroscopic data do not support the presence of a bridging hydride, although the hydrides are nonequivalent in the ^1H NMR spectrum. The complex promoted hydrosilylation of alkenes by a new mechanism, and to support the new mechanism, theoretical calculations were performed by Beddie and Hall.^{476a,b} The model complex cation, $[\text{Cp}(\text{H}_3\text{P})(\text{H})_2\text{Ru}(\text{SiH}_2)]^+$, was generated by “release” of the OMe_2 group from $[\text{Cp}(\text{H}_3\text{P})(\text{H})_2\text{Ru}(\text{SiH}_2)\cdot\text{OMe}_2]^+$. The basic features of the relevant core atoms contained a silylene linkage to $[\text{Ru}]$ and two hydrides that were depicted as bridging between Ru and Si with $\text{Si}\cdots\text{H}$ distances of 1.68 and 1.72 Å, respectively (this form was set with $\Delta G = 0.0$ kcal/mol), although no descriptor indicating an α -agostic interaction was suggested. In a later study, the influence of the theoretical method and basis sets used was published with essentially the same conclusion that the Glaser–Tilley pathway for hydrosilylation was energetically favored.^{476b}

5.6. Miscellaneous Examples and Unclassified Cases

There are some complexes that did not conform to any of the above categories as described by their respective authors but appear to exhibit a collection of properties consistent with either $\text{M}-\text{H}\cdots\text{Si}$ or with $\text{M}\cdots\text{HSi}$. Such examples are included in this section.

5.6.1. Additional SISHA Examples

In section 5.5.2, SISHA interactions were identified where the examples were exclusively those that contained the metal ruthenium. However, there is some evidence that the remaining two members of the same triad also exhibit such long-range interactions. Two examples are closely related to the polyhydrides discussed in section 5.5.2 in having the composition $\text{L}_3\text{H}_3\text{OsSiR}_3$ ($\text{L} = \text{PPh}_3$, $\text{R}_3 = \{\text{OCH}_2\text{CH}_2\}_3\text{N}$, **3-160**;²²¹ $\text{L}_3 = (\text{PPh}_3)_2(\text{CO})$, $\text{R} = \text{Me}$, **3-152**²²²). Both of these complexes were crystallographically characterized and exhibited a structure in which the L_3H_3 ligands exhibited a *fac*-geometry (octahedral) with the silyl group capping the H_3 face. In the more symmetrical complex, **3-160**, the Os–H distances were 1.52(3), 1.66(3), and 1.57(3) and the OsH \cdots Si distances were 2.06(4), 2.00(2), and 1.96(3), which are distances in accord with a SISHA assignment. The $^1\text{H}\{^31\text{P}\}$ -NMR spectrum was a singlet at room temperature and broadened when the temperature was lowered to -40°C . The T_1 values were consistent with a classical hydride complex. These observations are also in line with those reported for the related Ru complexes for which SISHA interactions were assigned. An interesting added feature was that the N center of the silatrane ligand in **3-160** does not form a bonding interaction with the silicon, as was the case in the silatrane precursor. This may be due to electron density transfer from the Os–H to the silicon center. In the more unsymmetrical complex, **3-152**, the Os–H distances were 1.58(9), 1.55(9), and 1.45(10) and the OsH \cdots Si distances were 1.980, 2.062, and 2.211, closely resembling those in **3-160**. The ^1H NMR spectrum at room temperature exhibited a broad resonance at -9.0 ppm for the three hydride ligands. However, at -60°C , these resolved into two multiplets that could be assigned to a triplet of triplets for the hydride *trans* to CO and a complex multiplet with twice the integrated intensity for the hydrides *trans* to the phosphines. Although the authors concluded there was no significant $\text{Si}\cdots\text{HOs}$ interaction, the results are again consistent with a SISHA classification.

Another example from the iron triad was the novel complex $[(\text{PhBP}^{\text{iPr}})_3\text{Fe}(\text{H})(\text{H}_2\text{SiPhMe})]$, **1-37**, formed from the reaction of $[(\text{PhBP}^{\text{iPr}})_3\text{FeMe}]$ and PhSiH_3 .⁴⁵ All three hydride positions were located in the difference Fourier map of the X-ray structure and refined. The Fe–H distances were 1.553(1), 1.482(1), and 1.566(2) Å and in this example the Fe–H \cdots Si distances were 1.464(1), 1.552(2), and 2.001(2) Å. A second complex, $[(\text{PhBP}^{\text{iPr}})_3\text{Fe}(\text{H})(\text{H}_2\text{SiMesMe})]$ (Table 1, footnote 40), was also crystallographically characterized with two molecules in the asymmetric unit. Two different Si–H distances were observed in each molecule with shorter distances of 1.56 and 1.62 Å, 1.67 and 1.74 Å, and longer distances of 2.14 and 1.97 Å for the SiPh and SiMes derivatives, respectively. However, the Fe–H distances as calculated from the CDB for the Mes derivative are 1.228 and 1.566 Å, the former of which is an unreasonable value. The mesityl complex exhibited NMR data analogous to that

Scheme 16

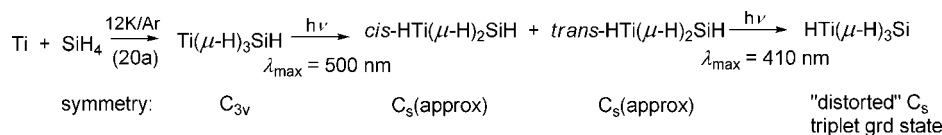


Table 15. Calculated Bond Parameters for $\text{H}_{1-x}\text{Ti}(\mu\text{-H})_y\text{SiH}_z$ ($x = z = 1, y = 3$; $x = 0, y = 2, z = 1$; $x = z = 0, y = 3$) in Å^{20a} (H_t = terminal; H_b = bridge)

complex	Ti–H _t	TiH _b	Si–H _t	Si–H _b	Ti–Si
H(Ti(μ-H))SiH ₂ ^a	1.750	200.6	1.514, 1.519	1.630	2.465
<i>cis</i> -H(Ti(μ-H) ₂)SiH	1.776	194.4	1.521	1.628	2.421
<i>trans</i> -H(Ti(μ-H) ₂)SiH	1.777	203.4	1.511	1.614	2.364
H(Ti(μ-H) ₃)Si	1.761	1.961, 1.991, 1.997		1.600, 1.632, 1.632	2.544

^a Highest energy form of all those calculated.

of **1-37**. The authors proposed that two 3-centered Fe–H–Si interactions were present in the solid state and one Fe–H(hydride). DFT calculations for all atoms in **1-37** were developed and the structure was minimized starting with the experimentally determined crystallographic coordinates. The resulting Fe–H and Si–H distances were similar to the X-ray structure and reproduced the one long and two short Si–H distances. A fluxional process of some type was suggested by the variable-temperature ¹H NMR spectrum, but the nature of the process was not identified. The hydride signals in both complexes exhibited ²⁹Si satellites with *J*_{SiH} coupling values of 68 and 70 Hz. However, since the complex was fluxional, the coupling must be averaged. If the ²*J*_{SiH(terminal)} is assumed to be zero, then the maximum ¹*J*_{SiH} values would be 102 for **1-37** and 105 for the mesityl derivative. An HMQC experiment confirmed that Si–H interactions were present in solution for both complexes. Although there are 3c/2e interactions in the solid state, all three hydrides appear to be chemically equivalent in solution. It is noteworthy that neither Ph₂SiH₂ nor Et₃SiH reacted with [(PhBP'Pr₃)FeMe].⁴⁵

Additional examples that could fit into the “SISHA” category are the complexes Cp*(OC)₂W(H)₂(SiHPhR) (R = Ph, H, Cl),⁴⁷⁷ which were formed as an isomeric mixture of a pseudo-octahedral form and a pseudo-trigonal-prismatic form, and two isomers were crystallographically characterized. The major isomer of Cp*(OC)₂W(H)₂(SiHPh₂) was the pseudo-octahedral form, and that of Cp*(OC)₂W(H)₂(SiH₂Ph) exhibited pseudo-trigonal-prismatic geometry. For Cp*(OC)₂W(H)₂(SiHPh₂), the distances between the silicon center and the hydrides on tungsten were 2.00(4) and 1.91(3) Å, and in Cp*(OC)₂W(H)₂(SiH₂Ph) only one WH...Si distance was specified, 2.02(4) Å. These values suggested a weak interaction such as those that have been described within the SISHA framework. Together these complexes exhibit four fluxional processes that are described in sections 6.1 and 6.3.

5.6.2. SiH₄ and M_{atoms}

A series of papers have been published describing the reactivity of metal atoms Ti,^{20a} Ni,²³ and Zn, Cd, and Hg²⁵ in a matrix doped with SiH₄. In each case, the species generated were studied by IR spectroscopy and supplemented by quantum chemical calculations. In the reaction of Ti with SiH₄, an initial adduct, Ti•SiH₄, was observed, which upon photolysis generated two other basic structures; the proposed structures are given in Scheme 16. A direct insertion product,

HTiSiH₃, was not observed experimentally. Attempts to model the initial adduct, Ti•SiH₄, resulted in a structure with insertion of the Ti atom into one of the Si–H bonds. The isomer, HTi(μ-H)SiH₂ (C₁ symmetry), had the highest energy of all the calculated minima for the various species, although the energy difference from the other forms was relatively small. On the basis of the closeness of the values of the wave numbers observed for Ti•SiH₄ to those of Al•SiH₄, a structure similar to that of Al•SiH₄ was proposed, Ti(μ-H)₃SiH as shown in Scheme 16. Table 15 summarizes the distances calculated for the indicated structures. Not unexpectedly, the bridging hydrides exhibited longer Ti–H_b and Si–H_b values than did the Ti–H_t and Si–H_t bonds, and the latter are independent of the number of bridging hydrides. The Ti–H_b bonds are 17–26 pm longer (~10–14% elongation) than the Ti–H_t bonds while the SiH_b bonds are 10–12 pm longer (~7% elongation) than the Si–H_t bonds. The calculated Ti–Si distances vary from 236 pm [*trans*-HTi(μ-H)₂SiH] to 254 pm [HTi(μ-H)₃Si], whereas the distances in solid Ti complexes ranged from 249 to 276 pm (Table 7). The IR bands were calculated and were in reasonable agreement with the observed bands. The Si–H_t bands are found near 2050 cm^{–1} for both *cis*- and *trans*-HTi(μ-H)₂SiH, and the Si–H_b and Ti–H_t bands combine near 1500–1550 cm^{–1}. Since the Ti–H_b bonds are elongated more than the Si–H_b bonds, it is tempting to classify these complexes as having a Si–H...Ti interaction.

A similar study of the reaction of Ni atoms with SiH₄ gave a very different result from Ti/SiH₄. The Ni reacted spontaneously with SiH₄ to give the insertion product HNiSiH₃.²³ The global minimum geometry was a C_s symmetric form. The calculated Ni–Si distance of 240 pm was somewhat outside the range observed in solid complexes (211–235 pm, Table 7). The Ni–H bond in this form was 144.1 pm (BP/SV(P)) with a calculated ν(Ni–H) of 2033 cm^{–1}, which was too weak to be observed. The ν_{sym}(Si–H) exhibited two bands and also a ν_{as}(SiH) band between 2000 and 2100 cm^{–1}, one of which may overlap with ν(Ni–H). The Si–H_t distances were ~152 pm (normal distance), but a unique feature of the structure was an acute H–Ni–Si angle that resulted in a Ni–H...Si distance of 227.3 pm. This H_b...Si distance is similar to some of those that occur in SISHA interactions (see Table 9) and, thus, suggests a weak Ni–H...Si interaction.

In another matrix isolation study, Zn, Cd, and Hg atoms were photolyzed in the presence of SiH₄.²⁵ Only one

silyl–metal species was reported, and it was the insertion product HMSiH_3 . The DFT calculation for a structure with C_{3v} symmetry in a singlet ground state gave M–Si distances of 238 (Zn), 255 (Cd), and 253 (Hg) pm, which are within the range of values observed in solid complexes for Zn and Hg (Table 7; there are only two values listed for Cd structures).²³

5.6.3. Unclassified Complexes

There are complexes with $\text{M}\cdots\text{H}\cdots\text{Si}$ interactions that do not fit the general description as described in sections 5.4 or 5.5 in contrast to the systems described earlier in section 5.6.1. There are seven cases where the authors have suggested alternate descriptions, and the structure of these complexes are also found in the structure section at the end of Table 9.

The first example is **1-19**, $\text{Cp}^*(\text{Cl})\text{HTa}[\text{PhSiH}_2\text{N}(\text{C}_6\text{H}_3\text{Me})_2\text{NSiPhHCl}]$, which was reported by Gountchev and Tilley in 1997.^{32b} The hydrides were located in the X-ray structure and gave the following pertinent parameters: Ta–H, 1.83(4), SiHClPh , 1.36(5), Ta–H \cdots Si, 1.86(4), which suggests a weak bonding interaction between the metal–hydride and the silicon center. There were three resonances in the ^1H NMR spectrum attributed to the two diastereotopic Si–H's of the SiH_2Ph group and one to the SiHPhCl group with $J_{\text{SiH}} = 208$ Hz (SiH_2Ph) and 272 Hz (SiHPhCl), but no value that could be attributed to Ta–H \cdots Si was reported. Two IR absorptions at ν (cm^{-1}) = 2152 and 2189 were assigned to SiH, and a third absorption at 1678 was assigned to TaH. This last absorption is in the region observed for many $\text{M}\cdots\text{H}\cdots\text{Si}$ interactions. Overall, an interpretation of an IHI interaction would be a consistent one for **1-19**, although this assignment was not made by the original authors.^{32b} Nikonov and co-workers have examined the products produced from the reaction of $\text{Cp}^*(\text{Pr}_2\text{MeP})\text{Fe}(\text{BH}_4)$ with a number of hydrosilanes in the presence of NEt_3 . The products with the general formulation $\text{Cp}^*(\text{Pr}_2\text{MeP})\text{FeH}_2\text{SiR}_3$ were observed.^{42a} The complexes where $\text{SiR}_3 = \text{SiMe}_2\text{Ph}$, SiHMePh , SiH_2Ph , and SiMe_2Cl were unstable in solution at room temperature. However, the products with $\text{SiR}_3 = \text{SiMeCl}_2$ and SiCl_3 (**9-47**) were isolated, and the solid-state structures were obtained. The FeH and Si \cdots H distances for the SiCl_3 complex were 1.35(3) and 1.88(3) ($J_{\text{SiH}} = 18.9$ Hz) Å, respectively. The unusually short Fe–H distance was attributed to the systematic foreshortening observed by the X-ray diffraction method. The DFT calculation for the model complex, $\text{Cp}(\text{Me}_3\text{P})\text{Fe}(\text{H})_2\text{SiMe}_3$, gives an equilibrium structure with two equivalent Si \cdots H interactions, which is not consistent with either a SISHA complex or an IHI complex. The authors favored a view in which the interaction of the silane with the iron center begins with a Si–H \rightarrow Fe donation and develops an interaction between the silyl and metal-bound hydride, providing the ending $\text{H}\cdots\text{SiR}_3\cdots\text{H}$ complex. The proposed explanation of the multicentral Si \cdots H interactions involved adduct formation between the hypervalent anion $[\text{H}_2\text{SiR}_3]^-$ and the cation $[\text{Cp}(\text{L})\text{Fe}]^+$.^{42a}

In the next case, $(\text{Cy}_3\text{P})_2(\eta^2\text{-H}_2)\text{Ru}(\text{H})\text{Cl}$ was reacted with $\text{HSiMe}_{3-n}\text{Cl}_n$, giving H_2 and products of the composition $(\text{Cy}_3\text{P})_2(\eta^2\text{-H}_2)\text{RuCl}(\text{SiMe}_{3-n}\text{Cl}_n)$ (**3-126b**) formed instead of a metal dihydride product.^{207b} These complexes were discussed earlier as cases where SISHA interactions were present (interaction of a H of the H_2 ligand with the silyl group). What is curious is the route from the starting Ru(II) complex to the ending Ru(II) complex. One of the proposed

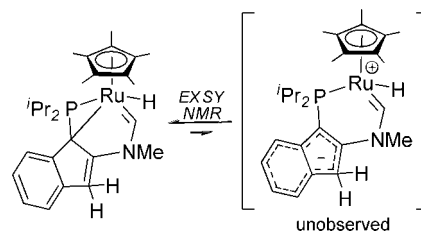


Figure 12. Formation of **16e** $\text{Cp}^*\text{Ru}(\kappa^2\text{-P}, \text{C})$ from the **18e** precursor $\text{Cp}^*\text{Ru}(\kappa^2\text{-P}, \text{C}, \text{C}')$ complex.^{47d}

pathways is coordination of the silane to the starting material to give the **18e** mixed σ -system $(\text{Cy}_3\text{P})_2(\text{H})\text{ClRu}(\eta^2\text{-H}_2)(\eta^2\text{-HSiMe}_{3-n}\text{Cl}_n)$. Loss of H_2 followed by OA of the silane would give the Ru(IV) dihydride, $(\text{Cy}_3\text{P})_2(\text{H})_2\text{RuCl}(\text{SiMe}_{3-n}\text{Cl}_n)$. Isomerization of the dihydride to $\eta^2\text{-H}_2$ would then give the observed product. Some support for this proposal is revealed in the reaction of $\text{HSiMe}_{3-n}\text{Cl}_n$ with deuterated starting material, $(\text{Cy}_3\text{P})_2(\eta^2\text{-D}_2)\text{Ru}(\text{D})\text{Cl}$, which provided $(\text{Cy}_3\text{P})_2(\eta^2\text{-HD})\text{RuCl}(\text{SiMe}_{3-n}\text{Cl}_n)$.^{207b}

Stradiotto and co-workers have been developing ligand sets that exhibit dynamic behavior such that a coordinatively unsaturated form is produced that would be capable of mediating bond-activation reactions. An example of such a system that was employed in a reaction with Ph_2SiH_2 to give **2-36f** was shown in Figure 12. This $\text{Cp}^*\text{Ru}(\kappa^3\text{-P}, \text{C}, \text{C}')$ complex undergoes a rather remarkable Ru–C(sp³) reversible bond-cleavage process in the generation of a presumed 16-electron species. The reaction of the **18e** $\text{Cp}^*\text{Ru}(\kappa^3\text{-P}, \text{C}, \text{C}')$ complex provided a kinetic product that involved the equivalent of OA to the 16-electron complex, and within 24 h, the kinetic product rearranged to the thermodynamic product **2-36f** (see structure section of either Table 2 or Table 9), which was isolated and characterized.^{47d} The solid structure of **2-36f** indicates the presence of a 4-membered “ring” that involves the sequence –Si–Ru–P–C(sp³)–, and bridging the Ru–Si edge is an unsymmetrical hydride bridge with Ru–H = 1.48(9) and an Si–H 1.90(8) Å. In general, the Ru–H distance in this system appears too short and the Si–H distance appears too long for the usual bridging hydride, although there are not many systems with which to compare the example. Consequently, the authors did not attempt at the time of the publication to explain the role that the hydride played.^{47d}

In another complex, $(\text{PNP})\text{Rh}(\text{H})(\text{SiClMe}_2)$ (PNP = bis(*o*-diisopropylphosphinophenyl)amide, a “pincer” ligand) (**3-212c**), the role of hydride also appears to be ambiguous. The hydride resonance was observed at –15.6 ppm with coupling to ^{29}Si , ^{103}Rh , and ^{31}P . The hydride was located in the X-ray structure, and the N–Rh–Si angle of 137° could be considered consistent with either a Y-shaped OA product or a nonclassical silane complex.^{254c} However, the SiMe_2Cl group is disordered with Cl exhibiting partial occupancy in the SiMe locations, thus precluding other possibilities such as an IHI interaction.

The last example, **3-245e**, $[(\text{POCOP})\text{Ir}(\text{H})(\eta^1\text{-HSiEt}_3)]^+[\text{B}(\text{C}_6\text{F}_5)_4]^-$, was formed from the pincer complex, $[(\text{POCOP})\text{Ir}(\text{H}(\text{acetone}))]^+[\text{B}(\text{C}_6\text{F}_5)_4]^-$, and Et_3SiH , which displaces the coordinated acetone in the starting iridium complex to form **3-245e**.^{266a} This unique complex, which was crystallographically characterized, contains an $\eta^1\text{-HSiEt}_3$ with an $\text{Ir–H}_{\text{term}} = 1.425(18)$, an $\text{IrH}_{\text{br}} = 1.94(3)$, and an $\text{Si–H}_{\text{br}} = 1.48(3)$. Two important parameters are an Ir \cdots Si distance equaling 3.346(1) Å, clearly outside of a bonding distance, and a Ir–H–Si angle of 157°, consistent with an end-on

η^1 -HSi coordination of the silane. Such an end-on approach of a silane in the OA of a silane to a metal center was first suggested by Schubert. Exchange of the terminal hydride and bridging hydride was observed in the room-temperature NMR data, but at $-70\text{ }^\circ\text{C}$ the static spectrum was obtained with two ^1H signals, one singlet at -4.9 with $J_{\text{SiH}} = 79$ and a triplet at -44.2 assigned to the terminal (Ir–H) hydride. The $J_{\text{SiH}} = 79$, which is also in the range of an η^2 -SiH complex, thus will require other characterization methods to reveal the nature of the SiH interaction.

All of the cases just described are unique and indicate that the interaction of metals with hydrosilanes is imperfectly understood.

5.7. Summary

The interactions of $\text{Si}\cdots\text{H}\cdots\text{M}$ have been categorized by the interaction with the longer hydrogen-to-element distance, i.e., $\text{Si}-\text{H}\cdots\text{M}$ (σ -interaction and agostic interactions) and $\text{M}-\text{H}\cdots\text{Si}$ (IHI and SISHA). The particular category into which a complex was placed followed those suggested by the original investigators based, in (too) many cases on incomplete characterization. A glance at the columns in Table 9 provides an overall view of what is “missing” in the characterization of the products produced from the reaction of hydrosilanes with transition metal complexes. The particular assignment made in an individual study can sometimes be based only on a chemical shift and/or a coupling constant. The problems of relatively small, observed values of the $J_{(\text{SiH})}$ coupling constant is complicated by the relative sign of the 1J vs 2J , the combination of which are involved in the actual value observed. The signs of each of these coupling constants are rarely obtained, which makes interpretation of $^{\text{obs}}J$ values less than ~ 20 Hz difficult (or impossible). This is more a difficulty in the case of $\text{M}-\text{H}\cdots\text{Si}$ interactions than it is in assessing $\text{Si}-\text{H}\cdots\text{M}$ interactions. The collection of simple IR data is curiously absent in many studies, and such data should be relatively simple to collect but perhaps not so easily interpreted, especially in cases where the bands are weak or red-shifted into a region where other absorptions occur. However, deuterated analogues can be very helpful in determining an assignment and have been used effectively in several complexes cited in this review. As mentioned in previous sections, X-ray data for $\text{M}-\text{H}/\text{M}\cdots\text{H}-\text{Si}$ and $\text{SiH}/\text{Si}\cdots\text{HM}$ distances have been used to categorize $\text{M}\cdots\text{H}\cdots\text{Si}$ interactions, even though such data can be imprecise for hydride ligands in the vicinity of heavier metal centers. Low-temperature data collection may improve the reliability of the measurement, but unfortunately, determining location of the hydrides is often not possible. Calculation methods are useful, but attention must be paid to the level of the calculation.

It is important to remember that the interactions of silicon, hydrogen, and the transition metal form a continuum, and it is unlikely that concrete borders can ever be established between possible structural assignments. Furthermore, it is unlikely that all the variations possible for these interactions have been experimentally established, but certainly future investigators should keep in mind that a range of characterization methods will be necessary to place their results in the context of nonclassical interactions.

6. Solution Processes Determined from NMR Data

In this section, the complexes that exhibit fluxional behavior in solution will be described. The specific complexes are found in Tables 1, 2, and 3, with VTNMR listed in the “Other” column as one of the methods of characterization. The most common cases where fluxionality was observed have involved complexes with hydrides, either on the metal and/or on silicon. These cases will be described initially for monometallic complexes (section 6.1) and then for bimetallic complexes (section 6.2). Earlier examples of fluxionality in bimetallic complexes were reviewed by Ogino and Tobita.⁴⁷⁸ Additional miscellaneous types of fluxional processes will be summarized in section 6.3.

Generally a fluxional process is signaled by a broadened resonance (averaged signal) in the NMR spectrum, whereupon lowering the temperature may lead to decoalescence. In some reports, this was all that supported the assignment of a fluxional process, and in other cases, the thermodynamic parameters were calculated from line-shape analysis or from EXSY, nuclear Overhauser enhancement spectroscopy (NOESY), $^1\text{H}-^{29}\text{Si}$ HMBC, and HMQC data. Support for a fluxional process has also been obtained from chemical studies. A more recent trend is the use of DFT calculations to flesh out the possible details of the fluxional process itself.

In sections 6.1 and 6.2, the material is organized in terms of the particular hydrides that undergo an exchange process and not in terms of the details of the process. However, some processes may have a commonality with the particular hydride exchange, and these cases are added to the subsection. For hydrides, some form of reductive elimination (RE) of H–Si is frequently invoked, and the RE can be either an intramolecular or intermolecular process in monometallic complexes. Subsequent steps then lead to exchange of hydrides. In a few cases, there may be more than one outcome for a particular fluxional process involving hydrides, and these are generally included together. In only a few cases is support for a particular proposal provided by calculation methods. Recently, a proposal for σ -complexes as a basis for σ -bond metathesis reactions has been suggested by Perutz and Sabo-Etienne and termed σ -CAM (σ -complex-assisted metathesis). A σ -CAM process does not require a change in oxidation state at the metal center as is typical for OA/RE cycles.⁴⁷⁹ Selected examples in the Perutz/Sabo-Etienne review concern the dynamics of hydride complexes that involve σ -complexes as postulated intermediates. Potential cases that might involve a σ -CAM process that were not included in the Perutz/Sabo-Etienne will be suggested in some of the complexes that are discussed in this section.

6.1. Monometallic Hydride Complexes

Several of the hydride complexes in this section involve those with one or more hydrides on the metal and/or one or more hydrides on silicon. The types of fluxional processes that have been observed/proposed run the gamut of possibilities: (section 6.1.1) exchange of a terminal MH with a terminal SiH on silicon; (section 6.1.2) exchange of a terminal MH with η^2 -H–Si; (section 6.1.3) exchange through intermolecular reductive elimination of HSi from the metal center; (section 6.1.4) exchange of two (or more) hydrides at the metal or of two hydrides on silicon; (section 6.1.5) exchange of σ -H–Si and terminal SiH; and (section 6.1.6)

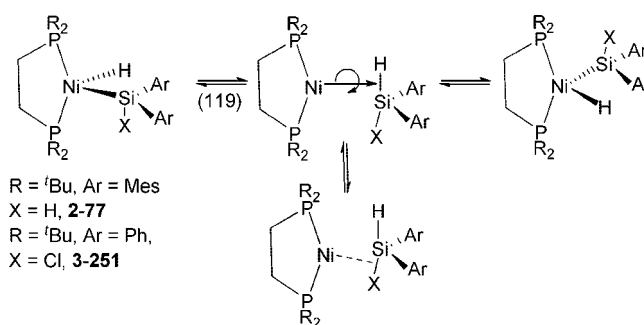
exchange of MH and MSi positions in the complex. These processes will be covered in the order just described.

6.1.1. H_b -[TM]-SiH_{a(term)} \rightleftharpoons H_a -[TM]-SiH_{b(term)} and Related Intramolecular RE in H-[TM]-SiR₃ Cases (Intramolecular Processes)

See section 6.1.3 for the related intermolecular process. The complex (dcpe)Pd(H)SiH(^tBu)₂, **2-78a** (stable in solution in the presence of excess free silane),^{120a} exhibited a novel fluxional behavior compared to its counterpart prepared from tertiary silanes whose features will be discussed in section 6.3. At low temperature (−80 °C), the spectrum of **2-78a** was consistent with a square-planar Pd(II) center with two ³¹P resonances, one of which was a doublet due to coupling with Pd–H. At room temperature, the *coupled* ³¹P NMR spectrum was observed as a broadened *triplet* and not the doublet that would be expected for a static square-planar complex. The observed triplet suggested that the P center was coupled to two equivalent protons resulting from a fluxional process that still occurred at room temperature. No Pd–H or Si–H resonances were observed in the ¹H NMR spectrum, but the exchanging protons were observed in the two-dimensional ¹H–²⁹Si HMQC and HMQC spectra. Thus, a dynamic process that exchanged Pd–H and Si–H could be demonstrated, but the nature of the process was suggested by DFT calculations of three rotational isomers of the model complex (dmpe)PdH(SiMe₂H). The rotational isomers considered were (a) a *trans* disposition of the hydrides PdH and SiH about the Pd–Si bond, **A**; (b) a *cis* disposition of the PdH and SiH about the Pd–Si bond, **B**; and (c) two hydrides bridging the Pd...Si and also located in the P₂PdSi coordination plane, **C**. Isomer **A** was the global minimum, and **C** was 6.9 kcal/mol higher in energy relative to **A**. It was proposed that this symmetrically bridged intermediate, **C**, was responsible for *both* the interchange about the Pd coordination environment and the observed SiH/PdH scrambling. Reductive elimination (discussed in section 6.1.5) to give (dmpe)Pd + Me₂SiH₂ was considerably less favored with a $\Delta E = 27.5$ kcal/mol and $\Delta G(298) = 16$ kcal/mol.

The Pd complexes, (dcpe)Pd(H)SiR₃ generated from tertiary silanes and [(μ -dcpe)Pd]₂, exhibited highly temperature-dependent NMR spectra.²⁷⁴ Only the complex where SiR₃ = SiPh₃ (**3-255**) could be isolated as the first stable mononuclear silylpalladium hydride and was crystallographically characterized. Three additional complexes (SiR₃ = SiPh₂Me, SiPhMe₂, and SiEt₃) were studied in solution, and the latter two are stable only in the presence of excess silane. Competition experiments, studied by ³¹P NMR, for the reaction of [(μ -dcpe)Pd]₂ with two different silanes established a stability order and K_e values (relative to the least stable complexes): SiR₃ = SiPh₃ (2400) > SiPh₂Me (310) > SiPhMe₂ (24) > SiEt₃ (1). The trends clearly show the effect of aryl substitution versus alkyl substitution on the stability of the Si–Pd–H series. The complexes also showed temperature-dependent ³¹P NMR spectra with a single ³¹P resonance, which broadened and reacoalesced to two resonances at −80 °C. An *intramolecular* interchange of coordination environments was proposed to explain the temperature dependence observed. The E_a , ΔH^\ddagger , and ΔS^\ddagger parameters were obtained for the protio complexes (SiR₃ = SiPh₃, SiPh₂Me, SiPhMe₂, SiEt₃) as well as for the deuterium analogues of the complexes with SiPh₃ and SiPh₂Me ligands. The values for the four (dcpe)Pd(H)(SiR₃) systems exhibited the following ranges (smallest for SiEt₃ and largest for SiPh₃):

Scheme 17

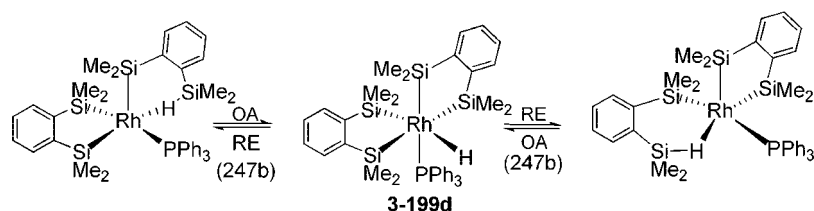


$E_a = 9.6(6)$ to $12.9(4)$ kcal/mol; $\Delta H^\ddagger = 9.2(6)$ to $12.4(4)$ kcal/mol; $\Delta S^\ddagger = -1(1)$ to $8.3(8)$ cal/(mol K). The deuterides have activation enthalpies that are 4–6 kcal/mol *less* than those of the hydrides and the activation entropies are ~ 17 – 25 cal/(mol K) more negative. This resulted in a crossover in the kinetic isotope effect (KIE; k_H/k_D) from $k_H/k_D = 0.13$ at -60 °C to 2.0 at -10 °C for **3-255**. The formation of a discrete well-defined Si–H σ -complex by reductive coupling followed by rotational interchange was proposed, resulting in both inverse and normal KIEs observed for the same complex.²⁷⁴

Another complex that undergoes reversible elimination of the silane is (dtbpe)Ni(μ -H)SiXAr₂ (dtbpe = 1,2-bis(di-*tert*-butylphosphino)ethane; Ar₂ = Mes₂ (**2-77**), Ph₂, X = H; Ph₂, X = Me, Cl).¹¹⁹ In C₆D₆ (but not THF-*d*₈), **2-77** is in equilibrium with free Mes₂SiH₂. In THF-*d*₈, however, the ¹H NMR spectrum showed that the four ^tBu signals were equivalent as were the two hydride resonances, and there was also a singlet in the ³¹P spectrum. Both J_{PH} (for SiH₂) and J_{SiP} in the ²⁹Si and ³¹P spectra were retained, indicating that the silane does not dissociate from the nickel center (on the NMR time scale). In addition, the product formed from Mes₂SiHD exhibited the same chemical shift for the Si–H proton in the ¹H NMR spectrum and for the Si–D in the ²H NMR spectrum, indicating that the two exchanged on the NMR timescale. The equilibrium with free silane was not observed in benzene for the other three complexes, although these were also fluxional. In the case of the complex formed from HSiPh₂Cl, the fluxional process was slow at 200 K, giving a ¹H spectrum consistent with the structure observed in the solid state with an upfield resonance for the hydride (a dd at -8.19 ppm) due to coupling to two inequivalent ³¹P nuclei. The two processes are demonstrated in Scheme 17. The features of the mechanism included a reversible RE through a Ni(0)- η^2 silane intermediate, rotation about the Ni–(H–Si) bond, followed by oxidative addition. With the secondary silane, another process that interchanged the two SiH positions also occurred, thus exchanging Ni–H_{term} and Si–H_{term} sites (Scheme 17).¹¹⁹

A reversible RE/OA sequence was also proposed to explain the fluxional behavior of (Ph₃P)Rh(SiMe₂C₆H₄-SiMe₂)(η^1 -HSi^aMe₂C₆H₄SiMe₂), **3-199d**, which exhibits a δ -agostic interaction in the solid state for the last of the four original HSiMe₂ groups that did not add to the metal center.^{247b} The Si^a...Rh distance is 3.082 Å, considered outside a bonding distance. At room temperature, the ¹H NMR spectrum shows no peak in the region -20 to -1 ppm attributable to a metal hydride; however, there was a resonance at -0.26 ppm with Si satellites ($J_{SiH} = 112$ Hz). The crystal structure indicated eight inequivalent Me groups (6 singlets and 2 doublets would be expected in the ¹H

Scheme 18



spectrum), but only four singlet signals were actually present in the rt spectrum, and dynamic behavior was observed at low temperature (183 K) where the signals were broad. The authors proposed a reversible RE/OA sequence shown in Scheme 18 to account for the broadening of the signals for the Me groups.^{247b}

In another unique system, **3-245e**, $[(\text{POCOP})\text{Ir}(\text{H})(\eta^1\text{-HSiEt}_3)]^+[\text{B}(\text{C}_6\text{F}_5)_4]^-$, the ^1H NMR signals for the Ir–H_{term} and the $\eta^1\text{-H-Si}$ are too broad to be observed at rt, but at 203 K, a static spectrum was obtained with a resonance at -4.9 (s, $^1J_{\text{SiH}} = 79$ Hz, $\eta^1\text{-H-Si}$) and at -44.2 (t, Ir–H), consistent with a square-pyramidal complex with an apical hydride (observed in the solid state). No mechanism was suggested for this exchange.^{266a}

6.1.2. $\text{H}_a[\text{TM}](\sigma\text{-H}_b\text{-Si}) \rightleftharpoons \text{H}_b[\text{TM}](\sigma\text{-H}_a\text{-Si})$

There are three groupings of complexes where exchange between a terminal metal hydride and the hydride of an $\eta^2\text{-HSiR}_3$ was proposed. In the first example, reaction of $\text{TpRuH}(\text{NCCH}_3)(\text{PPh}_3)$ with primary (H_3SiPh , to produce **1-40**), secondary (H_2SiEt_2 , to produce **2-37**; H_2SiPh_2 , Table 2, footnote 45), and tertiary silanes (HSiEt_3 , to produce **3-103**; $\text{HSi}(\text{OEt})_3$, HSiPh_3 , Table 3, footnote 117) gave complexes formulated as $\text{TpRu}(\text{PPh}_3)(\text{H}_2\text{SiR}_3)$ (Tp is the tridentate hydridotris(pyrazolyl)borate ligand,^{48a} indicating the uncertainty of the assignment as σ -complexes, $\text{Tp}(\text{Ph}_3\text{P})\text{-Ru}(\text{H}_a)(\eta^2\text{-H}_b\text{SiR}_3)$). The two hydrides (H_a and H_b) were equivalent down to -100 °C, indicating that a fluxional process averaged the signal for $\text{RuH}_{\text{term(a)}}$ and $\text{Ru}(\sigma\text{-H}_b\text{-Si})$. The complexes formed from primary and secondary silanes would also contain an SiH_{term} unit, but no exchange was observed between either hydride of the $\text{H}_a\text{Ru}(\sigma\text{-H}_b\text{-Si})$ unit with SiH_{term} . The nature of the fluxional process was suggested from an ab initio calculation at the B3LYP level for the model complex $[\{\text{HB}(\text{NH}=\text{N}=\text{CH}_2)_3(\text{H})(\text{PH}_3)\text{Ru}(\eta^2\text{-H-SiH}_3)\}]$ as four isomeric species (see Figure 7, section 5). The most stable isomer was the unsymmetrical “trans-dihydride” structure **A** shown in Figure 7. The other unsymmetrical isomer, **D**, with a nonclassical $\eta^2\text{-silane}$ coordination lies 1.9 kcal/mol above **A**. A simple “unsymmetric stretch” of $\text{H}\cdots\text{Si}\cdots\text{H}$ through a dibridged intermediate **B** (2 hydrides bridging the $\text{Ru}\cdots\text{SiR}_3$ similar to that proposed for the Pd complex, **2-78a**, described in section 6.1.1) interconverts enantiomeric pairs with a small reaction barrier. The interconversion between the enantiomers **A** and **D** had a calculated barrier of 7.5 kcal/mol, and the calculations also showed that the $(\eta^2\text{-H-Si})$ coordination was favored over $\eta^2\text{-H}_2$ coordination. This fluxional process could also be described as a $\sigma\text{-CAM}$ process,⁴⁷⁹ which was proposed after the publication of the study.

Another case involved the cation in the complex salt $[\text{Cp}^*(\text{Me}_3\text{P})\text{H}_a\text{Rh}(\eta^2\text{-H}_b\text{SiR}_3)]^+[\text{BAR}'_4]^-$ ($\text{Ar}' = 3,5\text{-(CF}_3)_2\text{C}_6\text{H}_3$; $\text{R} = \text{Ph, Me, Et}$ (**3-181b**)).²³⁹ The complexes were not isolated, but the hydride resonance at -10 ppm was integrated for 2H's and exhibited a J_{RhH} coupling but no ^{29}Si

satellites. The authors argued that, because the complex was fluxional, the J_{SiH} would be an average that could be a small number moving the satellites into the wings of the broad hydride resonance ($\nu_{1/2} \approx 50$ Hz), making them difficult to detect. Thus, the nonclassical representation was not necessarily precluded, and exchange of the terminal RhH and the bridging SiH was proposed. This result may also be described through the $\sigma\text{-CAM}$ process.⁴⁷⁹

One of the more unusual cases where the solid-state structure indicates a $\sigma\text{-H-Si}$ interaction but the solution structure appeared to differ was the complex **1-64** formed from the reaction of silicon “tridentate”, $[2\text{-(H}_3\text{SiC}_6\text{H}_4)_2\text{SiH}_2]$ and $(\text{depe})\text{Ni}(\text{PEt}_3)_2$.⁶⁵ The solid structure indicates that the original SiH_2 unit becomes bound to Ni with one of the two hydrogens bridging the Si–Ni bond with $\text{Si}\cdots\text{H} = 1.75(3)$ Å and $\text{Ni-H} = 1.47(3)$ Å. The room-temperature ^1H NMR spectrum showed one signal for $(\text{Si-H}_{\text{term}})$ at 5.67 ppm and another broad singlet at 2.61 for the two SiH_2 groups and the one bridging hydrogen. Thus, rapid exchange of five hydrogens takes place at room temperature, and the $^{29}\text{Si}\{^1\text{H}\}$ exhibited one triplet at 34.4 ppm for the $\text{SiH}(\text{H}_{\text{br}})$ group and one triplet at -2.3 ppm for the other two SiH_2 groups. In the ^1H -nondecoupled ^{29}Si spectrum, the downfield signal split into two with a $^1J_{\text{SiH}}$ of 173 Hz and the upfield signal coupled with five hydrogens with a $^1J_{\text{SiH}}$ of 80 Hz. At lower temperatures, the broad proton signal splits into two signals, one at -6.70 for the Ni–H signal and the other at 4.79 ppm for the four Si–H signals (SiH_2 groups). The low-temperature ^{29}Si NMR spectrum (^1H nondecoupled) showed a triplet due to coupling to two hydrogens with $^1J_{\text{SiH}} = 173$ Hz, but there was no change as observed for the $\text{SiH}(\text{H}_{\text{br}})$ signal. Since the two SiH_2 groups gave a single ^{29}Si signal, the complex was still considered fluxional at low temperature, although the hydrogens appear frozen. The structure in solution at low temperature was assumed to be a tetravalent tris(silyl)(hydrido)nickel(IV) complex, which was also consistent with the DFT calculations (see section 7.3.7).

Probably the best studied systems involved the novel complexes $[(\text{Cy}_3\text{P})_2(\text{H})_2\text{Ru}\{\eta^2\text{-(HSiMe}_2)_2\text{X}\}]$ ($\text{X} = \text{C}_6\text{H}_4$, **3-127**; O , **3-128**; NH , **3-132**; CH_2CH_2 , Table 3, footnote 141; as well as other systems listed in the footnotes) and $[(\text{Cy}_3\text{P})_2(\text{H})_2\text{Ru}\{\eta^2\text{-(HSiPh}_2)_2\text{O}\}]$ (Table 3, footnote 142).^{208,209,212,398} These complexes have two $\text{Ru}-(\eta^2\text{-H-Si})$ bonds where the silicon centers are also linked together (indicated by X in the general formula). The studies reported spectroscopic properties, various NMR experiments, structural data for selected examples, and calculations, which also included comments on the appropriateness of calculation methods. The complexes contain a “chelating” $\text{HSiR}_2\text{XSiR}_2\text{H}$ unit and the bulky phosphine, Cy_3P . The majority exhibited a novel octahedral geometry with the disilyl groups occupying *trans*-positions and the bulky phosphines occupying positions *cis* to each other (Figure 13). The complexes that were crystallographically characterized with these general structural features included $\text{R} = \text{Me}$, $\text{X} = \text{C}_6\text{H}_4$ (**3-127**),²⁰⁹ CH_2CH_2

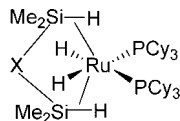


Figure 13. Complex with chelating $\text{HSiR}_2\text{XSiR}_2\text{H}$ with *trans*-silyl groups in an octahedral environment.²⁰⁸

(Table 3, footnote 141),²⁰⁸ and $-\text{OSiMe}_2\text{O}-$ (Table 3, footnote 141), as well as two additional examples ($\text{X} = \text{CH}_2\text{CH}_2$) where one or both of the PCy_3 groups were replaced by PPh_3 .²⁰⁸ The corresponding disilazane complex was a different structural type with the disilyl groups as well as the two phosphines and the two hydrides each *cis* to each other (an approximate C_{2v} disposition for the core P_2RuSi_2).²¹² The similarity of the VTNMR data for the disilazane- and disiloxane-derived complexes suggested that the same structure for both derivatives could be assumed.²⁰⁸

Additional NMR experiments and a more extensive discussion of the possible exchange mechanisms for $\text{RuH}_2\{[(\eta^2\text{-HSiMe}_2)_2](\text{CH}_2)_2\}(\text{PCy}_3)_2$ have been published,³⁹⁸ and selected results and conclusions are summarized first for this complex as a prototype for the complexes with this structure and secondly for the two systems with the C_{2v} disposition for the core P_2RuSi_2 ligands. The room-temperature ^1H NMR spectrum exhibited two high-field resonances attributed to the two $\eta^2\text{-SiH}$ hydrides (t, -8.21 ppm) and the two classical hydrides (m, -12.65 ppm). Coalescence of these two signals was obtained at 376 K, and the free energy of activation calculated from the rate of exchange at this temperature was 16.3 kcal/mol. At 273 K, NOESY/EXSY experiments showed negative nuclear Overhauser effect (NOE) cross-peaks, signaling a negligible exchange between these two sets of protons. However, between 297 and 333 K, EXSY spectra gave positive cross-peaks; thus, exchange between the two types of hydrides was established. NOE NMR experiments at four temperatures provided activation parameters (Eyring analysis) of $\Delta H^\ddagger = 18 \pm 2.6$ kcal/mol and $\Delta S^\ddagger = 3.3 \pm 8.1$ cal/mol. The entropy value suggested an intramolecular exchange process between the two sets of protons. Three possible mechanisms were considered and tested: (i) phosphine dissociation; (ii) formation of $\eta^2\text{-H}_2$ isomers; and (iii) decoordination of one of the $\eta^2\text{-HSi}$ bonds. The 1D NOE experiments for the complex in the presence of an equivalent of phosphine precluded phosphine dissociation as the mechanism. The calculations for the model $\text{RuH}_2\{[(\eta^2\text{-HSiMe}_2)_2](\text{C}_2\text{H}_2)\}(\text{PH}_3)_2$ showed that the exchange barrier for loss of phosphine was too high and was energetically unfavorable, although this might not have been the case for the sterically much larger PCy_3 ligand. The calculated barrier for decoordination of an $\eta^2\text{-HSi}$ bond was also too high, and mechanism (iii) could be eliminated. The X-ray structure of $\text{RuH}_2\{[(\eta^2\text{-HSiMe}_2)_2](\text{CH}_2)_2\}(\text{PCy}_3)_2$ exhibited two “short” $\eta^2\text{-HSi}$ bonds [1.73(3) and 1.78(4) Å] and four “longer” silicon-to-hydride distances [2.12(3), 2.13(3), 2.27(3), and 2.31(3) Å]. Four isomers of the model $\text{RuH}_2\{[(\eta^2\text{-HSiH}_2)_2](\text{C}_2\text{H}_2)\}(\text{PH}_3)_2$ were calculated (DFT; see Scheme 19 for structures) including the most stable isomer (**A**), which resembled the solid-state structure, and three other isomers (**B**, **C**, **D**) that were minima on the singlet potential energy surface, one of which contained *cis*-phosphines and *cis*-hydrides (**B**) and two additional isomers that had one and two $\eta^2\text{-H}_2$ ligands (**C** and **D**, respectively). The energies of the three isomers relative to **A** (0 kcal/mol) were **B** (7.3 kcal/mol), **C** (6.2 kcal/mol), and **D** (4.8 kcal/mol). Exchange of hydrogens can occur by rotation of the two dihydrogen

Scheme 19

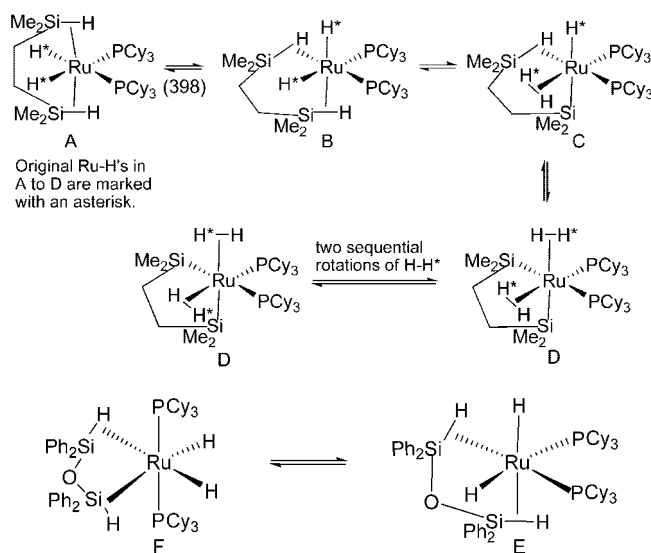


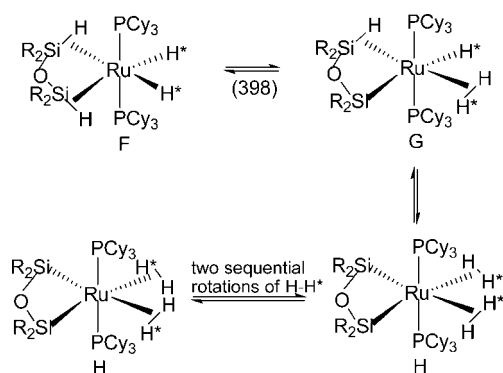
Figure 14. Isomers of $[(\text{Cy}_3\text{P})_2(\text{H})_2\text{Ru}\{(\eta^2\text{-(HSiPh}_2)_2\text{O)}\}]$.³⁹⁸

ligands in **D**, and the pathway in which the rotation occurs sequentially was energetically favored, as shown in Scheme 19.

The variable-temperature ^1H NMR study of the siloxane complexes, $[(\text{Cy}_3\text{P})_2(\text{H})_2\text{Ru}\{(\eta^2\text{-(HSiR}_2)_2\text{O)}\}]$ ($\text{R} = \text{Me}$ (**3-128**),²⁰⁸ Ph ,³⁹⁸ Table 3, footnote 142), revealed two fluxional processes. The exchange of the two $\eta^2\text{-H-Si}$ and the two RuH_{term} occurred with a lower ΔG^\ddagger of 11.4 and 12.2 kcal/mol ($\text{R} = \text{Me}$ and Ph , respectively) than was observed for the complexes with other linker atoms. The second process, with a slow exchange limit at 178 K, gave a ^{31}P NMR spectrum that was consistent with an arrested structure and a *cis*-disposition of the phosphine ligands.²⁰⁸ Subsequently, additional details of the ^{31}P spectral data for the second process, $[(\text{Cy}_3\text{P})_2(\text{H})_2\text{Ru}\{(\eta^2\text{-(HSiPh}_2)_2\text{O)}\}]$, were published.³⁹⁸ At 183 K, the ^{31}P NMR spectrum exhibited a singlet at $\delta = 42.4$ and a second signal corresponding to an AB pattern at $\delta = 44.9$ and 43.1. A $^{31}\text{P}\text{--}^1\text{H}$ correlation spectroscopy (COSY) spectrum allowed assignment of the signals that were consistent with the presence of two isomers as shown in Figure 14. The symmetrical isomer is associated with the singlet ^{31}P resonance and the unsymmetrical isomer with the AB multiplet present in the ^{31}P resonance. The ratio between **F** and **E** (shown in Figure 14) was 1:2, and the latter was the most thermodynamically stable. The EXSY spectra obtained at 193 K were consistent with both the exchange between the hydrides and the Si-H hydrogen atoms and between the two types of hydrides. However, the isomerization process between **F** and **E** prevented full analysis. The related study of $[(\text{Cy}_3\text{P})_2(\text{H})_2\text{Ru}\{(\eta^2\text{-(HSiMe}_2)_2\text{O)}\}]$ (**3-128**) indicated that only the equivalent of isomer **E** was present.³⁹⁸

A DFT analysis of the structures with the *one atom bridge* for the model complex $[\text{RuH}_2\{(\eta^2\text{-HSiH}_2)_2\text{O}\}(\text{PH}_3)_2]$ confirmed two minima that corresponded to **F** and **E** (Figure 14). In **E**, the two phosphines are *cis* but *trans* to the phosphines are different ligands, a hydride and the $\sigma\text{-Si-H}$ ligand. Consequently, the two calculated Si-H bonds (σ -coordinated to the Ru center) were different (1.784 and 1.596 Å) and the three $\text{Si}\cdots\text{H}_{\text{term}}\text{Ru}$ distances ranged from 2.125 to 2.193 Å while the fourth $\text{Si}\cdots\text{H}_{\text{term}}\text{Ru}$ was 4.181 Å. This contrasts to the previous case with a two-atom bridge where the X-ray and DFT data both indicated equivalent Si-H and $\text{Si}\cdots\text{H}$ distances. Calculations that are related to a possible

Scheme 20

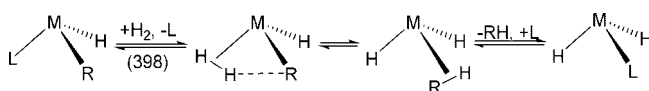


mechanism for exchange of the RuH and SiH bonds were developed for both isomers. The TS state for the hydride-exchange process for isomer **E** (modeled with $\text{RuH}_2[(\eta^2\text{-HSiH}_2)_2\text{O}](\text{PH}_3)_2$) was calculated to be only 3.7 kcal/mol above **E**, exhibited C_{2v} symmetry with a *trans*-disposition of the two $\eta^2\text{-SiH}$ groups, and had four $\text{Si}\cdots\text{H}$ distances that were almost equivalent and whose values correspond to SISHA interactions. The isomer **F**, in Figure 14, corresponded to coordination of the disiloxane in an early stage of activation (shorter Si—H bond) with no SISHA interactions. In two other isomers, **G** and **H** (Scheme 20), the Si—H_{br} bond to Ru is stretched (>3.5 Å), producing a H₂ ligand, and in the last isomer **H**, both Si—H_{br} are stretched, producing two H₂ coordinated ligands. The proposed exchange mechanism for isomer **F** is shown in Scheme 20. For this isomer, the two ($\eta^2\text{-SiH}$) bonds are converted successively to ($\eta^2\text{-SiH}$) ($\eta^2\text{-H}_2$) (**G**) and then to ($\eta^2\text{-H}_2$)₂ (**H**). Internal rotation of the dihydrogen ligands and return to ($\eta^2\text{-SiH}$) coordination completes the isomerization process.³⁹⁸

The disilazane complex, $[(\text{Cy}_3\text{P})_2(\text{H})_2\text{Ru}\{(\eta^2\text{-HSiMe}_2)_2\text{NH}\}]$ **3-132**, exhibited NMR data similar to that observed for the siloxane **3-128**.²¹² The first decoalescence (exchange of the RuH and SiH) is characterized by a $\Delta G = 11$ kcal/mol, and the second decoalescence had a $\Delta G = 9.1$ kcal/mol. Although not suggested by the authors, it is likely that the exchange processes for **3-132** and **3-128** are similar. In the case of **3-132**, however, an X-ray crystal structure was obtained that resembled isomer **E** in Figure 14. The activation of the two Si—H bonds appears to be similar as reflected in the closely related Ru—Si bond distances [2.395(2) and 2.434(2) Å] and the nearly identical $\sigma\text{-Si—H}$ bond lengths [1.91(5) and 1.93(5)], with the latter being at the usual limit assumed for σ -coordination. DFT calculations were performed at the B3LYP level, which gave two very different Ru—Si distances. The calculations were repeated using the B3PW91 functional for both the model $[\text{RuH}_2\{(\eta^2\text{-HSiH}_2)_2\text{NH}\}](\text{PH}_3)_2$ and the actual complex, $[(\text{Cy}_3\text{P})_2(\text{H})_2\text{Ru}\{(\eta^2\text{-HSiMe}_2)_2\text{NH}\}]$. The theoretical values for the latter closely matched parameters from the X-ray study. This appeared to be the first time in silyl—ruthenium chemistry where the choice of the functional for DFT calculations was necessary to reproduce the features of the complex that were measured in the solid state.

Complexes of the general formula $[(\text{R}_3\text{P})_2(\text{H})_2\text{Ru}\{(\eta^2\text{-HSiMe}_2)_2\text{X}\}]$ appear to be stabilized by two $\eta^2\text{-H—Si}$ groups and by weak $\text{H—Si}\cdots\text{H}$ interactions that are referred to by the term SISHA interactions. It was the breaking of the SISHA interactions that was the most energetically demanding step in the exchange between the two types of

Scheme 21



hydrides. Secondary interactions between halosilyl ligands and hydrides were described by Nikonov, but the SISHA interactions occur in the absence of electron-withdrawing substituents. Scheme 21 highlights how the SISHA interactions can lead to formation of new σ -bonds without decoordination of the ligand.³⁹⁸

For the complex **3-134b**, $\text{H}_2\text{Ru}\{\eta^2\text{-HSiMe}_2\text{CH}_2(o\text{-C}_6\text{H}_4)\text{PPh}_2\}_2$, the rt ^1H NMR spectrum exhibited one broad signal at -7.8 ppm. Decoalescence occurred at 273 K, and at the low-temperature limit (193 K), two broad signals were observed at -5.52 and -10.4 (AA'XX') ppm. The fluxional process is attributed to the ε -agostic $\eta^2\text{-H—Si/Ru—H}$ exchange with $\Delta G^\ddagger = 11$ kcal/mol.^{213c}

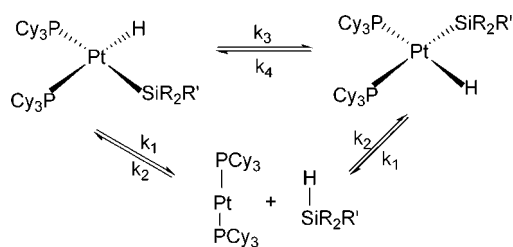
6.1.3. $\text{H}[\text{TM}]\text{SiH} \rightleftharpoons [\text{TM}] + \text{H}_2\text{Si}$

This section involves an intermolecular RE process. The intramolecular RE was described in section 6.1.1. The fluxional behavior of a seven-coordinate complex, $(\text{Me}_3\text{P})_3(\text{H})_2\text{Ru}(\text{SiMe}_3)_2$, **3-123**, related to complexes **1-41** and **2-40** (which will be described further in part 6.1.4) has been reported.⁴⁹ In contrast to **1-41** and **2-40**, several other intermolecular processes occurred on raising the temperature from 150 K, and from line-shape analyses, two processes were identified. The lower-energy process involved intramolecular exchange of the two RuH's and a second process that took place with a higher barrier that involved intermolecular exchange with free (excess) HSiMe_3 and was proposed to occur by reversible Si—H reductive elimination to give the intermediate **16e** $(\text{Me}_3\text{P})_3(\text{H})\text{RuSiMe}_3$. The equilibrium constant for dissociation of Me_3SiH from **3-123**, $(\text{PMe}_3)_3\text{Ru}(\text{SiMe}_3)_2\text{H}_2 \rightleftharpoons (\text{Me}_3\text{P})_3(\text{H})\text{RuSiMe}_3 + \text{HSiMe}_3$, was determined for several temperatures from the ^{31}P NMR spectrum and provided the thermodynamic parameters from the temperature dependence: $\Delta H_{\text{SiH-elim}} = 11.2 \pm 0.6$ kcal/mol and $\Delta S_{\text{SiH-elim}} = 40 \pm 2$ cal/(mol K), consistent with the proposed dissociation process. From ^1H NMR line-shape analysis, the activation parameters for HSiMe_3 dissociation were determined: $\Delta H_{\text{SiH-elim}}^\ddagger = 9.2 \pm 0.6$ kcal/mol and $\Delta S_{\text{SiH-elim}}^\ddagger = -9 \pm 3$ cal/(mol K); $\Delta H_{\text{SiH-add}}^\ddagger = -1.8 \pm 0.8$ kcal/mol and $\Delta S_{\text{SiH-add}}^\ddagger = -31 \pm 3$ cal/(mol K).⁴⁹

One of the most interesting aspects of the study was the estimation of the thermodynamic preference for SiH, $\beta\text{-CH}$, or H_2 oxidative addition to **16e** $(\text{Me}_3\text{P})_3(\text{H})\text{RuSiMe}_3$, which ultimately was dominated by entropy contributions and steric effects. Addition of H_2 was the most favorable at all temperatures studied, but the dominance of intramolecular $\beta\text{-CH}$ versus intermolecular SiH addition were dependent on temperature. Below 250 K, the free energy for the oxidative addition followed the order (from most to least favorable) $\Delta G_{\text{HH-add}} \ll \Delta G_{\text{SiH-add}} < \Delta G_{\text{CH-add}}$, but above 250 K, the preference for $\beta\text{-CH}$ addition over SiH activation was reversed and the order became $\Delta G_{\text{HH-add}} \ll \Delta G_{\text{CH-add}} < \Delta G_{\text{SiH-add}}$. The authors propose that the “relative enthalpies are interpreted in terms of strong SiH σ -complex formation—and much weaker CH coordination—in the transition state for oxidative addition”.⁴⁹

The broad, room-temperature SiH ^1H NMR resonance for the silyl capped complex $[\text{PhBP}'_3]\text{IrH}_3(\text{SiH}_2\text{Et}_2)$, $(\text{PhBP}'_3 = \text{PhB}(\text{CH}_2\text{P}^i\text{Pr}_2)_3)$, **2-75a**, suggested a possible fluxional

Scheme 22



process that could be attributed to reversible elimination of Et_2SiH_2 .¹¹¹ To test this possibility chemically, two reactions were performed, one involving D_2 and the other involving addition of phosphine. After addition of D_2 to a solution of **2-75**, deuterium was incorporated into both the SiH and IrH sites (reaction required heating). Addition of 1 equiv of PMe_3 resulted in quantitative formation of 1 equiv of Et_2SiH_2 and no evidence for elimination of H_2 . No NMR data at other temperatures were reported; thus, this example has more indirect support for reversible elimination of the silane.¹¹¹

Another complex that underwent reversible elimination of the silane was $(\text{dtbpe})\text{Ni}(\mu\text{-H})\text{SiXAr}_2$ (dtbpe = 1,2-bis(*tert*-butylphosphino)ethane; Ar_2 = Mes_2 (**2-77**), Ph_2 , X = H; Ph_2 , X = Me, Cl) (discussed in section 6.1.1).¹¹⁹ In C_6D_6 (but not $\text{THF-}d_8$), **2-77** was in equilibrium with free Mes_2SiH_2 . Both J_{PH} (for SiH₂) in **2-77** in the ^1H spectrum and J_{SiP} in the ^{29}Si and ^{31}P spectra were retained, indicating that the silane does not dissociate from the nickel center (on the NMR time scale), and this case was discussed previously in section 6.1.1.

The Pt–H and SiH signals for the square-planar platinum complex *cis*-(Cy_3P)₂Pt(H)SiHMe₂ (**2-95**) are broad in the ^1H NMR spectrum.^{11,12} Because of the overlap of the Pt–H–Si–H protons with the cyclohexyl resonances during the VT studies, ^1H EXSY experiments were used to verify the exchange of the Pt–H and Si–H signals. The EXSY experiments indicated exchange between the Pt–H hydrides with the Si–H hydrides of *free* Mes_2SiH_2 , which were also supported by experiments with Mes_2SiD_2 . No exchange with excess free phosphine was observed. Thus, the data appeared to be consistent with an intermolecular mechanism involving hydrogen exchange via a rate-determining elimination of Mes_2SiH_2 , which does not require prior dissociation of a phosphine ligand.¹²

However, the situation with less bulky silyl groups as in *cis*-(Cy_3P)₂Pt(H)SiHPh₂ (**2-94**) is more complex (a total of 11 complexes were studied, but **2-94** will be used to illustrate the general features).¹²⁹ In this case, the phosphines undergo mutual exchange while retaining P–H spin correlation, indicating an intramolecular process. A second intermolecular dynamic process competes with the intramolecular process and required loss of P–H coupling. Two possibilities were considered: dissociative exchange between **2-94** and free phosphine or dissociative exchange between **2-94** and free silane (or a combination of these two; Scheme 22). In one case, free silane could be detected at 315 but not at 280 K. No exchange between SiH and PtH was detected in EXSY experiments. Evidence for RE of silane was found from line broadening, EXSY experiments, silane exchange, and isotope labeling. The barrier for reductive elimination increased in the sequence of silyl substituents, SiMe_2Et (Table 3, footnote 294) < SiPh_3 (**3-278a**) < SiPh_2H (**2-94**). The authors concluded that the TS^\ddagger for phosphine exchange and that for RE (in **2-94**) of silane both involved an $\eta^2\text{-H-SiHPh}_2$ but

that the geometry of the TS^\ddagger for each of these two processes must be distinct, although no suggestion was presented for the difference between the two. The standard enthalpy for the RE of silane was determined for two examples and was 7.6 ± 0.5 and 15 ± 2 kcal/mol for the SiMe_2Et and SiPh_3 complexes, respectively.¹²⁹

Another complex where the possibility of a RE/OA of HSiR_3 was proposed was for the novel ligated complex, $(\text{Gaddp})_2\text{Pt}(\text{H})\text{SiEt}_3$ (ddp = 2-{(2,6-diisopropylphenyl)amino}–4-{(2,6-diisopropylphenyl)imino}–2-pentene), **3-278b**.^{298a} The rt NMR spectrum shows that, other than the $\gamma\text{-C}'$ s, all other ddp signals are separated, indicating two chemically inequivalent ligands with local C_s symmetry but broadened, suggesting a fluxional process. At 70 °C, only one set of signals is present. Either the fluxional process involves RE/OA of HSiEt_3 or dissociation/association of a $\text{Ga}(\text{ddp})$ ligand. However, the catalytic deuteration of HSiEt_3 by the C_6D_6 solvent favors the reversibility of silane addition.^{298a}

6.1.4. $\text{H}_a[\text{TM}]\text{H}_b$ or $[\text{TM}]\text{H}_a\text{H}_b\text{Si}$ Exchange

The three reported cases for exchange of the position of hydrides in a silyl–metal complex are derived from reaction of a metal precursor with a tertiary silane. The three cases include $\text{Cp}'(\text{H})_3\text{IrSiEt}_3$ (Cp' = $\text{C}_5\text{H}_4\text{CH}_2\text{CH}_2\text{OMe}$, **3-232**),²⁶⁰ $\text{Tp}^{\text{Me}_2}(\text{H})_3\text{IrSiEt}_3$ (**3-242a**),^{264a} and $(\text{Me}_3\text{P})_3(\text{H})_2\text{Ru}(\text{SiR}_3)_2$ (SiR_3 = SiH_2Ph , **1-41**; SiHPh_2 , **2-40**; SiMe_3 , **3-123**).⁴⁹ A fourth example involved complexes from an addition reaction to the multiple bond of a $\text{W}=\text{Si}$ complex to produce $\text{Cp}^*(\text{OC})_2\text{W}(\text{H})_2(\text{SiHPhR})$ (R = Ph, H, Cl) and may be considered to be formally derived from a secondary silane or from tertiary silanes.⁴⁷⁷

The ^1H NMR spectrum of **3-232**, $\text{Cp}'(\text{H})_3\text{Ir}(\text{SiEt}_3)$ (Cp' = $\text{C}_5\text{H}_4\text{CH}_2\text{CH}_2\text{OMe}$), exhibited a singlet resonance for the hydrides that decoalesce between 243 and 233 K to give an AB_2 spin system at 193 K.²⁶⁰ At low temperature, a rigid structure was formed with a four-legged piano-stool geometry and the Cp' group occupying the 3-membered face. The hydride ligand that is transoid to the silyl group was assigned to H_A , which exchanged with the two adjacent H_B . Line-shape analysis provided rate constants, and the activation parameters were obtained from the Eyring analysis: ΔH^\ddagger = 11.8 ± 1 kcal/mol and ΔS^\ddagger = 1.8 ± 2.5 cal/(mol K). The entropy value is consistent with an intramolecular process and may be another variant of a $\sigma\text{-CAM}$ process. An interesting feature of **3-232** is the stepwise exchange of HIr with C_6D_6 to give **3-232-*d*₃** (IrD_3) and then **3-232-*d*₇** (IrD_3 and $\text{C}_5\text{D}_4\text{R}$) after a longer period of time.²⁶⁰ A second complex, $\text{Cp}'(\text{H})_2\text{Ir}(\text{SiEt}_3)_2$ (**3-233**, transoid silyl groups), was also isolated, but the ^1H NMR spectrum was temperature invariant. A second iridium system, $\text{Tp}^{\text{Me}_2}(\text{H})_3\text{IrSiEt}_3$ (**3-242a**), which contained an octahedral *fac*- N_3IrH_3 core with the silyl group capping the H_3 face, was reported to give a singlet hydride resonance, and the three pyrazolate arms of Tp^{Me_2} were equivalent down to -80 °C.^{264a} The structure in the solid state exhibited a mirror plane that contained one of the pyrazolyl rings, the Ir, Si, and one H. The two nonequivalent Ir–H bonds are equal within experimental error. The coupling constant J_{SiH} was only 6 Hz; thus, the authors concluded that there was no significant Ir–H...Si interaction and also did not speculate as to whether or not there was a fluxional process.

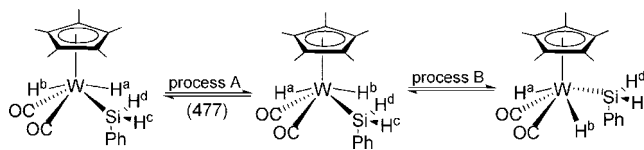
When $(\text{PMe}_3)_3\text{Ru}(\text{SiMe}_3)\text{H}_3$ was treated with excess H_3SiPh or H_2SiPh_2 , new seven-coordinate complexes $(\text{PMe}_3)_3(\text{H}_2\text{Ru}(\text{SiR}_3)_2$ [SiR_3 = SiH_2Ph (**1-41**); SiHPh_2 (**2-**

40)] formed.⁴⁹ These new complexes exhibited NMR data that were consistent with a pentagonal-bipyramidal geometry with axial phosphines as was observed in the solid-state structure of **1-41**. As is the case for most seven-coordinate complexes, **1-41** and **2-40** are fluxional, and the pairs of inequivalent hydride and $\text{SiH}_x\text{Ph}_{3-x}$ ligands undergo intramolecular exchange (summarized in section 6.1.4). From line-shape analysis of the VT ^1H NMR data, the activation parameters for the intramolecular exchange were determined to be $\Delta H^\ddagger = 9.3 \pm 0.3$ (**1-41**), 9.9 ± 0.6 (**2-40**) kcal/mol with $\Delta S^\ddagger = -26 \pm 1$ (**1-41**), -13 ± 2 (**2-40**) cal/(mol K). Complex **1-41** does not undergo intermolecular exchange with free PhSiH_3 (presumably this is also the case for **2-40**/ H_2SiPh_2). The related system, **3-122** $[(\text{Me}_3\text{P})_3(\text{H})_2\text{Ru}(\text{SiMe}_2\text{CH}_2\text{CH}_2\text{SiMe}_2)_2]$, formed from the chelating bis-silane, $\text{HMe}_2\text{SiCH}_2\text{CH}_2\text{SiMe}_2\text{H}$, has different spectral features and is highly fluxional in solution even at 150 K. In the solid state, the 7-coordinate complex has a “*fac*”-like arrangement of the three phosphine ligands, as well as *cis*-hydrides and a chelating silane that has one Si group bonded to the Ru center *trans* to phosphine, and the second Si group bisects the two hydrides.⁴⁹

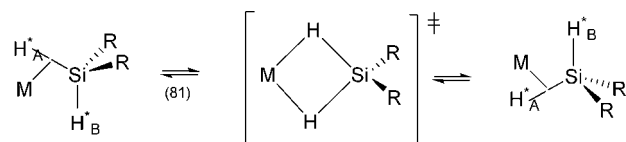
For the complex $(\text{Me}_3\text{P})_3(\text{H})_2\text{Ru}(\text{SiMe}_3)_2$ (**3-123**), VTNMR experiments indicated that two independent processes occurred. The higher energy barrier was associated with intermolecular exchange with free HSiMe_3 and was described in section 6.1.3, and the lower-energy process was associated with an intramolecular exchange of the two Ru–H’s (and the two silyl groups). This lower-energy process was similar to that described for **1-41** and **2-40** but with significantly lower activation parameters, $\Delta H^\ddagger = 6.5 \pm 0.6$ kcal/mol and $\Delta S^\ddagger = -4 \pm 2$ cal/(mol K).⁴⁹

The next example in this section involves the sets of isomers that were produced from one of two reactions involving reduction of *cis*- $\text{Cp}^*(\text{OC})_2(\text{H})\text{W}=\text{SiRPhDo}$ [Do = THF; R = Ph (Table 2, footnote 26) or H (**1-29b**)] with LiAlH_4 to give the tungstate (hydride added to the silicon center) followed by protonation with $\text{CF}_3\text{CO}_2\text{H}$ to give the polyhydride complexes $\text{Cp}^*(\text{OC})_2\text{W}(\text{H})_2(\text{SiHPhR})$ (R = Ph, H).⁴⁷⁷ Addition of HCl to the tungsten–silylene precursor gave $\text{Cp}^*(\text{OC})_2\text{W}(\text{H})_2(\text{SiHPhCl})$.⁴⁷⁷ The crystal structure of the major form of the R = Ph isomer verified a pseudo-octahedral geometry, and the major form when R = H exhibited a pseudo-trigonal-prismatic geometry. Thus, it was assumed that all three sets of isomers contained a 6-coordinate octahedral form and a trigonal-prismatic form: the ratio of octahedral/trigonal prismatic forms (-51°C) = 89/11 (R = Ph); 37/63 (R = H); 94/6 (R = Cl). These complexes, all together, exhibited four different fluxional processes including (a) an equilibrium between the two geometrical forms; (b) hydride site exchange for the pseudo-trigonal-prismatic form where R = H, Cl; (c) hydride site exchange for the pseudo-octahedral form where R = Cl; and (d) averaging of the diastereotopic SiH signals in the pseudo-trigonal-prismatic form (R = H). The equilibrium process (a) will be described in section 6.3, and processes (b)–(d) will be described in the current section. The hydride exchange in the pseudo-trigonal-prismatic isomer for the R = H complex is shown as process A in Scheme 23, and the process for the R = Cl complex is similar. The parameters obtained from variable-temperature ^1H NMR are $\Delta H^\ddagger = 9.8 \pm 0.6$ kcal/mol and $\Delta S^\ddagger = 0.3 \pm 2.1$ eu for the R = H complex; process B, which involves SiH site exchange (for the diastereotopic SiH; enantiomer interconversion, process B, Scheme 23) was

Scheme 23



Scheme 24



also evaluated for the R = H pseudo-trigonal-prismatic complex, and those parameters were $\Delta H^\ddagger = 8.0 \pm 0.9$ kcal/mol and $\Delta S^\ddagger = 3.1 \pm 3.8$ eu. The hydride site exchange in the pseudo-octahedral complexes was probably present in all three of the complexes but could only be observed in a complex with a Si center that was chiral, as was the case for the R = Cl complex. The parameters estimated by spectral simulation were $\Delta H^\ddagger = 8.1 \pm 0.6$ kcal/mol and $\Delta S^\ddagger = 3.2 \pm 2.4$ eu for R = Cl. The authors did not speculate as to the nature of any of these processes (b, c, d).⁴⁷⁷

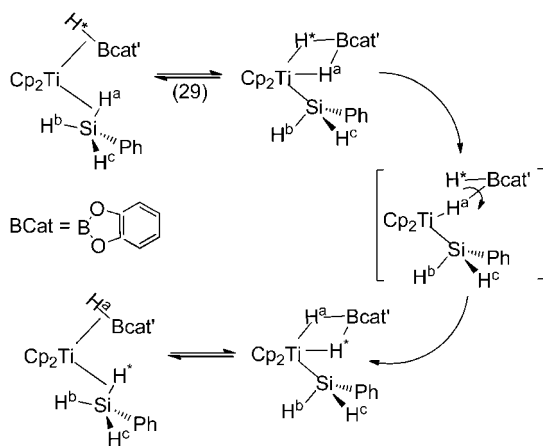
In an attempt to observe a simple OA of a hydrosilane to Co(I) in the pincer complex PNPCo ($\text{PNP} = (\text{Bu}_2\text{PCH}_2\text{SiMe}_2)_2\text{N}^-$) to produce $(\text{PNP})\text{Co}(\text{H})(\text{SiR}_3)$, a much more complicated silylene product was obtained, **1-54a**, $\text{Bu}_2\text{PCH}_2\text{Me}_2\text{SiNSiMe}_2\text{CH}_2/\text{Bu}_2\text{P}(\text{H})\text{Si}=\text{Co}(\text{H})_3(\text{SiH}_2\text{Ph})_2$ (crystallographically characterized).^{57ab} In the ^1H NMR spectrum (298 K), resonances for the diastereotopic SiHs were observed for both SiH_2Ph groups, a silylene hydrogen, and a broad hydride resonance of intensity 3. Typical of a 7-coordinate complex, rapid fluxionality was observed that was attributed to hydride migration among inequivalent sites, which did not include site exchange between the two SiH_2Ph groups. There was no exchange between any SiH and any CoH. No mechanism was proposed for the exchange.^{57a, b} The slow hydride-exchange regime was not reached at 203 K, the lowest temperature reported in the study.

6.1.5. $[\text{TM}]-\sigma\text{-H}_a\text{-Si-H}_{b(\text{term})} \rightleftharpoons [\text{TM}]-\sigma\text{-H}_b\text{-Si-H}_{a(\text{term})}$ or Two Diastereotopic $\text{SiH}_{(\text{term})}$

The exchange of hydrides at silicon has been reported for the complexes $\text{M}(\text{CO})_5(\eta^2\text{-H}_2\text{SiPh}_2)$ (M = Cr, **2-8**; Mo, **2-12**; W, **2-23**).⁸¹ At low temperatures, two sharp resonances were observed (Cr, 220 K; Mo, 185 K; W, 220 K) that broadened on warming, although coalescence of the resonances was not observed due to decomposition of the complexes at higher temperatures. Line-shape analysis provided the following activation parameters for the series: $\Delta H^\ddagger = 8\text{--}10$ kcal/mol and $\Delta S^\ddagger \approx -5$ eu. The J_{SiH} values varied from 98 to 111 Hz (largest value for the Mo complex). No line broadening of excess free silane was observed, indicating that dissociation of the bound silane did not occur. The mechanism proposed for the exchange involved the formation of a species where both Si–H bonds are coordinated to the metal center (Scheme 24). The observation of rapid SiH exchange in these carbonyl complexes was attributed to the electrophilic nature of the metal center.⁸¹

Another example of exchange of hydrides at silicon was discussed earlier in section 6.1.4 and is shown in Scheme 23 (process B). A transition state similar to that proposed for $\text{M}(\text{CO})_5(\eta^2\text{-H}_2\text{SiPh}_2)$ was not considered.

Scheme 25



The complex $\text{Cp}_2\text{Ti}(\eta^2\text{-H-SiH}_2\text{Ph})(\eta^2\text{-H-Bcat-4'-Bu})$, **1-14a**, is unique in that it contains two different $\sigma\text{-H-El}$ interactions.^{29a} Two-dimensional ^1H NMR spectroscopy provided evidence for both the exchange between the $\eta^2\text{-H-Si}$ and the $\eta^2\text{-H-B}$ hydrides but also between the $\eta^2\text{-H-Si}$ and the remaining noncoordinated hydrides at silicon. Deuterium labeling of the boron unit showed that the label scrambled into the silicon unit most likely through a bidentate–monodentate equilibrium, where rotation about the monodentate Ti-H-B bonds would exchange the label with silicon (Scheme 25). The deuterium label could then exchange with the noncoordinated silicon hydrides by a turnstile rotation.^{29a}

6.1.6. $\text{H-[TM]-Si} \rightleftharpoons \text{Si-[TM]-H}$

The last process to be considered for mononuclear hydride complexes is the exchange of hydride and silyl sites at the metal center. Two basic systems, with variations in silyl substituents, have been reported to undergo this type of exchange: $\{(\eta^5\text{-C}_5\text{H}_4\text{CH}_2\text{CH}_2\text{P})(\text{t-Bu})_2\}\text{HCoSiR}_3$ [$\text{SiR}_3 = \text{SiPhH}_2$, **1-53**; SiPh_2H , **2-51**; SiPhMeH , **2-50**; SiPh_3 , **3-164a**]⁵⁶ and $\text{CpRh}(\text{C}_2\text{H}_3\text{CO}_2\text{t-Bu})\text{HRhSiR}_3$ [$\text{R}_3 = \text{HEt}_2$, **2-57b**; Et_3 , **3-179**; Me_3 , $(\text{OMe})_3$, Me_2Cl (Table 3, footnote 189)].¹⁸⁹

For the racemic mixture of $\{(\eta^5\text{-C}_5\text{H}_4\text{CH}_2\text{CH}_2\text{P})(\text{t-Bu})_2\}\text{HCoSiPh}_2\text{H}$ (**2-51**),⁵⁶ the Co-H resonance exhibited a doublet in the ^1H spectrum and no coupling to the Si-H proton in the H,H COSY spectrum. However, for **1-53**, the Co-H signal appeared as a doublet of doublets and the H,H-COSY showed coupling to ^{31}P but also only one coupling from the Co-H to a Si-H . The silyl–cobalt products, **1-53**, **2-51**, **2-50**, and **3-164a**, are chiral at cobalt and were assumed to be formed as racemic mixtures. To possibly rationalize the role of the different hydrogens in **1-53**, the reaction of the cobalt precursor with the prochiral silane PhMeSiH_2 was studied to determine possible diastereoselectivity in such a system. The oxidative addition product (**2-50**) provided a diastereomeric mixture of *rac*-(*RS/SR*) and *rac*-(*SS/RR*) with a diastereomeric excess (de) of 23%. The Si-H , Co-H coupling was not observed, and P-H , Si-H coupling was observed only in the P decoupled ^1H NMR spectrum. Although a crystal structure of **2-50** was obtained, the pertinent Co-H could not be located and its position was calculated.⁵⁶

The *tert*-butyl groups at P are diastereotopic, and VT-NMR experiments for the Me region of both the ^1H and ^{13}C NMR spectra provided the following free enthalpies of activation

for loss of diastereotopicity of the *tert*-butyl groups: 16.3 (**1-53**), 15.4 (**2-51**), and 14.9 (**2-50**) kcal/mol. Several other NMR techniques (H,H COSY , HSQC, HMBC, P,H correlated spectroscopy, and $^{31}\text{P}\{^1\text{H}\}$ and $^1\text{H}\{^{31}\text{P}\}$ NMR) also were used in assigning the fluxional process. The sequence proposed to account for the observed NMR data involved three steps: (i) decomplexation of the phosphine; (ii) a probable exchange of Co-H and Co-Si positions; and (iii) recomplexation of the phosphine.⁵⁶ However, the ^{31}P NMR data did not detect the presence of a decoordinated sidearm.

For the last example, $\text{CpRh}(\text{C}_2\text{H}_3\text{CO}_2\text{t-Bu})(\text{H})\text{RhSiR}_3$ ¹⁰² [$\text{R}_3 = \text{HEt}_2$, **2-57b**; Et_3 , **3-179**; Me_3 , $(\text{OMe})_3$, Me_2Cl (Table 3, footnote 189)], the complexes were studied in solution only. All five of the complexes were generated as a mixture of two pairs of interconverting isomers. The silyl group and the hydride exchanged positions relative to the orientation of the alkene substituent, $\text{H}_2\text{C}=\text{CHCO}_2\text{t-Bu}$ (in all cases, the $\text{CO}_2\text{t-Bu}$ substituent was pointed towards the Cp -ring). No exchange of the bound silane or the acrylate ligand with free silane or free acrylate was observed; therefore, the exchange of the silyl group and the hydride was judged to be intramolecular. A reductive elimination of the silane was proposed, forming $\eta^2\text{-Rh-H-Si}$ as an intermediate or TS, followed by rotation about the $\sigma\text{-H-Si}$ and reoxidative addition. The activation parameters for both the forward and reverse isomerizations were measured for **2-57b** and **3-179** (and the related SiMe_3 complex). The values for **3-179** for the isomerization from Rh-H located *cis* to the ester group of the coordinated alkene to the silyl group occupying this *cis*-position were found to be as follows: $\Delta H^\ddagger = 14.4 \pm 0.5$ kcal/mol, $\Delta S^\ddagger = 1.9 \pm 2.2$ cal/(mol K), $\Delta G_{253}^\ddagger = 13.9 \pm 0.02$ kcal/mol, $K_{\text{eq}} = 2.35$ at 223 K. The values for **3-179** and the related SiMe_3 complex were similar. The stability of the $\text{CpRh}(\text{C}_2\text{H}_3\text{CO}_2\text{t-Bu})\text{HRhSi}(\text{OMe})_3$ complex (Table 3, footnote 189) was reversed relative to **3-179** with a $K_{\text{eq}} = 0.83$ at 223 K. In this case, the interconversion process was believed to be more complex than a simple rotation, and a discrete $\eta^2\text{-Rh-H-Si}$ may be formed that existed in two conformations (whose nature was not specified).¹⁰²

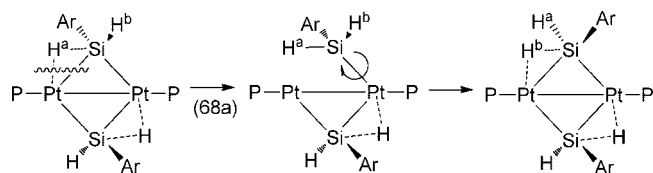
6.2. Bimetallic Metal Hydride Complexes

The complexes in this category may have $\text{Si-H}_{\text{term}}$, M-H_{term} , and hydrides that bridge a Si-M bond or a M-M bond. There are variations that may be related to the mononuclear complexes such as described in (section 6.2.1) $\text{Si-H}_{\text{term}}$ and $\text{Si-H}_{\text{br}}\text{-M}$ exchange and (section 6.2.2) M-H_{term} and $\text{Si-H}_{\text{br}}\text{-M}$ exchange in addition to processes that are unique to a bimetallic complex, (section 6.2.3) $\text{Si-H}_{\text{br}}\text{-M}$ exchange and $\text{M-H}_{\text{br}}\text{-M}$ exchange, and (section 6.2.4) exchange of two bridging hydrides, $\text{M-(H}_{\text{br}})_2\text{-M}$.

6.2.1. $\text{Si-H}_{\text{term}}$ and $\text{Si-H}_{\text{br}}\text{-M}$ Exchange

The complexes $\{(\text{Ph}_3\text{P})\text{Pt}[\mu\text{-}\eta^2\text{-H-Si}(\text{Ar})\text{H}]\}_2$ [$\text{Ar} = 2,4,6\text{-(MeO)}_3\text{C}_6\text{H}_2$ (**1-73**), $2,4,6\text{-Me}_3\text{C}_6\text{H}_2$ (Table 1, footnote 85), and $2\text{-}^i\text{Pr-6-Me-C}_6\text{H}_2$ (**1-78**)] undergo exchange of the terminal SiH and the bridging SiH with coalescence temperatures between 342 and 356 K that translate to ΔG^\ddagger values $\sim 15\text{--}17$ kcal/mol.^{68ab} The exchange of the hydrides also leads to *cis/trans*-isomerization of the groups on silicon. The proposed mechanism for this exchange is shown in Scheme 26 and involves reductive elimination of $\text{H}_{\text{br}}\text{Si}$ followed by rotation of the silyl group formed around the Si-Pt bond

Scheme 26



and finally OA of the previously terminal H_B to the original Pt center.^{68a}

6.2.2. $M-H_{term}$ and $Si-H_{br}-M$ exchange

This exchange variation involved complexes of the type $(Ph_3P)_2(H_a)Pt(\mu-SiR_2)(\mu-\eta^2-H_bSiR_2)Pt(PPh_3)$, where $Ar_2 = C_{12}H_8Si$ (Table 2, footnote 117; silafluorene) and $R = C_{20}H_{24}$ (**2-103**, di-*tert*-butylsilafluorene) are illustrative examples.^{127c} From variable-temperature ^{31}P NMR experiments, the coalescence temperatures were found to correspond at 260 K to a ΔG^\ddagger value ~ 12 kcal/mol and at 288 K to a ΔG^\ddagger value ~ 11 kcal/mol. The mechanism proposed for the fluxional process involved loss of PPh_3 from the $(Ph_3P)_2(H_{term})Pt$ site and reassociation of the PPh_3 to the $Pt(PPh_3)$ site with transformation of the terminal $Pt-H_{term}$ to a bridging $Pt \cdots H_{br} \cdots Si$ unit and the former bridging hydride (associated with the original $Pt-PPh_3$ unit) to a $Pt-H_{term}$. The process equilibrates the two different phosphorus and hydride sites in the complex.^{127c} The same type of process was reported for the complex where R is Me.^{284c} The dynamic behavior involved either intra- or intermolecular exchange of PPh_3 between the two Pt sites. In both cases, the solid structure differed from the solution structure in that, in the solid, the two Pt centers are bridged by 2 $SiHR_2$ groups, whereas in solution, one of the $SiHMe_2$ groups is converted to a bridging $SiMe_2$ and a terminal $Pt-H$ forms.

It is possible that the palladium dimer, $[(Me_3P)Pd](\mu-\eta^2-H-SiPh_2)_2[Pd(PMe_3)_2]$, **2-79a**,^{121a,b} undergoes a process similar to that described in the previous paragraph for the silafluorene complex and **2-103**. For **2-79**, there is a single resonance for the two hydrides and the three phosphines. However, at -90 °C, there are two resonances for the hydrides and two for the phosphines. The 1H NMR spectrum exhibited a doublet (1.24 ppm) and a triplet (-2.34 ppm) of equal intensity, indicating that the two SiH hydrogens are magnetically inequivalent. The authors suggested that the fluxional behavior could occur by intra- or intermolecular exchange of coordinated PMe_3 but did not speculate on the possible details of the process. Although the J_{SiH} coupling constant values are nearly identical, it is possible that the phosphine migration from the $Pd(PMe_3)_2$ site to the $PdPMe_3$ site results in a change in the role of the $Si-H$ from $Si-H_{br}-Pd$ to $Pd-H_{term}$ as proposed for **2-103** and the silafluorene complex. The more symmetrical palladium dimer, $[(Me_3P)Pd]_2(\mu-\eta^2-H-SiPh_2)_2$, **2-81**, exhibited solution data consistent with the solid-state structure from 25 to -90 °C.^{121a,b}

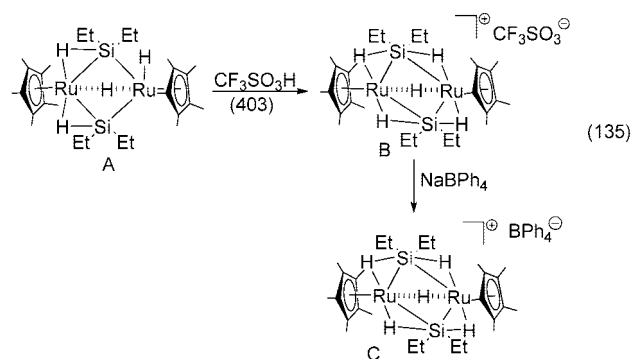
6.2.3. $Si-H_{br}-M$ and $M-H_{br}-M$ Exchange

The complex $\{Cp^*Ru(\mu-H^b)(\mu-H^c)\}_2\{\mu-\eta^2:\eta^2-H^a-SiMe_2(CH=CH_2)\}$ (**3-138**) contained one SiH and two nonequivalent hydrides bridging the two Ru centers. The complex exhibited one 1H signal for all three hydrides at 30 °C and three signals at -70 °C.²¹⁴ Since all three hydride signals broadened at the same time on warming the sample

from -70 °C, it is likely that the site exchange occurred randomly and that the rates of H^a/H^b , H^b/H^c , and H^c/H^a exchange were equal. The estimate for the ΔG^\ddagger value was 12.6 ± 0.1 kcal/mol at 0 °C ($\Delta H^\ddagger = 12.4 \pm 0.4$ kcal/mol; $\Delta S^\ddagger = -0.9 \pm 1.5$ cal/(mol K)). The ΔH^\ddagger and ΔS^\ddagger values for the related derivative, $\{Cp^*Ru(\mu-H^b)(\mu-H^c)\}_2\{\mu-\eta^2:\eta^2-H^a-SiMePh(CH=CH_2)\}$ (Table 3, footnote 153) as a mixture of diastereomers, were similar to those for **3-138**. For both complexes, a second process occurred at temperatures >30 °C, which was attributed to inversion of the $H-Si-C=C$ unit.²¹⁴

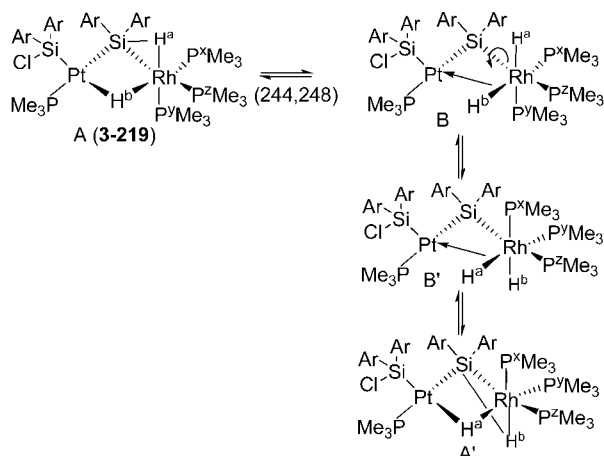
The complex $(Cp^*Fe)_2(\mu-H)_2(\mu-\eta^2:\eta^2-H_2Si^iBu_2)$ (**2-34**) exhibited a singlet for the hydrides at room temperature but two sharp singlets at -110 °C, consistent with an exchange between $Fe-H_{br}-Si$ and $Fe-H_{br}-Fe$.^{93,94} The authors proposed an exchange through $Si-H$ bond cleavage (RE). The free activation energy at the coalescence temperature was $\Delta G^\ddagger(-50$ °C) = 8.6 kcal/mol. The corresponding complex prepared from iPr_2SiH_2 also exhibited a broad singlet at room temperature for the hydrides.

Another complex that undergoes $Si-H_{br}/Ru-H_{br}-Ru$ exchange is the “dimer” produced in eq 135. The dimer B (eq 135) was formed by protonating the complex A with triflic acid followed by exchange of the triflate anion with BPh_4^- to give the dimer C. The cationic ruthenium dimer gave a singlet hydride resonance at 298 K and two peaks at 173 K in a ratio of 1:4, indicating site exchange between the $Si-H_{br}(2)/M-H_{br}-M$ sites. The slight broadening of the second resonance suggested that site exchange between the two different $Si-H_{br}$ sites was still present at 173 K, although no mechanism for either process was proposed.⁴⁰³



The last example in this grouping involved a heterobimetallic dimer, $[(Me_3P)(ClAr_2Si)Pt](\mu-H)(\mu-\eta^2-H-SiAr_2)[Rh(PMe_3)_3]$ (**3-219**, $Ar = C_6H_4F-p$), where a hydride bridged the $Pt-Rh$ bond and the $\eta^2-H-SiAr_2$ was associated with the Rh center.^{244,258} The 1H and the $^{31}P\{^1H\}$ spectra from -90 to -10 °C indicated a fast exchange between two of the three PMe_3 ligands at Rh with the two bridging hydrido ligands and a second process at a slower exchange rate due to the third PMe_3 exchanging with the other two PMe_3 ligands at Rh. A possible mechanism for the fast-exchange process is shown in Scheme 27. Cleavage of the $Pt-H_{br}$ bond (OA of H_{br} to Rh) places two hydrides on the Rh center. Rotation about the $Si-Rh$ bond and reformation of the $Rh-H_{br}-Rh$ and $\eta^2-H-SiAr_2$ bonds exchanges both the hydride and the two phosphine sites. The ^{31}P NMR signal for the $Pt-PMe_3$ unit does not exhibit broadening in the temperature range studied; thus, the activation and formation of the $Si-H$ bond must take place only at Rh. No explanation was provided for the second phosphine exchange.²⁴⁴

Scheme 27



6.2.4. Exchange of $M-(H_{br})_2-M$

Protonation of $\{Cp^*Ru(\mu-\eta^2-HSiPh_2)\}_2(\mu-H)(H)$ with triflic acid produced a dimer with two hydrides bridging the two Ru centers, $\{Cp^*Ru(\mu-H)\}_2\{\mu-SiPh(OCOCF_3)\}(\mu-SiPh_2)$, and this complex provided the starting point for the preparation of two other Si-substituted complexes $[\{Cp^*Ru(\mu-H)\}_2\{\mu-SiPh(OR)\}(\mu-SiPh_2)]$ ($R = Me, H$).⁴⁵³ All three complexes exhibited fluxional behavior and were compared to the alkyl/aryl-substituted analogues, **3-136** and **3-137e**.⁹⁸ The hydride ligands (in all five complexes) mutually exchange coordination sites, and a *cis*-bis(μ -silylene) intermediate was proposed as an intermediate (see D in Scheme 28 for proposed mechanism). The activation parameters for the five complexes are the same within experimental error, and ΔG^\ddagger_{300K} values range from 11.8 to 13 kcal/mol. Thus, it was concluded that substituents at the bridging silyl group did not exert an electronic influence on the activation parameters for the hydride site exchange. However, electron-withdrawing substituents at the bridging silicon caused a decrease in both ΔH^\ddagger and ΔS^\ddagger in comparison to the methyl groups in **3-136** and **3-137e**. Thus, the site exchange, which was depicted as involving formation and cleavage of an η^2 -Si-H bond (A, C, E, or F in Scheme 28), was influenced by the electronic nature of the substituents. The “silyl” complex would be formed by reductive coupling of the μ^2 -silylene and the bridging hydride, $Ru-H_{br}-Ru$. Rotation about the silyl-ruthenium bond and oxidative addition of Si-H provides the *cis*-bis(μ -silylene) intermediate.⁴⁵³

Another ruthenium complex that exhibits fluxional behavior is **3-144b**, $[(OC)_{10}Ru_3(Xantsil)(\mu-H)_2]$ (see structure section of Table 3), which was formed from reaction of $Ru_3(CO)_{12}$ with $H_2[Xantsil]$.^{177b} The 1H NMR spectrum exhibits two upfield resonances at -14.94 and -16.27 ppm, indicating two inequivalent bridging hydrides. At 295 K, there are two broad singlets for both the CMe_2 and the $SiMe_2$ groups of the coordinated Xantsil ligand, and these signals sharpen on lowering the T . The $T_c = 307$ K and $\Delta G^\ddagger = 16$ kcal/mol, which was attributed to inversion of the puckered chelate ring. The ^{29}Si NMR spectrum contains one resonance at 7.2, and it was concluded that there was another dynamic process that was too fast to be detected by NMR. This process was believed to involve switching of a bridging $Ru-H-Ru$ from one triangular side of the Ru_3 unit to the adjacent unoccupied side. Fluxionality of the mononuclear complexes $[(OC)_4M]Xantsil$ ($M = Fe$ (**3-72b**), Ru (**3-104**), Os (**3-151a**)) was also attributed to inversion of the puckered chelate Xantsil ligand.^{177b}

The presence of bridging hydrides, either between metals or between metal and silicon, does not necessarily result in fluxional behavior. For instance, the vanadium dimer, $Cp^*_2H_2Ta_2(\mu-ArNSiHPh)_2$ (**1-20b**, $Ar = 2,6\text{-}i\text{-Pr}_2C_6H_3$), did not exhibit exchange of any hydrides in the temperature range from -60 to 95 °C,³³ and the palladium complex $Pd_3[o-(HSi)(H_2Si)C_6H_4]_2[o-(HSi)C_6H_4](depe)_2$, **2-84**, exhibited no dynamic behavior between -80 and 50 °C.¹²³ The complex **2-36c**, $Fe_2(\eta-H_2SiPh_2)(edt)(CO)_2(dppv)$ [$edt = \text{ethanedithiolate}$; $dppv = cis\text{-}C_2H_2(PPh_2)_2$], exhibited no evidence in the NMR spectral data for fluxional behavior over the temperature range -80 to 20 °C.^{95c}

6.3. Miscellaneous Processes

In this section are described processes that have been proposed to explain fluxional behavior in complexes that do not have SiH or MH bonds, or if such bonds are present, they do not appear to be responsible for the fluxional process that is described.

6.3.1. Exchange of a Classical Silyl Ligand with Added Silane

The reaction of $(ArN=)_2Mo(PMe_3)_3$ with $PhSiH_3$ produced a Mo-centered trigonal-bipyramidal complex with one classical $-H_2SiPh$ group and one β -agostic $\eta^2-H-SiHPh$ group (**1-25b**).^{36b} The complex was fluxional at room temperature but at 223 K showed the presence of the agostic Si-H (br m, $J_{SiH} = 113$ Hz) and its companion SiH_{term} (d, $J_{SiH} = 245$ Hz) as well as resonances for the diastereotopic protons of the classical $-H_2SiPh$ group. The IR spectrum showed three absorptions in the classical SiH stretching region (2014 to 2165 cm^{-1} in this case) and one red-shifted absorption at 1694 cm^{-1} attributed to the agostic H-Si. The $^1H-^1H$ EXSY spectrum demonstrated exchange between free $PhSiH_3$ and the classical PhH_2Si group but not the nonclassical PhH_2Si group. However, when $PhSiD_3$ was added, a statistical distribution of D at all silicon centers was determined, which suggests both silyl groups may exchange with the free silane, although it is also possible that deuterium could be transferred from the classical $PhSiD_2$ group to the nonclassical group. When a second silane, $m\text{-TolSiH}_3$, was added, only the complex (**1-25c**) with the $m\text{-TolSiH}_2-$ group replacing the classical $PhSiH_2$ group was observed.^{36b}

6.3.2. Exchange through $M=Si$ Intermediates

There are three types of complexes where a fluxional process was explained by a rearrangement that involved formation of a terminal silylene ligand. Two related complexes were $Cp(OC)_2Mo\{(\text{SiMe}_2)\cdots X\cdots(\text{SiMe}_2)\}$ ($X = OMe$, **3-32**; $X = NEt_2$, Table 3, footnote 45),¹⁵¹ in addition to two entirely different types of complexes, $(OC)_2Re(\mu-C_5H_4-C_5H_4)(\mu-SiPh_2)Re(CO)_2$, **2-31**,⁹¹ and $\{(Cp^*Ru)_2(\mu-H)\}_2(\mu-SiPhMe)(\mu-SiMe_2)$, **3-137e**.⁹⁸

The bridged silylene complexes for $Cp(OC)_2M\{(\text{SiMe}_2)\cdots X\cdots(\text{SiMe}_2)\}$ [$M = Cr$ (**3-27**); Mo (**3-32**)] were formed upon photolysis of $CpM(CO)_3Me$ in the presence of $HSiMe_2SiMe_2Do$.¹⁵¹ Similar reactions and product complexes were reported earlier for W.⁴⁸¹ In each of the complexes, the $SiMe_2$ groups exhibited two singlets (and two overlapping triplets for the $X = NEt_2$ group) at 250 K, as would be expected from the solid-state structures. On warming, these signals broadened and coalesced to

Scheme 28

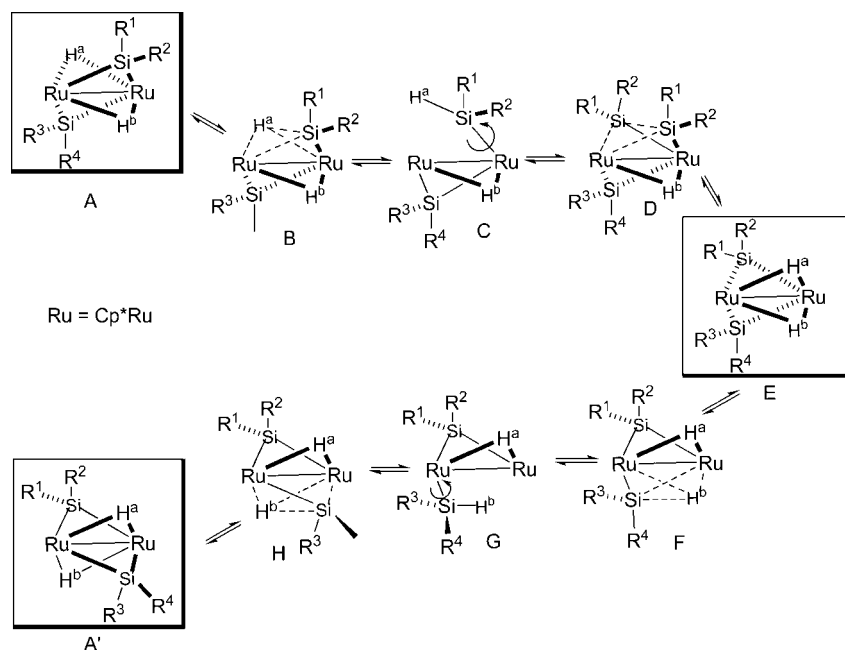
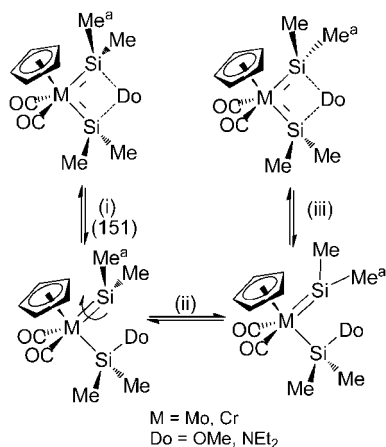


Table 16. Thermodynamic Parameters for Fluxional Process for $\text{Cp}(\text{OC})_2\text{M}(\text{SiMe}_2)\cdots\text{X}\cdots(\text{SiMe}_2)$ ^{151,481}

X	Mo		W	
	ΔH^\ddagger , kcal/mol	ΔS^\ddagger , cal/(mol K)	ΔH^\ddagger , kcal/mol	ΔS^\ddagger , cal/(mol K)
OMe	14.6(1.1)	2.8(3.6)	16.8(0.5)	9.5(1.8)
NEt ₂	15.5(0.8)	5.5(1.2)	17.4(0.8)	11.7(2.5)

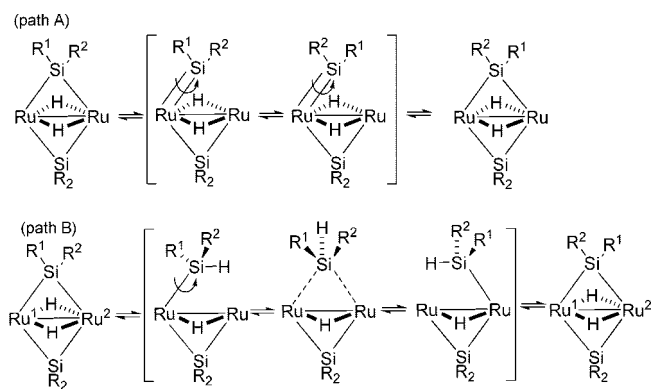
Scheme 29



become a singlet for the SiMe_2 groups (a quartet and a triplet for the NEt_2 group). Unfortunately, decomposition of the Cr analogue, **3-27**, occurred during the VT NMR experiment and prevented the determination of the thermodynamic parameters for the Cr complex. From the VT ^1H NMR spectra of the SiMe_2 group, band-shape analysis provided the parameters summarized in Table 16. The mechanism proposed for exchange of Me groups at silicon is shown in Scheme 29 and involves (i) the cleavage of a Si–Do bond to form a terminal (base free) silylene, (ii) rotation about $\text{M}=\text{Si}$, and (iii) the reformation of the Si–Do bond to the same silylene ligand.¹⁵¹

Two mechanisms have been proposed to explain the sharper signals for $(\text{OC})_2\text{Re}(\mu\text{-C}_5\text{H}_4\text{-C}_5\text{H}_4)(\mu\text{-SiPh}_2)\text{Re}(\text{CO})_2$, **2-31**,⁹¹ at low temperature that broadened

Scheme 30



above room temperature. The two low-field Fv signals coalesced at 307 K and gave an estimate for ΔG^\ddagger of 15.2 ± 0.5 kcal/mol. The process could involve a bridging to terminal silylene/carbonyl migration in a “merry-go-round” fashion with rapid C–Si bond rotation or a more simple double-turnstile motion at the respective metals that is tantamount to a “swinging through” of the silyl group from one side of the Fv ligand to the other.⁹¹

The hydride fluxionality observed in $\{(\text{Cp}^*\text{Ru})_2(\mu\text{-H})\}_2(\mu\text{-SiPhMe})(\mu\text{-SiMe}_2)$, **3-137e**,⁹⁸ was discussed previously in section 6.2.4. Another site-exchange process for **3-137e** was observed at higher temperature that involved the bridging SiMe_2 group. Line-shape analysis indicated that this site-exchange process for the methyl groups took place independently of the hydride ligands, yielding the parameters $\Delta H^\ddagger = 16.5 \pm 0.7$ kcal/mol and $\Delta S^\ddagger = -7.8 \pm 2.1$ cal/(mol K). Two possible pathways were suggested, one of which involved isomerization of the $\mu\text{-SiMe}_2$ (or $\mu\text{-SiMePh}$) to a terminally bound silylene, rotation around the $\text{Ru}=\text{Si}$ bond, followed by reforming of the bridging silylene (path A). In the second mechanism (path B), reductive elimination of HSi takes place to form a silyl (Scheme 30), followed by a 1,2-silyl shift to the adjacent Ru center, and then oxidative addition of the HSi to the original Ru center.⁹⁸

6.3.3. Hindered M–Si Rotation

A complex with a cyclic diaminosilylene ligand, $[N_3]Ru(H)(Cl)\{Si(NN)\}$ (**3-134e**) was generated by a sequential (reversible) activation of the SiH bond and a 1,2-migration of the Cl from Si to Ru of $H(Cl)Si(NN)$ ($NN = o-(^iBuCH_2N)_2C_6H_4$) when added to the ruthenium precursor, $\{[N_3]Ru\}_2(\mu-N_2)$.^{213b} The X-ray structure indicated that the silicon center was slightly pyramidal and that the Ru–Si bond was at the shorter end of the Ru–Si bonds (Table 7). The 1H NMR spectrum below room temperature (285 K) exhibited diastereotopic neopentyl CH_2 groups and no symmetry along either the H–Ru–Cl or the N–Ru–N axes. The coalescence of the various pairs of imine, methylene, and neopentyl resonances was observed between 313 and 345 K. These observations were interpreted as indicating hindered Ru–Si bond rotation and slow inversion at the slightly pyramidal silicon center. Heterocyclic silylenes appear to be strong σ -donors but poor π -acids. Although no calculations were performed for complex **3-134e**, for a related ruthenium silylene complex, DFT calculations indicated that the highest occupied molecular orbital (HOMO) that resided on ruthenium had the appropriate symmetry to back-bond into a vacant Si “p” orbital but that the LUMO was localized on Ru and not on Si, consistent with the silylene ligand being principally a σ -donor.^{393a} The short Ru–Si bond was attributed to a strong electrostatic interaction between an electron-rich metal center and an electrophilic silicon center.

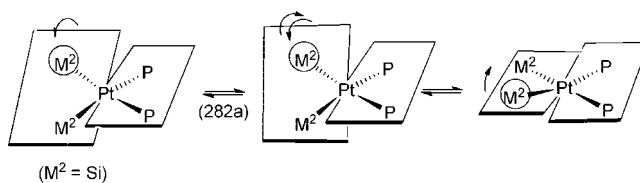
The square-planar complex, $trans-(Cy_3P)_2Pt(H)(SiHMe_2)$ (Table 2, footnote 106) produced from the reaction of H_2 with the silylene complex $(Cy_3)_2Pt=SiMe_2$, was fluxional according to the variable-temperature ^{31}P data, and the fluxionality was attributed to restricted rotation about the Pt–Si bond with a rotational barrier $\Delta G^\ddagger = 15.8 \pm 0.4$ kcal/mol.¹²

Free rotation about the $W=Si$ bond in $Cp'(OC)_2(H)W=Si(H)\{C(SiMe_3)_3\}$ (**1-29a**) does not appear to occur as there are two independent hydride signals at room temperature.^{38a} However, a single carbonyl resonance was observed at room temperature but two signals were observed at 183 K ($\Delta G^\ddagger = 9.8$ kcal/mol), indicating rapid exchange of carbonyl groups at room temperature. No mechanism for this exchange was suggested, but whatever process occurs apparently does not involve the hydrides.

6.3.4. Isomerization in Square-Planar Complexes

Two rhodium examples exhibited an equilibrium between an 18e form and a 16e form. The 18e complex $(Me_3P)_4RhSiHPh_2$ (**2-58**) exhibited 2 resonances in the ^{31}P spectrum at 213 K in a 3 to 1 ratio consistent with a 5-coordinate rhodium center where the silyl substituent occupies the apical position.¹⁰⁷ At 173 K, however, there are 3 resonances, including one due to free PMe_3 , in addition to 2 broad resonances in a 2:1 ratio, suggesting exchanging ligands in a square-planar, 16e complex. The 18e complex, $mer-(Me_3P)_3H(Cl)RhSiPh_3$ (**3-186**) exhibited 1H and ^{31}P spectra, consistent with the presence of **3-186** only at 203 K.²⁴³ At 298 K, the ^{31}P spectral data indicated the presence of **3-186** and another broad signal that was tentatively assigned to a mixture of Rh(I) complexes, and the 1H NMR spectrum indicated the presence of $HSiPh_3$. Thus, an equilibrium between $HSiPh_3$ and unassigned Rh(I) complexes appears to take place at room temperature.

Scheme 31



Two mononuclear platinum complexes exhibited fluxional properties. When 2 equiv of Ph_2SiH_2 were reacted with $cis-(Me_3P)_2PtEt_2$, the initial isolated product was $trans-(Me_3P)_2Pt(SiHPh_2)_2$ (**2-87**).¹²⁵ However, when the *trans*-product was redissolved in solvent, an equilibrium between the *trans*- and *cis*-forms was observed by 1H NMR spectroscopy. The ratio of the two forms was about 1:1 in C_6D_6 but changed to a *cis/trans* ratio of $\sim 3:1$ in CD_2Cl_2 and 2.8:1 in $THF-d_8$ at room temperature. The equilibrium was temperature dependent in CD_2Cl_2 or $THF-d_8$ (-50 to $10^\circ C$), but a negligible temperature dependence was observed in C_6D_6 . The following thermodynamic parameters were reported: $\Delta H^\ddagger = 1.4(0.7)$ kcal/mol and $\Delta S^\ddagger = 1.6(0.2)$ cal/(mol K) in CD_2Cl_2 and $\Delta H^\ddagger = 0.91(0.5)$ kcal/mol and $\Delta S^\ddagger = 0.84(1.4)$ cal/(mol K) in $THF-d_8$ at 298 K. Although the study demonstrated that added PMe_3 did not significantly alter the rate of *trans-cis* isomerization, which should eliminate an associative pathway, no explanation was developed to explain the observed process.¹²⁵ In a related system, $cis-(PhMe_2P)_2Pt(SiMePh_2)_2$ (**3-264**), the ^{31}P NMR spectrum at 203 K exhibited satellite peaks with $^2J_{PSi}$ due to both *cis*- and *trans*-silyl groups.^{282a,b} On warming, the satellite peaks broadened and coalesced at 263 K. The fluxional process was reversible and the $^1J_{P-Pt}$ value was maintained from 243 to 283 K, providing the parameters $\Delta H = 14 \pm 0.5$ kcal/mol and $\Delta S = 4.1 \pm 2$ cal/(mol K). A similar fluxional behavior was also observed for $cis-(PhMe_2P)_2Pt(SiFMe_2)_2$.^{282a} In the fluxional process for each of these two platinum complexes, the spin–spin coupling between the P, Si, and Pt nuclei was retained; therefore, a dissociative or consecutive displacement mechanism that involved either Pt–Si or Pt–P bond cleavage could be eliminated. A twist-rotation through a pseudo-tetrahedral intermediate was proposed as shown in Scheme 31. The square-planar complex, $[Rh(\kappa^2-Si,P)-Me_2Si(CH_2)_2PPh_2](PMe_3)_2$ (prepared from addition of MeLi to **3-197**), was also fluxional in $tol-d_8$, exhibiting intramolecular exchange of the two PMe_3 ligands. However, a mechanism for the exchange was not proposed.^{246,282a,b}

The most interesting fluxional process for a square-planar complex was the one reported by Fink and coworkers for $(dcpe)Pd(H)(SiH^tBu_2)$ (**2-78a**) described in section 6.1.1 and in this section for $(dcpe)Pd(SiMe_2H)_2$ (see compound **19-3** in Table 19 (section 8.2.1)) and its deuterium analogue.^{120a} The $^{29}Si\{^1H\}$ NMR spectrum of **19-3** exhibited a doublet of doublets at 203 K, consistent with the X-ray structure, which showed little distortion from a square-planar geometry. On raising the temperature the signals change to a triplet, suggesting rapid exchange of the silicon nuclei. The complex **19-3** showed a significant deuterium isotope effect for the interchange of the two silyl groups. Line-shape analysis from the ^{31}P NMR spectrum gave the activation parameters $E_a = 14.1(7)$ kcal/mol, $\Delta H^\ddagger = 13.6(7)$ kcal/mol, and $\Delta S^\ddagger = -0.7(5)$ cal/(mol K) for the protio system and $E_a = 17.7(8)$ kcal/mol, $\Delta H^\ddagger = 17.1(8)$ kcal/mol, and $\Delta S^\ddagger = 11(2)$ cal/(mol K) for the deuterio system. The KIE (k^H/k^D) was 1.37

at $-20\text{ }^{\circ}\text{C}$ and 0.85 at $20\text{ }^{\circ}\text{C}$. The authors concluded that the silyl groups were not just spectators but underwent electronic changes that affected the Si–H bond. The most likely intermediate proposed was a Si–Si σ -complex and represented the first example of an intermediate with an unsupported Si–Si interaction.^{120a}

6.3.5. Isomerization in 5- and 6-Coordinate Geometries

Observations of equilibria between geometries associated with the same coordination number are rather rare. The fluxional process shown in Scheme 31 shows an isomerization of a square-planar complex that appears to go through a transition state that involves a tetrahedral form. There was also a case where an equilibrium was established between two stable isomers of the 6-coordinate complex $\text{Cp}^*(\text{OC})_2\text{W}(\text{H})_2(\text{SiXPhR})$ [$\text{X} = \text{H}$, $\text{R} = \text{Ph}$ (formed from **2-20** and LAH, Table 2, footnote 26); $\text{X} = \text{R} = \text{H}$ (formed from addition of LAH to **1-29b**); $\text{X} = \text{Cl}$, $\text{R} = \text{Ph}$ (addition of HCl to **2-20**)].⁴⁷⁷ The hydride-exchange processes for these complexes were discussed earlier in section 6.1.4. The activation parameters were also reported for the equilibrium between the pseudo-octahedral and pseudo-trigonal-prismatic forms for the $\text{R} = \text{H}$ complex in toluene- d_8 : $\Delta H^\ddagger = 13.5 \pm 0.7\text{ kcal/mol}$ with $\Delta S^\ddagger = -1.1 \pm 1.7\text{ eu}$. Of the four dynamic processes, the equilibrium between the two geometrical forms has the highest activation barrier.⁴⁷⁷

Exchange of silyl groups in bis-silyl–metal complexes does not appear to be very common but was observed for the 5-coordinate complex, $(\text{PrPDI})\text{Fe}(\eta^2\text{-HSiH}_2\text{Ph})_2$ [$\text{PrPDI} = (2,6\text{-CHMe}_2)_2\text{C}_6\text{H}_3\text{N}=(\text{CMe}_2)_2\text{C}_5\text{H}_3\text{N}$] (**1-36**).^{44a} The solid-state structure showed a square-pyramidal geometry with one of the $\eta^2\text{-HSiH}_2\text{Ph}$ groups in the apical position and the other in the basal plane. The low-temperature, static NMR spectra were consistent with the C_s symmetry observed in the solid (an idealized mirror plane of symmetry bisects the basal silane ligand). As the temperature was raised, the silane signals broadened, suggesting a fluxional process at $>253\text{ K}$. A process was proposed that involved a Berry pseudorotation where the apical and basal silanes are equivalent by a rocking motion through the plane containing the iron center.^{44a}

7. Bonding and Calculations

Calculations have been reported as an additional characterization method to support a structure assignment, and such cases were indicated earlier in Tables 1, 2, 3, and 9. Several of the calculation results have been mentioned in the discussion of complexes with nonclassical interactions in section 5. However, in the current section, the publications whose focus is on calculations, especially for σ -complexes and nonclassical systems, as well as commentaries on bonding aspects will be described first (sections 7.1 and 7.2) followed by specific cases introduced by triad (section 7.3)

7.1. σ -Complexes: Comparison of H_2 and HSi

Scheme 15 in section 5 illustrates a range of interactions identified in $\sigma\text{-H}_2$ complexes and the variations that have been identified for the range of silyl–transition metal complexes produced from hydrosilanes. Computational studies of transition metal polyhydrides have been reviewed and summarized by Lledós and Eisenstein and their respective

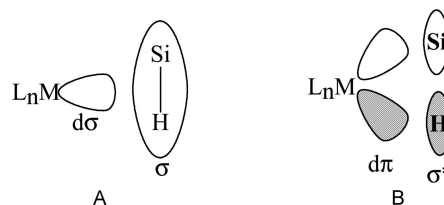


Figure 15. (A) $\text{M}-(\eta^2\text{-HSi})$ σ -bonding interaction. (B) $\text{M}-(\eta^2\text{-HSi})$ back-bonding interaction into Si–H.^{1a}

co-workers and include factors influencing formation of H_2 complexes versus the dihydride form.⁴⁸²

The principles of σ -bond coordination/activation in terms of the Dewar–Chatt–Duncanson (DCD) model have been well-summarized by Kubas both in his monograph^{5c} and in reviews^{5d,455,460a} as well as by Lin.⁴⁸³ Kubas defines a σ -complex as a side-on, three-centered interaction of the bonding electron pair of H_2 or other $\text{X}-\text{Y}$ bond with a metal.^{460a} Although any $\text{X}-\text{Y}$ bond can coordinate to a metal center if the steric and electronic factors are favorable, the more general examples include H_2 , $\text{El}-\text{H}$ ($\text{El} = \text{group 14, B, and P}$), and a few $\text{C}-\text{El}$ bonds ($\text{El} = \text{C, Si, P, B, N}$).

The DCD model adapted for σ -complexes involves coordination of a σ -bond of the ligand to an empty metal orbital and back-donation (BD) of metal electrons into the σ^* -orbital of the ligand (Figure 15). Strong back-bonding from the metal ultimately breaks the σ -bond and leads to the OA of the ligand to the metal center. Scheme 15 shows a range of interactions of $\text{H}-\text{H}$ and of $\text{Si}-\text{H}$ with a metal center. When are the bonds in $\text{H}-\text{H}$ and $\text{Si}-\text{H}$ considered “broken”? From theoretical analysis, this occurs for $\text{H}-\text{H}$ when the distance between the two hydrogens in the complex is 1.48 \AA (distance in free H_2 is 0.74 \AA). Although little $\text{H}-\text{H}$ bonding interaction is still present when $d_{\text{HH}} > 1.1\text{ \AA}$,^{455,484} distances up to 1.6 \AA have been suggested for complexes categorized as compressed dihydrides. In between the limits set by free H_2 and 1.6 \AA , three types of complexes have been identified: (a) the “true” H_2 complex, (b) the elongated H_2 complex, and (c) the compressed dihydride, each of which have their unique structural and spectroscopic features. In the case of $\text{Si}-\text{H}$ interactions, the bond distance range relative to that in “free” SiH compared to a complexed silyl hydride appears to span $\sim 1\text{ \AA}$ ($1.4\text{--}2.4\text{ \AA}$), and four types of complexes have been claimed or identified: (a) σ -complex, (b) α - through ϵ -agostic complexes as well as longer-range interactions, (c) IHI, and (d) SISHA (see Scheme 15), each of which have distinctive (but not necessarily unique) characteristics as outlined in section 5.

One of the features that distinguishes $\text{M}-\text{H}-\text{Si}$ (and other $\text{M}-\text{H}-\text{X}$ linkages) from $\text{M}-\text{H}_2$ is that the interaction with the silane is asymmetric with Si further from the metal center than is the H. With an $\text{M}-\text{H}-\text{Si}$ angle near 90° , $\text{M}-\text{H}-\text{Si}$ appears to resemble a hydride-bridged system. A second difference is that the $\text{Si}-\text{H}$ bond is more basic than $\text{H}-\text{H}$ and thus is a better σ -donor; because there is a better energy match of the SiH σ^* -orbital with the “d” orbitals of the metal, $\text{Si}-\text{H}$ is also a better π -acceptor. In contrast to the simplest ligand, dihydrogen, substituents at silicon (in addition to variations at the metal center) can alter both the σ -donor and π -acceptor capability in a σ -silane. In characterized complexes, the metal–silane interaction appears to be arrested further along the reaction coordinate towards OA than is found in metal–dihydrogen complexes.^{5d,483}

The role of dihydrogen complexes and other σ -bonded complexes has been outlined by Kubas.^{460a} That paper has a

good summary of the general features of σ -complexes and how their reactions are relevant to both homogeneous and heterogeneous catalysis. Sakaki has reviewed the theoretical studies of interelement linkages with transition metal complexes.⁴⁸⁵ The work focuses more on boron chemistry but has a section on Pt–EtH₃ and Pd–EtH₃ bond energies for El = group 14 elements in terms of the sp^3 -orbital energies of El.⁴⁸⁵ Also included is a discussion of the role of hypervalency in the reductive elimination of Pd(EtH₃)(η^3 -C₃H₅)(PH₃) (El = C, Si, Ge, Sn) where the new bond to the allyl carbon atom can be made while keeping the bonding interaction of El with Pd (thus utilizing the role of hypervalency for the heavier group 14 elements). Braunstein has described a potential relationship between C, Si, and P in nonclassical bonding modes. Each of the donor atoms is sp^3 -hybridized, and the ligands are related to each other by the isolobal analogy: (CR₃)[−] \neq (SiR₃)[−] \neq (PR₃).^{5b} Frenking and Fröhlich have reviewed the bonding in transition metal compounds, and the review includes sections on H₂ complexes as well as carbene complexes and their heavier group 14 analogues, although the most recent reference was 1996.⁴⁸⁶

7.2. Long-Range Bonding Interactions

Although the DCD model may be effective for σ -complexes and agostic complexes, other bonding models have been proposed especially for nonclassical interligand interactions designated earlier in sections 5.5.1 and 5.5.2 as IHI and SISHA, respectively (see also Scheme 15). These have been recently reviewed by Nikonov^{5a,c} and are also included in Lin's review.⁴⁸³ The basis of the difference in approach relative to the DCD model can be attributed to the tendency of silicon to become hypervalent. Examples of the types of complexes that fit the IHI or SISHA category were discussed in section 5.5 and are listed in Table 9.

The view proposed by Nikonov was based on MO theory and implies a delocalized covalent interaction in systems where there are two (or more) hydrides and a silicon unit associated with the metal center.^{5a,c} In this approach, the two hydrides and the silyl unit were considered one molecular fragment with the silicon atom in the center of an open triangle. This unit bears a negative charge and thus produced an MO pattern analogous to the trihydrogen anion (H₃)[−]. As an example, the complex reported by Sabo-Etienne and co-workers that was originally formulated as [(Cy₃P)₂(H)₂Ru(η^2 -H₂)(η^2 -HSiPh₃)]^{210a} and later described in terms of a SISHA interaction⁴⁵² could also be described with the hypervalent fragments (H₂SiPh₃)[−] and the metal fragment [(Cy₃P)₂(H)₂Ru(η^2 -H₂)]⁺. The complex exhibited pseudo-octahedral geometry with the *cis*-phosphines in a position *trans* to the two coordination sites occupied by the (η^3 -H₂SiPh₃) ligand (silyl group bridges the H–H edge). The (η^3 -H₂SiPh₃) ligand can also be compared to a (η^3 -H₂BR₂) borate ligand. The nonclassical (H₂SiR₃)[−] ligand could be formed in the coordination sphere of the metal under conditions that favor (η^2 -HSiR₃) σ -complexes when back-donation from the metal is relatively weak. Another example, [(Ph₃P)₃(H)₃M(SiPyr₃)] (M = Ru, Os; Pyr = pyrrolyl), which may be considered an octahedral complex with the SiPyr₃ group capping the H₃-face could also be viewed as an interaction between the silicon fragment H₃SiR₃^{2−} and the metal fragment [(R₃P)₃M]²⁺. In this case, the qualitative MO orbitals for H₃SiR₃^{2−} would involve a combination of the closed form of the trihydrogen ion [H₃][−] with the MO of the SiR₃[−] ion.

The SiH interaction would be retained if back-donation into {H₃–Si}^{*} is incomplete.^{5a,c}

Another type of hypervalent interaction is found in cases where a M–H bond is *cis* to a SiR₃ substituent as in Cp₂(H)NbSi(HSiR₃), which may be considered as a combination of (H₂SiR₃)[−] and Cp₂Nb⁺, although the interaction is a function of the substituents on Si. In the case where R is an alkyl and/or aryl group, there is effective back-donation from a metal orbital into the antibonding orbital of the H₂SiR₃[−] fragment, producing a classical monosilyl dihydride without SiH interaction.^{5c} When there is a good leaving group X at the silicon center, the metal hydride functions as a “nucleophile” interacting with the silicon center by transferring electron density into the (Si–X)^{*} antibonding orbital. This transforms the silicon center into a pseudo-trigonal-bipyramidal environment with the hydride and the X group occupying apical sites, giving rise to an interligand hypervalent interaction (IHI). The consequence of the transfer of electron density from the metal hydride is to elongate the Si–X bond and to provide more “s” character to the most electropositive equatorial group that can include the ML_{*n*} fragment, thus producing a shorter M–Si bond. The interligand M–H...Si contacts generally range from 1.8 to >2.0 Å. DFT calculations^{142,487} indicate that the M–H bond involved is elongated, and this is supported by NMR relaxation measurements as well as by neutron diffraction studies.^{145a}

Lin has suggested that, in silyl hydride complexes, if a silyl group and a hydride are in positions *cis* to each other, some type of interaction should always be expected. He suggested that silicon-to-hydrogen distances in the range 1.9–2.1 Å represent a strong attractive interaction, whereas those with distances from 2.1 to 2.5 Å should be considered as weak attractive interactions.⁴⁸³

7.3. Theoretical Calculations: Specific Cases

Theoretical calculations are performed for a variety of reasons including rationalization of structural properties, particularly when hydrogen ligands are involved. In some cases, the calculations are performed to identify what could be the most stable isomer when several isomers are possible. This has been done particularly for multiply bonded silicon complexes and includes silylenes as well as silenes and silynes. Another common reason for calculations is to determine the location of hydrides and the role of the hydride especially when the hydrides could not be located in the X-ray determination.

The following discussion is organized in terms of the triads from titanium through copper. The reader should consult the original papers for the details associated with the calculations.

7.3.1. Ti Triad

Titanium complexes for which calculations (Gaussian 98) were performed included Cp₂(Me₃P)Ti(η^2 -HSiMeCl₂) (**3-1**) and the related derivatives formed from HSiMeRCl (R = Ph, Me) and HSiCl₃.^{20b} The comparison between the X-ray data for isolated complexes and DFT calculations was summarized earlier in Table 12. The model for the calculations was the rotamer with the hydride *trans* to a chloride, and the trends in the calculated (as well as experimental) bond distances were those expected for an IHI interaction (see section 5.5.1). For the rotamer where the Me group is *trans* to the hydride, the Ti–Si and Si–H bond distances

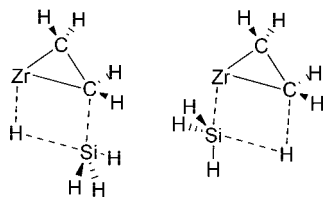


Figure 16. Proposed Si–H σ -bond activation in the Cp_2Zr -catalyzed hydrosilylation of ethylene.^{489a}

were longer and weaker, whereas the Ti–H bond was shorter and stronger. In this case, the results for this constrained model were best described as a stretched silane σ -complex and not an IHI interaction, as would be expected in complexes with electropositive R substituents.

The experimental study of the oxidative insertion of titanium atoms into the SiH bond of SiH_4 in an Ar matrix was monitored by IR spectroscopy and showed the formation of both dihydride-bridged complexes, *cis*- and *trans*- $\text{HTi}(\mu\text{-H})_2\text{SiH}$, as well as the trihydride-bridged $\text{HTi}(\mu\text{-H})_3\text{Si}$.^{20a} Quantum mechanical calculations indicated that the trihydride-bridged complex was the global minimum with a triplet ground state where the two unpaired SOMO's were associated with the titanium center. The calculated parameters for $\text{H}_{1-x}\text{Ti}(\mu\text{-H})_y\text{SiH}_z$ [$x = 0, z = 2, y = 1$; $x = 0, y = 2, z = 1$ (*cis*-**1-2a** and *trans*-**1-2a**); $x = z = 0, y = 3$ (**1-2b**)] were summarized earlier in Table 15.^{20a} The insertion reactions of the cationic metal species $\text{Ti}^+(\text{F})^{488a}$ and $\text{Zr}^+(\text{D})^{488b}$ into an SiH of SiH_4 (and other EIH bonds) were studied by ab initio molecular orbital calculations. The reaction proceeds through an ion–molecule complex, M^+-SiH_4 , with C_{3v} symmetry for $\text{M}^+ = \text{Ti}^+$ and two isomers for $\text{M}^+ = \text{Zr}^+$, one of which exhibited η^3 -coordination with C_s symmetry and the other of which exhibited η^2 -coordination with C_{2v} symmetry. In the transition state, one of the Si–H bonds elongates, producing a 3-center, 4-electron transition state (C_s symmetry), which leads to hydrogen migration and formation of two closely related insertion isomers, $\text{H}-\text{M}^+-\text{SiH}_3$. The insertion barrier was found to be lower and the insertion reaction was found to be more exothermic for Zr^+ than for the corresponding Ti^+ system.^{488a,b}

Calculations involving hydrosilylation mechanisms will not be covered in the current review unless there are results relative to the type of interaction of an SiH with a metal center. The majority of the papers on hydrosilylation mechanisms involve group 10 metals, and these may be found in section 7.3.7. The theoretical study [DFT and MP2MP4(SDQ)] of Cp_2Zr -catalyzed hydrosilylation of ethylene does introduce a mechanism that includes a new type of Si–H σ -bond activation.^{489a,b} The mechanism differs from that normally invoked for electron-rich metals. The Chalk-Harrod and modified Chalk-Harrod mechanisms involve insertion of ethylene into a M–H bond and into a M–Si bond, respectively. In the mechanism proposed by Sakaki and co-workers for hydrosilylation of ethylene, $\text{Cp}_2\text{Zr}(\text{C}_2\text{H}_4)$ reacts with SiH_4 to produce $\text{Cp}_2\text{Zr}(\text{H})(\text{CH}_2\text{CH}_2\text{SiH}_3)$ and $\text{Cp}_2\text{Zr}(\text{CH}_2\text{CH}_3)(\text{SiH}_3)$ through the σ -bond metathesis intermediates shown in Figure 16. Direct reductive elimination to give the product, $\text{H}_3\text{SiCH}_2\text{CH}_3$, requires a high barrier and is endothermic. Thus, an ethylene-assisted Si–C reductive elimination was proposed. The difference between the mechanism for Cp_2Zr and the Chalk-Harrod mechanism for $\text{Pt}(0)$ and $\text{Rh}(\text{I})$ is attributed to an occupied d orbital on Cp_2Zr that is too high in energy.^{489a,b}

The nature of the multiple bonding in $\text{H}_2\text{Ti}=\text{ElH}_2$ ($\text{El} = \text{C}, \text{Si}$) was probed by the multiconfiguration SCF method.^{490a} The planar structure for both molecules has a singlet ground state. In the case of a doubly bonded species, the π and π^* NOON (natural orbital occupancy numbers) changes from 2.0 and 0.0, respectively, to about 1.0 and 1.0 as the π -bond is broken. In the planar form of $\text{H}_2\text{Ti}=\text{CH}_2$, however, the π -orbital NOON increases from 1.74 to 1.88 as rotation occurs and is accompanied by a bond-distance decrease. In contrast, the π -orbital NOON for $\text{H}_2\text{Ti}=\text{SiH}_2$ decreases from 1.6 to 1.0 and the π -bond is broken. At the highest level of theory, the $\text{Ti}=\text{C}$ bond energy was 83.4 kcal/mol whereas that for $\text{Ti}=\text{Si}$ was 56.9 kcal/mol.^{490a}

The reaction of $\text{Cp}_2\text{Hf}(\text{SiMes}_2\text{H})\text{Me}$ with $\text{B}(\text{C}_6\text{F}_5)_3$ resulted in methide extraction to produce the silyl product, $\text{Cp}_2\text{Hf}(\eta^2\text{-SiHMe}_2)(\mu\text{-Me})\text{B}(\text{C}_6\text{F}_5)_3$, which was characterized by spectroscopic methods, but no X-ray structure was reported.^{307c} The unusual feature of the complex was an α -agostic Si–H interaction. The gas-phase structure was modeled with both $\text{Cp}_2\text{HfSiH}_3^+$ and $\text{Cp}_2\text{HfSiH}(\text{2,6-Me}_2\text{C}_6\text{H}_3)_2^+$, which reproduced the α -agostic Si–H unit. The geometry about the silicon center was distorted to trigonal monopyramidal with the bridging hydride in the pseudoaxial position. The sum of the angles at silicon was nearly 360° , with Si–H_{br} and Hf–H_{br} distances of 1.67 and 2.02 Å, respectively, for the $\text{HfSiH}(\text{2,6-Me}_2\text{C}_6\text{H}_3)_2^+$ cation.

It is noteworthy that the calculations reported for the isoelectronic neutral compound $\text{Cp}_2\text{ScSiH}_3$ do not exhibit an α -agostic Si–H feature nor does the crystallographically characterized complex, $\text{Cp}^*\text{ScSiH}_2\text{SiPh}_3$ (**1-9**).^{26b}

7.3.2. V Triad

In the ultrafast IR study of Si–H bond activation by the complex $\eta^5\text{-CpV}(\text{CO})_4$ (promoted by photolysis) in neat HSiEt_3 , the intermediates were calculated by DFT methods utilizing HSiH_2CH_3 as a model. The results were briefly presented in section 3.2.2 and shown in eq 43.^{141,165b} Photolysis produced both triplet and singlet $\eta^5\text{-CpV}(\text{CO})_3$. The triplet form reacts directly by a concerted spin crossover/solvation through the SiH bond to give $\text{Cp}(\text{OC})_3\text{V}(\eta^2\text{-HSiEt}_3)$. The uncoordinated singlet is solvated by the hydrocarbon substituent on silicon and then more slowly rearranges to the same σ -complex that was observed from the triplet form.

The study of how substituents effect the interaction between a metal and the HSi unit has been studied for two sets of complexes: $\text{CpL}_2\text{M}(\text{HSiR}_3)$ ($\text{M} = \text{Mn}, \text{Tc}, \text{Re}$; see next section) and the bent metallocenes, both $\text{Cp}_2\text{M}(\text{SiCl}_n\text{H}_{3-n})_2(\text{H})$ (symmetrical structures) and $\text{Cp}_2\text{M}(\text{SiCl}_n\text{H}_{3-n})(\text{H})\text{X}$ ($\text{X} = \text{H}, \text{Me}, \text{Cl}$; asymmetrical structures) where $\text{M} = \text{Nb}, \text{Ta}$ for both sets of compounds.^{142,483,487} The two research groups involved do not appear to agree in some cases on the interpretation of the bonding interaction. The structural parameters for isolated Nb complexes were summarized earlier in Table 13.

The nature of the interactions in $\text{Cp}_2\text{M}(\text{SiR}_3)\text{HX}$ ($\text{M} = \text{Nb}, \text{Ta}$; $\text{X} = \text{SiR}_3, \text{Cl}, \text{H}, \text{CH}_3$) were studied by ab initio calculations at the MP2 level.⁴⁸⁷ The results for $\text{Cp}_2\text{Nb}(\text{SiClH}_2)\text{H}(\text{SiClH}_2)$ indicated a symmetrical displacement of the silyl ligands about the hydride with an $\text{H}\cdots\text{Si}$ distance of 2.154 Å compared to the value of 2.076(3) Å^{145a} determined by neutron diffraction. Plots of the Laplacian of the valence electron density in the series $\text{Cp}_2\text{Nb}(\text{SiCl}_n\text{H}_{3-n})\text{H}(\text{SiCl}_n\text{H}_{3-n})$ ($n = 0-3$) did not show any

observable $\text{H}\cdots\text{Si}$ bond paths, although the electron density around H was polarized toward both silyl ligands. The spherical appearance of the Laplacian at the Nb (or Ta) center indicated that the metal has a d^0 configuration, which is most consistent with a classical silyl–hydrido–silyl complex.⁴⁸⁷ It was concluded, however, that the in-plane substituents in the assumed C_s symmetry used in the calculations did play an important role in determining the extent of the $\text{H}\cdots\text{Si}$ interaction. In contrast, calculations for the $\text{Cp}_2\text{M}(\text{SiCl}_n\text{H}_{3-n})\text{-HCl}$ complexes indicated a shorter $\text{H}\cdots\text{Si}$ interaction, and the combined influence of a terminal M-Cl and an in-plane Si-Cl substituent significantly strengthened the $\text{H}\cdots\text{Si}$ interaction. In this case, the Laplacian plots for all complexes with one or more Cl substituents indicate a curved path for the $\text{H}\cdots\text{Si}$ interaction with an electron density distribution about the metal center that was consistent with a d^2 configuration, and thus, the complexes may be viewed as nonclassical with an η^2 -silane coordination.⁴⁸⁷ The authors viewed the formation of an η^2 -silane coordination in the absence of a strong π -acceptor ligand a surprising result and indicated that the factors influencing the strength of the $\text{H}\cdots\text{Si}$ interaction are different from those of the mid-transition metals. Complexes $\text{Cp}_2\text{MXH}(\text{SiCl}_n\text{H}_{3-n})$, $\text{X} = \text{H}$ or CH_3 , in which both ligands exhibit little π -bonding character, were also examined. When $\text{X} = \text{H}$, neither an $\eta^2\text{-H}_2$ nor an $\eta^2\text{-H}\cdots\text{Si}$ coordination was observed in the Laplacian plots and the density at the metal was consistent with a classical complex for both the Nb and Ta complexes. The results for $\text{X} = \text{CH}_3$ appear to be in between those observed for $\text{X} = \text{H}$ and $\text{X} = \text{Cl}$. The authors concluded that “using the criterion of Bader’s atoms-in-molecules theory, a ‘boundary’ between nonclassical η^2 -silane and classical hydridosilyl complexes can be placed at a $\text{H}\cdots\text{Si}$ distance of $\sim 2.0 \text{ \AA}$.”⁴⁸⁷

The theory of IHI interactions from both a qualitative description and from ab initio calculations was imbedded in a synthesis/characterization study reported by Nikonov, Vyboishchikov, and co-workers in 1999.¹⁴² The DFT calculations were performed with optimization at the BP86 level for the model mono- and bis(silyl) complexes $[\text{Cp}_2\text{NbH}_{3-m}(\text{SiH}_n\text{Cl}_{3-n})_m]$ ($m = 1, 2$; $n = 2, 3$) as well as for the actual complex, $\text{Cp}_2\text{Nb}(\text{SiMe}_2\text{Cl})\text{H}(\text{H})$ (**3-12b**). The authors concluded that the IHI interaction in the SiH_3 complexes ($n = 3$) was weak and that the hydrogen was the “boundary” substituent on silicon, for which nonclassical Si-H hypervalent interaction was possible. They also concluded that tantalum compounds (not calculated in this study) might have weak IHI interactions between silicon and hydride ligands. The NBO analysis, however, did not indicate any Si-H bond in the calculated structures because the interaction was too weak to be observed within the standard NBO program thresholds. The higher Nb–Si NBO bond orders for the chlorosilyl complexes compared to the silyl complexes as well as lower Si–Cl bond orders for the chlorosilyl complexes were interpreted as providing support for the IHI interaction. Within Bader’s atoms-in-molecules theory, a “bond path” was observed between Si and H atoms only in the two complexes with the strongest IHI interaction. Nikonov, Vyboishchikov, and co-workers, in addressing the difference between their calculations and those of Lin, suggested that “the results of analysis of Laplacian maps can depend on the level of calculation and that care should be taken in making deductions based only on the qualitative analysis of Laplacian maps”. Similar cautionary statements

have been made by others on calculations for other systems. In summarizing his work in his 2002 review,⁴⁸³ Lin points out that if detailed structural characteristics among the Nb complexes are to be compared, the parameters in the NbHSi triangle must be taken as a whole and that the various values cannot be isolated.

DFT calculations were made for the two isomers of $[\text{Cp}(\text{Me}_3\text{P})\text{ClNb}\{\eta^3\text{-N}(\text{Ar})\text{SiMe}_2\text{H}\}]$ ($\text{Ar} = 2,6\text{-C}_6\text{H}_3\text{Pr}_2$, **3-17** and **3-18**, isomers differing by exchange of PMe_3 and Cl locations), both of which have a four-legged piano-stool structure where the isomers are derived from the interchange of the *cis*- Me_3P and Cl ligands.^{147a} The spectroscopic data are consistent with a β -hydride interaction. The X-ray structure of **3-18** was of insufficient quality to locate the hydride, and thus, calculations were developed to locate the hydrides in model compounds and to address the nature of the Si-H and the Si-M interactions. The results were briefly described in section 5.4.2. What is interesting about this case is that three levels of models were calculated before obtaining results that seemed to correlate with the crystal structure data. The models for the isomer with the Cl substituent *trans* to the Si-H bond in order of complexity were $\text{Cp}(\text{H}_3\text{P})\text{ClNb}\{\text{N}(\text{H})\text{SiH}_2\text{-H}\}$, $\text{Cp}(\text{H}_3\text{P})\text{ClNb}\{\text{N}(\text{Ph})\text{-SiH}_2\text{-H}\}$, and $\text{Cp}(\text{Me}_3\text{P})\text{ClNb}\{\text{N}(\text{Ph})\text{SiMe}_2\text{-H}\}$. The modeling of the phosphine ligand was most important in providing Nb–H and Si–H distances that came the closest to the X-ray structure with $\text{Nb-H}_{\text{calc}} = 1.87 \text{ \AA}$ ($1.91(5) \text{ \AA}_{\text{exp}}$) and $\text{Si-H}_{\text{calc}} = 1.73 \text{ \AA}$ ($1.52(5) \text{ \AA}_{\text{exp}}$). For the isomer with PMe_3 and Cl interchanged, the $\text{Nb-H}_{\text{calc}} = 2.06 \text{ \AA}_{\text{calc}}$ and $\text{Si-H}_{\text{calc}} = 1.57 \text{ \AA}$. The authors concluded that the two isomers were best described as a β -agostic silylamine with a d^2 , Nb(III) center. Although the energies of the two isomers are relatively close, that of the isomer with PMe_3 *trans* to the Si-H was more stable (it is also the isomer produced experimentally over the longest reaction time). The NBO analysis of the isomer with Cl and SiH *trans* indicated an Nb–H bond but no Si–H bond, whereas the reverse was true for the isomer with PMe_3 *trans* to SiH.

The tantalum complex, formed in a similar way from $\text{CpTa}(\text{=NAr})(\text{PMe}_3)_2$ and HSiClMe_2 , appeared to prefer a d^0 , Ta center with an IHI interaction between Si and HTa in the products, **3-25a** and **3-26a**.^{147a} Additional examples of related complexes $\text{Cp}(\text{ArN})\text{Ta}(\text{PMe}_3)(\text{H})(\text{SiR}_3)$ ($\text{Ar} = 2,6\text{-C}_6\text{H}_3\text{Pr}_2$; $\text{SiR}_3 = \text{SiPhMeH}$ (**2-3b**),^{32a} SiMeCl_2 (**3-26a**), and SiCl_3 (Table 3, footnote 38) were also reported as well as SiMePhCl .^{147b} The X-ray structure of **3-26a** exhibited two different Si–Cl bond distances. The in-plane Si–Cl (Cl *trans* to the hydride on Ta) was longer than the out-of-plane SiCl, consistent with the donation of electron density from the hydride into the antibonding orbital of Si–Cl bond and characteristic of an IHI interaction. DFT calculations (Gaussian 98 program package) for the four model complexes $\text{Cp}(\text{MeN})\text{Ta}(\text{PMe}_3)(\text{H})(\text{SiH}_{3-n}\text{Cl}_n)$ ($n = 0\text{--}3$) revealed a minimum in the $\text{Si}\cdots\text{H}$ distance for the SiH_2Cl complex as well as the longest Si–Cl in-plane distance, again, what is expected for the IHI interaction being the strongest in the monochloro-substituted case. The atom-weighted bond orders (BO) and Wiberg bond indices (WBI) also showed a maximum for the Si-H-Ta interaction in the SiH_2Cl complex with a minimum for the in-plane Si–Cl bond, thus indicating the strongest Si–H–Ta IHI interaction in the halogenated complexes for the SiH_2Cl derivative. Another feature in the series of isolated complexes was the J_{SiH} values, which increased in the sequence SiPhMeH (14 Hz) to

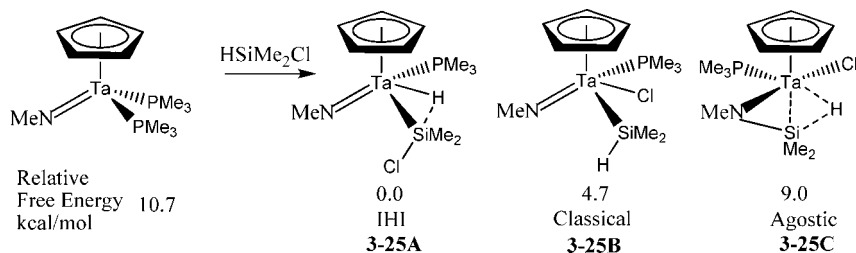


Figure 17. Relative free energies of products from reaction of HSiMe_2Cl and $\text{Cp}(\text{ArN}=\text{Ta})(\text{PMe}_3)_2$ (DFT calculations).^{147b}

SiMeCl_2 (40 Hz) and then again to the SiCl_3 complex (50 Hz), which is essentially the opposite of that observed for the usual $\sigma\text{-Si-H}$ complex.^{78a} The increase in J_{SiH} in the order observed should indicate an increase in the strength of the Si-H interaction but, in this system, was not consistent with the results of the calculations. The authors concluded that “an increase in the magnitude of J_{SiH} does not necessarily correspond to a stronger bonding interaction between these two ligands”.^{78a}

A second publication reported the use of cyclopentadienyl-imido ligand sets, $\text{Cp}(\text{ArN}=\text{Ta})(\text{PMe}_3)_2$ ($\text{Ar} = 2,6\text{-diisopropylphenyl}$ and $2,6\text{-dimethylphenyl}$) with $\text{HSiR}_n\text{Cl}_{3-n}$, including compounds prepared previously as well as new complexes ($\text{Ar} = 2,6\text{-diisopropylphenyl}$, HSiPhMeCl ; $\text{Ar}' = 2,6\text{-dimethylphenyl}$, HSiClMe_2 , HSiClPhMe , HSiCl_2Me , HSiClPh_2).^{147b} The hydride complexes, $\text{Cp}(\text{ArN}$ or $\text{Ar}'\text{N})\text{Ta}(\text{PMe}_3)(\text{H})(\text{SiR}_3)$ when one of the R substituents is Cl, rearrange or decompose to $\text{Cp}(\text{ArN})\text{Ta}(\text{PMe}_3)(\text{Cl})(\text{SiHR}_n\text{Cl}_{3-n})$ if PMe_3 is present (additional decomposition takes place in certain of the cases). The authors were successfully able to measure the sign of the coupling constant between the hydride and the silicon in four cases. The sign was negative for the complexes produced from HSiMePhCl , HSiMeCl_2 , HSiCl_3 (2,6-diisopropylphenyl), and HSiMeCl_2 (2,6-dimethylphenyl), demonstrating the existence of a $\text{Si}\cdots\text{HTa}$ interaction. The sign on the complex produced from H_2SiMePh , however, was positive, indicating a classical complex.^{147b}

Calculations for three model complexes from reaction of $\text{Cp}(\text{MeN}=\text{Ta})(\text{PMe}_3)_2$ with HSiMe_2Cl (Figure 17) showed that the IHI complex (*trans* rotamer, **3-25A**) was the most thermodynamically stable.^{147b} The corresponding *cis*-rotamer (chloride substituent at Si is *cis* to the hydride; not shown in Figure 17) is 3.0 kcal/mol less stable as a result of the loss of the IHI interaction. The agostic d^2 complex, **3-25C**, is the least stable product, lying 9 kcal/mol above **3-25A**. In contrast to the lowest-energy product calculated for HSiMe_2Cl , the lowest-energy product for HSiMeCl_2 is the related classical complex corresponding to **3-25B**, although the IHI complex (related to **3-25A**) is separated by <1 kcal/mol.^{147b}

Two mechanisms were calculated for the addition of silane, HSiMe_2Cl , to the model complex $\text{Cp}(\text{MeN}=\text{Ta})(\text{PMe}_3)_2$. In the calculated dissociative mechanism, a PMe_3 is lost through a transition state 49.3 kcal/mol higher in energy relative to the starting complex (at 10.7 kcal/mol) to give $\text{Cp}(\text{MeN}=\text{Ta})(\text{PMe}_3)$ (A in Figure 18), which could then undergo addition of the silane to afford the complex shown as **3-25A** in Figure 17. In the associative pathway, two directions of attack were considered. One of these is where the silane added to the metal–nitrogen bond such that, in the TS, the chloride on silicon was *trans* to nitrogen and *cis* to the hydride on the silicon center (C in Figure 18) and leads to a species with a pentacoordinate silicon center and

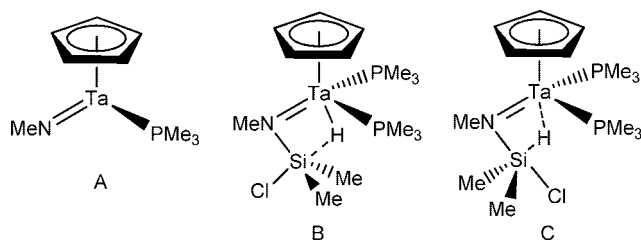


Figure 18. Calculated intermediates in reaction of $\text{Cp}(\text{MeN}=\text{Ta})(\text{PMe}_3)_2$ with HSiMe_2Cl : (A) dissociative mechanism, (B and C) associative mechanism.^{147b}

$\text{Si-H}\cdots\text{M}$ agostic bonding (and two PMe_3 groups). The second pathway involved addition of the silane such that the chloride is *trans* to the hydride and *cis* to the nitrogen center, giving a pentacoordinate silicon center with an IHI type interaction (B in Figure 18). Although B is the most stable structure, the barrier to its formation is very high. Loss of PMe_3 would be required to provide either **3-25A** or **3-25B**, but formation of **3-25C** requires a chloride migration from Si to Ta. These steps were not included in the calculations. In the case of addition of HSiMeCl_2 , both complexes corresponding to **3-25A** and **3-25B** are formed (except that one Me is replaced by a Cl), and the two isomers are of almost equal stability (the agostic form, **3-25C**, is higher in energy).^{147b}

Similar DFT calculations were reported for the corresponding Nb complex.^{32a} In this case, the associative mechanism for silane addition to $\text{Cp}(\text{RN}=\text{Nb})(\text{PMe}_3)_2$ is thermodynamically comparable to the dissociative mechanism for HSiClMe_2 and is the preferred mechanism for HSiCl_2Me .

The last system involves calculations for the ditantalum complexes $\text{Cp}^*_2(\text{ArN}=\text{Ta})_2\text{H}_2(\mu\text{-ArNSiHPh})$ ($\text{Ar} = 2,6\text{-}^i\text{Pr}_2\text{C}_6\text{H}_3$, **1-20a**; paramagnetic) and $\text{Cp}^*_2\text{Ta}_2\text{H}_2(\mu\text{-ArNSiHPh})_2$ ($\text{Ar} = 2,6\text{-}^i\text{Pr}_2\text{C}_6\text{H}_3$, **1-20b**; diamagnetic).³³ X-ray structures were reported for both complexes, but the hydrides were not located for **1-20b**. Therefore, to determine the most probable position of the Ta–H, calculations were performed at the density functional level for a series of model isomers. The 14 models were based upon three groups of $\text{Cp}_2\text{Ta}_2\text{H}_2(\mu\text{-HNSiH}_2)_2$ isomers: (a) five isomers with both hydrogen atoms positioned endo to the Cp rings; (b) six isomers where both hydrogen atoms were positioned exo to the Cp rings; and (c) three isomers in which one hydrogen atom was positioned exo to the two Cp rings. A bis- μ -dihydride (a-type isomer) was the lowest-energy structure; two isomers of the b-type were 7.9 and 5.8 kcal/mol higher in energy than the lowest-energy structure; and one isomer of c-type was 7.3 kcal/mol above the lowest-energy structure (the core structures are shown in Figure 19). The c-type isomer contained one terminal hydride and one bridging hydride, consistent with the ~ 12.5 ppm difference observed for the hydrides in the ^1H NMR spectrum. The 140-atom potential surface of **1-20b**

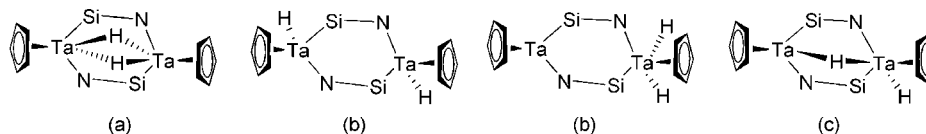


Figure 19. Representative core structures of isomers of **1-20b** utilized for calculations. In type (a), the hydrides are endo to the Cp rings. In type (b), both hydrides are exo to the Cp rings. In type (c), one hydride is exo to the two Cp rings.³³

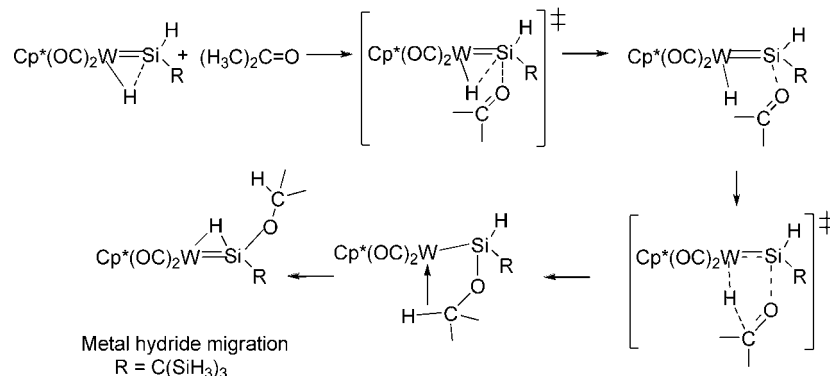


Figure 20. Calculated lowest-energy sequence for reaction of acetone with **1-29**.^{490b}

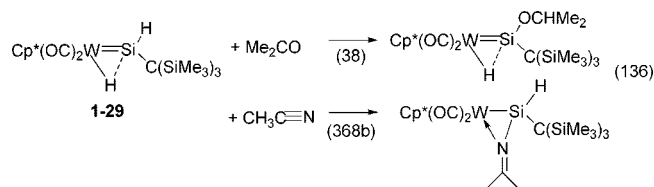
was then calculated for the same four lowest-energy conformers found for the model complex. The lowest-energy structure became the c-type isomer, although it was only 1 kcal lower than the a-type isomer. The calculations for the real ligands were in closer agreement with the X-ray structure. Of the four isomers, only two have hydrides in distinct environments; because the c-type isomer contained one bridging and one terminal hydride, it was chosen as the most likely candidate. The best-fit superposition of the X-ray structure and the calculated gas-phase structure was obtained for the a-isomer, but the fit for the c-isomer was very close (Figure 19). The calculated H–H distances for the c-isomer also fit the experimental NOE data (with one exception). The c-type isomer was chosen as the best candidate in terms of energy and agreement with the observed spectroscopic data. Thus, the ditantalum dihydride **1-20b** was a rare case of a dinuclear metal complex that exhibited an asymmetrical distribution of hydride ligands. The full-scale calculation (127 atoms) for **1-20a** was also performed, and the complex exhibited structural features similar to **1-20b** with a terminal and a bridging hydride ligand. Mayer bond orders were reported for both complexes. The Ta–Ta bond was weak with a calculated bond order in **1-20a** of 0.13 and in **1-20b** of 0.38. The authors concluded that a truncated ligand system could not produce the key aspects of the bonding in the Ta₂ complexes even though “surrogate” ligands are often used in theoretical calculations for organometallic complexes.³³

7.3.3. Cr Triad

The nature of the bonding in silylene complexes continues to be of interest. Tilley and co-workers reported the isolation of the cationic silylene, [Cp*(dmpe)(H)₂W=SiMe₂][B(C₆F₅)₄] (**2-21**),^{39,86} and Frenking and co-workers⁴⁷⁵ reported calculation results (nonlocal DFT level of theory) obtained for [Cp(PH₃)₂W(H₂SiMe₂)]⁺, which was used as the model for the cation in the isolated salt. The optimized geometry when the model was constrained to C_s symmetry provided a structure with classical W–H hydride bonds, but there were additionally four other structures having up to two bridging hydrides (nonclassical forms) that were <5 kcal/mol higher in energy than the classical form. Thus, the energy differences between the classical and nonclassical forms were

small and the W(H₂SiMe₂) unit was predicted to be fluxional. Therefore, it was not possible to classify the complex cation as either classical or nonclassical. The energy decomposition analysis (EDA) indicated that the electrostatic interaction in W–SiMe₂ was slightly higher than the covalent character. The EDA results also indicated a small π -contribution (<10%) to the W–Si bonding; thus, the silylene functions primarily as a σ -donor and the W has a formal oxidation state of +4. DFT calculations (B3LYP level) were also reported for the neutral silylene complex Cp*(OC)₂(H)W=Si(H){C(SiMe₃)₃}, **1-29a**.^{38a} The energy-minimized structure for the model complex [Cp(OC)₂(H)W=Si(H){C(SiH₃)₃}] closely matched that of the X-ray crystal structure of **1-29a**. The NLMO/NPA bond orders were W–Si = 1.518, W–H = 0.511, and Si–H in the W–H–Si bridge = 0.476. The latter two distances supported a 3c-2e W–H–Si interaction.^{38a} The reactivity patterns of **1-29a** (and the related Cp* complex, Table 1, footnote 30) have also been of interest, as these silylene complexes react stoichiometrically with acetone^{38a} and acetonitrile^{368b} to give hydrosilylation products, although differing in nature (eq 136). Four different mechanisms were calculated for the model [Cp(OC)₂(H)W=Si(H){C(SiH₃)₃}] by Wu and co-workers, including metal hydride migration (originally proposed by Tobita), silyl hydride migration, silyl migration, and the Glaser–Tilley mechanism.^{490b} The lowest-energy pathway for the reaction with acetone was metal hydride migration outlined in Figure 20. The second transition state depicted in Figure 20 was the one higher in energy. The silyl migration mechanism for the reaction with acetone was higher in energy and more complex with six transition states. The lowest-energy pathway in the reaction of the model complex with CH₃CN, however, involved the silyl migration route and also had six different transition states, with the last transition state being the highest in energy. The silyl migration mechanism is analogous to the modified Chalk–Harrod mechanism that has been proposed for the hydrosilylation of olefins. The authors also explored the possibility of making the hydrosilylation reactions with neutral tungsten complexes catalytic. However, the energetics involved in returning the hydrosilylation products to the starting complex, [Cp(OC)₂(H)W=Si(H){C(SiH₃)₃}], were too high;

thus, the likelihood of the neutral tungsten–silylene complexes catalyzing hydrosilylation of unsaturated organic molecules was considered small.³⁹⁰



The reaction of the stable silylene $\text{Si}[\text{t-BuNCH}=\text{CHNBu}]$ with Cp_2MH_2 ($\text{M} = \text{Mo}, \text{W}$) resulted in the expected insertion of the silylene into the $\text{M}-\text{H}$ bond to form $\text{Cp}_2(\text{H})\text{M}-\{\text{HSi}[\text{t-BuNCH}=\text{CHNBu}]\}$.³⁷² However, with the precursor $\text{Cp}_2\text{Mo} \leftarrow \text{PET}_3$, displacement of the phosphine occurred to give the silylene complex. The $\text{Mo}-\text{Si}$ bond in the former complex was 2.538(3) Å, which corresponds to a single bond. The silylene complex, however, had a significantly shorter $\text{Mo}-\text{Si}$ bond length of 2.4125(13) Å, which is about the middle of the $\text{Mo}-\text{Si}$ range reported in Table 7. The authors argue that back-bonding from the HOMO of the Cp_2Mo fragment and the “p” orbital on the silicon in the complex is not possible because these are orthogonal to each other.

The reaction of $\text{Cp}'(\text{OC})_2(\text{MeCN})\text{W}(\text{Me})$ ($\text{Cp}' = \text{Cp}^*, \text{C}_5\text{Me}_4\text{Et}$) with $\text{HPh}_2\text{Si}(\text{C}\equiv\text{C}^t\text{Bu})$ produced a novel complex that was described as a silylene hybrid, $\text{Cp}'(\text{OC})_2\text{W}-(\text{C}\equiv\text{C}^t\text{Bu})(\text{SiPh}_2)$ (**3-43**).^{160a} The complex was viewed as representing an intermediate state between coordination of the triple bond to the silylene center and coordination of the $\text{C}-\text{Si}$ bond of the silacyclopropene ring to the metal center. Subsequently, Sakaki and co-workers published a theoretical study (DFT, MP2 to MP4(SDTQ), and CCSD(T) methods) for the model complex, $\text{Cp}(\text{OC})_2\text{W}(\text{C}\equiv\text{CH})(\text{SiH}_2)$, in an attempt to clarify the nature of the bonding in **3-43a**.^{338a} The calculations showed that the silylene group interacted with both the metal center and the acetylide group. The orbitals for the model resemble those observed in the interaction of a silylene and acetylene, leading to the formation of silacyclopropene. In this case, charge transfer occurs from the π -orbital of the acetylide unit into the empty p-orbital of the silylene and from the lone pair (sp^2) of the silylene into the π^* -orbital of the acetylide. The unit $\text{CCH}(\text{SiH}_2)$ is then trapped by the W center in the path to silacyclopropene from silylene and acetylene. The final product was formed after several steps, each of which was calculated. In the last step, $\text{Cp}(\text{OC})_2\text{W}[\text{Si}(\text{H})_2\text{C}\equiv\text{CH}]$ converted to $\text{Cp}(\text{OC})_2\text{W}(\text{C}\equiv\text{CH})(\text{SiH}_2)$ through an $\alpha\text{-Si}-\text{C}$ σ -bond activation by a 1,2-alkynyl shift as a result of the bonding interactions of the π - and π^* -orbitals of the acetylide. The nonbonding, π -orbital of the H_2SiCCH unit bore an analogy to the propargyl group, but the π -conjugation between Si and C centers was considered very weak.^{338a}

Later, Sakaki and co-workers published a theoretical study of the system related to **3-43**, $\text{Cp}^*(\text{OC})_2\text{W}(\eta^3\text{-Me}_2\text{SiCHCMe}_2)$ (**3-42**), utilizing the models $\text{Cp}(\text{OC})_2\text{W}(\eta^3\text{-H}_2\text{SiCHCH}_2)$ (**1**) and $\text{Cp}(\text{OC})_2\text{W}(\text{CH}=\text{CH}_2)(\text{SiH}_2)$ (**2**).^{338b} The relationship between forms of **3-42** and **3-43** is shown in Figure 21. The complexes **3-42A** and **3-43A** are related, as are **3-42B** and **3-43B**. Complex **3-43A** converted readily to **3-43B**, the form that was isolated experimentally. However, **3-42A** was lower in energy than **3-42B**, and **3-42A** was the form that was isolated. The $\text{Si}-\text{C}$ bond in **3-42A** is

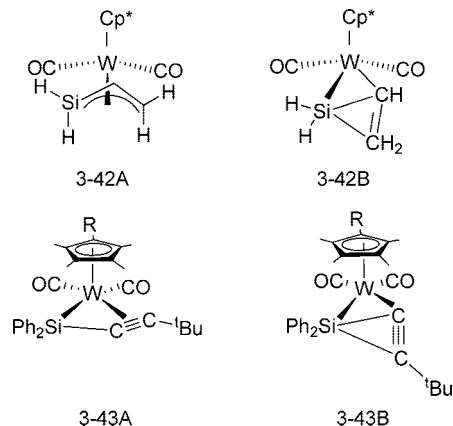


Figure 21. Comparison of η^3 -silaallyl/ η^3 -vinylsilyl complex (**3-42A**) and tungsten vinyl silylene complex (**3-42B**) with η^3 -1-silaalkynyl complex (**3-43A**) and tungsten acetylide silylene complex (**3-43B**).^{338b}

weak, but the $\text{W}-(\eta^3\text{-H}_2\text{SiCHCH}_2)$ interaction is strong. The W -vinyl and silylene–vinyl interactions are very weak in **3-42B**. Conversely, the $\text{Si}-\text{C}$ bond is strong for **3-43A**, but the $\text{W}-(\eta^3\text{-H}_2\text{SiCCH})$ interaction is weak and the W -acetylide and silylene–acetylide interactions are very strong in **3-43B**. Thus, the complex **3-42A** is more stable than **3-42B** but **3-43A** is less stable than **3-43B**.

An unusual way to make a silyl–metal hydride was reported by Berry and co-workers from reaction of $\text{Cp}_2\text{W}(\eta^2\text{-Me}_2\text{Si}=\text{CH}_2)$ with H_2 to give $\text{Cp}_2\text{W}(\text{SiMe}_3)\text{X}$.^{338c} At the time, a mechanism was suggested where SiMe_2 migrates from W to the Cp ring, generating a 16e intermediate. Calculations have been performed for three possible pathways, and the migration of the silicon group, indeed, provided the lowest-energy pathway.^{338d} It was proposed that relief of strain in the calculated transition state shown in Figure 22, forming the indicated intermediate, may be mainly responsible for this favored pathway.

A combined effort of the synthesis group of Kubas and the theoretical group of Lledós provided a comprehensive study of the OA of $\text{EH}_{4-n}\text{Ph}_n$ ($\text{E} = \text{Si}, \text{Ge}$) to $\text{Mo}(\text{CO})_2(\text{diphosphine})_2$ from the standpoint of both the reaction chemistry and the computational aspects (ab initio DFT with the B3LYP functional).^{21b} The results for one example were briefly summarized earlier as Case 1 of section 5.3. The model complexes employed were $\text{Mo}(\text{CO})(\text{EH}_{4-n}\text{vin})_n(\text{dhpe})_2$ ($n = 0-3$; $\text{E} = \text{Si}, \text{Ge}$; only the silicon cases will be presented here) where the vinyl group was used as a surrogate for the phenyl substituent actually used in the reaction chemistry. The bidentate, dhpe ($\text{H}_2\text{PCH}_2\text{CH}_2\text{PH}_2$), was used in place of dppe and depe to simplify the calculations. The test calculations using the actual silane, H_3SiPh , showed that the vinyl substitution led to almost identical results for all three isomers (see Figure 23) employed in the calculations. The three isomers included the pseudo-octahedral σ -complex *a* with the silane *cis* to the CO , a seven-coordinate pentagonal-bipyramidal OA product *b*, and a pseudooctahedral complex *c* with the silane *trans* to CO (see Figure 23). The calculated $\text{Mo}-\text{E}$ and $\text{Mo}-\text{H}$ distances are similar for isomers *a* and *b* for all $\text{EH}_{4-n}\text{vin}_n$. The isomers with structure *a* were described as arrested intermediates with an advanced stage of OA toward isomer *b*. Isomer *c*, however, appears to be at the early stage of OA between an η^1 and an η^2 σ -complex. The isolated complexes formed in this series vary from OA to a σ -complex, and the free energy difference between

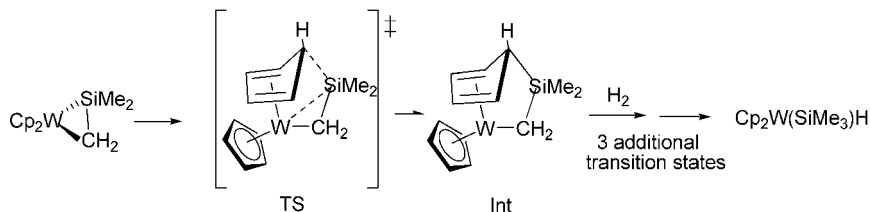


Figure 22. Lowest-energy pathway calculated for the transformation of the tungsten silaethylene complex to a silyltungsten hydride on reaction with H_2 .^{338d}

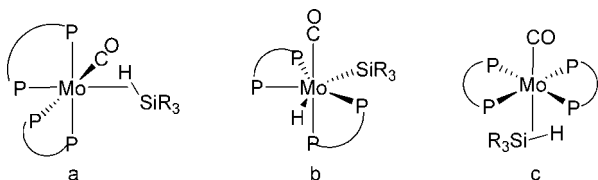


Figure 23. Models of complexes **2-13** and **2-14** used for DFT calculations. $\text{P}\cap\text{P}$ = dhpe.^{21b}

isomer *a* and isomer *b* can be nearly 0 as it is for the real system, $(\text{depe})_2(\text{CO})\text{Mo}(\text{SiH}_4) \neq (\text{depe})_2(\text{CO})\text{Mo}(\text{H})(\text{SiH}_3)$ (**1-3d**). In general, the cleavage of the H–Ge bond in hydrogermanes occurs further along the OA pathway than do those of hydrosilanes or dihydrogen, but the homolytic σ -bond cleavage appears to be similar for Si–H and H–H.

Two studies report calculations performed for two complexes that exhibit a β -agostic interaction: $(\text{Me}_3\text{P})_2(\text{ArN}=\text{C})\text{CIMO}[\text{N}(\text{SiMe}_2\text{R})\text{Ar}']$ ($\text{Ar}' = 2,6\text{-Me}_2\text{C}_6\text{H}_3$; $\text{R} = \text{Me}$, **3-37a**,^{155a} Cl) and the carbene complex $(\text{OC})_4\text{W}=\text{C}(\text{NMe}_2)\text{SiMe}_2\text{H}$ ($\text{Mes} = 2,4,6\text{-Me}_3\text{C}_6\text{H}_2$).^{496a} The complexes **3-37a** and the $-\text{SiCl}_2\text{Me}$, its Cl analogue (Table 3, footnote 46), are formed from reaction of $\text{HSiCl}(\text{Me})\text{R}$ with $(\text{Ar}'\text{N})_2\text{Mo}(\text{PMe}_3)_3$. The X-ray structures show that the two complexes are isomorphous and exhibit similar Mo–Si, Mo–H, and Si–H bond distances. However, the $^1J_{\text{SiH}}$ values for the $\text{R} = \text{Me}$ (97 Hz) complex versus the $\text{R} = \text{Cl}$ (129 Hz) differ by 32 Hz, which suggests a strengthening of the Si–H interaction in the latter case, which is not consistent with the observed bond distances. To try to determine the origin of the conflicting results, DFT calculations were performed for the model complexes $(\text{Me}_3\text{P})_2\text{CIMO}[\text{N}(\text{SiMe}_{2-n}\text{Cl}_n\text{H})\text{Me}]$ ($n = 0, 1, 2$).^{155a} The optimized structures gave parameters that are close to those obtained from the X-ray study. As the number of Cl substituents increased in the series, the Mo–Si bond lengths decreased only marginally, although the Wiberg bond indices (WBI) are consistent with a weaker bond (0.1471 for $n = 0$, 0.1445 for $n = 1$, and 0.1426 for $n = 2$). The Si–H bond actually strengthens in the series with WBI = 0.5830 ($n = 0$) to 0.6649 ($n = 2$), and the W–H bond weakens. The results of the AIM analysis also suggested a weakening of the Mo–H bond. The results were rationalized by a DCD model adjusted in accordance with Bent's rule.^{155b} The substitution of electron-donating Me groups with electron-attracting Cl groups provides greater “s” character in the Si–H bond, causing the bond to shorten and to decrease the σ -donor strength.

The 16e carbene complexes $(\text{OC})_4\text{W}=\text{C}(\text{NRR}')\text{Si}(\text{Ar})_2\text{X}$, produced from CO loss during photolysis of the 18e precursor, $(\text{OC})_5\text{W}=\text{C}(\text{NHR})(\text{SiAr}_2\text{X})$, are stabilized by the interaction of a silicon substituent with the W center. To ascertain the details of the intermolecular interaction and the potential role of steric and electronic factors, DFT calculations were reported for four model complexes $(\text{OC})_4\text{W}=\text{C}(\text{NH}_2)\text{SiH}_2\text{R}$ ($\text{R} = \text{H}, \text{Ph}, \text{Me}, \text{CMe}=\text{CHMe}$).¹⁶⁴ The model structures either started with the known crystal-

lographically determined structures or a structure where the angles about the carbene C were set at 120° . Both of these initial points led to the same global minimum. The bond lengths and angles agreed with the experimental values obtained from the X-ray structure. The results indicated that there were no steric reasons for the distorted arrangement about the carbene C but that electronic reasons could be responsible for the agostic interaction. The metal d_{z^2} orbital was thought to be responsible for the intramolecular interaction in the 16e complex. The stabilization resulted from the agostic interaction with a $\sigma\text{-H-Si}$ or with π -orbitals of a phenyl or olefin group. The Si–H bond was located in the W–C–Si plane as was the case for the solid-state structure of $(\text{OC})_4\text{W}=\text{C}(\text{NMe}_2)\text{SiMe}_2\text{H}$. The electron density plot showed that both H and Si are involved in the delocalized, occupied d_{z^2} orbital. Thus, the Si–H bond is the electron donor to the metal. In the case of $(\text{OC})_4\text{W}=\text{C}(\text{NH}_2)\text{SiH}_2\text{R}$ ($\text{R} = \text{Ph}, \text{CMe}=\text{CHMe}$), stabilization occurred either through the *ipso*-carbon of the phenyl ring or by coordination of the double bond of $\text{CMe}=\text{CHMe}$, but the interaction of the phenyl substituent was much weaker than that of the butenyl group.

Computational methods were used to support structure assignments for the products produced when the laser-ablated group 6 metal atoms interacted with SiH_4 in an argon or neon matrix.^{21a} The study provided an interesting comparison of the most stable product(s) obtained throughout the triad. The products were identified from M–H and Si–H stretching modes in the experimental IR spectra compared to the corresponding products produced from SiD_4 . The frequencies and intensities were computed with B3LYP density functional and the 6-311++ G(3df,3pd) basis sets for Si and H. Geometries were fully relaxed during optimization for the silyl metal hydride, H_3SiMH , the silylidene, $\text{H}_2\text{Si}=\text{MH}_2$, and the silyldiyne, $\text{HSi}\equiv\text{MH}_3$. Energies were calculated in kcal/mol relative to the metal atom + silane. The lowest-energy structures for Cr and Mo were $\text{H}_3\text{Si-MH}$ ($\text{M} = \text{Cr}$, slightly endothermic; Mo, exothermic). The silylidene form for Mo was isoergic with the reagents, and the silyldiyne form was somewhat exothermic (3 kcal/mol relative to the starting reagents), although the authors suggested that, with higher-level calculations, the silyldiyne could be the lowest-energy structure. The lowest-energy form for the open structures for W was the silyldiyne (–30 kcal/mol), but the silyl metal hydride was relatively close in energy (–28 kcal/mol). A bridged tungsten dihydride silylidene was found that was 9 kcal/mol lower in energy than the “open” silyldiyne; however, the calculated frequencies for this isomer did not fit the observed spectrum. The silyl metal hydrides all had a C_s structure; the silylidenes have a plane of symmetry making both SiH bonds and the two M–H bonds equivalent with no agostic distortion. The calculated Si=Mo bond distance was 2.334 Å, which is reasonably close to the observed value of 2.288 Å in the more decorated complex, $\text{Cp}^*(\text{dmpe})(\text{H})\text{Mo}=\text{C}(\text{SiH}_3)_2$.

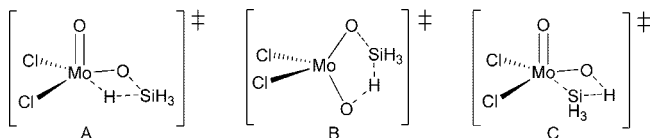


Figure 24. Transition states for SiH activation by MoCl_2O_2 : (A) [2+2]-addition to $\text{M}=\text{O}$; (B) [3+2]-addition to $\text{M}=\text{O}$; and (C) [2+2]-heterolytic addition to $\text{M}=\text{O}$.^{496b}

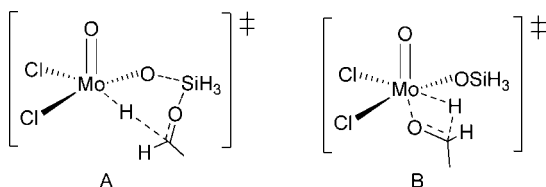


Figure 25. Transition states for reduction of aldehyde by $[\text{MoCl}_2(\text{H})(\text{O})(\text{OSiH}_3)]$: (A) concerted reduction and (B) classical reduction.^{496b}

$\text{Si}(\text{Cl})\text{Mes}$, (**2-11**).^{82a} The silylidyne ($\text{M} = \text{Mo}, \text{W}$) are calculated to have C_{3v} symmetry. The calculated $\text{Si}\equiv\text{Mo}$ was 2.145 Å compared to 2.219 Å measured for the isolated complex $[\text{Cp}^*(\text{dmpe})(\text{H})\text{Mo}=\text{SiMe}_3]^+[\text{B}(\text{C}_6\text{F}_5)_4]^-$.^{82a} The silyne is polarized differently from the corresponding carbyne as the natural charges on the $\text{H}-\text{Si}-\text{W}$ sequence are -0.16 , -0.51 , and 0.22 compared to 0.17 , -0.033 , and 0.75 for the $\text{H}-\text{C}-\text{W}$ sequence. The polarization reduces the “s” character in the $\text{Si}-\text{H}$ bond to $\sim 40\%$ with the remainder in the $\sigma\text{-Si}-\text{W}$ bond. In both systems, the π -bonds are valence np-tungsten 5d. The effective bond orders (EBOs) calculated by pure BPW91 DFT were 2.84 for $\text{Si}\equiv\text{Mo}$ and 2.89 for $\text{Si}\equiv\text{W}$ with a slightly stronger triple bond for the heaviest group 6 metal.^{21a}

Recent studies have shown that high oxidation state metals may be hydrosilylation catalysts. For example, $[\text{MoCl}_2\text{O}_2]$ catalyzes the hydrosilylation of aldehydes and ketones, as does $[\text{Re}(\text{O})_2(\text{PPh}_3)_2]$ (see section 7.3.4). Since the molybdenum complex is in the highest oxidation state for that triad, an oxidative addition reaction with the silane is precluded. Thus, how does the $\text{Si}-\text{H}$ bond become activated to promote the reduction reaction and do other metals in high oxidation states follow suit? In the calculation study for a catalyzed hydrosilylation of an aldehyde by $[\text{MoCl}_2\text{O}_2]$, three pathways involving [2+2]- and [3+2]-additions for the activation of the $\text{Si}-\text{H}$ bond were considered and the transition states are depicted in Figure 24.^{496b} The final step in the sequence produces $[\text{MoCl}_2(\text{H})(\text{O})(\text{OSiH}_3)]$ from A, $[\text{MoCl}_2(\text{OSiH}_3)(\text{OH})]$ from B, and $[\text{Mo}(\text{Cl})_2(\text{O})(\text{OH})(\text{SiH}_3)]$ from C. The lowest-energy pathway was found to be through the transition state A in Figure 24, and it was used to calculate the free energy profiles for the concerted reduction of the aldehyde (through transition state A in Figure 25) and the classical reduction (through transition state B in Figure 25) followed by silyl migration and loss of the silyl ether, $\text{H}_3\text{SiOCH}_2\text{CH}_3$. The energies of the two mechanisms are similar for the gas-phase calculation, but if solvent effects are included and HSiMe_3 is used as the silane, the classical mechanism is favored. However, the energy of a radical pathway then becomes competitive.^{496b}

7.3.4. Mn Triad

One of the earlier nonclassical complexes where the SiH interaction was studied as a function of the silicon substituents was based on $\text{Cp}'(\text{OC})_2\text{Mn}(\text{HSiR}_3)$, and these earlier studies were summarized by Schubert.⁴ Of particular interest has been the complex formed from $\text{HSiR}_3 = \text{HSiCl}_3$. Earlier

PES studies were interpreted in terms of full oxidative addition of HSiCl_3 to give $\text{Cp}'(\text{OC})_2(\text{H})\text{MnSiCl}_3$ where Mn exhibits a d^4 configuration, although some residual $\text{Si}\cdots\text{H}$ interaction might remain.^{492a-c} However, some question remains as to whether the assignment of a classical HSiCl_3 complex was correct. One of the reasons behind this uncertainty is the interpretation of the J_{SiH} values for $\text{Cp}'(\text{OC})_2(\text{H})\text{MnSiCl}_3$ compared to the complexes formed from other hydrosilanes. The value observed for J_{SiH} of the HSiCl_3 complex is in the range that has been assigned to silane σ -complexes. However, the J_{SiH} for free HSiCl_3 is ~ 400 Hz, whereas for most other hydrosilanes the uncomplexed J_{SiH} values usually range near 200 Hz. Thus, the extent of the change upon complexation of HSiCl_3 is much larger than for other hydrosilanes. Five separate studies including calculations of various model compounds, generally based on more sophisticated calculations than used in the earlier studies, have been published, some of which suggest a nonclassical interpretation for $\text{Cp}'(\text{OC})_2(\text{H})\text{MnSiCl}_3$. The more recent calculations (2000–2008) include a frontier orbital model study with modern density functional methods and more extensive basis sets,⁴⁹³ as well as an AIM study.⁴⁹⁴ There is by no means uniform agreement amongst these studies, and only the basic aspects of the arguments will be presented below. A time-dependent DFT method⁴⁹⁵ has also been used to develop an approach to transition metal hydrosilane complexes using the model complex $[\text{Cp}(\text{OC})_2\text{Mn}(\text{SiH}_4)]$.

The earliest of the five reports was that of Lin and coworkers.⁴⁵⁸ A series of model complexes $\text{Cp}(\text{OC})_2\text{Mn}[\eta^2\text{-H}(\text{SiCl}_n\text{H}_{3-n})]$ ($\text{M} = \text{Mn}(2), \text{Tc}(3), \text{Re}(4); n = 1$ (a), 2 (b), 3 (c)) were calculated at the MP2 and B3LYP levels.⁴⁵⁸ The bond lengths for $\text{M}\cdots(\eta^2\text{-HSi})$ for 2c (i.e., $\text{Cp}(\text{OC})_2\text{Mn}[\eta^2\text{-HSiCl}_3]$) were in good agreement with the X-ray structure for $\text{MeCp}(\text{OC})_2\text{Mn}(\eta^2\text{-HSiCl}_3)$. Geometry optimization for $\text{Cp}(\text{OC})_2\text{Mn}(\eta^2\text{-HSiFH}_2)$ as a model for the complex $\text{MeCp}(\text{OC})_2\text{Mn}(\eta^2\text{-HSiFPh}_2)$ that had been structurally characterized by neutron diffraction also showed good agreement in bond lengths. The calculations indicate that successive substitution of H atoms by Cl atoms resulted in a decrease in the $\text{M}-\text{Si}$ distance of >0.05 Å as n changed from 1 to 3, although the $\text{M}-\text{H}$ distance appeared to remain constant. The change in $\text{Si}\cdots\text{H}$ distances were a function of the calculation level and showed either little change (B3LYP) or a modest decrease (MP2). However, the $\text{Si}\cdots\text{H}$ distances increased from Mn to Tc to Re with $\text{Si}\cdots\text{H}$ distances >2.0 Å for Re. The authors attributed the increasing distance to an increase in classical character for the heavier elements (i.e., OA). The dissociation energies for the silane from the metal center were also calculated with slightly different results as a function of the calculation method. Not unexpectedly, the dissociation energies increased with increasing Cl substitution at silicon, which would result from the increase in $\text{M}-\text{Si}$ interactions and should not be attributed to the $\text{H}-\text{Si}$ interaction.⁴⁵⁸

In earlier studies, Lichtenberger had proposed a frontier molecular orbital model that accounted for the original electronic structure as well as photoelectron data, and even with more modern computational tools, the model was substantially correct.⁴⁹³ The LUMO for the model $[\text{Cp}(\text{OC})_2\text{Mn}]$ fragment is predominantly a Mn d_{z^2} , which is a strong acceptor for an incoming ligand on the z axis, and the HOMO is a predominantly metal d_{yz} orbital, which can participate in π -back-bonding to the ligand on the same

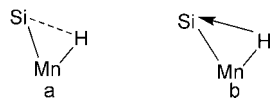


Figure 26. Valence bond depictions of a residual Si–H interaction in $\text{Cp}(\text{CO})_2\text{MnHSiCl}_3$.⁴⁹³

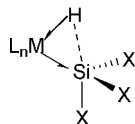


Figure 27. Depiction of residual Si–H interaction in $\text{Cp}(\text{OC})_2\text{Mn}(\text{HSiCl}_3)$ in the calculation by Lin and co-workers⁴⁵⁸ as depicted by Nikonov.^{497a}

axis. The interaction of these frontier orbitals with HSiCl_3 produced an antisymmetric combination of the Mn–Si and Mn–H bonds that were localized more on the silicon center. The calculated and experimental Mn–H distances (1.570 and 1.471, respectively) are in the range of a “normal” covalent Mn–H bond. Since values for M–H determined by X-ray diffraction are systematically short, the agreement is considered good. The calculated H–Si bond population in the model complex is reduced by 75% relative to the calculated bond population in HSiCl_3 . From a comparison of the J_{SiH} values observed for $\text{Cp}'(\text{OC})_2(\text{H})\text{MnSiCl}_3$ and for the classical complex $(\text{OC})_4(\text{H})\text{Fe}(\text{SiCl}_3)$, the formation of $\text{Mn}(\text{H})\text{-(SiCl}_3)$ was considered $\sim 80\%$ complete and the oxidative addition is considered 85% complete in agreement with the 75% loss of Si–H bond population in the electronic structure calculations. From a valence bond model, the experimental Si–Mn–H angle suggested that the silyl and hydride ligands were at optimum coordination sites for the metal d hybrid orbitals with donation of hydride density toward the silyl ligand as shown in Figure 26. This representation is consistent with the prediction of Lin⁴⁸³ that when Si and H are *cis* to each other, some residual bonding interaction between the two centers will be observed. A more lengthy analysis utilizing the quantum theory of atoms in molecules (QTAIM) was published by Bader and co-workers,⁴⁹⁴ which complemented the study by Lichtenberger. Although the arguments are more complex, Bader et al. conclude that “the addition complex, while structurally anchored by the Mn–H bond path, is characterized by a flexible interaction of the $-\text{SiCl}_3$ group with the Mn and H atoms of the $\text{CpMn}(\text{CO})_2\text{H-}$ group.”⁴⁹³

The classical versus nonclassical question for $\text{Cp}(\text{OC})_2\text{Mn}(\text{HSiCl}_3)$ was also addressed by Nikonov, who argued that, because the J_{SiH} for HSiCl_3 was significantly larger than that observed for HSiR_3 ($\text{R} = \text{alkyl, aryl}$), then if bonding between the H and Si remained in the HSiCl_3 complex, “the J_{SiH} value for the *same degree of oxidative addition* of the Si–H bond to the metal should be higher than the coupling constant in a complex of HSiR_3 .”^{497a} Thus, comparable values for coupling constants could be observed for both $\text{L}_m\text{Mn}(\text{HSiCl}_3)$ and $\text{L}_m\text{Mn}(\text{HSiR}_3)$, although the degree of Si–H oxidative addition would not be the same. Nikonov also suggested that some residual Si–H bonding also occurred and formation of a nonclassical silane complex $\text{Cp}(\text{OC})_2\text{Mn}(\text{HSiCl}_3)$ was consistent with Lin’s calculation⁴⁵⁸ and the formulation shown in Figure 27.^{497a}

In the most recent discussion of the bonding in $\text{Mn}(\eta^2\text{-SiH})$ complexes involving charge density analysis, Scherer, McGrady, and co-workers examined the relevant distances in three complexes: $\text{Cp}'\text{Mn}(\text{CO})_2(\eta^2\text{-HSiXPh}_2)$ ($\text{X} = \text{H, F}$),

both of which have been studied by neutron diffraction methods,^{89a,b} and compared the results to the third complex, $\text{Cp}'\text{Mn}(\text{CO})_2(\text{HSiCl}_3)$. The Si–H distances in the two HSiX-Ph_2 complexes are identical within the range of experimental error as are the Mn–H distances. The HSiCl_3 complex is classified as an oxidative addition product by PE spectrum, but the similarity in the SiH, MnH, and $\text{Mn}\cdots\text{H}\cdots\text{Si}$ angle for the three complexes does not support the OA assignment. Only the $\text{Mn}\cdots\text{Si}$ distance appears to discriminate between the HSiFPh_2 and HSiHPh_2 complexes and that of the HSiCl_3 complex. The authors proposed that the addition of the Si–H to the Mn center may occur in an asymmetric manner (with the hydride “leading”); thus, the three complexes are all products of asymmetric OA but with various stages of Si–Mn bond formation. A full paper contains an extensive discussion of the calculation methods utilized in the study.^{89d} The overall result is that the stage of OA was controlled by the substituents on the 5-coordinate silicon but mainly by the ligand *trans* to the $(\eta^2\text{-SiH})$.^{89a} The formation of Mn–Si and the activation of the $\eta^2\text{-HSi}$ are controlled by the extent of $\text{Mn} \rightarrow \sigma^*(\text{X-Si-H})$ back-donation, which, in turn, increases with increasing electron-withdrawing character of the X substituent in the position *trans* to the coordinated Si–H bond. The theoretical charge density studies demonstrate that all three atoms of the $\text{Mn}(\eta^2\text{-HSi})$ unit contribute to a similar extent to the density at the Mn–Si bond critical point.

The model complex, $[\text{Cp}(\text{OC})_2\text{Mn}(\text{SiH}_4)]$, was studied by time-dependent DFT methods (B3LYP).⁴⁹⁵ The silicon was constrained to tri-*n*-butyl phosphate (TBP) coordination as a donor–acceptor complex (related to Nikonov’s approach) with the metal unit in an equatorial position, and the structure was then allowed to relax to the minimum-energy structure. The minimum-energy structure obtained was that which resulted from migration of an equatorial hydrogen atom to a bridging position between the Mn and Si atoms. The results were interpreted in terms of a pseudo-Jahn-Teller interaction in the TBP geometry. The possible influence of substituents at silicon on the structure was not addressed in this report.

The nonclassical bonding of HSiR_3 ($\text{R} = \text{more electro-positive substituent}$) with $[\text{Cp}'\text{Mn}(\text{CO})_2]$ is accepted, but the nature of the bonding when HSiR_3 contains a more electro-negative substituent still seems to have engendered differences in interpretation, one of which favors a hypervalent silicon model. The weight of the evidence favors a greater degree of oxidative addition to the Mn center for HSiCl_3 , but what appears to be at issue is the extent of residual interaction between the hydride and the silicon center, although the arguments of Lichtenberger and Bader seem to be more persuasive for some residual donation of Mn–H to Si.

The Si–H activation by the photolysis product formed from $\eta^5\text{-CpM}(\text{CO})_3$ ($\text{M} = \text{Mn, Re}$) in neat Et_3SiH was studied by Harris and co-workers by femtosecond and nanosecond pump-probe spectroscopic methods^{165a} as described earlier for the $\eta^5\text{-CpV}(\text{CO})_4/\text{Et}_3\text{SiH}$.¹⁴¹ As in the V case, photolysis of $\eta^5\text{-CpMn}(\text{CO})_3$ led to both singlet and triplet states of $\eta^5\text{-CpMn}(\text{CO})_2$ with the former being the higher-energy state, but for $\eta^5\text{-CpRe}(\text{CO})_3$, only a singlet state was observed. In both cases, the unsaturated carbonyls were solvated by Et_3SiH through either the Si–H or the C–H of an ethyl group. The intermediates were modeled by complexation of the $\eta^5\text{-CpMn}(\text{CO})_2$ fragment with ethane and the final products by $\eta^5\text{-CpMn}(\text{CO})_2(\text{H})(\text{SiH}_2\text{CH}_3)$,

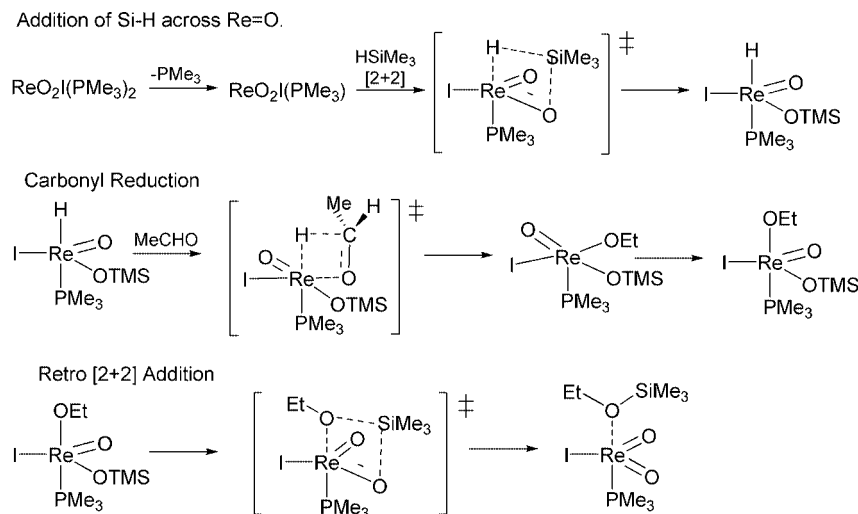


Figure 28. Lowest-energy pathway for reduction of RCHO by R_3SiH by $\text{ReO}_2\text{I}(\text{PMe}_3)_2$.^{497e}

optimized at the MP2/lan12dz level of theory. The solvation through Si-H led directly to the final products, a σ -complex, $\text{Cp}(\text{OC})_2\text{Mn}(\eta^2\text{-HSiEt}_3)$, for the Mn case and to the OA addition product for Re, $\text{Cp}(\text{OC})_2\text{Re}(\text{H})(\text{SiEt}_3)$. The calculated Si-H bond lengths in the products were 1.90 Å for Mn and 2.35 Å for Re. The authors viewed the $\text{Si} \cdots \text{H}$ distance in the Re complex as indicating complete cleavage of the Si-H bond, although Lin⁴⁸³ has argued that this could still indicate a weak attractive interaction. One of the most interesting results was the measurement of the time scale for Si-H bond cleavage, which was 4.4 ± 2.6 ps compared to 230 s for a $\text{sp}^3\text{-C-H}$ bond and which implies a very low barrier for the Si-H reaction.^{165a}

High-valent rhenium complexes have been developed as popular catalysts for the reduction of carbonyls by hydrosilanes. Active catalysts include Re_2O_7 , MeReO_3 , CpReO_3 , $[\text{ReO}_2\text{Cl}(\text{DMSO})_2]$, $[\text{ReO}_2\text{Me}(\text{PhC}\equiv\text{CPh})]$,^{497b} and $[\text{ReOCl}_3\text{-(PPh}_3)_2]$,^{308b,497b}, $[\text{Re}(\text{O})(\text{hoz})_2][\text{TFPB}]$ ($\text{hoz} = 2\text{-(2'-hydroxyphenyl)-2-oxazoline(-)}$), $\text{TFBP} = [\text{B}(\text{C}_6\text{F}_5)_4]$,^{497c} $[\text{Re}(\text{O})(\text{salen})(\text{Solv})][\text{B}(\text{C}_6\text{F}_5)_4]$ (salen , dianion of 1,2-bis(salicylidene)ethylene-diamine; salpn , dianion of 1,3-bis(salicylidene)propyldiamine),^{497d} and $[\text{Re}(\text{O})(\text{salpn})(\text{Solv})][\text{B}(\text{C}_6\text{F}_5)_4]$.^{497d} Abu-Omar and co-workers favored a reaction of the hydrosilane with the rhenium complex through formation of a $\eta^2\text{-H-SiR}_3$ interaction with an empty coordination site at the metal,^{308b,497c,d} and Royo and Romão considered both a $[2+3]$ -addition to the ReO_2 unit and a $[2+2]$ -addition across one of the M=O bonds.^{497b} However, in none of these papers was a speculated mechanism supported by calculation methods. A computational study by Wu and coworkers used the model $\text{ReO}_2\text{I}(\text{PMe}_3)_2$ with the smaller phosphine replacing PPh_3 in the actual catalyst to determine the lowest-energy pathway for the sequence: (1) addition of the Si-H bond to one of the two ReO_2 bonds; (2) reduction of the carbonyl; and (3) retro- $[2+2]$ -addition.^{497e} The lowest-energy pathway was calculated to start with a $[2+2]$ -dissociative mechanism as shown in Figure 28, followed by carbonyl reduction and a retro- $[2+2]$ -addition to provide the product EtOSiMe_3 and regenerate the catalytically active complex. Other higher-energy pathways are described by the authors as were calculations using the silanes H-SiCl_3 (a commonly used hydrosilylation substrate) and silacyclobutane, $(\text{CH}_2)_3\text{SiMeH}$, as substrates. The barriers for the dissociative $[2+2]$ were decreased with these two silanes; however, a $[2+2]$ -addition of a Si-Cl

bond to the Re=O bond was lower in energy than the addition of the HSi bond in HSiCl_3 , suggesting that this silane would not be a good substrate to use with high-valent oxometal complexes. Calculations for monooxo rhenium complexes were also briefly described, but the results indicated that such systems would not be as effective as the dioxo complexes due to a stronger Re=O bond in the monooxo complexes. Several other Si-H activation processes were also calculated including a metathesis-like pathway, but none were competitive with the cycle developed for $\text{ReO}_2\text{I}(\text{PMe}_3)_2$. The metathesis pathway was proposed by Abu-Omar and co-workers for the cationic complex, $[\text{ReO}(\text{hoz})_2]^+$,^{497c} and Wu and co-workers suggested that it was possible that cationic complexes may operate by a different mechanism.

7.3.5. Fe Triad

DFT calculations for a series of related complexes of the iron fragment $[\text{Cp}(\text{L})\text{Fe}]$ ($\text{L} = \text{CO}, \text{PR}_3$) were developed to probe for potential nonclassical interactions.⁴⁷¹ The model systems studied included $[\text{Cp}(\text{OC})\text{Fe}(\text{SiMe}_n\text{Cl}_{3-n})_2\text{H}]$, $[\text{Cp}(\text{Me}_3\text{P})\text{Fe}(\text{SiMe}_n\text{Cl}_{3-n})_2\text{H}]$, $[\text{Cp}(\text{OC})\text{Fe}(\text{SiMe}_n\text{Cl}_{3-n})\text{H}(\text{Me})]$, and $[\text{Cp}(\text{OC})\text{Fe}(\text{SiMe}_n\text{Cl}_{3-n})\text{H}_2]$ ($n = 0-3$ for all 4; total of 12 complexes). Except for $[\text{Cp}(\text{OC})\text{Fe}(\text{SiCl}_3)_2\text{H}]$,⁴⁹⁸ the compounds have not been reported. The complex $[\text{Cp}(\text{OC})\text{Fe}(\text{SiCl}_3)_2\text{H}]$ was one of the first for which an experimental measurement was reported for J_{SiH} , and the value of 20 Hz was subsequently viewed as indicating no interaction between the hydride and silyl ligands. One of the reasons for the calculation study was the determination of the conditions for formation of a classical ligand set $\text{R}_3\text{Si}(\text{H})(\text{X})$ versus a nonclassical set $(\text{R}_3\text{Si})(\eta^2\text{-HX})$.⁴⁷¹ A range of interactions was indicated from the calculations for the 12 complexes. For $[\text{Cp}(\text{OC})\text{Fe}(\text{SiMe}_n\text{Cl}_{3-n})_2\text{H}]$ ($n = 0-3$), the calculated structures converged to a nearly symmetric C_s geometry. For $[\text{Cp}(\text{OC})\text{Fe}(\text{SiCl}_3)_2\text{H}]$, the calculated and observed geometries agreed. Overall, the Si-H distances varied only from 2.030 to 2.075 Å in the series and were consistent with some attractive interaction between the silyl and hydride ligands. The authors suggested that the complexes could be described as edge-bridged pseudo-octahedral compounds rather than piano-stool complexes if the Cp ligand was viewed as occupying a face of the octahedron. The complex could then be described by an MO interaction

diagram between $(\text{R}_3\text{Si}-\text{H}-\text{SiR}_3)^-$ and the cationic metal fragment, $[\text{Cp}(\text{OC})\text{Fe}]^+$, thus bearing an analogy to H_3^- as Nikonov had described earlier (section 7.2), and would account for distortion from the ideal piano-stool geometry.^{5a} Mayer bond orders (MBOs) and Wiberg bond orders (WBOs) were determined and fell within the range 0.146–0.192 for the MBO calculations. The WBOs were slightly larger and ranged from 0.202 to 0.208, also supporting some bonding interaction between the silyl and hydride ligands. When PMe_3 replaced the CO ligand to give $[\text{Cp}(\text{Me}_3\text{P})\text{Fe}(\text{SiMe}_n\text{Cl}_{3-n})_2\text{H}]$ complexes, the structures were best viewed as having an edge-bridged distorted octahedral geometry. In this case, however, the Si–H distances were shorter and the complexes were asymmetric with two different Si–H distances. No explanation was proposed for the strengthening of the Si–H interactions in the phosphine-substituted complex. The interligand bonding in the two sets of complexes was considered different to that observed in silane σ - or IHI complexes.

The $[\text{Cp}(\text{OC})\text{Fe}(\text{SiMe}_n\text{Cl}_{3-n})\text{H}(\text{Me})]$ compounds exhibited very short Si–H separations in the range 1.822–1.856 Å and, thus, were considered consistent with σ -complexes. A bond critical point between H and Si confirmed this nonclassical Si–H bonding. Results for the last set of complexes, $[\text{Cp}(\text{OC})\text{Fe}(\text{SiMe}_n\text{Cl}_{3-n})\text{H}_2]$, fell into three groups: (a) large Si–H separations (~ 2.25 Å) and H–H distances ~ 1 Å consistent with a dihydrogen complex (favored by electron-withdrawing substituents as silicon); (b) nonclassical bis(hydride) complexes with some Si–H interactions; and (c) $[\text{Cp}(\text{OC})\text{Fe}(\text{SiMe}_2\text{Cl})\text{H}_2]$, which coexists with its dihydrogen isomer and was similar to that observed in hydride(dihydrogen) complexes with a *cis* effect. The bonding in this last case was considered electron deficient. Thus, there appears to be a range of Si–H–M interactions supported by the $[\text{Cp}(\text{OC})\text{Fe}]$ fragment. The results of the AIM analyses indicated a Si–H bond path if the Si–H distance was less than ~ 1.9 Å. At longer distances, the bond path disappears into M–H and M–Si bonds even though Mayer bond indices may be >0 .⁴⁷¹

Also included in this report were calculations of hydride chemical shifts and coupling constants for the hydride and silyl ligands in the 12 complexes.⁴⁷¹ The value of $^{\text{obs}}J$ was also reported for the computed coupling constant averaged according to the Boltzmann distribution, since the computed J_{SiH} constants depended on the orientation of the silyl ligand. As discussed previously, the sign of J_{SiH} is important for the determination of the presence of Si–H–M nonclassical bonding, and if the sign is negative, then a direct one-bond H–Si is indicated. The sign of $^{\text{obs}}J_{\text{SiH}}$ was reported for 8 of the 12 complexes and all but one were negative, although the value of the last complex was small enough to be outside the accuracy of the calculation. The signs of $^{\text{obs}}J_{\text{SiH}}$ for the “dihydride” complexes were also negative, even though in these complexes essentially no Si–H interaction was revealed in the calculations. The next task will be to synthesize the complexes based on the $\text{Cp}(\text{OC})\text{Fe}$ fragment to see if the computational predictions of the various roles for $\text{Fe}\cdots\text{H}\cdots\text{Si}$ can be matched by generation and/or isolation of complexes.

A DFT study of catalytic silane alcoholysis at a $[\text{Cp}(\text{OC})(\text{R}_3\text{P})\text{Fe}]^+$ center included formation of $[\text{Cp}(\text{OC})(\text{R}_3\text{P})\text{Fe}(\eta^2\text{-H}-\text{SiR}_3)]^+$ in the first step of the catalytic cycle.^{499a} The model used in the calculations (BP86/AE1) was $[\text{Cp}(\text{OC})(\text{H}_3\text{P})\text{Fe}(\eta^2\text{-H}-\text{SiH}_3)]^+$ with the coordinated Si–H = 1.780 Å and the Fe–H = 1.542 Å and similar to

the related neutral complex of manganese, $\text{Cp}'(\text{OC})(\text{Me}_3\text{P})\text{Mn}(\eta^2\text{-H}-\text{SiHPh}_2)^{499b}$ in the solid. As the MeOH approaches the silicon center in the cationic complex, the Si–Fe is practically cleaved (Si–Fe = 2.903 Å) and the Si–H shortens (Si–H = 1.705 Å) in the nearly trigonal-bipyramidal coordination geometry about the Si (H–Si–O = 163°).

Calculations were reported in synthesis/characterization papers for two sets of complexes to clarify the role of the hydrides. One set involved the tripodal ligands, tris(phosphino)borate in the iron complex **1-37**⁴⁵ and hydridotris(pyrazolyl)borate^{48a} in the ruthenium complexes **1-40**, **2-37**, and **3-103**. Another set involves ruthenium complexes containing the general unit $(\text{Cy}_3\text{P})_2(\text{H})_2\text{Ru}(\text{silane})$ in **3-127**,^{208,209,500} **3-128**,^{208,209} **3-129**,^{101,210a} and **3-132**,²¹² as well as the related dimers **2-45**^{100,101} and **3-144a**¹⁰¹ and still another set of novel complexes formed from reactions of $(\text{Cy}_3\text{P})_2(\text{H})_2\text{Ru}(\eta^2\text{-H}_2)_2$.

DFT calculations (B3LYP/LACVP**) for $[(\text{PhBCH}_2\text{P}'\text{Pr}_3)\text{-Fe}(\text{H})(\eta^3\text{-H}_2\text{SiPhMe})]$, **1-37**, gave two short (1.47–1.55 Å), one long $\text{Si}\cdots\text{H}$ (2.07 Å), and three Fe–H distances between 1.48 and 1.57 Å that were in good agreement with the X-ray determination and consistent with an $\eta^3\text{-H}_2\text{SiR}_2$ arrangement in the complex.⁴⁵ The NBO analysis predicted two Si–H bonding orbitals, one Fe–H bonding orbital, and no bonding orbital between Si and Fe, thus leading to the assignment of the two indicated Si–H short bonds to an η^3 -silane adduct of an Fe(II) hydride and not that of an Fe(IV) silylene trihydride.⁴⁵

Although Fe(II) complexes appear to be classical hydrides, Fe(I), Fe(III), and many Fe(IV) complexes contain $\eta^2\text{-HSiR}_3$. The reaction of hydrosilanes with $\text{Cp}(\text{MePr}_2\text{P})\text{FeH}$ does not appear to occur through the more conventional OA or silane σ -complexation but starts with $\text{Si}-\text{H} \rightarrow \text{Fe}$ donation and ends with a structure with $\text{H}\cdots\text{SiR}_3\cdots\text{H}$ bonding (see, for example, **1-33a**, **3-68a**, and Table 3, footnote 74).^{42a} DFT calculations indicated that the activation proceeds without a barrier and begins at an $\text{Fe}\cdots\text{Si}$ separation of 3.0 Å. The final structure shows the presence of two simultaneous, equivalent $\text{Si}\cdots\text{H}$ interactions with an Si–H distance of 2 Å and $\text{MI} = 0.18$. It also appears that the extent of the bonding interaction is independent of the other substituents on silicon or on the orientation of the silyl group (model complexes, $\text{Cp}(\text{Me}_3\text{P})\text{FeH}_2(\text{SiMe}_{3-n}\text{Cl}_n)$ ($n = 0-3$). The calculated J_{SiH} values varied from ~ 0 to 40 Hz (experimental values were close to 20 Hz) and are negative, which supports direct Si–H bonding. The authors preferred a bonding description involving a hypervalent anion $[\text{H}_2\text{SiR}_3]^-$ and the metal fragment $[\text{Cp}(\text{L})\text{Fe}]^+$.^{42a}

The NMR data for the six isolated complexes of the general formula $\text{TpRu}(\text{PPh}_3)_2\text{H}_2\text{SiR}_3$ did allow assignment of the stereochemistry around the metal center. Calculations (B3LYP level) for four isomers of $\text{TpRu}(\text{PPh}_3)_2\text{H}_2\text{SiR}_3$ utilizing the model $[\text{HB}(\text{NH}-\text{N}=\text{CH}_2)_3]\text{Ru}(\text{PPh}_3)_2\text{H}_2\text{SiH}_3$ were described in Case 2 in section 5.3, and the basic aspects of the isomers that were calculated are illustrated in Figure 7. The most stable isomer is shown as **A** in Figure 7 (described as an unsymmetrical *trans*-dihydride). There were two Ru–H distances of 1.610 and 1.629 Å; the more stretched Ru–H hydride was 1.823 Å from silicon, and the shorter hydride distance from silicon was 2.108 Å. Initially, this longer Ru–H \cdots Si distance was interpreted as showing the absence of significant Si–H interaction, but it is within the distance found in complexes that exhibit SISHA interactions. A second isomer (**D** in Figure 7) also exhibited an

η^2 -silane coordination and was 1.9 kcal/mol higher in energy than isomer **A**. The two isomers are in equilibrium with a 7.5 kcal/mol barrier between the two forms. The possibility of a nonclassical η^2 -H₂ coordination was also eliminated.^{48a}

The second set of complexes started with the isolation of the novel [RuH₂{(η^2 -HSiMe₂)₂X}(PCy₃)₂] (X = C₆H₄, **3-127**; O, **3-128**) complexes with a *trans*-spanning chelating silane, as reported first in 1997²⁰⁹ with the full paper including additional examples appearing in 1999.²⁰⁸ The factors that influenced the stability of the *trans*-bis(H \cdots Si) arrangement in this series of complexes was explored in DFT calculations of the model [RuH₂{(η^2 -HSiH₂)₂CH=CH}(PH₃)₂]. The geometry optimizations were performed with overall *C*_{2v} symmetry (*C*₂ axis bisecting the P–Ru–P angle) as well as with *C*₁ symmetry. For comparison, the unchelated analogue, [RuH₂(η^2 -HSiH₃)₂(PH₃)₂], was also optimized with both *C*_{2v} and *C*₁ symmetries. The structure of the chelated complex with *C*_{2v} symmetry was in reasonable accord with bond distances observed in **3-127**, although the P–Ru–P angle was 14° smaller than the experimental value of 109°. Optimization with PMe₃ ligands instead of PH₃ reduced the angle difference to 10°. The analysis of the Laplacian of the valence electron density suggested weakened H_{ax} \cdots Si “bonds” indicating a significant degree of Ru \rightarrow (H \cdots Si)* back-donation. The NBO analysis showed an ON of \sim 1.5, indicating occupation of the H \cdots Si antibonding orbital and also consistent with the observed/calculated distances. The unchelated model complex exhibited a distortion of the two H \cdots Si coordinated units, similar to the chelated system but with somewhat less σ^* -back-donation. Relaxing the symmetry constraints did not produce a new structure for [RuH₂{(η^2 -HSiH₂)₂CH₂CH₂}(PH₃)₂], but for the unchelated complex, another isomer was located that was 1.6 kcal/mol more stable than the *C*_{2v} isomer and had a structure intermediate between the one with *C*_{2v} constraints and a square antiprism. The structural features of **3-127** were rationalized by a qualitative molecular interaction scheme, which included the distortion of the nearly *trans*-dihydride configuration observed in the actual complex. In the undistorted complex, the two Si–H bonds would compete for σ^* -back donation. In the distorted complex, utilization of the d_{yz} and d_{x²–y²} is possible with the H \cdots Si σ^* -orbitals in a cooperative rather than a competitive interaction. The HOMO, mainly the d_{xz} orbital, is not affected by the distortion. The *C*_{2v} symmetry observed in these complexes is a balance of electronic, structural, and steric factors.⁵⁰⁰ In the full report, DFT calculations (discussed briefly as Case 5 in section 5.3) by means of two hybrid functionals B3LYP and B3PW91 also used the same model, [RuH₂{(η^2 -HSiH₂)₂X}(PH₃)₂] (X = (CH)₂, C₆H₄, (CH₂)_n, O, and OSiH₂O).²⁰⁸ Five isomers with pseudo-octahedral geometry are possible in principle, but the two with mutually *trans*-hydrides were considered too high in energy. Therefore, three structures (X = C₆H₄) were characterized on the singlet potential energy surface: **A** with *cis*-hydrides and *cis*-phosphines, **B** with a *cis*-HSi \cap SiH, two *cis*-phosphines that are each *cis* to a hydride, and **C** with a *cis*-HSi \cap SiH, *cis*-hydrides, and *trans*-phosphines. A comparison of the two levels of calculation showed only trivial differences. The relative energies of the three isomers for the complex with X = CH₂CH₂ were also similar. Isomer **A** was the lowest energy form with the Si–H bonds participating in the η^2 -coordination mode elongated by \sim 24%. Isomer **B** (*C*₁ symmetry) was 7.6 kcal/mol less stable than **A**, but the

coordinating Si–H bonds are *trans* to two different substituents; thus, the Si \cdots H distances are different with one bond (*trans* to a hydride) much more activated than the other. Isomer **C** (*C*_{2v}) has a calculated P–Ru–P angle of \sim 170° with a Si–H stretch of only 15%, thus less activated than in the other two isomers. Isomer **C** lies 11 kcal/mol above isomer **A**. For the remaining complexes, RuH₂{(η^2 -HSiH₂)₂(CH₂)_n}(PH₃)₂ (*n* = 1–4), only the structure corresponding to **A** was optimized (B3LYP level). The optimized geometry for *n* = 2 with *C*_{2v} symmetry was a transition state. The minimum, 3.30 kcal/mol below the transition state, exhibited *C*₂ symmetry, as did the complexes with *n* = 3 or 4. The complexed Si–H bond distance was comparable to that of isomer **A** for [RuH₂{(η^2 -HSiH₂)₂CH₂CH₂}(PH₃)₂], indicating a similar degree of activation. The complex where *n* = 1 with unconstrained optimization gave a *C*₁ structure. The complex with X = O also gave a minimum with no symmetry and the chelate with *cis* (η^2 -H–Si) coordination, one *trans*-HRuP, and one *cis*-HRuP. Thus, the H–Si *trans* to the phosphine was more activated than the H–Si *trans* to the hydride. With X = OSiH₂O, whose minimized structure also belongs to *C*₁ symmetry, both coordinated Si–H bonds are activated to approximately the same degree. The binding energies for the eight complexes show a variation from 31.0 to 44.9 kcal/mol, and the authors concluded that the electronic binding energies differ as a function of the bridging group X.⁵⁰⁰

At a later date, the related disilazane complex **3-132**, [(Cy₃P)₂H₂Ru{(η^2 -HSiMe₂)₂NH}] was reported²¹² and had a structure similar to the calculated structure for the related siloxane complex. However, in the case of **3-132**, an X-ray crystal structure was obtained that verified the *cis* arrangement for the chelate, and all the hydrides in the coordination sphere of the metal could be located. When the silazane structure was compared to the calculated model (DFT/B3LYP level; see also discussion in section 6.1.2) for [RuH₂{(η^2 -HSiH₂)₂O}(PH₃)₂], it became obvious that there was a poor match between the X-ray parameters and the calculated parameters. Therefore, the disilazane complex was calculated using the B3PW91 functional, where the agreement was better for the optimized disilazane isomers [(H₃P)₂-H₂Ru{(η^2 -HSiH₂)₂NH}] as well as the actual complex [(Cy₃P)₂H₂Ru{(η^2 -HSiMe₂)₂NH}]. The disiloxane isomer [(H₃P)₂H₂Ru{(η^2 -HSiH₂)₂O}] was also recalculated with the B3PW91 functional. With the actual complex, the calculated (B3PW91) Ru–Si distances were 2.416 and 2.490 Å compared to 2.395(2) and 2.434(2) determined by X-ray diffraction, and the coordinated η^2 -H–Si had bond lengths of 1.922 and 1.775 Å compared to the X-ray values of 1.93(5) and 1.91(5) Å, respectively, indicating a similar degree of activation in the *cis*-coordinated chelate. The choice of DFT calculation can be critical in attempts to obtain a calculated structure that is similar to X-ray data (or, for that matter, to determine a suitable structure in the absence of either X-ray data or when hydrides cannot be located).²¹²

Several other reactions of RuH₂(η^2 -H₂)₂(PCy₃)₂ with a variety of hydrosilanes (including the chelating disilyl complexes in the previous two paragraphs) have been reported by Sabo-Etienne and co-workers, and calculations have been included for the majority of the novel complexes that have been produced; these calculations and will be described in the following paragraphs.

Calculations (B3LYP) for the complex (Cy₃P)₂(H)₂(η^2 -H₂)Ru(η^2 -HSiPh₃) (**3-129**; produced from the reaction with

HSiPh₃) were conducted using (H₃P)₂(H)₂(η^2 -H₂)Ru(η^2 -HSiH₃) as the model.^{101,210a} Geometry optimization led to five singlet local minima of which the isomer with C₁ symmetry resembled the general features of the X-ray structure (*cis*-phosphines and *cis*-terminal hydrides). The two nonbonded interactions between the silicon and the two classical hydrides (Si...H distances are >2.0 Å) appear to stabilize the geometry by a weak attractive interaction revealed in the Mulliken population analysis. Similar interactions were later described with the term SISHA, but this appears to be one of the earlier examples of this effect.

When PhMeSiH₂ reacted with RuH₂(η^2 -H₂)₂(PCy₃)₂, disproportionation of the silane occurred and the SiH₄ produced was "trapped" as the complex (PPr₃P)(H)₂Ru(SiH₄)Ru(H)₂-(PPr₃)₂ (Table 2, footnote 52).^{100,101} The complex was modeled by Ru₂H₄(SiH₄)(PH₃)₂, which generated an optimized structure with D_{3d} symmetry that was the minimum on the singlet potential energy surface and agreed with the overall structure obtained from the X-ray data. The calculated Si-H distances are in good agreement with those in the solid state and are stretched 3% by comparison to uncomplexed SiH₄. The reduction of the Wiberg bond indices for the σ -coordinated H-Ru compared to the classical Ru-H bonds reflected the stronger coordination of the former H-Ru bond to silicon. Each Si-H interaction of SiH₄ in the complex reflected a σ -donation to a ruthenium and back-bonding interaction from the second ruthenium. Calculations for the complex Ru₂H₂(μ - η^2 : η^2 -H₂Si(OMe)₂)₃(PCy₃)₂ (**3-144a**, formed from Ru₂H₄(μ - η^2 : η^2 : η^2 : η^2 -SiH₄)(PCy₃)₄ and xs HSi(OMe)₃) were reported at both the DFT/B3LYP and BPW91 levels for the model Ru₂H₂(μ -H₂Si(OH)₂)₃(PH₃)₂ and at the DFT/B3LYP levels for Ru₂H₂(μ -H₂Si(OH)₂)₃(PMe₃)₂, Ru₂H₂(μ -H₂Si(OMe)₂)₃(PH₃)₂, and Ru₂H₂(μ -H₂Si(OMe)₂)₃(PH₃)₂ (with "f" orbital contributions). The overall B3LYP-optimized geometry does not change much in the four model compounds. Each silane bridges the Ru-Ru bond, and the two Si-H bonds are coordinated to the two ruthenium centers with different activation modes (14–20% elongation).¹⁰¹

Two chelates of the type P \cap Si were also reacted with RuH₂(η^2 -H₂)₂(PCy₃)₂ to provide novel mononuclear complexes.^{213c} With Ph₂P(*o*-C₆H₄CH₂SiMe₂H), three different complexes formed: H₂Ru{ η^2 -HSiMe₂CH₂(*o*-C₆H₄)PPh₂}₂, ***3-134b**, with ϵ -agostic SiH interactions, Ru[η^2 -H-SiMe₂(CH(C₆H₄)PPh₂)₂], ***3-134c**, with β -agostic SiH interactions, and RuH{ η^2 -H-SiMe₂CH₂(*o*-C₆H₄)PPh₂} {(η^2 -H-SiMe₂)CH(*o*-C₆H₄)PPh₂}, ***3-134d**, with both ϵ - and β -agostic interactions. Support for key aspects of the assigned structures for these novel complexes was obtained from DFT calculations at the B3PW91 level for a model complex where the PPh₂ unit in **3-134b** was replaced with PH₂. Two isomers calculated for **3-134b** indicated that the isomer with *cis* disposition of the phosphine ligands was the lower in energy of the two. The calculations for **3-134b** gave a value for the Si-H bond length of 1.709 Å, which corresponds to the average of 1.70 Å observed for the two Si-H bonds obtained from X-ray diffraction and is considered in the typical range of η^2 -H-Si bonds. The computed structure is consistent with the ground-state structure shown in the structure section of Table 3 for **3-134d**.^{213c}

The second chelate of the type P \cap Si, Ph₂PCH₂OSiMe₂H, gave a complex with the composition Ru(PPh₂CH₂-OSiMe₂H)₃, ***3-130b**, upon reaction with RuH₂(η^2 -H₂)₂(PCy₃)₂.^{211b} In this case, there is a dangling Me₂SiH group on one of the chelates, and each of the SiMe₂H of the

other two chelates exhibits a different type of Si-H activation. DFT calculations used the *Gaussian 03W* programs with B3PW91 functional for the model complex Ru(H₂PCH₂OSiMe₂H)₂(PH₃) (PH₃ was used to model the η^1 -coordinated phosphinosilane). The dissymmetry associated with the remaining two Si-H bonds was reproduced in the calculation. The WBI for one SiH was 0.15 and for the other Si-H was 0.33 with a RuSi for the former = 0.42 and for the latter = 0.34. The authors concluded that the complex cannot be viewed as a Ru(IV) dihydride species because Si-H bonding is clearly present. However, the observed structure is not that expected for a d⁶ complex with an ideal octahedral geometry and should be better viewed as intermediate between the two arrested structures, as shown in the structure section of Table 3 for **3-130b**.

The reaction of a related Ru(η^2 -H₂) complex, RuClH(η^2 -H₂)(PCy₃)₂, with HSiMe_{3-n}Cl_n provided the complexes RuCl(SiMe_{3-n}Cl_n)(η^2 -H₂)(PCy₃)₂ (see **3-126b** for the RuSiMeCl₂ complex).^{207b} Calculations for the model complex where PMe₃ was used in place of PCy₃ support the formulation of a pseudo-octahedral structure with P-Ru-P angle of ~160° and η^2 -H₂, Cl, and the silyl group *trans* to an empty site. A SISHA interaction was calculated and experimentally determined in the X-ray structure with Si...H distances of 2.204 (DFT) and 2.25(2) (X-ray). The calculations also provide evidence that could be interpreted in terms of σ -CAM mechanism.

Systems with Si=X bonds have been the subject of calculations for both X = Ru^{501a,b} and Os,^{55,501b} although catalytic hydrosilylation was the main focus of one of the studies.⁵⁵ The experimental trapping of Si=C by organometallic ruthenium units has also included results of calculations. Arnold has reported calculations (B3PW91 hybrid functional) for CpL₂Ru=SiX₂⁺ (L = PH₃, PMe₃, CO; X = H, Me, SH) as a model for complexes that have been isolated by Tilley and coworkers and in an effort to rationalize why it has been so difficult to isolate base-free examples of metal silylenes.^{501a} The qualitative orbital interaction of a SiX₂ fragment with a CpL₂Ru⁺ fragment indicated less stabilization of silylene orbitals compared to the related carbene, and thus, the orbitals are not stabilized as well as those of the carbene. The Fenske-Hall calculations indicate that [Cp(Me₃P)₂Ru=SiR₂]⁺ should possess a real Si=Ru double bond. The optimized geometries using BP3PW91 hybrid functional for five model complexes gave Ru-Si distances from 2.215 to 2.259 Å, in reasonable agreement with the base-free structure of [Cp*(Me₃P)₂Ru=SiMe₂][B(C₆F₅)₄].^{499c} The NBO results indicate that all of the Ru-Si cationic complexes consist of a Ru-Si single bond, with some enhancement through a π -bond from donation of a Ru electron pair into the p-orbital on silicon. The natural charges are influenced by the nature of the substituents at silicon with a lower electron population at silicon when methyl substituents are present, causing the silylene to be a weaker donor to the metal center. The p-orbital populations are not perturbed by changing substituents at silicon, suggesting that the charge differences at the metal and silicon centers are a result of changes in the σ -framework. Overall, CpRu silylenes have dative Si \rightarrow Ru σ -bonds with small Ru \rightarrow Si π -back-bonding. The silicon is an electron-deficient center, and even with an electron-rich center as in Cp(R₃P)₂Ru, there is insufficient back-bonding to silicon to give a good π -bond. Arnold suggested that replacing the Cp with a neutral ligand that could donate six electrons giving a neutral complex may

provide a solution. Bulky ligands need to be avoided to prevent a destabilizing twist of the Ru=Si bond, but this, of course, could lead to a highly reactive silylene system.^{501a} The first neutral hydrido(hydrosilylene) complex, $[\text{Cp}^*(\text{OC})(\text{H})\text{Ru}=\text{Si}(\text{H})\{\text{C}(\text{SiMe}_3)_3\}]$ ^{393a} in which there appears to be no interaction of the Ru–H with the silylene silicon stands in contrast to previous observations of the W–H interaction with the silylene silicon in $[\text{Cp}^*(\text{OC})_2(\text{H})\text{W}=\text{Si}(\text{H})\{\text{C}(\text{SiMe}_3)_3\}]$ (Table 1, footnote 30).^{38a} DFT calculations were conducted in an effort to determine the difference in these two systems. The W–H bonding orbital could overlap with the vacant p-orbital on the silylene silicon, but the Ru–H bonding orbital (model used SiH_3 to replace SiMe_3) was actually directed away from the silylene p-orbital; thus, no significant interaction occurred. The difference was attributed to the different geometries at the two metal centers: that for W was a three-legged piano-stool geometry while the Ru center exhibited four-legged piano-stool geometry.^{393a}

The donor alkoxy-bridged bis(silylene)–ruthenium complex, $\text{Cp}(\text{OC})\text{RuSiMe}_2\text{SiMe}_2\text{OMe}$, reacts with MeOH to give the bis(silyl)–ruthenium hydride, $\text{Cp}(\text{OC})\text{RuH}(\text{SiMe}_2\text{OMe})_2$, although this is unlikely to be a general route to such complexes. The mechanism of the ring-opening was studied by DFT methods.^{501d} Four steps in the mechanism were identified starting with formation of hydrogen bonding between the bridging alkoxy group and MeOH, followed by ring-opening of a Ru–Si–O–Si four-membered ring. The hydrogen-bonded intermediate converts to a 6-membered ring where hydrogen bridges the two SiOMe groups and the hydroxyl hydrogen migrates to the ruthenium center in the rate-determining step.

Parameters for the model neutral and charged osmium silylene complexes, $\text{Cp}(\text{H}_3\text{P})(\text{H})\text{Os}=\text{SiH}_2$ (**A**) and $[\text{Cp}(\text{H}_3\text{P})(\text{H})_2\text{Os}=\text{SiH}_2]^+$ (**B**), respectively, were calculated (DFT B3LYP) in the hydrosilylation of ethylene to shed light on why the neutral complex $[\text{Cp}^*(\text{Pr}_3\text{P})(\text{H})\text{Os}=\text{SiH}(\text{trip})]$ (**1-50**) was much less reactive than the cationic complex $[\text{Cp}^*(\text{Pr}_3\text{P})(\text{H})_2\text{Os}=\text{SiH}(\text{trip})][\text{B}(\text{C}_6\text{F}_5)_4]$ (prepared from **1-47** on treatment with $\text{LiB}(\text{C}_6\text{F}_5)_4$)⁵⁴ towards promotion of hydrosilylation of 1-hexene.⁵⁵ The coordination of ethylene to **A** was ~ 8 kcal/mol higher in energy than for the coordination to **B**, and the TS_1 for the insertion of ethylene into the Si–H bond was considerably higher for **A** than for **B**. The LUMOs for both **A** and **B** are primarily silicon p-orbitals, but the LUMO–HOMO energy gap is small for **B**, allowing for better binding of ethylene in **B**. The difference in reactivity may result from resonance contributors such as $[\text{Os}=\text{SiH}_2] \leftrightarrow [\text{Os}^+-\text{SiH}_2^-]$ for **A** and $[\text{Os}=\text{SiH}_2] \leftrightarrow [\text{Os}^+-\text{SiH}_2^-]$ for **B** that place a positive charge at silicon, making it more boron-like (as in a hydroborate). The increase in positive charge on silicon increases Os(II) character for **A** and Os(IV) character for **B**. The Os(IV)/Os(II) distribution was calculated to be $\sim 10/1$ for **A** but $\sim 1/1$ for **B**.

The substituent effect on the silicon–metal bond for four base-stabilized silylene complexes and two base-free ruthenium silylenes was examined by Hartree-Fock ab initio calculations.^{501b} For the complex originally formulated as $\text{Cp}^*(\text{Me}_3\text{P})_2\text{Ru}=\text{Si}[\text{S}(\text{Tol-}p)]\{\text{Os}(\text{CO})_4\}$,^{501c} the overlap population indicated that a better description would be a Si–Ru single bond, a Si=S bond, and a partial double bond for Si–Os. The atomic charge at silicon was the most positive for $[\text{Cp}(\text{Me}_3\text{P})_2\text{Ru}=\text{SiMe}_2]^+$, indicating a significant amount

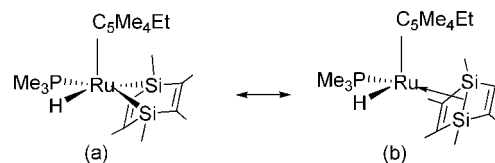


Figure 29. Resonance structures for **3-99**.^{189a}

of electron density in the silicon–ruthenium overlap region. The base-stabilized silylene complexes were of the general form $\text{Cp}^*(\text{Me}_3\text{P})_2\text{RuSiX}_2\cdot\text{Z}$ [$\text{X} = \text{Me}$, $\text{Z} = \text{NCMe}$; $\text{X} = \text{S}(\text{Tol-}p)$, $\text{Z} = \text{NCMe}$, OTf ; $\text{X} = \text{OTf}$, $\text{Z} = \text{S}(\text{Tol-}p)$]. Only $[\text{Cp}^*(\text{Me}_3\text{P})_2\text{RuMe}_2\cdot\text{NCMe}]^+$ had Ru=Si multiple-bond character. The best X groups for promoting multiple-bond character between the metal and the silicon would be methyl followed by the triflate group, and the worst was $\text{S}(\text{Tol-}p)$, as it preferentially formed the multiple bond to silicon. The best base-stabilizing “Z” groups for promoting silylene character were NCMe and OTf^- .^{501b} The bonding in the coordinatively unsaturated ruthenium–silylene complex,³⁹³ $\text{RuCl}(\eta^3\text{-dcpb})(\text{SiL}^{\text{N}_2})$ (dcpb = bis(dicyclohexyl)-1,4-phosphinobutane; $\text{SiL}^{\text{N}_2} = \text{Si}[\text{tBuNCH}=\text{CHN}^+\text{tBu}]$), was described in section 6.3.

An important area of study in organosilicon chemistry involves methods of formation and stabilization of compounds with multiple bonding between silicon and elements other than a metal. One opportunity for stabilization could be the complexation of $\text{Si}=\text{El}$ within a transition metal complex. This has been accomplished by Tilley and co-workers in ruthenium complexes of silabenzene and disilabenzene (**3-99a**; eq 14).^{189a} Two resonance structures (Figure 29) could describe the bonding in the disilabenzene complex of the $\text{Cp}^*(\text{Me}_3\text{P})(\text{H})\text{Ru}$ ($\text{Cp}^* = \text{C}_5\text{Me}_4\text{Et}$) fragment: (a) a Ru(IV) center bound to two silyl ligands that do not interact and (b) a Dewar-disilabenzene with a Si–Si bond coordinated to Ru. The Si–Si separation in the crystal structure was 2.621(2) Å, which is longer than the Si–Si bond distance of 2.244(2) Å in a known disilabenzene; thus, calculations (DFT) were developed for the model $\text{Cp}(\text{H}_3\text{P})(\text{H})\text{Ru}(\eta^2\text{-hexamethyl-1,4-disilabenzene})$ to clarify the nature of the interaction between Ru and the disilabenzene. The relevant distances from the calculated structure are in agreement with the parameters from the X-ray structure. Three of the calculated molecular orbitals exhibited Si–Ru bonding character. One of these MO's is a σ -type orbital that is bonding between the Ru and each of the Si centers but with a node between the two silicons consistent with resonance structure a in Figure 29. The other two MOs are C–C π -bonding orbitals with Ru–Si bonding character and no nodes between the Si–Si centers, consistent with a weak interaction of the Si–Si bond with the Ru center suggested in resonance structure (b, Figure 29). The Ru–Si bonding in the latter two MOs was studied further by interaction of the HOMO obtained for the isolated disilabenzene constrained to the geometry observed in the isolated ruthenium complex.

This HOMO exhibited weak Si–Si σ -bonding character. The contribution of the Si–Si bonding orbital to the Ru–Si bonding was determined through construction of MOs from the Si–Si σ -bonding orbital and those of the $\text{Cp}(\text{H}_3\text{P})\text{RuH}$ fragment. The results were interpreted as showing constructive overlap between the Si–Si σ -bonding orbital and the d orbitals of the Ru center. The MBO calculation gave a Si–Si BO = 0.17 and Ru–Si bond orders of 0.53 and 0.48.^{189a}

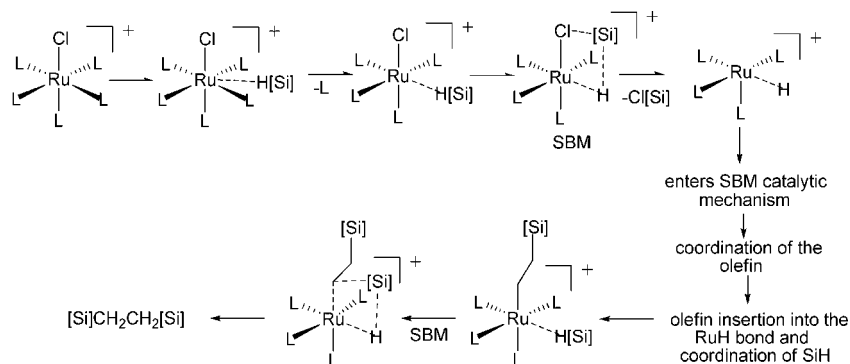


Figure 30. Generation of the calculated catalytic intermediate for hydrosilylation promoted by $[\text{RuCl}(\text{NCCH}_3)_5]^+$ as well as the hydrosilylation sequence through SBM.^{502b}

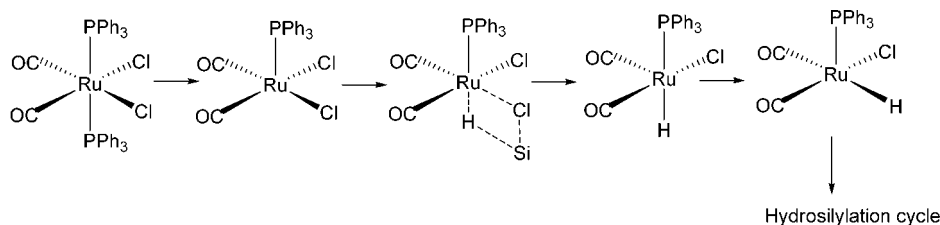


Figure 31. Formation of the catalytically active species for the hydrosilylation cycle from the precursor, $\text{RuCl}_2(\text{CO})_2(\text{PPh}_3)_2$.^{502c}

Glaser and Tilley reported a novel hydrosilylation mechanism using a cationic ruthenium–silylene catalyst.⁵⁴ The key step involved alkene insertion into a silicon–hydrogen bond of the cationic silylene, $[\text{Cp}^*(\text{Pr}_3\text{P})(\text{H})_2\text{Ru}=\text{Si}(\text{H})\text{Ph}]^+$, that is remote from the metal site and that involved concerted addition of the Si–H bond of the silylene across the C=C bond of the olefin. Beddie and Hall subsequently published theoretical support for the proposed mechanism using $[\text{Cp}(\text{H}_3\text{P})(\text{H})_2\text{Ru}(\text{SiH}_2)]^+$ as a model first in a communication^{476a} followed by a full paper.^{476b} In the full paper, both DFT and WFT methods were used with a series of basis sets to determine if the computational methodology influenced the relative energies of the key intermediates and transition states for the Glaser–Tilley (GT) mechanism versus the more commonly invoked Chalk–Harrod (CH) mechanism for hydrosilylation. The DFT methods in a range of basis sets indicated that the GT pathway was energetically favored. However, the CCSD(T) calculations favored the CH pathway for smaller basis sets, and when extrapolated to larger basis sets, the GT pathway was favored. The authors speculated that the differences in the two calculation methods could be attributed to basis set effects.^{476b} In another study concerned with the metal-catalyzed hydrosilylation of acetylenes with the cationic Ru complex $[\text{Cp}^*\text{Ru}(\text{MeCN})_3]^+$, calculations showed that the Ru directs addition of the silane to the alkyne and hydride insertion was favored over silyl insertion.^{502a}

Tuttle, Thiel, and co-workers have published two DFT studies on olefin hydrosilylation catalyzed by two different ruthenium complexes, $[\text{RuCl}(\text{NCCH}_3)_5]^+$ ^{502b} and $\text{RuCl}_2(\text{CO})_2(\text{PPh}_3)_2$.^{502c} Both of these studies developed the sequence that led from the initial complex to the catalytically active species and then the lowest-energy pathway leading to the formation of the hydrosilylation product $(\text{MeO})_3\text{SiCH}_2\text{CH}_2\text{Si}(\text{OMe})_3$ (from $\text{HSi}(\text{OMe})_3$ and $\text{CH}_2=\text{CH}_2$). A total of 10 different pathways with catalytic cycles and induction steps were examined for the latter complex, and the Chalk–Harrod (CH), Glaser–Tilley, and σ -bond metathesis mechanisms were examined for the former complex. A σ -bond metathesis mechanism was most consistent and was the most favored

for both complexes, and both involved replacement of a chloride by a hydride in the steps leading to the proposed catalytically active species.

When PhMeSiH_2 is added to RuCl_3 in acetonitrile, reduction takes place and the salt $[\text{RuCl}(\text{NCCH}_3)_5]^+[\text{RuCl}_4(\text{NCCH}_3)_2]^-$ is produced, which functions as a catalyst in the hydrosilylation of CO_2 by secondary and tertiary silanes. The calculations were developed to shed light on the mechanism of hydrosilylation promoted by this complex. For the system to work, the active form would require the dissociation of at least one of the six ligands in the octahedral cation and in the classical CH mechanism as well as the modified CH mechanism (mCH), but the barrier to removal of two CH_3CN ligands is too high. An alternative mechanism was calculated where the hydrosilane displaced an acetonitrile ligand (lowering the energy barrier from ~ 70 to 23.5 kcal/mol. Shown in Figure 30 is the sequence calculated for replacement of the chloride ligand with a hydride (see section 3.7 for other examples of transfer of hydride from silicon to the metal, although these do not include any mechanistic suggestions). The square-pyramidal hydride complex then enters into a catalytic cycle that involves a SBM intermediate, which was lower in energy than either the CH or mCH mechanisms and is also shown in Figure 30.^{502b}

There are five isomers of $\text{RuCl}_2(\text{CO})_2(\text{PPh}_3)_2$,^{502c} and the lowest-energy isomer calculated had *trans*-phosphines with *cis*-chlorides and *cis*-carbonyls (cct isomer) and was the isomer observed in the X-ray structure. To open a coordination site, loss of a ligand must occur, and of the four pathways considered (CO loss or PPh_3 loss, as Cl^- loss was too high in energy), the loss of PPh_3 was more favorable than CO dissociation, but removal of a second PPh_3 was enthalpically too high. Therefore, another sequence involving replacement of $\text{Ru}-\text{Cl}$ with $\text{Ru}-\text{H}$ through a SBM reaction was calculated as shown in Figure 31, where a shift of the hydride ligand from an axial to an equatorial position produces the catalytically active species and formation of the hydride form represents the rate-determining step in the activation barrier to the hydrosilylation cycle. The hydrosi-

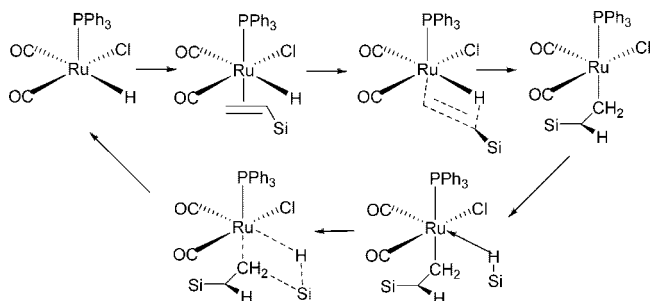


Figure 32. Hydrosilylation sequence through two SBM steps.^{502c}

lylation cycle (Figure 32) involves coordination of the olefin to the vacant axial site in the catalytically active species, transfer of the hydride to the α -C of the olefin through a SBM TS, followed by coordination of HSi to the open site just created and a second SBM TS, which leaves the hydride on the metal, and then the product $\text{SiCH}_2\text{CH}_2\text{Si}$ is formed.^{502c}

The ruthenium–silylene complex $[\text{Cp}^*(\text{Pr}_3\text{P})(\text{H})_2\text{Ru}=\text{Si}(\text{H})\text{Ph}\cdot\text{OEt}_2][\text{B}(\text{C}_6\text{F}_5)_4]$ synthesized by Glaser and Tilley exhibits an unusual hydrosilylation pathway in that direct insertion of an alkene occurs into the SiH bond and not into the Ru–H bond. Thus, a new mechanism was developed (GT mechanism) as outlined in Figure 33. There is no experimental “proof” for the intermediates shown in Figure 33; thus, a calculation study might provide insight into this new type of hydrosilylation mechanism. A DFT (B3LYP) study for the model cation, $[\text{Cp}^*(\text{H}_3\text{P})(\text{H})_2\text{Ru}=\text{Si}(\text{H})\text{Ph}]^+$, and ethene as the model olefin was reported by Böhme.^{502d} In the experimental complex, ether is weakly bound to the cation $[\text{Cp}^*(\text{Pr}_3\text{P})(\text{H})_2\text{Ru}=\text{Si}(\text{H})\text{Ph}\cdot\text{OEt}_2]$, and the calculated free energy difference for cleavage of an ether molecule in the model cation was 2 kcal/mol. The computations for the ether-free model cation indicated that the two metal hydrides bridge the Ru–Si bond and there are three-centered Ru–H–Si bonds. The bridging hydrogen atoms appear to be bound to both Ru and Si with approximately the same strength. Calculations for the hydrosilylation cycle are shown in Figure 33. Böhme’s calculations confirm the hydrosilylation mechanism originally proposed by Glaser and Tilley. The catalytically active complex has a nonclassical η^3 -bonded silane ligand.^{502d}

Osmium tetroxide oxidizes tertiary silanes to silanols in the presence of excess pyridine.^{502e} The reaction of OsO_4 with SiH_4 and Me_3SiH was studied by DFT (B3LYP) methods. In the presence of pyridine, an $\text{OsO}_4\cdot\text{py}$ is formed and four pathways for addition of the silane were tested: hydrogen atom abstraction, hydride transfer, and [2 + 2]- or [3 + 2]-mechanisms. In this case, the ΔH^\ddagger calculated for the [3 + 2]-pathway was 4 kcal/mol, whereas for the [2 + 2]-pathway, the value was 34 kcal/mol, in contrast to the results for the ReO_2 system described in section 7.3.4 where the [2 + 2]-route was favored.

7.3.6. Cobalt Triad

Several papers dealing with calculations and with no synthetic aspects have appeared, three of which address predictions of potentially stable complexes with structural motifs that have yet to be isolated. The first of these to be discussed was concerned with the calculation of the relative energies of isomers of the 16e complex cation, $[\text{Cp}^*(\text{H}_3\text{P})\text{IrSiHR}_2]^+$ and $[\text{Cp}^*(\text{H}_3\text{P})\text{IrSiR}_3]^+$ ($\text{R} = \text{H}, \text{CH}_3, \text{SiH}_3, \text{Cl}$).⁵⁰³ The isomers that were considered are shown in

Figure 34 and include a terminal silyl group, various bridged and non-bridged silylene forms, including an isomer where hydrogen bridges two silylenes, and finally silene complexes. This particular model was based on the experimental iridium complexes $[\text{Cp}^*(\text{Me}_3\text{P})\text{Ir}(\text{HSiR}_2)]^+$, which appear to undergo silene/silylene interconversion within the coordination sphere of the metal, as investigated by Tilley and co-workers.^{116,117a,183,343a,503}

The geometry optimizations were conducted without symmetry restrictions; for the 10 complexes that were calculated, only one, $[\text{Cp}^*(\text{H}_3\text{P})\text{IrSiCl}_3]^+$, had a single isomer, and the remainder exhibited up to seven isomers whose relative energies varied from ~ 1 to ~ 24 kcal/mol above the lowest-energy isomer.⁵⁰³ The very interesting results are summarized briefly in the following points.

(a) A terminal silyl group was never a favored structure for the 16e iridium complexes. A structural reorganization occurred to occupy the empty coordination site. This contrasts to square planar 16e complexes of platinum (see section 7.3.7).

(b) The $\text{HM}=\text{Si}<$ form was a true minimum for all $-\text{SiHR}_2$ groups and was the most stable isomer when R was a π -donor group ($\text{R} = \text{CH}_3, \text{Cl}$).

(c) $(\text{H}_3\text{Si})(\text{H})\text{Si}=\text{M}(\text{SiH}_3)$ is lower in energy than $(\text{H}_3\text{Si})_2\text{Si}=\text{MH}$ as the silyl group is the stronger σ -donor. The energy difference between two silylene isomers is relatively small, but strong σ -donor groups ($\text{SiH}_3, \text{CH}_3, \text{H}$) can occupy terminal sites if the silyl groups are stabilized by π -donors ($\text{Cl}, \text{SiH}_3, \text{CH}_3$).

(d) The $\text{Ir}=\text{Si}$ moiety is polarized $\text{Ir}^{\delta-}-\text{Si}^{\delta+}$, and from the NBO analysis, the $\text{Ir}(5d)$ orbital contains $1.8 e^-$, the $\text{Si}(3p)$ has an average of $0.37 e^-$ (range, 0.33 – $0.50 e^-$), and the Ir-5d population does not vary much with the nature of the substituents on silicon. The observation that the sum of the population of the two orbitals is not 2 suggests that the Ir–Si π -component dominates over an interaction with the silicon substituents.

(e) A consequence of the bond polarity suggests that the silicon center is electron deficient, and thus, bridged structures are preferred by analogy to base-free and base-complexed silylenes that have been isolated. All the groups ($\text{H}, \text{CH}_3, \text{SiH}_3$, and Cl) can occupy a bridging position, but a hydrogen-bridged species was never observed as a stable isomer.

(f) More diverse bridging situations were found for $\text{SiH}(\text{SiH}_3)_2$ than for $\text{SiH}(\text{CH}_3)_2$, and this was attributed to the ability of silicon to become hypervalent.

(g) Silylene forms were favored more by iridium than by platinum (see section 7.3.7), because Ir(III) was more effective at back-bonding than was Pt(II) and, thus, stabilized the silylene more efficiently.

There are certainly many examples of metal complexes that contain terminal silyl groups, but, in general, there are few that contain a $-\text{SiH}_3$ group and none that contain a $-\text{SiH}(\text{SiH}_3)_2$ unit. Several examples of complexes where a hydride bridges a metal–silylene have been reported, and one, $\text{Os}=\text{SiH}_2$ system (**1-51**), has been isolated.⁵⁰ Although simplification of SiR_3 with a SiH_3 group assists making calculations more practical, such groups are not likely to be found in isolable (stable) compounds. Therefore, a major question still remains, and that is what substituents at silicon could be explored that would generate some of the novel bridged units for silylene and silenes as shown in Figure 34. The fact that these isomers seem to be relatively stable

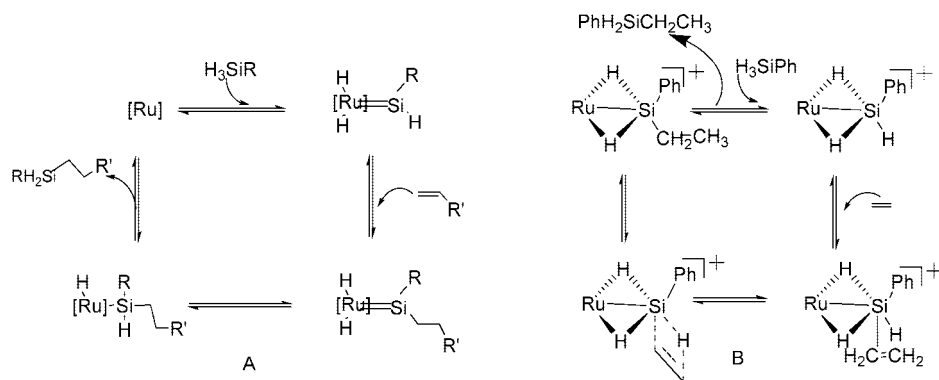


Figure 33. Comparison of hydrosilylation mechanisms: (A) GT proposal and (B) calculated by Böhme.^{502d}

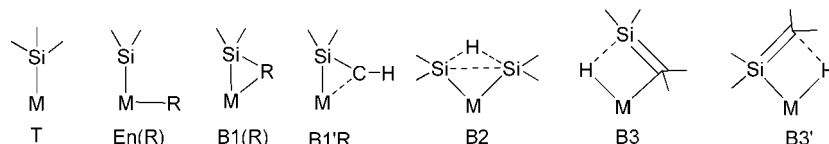


Figure 34. Bonding modes studied computationally for $[(\text{dhpe})\text{Pt}(\text{SiHR}_2)]^+$ and $[(\text{dhpe})\text{PtSiR}_3]^+$.⁵⁰³ T = terminal silyl, En = doubly bonded silylene, and B = bridged structure.

suggest that an effort should be made to explore these possibilities.

In an additional study, Webster and Hall explored calculations in an effort to find a ligand combination that would stabilize an Ir(V) complex with adjacent Ir–X and Ir–H bonds where X = C, Si, Sn, but their main focus was a system where X = C.^{504a} The types of ligands studied included Cp^- variations, carboranes, alternative phosphines, silanes, and stannanes as well as chelating ligands. Unfortunately, the goal of finding a ligand set that was capable of “trapping” an Ir(V) intermediate from C–H activation by Ir(III) was not achieved. However, the calculations showed that $[\text{Cp}(\text{R}_3\text{P})\text{Ir}^{\text{III}}\text{SiH}_3]^+$ (R = H, CH_3) reacts with silane to form $[\text{Cp}(\text{R}_3\text{P})\text{Ir}^{\text{V}}(\text{SiH}_3)_2\text{H}]^+$, which was more stable than the reactants. Calculations also showed that the Ir^V complex could be formed by Si–H activation of a silane by $[\text{Cp}(\text{R}_3\text{P})\text{Ir}^{\text{III}}\text{CH}_3]^+$ or by Si–H activation of a second equivalent of silane.^{504a}

In a study of a series of formally Rh(V) complexes, $\text{Cp}(\text{H})_2\text{Rh}(\text{SiMe}_3)_2$, $\text{CpHRh}(\text{SiMe}_3)_3$, $\text{Cp}(\text{H})\text{Rh}(\text{SiMe}_3)_2(\text{SiEt}_3)$, and $[\text{Cp}(\text{PMe}_3)(\text{H})\text{Rh}(\text{SiMe}_3)_2]^+$, calculations were performed to determine whether these high oxidation state complexes with H and SiR_3 ligands formed classical complexes, consistent with a Rh(V) oxidation state, or whether the oxidation state is lowered to Rh(III) by formation of a σ -interaction. The model used for the DFT study was $[\text{Cp}(\text{Me}_3\text{E})(\text{X})\text{Rh}(\text{SiMe}_3)_2\text{H}]^n$ (E = Si, X = H, $n = 0$; E = Si, X = SiMe_3 , $n = 0$; E = P, X = SiMe_3 , $n = +1$; E = P, X = H, $n = +1$).^{504b} The four actual complexes will be summarized in turn in the next paragraphs.

The complex $\text{CpRh}(\text{SiEt}_3)_2\text{H}_2$ was originally characterized by a ND study, and the piano-stool structure has one pair of *trans*-silyl ligands and one pair of *trans*-hydride ligands, although there is some asymmetry in the $\text{Si}\cdots\text{H}$ contacts with an average for one pair of 2.36 Å and for the other pair, 2.29 Å. The calculated J_{SiH} values are negative, which indicates some residual $\text{Si}\cdots\text{H}$ bonding, and the Mayer indices for these $\text{Si}\cdots\text{H}$ interactions fall in the range 0.09–0.11, suggesting a weak bonding interaction. The minimum energy structure may be consistent with a Rh(V)

complex, but a flat potential for the residual Si–H interaction indicates that “oxidation state” has little meaning in this system.^{504b}

For the actual complex $\text{CpHRh}(\text{SiMe}_3)_3$, calculations showed a distorted piano-stool structure, the hydride is *cis* to two silyl groups, and the $\text{Rh}-\text{Si}_{\text{cis}}$ bond lengths are slightly longer than the $\text{Rh}-\text{Si}_{\text{trans}}$ (2.448 and 2.438 Å compared to 2.410 Å). The two Si–H distances are 1.995 and 2.073 Å with Mayer indices of 0.18 and 0.14, respectively. The complex gives rise to equivalent ^1H , ^{13}C , and ^{29}Si NMR resonances of the silyl groups down to 197 K, and a structure was proposed that is a pseudo-octahedron capped on the Si–Si edge by a hydride, which can wander from one edge to another on the RuSi_3 face. The calculated J_{SiH} values have a negative sign for the silicons that are *cis* to the hydride but a positive sign for the *trans* silicon. The complex is not viewed as one having a σ -silane interaction but has delocalized Si–H interactions between the hydride and the two adjacent *cis*-silyl groups.^{504b}

An exact model was used for the real complex, $\text{Cp}(\text{H})\text{Rh}(\text{SiMe}_3)_2\text{SiEt}_3$, which also shows equivalent ^1H , ^{13}C , and ^{29}Si resonances of the SiMe_3 groups. The structure assumed was the same as the previous example with the hydride on the $\text{Me}_3\text{Si}\cdots\text{SiEt}_3$ edge or the $\text{Me}_3\text{Si}\cdots\text{SiMe}_3$ edge, but the hydride is asymmetrically placed (distances to each of the *cis*-Si groups are not equal). A delocalized $\text{Si}\cdots\text{H}$ interaction was also assumed for $\text{Cp}(\text{H})\text{Rh}(\text{SiMe}_3)_2\text{SiEt}_3$.^{504b}

The model for the actual complex $[\text{Cp}^*(\text{Me}_3\text{P})(\text{H})\text{Rh}(\text{SiMe}_3)_2]^+$ ²³⁹ replaced the Cp^* with Cp. However, calculations for the actual complex were also developed, and the results differed from those for the model. In the actual complex, the silyl ligands are equivalent down to -60°C and the hydride signal is flanked by ^{29}Si satellites. In the original report, a fast degenerate exchange between two forms of a Rh(III) η^2 -silane complex was proposed. Two isomers of $[\text{Cp}(\text{Me}_3\text{P})(\text{H})\text{Rh}(\text{SiMe}_3)_2]^+$ were calculated: a bis-silyl complex with the hydride *trans* to the phosphine and the second a silyl silane σ -complex, $[\text{Cp}(\text{Me}_3\text{P})(\eta^2\text{-H}-\text{SiMe}_3)(\text{SiMe}_3)]^+$. The σ -complex was the one higher in energy, and the hydride was not located on the Si–P edge but inside the Si_2P triangle; the structure would be best

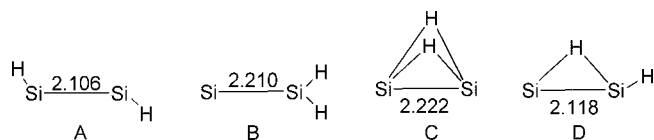


Figure 35. Valence isomers of Si_2H_2 used to calculate stability of complexes of Rh(I) and Pt(0). A is an acetylene-type with a SiSi triple bond, B is a vinylidene type with a SiSi double bond, and C and D contain 2 and 1 bridged hydrides, respectively.⁵⁰⁵

described as a three-legged piano-stool complex. A short Si–H distance of 1.682 Å suggests a bonding that is characteristic of silane σ -complexes. With the actual complex with Cp^* as a ligand, two isomers were calculated. The most stable isomer was the bis(silyl) complex, which has a stronger Si–H interaction as indicated by the two $\text{Si}\cdots\text{H}$ distances of 1.909 and 2.099 Å with Mayer indices of 0.20 and 0.11, respectively. The second isomer exhibits an end-on $\text{Rh}\cdots\text{H}\cdots\text{Si}$ silane coordination with $\text{Rh}\cdots\text{H}$ and $\text{Si}\cdots\text{H}$ distances of 1.754 and 1.599 Å, respectively. Substitution of the ring with Me groups increases the $\text{Si}\cdots\text{H}$ interaction. The model for the last complex, $[\text{Cp}^*\text{Rh}(\text{SiMe}_3)(\text{H})_2(\text{PMe}_3)]^+$,²³⁸ also used Cp in place of Cp^* . The calculated structure was distorted with the hydride ligands shifted away from the phosphine towards the silyl groups. Since one of the Si–H distances was shorter than the other, the authors suggested that the complex was better described as a stretched silane σ -complex with a second, weaker $\text{Si}\cdots\text{H}$ interaction. The actual complex was fluxional down to -80°C , and no ^{29}Si satellite peaks were observed. The calculated J_{SiH} values carry a negative sign consistent with the presence of direct Si–H bonding. The series of complexes display a range of interligand $\text{Si}\cdots\text{H}$ interaction, and none appear to have a +5 oxidation state but are characterized by multicentral Si–H interactions.^{504b}

A continuing challenge in multiple-bonded silicon chemistry is to determine whether there are transition metal systems that can stabilize disilenes or disilynes. A theoretical investigation (DFT with the B3LYP functional) has been reported for the interaction of various isomers of Si_2H_2 with 14e transition metal fragments such as $\text{RhCl}(\text{PMe}_3)_2$.⁵⁰⁵ The valence isomers of Si_2H_2 that were included in this study are shown in Figure 35, and the calculations were performed to determine which of these isomers could lead eventually to an isolable complex containing the Si_2H_2 unit. The most stable complex of $\text{RhCl}(\text{PMe}_3)_2\cdot\text{Si}_2\text{H}_2$ appeared to be the vinylidene form (containing the structure B in Figure 35), although the most stable of the Si_2H_2 forms itself is the dibridged Si_2H_2 species (C in Figure 35). The $\text{Si}\equiv\text{Si}$ triple bond of A (Figure 35) and the $\text{Si}=\text{Si}$ double bond of B become double and single, respectively, on coordination to the Rh(I) center. The relative energy of the $\text{RhCl}(\text{PMe}_3)_2\cdot\text{Si}_2\text{H}_2$ isomers indicated that A–Rh isomerized to D–Rh with a small activation barrier and D–Rh isomerized to an edge-on isomer with an even lower barrier. This suggests that, experimentally, the rhodium complex of B could be accessible from any of the other three isomers should any of these complexes be generated.⁵⁰⁵

One of the few theoretical studies that deals with dinuclear complexes includes the model $\text{Rh}_2(\text{Si}_2\text{H}_4)(\text{PH}_3)_4$ as well as the corresponding Pd and Pt analogues that will be discussed in the next subsection.⁵⁰⁶ The rhodium complex was a model for the dinuclear complex, $\text{Rh}_2(\text{SiRR}')_2(\text{dippe})_2$, isolated from the reaction of $\text{Rh}_2(\text{H})_2(\text{dippe})_2$ with PhMeSiH_2 (**2-67**).¹¹⁴ Two possible views of the bonding in the central four-

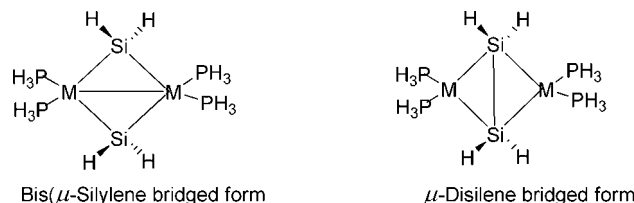


Figure 36. Structures of metal complexes of composition $\text{M}_2(\text{Si}_2\text{H}_4)(\text{PH}_3)_4$ ($\text{M} = \text{Rh}, \text{Pd}, \text{Pt}$) used in the theoretical study of the electronic structure and bonding nature of such derivatives.⁵⁰⁶

membered ring include a μ -disilene-bridged dinuclear complex with a $\text{Si}=\text{Si}$ double bond (generally written with a line between the two silicon centers) or a bis(μ -silylene)-bridged dinuclear complex with four Rh–Si bonds and no Si–Si bond (structure is usually written with a Rh–Rh bond) (see Figure 36). In this study, the geometries were optimized by the DFT method, where the B3LYP functional was used, with the aim of obtaining the electronic structure and bonding as well as to determine the possible interconversion between the two forms.⁵⁰⁶

The calculations⁵⁰⁶ for $\text{Rh}_2(\text{Si}_2\text{H}_4)(\text{PH}_3)_4$ showed an occupancy number of 0 for the Si–Si bond, 1.674e for the Rh–Si σ -bond, and 0.466e for the Rh–Si σ^* -bond as well as 0 for the Rh–Rh bond, as was assumed in the original isolated complex.¹¹⁴ The orbitals on silicon and the metal center involved in the bonding interaction are shown in Figure 37. The lowest-energy HOMO involves the bonding couple $d_\sigma-d_\sigma$ of the two metals, which also forms a bonding interaction with the 2sp^2 -Si orbitals of the bridging silicon units (B in Figure 37). The unoccupied p-orbital of SiH_2 overlaps with the d_π -orbitals of the metals in a bonding HOMO (higher in energy) and corresponds to the π -back-donation illustrated in (A) in Figure 37. In a higher-energy HOMO (not shown), the sp^2 orbital of one SiH_2 group overlaps with the sp^2 of the second SiH_2 group in an antibonding interaction since the sp^2 orbital is double occupied (C). The highest-energy LUMO involves an antibonding overlap between the sp^2 orbitals of silicon and the $d_\pi-d_\pi$ bonding couple of the Rh–Rh unit. The net result is that the silylene forms three bonding interactions illustrated in Figure 37. The $d_\sigma-d_\sigma$ of a higher energy HOMO (not shown) exhibited antibonding overlap with the empty p-orbital of the SiH_2 unit, but in a bonding way. Consequently the Rh–Rh bonding interaction becomes weak and the Rh–Si interaction becomes stronger as reflected in the NBO analysis. Reduction of the Rh(0) dinuclear complex produced geometry changes, decreasing the Si-to-Si distance from 3.872 to 2.541 Å and increasing the Rh-to-Rh distance from 2.941 to 4.200 Å. The occupation number of the Rh–Si bond becomes 0, the π - and π^* -orbitals of $\text{Si}=\text{Si}$ become 1.531 and 0.691 e^- , respectively, and the complex has converted to a μ -disilene-bridged dinuclear rhodium complex. All the d-orbitals in $[\text{Rh}_2(\mu\text{-Si}_2\text{H}_4)(\text{PH}_3)_4]^{2-}$ are doubly occupied.⁵⁰⁶

Calculations have also been incorporated into synthesis papers. The Co^{V} complex $\text{Cp}^*(\text{H})_2\text{Co}(\text{SiPh}_2\text{H})_2$ (**2-52a**) was crystallographically characterized, but the hydrides could not be located.¹⁰³ The DFT calculations (B3LYP) gave a Co–Si distance of 2.29 Å compared to the experimentally determined 2.26 Å as well as a pseudo-square-pyramidal structure. From the calculated $\text{H}\cdots\text{H}$ distance of 2.28 Å and $\text{H}\cdots\text{Si}$ distances of 2.24 and 2.25 Å, the authors favored a complete oxidative addition of both equivalents of Ph_2SiH_2 to the starting materials, $\text{Cp}^*\text{Co}(\eta^2\text{-H}_2\text{C}=\text{CHR})$ ($\text{R} = \text{H}, \text{SiMe}_3$). Since the hydrides and the silicon centers are *cis* to each

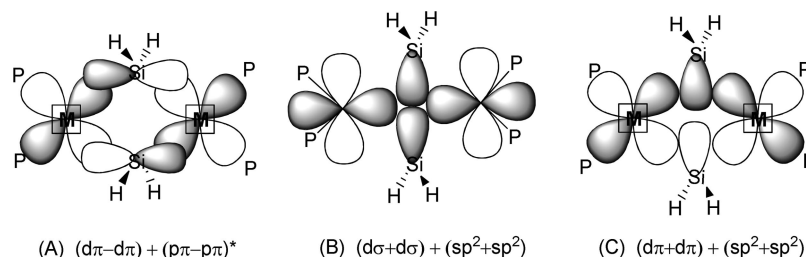


Figure 37. Bonding interactions in $[\text{Rh}_2(\mu^2\text{-SiH}_2)_2(\text{PH}_3)_4]$.⁵⁰⁶ (A) Bonding interaction of the unoccupied p-orbital of SiH_2 with doubly occupied dp-orbital of Rh. (B) Bonding interaction between the sp^2 -orbitals of two SiH_2 groups and the ds - ds bonding couple of the Rh-Rh unit. (C) Antibonding overlap of the sp^2 -orbitals of two SiH_2 groups and bonding overlap of the dp-orbital of Rh and the same sp^2 -orbitals on Si.

other, some residual interaction may be present (as in SISHA), although there were no silicon satellites observed for the Co-H signal.¹⁰³

In the mono(silyl)- and bis(silyl)-*o*-carboranes that are chelated to a $\text{Cp}^*(\text{H})_2\text{Ir}$ fragment in **3-228**, **3-229**, and the related complex formed from *o*-(HMe_2Si) $_2\text{C}_6\text{H}_4$, **3-231**, the basic structure was that of a four-legged piano-stool geometry with the Cp^* ligand in an apical position.¹⁷² The crystal structures of **3-228** and **3-231** were reported. The positions of the hydrides were determined from difference maps but were not refined in the case of **3-228**. DFT calculations were obtained for all three structures, and the geometry optimization provided the same *cisoid*-orientation for the chelate in **3-228** as observed in the X-ray structure and the *transoid*-orientation for both **3-229** and **3-231** (also consistent with the X-ray structure for **3-230**) as the lowest-energy structures. The calculated Ir-Si distances (X-ray value if reported) were 2.404 Å (**3-228**; 2.380(2) Å), 2.354 Å (**3-229**), and 2.364 Å (**3-231**, 2.359(1) Å). The calculated Ir-H distances were 1.568, 1.579, and 1.581 Å for **3-228**, **3-229**, and **3-231**, respectively. The X-ray value obtained for Ir-H in **3-231** was 1.649 Å.¹⁷²

The silylene complex, $[(\text{PNP})(\text{H})\text{Ir}=\text{SiH}(\text{Mes})]\text{-}[\text{B}(\text{C}_6\text{F}_5)_4]$,⁶¹ could not be isolated as a crystalline solid, and DFT calculations (B3LYP/LANL2DZ) were conducted to obtain information concerning the geometric and electronic structures. Three rotamers were calculated where the main difference involved the H-Ir-Si-H dihedral angle (32°, 122°, and 161°). The lowest-energy rotamer was that with a dihedral angle of 122°. The NBO analysis indicates essentially no interaction between the IrH and the Si center. Each rotamer had a trigonal-planar environment for the Si center and an angle sum of 360° with Si-Ir bond lengths between 2.27 and 2.29 Å (these would be on the short end of Si-Ir bond lengths; see Table 7). The LUMO is localized mainly on the silylene portion and contained considerable character from a silicon p-orbital. The HOMO is dominated by the PNP ligand backbone. The NBO analysis supports the localization of the cationic charge on Si, which leads to alkene insertion into the Si-H bond.⁶¹

7.3.7. Nickel Triad

Several publications detailing calculations with bonding modes in Ni triad complexes have been published, some of which model previously isolated and characterized examples. The possible structures of $[(\text{dhpe})\text{Pt}(\text{SiHR}_2)]^+$ have been examined⁴⁶⁶ in a study that is closely related to that reported for the iridium complex, $[\text{Cp}(\text{H}_3\text{P})\text{IrSiR}_3]^+$,⁵⁰³ discussed in the previous section. Three studies were concerned with silyl- and silylene-bridged dinuclear complexes of Pd and Pt,^{456,507} and of Rh, Pd, and Pt,⁵⁰⁶ where the Rh example was

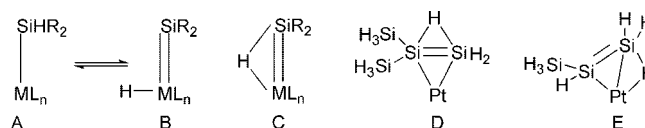


Figure 38. Model isomers for DFT calculations used to determine the lowest-energy tautomer for a series of complexes, $[(\text{dhpe})\text{Pt}(\text{SiHR}_2)]^+$ ($\text{R} = \text{H}, \text{CH}_3, \text{SiH}_3, \text{Cl}, \text{OMe}, \text{SMe}, \text{NMe}_2$) and $[(\text{dhpe})\text{Pt}(\text{SiR}_3)]^+$ ($\text{R} = \text{CH}_3, \text{Cl}$).⁴⁶⁶

discussed in the previous section. The stabilization of Si_2H_2 discussed for rhodium⁵⁰⁵ also included results for Pt, and the results for Pt and Pd cases will be summarized in this section. Theoretical studies of silyl-bridged dinuclear complexes of Pd and Pt have also been presented.^{456,507} There were more papers reporting calculations for group 10 elements than for any other group (although calculations for Ru complexes are increasing). The results will be summarized in the following order:

Section 7.3.7.1: Mononuclear complexes mainly featuring “unknown” compounds or compounds where the basic structural motif is known but not necessarily the specific examples for which the calculations were performed. The types of questions addressed involved how transition metals can stabilize multiple bonds to silicon or how substituents at silicon affect the stability of the complex.

Section 7.3.7.2: Dinuclear complexes where at issue is whether there are M-M bonds or Si-Si bonds.

Section 7.3.7.3: OA and RE. These are two processes that influence reactivity and also are invoked in catalytic cycles. However, the catalytic cycle itself is not the focus.

Section 7.3.7.4: Silylene complexes. The questions usually addressed here involve the factors that influence the stabilization of base-free silylenes.

Section 7.3.7.5: Cases from Tables 1, 2, and 3. Individual compounds that have not been presented in earlier subsections are presented here.

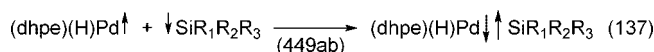
7.3.7.1. Mononuclear Complexes. The calculations for $[(\text{dhpe})\text{Pt}(\text{SiHR}_2)]^+$ ($\text{dhpe} = \text{H}_2\text{PCH}_2\text{CH}_2\text{PH}_2$; $\text{R} = \text{H}, \text{Me}, \text{SiH}_3, \text{Cl}, \text{OMe}, \text{NMe}_2$) were carried out in order to evaluate the energies and the stereochemistry of the possible structures.⁴⁶⁶ The basic structures that were probed are shown in Figure 38. The structures A (silyl form) and B (hydrido/silylene form) could be valence tautomers separated by a transition state, and determining the factors that would favor one structure over the other was one of the aims of the study. It was found that the structural preferences vary with R.⁴⁶⁶

For $\text{R} = \text{H}$, two minima were found with one of type A ($\text{R} = \text{H}$), which exhibited a SiMP_2 core that is T-shaped (one P of dhpe is *trans* to the empty coordination site), and the other which has two different Si-H distances and is related to structure C ($\text{R} = \text{H}$) with a bridging hydride that

is almost equally bonded to Pt and to Si. No structure corresponding to B with a terminal hydride could be located as a minimum on the potential energy surface. For R = Me, the most stable minimum corresponded to structure B (R = Me) with a Pt–H distance that was similar to a terminal hydride and a Pt–Si distance that is appropriate for a silylene derivative. No terminal complex (A) nor a bridged hydride structure (C) was located as a minimum, but a secondary minimum with a CH₃ group bridging Pt and Si was calculated. In contrast, when R = SiH₃, the most stable structure contained a disilene, (H₃Si)₂Si=SiH₂, coordinated to the Pt center with a hydride bridging the double bond (Figure 38D), and 5 kcal above this structure was one with a (H₃Si)(H)Si=SiH₂ ligand (Figure 38E) and hydrogen bridging a Pt–Si bond. If X in [(dhpe)Pt(SiHX₂)]⁺ was Cl, OMe, SMe, or NMe₂, all could potentially stabilize the silylene group through π -donation into the empty p-orbital on silicon. For the SiHCl₂ and SiH(NMe₂)₂ ligands, the preferred structure was of type B, but for X = Cl, a structure with a Cl bridging the Pt–Si bond was only slightly above that of B. The most stable structure for the SiH(OMe)₂ was also of type B, but there were several other minima due to additional conformational possibilities for the OMe unit. When X was changed to SMe, the more stable structure was of type C with a bridging SMe group (replacing the bridging hydride), but the energy of isomer of type B was <2 kcal/mol higher in energy. The authors concluded that care needed to be exercised in computational studies for determining the minimum structure for silicon–transition metal complexes because such complexes are sensitive to the nature of *all* the elements in the system when compared to the corresponding carbon complexes.⁴⁶⁶

An important question in silyl–transition metal chemistry involves how substituents at either silicon or the metal center influence stability, structure, and reactivity of the complex. This type of question is infrequently addressed experimentally but could potentially be determined through computational methods. This was the case as reported by Jacobsen and Fink for substituent variations on silicon in the model complex (dhpe)(H)MSiR¹R²R³ (M = Pd, Pt) by density functional calculations (PW91).^{449a} Included were 22 variations of R₁R₂R₃ for Pd and 11 for Pt. The geometry was optimized based on X-ray parameters for the known complex (dcpe)(H)PdSiPh₃ and the related Pt complex. The experimental and the calculated structures indicated two Pd–P bond lengths with the longer length associated with the phosphorous that was *trans* to the silicon substituent. The relative stability order for (dcpe)(H)PdSiR₃ complexes was established by earlier NMR experiments and described in section 6.1.1: SiR₃ = SiPh₃ > SiPh₂Me > SiPhMe₂ > SiEt₃.²⁷⁴ To establish how substitution patterns influence Si–Pd and Si–Pt bond energies, ΔE_{RE} were calculated from changes in total bond energy for the RE of HSiR₃ from (dhpe)(H)–Pd(SiR₃). The ΔE_{RE} values ranged from 19 kcal/mol for SiMe₃ to 30 kcal/mol for SiCl₃. Substitution of hydrogen by halogen or phenyl groups resulted in an increase in reaction energy whereas methyl groups provided a lower energy. If the free energies of reaction are determined by the difference in energy of bonds broken and formed, K_e can be estimated for (dhpe)PdH(SiR₃) + HSiR'₃ \rightleftharpoons (dhpe)PdH(SiR'₃) + HSiR₃. The relative stability order thus generated was PdSiPh₃ > PdSiPh₂Me > PdSiPhMe₂ > PdSiMe₃, which was the same trend observed in the NMR experiments.^{449a}

The bond-forming reaction associated with the process shown in eq 137 is referred to as the bond-snapping energy, BE_{snap},^{449b} and may be considered an approximation of a bond enthalpy term, which can then be translated into bond strength. For homosubstituted complexes [Pd]–SiR₃, the bond-snapping energy, BE_{snap}, led to the following ranking: R = F > Cl > Ph > H > Me. The BE_{snap} can be partitioned into two main components, steric repulsion, ΔE^0 , and orbital interaction, ΔE_{int} . The values obtained after partitioning the BE_{snap} gave an order for the stabilizing orbital interaction ΔE_{int} that corresponded to Cl > F > Ph > H > Me and for the destabilizing steric repulsion, ΔE^0 , that corresponded to Cl > H > Ph > Me > F. The values obtained showed that the complex [Pd]–SiF₃ was an interesting example in that it displayed the strongest Pd–Si bond but not the strongest orbital interaction. Since [Pd]–SiHF₂ exhibited an orbital interaction greater than the value for [Pd]–SiF₃ and a steric repulsion larger than the value for [Pd]–SiH₃, it was concluded that other secondary bonding interactions were important and it was concluded that an interaction of Pd–H with the silyl center in addition to Pd–Si bonding could account for the observation. The calculated geometric parameters indicated an Si...H–[Pd] separation that ranged from 1.90 Å ([Pd]–SiHF₂) to 2.33 Å for ([Pd]–SiCl₃). The larger value for the Si–H separation in the SiCl₃ ligand case contrasts to that of IHI cases, but the smaller distances are in line with Lin's prediction that an interaction appears to occur between the hydride in M–H with the silicon of M–Si if these units are in adjacent (*cis*) positions.⁴⁸³ In line with the Si...H[Pd] separation are the H–Pd–Si angles, which range from 53° ([Pd]–SiHF₂) to 70° in ([Pd]–SiCl₃). The Hirshfeld charge analysis indicated a charge flow from [Pd] to SiR₁R₂R₃, producing a polar Pd–Si bond. A large value for the charge flow corresponded to a short Pd–Si bond separation.^{449a}



The Pt complexes, (dhpe)(H)Pt(SiR₁R₂R₃), also exhibit two different Pt–P distances, Pt–H distances between 1.60 and 1.61 Å, Si...H separations from 2.57 to 2.63 Å, and H–Pt–Si angles from 77 to 81°. The optimized geometries do not support a secondary [Pt]–H...Si bonding interaction. The Pt–Si bond energy was ~6.0 kcal/mol higher than that of the Pd–Si bond energies leading to an expectation that the platinum complexes would be more stable and exhibit less fluxionality. The $\Delta E_{\text{RE}}(\text{Pt})$ was ~23 kcal/mol higher than that of $\Delta E_{\text{RE}}(\text{Pd})$. A set of SiR increments can be derived for ΔE_{RE} , which vary from 7.4 (R = H) to 10 (R = Cl) kcal/mol for Pd complexes and from 15 (R = H) to 20 (R = Cl) kcal/mol for Pt. The values for Pt are consistently larger by 7.4 kcal/mol (R = H, Me, Ph) and 7.9 kcal/mol (R = Cl, F), leading to the conclusion that an inherent transition metal effect on the energies of RE exists. The authors demonstrated that the differences in the Pt–Si bond relative to Pd–Si lie in the consideration of relativistic effects. A relativistic stabilization for Pd–Si was found to be 26 kcal/mol but for Pt it is 13 kcal/mol, thus producing stronger Pt–Si and Pt–H bonds. The authors concluded that: “Whereas the Pd–Si and Pd–H bond energies are fairly well approximated in nonrelativistic calculations, the nature of the Pd–H and Pd–Si bond changes significantly when relativistic contributions are either included or omitted.”^{449a}

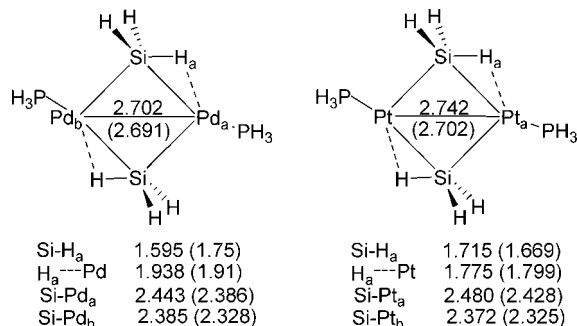


Figure 39. Optimized geometries for $M_2(SiH_3)_2(PH_3)_2$ ($M = Pd, Pt$) showing bond distances in Angstroms with experimentally determined values in parentheses for comparison.⁴⁵⁶

The calculations for the stabilization of an isomer(s) of Si_2H_2 by Rh were described in the previous section, but the calculations were also performed for the Pt(0) complex.⁵⁰⁵ In the Pt case, the complex of $(R_3P)_2Pt$ with the 2H-bridged Si_2H_2 species (isomer C in Figure 35) was almost the same energy as that of the vinylidene isomer (B in Figure 35). The complex of the acetylene-type isomer was moderately less stable, but the acetylene-type Si_2H_2 is distinctly less stable. It was proposed that the vinylidene isomer could possibly be synthesized as a mixture with the 2H-bridged Si_2H_2 species.⁵⁰⁵

7.3.7.2. Dinuclear Complexes. The study of silylene-bridged dinuclear complexes, $M_2(Si_2H_4)(PH_3)_4$ discussed in the previous section (7.3.6) for Rh also included the Pd(0) and Pt(0) analogues.⁵⁰⁶ The Rh(0) complex was classified as a bis(μ -silylene)-bridged complex (see Figure 36). Since two additional electrons have been added for the Pd and Pt analogues, the d_σ - d_σ antibonding orbital is now doubly occupied as was the case for $[Rh_2(\mu-SiH_2)_2(PH_3)_4]^{2-}$, and thus, there was no M-M σ -bond in either the Pd(0) or Pt(0) complexes. The occupation number of the Pd-Si bond was 0, but that of the Si-Si bond indicated that the complex should be characterized with a μ -disilene-bridged form, $Pd_2(\mu-Si_2H_4)(PH_3)_4$. The occupation numbers for the Pt analogue depended on the basis sets used, but the occupation number was 0 for the π - and π^* -interactions of the Si=Si bond for all levels of calculations. Therefore, the Pt complex was characterized as a bis(μ -silylene)-bridged complex with a weak Si-Si bonding interaction. The calculated structures after a two-electron oxidation for both the Pd and Pt complexes provided $[M_2(\mu-SiH_2)_2(PH_3)_4]^{2+}$ with a M-M σ -bond. The two-electron oxidation of the Pd(0) and Pt(0) complexes was predicted to be achievable with an oxidant such as Cl_2 .

The bonding nature of the Pd(I) and Pt(I) complexes, $M_2(\mu-\eta^2-H\cdots SiH_2)_2(PH_3)_2$, as models for complexes of the composition $M_2(HSiR_2)_2(PH_3)_2$ ($R = \text{aryl, etc.}$) was also the subject of theoretical studies (DFT, MP2 to MP4(SDQ), and CCSD(T) methods).⁴⁵⁶ The objectives included a determination of how the 3c-2e and agostic interactions were formed in $M_2(SiH_3)_2(PH_3)_2$, how these interactions might determine the geometry and bonding nature of the dinuclear complexes, and a determination of any differences between the Pd and Pt analogues. The optimized geometries are shown in Figure 39.⁴⁵⁶

The Pd-Pd and Pd-H distances agree with the experimental values, but the Pd-Si bond lengths are longer and the Si-H bond length is much shorter than the experimental values.^{121a,b,122} The optimized Si-H, 1.595 Å, for the Pd

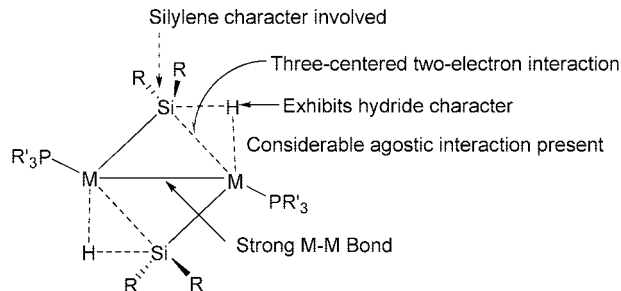


Figure 40. Summary of the major bonding features in the dimers $M_2(SiH_3)_2(PH_3)_2$ as determined by calculations.⁴⁵⁶

system exceeds that of the average Si-H bond length (1.5 Å), suggesting that an agostic interaction with the metal center could be present, although it appeared to be a stronger interaction for the Pt complex than for the Pd complex. The calculated NMR chemical shifts indicated that the SiH_3 in $Pd_2(SiH_3)_2(PH_3)_2$ was in between that of a silyl and a silylene group. The differences between the Pd and Pt complexes are moderate, and the bonding nature appeared to be the same and is depicted in Figure 40. The stronger Pt-Pt bond and the agostic interactions in the Pt complex were attributed to the larger size of the d-orbitals on Pt.⁴⁵⁶

An earlier study of the bonding in $[L_nM(\mu-\eta^2-HSiR_2)]_2$ ($M = Pd, Pt, Rh, Fe, W$ and Ti ; $L = PH_3$ or CO) by DFT (B3LYP) methods was reported by Choi and Lin.⁵⁰⁸ The calculated structural features for the Pt and Pd complexes agreed with the X-ray determined structures $[(C_6H_{11})_3PPt(\mu-\eta^2-HSiMe_2)]_2$ ⁵⁰⁹ and $[(Me_3P)Pd(\mu-\eta^2-HSiPh_2)]_2$ (**2-81**)^{121a} except for the M-P distances, which were overestimated in the calculation. The metal centers exhibited a distorted square-planar arrangement, and the metal center could be viewed as a mononuclear η^2 -silane complex with one of the organic substituents at Si replaced by a metal fragment. The $M\cdots H$ distances were longer than a normal terminal metal-hydride distance (<1.70 Å for both metals). The shorter $Si\cdots H$ distances seem to indicate that the bis(μ - η^2 -silane) complexes are more nonclassical than their mononuclear analogues. The shorter $Si\cdots H$ distance was attributed to a decrease in $metal(d) \rightarrow Si-H(\sigma^*)$ due to a metal substituent that makes the Si center more electron rich and weakens the back-donation from the metal. In a qualitative sense, if the dinuclear complex is considered as two T-shaped ML_3 units with an a_1 frontier fragment orbital that forms the M-M bonding orbital, and the t_{2g} set and d_{z^2} are a set of 8 nonbonding MOs, then occupation of the 8 orbitals along with the M-M bonding orbital gives a dinuclear complex with a 30-electron count and each metal center has a 16-electron count (when the metal-metal bond is present). Similar complexes of Fe, Rh, W, and Ti, conforming to a 18-electron count for the metals, were also discussed.⁵⁰⁸

In a study, reported earlier, the nature of the four-membered ring structures for $M_2(\mu-EH_2)_2(P_2)_2$ ($M = Pd, Pt$; $E = Si, Ge$; $P_2 = (PH_3)_2$ or $H_2PCH_2CH_2PH_2$) was studied by Sakaki and co-workers, although only the silicon complexes will be discussed here.⁵⁰⁷ The calculations (DFT) also revealed a difference between the bonding in the Pd complexes versus the Pt complexes. For $Pt_2(SiH_2)_2(P_2)_2$, the complex should be described as a di(μ -silylene) dinuclear platinum(0) complex with a Pt_2E_2 four-membered ring. This assignment was determined from occupancy numbers of σ - and π -NBOs of the Si-Si bond that were zero, whereas the occupancy number of the Pt-Si bonding NBO was 1.80–1.84 and the antibonding counterpart was 0.42–0.46. The Lapla-

cian indicated no electron density between the two silicon centers but a bonding interaction between the Pt and Si atoms. For the Pd analogue, however, a μ -disilene-bridged dinuclear palladium(0) description was more appropriate because both the Laplacian of electron density and the NBO analysis were consistent with the presence of a Si–Si bond. The difference between the Pd and Pt cases was attributed to a d-orbital on Pt(0) that was higher in energy than the Pd(0) d-orbital; thus, the π -back-donation between Pt(0) and disilane is stronger than in the Pd(0) case, and the Si–Si bond of the Pt(0) complexes is weakened to a greater extent than that of the Pd(0) counterpart. Calculations were also performed for $M(\text{Si}_2\text{H}_4)(\text{P}2)$ ($M = \text{Pd}, \text{Pt}$) where the Pt complex was a three-membered metallacycle with a Si–Si single bond and Pt–Si covalent bonds. The Pd(0) analogue, however, was characterized as a disilene complex with a Si=Si double bond coordinated to the metal center.⁵⁰⁷ The complexes seem to conform to the DCD model described earlier in this section.

For hydrido-bridged diplatinum precatalysts used for hydrosilylation of alkynes, the model complex $[(\text{H}_3\text{P})(\text{H}_3\text{Si})\text{Pt}(\mu\text{-H})_2]_2$ was calculated (DFT/B3LYP).⁵¹⁰ The dimer exhibited C_{2h} symmetry and slightly asymmetric Pt($\mu\text{-H}$)₂Pt bridges with a difference of 0.03 Å for Pt–H and H \cdots Pt distances. The SiPtP angle of 90.7° is consistent with a square planar environment about Pt, although distorted by the hydride bridges. The Si \cdots H_{br} distance was ~ 2.75 Å, which the authors viewed as a weak interaction although the value was outside the normal range for weak interactions described in section 5. The calculated Pt \cdots Pt distance was 2.742 Å, which is longer than the sum (2.62 Å) of the covalent radii. The predicted dissociation energy was found to be 25.4 kcal/mol.⁵¹⁰ Other aspects of the catalytic cycle for hydrosilylation are discussed in section 7.3.6.

The calculations for the stabilization of an isomer(s) of Si₂H₂ by Rh were described in the previous section, but the calculations were also performed for the Pt(0) complex.⁵⁰⁵ In this case, the complex of (R₃P)₂Pt with the 2H-bridged Si₂H₂ species (isomer C in Figure 35) was almost the same energy as that of the vinylidene isomer (B in Figure 35). The complex of the acetylene-type isomer was moderately less stable, but the acetylene-type Si₂H₂ is distinctly less stable. It was proposed that the vinylidene isomer could possibly be synthesized as a mixture with the 2H-bridged Si₂H₂ species.⁵⁰⁵

7.3.7.3. Oxidative Addition and Reductive Elimination.

The reaction of $[(\text{P}\cap\text{N})\text{PtMe}_2]$ ($\text{P}\cap\text{N} = (\kappa^2\text{-P},\text{N})\text{-Me}_2\text{N}(\text{CH}_2)_3\text{PPh}_2$) with HSiEt₃ resulted in immediate formation of $[(\text{P}\cap\text{N})\text{Pt}(\text{H})\text{Me}]$ and MeSiEt₃ followed by formation of $[(\text{P}\cap\text{N})\text{Pt}(\text{SiEt}_3)\text{Me}]$ (**3-283**).²⁹⁰ The proposed sequence involved two separate steps, OA of Et₃SiH to the starting complex and RE of MeSiEt₃ to produce $[(\text{P}\cap\text{N})\text{Pt}(\text{H})\text{Me}]$, the OA/RE of which gave the observed silyl-substituted Pt complex. This speculation was confirmed by DFT calculations using H₂PCH₂CH₂NH₂ as a model for P \cap N and SiH₄ as the model for the silane. In each step, a 6-coordinate intermediate was found and the geometry was optimized. The first OA produced an octahedral Pt(IV) with a SiH₃ *cis* to both Me groups, allowing for RE of CH₃SiH₃. The OA of HSiEt₃ to $[(\text{P}\cap\text{N})\text{Pt}(\text{H})\text{Me}]$ also produced an octahedral Pt(IV) complex where the two H's are *cis*, allowing for reductive elimination of H₂. Both RE reactions were exothermic. In the actual experiment, both MeSiEt₃ and CH₄ were observed in the reaction mixtures. The difference

between the first and second steps was attributed to the different *trans* effects in the Pt(IV) intermediates.²⁹⁰

The oxidative addition of Si–H and Si–C σ -bonds to Pt(0)⁵¹¹ and reductive elimination of Si–C from Pt(II) centers^{512,513a} and Pd(II) centers⁵¹⁴ have been the subject of several calculations because of the relevance to hydrosilylation mechanisms. The generally accepted mechanism for hydrosilylation of olefins and alkynes involves the Chalk-Harrod or modified Chalk-Harrod catalytic cycle, which includes OA of SiH₄ to the metal center, coordination of the olefin, insertion of the olefin into either M–Si or M–H, followed by RE of Si–C. All the steps in the cycle have been studied theoretically, and Sakaki and co-workers have reviewed the work published as of early 1998.^{515a} The theoretical studies in this section will focus on publications from 1998 to 2008.

The OA of CH₄ and its heavier congeners (AH₄) with uncoordinated Pd(0) was studied by relativistic density functional theory by van Stralen and Bickelhaupt.^{515b} The authors wished to establish the trends in activation and reaction enthalpies for A–H in a direct oxidative insertion (OxIn) and to determine if there was an alternative S_N2-type mechanism for A–H bond activation. The insertion of Pd into A–H (A = Si, Ge, Sn, Pb) proceeded spontaneously without formation of a stable reactant complex and without a transition state and was overall exothermic. This was viewed as consistent with the experimental observation of a spontaneous reaction of SiH₄ and Ni in the matrix (at 12 K) that was reported by Himmel (see **1-5**).²³ The barrier-free insertion of Pd contrasts with the results for Pd(PH₃)₂ and SiH₄ calculated earlier by Sakaki et al., where a reactant complex formed prior to the transition state for insertion into the Si–H bond.^{515c} A second reaction channel was calculated for a route that involved nucleophilic attack of Pd at the A-center opposite to the A–H bond that was activated in an earlier stage. This route results in dehydrogenation of AH₄ to give PdAH₂ by a 1,1-elimination, but this process was less exothermic than OxIn (formation of H₃APdH).^{515b}

Sakaki and co-workers addressed the transition state on OA of Si–H and of Si–C (and the corresponding carbon compounds) to Pt(PH₃)₂ (with a linear P–Pt–P geometry) by ab initio methods (MO/MP2-MP4SDQ, CCD, and CCSD).⁵¹¹ These calculations revealed that the OA of Si–H σ -bonds occurred through a planar TS that was predicted from the orbital interaction diagram, but the OA of SiH₃CH₃ took place through an unexpected nonplanar TS. The interesting feature for OA of Si–C was that the Si–C approached parallel to the P–Pt–P axis, and as the Si–C lengthens, the Si–C bond pivoted and became approximately perpendicular to the PtP₂ plane. After the TS, the Pt d-orbital populations started to decrease, indicating charge transfer from Pt to Si–C, which would be required to break the bond. The Pt–P bonds lengthen to stabilize the singlet state, and the Pt–Si and Si–C distances shorten to those observed in the product. Thus, an electronic factor is not responsible for the nonplanar TS, but it is most likely due to a steric factor. An electronic factor does stabilize the planar TS relative to the nonplanar TS. Not unexpectedly, the OA of Si–C has a higher *E*_a than does OA of H–Si. In a separate report, Sakaki and co-workers calculated the Pt(PH₃)₂-catalyzed reaction of SiH₄ with C₂H₄ in which a *cis*–*trans* isomerization of (H₃P)₂Pt(H)(SiH₃) played a role. The isomerization was promoted by complexation with ethylene, producing a 5-coordinate intermediate that undergoes Berry pseudo-

rotation resulting in the *cis*–*trans* isomerization with a barrier similar to that of the rate-determining step of the Chalk–Harrod mechanism without the *cis*–*trans* isomerization. The results suggested that the ethylene-promoted *cis*–*trans* isomerization cannot be ruled out as a possible mechanism.⁵¹¹

A related study was reported a few years later for the mechanism of the same reaction [SiH_4 and $\text{Pt}(\text{PH}_3)_2$] using fully optimized DFT methods (performed without symmetry constraints) and ab initio molecular dynamics (AIMD) simulations.⁵¹⁶ In this study, however, the SiH_4 bond did not lie in the P–Pt–P plane in the TS, but SiH_4 approached the metal center in an out-of-plane trajectory with a dihedral angle between the Pt–Si–H and P–Pt–P planes of $\sim 52^\circ$. This could conceivably result in formation of a *trans*– $(\text{H}_3\text{P})_2\text{Pt}(\text{H})(\text{SiH}_3)$. The bonds and angles in the TS did not differ much from those in the reactants. The OA is exothermic ($\Delta E = -22.2$ kcal/mol) for the production of the *cis*-isomer, and the *trans*-isomer was 11.7 kcal/mol higher than the *cis* isomer. The dynamics simulation indicated that the formation of the incipient Pt–H bond occurred before the Si–H bond was broken and that the OA led directly to the *cis* square-planar product.⁵¹⁶

In another study of OA, Thiel and co-workers used $(\text{COD})\text{Pt}(\text{CCH})_2$ as a model for a real precatalyst (where H is an R group in the experimental alkyne) for hydrosilylation of C_2H_4 with HSiMe_3 .⁵¹⁷ The Chalk–Harrod mechanism requires three sites to be occupied to form $[\text{Pt}^{\text{II}}](\text{H})(\text{SiR}_3)(\text{C}_2\text{H}_4)$ before the ethylene-insertion step. If a 6-coordinate Pt^{II} center was assumed, then the remaining three sites could be occupied by the ligands from the original precatalyst. In the current case, decooordination of $(\text{COD})\text{Pt}(\text{CCH})_2$ would be required. Three possible reactions of the catalyst precursor to give an appropriate $\text{Pt}(0)$ catalyst were considered that involved 20 individual platinum complexes (24 including isomers). The three reactions that led to a 3- or 4-coordinate Pt complex that can enter a Chalk–Harrod cycle included: (a) sequence 1, OA of HSiMe_3 to the catalyst precursor to give a 6-coordinate complex followed by RE of $\text{HC}\equiv\text{CSiMe}_3$ or $\text{HC}\equiv\text{CH}$ to give $(\text{COD})\text{Pt}(\text{CCH})(\text{R})$ ($\text{R} = \text{H}, \text{SiMe}_3$), which then must undergo OA of another HSiMe_3 and RE of $\text{HC}\equiv\text{CR}$ to give $(\text{COD})\text{Pt}(\text{H})(\text{SiMe}_3)$; (b) sequence 2, decooordination of one of the double bonds in COD giving $(\eta^2\text{-COD})\text{Pt}(\text{CCH})_2$; and (c) sequence 3, addition of ethylene to the precatalyst to give the π -complex, $(\text{COD})\text{Pt}(\text{C}_2\text{H}_4)_2(\text{C}_2\text{H}_4)$, which undergoes RE of $\text{HC}\equiv\text{C–C}\equiv\text{CH}$ to give $(\text{COD})\text{Pt}(\text{C}_2\text{H}_4)$. Two plausible pathways were calculated for entering a Chalk–Harrod cycle. One was initiated as in sequence 1 and involved four steps (2 OA and 2 RE) with the rate-determining step being the initial OA of HSiMe_3 with a barrier of 26.8 kcal/mol. The second pathway involved sequence 3 where the RE of $\text{HC}\equiv\text{C–C}\equiv\text{CH}$ was rate-limiting with a barrier of 26.4 kcal/mol. The subsequent two steps involved OA of HSiMe_3 and coordination of C_2H_4 and insertion of C_2H_4 into Pt–H . According to the calculations, sequence 2 was not mechanistically relevant.⁵¹⁷

Hydride-bridged diplatinum complexes have been used as precatalysts for hydrosilylation, and the structural features of the model complex $[(\text{H}_3\text{P})(\text{H}_3\text{Si})\text{Pt}(\mu\text{-H})_2]_2$ were described in the previous subsection (7.3.7). For the first step in the hydrosilylation of acetylene, the structure of the monomer, $[(\text{H}_3\text{P})\text{PtH}(\text{SiH}_3)]$, that would be generated from the dimer was calculated.⁵¹⁰ The monomer exhibited a planar T-shaped structure with the Pt–H *trans* to the phosphine

ligand. The $\text{Si}\cdots\text{H}$ separation distance was 2.40 Å, suggesting a weak $\text{Si}\cdots\text{H}$ interaction between these *cis*-oriented Pt substituents. The LUMO corresponded to a dsp^2 -hybridized orbital of Pt directed to the open coordination site (*trans* to the silyl group), thus allowing interaction with an incoming olefin or alkyne. The addition of an alkyne resulted in formation of an intermediate $[(\text{H}_3\text{P})(\text{H}_3\text{Si})\text{HPt}(\text{HC}\equiv\text{CH})]$. The next step was migratory insertion of the ethyne into the adjacent Pt–H bond, giving a T-shaped $[(\text{H}_3\text{P})(\text{H}_3\text{Si})\text{-Pt}(\text{CH}=\text{CH}_2)]$ with an activation barrier of 10.8 kcal/mol. The T-shaped complex added another mole of acetylene and reductively eliminated $(\text{H}_3\text{Si})\text{HC}\equiv\text{CH}_2$ to produce $[(\text{H}_3\text{P})\text{Pt}(\text{HC}\equiv\text{CH})]$, and the latter reentered the cycle upon OA of HSiH_3 .⁵¹⁰

RE elimination of Si–C is the last step in the Chalk–Harrod and modified Chalk–Harrod mechanisms for hydrosilylation of olefins. The reductive elimination step has been calculated by the groups of Sakaki^{512,513a} and Frenking⁵¹⁸ in the presence of ethylene and the group of Sugimoto⁵²⁰ in the presence of an alkyne. In both cases, elimination from a 4-coordinate versus a 5-coordinate Pt center was calculated, and the elimination from the 4-coordinate Pt was the one lower in energy. The three groups refer to the experimental results of Ozawa and co-workers, who observed that RE of MeSiPh_3 occurred more rapidly from $[(\text{Me}_2\text{PhP})_2\text{Pt}(\text{Me})(\text{SiPh}_3)]$ in the presence of alkynes.^{519a,b} The mechanism proposed by Ozawa involved replacement of a phosphine in $[(\text{Me}_2\text{PhP})_2\text{Pt}(\text{Me})(\text{SiPh}_3)]$ by the alkyne followed by the RE as the rate-determining step.^{519a,b} The purpose of the Frenking study was to investigate the proposed mechanism and to probe whether a 5-coordinate species involving the alkyne was a possible pathway, as well as to determine the nature of the phosphine displacement in the first step. Calculations for the starting model complex, *cis*– $[(\text{H}_3\text{P})_2\text{Pt}(\text{CH}_3)(\text{SiH}_3)]$, gave structural parameters in agreement with those of the experimental bond lengths determined for *cis*– $[(\text{MePh}_2\text{P})_2\text{Pt}(\text{Me})(\text{SiPh}_3)]$.^{519a} The study demonstrated the following:

(1) The RE proposed by Ozawa et al.^{519b} was supported by the calculated results and the rate-determining step occurred through a 4-coordinate TS, and although possible, the 5-coordinate TS was higher in energy.

(2) The first step was association of the alkyne with $[(\text{H}_3\text{P})_2\text{Pt}(\text{CH}_3)(\text{SiH}_3)]$ to form a trigonal-bipyramidal species with Me and PH_3 in axial positions, which then eliminated PH_3 to give 4-coordinate Pt where the alkyne has replaced the PH_3 that was *trans* to the SiH_3 group (another example of the larger *trans*-effect of a silyl group); it then proceeds to the TS where the Si–C bond was developed followed by elimination of CH_3SiH_3 and PH_3 to give $[\eta^2\text{-HC}\equiv\text{CH}]\text{PtPH}_3$.

(3) Calculated activation barriers for the model compounds are in good agreement with the experimental values reported by Ozawa et al.

(4) The energies calculated by the B3LYP and CCSD(T) methods showed that the relative stabilities of complexes with different coordination numbers is poorly reproduced by the B3LYP method.

Sakaki and co-workers also showed that RE from $[(\text{H}_3\text{P})(\text{C}_2\text{H}_4)\text{Pt}(\text{CH}_3)(\text{SiH}_3)]$ was lower in energy than RE from $[(\text{H}_3\text{P})_2(\text{C}_2\text{H}_4)\text{Pt}(\text{CH}_3)(\text{SiH}_3)]$ and provided more details concerning the insertion of olefin into the Pt–H and Pt–SiR_3 bonds as well as subsequent isomerization of the ethylene-insertion product.⁵¹²

A few years later, Sakurai and Sugimoto⁵²⁰ reported a DFT study of the alkyl group dependence on C–Si reductive eliminations from $[(\text{Me}_3\text{P})_2\text{Pt}(\text{R})(\text{SiPh}_3)]$ ($\text{R} = \text{Me}, \text{Pr}$), which was prompted by the results of Ozawa and co-workers, who showed that when $\text{R} = \text{Et}, \text{Pr}$, or Bu the RE rates were much smaller than the rate when $\text{R} = \text{Me}$.⁴²⁷ The optimized geometry agreed with the experimental values,^{519b} although all the calculated bonds to Pt were longer than the experimental values. The slower rate for the Pr complex was attributed to steric effects between the Pt–alkyl group and the SiPh_3 substituent as well as R–Si bond energy differences. If the ligands in the Pt complex are bulky, the TS geometry becomes more like the product in order to relax the steric repulsion and the energy difference in the Si–Me and Si–Pr, formed in the product, becomes more significant in determining the activation energy.⁵²⁰

Reductive elimination of C–X from the Pd center in $[(\text{H}_3\text{P})\text{Pd}(\text{XH}_3)(\eta^3\text{-C}_3\text{H}_5)]$ ($\text{X} = \text{C}, \text{Si}, \text{Ge}, \text{Sn}$) was investigated by MP2-MP4(SDQ) and CCSD(T) methods.⁵¹⁴ The calculations for the starting complex show that the C^3 of the allyl group positioned *trans* to XH_3 is longer than the C^1 bond that is positioned *trans* to PH_3 because XH_3 exhibits a stronger *trans* influence than does PH_3 . The $\text{C}^1\text{--C}^2$ distances were 1.443–1.452 Å and the $\text{C}^2\text{--C}^3$ bonds were 1.395–1.400 Å, indicating a slight distortion of the η^3 -allyl group to an η^1 -allyl structure. In the transition state for C–X ($\text{X} = \text{Si}, \text{Ge}, \text{Sn}$) elimination, the C–X bond is $\sim 80\%$ formed. This calculation suggests that the C–X bond forms without the Pd– XH_3 bond breaking and is attributed to hypervalency that can occur with the heavier group 14 elements. The energy of activation for RE of $(\eta^3\text{-C}_3\text{H}_5)\text{--XH}_3$ is higher than that of $\text{CH}_3\text{--XH}_3$ RE and is attributed to the higher bond energy of Pd– $(\eta^3\text{-C}_3\text{H}_5)$.⁵¹⁴

The exchange of C–Cl and Si–H was catalyzed by $[(\kappa^2\text{-P}, \text{N})\text{-Ph}_2\text{PCH}_2\text{CH}_2\text{NMe}_2]\text{PtMeCl}$ to give C–H and Si–Cl products.⁵²¹ The mechanism for this transformation was investigated through DFT calculations (B3LYP), which were performed in two stages. In the first stage, the reaction was modeled with SiH_4 and $\text{H}_2\text{NCH}_2\text{CH}_2\text{PH}_2$ with the two isomers of $[\text{P}\cap\text{NPtMeCl}]$.⁵²² The most stable isomer, $[\text{P}\cap\text{NPtMeCl}]$ (P and Cl *trans*), and SiH_4 (the model silane) required 23.6 kcal/mol to reach the TS leading to a 6-coordinate OA product with H_3Si *trans* to the CH_3 group, which was 16.4 kcal/mol higher in energy than the starting components. In contrast, the less-stable isomer (P and Cl *cis*) required 22.7 kcal/mol to reach a similar TS, but the 6-coordinate Pt(III) complex (SiH_3 and Cl *trans*) was formed with release of 13.1 kcal/mol. Since the energy difference between *trans*- and *cis*-forms is < 10 kcal/mol, the two could be present in an equilibrium. The second stage of the mechanism used the models SiH_4 and the nonchelated system, *cis*- $[(\text{H}_3\text{P})(\text{H}_3\text{N})\text{PtMeCl}]$ (P and Cl *cis*). The OA of SiH_4 gives a TS that relaxed to an octahedral Pt(III) complex with Si and Cl *trans* to each other. To react further, the octahedral complex must lose the ligand (equivalent to decoordination of the N-end of the $\text{P}\cap\text{N}$ chelate) to give a distorted trigonal bipyramid in an endothermic process. The SiH_3 group must move towards the Cl ligand to reductively eliminate H_3SiCl and provide the 3-coordinate complex $[(\text{H}_3\text{P})\text{PtMeH}]$, which then undergoes OA of CH_3Cl and RE of CH_4 to complete the cycle after recoordination of NH_3 to give the 4-coordinate complex in an exothermic step.⁵²²

How the chemistry of organo(silyl)platinum(II) complexes is relevant to catalysis has been reviewed by Ozawa.^{513b} In

this review, three types of processes are categorized that result in C–Si bond formation by RE from $\text{R}(\text{SiR}')_3\text{PtL}_2$ complexes.

7.3.7.4. Silylene Complexes. The isolation of stable silylenes such as 1,3-dialkyl-1,3,2-diazasilol-2-ylidene and variations of this basic structure collectively referred to as N-heterocyclic silylenes or NHSi have led to investigations of their reactivity with metal precursors with the objective of isolating stable, base-free metal silylene complexes. Isolation of such complexes has been reported for Cr, Mo, W, Fe, Ru, Rh, Ni, Pd, Pt, and Lu (see Table 8 for examples). The NHSi ligand contains a lone pair in an approximate sp^2 orbital in the same plane as the directly attached substituents, and this lone pair functions as a σ -donor ($\text{R}_2\text{Si} \rightarrow \text{ML}_n$). An empty p-orbital orthogonal to the lone pair can function as an electron-pair acceptor ($\text{R}_2\text{Si} \rightarrow \text{ML}_n$) through π -back-donation. Thus, the silylene ligand bears an analogy to a phosphine ligand.

A theoretical study of base-stabilized silylene complexes examined the substituent effects on the silicon–metal bond for base-free complexes of Os, Ru, Ni, and Pt (as well as four base-stabilized ruthenium complexes) and employed Hartree-Fock ab initio molecular-orbital calculations.^{501b} The Ni complex, $(\text{OC})_2\text{Ni}[\text{Si}\{\text{t-BuNCH}=\text{CHNt-Bu}\}]_2$, exhibited the largest silicon–metal overlap (0.454 electrons) of all the complexes studied. In Arnold's study of ruthenium silylenes^{501a} cited earlier (section 7.3.5), the problem of generating base-free silylene complexes was attributed to the small stabilization of the metal fragment frontier orbitals when bonding to the silylene unit. However, in the case of Ni, the electronegativity value is 1.8 (Pauling scale) relative to 2.2 for Ru, Os, and Pt; thus, the valence orbitals of the more electropositive Ni should have a higher energy, leading to a greater overlap population.

A more recent calculation study compared the effects of replacing NHCs with NHSi's at a Pd(0) center.⁵²³ The authors sought to explain the unusual experimental observation that the stronger bound NHC in $\text{Pd}(\text{CNH})_2$ exchanged rapidly with NHSi to give $\text{Pd}(\text{SiNH})_3$. The structures were optimized (density functional hybrid model Becke3LYP) first for complexes where the substituent at the N-centers were Me groups and then with the actual system where the substituent was a t-Bu group. With the Me group model in the 2-coordinate system, the NHC complex was more stable than either $\text{Pd}(\text{NHC})(\text{NHSi})$ or $\text{Pd}(\text{NHSi})_2$, although in the 3-coordinate system, the $\text{Pd}(\text{NHC})(\text{NHSi})_2$ complex was more stable than either $\text{Pd}(\text{NHC})_2(\text{NHSi})$ or $\text{Pd}(\text{NHC})_3$. The steric interactions are less in the case of a NHSi and it is unclear why the replacement reaction would take place even though the bond strength was lower. To account for the experimental observations, the calculations were performed on the actual system with t-Bu substituents at nitrogen. The calculated Pd–C bond strength in $\text{Pd}(\text{NHC})_2$ (t-Bu substituents) was lower, and thus, replacement of NHC by NHSi was possible. The main message here was that the NHC–metal bond was influenced by the steric bulk at the N-center and that calculations with real systems and not model compounds may be necessary to reproduce the experimental observations.

The dialkylsilylene shown in Figure 41A reacted with $[(\text{Cy}_3\text{P})_2\text{Pd}]$ to give the 14-electron, bis(silylene) complex shown in Figure 41B.^{421d} The Si–Pd–Si angle determined in the X-ray structure was nearly linear (179°), and the geometry about the two silicon centers was planar. No agostic

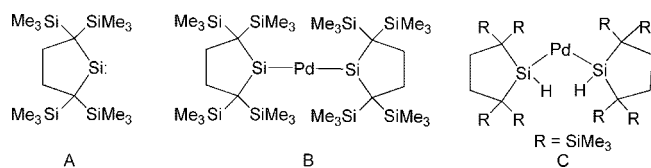


Figure 41. (A) Dialkylsilylene; (B) Pd complex of disalkylsilylene A; and (C) hydrogenation product of the bissilylenepalladium complex B.^{421d}

interactions with the protons of the SiMe₃ groups were observed. The reaction of the [(silylene)₂Pd] complex with H₂ gave the novel 12e dicoordinate Pd complex shown in Figure 41C; in this case, the Si–Pd–Si angle was 97° with no Si–H···Pd interactions, but there are agostic interactions between the hydrogens of the CH₃ groups and the Pd center. These agostic interactions do not appear to be retained in solution. The *J*_{SiH} value and the *ν*_{SiH} band are both in the range that is typical of a hydrosilyl–transition metal complex. DFT calculations for the model complex, [(Me₂Si)₂Pd], indicate that the optimized geometry gave a Si–Pd–Si angle of 116.7°. The angle of the optimized geometry increases as the bulk of the silylene ligand increases. The skeleton for the 14e [(silylene)₂Pd] complex is intrinsically bent due to π -back-donation. The linear skeleton for the silylene complex B shown in Figure 41 may be due to steric effects of the bulky silylene ligands. Calculations for the 12e complex C in Figure 41 were not reported, although the simpler case with two hydrosilylacyclopentane ligands bonded to Pd was strongly bent with a Si–Pd–Si angle of 95.7° as predicted on the basis of a qualitative analysis of the Walsh diagram.^{421d}

The elimination of the cationic species, {MeSi[MeNCH=CHNMe]}⁺, from the 4-coordinate model cationic Pd complex, [(H₃P)₂(CH₃)Pd(SiHN)]⁺ (and the corresponding C and Ge systems), has been the subject of calculations (B3LYP DFT level).⁵²⁴ Although this could be viewed as a RE reaction, the pathway was somewhat different from those described earlier in this section. The activation barrier for the coupling of the silylene and the Me group was much lower than that predicted for the carbene ligand. In the TS, the Me group bridges the Pd–Si bond and the C center is almost equidistant from both Pd and Si. After migration, a 3-coordinate Pd complex was produced, and the Si center has become tetrahedral with a bond distance to Pd that was typical of a sp³-Si-to-Pd bond. Thus, the authors favored a description of a migration of the Me group to the silylene to give an anionic silyl ligand instead of a RE. The separated silicenium cation and Pd(PH₃)₂, however, have a higher energy than both reaction products and the starting complexes. To determine whether a solvent would promote the reaction, the reaction was recalculated with addition of a THF molecule. Two pathways were found where the THF was positioned either between the Si and a P or between the C and a P ligand. Neither the starting complex nor the TS structure for the Me migration was significantly perturbed by the addition of the THF. The energy of the separated silicenium ion and Pd(PH₃)₂ was reduced with THF as a result of the donor interaction of THF with the silicenium ion. The results of the calculation showed that the energy required for migration of an alkyl group from Pd to the silylene ligand lowered the energy of the product to such an extent that RE became feasible.⁵²⁴ A DFT study of σ - and π -bond activation of Pd=Si bonds in the model silylene complex, (H₂PCH₂CH₂PH₂)Pd=SiH₂ (and the C and Sn analogues), has also been published.⁵²⁵

7.3.7.5. Cases from Tables 1, 2, and 3. A study of the kinetics of the exchange of dppe for the monodentate phosphines in *cis*-[(PhMe₂P)₂Pt(SiMePh₂)₂] suggested that the reaction occurred by a dissociative process.⁵²⁶ DFT calculations for a series of model complexes [(R₃P)₂Pt(SiH₃)₂] (R = H, Me) and [(R₃P)₂Pt(SiMe₃)₂] (R = H, Me) provided structural parameters including PPtP/SiPtSi dihedral angles and total binding energies. The calculations for the dissociative process provide an estimate for the Pt–PH₃ bond energy that was 7.2 kcal/mol for *cis*-[(H₃P)₂Pt(SiMe₃)₂] and 23 kcal/mol for Pt–PMe₃ in *cis*-[(Me₃P)₂Pt(SiMe₃)₂]. The latter value was considered in “reasonable” agreement with the experimental value of 28.15 kcal/mol, and an even closer agreement of the Pt–PR₃ bond energy was expected for the actual phosphine, PMe₂Ph. The structure of *cis*-[(PhMe₂P)₂Pt(SiMePh₂)₂] exhibited a dihedral angle between the PtP₂ and PtSi₂ planes of 38°, ^{282a} the same value calculated for *cis*-[(Me₃P)₂Pt(SiMe₃)₂]. The distortion from planarity in these P₂PtSi₂ complexes could be attributed to four tertiary ligands at the Pt center, but it has been demonstrated that the more sterically demanding SiPh₃ ligand actually gave rise to a smaller dihedral angle.²⁸¹ The calculations⁵²⁶ showed that the larger twist angles in the four calculated complexes come from replacing the hydrogen substituents at the silicon with the larger Me groups. The increasing twist angles appear to be related to greater electron donation and stronger binding of silyl ligands and, thus, were not purely steric in origin. The steric strain caused by the tertiary ligands can be decreased by a twist of two ligands out of the plane, which results from the hybridization that occurs when two strong σ -donors occupy *cis*-positions. In the C_{2v} symmetry of an idealized square-planar complex, the s and d_{x²–y²} orbitals have a₁ symmetry and the p_x and p_y have b₁ and b₂ symmetries. If two ligands are better σ -donors, then these ligands interact more strongly with the orbitals of a₁ symmetry and decrease the contribution of the a₁ orbitals to the bonding of the *trans* ligands. The two Pt–Si bonds have high “s” character, and a tetrahedral twist of these two ligands does not reduce the overlap to any large extent.^{281a,526} If the silicon center contains electron-withdrawing substituents, the b₁ orbital becomes more prominent, reducing the dihedral angle.²⁸¹

Distortions from planarity were also observed in the complexes formed from a more complex P \cap N ligand in two (bistrichlorosilyl)Pd complexes, **3-258**, and a variant of the pyrazole ring with a mesityl substituent (Table 3, footnote 272).²⁷⁷ Two anomalous features were revealed in the solid-state structures: (i) PPdN/SiPdSi dihedral angles of ~18° for **3-258** and 34° for the mesityl substituted P \cap N ligand; and (ii) unusually long Pd–P bond lengths of 2.4559(16) in **3-258** and 2.504(2) in the mesityl derivative. A DFT calculation involved a combined QM/MM method in order to sort out electronic and steric effects. Six models were examined, and in the case of three of the models, a region was defined for the QM calculations and the portion outside of the region was treated by molecular mechanics force field. The full QM optimization of the mesityl-substituted derivative gave parameters that were in the closest agreement with the solid-state structure, which included a correspondence with the Pd–P bond distance as well as the P–Pd–N/Si–Pd–Si dihedral angle. The strong *trans*-influence of the trichlorosilyl substituent accounts for a part of the Pd–P bond elongation, but the steric interaction between the PPh₂ and the mesityl group was considered primarily responsible for

the long bond. The deviation from square-planar geometry at the Pd center was attributed entirely to steric factors.²⁷⁷

As mentioned earlier, calculations were performed for complexes when the role of the hydride appeared to be ambiguous. One of the more interesting cases is that of **1-64**, (depe)Ni[η^2 -H-SiH(C₆H₄SiH₂)₂], which appears to contain a Ni \cdots H \cdots Si interaction in the solid state, but the low-temperature solution NMR data suggested that the complex was better described as a tetravalent tris(silyl)(hydrido)nickel derivative.⁶⁵ The structure was fully optimized (DFT/B3LYP) to give a geometry consistent with a distorted octahedral Ni(IV) complex with the three Si centers occupying a face and the hydride occupying a coordination site at Ni. The Si-H_{br} distance, 1.75(3) Å observed in the solid state, was calculated to be 2.362 Å, which the authors viewed as nonbonding. The calculated Ni-Si distance for the relevant silicon was 2.266 Å, whereas the distance for the same bond in the solid structure was 2.3480(8) Å (the longest recorded Ni-Si distance, see Table 7). Although the authors offer one interpretation for the calculated Si-H_{br} distance, the distance is within the range of a weak interaction (proposed by Lin⁴⁸³ or a SISHA⁴⁵² interaction).

The usefulness of DFT calculations in complexes where the interpretation of the data is ambiguous became important in resolving the question as to whether the trinuclear palladium complex **2-84** contained a Pd(VI) center with six silyl ligands or a Pd(II) center with two silyl ligands and two coordinated Si-Si bonds.¹²³ Tanaka and co-workers reported this unusual complex and provided the two alternative representations but strongly favored the presence of a Pd(VI) center.¹²³ Shortly thereafter, two groups reported the results of theoretical calculations although using somewhat different models.^{527,528} The X-ray parameters for **2-84** showed that there were two Si-Si distances of 2.49 and 2.59 Å, which are similar to those found in the well-known disilane, Ph₃Si-SiPh₃ (2.52 Å⁵²⁹). Alvarez and co-workers determined the continuous symmetry measures, which provide an estimate of the deviation of a coordination sphere relative to an ideal polyhedron, and showed that there was no correspondence to an octahedron or to a trigonal prismatic environment but a good correspondence with a square-planar arrangement if the centroid to two Si-Si bonds was considered for two of the coordination sites. Alvarez et al. carried out DFT calculations for the model octahedral complex [Pd(SiH₃)₆] with geometry optimization assuming each pair of *trans* silyl groups to be equivalent, which gave all Pd-Si lengths of 2.491–2.497 Å but no Si \cdots Si distances <3.5 Å and a triplet state more stable than the singlet. There was no indication in the original publication¹²³ that **2-84** was paramagnetic. A second model, [Pd(SiH₃)₂(η^2 -Si₂H₆)₂], with a square-planar environment of C₂ symmetry was also calculated, which gave a much more stable complex than the octahedral one calculated. Three other models with differently substituted methyl disilanes gave similar results. The authors also optimized the trinuclear complex, substituting 2PH₃ groups for the original chelate and the benzo groups replaced by HC=CH linkers, which gave Si-Si and Pd-Si distances in agreement with the experimental data. The elongation of the Si-Si distance could be accounted for within the Dewar-Chart-Duncanson model with a σ (Si-Si) MO donating a pair to the metal and a σ^* (Si-Si) MO accepting back-bonding electron density from π -type metal orbitals.⁵²⁸ The parallel study performed by Cramer and co-workers⁵²⁷ performed preliminary calculations on PdF_x (*x* =

2, 4, 6) before computing optimized geometries and Mayer bond orders for singlet ground states of [Pd(SiH₃)_x] (*x* = 2, 4, 6). The results for the *x* = 4 system gave long Pd-Si bonds and two Si-Si bond distances with a Mayer BO of 0.43, demonstrating a tendency to multicenter delocalized bonding even for Pd(IV). The HOMO calculated for the Pd₃Si₆ framework of **2-84** was dominated by Si-Si σ -bonding between two sets of silicon centers; thus, the assignment of the central Pd in **2-84** as Pd(VI) was not considered warranted. A commentary on hexacoordinate silyl-palladium complexes has also been published by Kostic.⁵³⁰

DFT calculations were also obtained for the model complex (dmpe)PdH(SiMe₂H) to rationalize the fluxional behavior of the actual complex (depe)Pd(H)SiH(^tBu)₂ (**2-78a**). A dynamic process exchanged the Pd-H and the Si-H in **2-78a**.^{120a} The calculations revealed that the symmetric intermediate with two hydrides bridging the Pd-Si bond was the most likely for the observed Si-H/Pd-H scrambling. This case was described in more detail in section 6.1.1.

The calculations for the reaction of Ni⁺ and SiH₄ in the gas phase⁵³¹ were described in section 5.4.2 and the structure of the matrix-isolated product from insertion of Ni atoms into SiH₄ was described in 5.6. DFT calculations were mentioned in the study of stable *trans*-isomers of Pt(Cab^{P,Si}) (**3-256a**, **3-257a**)^{276a} and for [(Pt(μ -SiPh₂)(PMe₃))₃] (**3-298a**),^{298b} but with insufficient detail to be included.

7.3.8. Cu

One of the earliest theoretical studies of NHC's, NHSi's, and NHGe's during this review period was reported in 1998 by Boehme and Frenking for complexes of MCl (M = Cu, Ag, Au).⁵³² The calculations were performed at the MP2 level for the model ligand, X[HNCH=CHNH] (X = C, Si, Ge). On complexation to the metal centers, the N-X-N angles become larger and the X-N bond lengths become shorter than in the free ligands. The bond dissociation energies followed the order Au > Cu > Ag and for C > Si > Ge. The most important finding was that the σ -donation was always greater than the π -back-donation. The NHC was a pure σ -donor, and although σ -donation dominates for both the NHSi and NHGe ligands, back-donation to NHSi and NHGe becomes stronger in their complexes. Although the p(π) population of the X center is increased in the complexes, this is due to stronger N \rightarrow X π -donation, which also explains the N-X bond shortening mentioned above. The metal-ligand bonds were found to be largely ionic but have some covalent contribution. The [HNCH=CHNH]X-MCl bond was primarily the result of a Coulombic attraction between the positively charged metal centers and the lone-pair electrons of the ligand donor. The covalent contribution was a result of donation of the donor lone-pair electrons to the M-Cl σ^* orbital. At the time of publication of the theory paper, there were no known NHSi or NHGe complexes of Cu, Ag, or Au. Since then, a Cu(I) complex of NHSi has been isolated,⁴⁰⁸ but the complex is 4-coordinate not 2-coordinate as in the theoretical study. Nonetheless, two parameters are relevant for [I(Ph₃P)₂Cu(SiNN)] (SiNN = (NCH₂^tBu)₂C₆H₄-1,2)⁴⁰⁸ where the Si-N distances were 1.716(9) and 1.736(9) Å and the Cu-Si distance was 2.289(4) Å compared to the calculated value of Si-N = 1.736 Å and of Cu-Si = 2.137 Å for the model complex, ClCu[Si{HNCH=CHNH}]. The calculated Cu-Si distance is underestimated, but this could be due to the difference in coordination numbers for the Cu(I) center.

Silanes are adsorbed onto gold surfaces and have been studied by Banaszak Holl and co-workers, experimentally, in depth,^{71a,b,c,d} and, more recently, by DFT calculations.^{71e} The primary alkylsilanes chemisorb on a Au(111) surface with cleavage of the three Si–H bonds and formation of three Si–Au bonds. The experimental work was done with longer-chain R groups but the calculations used MeSiH₃. The calculations explored four adsorption configurations: (i) adsorption at the Au(111) “threefold hollow” site, (ii) adsorption atop a single Au atom, (iii) adsorption in a surface vacancy, and (iv) adsorption at a bridge site. The calculations indicated that (i) and (iii) are the preferred sites and that both sites contain Si in a distorted tetrahedral geometry. The hollow site (i) is energetically favorable, but with high coverage, the top site (iii) becomes more stable.

8. Oxidative Addition Reactions of Other Si–X Bonds

8.1. Lanthanides/Actinides

Reactions of organohydrosilanes with lanthanides can lead to silyl–lanthanide complexes, transfer of the hydride from the silane to the lanthanide center, cleavage of a C–Si bond particularly in PhSiH₃, or formation of a Ln–SiH₃ complex. β -Agostic interactions have played a dominant role in the lanthanide complexes that contain the amide group –N(SiHMe₂)₂. Since Y and La complexes have often been treated with the lanthanides due, in part, to the common oxidation state of +3 in their complexes, these two elements from the Sc triad are also treated in this section. The reactions that have resulted in the formation of a Ln–Si bond are given in Table 1, and the complexes with β -agostic interactions are listed in Table 17 (7 of the 15 listings involve Y, but the footnotes list related lanthanide derivatives reported in the respective references).

8.1.1. Silyl Complexes of Lanthanides/Actinides

The general lanthanide starting materials are similar to those discussed for transition metals (Tables 1, 2, 3) and include Ln–H, Ln–Ar, and Ln–R precursors. When Cp*₂SmCH(SiMe₃)₂ was reacted with PhSiH₃, redistribution of the silane occurred, yielding SiH₄ and Ph₂SiH₂ as well as benzene along with a very insoluble Sm(III) trimer, [Cp*₂SmSiH₃]₃ (**1-81**), which represents the first f-element-SiH₃ derivative.⁷² Crystals suitable for X-ray analysis could not be obtained, the Si–H hydrogens were not observed in the ¹H NMR spectrum because of the paramagnetic Sm(III) center, and the parent ion was not observed in the EI mass spectrum although the IR data showed ν (SiH) stretching frequencies consistent with the presence of a SiH₃ group. The trimer structure was assigned on the basis of analogy to samarium trimers produced from the reaction of Cp*₂SmCH(SiMe₃)₂ with Ph₂SiH₂.⁵³³ Lewis bases reacted with **1-81** to give isolable base adducts of the monomer, although these were not very stable.⁷² A similar product mixture was obtained from reaction of [Cp*₂Sm(μ -H)]₂, and the hydride may be the actual species that promoted redistribution through Si–C bond cleavage. Reaction of [Cp*₂SmPh] with PhSiH₃ gave 80% Ph₂SiH₂ (+ 20% benzene) and produced 80% [Cp*₂Sm(μ -H)]₂ as determined in solution.⁷³

The cleavage of a Si–C bond in PhSiH₃ by samarium hydride was assumed to give Cp*₂SmPh, although this was

not observed as an intermediate. To provide support for the “transfer” of an aryl group from Si to Sm, other arylsilanes were examined that might produce a more stable Cp*₂SmAr that could be isolated. This goal was achieved through reaction of the primary silanes C₆F₅SiH₃ and (*o*-MeOC₆H₄)SiH₃. The reaction of 1 equiv of C₆F₅SiH₃ with [Cp*₂Sm(μ -H)]₂ gave quantitative conversion of the silane to [Cp*₂Sm(μ -C₆F₅)]₂ by comparison to an authentic sample prepared by an alternate route. The reaction of (*o*-MeOC₆H₄)SiH₃, however, gave the monomer **1-82** with a chelated *o*-MeO group, but the complex decomposed on isolation attempts.⁷³ Related reactions of [Cp*₂Lu(μ -H)]₂ with PhSiH₃ gave a number of lutetium-containing products that were not identified, but the results indicated a preference for hydride transfer by the silane to lutetium rather than phenyl transfer. The reaction with C₆F₅SiH₃ again gave quantitative transfer of the aryl group to give Cp*₂LuC₆F₅, which was stable enough to be isolated. In the case of the reaction of (*o*-MeOC₆H₄)SiH₃ with [Cp*₂Lu(μ -H)]₂, the monomer **1-83** was formed, isolated, and crystallographically characterized. The reaction of the lutetium precursor, [Cp*₂LuMe]₂, with ArSiH₃ gave similar results but were not as clean as those produced with the hydride precursor.⁷⁴

The lanthanide(II) complexes, Cp*₂Ln(THF)₂, reacted with KH/H₃SiPh to give the polymeric silyl-containing complexes [Cp*₂Ln(SiH₃)(THF)Cp*K(THF)]_n (Ln = Eu (**1-84**), Sm, and Yb).^{75a} The reaction required cleavage of the Si–Ph, just as was the case in the reactions studied by Tilley and co-workers for Sm and Lu.

Two silylene complexes of lanthanides (Sm,⁴⁴² Yb^{443a}) were reported during the review period, although these were not prepared from reaction of a hydrosilane but from the direct reaction of a stable silylene.

Only one example of an actinide silyl species was reported during this review period, and it was prepared by a salt metathesis reaction of IU[N(^{*i*}Bu)Ar]₃ (Ar = 3,5-C₆H₃Me₂) with (THF)₃LiSi(SiMe₃)₃.^{443b} The product, [(^{*i*}Bu)ArN]₃USi(SiMe₃)₃, was isolated and crystallographically characterized, giving the first U–Si bond distance (3.091(3) Å) for a molecular system. DFT calculations provided a description of the U–Si bonding MO, which was mainly derived from a valence Si-*p_z* and a U *d_{z²}*.

8.1.2. Reactions That Involve Transfer of Hydride from Hydrosilanes

The use of hydrosilanes as reducing agents for transition metal complexes was discussed in section 3.7. Thus, the use of hydrosilanes to transfer hydride to lanthanides is not unexpected, and this role was described in the previous subsection. In some cases, the lanthanum hydride was isolated and two examples have been reported by Hou and co-workers.^{328,330a} The addition of Cp*₂Sm(THF)₂ to KCH(SiMe₃)₂ in THF provided [Cp*₂Sm(CH(SiMe₃)₂)Cp*K(THF)₂]_n, which was then reacted with PhSiH₃ to give the first dihydrido Ln(III) complex, [Cp*₂Sm(μ -H)]₂[(μ -H)–K(THF)₂]₃, and (Me₃Si)₂CHSiH₂Ph. The X-ray structure showed that this polyhydrido Sm(III)/K cluster complex consisted of six “Cp*₂SmH₂” and three “KH(THF)₂” units. The hydride ligands were located and refined.³²⁸ By a similar strategy, (Cp')Lu(CH₂SiMe₃)₂(THF) (Cp' = C₅Me₄SiMe₃) reacted at –30 °C with PhSiH₃ to give [Cp'Lu(CH₂SiMe₃)(μ -H)(THF)]₂, which, when treated with additional PhSiH₃ in Et₂O at room temperature, provided the tetramer, [Cp'Lu(μ -H)]₄, and (Me₃Si)₂CHSiH₂Ph.^{330a} Recrystallization from

Table 17. Complexes with β -Agostic La \cdots HSi Interactions

compound	starting metal complex	color % yield m.p., °C	NMR				ref ⁵
			solvent (temp., °C) ^f	¹ H Si–H ²	²⁹ Si ³	other ^d	
17-1 (C ₅ Me ₄ H) ₂ Y[N(SiHMe ₂) ₂]	Y[N(SiHMe ₂) ₂] ₃ (THF) ₂ + C ₅ Me ₄ H ₂ + heat	colorless 85%	C ₆ D ₆	3.94 (oct) ³ J _{HH} \approx ³ J _{YH} = 2.7		¹³ C IR EA X-ray ¹³ C IR	345b
17-2 Cp* ₂ Y[N(SiHMe ₂) ₂]	Y[N(SiHMe ₂) ₂] ₃ (THF) ₂ + C ₅ Me ₅ H + heat	colorless 76%	C ₆ D ₆	4.07 (oct) ³ J _{HH} \approx ³ J _{YH} = 2.7		EA X-ray ¹³ C IR	345b
17-3 Me ₂ Si(C ₅ Me ₄) ₂] YN(SiHMe ₂) ₂ ⁶	M[N(SiHMe ₂) ₂] ₃ + [Me ₂ Si(C ₅ H ₄ H) ₂]	colorless 82%	C ₆ D ₆	4.00 (dssept) ¹ J _{YH} = 2.9 ¹ J _{SiH} = 147	–19.87 (NSi) –32.45 (Si _{br})	EA X-ray ¹³ C IR MS	539
17-4 [Me ₂ C(Ind) ₂] ₂ Y[N(SiHMe ₂) ₂]	Y[N(SiHMe ₂) ₂] ₃ (THF) _x + [Me ₂ C(IndH) ₂]	yellow 14%	C ₆ D ₆	3.56 (d sept), ¹ J _{SiH} = 152, SiH)		[EA] ¹³ C IR MS [EA] ¹³ C IR MS EA ¹³ C	539
17-5 [Me ₂ Si(2-Me-4- Ph- Ind) ₂ M[N(SiHMe ₂) ₂] M = Y ⁷	Y[N(SiHMe ₂) ₂] ₃ (THF) _x + Me ₂ Si(2-Me-4-Ph-Ind ⁸ dH) ₂	lemon yellow 11%	C ₆ D ₆	4.31 (dsept) ¹ J _{SiH} = 148		MS [EA] ¹³ C IR MS EA ¹³ C	539
17-6 <i>rac</i> -[Me ₂ Si(2-Me-BenzInd) ₂]- MN(SiHMe ₂) ₂ M = Y ⁸	Y[N(SiHMe ₂) ₂] ₃ (THF) _x + Me ₂ Si(2-Me-Benz–IndH) ₂	lt. yellow 72%	C ₆ D ₆	2.65 (dsept) ¹ J _{SiH} = 133	–15.90 (d) –26.61 (Si _{br})	⁸⁹ Y IR MS [EA] X-ray	539
17-7 [Me ₂ Si(Fluo) ₂] YN(SiHMe ₂) ₂ ⁹	Y[N(SiHMe ₂) ₂] ₃ (THF) _x + Me ₂ Si(FluoH) ₂	orange 35% ¹⁰	C ₆ D ₆	3.21 (sept)			539
17-8 [C ₅ Ph ₄ H] ₂ La[N(SiHMe ₂) ₂]	La[N(SiHMe ₂) ₂] ₃ (THF) ₂ + C ₅ Ph ₄ H ₂ + heat	yellow 78%	C ₆ D ₆	4.58 (sp) ³ H _{HH} = 2.7		¹³ C IR EA X-ray ¹³ C	345b
17-9 Sm{[μ -N(SiHMe ₂) ₂] ₂ - Sm[N(SiHMe ₂) ₂]}{thf} ₂	Sm[N(SiMe ₃) ₂] ₂ (THF) ₂ + HN(SiHMe ₂) ₂	black >95%	C ₄ D ₈ O	–12.18 (s, 1H) –2.67 (s, 6H)		IR ¹³ C IR MS [EA] X-ray ¹³ C	541a
17-10 [Me ₂ Si(2-MeInd) ₂ M- N(SiHMe ₂) ₂] M = Lu ¹⁰	Lu[N(SiHMe ₂) ₂] ₃ (THF) _x + Me ₂ Si(2-Me–IndH) ₂	lemon yellow 32%	C ₆ D ₆	3.29 (sept) ¹ J _{SiH} = 146		IR MS EA X-ray ¹³ C	539
17-11 Nd[N(SiHMe ₂) ₂] ₃ 2nhc ¹¹	Nd[N(SiHMe ₂) ₂] ₃ (thf) _n + 2nhc	green 69%	C ₆ D ₆	7.62 (br s)		IR ¹³ C IR MS(Cl) EA X-ray ¹³ C	541b
17-12 Nd[N(SiHMe ₂) ₂] ₃ (<i>o</i> -phen) ¹²	Nd[N(SiHMe ₂) ₂] ₃ (thf) _n + <i>o</i> -phen	–89%	C ₆ D ₆	–1.03 (s)		IR MS(Cl) [EA] X-ray ¹³ C	541b
17-13 Sc[N(SiHMe ₂) ₂] ₃ (<i>o</i> -phen)	Sc[N(SiHMe ₂) ₂] ₃ (thf) _n + <i>o</i> -phen	89%	C ₆ D ₆	5.34 (h)		IR EA X-ray ¹³ C	541b
17-14 Y[N(SiHMe ₂) ₂] ₂ - [μ - N(SiHMe ₂) ₂] ₂	[YMe ₃] _n + 3HN(SiHMe ₂) ₂	colorless 41%	C ₇ D ₈	4.89 (m)		IR EA X-ray ¹³ C IR EA X-ray	541c

Table 17. Continued

compound	starting metal complex	color % yield m.p., °C	NMR			
			solvent (temp., °C) ¹	¹ H Si–H ²	²⁹ Si ³	other ⁴ ref ⁵
17-15 {Y[N(SiHMe ₂) ₂] ₄ Li} ₂	Y(OTf) ₃ + 4LiN(SiHMe ₂) ₂	colorless 77%	C ₆ D ₆	4.78 (h)		¹³ C IR EA X-ray

¹ Ambient temperature unless otherwise noted. Temperatures are in °C. ² In ppm. Coupling constants in Hz. Assignments: s, singlet; d, doublet; t, triplet; q, quartet; quin, quintet; sept, septet; m, multiplet; br, broad; vt, virtual triplet. ³ ¹J_{SiH} coupling constants were determined either from ²⁹Si satellites in the proton spectrum or from proton-coupled ²⁹Si data. The former appear in the SiH column, and the latter appear in the ²⁹Si column. ^{3,29}Si may have been determined by direct observation, INEPT or DEPT, or 2D ²⁹Si–¹H correlation. These methods are not distinguished in the table. ⁴ Will contain other characterization methods including spectroscopic, X-ray, and calculations if reported. If elemental analyses were reported, this will be indicated by EA. If analysis is outside ±0.5% of calculated percentage value for carbon, this will be indicated by the symbolism [EA]. ⁵ Some data have been retrieved from the Supplemental Data associated with the indicated reference. ⁶ Additional derivative, M = La (X-ray). ⁵³⁹ ⁷ Additional derivative, M = La (*rac*). ⁵³⁹ ⁸ Additional derivatives, M = La, Lu (X-ray). ⁵³⁹ ⁹ Mixture with unreacted bis(fluorene) and a complex containing a monocoordinated bis(fluorene). ⁵³⁹ ¹⁰ Additional derivatives, M = Sc, Y (X-ray), La, Nd. ⁵³⁹ ¹¹ La analogue also reported. Also included were *N*-methylimidazole complexes of La and Nd, Ph₃PO complexes of La, Nd, and Pr, tmeda complex of La, and dmpe complex of Nd. ^{541b} ¹² La and Sc analogues also reported. ^{541b}

THF gave the THF solvate, which was crystallographically characterized. In both complexes, the four core lutetium centers form a tetrahedron. The addition of PhSiH₃ to Ln(η^5 : η^1 -C₅Me₄SiMe₂NR)(CH₂SiMe₃)(THF) (R = CMe₃, CMe₂Et; Ln = Lu, Yb, and also Y) provided the dimers [Ln(η^5 : η^1 -C₅Me₄SiMe₂NR)(THF)(μ -H)]₂.³²⁹ The transfer of hydride from a hydrosilane to a lanthanide center has also been invoked in catalytic cycles for hydrosilylation and dehydrogenative silylation as in the formation of silyl amines,⁵³⁴ hydrosilylation of imines⁵³⁴ and olefins,^{332a,535–537} and dehydrocoupling of amines with silanes.⁵³⁸

8.1.3. Complexes with β -H...Si interactions

Anwender and co-workers have introduced the use of the –N(SiHMe₂)₂ ligand into organolanthanide chemistry, and both homoleptic and lanthanidocene complexes that contain the –N(SiHMe₂)₂ ligand have been reported (Table 17), with the crystallographic data in Table 18. One of the earlier complexes was prepared by a *trans*-silylation reaction of Sm[N(SiMe₃)₂]₂(THF)₂ and HN(SiHMe₂)₂. The X-ray structure showed that the complex had an oligomeric trinuclear composition, Sm{[μ -N(SiHMe₂)₂]₂Sm[N(SiHMe₂)₂](THF)}₂, with a Sm...Sm...Sm bent arrangement and a central Sm center that had a distorted tetrahedral SmN₄ core. All of the SiHMe₂ groups exhibit Si–H...Sm β -agostic interactions.^{541a} When the disilazane HN(SiHMe₂)₂ was added to [YMe₃]_n, a colorless oil was obtained from which the dimer, {Y[N(SiHMe₂)₂]₂[μ -N(SiHMe₂)₂]}₂, was obtained as a colorless solid (41%; other unidentified silylamide ligand products were observed in the original oil). The X-ray structure revealed an asymmetrically bridged molecule with two different Y–N bond distances that averaged 2.249 Å for the terminal amide bonds and 2.479 (av) Å for the bridging amide bonds. Several Y...SiH β -agostic interactions were present and one of the bridging N(SiMe₂H)₂ exhibits a β -diagnostic interaction with both metal centers. The IR spectrum shows two SiH stretching frequencies at 2095 (nonagostic) and 1931 cm^{–1} (agostic), supporting the presence of agostic interactions in the solid. However, there is only one signal at 4.89 ppm in the ¹H NMR spectrum for the SiH of the silylamide ligands, indicating that the weak agostic interaction does not persist in solution.^{541c}

Several variations of biscyclopentadienide and *ansa*-lanthanidocenes have been prepared from Ln[N(SiHMe₂)₂]₃-(THF)_x, and the appropriate Cp-type precursor (examples are

given in Tables 17 and 18).⁵³⁹ The IR spectra of the metallocene bis(dimethylsilyl)amide typically contain an Si–H stretching frequency that was shifted >200 cm^{–1} to lower energy compared to the noncomplexed ligand. The Si–H signal in the ¹H NMR spectra was also shifted upfield upon complexation but was still downfield of TMS. The ¹J_{SiH} values range from 133 to 148 Hz for the lanthanidocene complexes.⁵³⁹ The –NSiR₂H β -agostic interactions in *transition* metal complexes tend to have Si–H chemical shifts that are upfield of TMS and coupling constants that are closer to 100 Hz (see Table 9). In the *ansa*-metallocenes, both SiH groups of the coordinated amide interact with the metal center and the H...Yb...H interaction persists in solution.⁵³⁹ The presence of Y...H coupling was demonstrated by ⁸⁹Y NMR spectroscopy, and the ⁸⁹Y signal is strongly temperature dependent. The agostic rigidity of the amide was also supported by ¹H NMR-NOE spectroscopy. The structures of five of the lanthanidocene complexes (one La, two Y, and two Lu systems) were reported. The observed Ln...Si distances ranged from 3.028(1) to 3.246(1) Å and resemble previously reported Ln–Si σ -bond distances. The Ln...H distances ranged from 2.38(3) to 2.70(3) Å and appear to be at the upper end of covalent Ln–H bonds that had been previously reported. The Si–N–Si angle in the coordinated amide ranged from 144 to 161°, also consistent with a strong symmetric interaction with the Ln center of the two Si–H groups.⁵³⁹

In a later publication, the Anwender group demonstrated that, when the Cp' ligands were bulky in Cp'₂Ln(SiHMe₂)₂ (Cp' = C₅Me₅, Me₄C₅H, and Ph₄C₅H), the double agostic interaction was suppressed and the two SiHMe₂ groups exhibited different bonding modes with IR stretching frequencies consistent with a complexed and noncomplexed SiH group in the three complexes that were prepared (including **17-1**, **17-2**, and **17-8**).⁵⁴⁰ The crystal structure of **17-2** demonstrated the asymmetric β -SiH monoagostic bonding of the amide ligand.⁵⁴⁰ Removal of only one Me group in the coordinated Cp' ligand in **17-1** resulted in a Y...SiH bonding that was described as intermediate between the monoagostic complex **17-2** and the diagnostic interaction in **17-10**. Replacement of the Me groups of the Cp rings in **17-1**, with Ph groups, produced the La complex, which had two crystallographically independent molecules that exhibited different coordination modes. One molecule had angles similar to those in the monoagostic interaction in **17-2** but

Table 18. Structural Data for Silyl Lanthanide Complexes with β -Agostic Interactions

complex	temp (K)	M–H (Å)	SiH (Å)	M–Si (Å)	ref
17-1 (C ₅ Me ₄ H) ₂ Y[N(SiHMe ₂) ₂]	173	2.57(3) 2.89(3)	1.48(3) 1.48(2)	Y···Si 3.1213(6) 3.2887(5) ^a	345b 540
17-2 Cp* ₂ Y[N(SiHMe ₂) ₂]	293	2.40(3) 3.37(3)	1.50(3) 1.36(3)	Y···Si 3.0505(8) 3.5365(7) ^a	345b 540
17-3 [Me ₂ Si(2-MeInd) ₂ Y–N(SiHMe ₂) ₂]	163	2.54(2) 2.54(2)	1.39(3) 1.38(4)	Y···Si 3.082(1) 3.082(1) 3.387(1) ^b	539
[Me ₂ Si(2-MeInd) ₂ LuN(SiHMe ₂) ₂] ^c	273	2.63(2), 2.63(2)	1.42(5), 1.42(5)	Lu···Si 3.116(1) 3.116(1) 3.347(1) ^b	539
17-6 <i>rac</i> -[Me ₂ Si(2-Me-4,5-Benz-Ind) ₂]YN(SiHMe ₂) ₂	193	2.37(3) 2.38(3)	1.45(3) 1.47(3)	Y···Si 3.028(1) 3.034(1) 3.416(1) ^b	539
<i>rac</i> -[Me ₂ Si(2-Me–Benz–4,5-Benz-Ind) ₂]LuN(SiHMe ₂) ₂ ^c	293	3.05(2) 2.66(2)	1.45(2) 1.45(2)	Lu···Si 3.277(2) 3.041(2) 3.384(2) ^b	539
17-8 [C ₃ Ph ₄ H] ₂ La[N(SiHMe ₂) ₂]	173	2.78(9) 2.59(6) 3.21(9) 4.83(6)	1.48(9) 1.67(8) 1.43(6) 1.56(6)	La···Si ^d 3.261(2) 3.472(2)	345b, 540
[Me ₂ Si(C ₅ Me ₄) ₂]LaN(SiHMe ₂) ₂ ^e	193	2.70(3) 2.66(4)	1.39(3) 1.38(4)	3.193(2) 3.889(3) La···Si 3.246(1) 3.244(1) 3.494(1) ^b	539
17-9 Sm{ μ -[N(SiHMe ₂) ₂] ₂ Sm–[N(SiHMe ₂) ₂](thf) ₂ }	173	2.75 (av)		Sm···Si, 3.2317(9)–3.342(1)	541a
17-10 [Me ₂ Si(2-MeInd) ₂ LuN(SiHMe ₂) ₂]	273	2.63(2) 2.63(2)	1.42(5) 1.42(5)	Lu···Si 3.116(1) 3.116(1) 3.347(1)	539
17-11 Nd[N(SiHMe ₂) ₂] ₃ •2nhc	193	2.7785 2.956 2.958 3.622 3.628 3.628	1.365 1.385 1.405 1.414 1.442 1.453	3.3051(1) 3.2511(8) 3.287(9) 3.269 3.658 3.780	541b
17-12 Nd[N(SiHMe ₂) ₂] ₃ •(<i>o</i> -phen)	123	2.666 2.974 3.045 3.055 3.198 3.485	1.392 1.394 1.399 1.407 1.424 1.430	3.2055(3) 3.3255(3) 3.3540(6) 3.391 3.428 3.724	541b
17-13 Sc[N(SiHMe ₂) ₂] ₃ (<i>o</i> -phen) ^f	123K	2.644 2.645 3.048 3.313 3.316 3.409	1.470 1.470 1.469 1.469 1.470 1.469	3.0359(3) 3.0467(3) 3.2119(3) 3.498 3.517 3.333	541b
17-14 {Y[N(SiHMe ₂) ₂] ₂ [μ -N(SiHMe ₂) ₂] ₂ }	123	2.41(3) ^g 2.43(3) 2.44(3) 2.47(3) 2.49(3) 2.57(3)	1.44(3) ^g 1.45(3) 1.46(3) 1.40(3) 1.45(3) 1.46(3) 1.47(3)	3.0521(7) 3.0569(7) 3.0929(7) 3.1012(7) 3.1375(7) 3.1620(7) 3.1990(7)	541c
17-15 {Y[N(SiHMe ₂) ₂] ₄ Li} ₂	123			3.0283(7) 3.0458(6) 3.1608(7) 3.1863(7)	541b

^a Noncoordinating SiH. ^b Distance of metal to the silicon bridging the two Cp rings. ^c Table 17, footnote 8. ^d Two independent molecules in the unit cell. ^e Table 16, footnote 6. ^f It should be noted that the Sc···Si distances in [(2-Me–Ind)₂Sc{N(SiMe₃)₂}] are reported to be 3.005(1) and, for the cationic species, [(2-MeInd)Sc{N(SiMe₃)₂}(PhNMe₂)₂]⁺[B(C₆F₅)₄], 2.893(1) as a result of the presence of bridging SiMe–Sc groups.^{541d} ^g Values are given only for the bridging hydrides.

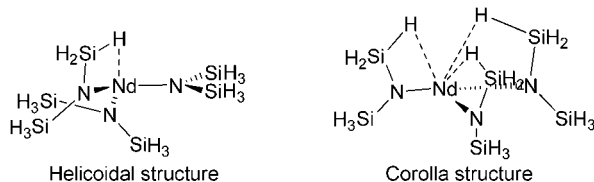


Figure 42. Optimized structures for $\text{Nd}[\text{N}(\text{SiH}_3)_2]_3$ illustrating the two different β -agostic Si–H interactions.⁵⁴²

with a smaller difference ($\sim 0.2 \text{ \AA}$) in the $\text{Ln} \cdots \text{Si}$ contacts. The second molecule showed a much more pronounced monoagostic interaction with $\sim 0.7 \text{ \AA}$ difference in $\text{Ln} \cdots \text{Si}$ distance. However, all three complexes exhibited only one signal for the Si–H proton in solution.⁵⁴⁰

Adducts of $\text{Ln}[\text{N}(\text{SiMe}_3)_2]_3(\text{THF})_n$ ($\text{Ln}_{(n=2)} = \text{La, Nd, Pr}$; $\text{Ln}_{(n=1)} = \text{Sc}$) were prepared on reaction with Ph_3PO (La, Nd, Pr), *N*-methylimidazole (La, Nd), NHC (La, Nd (**17-11**)), dmpe (Nd), tmeda (La), and phen [La, Nd (**17-12**), Sc (**17-13**)], and three of the complexes were crystallographically characterized (Table 18). In addition, the -ate complex, $\{\text{Y}[\text{N}(\text{SiHMe}_2)_2]_4\text{Li}\}_2$ (**17-15**), was prepared from the reaction of $\text{Y}(\text{OTf})_3$ with 4 equiv of $\text{LiN}(\text{SiMe}_3)_2$ and was crystallographically characterized.^{541b} The complexes also exhibited a ν_{SiH} stretching frequency from 2018 to 2108 cm^{-1} that contained low-energy shoulders in the region 1900–2000 cm^{-1} that were assigned to weak agostic interactions (strong agostic interactions fall between 1700 and 1900 cm^{-1}). The Si–H resonance in the adducts was shifted to lower field in the presence of a donor ligand stronger than THF. The Fourier transform infrared (FTIR) and ^1H NMR data provided the following donor capability to the $\text{Ln}(\text{III})$ center: $\text{THF} < 1,3\text{-dimethylimidazolin-2-ylidene (NHC)} < N\text{-methylimidazole} < \text{triphenylphosphine oxide} < 1,10\text{-phenanthroline}$. When donor molecules are absent, $\text{M}[\text{N}(\text{SiMe}_2\text{H})_2]$ forms an -ate complex.

8.1.4. Theoretical Calculations

Three papers using DFT(B3PW91) theoretical calculations have been published by Eisenstein and co-workers.^{542,543a,b} In section 7, there were a few examples of calculations where simplified models did not reproduce adequately the features of the known structure. Maron and Eisenstein report on the entire series of lanthanides that were examined with the model $\text{Ln}[\text{N}(\text{SiH}_3)_2]_3$.⁵⁴² An objective of the study was to determine if the SiH_3 substitution was adequate for describing $\text{Ln}[\text{N}(\text{SiMe}_3)_2]_3$, for which several structures are known within the series. Two levels of calculations were involved, one without any polarization function on the silicon center and comparable calculations including a polarization function. Without the polarization function, the $\text{Ln}-\text{N}$ bond lengths were too short and the $\text{N}-\text{Si}$ distances were too long when compared to available experimental data. However, the helicoidal shapes of the actual $(\text{Me}_3\text{Si})_2\text{N}-$ ligand systems were reproduced. The calculation without polarization functions for the $-\text{N}(\text{SiH}_3)_2$ model complex indicated that β -agostic Si–H interactions were absent. The calculations, including a set of polarization functions, gave two structures, both of which had the key distances in agreement with the experimental data. The two optimized structures are shown in Figure 42. One of the structures was helicoidal but also exhibited a β -agostic Si–H interaction (Nd system), which does not exist in the experimental structure. The second structure was a corolla with three β -agostic Si–H interactions, and this structure was calculated to be 10 kcal/

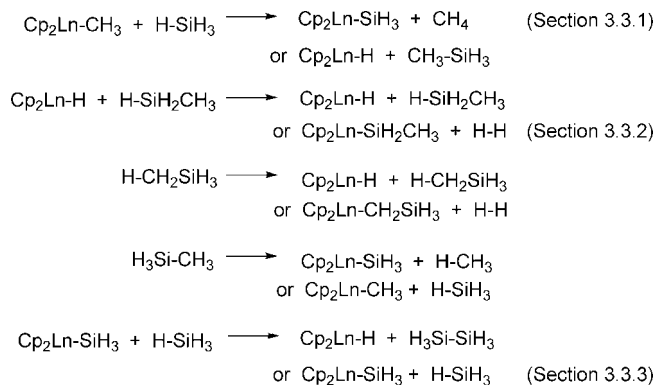


Figure 43. Selected σ -bond activation reactions studied by DFT calculations in reactions of Cp_2LnR with SiH_4 and $\text{H}_3\text{C}-\text{SiH}_3$.^{543b}

mol more stable than that of the helicoidal structure. Thus, the electron deficiency of the metal was not the only requirement for the agostic interaction. The authors point out that the calculations do not agree with the experimental results, and thus, substituting SiH_3 for SiMe_3 does not produce a valid model because interactions that could not take place in the real complex resulted.⁵⁴²

Lanthanide complexes, particularly those with a metallocene structure, have been employed in activation of an assortment of bonds including Si–H and Si–C bonds. Since the $\text{Ln}(\text{III})$ center in Cp_2LnX has an empty 5d-shell and a stabilized 4f-shell, activation of bonds does not proceed by an OA mechanism. To explore the bond transformation through a 4-center σ -bond metathesis route, Maron and Eisenstein examined the activation of SiH_4 by Cp_2LnH at the DFT-B3PW91 level of theory (including a polarization function for the silicon atom).^{543a} For a realistic model system, solvent effects were neglected, the monomeric form of Cp_2LnH was assumed, and C_5H_5 replaced the more frequently used Cp^* ligand. The reactions included H/H exchange and silylation (to form $\text{Cp}_2\text{LnSiH}_3$) through a single-step σ -bond metathesis mechanism. In the H/H exchange, the TS state is preceded by formation of an adduct, $\text{Cp}_2\text{Ln}(\eta^2\text{-H}-\text{SiH}_3)(\text{H})$, which then forms a dihydride-bridged TS before losing SiH_4 to give the equivalent adduct where the positions of the $\text{Ln}-\text{H}$ and $\text{Ln}(\eta^2\text{-H}-\text{SiH}_3)$ are reversed. Dissociation of the SiH_4 gives the exchange of hydride at the Ln center. The adduct may be viewed as formed from addition of a hydride to SiH_4 to give a trigonal-bipyramidal silicon environment as in SiH_5^- , whereas in the TS, the silicon center exhibited a square-based pyramidal geometry and the change from the adduct to the TS involved a “turnstile” rotation of the SiH_3 fragment relative to the bridging two hydrogens. The production of $\text{Cp}_2\text{LnSiH}_3$ is exogenic by -47 kcal/mol for $\text{Ln} = \text{La}$. The adduct, $\text{Cp}_2\text{Ln}(\eta^2\text{-H}-\text{SiH}_3)(\text{H})$, was again formed and proceeded to the 4-centered TS in which the H_3Si group was now α to the Ln center. In this case, the adduct formed after the transition state was $\text{Cp}_2\text{Ln}(\text{SiH}_3)(\eta^2\text{-H}_2)$, which then lost H_2 to give $\text{Cp}_2\text{Ln}(\text{SiH}_3)$. Thus, there are two possible views of SiH_4 in the adduct: (i) side-bonded to $\text{La}(\eta^2\text{-SiH}_4)$ with an additional agostic Si–H bond or (ii) η^3 -bonding of the HSiH_3 group.^{543a}

In a related study, σ -bond activation by lanthanocene complexes, Cp_2LnR ($\text{R} = \text{CH}_3, \text{H}, \text{SiH}_3$), with SiH_4 and H_3CSiH_3 through a σ -bond metathesis mechanism was explored.^{543b} Selected reactions that were the target of the DFT calculations are shown in Figure 43 where the relationship to similar reactions covered earlier in section 3 for

transition metals is indicated to show the parallels between the two sets of metals. The 4-centered intermediate characteristic of the σ -bond metathesis intermediate is generally preceded by adduct formation involving a coordinated Si–H, C–H, or Si–C. Because in a precursor such as $\text{Ln}-\text{CH}_3$ the product could be CH_3SiH_3 , the potential reactions of the methylsilane were also calculated. The nature of the lanthanide atom on the energy profiles was small; thus, $\text{Ln} = \text{La}$ was the only metal studied. No preference for a silyl group at either the α - or β -sites was shown in the transition state. The substitution of SiH in SiH_4 by a CH_3 group does not change the reactivity of the Si–H bond. In the reaction of SiH_4 with $\text{Cp}_2\text{LnSiH}_3$, the thermodynamic preference is for a silyl exchange reaction over the equivalent of dehydrocoupling (formation of a Si–Si bond). The activation energy for the cleavage of an Si–C bond by Cp_2LnH is greater than the cleavage of the Si–H bond. Thus, alkylsilanes will react via the Si–H bond rather than the Si–C bond.^{543b}

The β -diagnostic interaction in C_2 -symmetric *ansa*-lanthanidocene complexes were the subject of DFT calculations by Herrmann and co-workers.⁵⁴⁴ Two models were utilized for the $\text{Ln}\cdots(\text{Si}-\text{H})$ β -diagnostic interaction observed in the complexes described in section 8.1.3. The *ansa*-metallocene structure was initially simplified to $[\text{H}_2\text{Si}(\text{Cp})_2\text{LnN}(\text{SiH}_3)_2]$ ($\text{N}(\text{SiH}_3)_2 = \text{dsa}$; type 1a/1b), and then calculations were performed with the actual ligand $\text{N}(\text{SiHMe}_2)_2$ (bdsa, type 2a/2b) and then with $\text{Cp}'' = \text{C}_5\text{Me}_4$ (type 3a) as representative of the substituted cyclopentadienyl rings. A C_{2v} symmetry with a symmetrical diagnostic interaction was assumed for type 1a/2a/3a and C_s symmetry for an asymmetric coordination in type 1b/2b (one agostic and one nonagostic interaction), and the calculations were performed for $\text{Ln} = \text{La}$ as a representative example. The SiHR_2 ligands exhibited an elongation of the agostic SiH_a and a contraction of the $\text{N}-\text{Si}-\text{H}_a$ angle in all models. Because of uncertainties in hydrogen placements, the authors viewed the $\text{Si}-\text{N}-\text{Si}$ angle as the only parameter to compare with experimental values. This angle widens in the β -diagnostic interaction (also observed in the crystal structure data) and varied from 154.5 to 159.6° depending on the basis set used, but these are all in agreement with the observed value of 154.9°⁵³⁹ observed for $[\text{Me}_2\text{Si}(\text{C}_5\text{Me}_4)_2][\text{La}(\text{N}(\text{SiHMe}_2)_2)]$. An attempt to locate a C_s symmetric minimum structure for 1b (one long and one short Si–H bond) was unsuccessful, nor was it successful for the bdsa complex, 2b. Although the elongation of the agostic–SiH was only 0.05 Å, the $\text{La}^{3+} d^0$ configuration precludes any metal-to-(Si–H) back-donation, accounting for the weaker interaction calculated.

The possibility of the symmetric diagnostic interaction for types 1 and 2 complexes was also investigated for the series La, Y, Sc, Lu. For La, only the diagnostic structure was observed; for Y and Lu, both the mono- and diagnostic modes were found; and for Sc, only the monoagostic mode was found. In the bdsa systems, the only stable geometry for Y was 2a, but both 2a and 2b geometries were found. The authors concluded that the size and accessibility of the area involved in the coordination of the ligands to the central metal played the decisive role in determining the dominant species in the equilibrium $1/2a (\text{Ln}) \rightleftharpoons 1/2b (\text{Ln})$. Also calculated were natural atomic partial charges and Wiberg bond orders.⁵⁴⁴

DFT calculations⁵⁴⁵ were conducted for the models $\text{Ln}[\text{CH}(\text{SiR}_2\text{R}')(\text{SiR}_3)]_3$ ($\text{Ln} = \text{La}, \text{Sm}$; $\text{R} = \text{R}' = \text{Me}$; $\text{R} = \text{H}$, $\text{R}' = \text{Me}$; $\text{R} = \text{R}' = \text{H}$) for $\text{Ln}[\text{CH}(\text{SiMe}_3)_2]_3$, where the

crystal structures⁵⁴⁶ for the lanthanum and samarium complexes exhibited an unusual pyramidal coordination geometry. The calculations showed that the structural change was the result of β -Si–C agostic interactions. The simplest model, $\text{Ln}[\text{CH}(\text{SiH}_3)_2]_3$, did not accurately describe the real molecule as the β -Si–C agostic interactions were replaced by β -Si–H agostic interactions. However, the other two models correctly reproduced the features of the reported complexes. Inclusion of polarization functions did not change the basic description of the molecular features.

8.2. Oxidative Additions of Other Si–El Bonds

The section includes a sampling of oxidative additions that have been reported for Si–El bonds other than $\text{El} = \text{H}$. The examples are summarized in Table 19, and for those complexes that have been crystallographically characterized, the pertinent metal–silicon bond information appears in the appropriate footnote to Table 6. The oxidative additions are summarized in the order: section 8.2.1, Si–Si; section 8.2.2, Si–C; section 8.2.3, Si–El ($\text{El} = \text{Sn}, \text{B}, \text{S}$); section 8.2.4, Si–X ($\text{X} = \text{halogen}$).

8.2.1. Si–Si Bonds

The activation of Si–Si bonds by transition metal complexes has been reviewed by Ito and Sugimoto.^{555,556} Although the cases covered are in references prior to 1998, there are a surprising number of examples including insertion of low-valent metals into a Si–Si bond, double OA, and silyl or silylene migrations to name a few. Table 19 illustrates similar reactions. The complex **19-4** was most likely obtained from RE of diphenylsilylcyclobutane from the metal precursor, thus forming a $\text{Pd}(0)$ species that could insert into the SiSi bond of 1,2-tetramethyl–disilacyclopentane, and the case for insertion into SiSi bond in formation of **19-3** was more direct because a $\text{Pd}(0)$ precursor was employed in the reaction.^{120a} An unusual insertion of $\text{Pd}(0)$ and of $\text{Pd}(\text{II})$ into the Si–Si bonds of a trisilasp[4.4]nonane⁴¹⁸ was reported, and the products, **19-5** and **19-6**, are shown in Figure 44 and Table 19. An X-ray structure of the Cp^* analogue of **19-6** verified the structure shown in the figure.

Chelate-assisted OA of Si–Si bonds was illustrated in the insertion of $\text{Pt}(0)$ into the Si–Si bond in the disilane, $\text{Ph}_2\text{P}(\text{CH}_2)_x\text{SiMe}_2\text{SiPh}_3$ ($x = 1, 2$), to form **19-7** and **19-8**.⁴²⁸ The course of the conversion in the reaction of the bis(*o*-carboranyl)disilane with $\text{Pt}(\text{PET}_3)_3$ to give the silyl-chelated derivative **19-10** was much less obvious.⁴²⁴ In **19-9**, insertion of Pt into the Si–Si bond of a 1,2-disilacyclohexane as suggested by the authors in the sequence leading to the 1,4-dimethyl-1,2,3,4-tetraphenyl-1,4-disilacyclooct-2-ene products is certainly plausible, but such a complex or intermediate was not characterized.^{547c} In the $\text{Cu}(\text{I})$ -catalyzed disilylation of alkylidene malonates, transfer of R_3Si from R_3SiSiR_3 to a $\text{Cu}(\text{I})$ center to give the intermediate $[\text{R}_3\text{SiCu}]$, **19-11**, was proposed through activation of the disilane in the presence of dimethylformamide (DMF).⁵⁴⁸ The addition of the Si–Si bonds of 5-membered and benzo-condensed 6-membered cyclic disilanes to arynes was catalyzed by a combination of $\text{Pd}(\text{OAc})_2$ and a large excess of *t*-OctNC.⁵⁵⁸ The catalytic cycle proposed for this transformation involved insertion of $\text{Pd}(0)$ into the Si–Si bond. Baumgartner and co-workers reported reactions of oligosilylalkynes with $\text{Co}_2(\text{CO})_8$ in which Si–Si bond activation appears to occur in the coordination sphere of the cobalt atoms.²³³ An example is

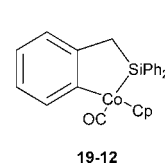
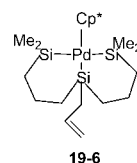
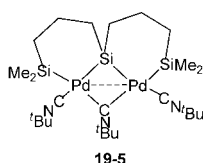
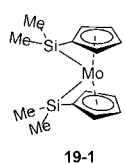
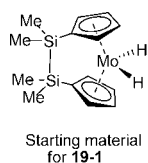
Table 19. Reactions of Si–Si, Si–El, Si–C, and Si–X Bonds with Transition Metal Complexes (Structures are Shown at the End of the Table for Compounds Marked with an Asterisk)^{†,‡}

compound	reactants	% yield, color m.p., °C	NMR				ref ⁵
			solvent (temp.) ²	¹ H M–H ³	²⁹ Si ^{1,3}	other ⁴	
Si–Si bonds							
*19-1 C ₅ H ₄ SiMe ₂ MoSiMe ₂ C ₅ H ₄	[X(C ₅ H ₄) ₂]MoH ₂ X = Me ₂ SiSiMe ₂ <i>hν</i>	75 yellow	C ₆ D ₆		–14.76	¹³ C EA X-ray	547a
19-2 (OC) ₃ Fe(<i>η</i> ⁴ - [Ph ₄ C ₄]Si-(SiMe ₃)Me	Fe(CO) ₅ + [Ph ₄ C ₄]Si(SiMe ₃) ₃	25 red 190–192	CDCl ₃		–20.1 (SiMe)	¹³ C IR X-ray	547b
19-3 (dcpe)Pd(SiMe ₂ H) ₂ ⁶	[(dcpe) ₂ Pd] + HMe ₂ SiSiMe ₂ H		C ₇ D ₈		18.4 (SiMe ₃) 80 °C –15 (t)	¹³ C 7 X-ray	120a,b
19-4 (dmpe)Pd[SiMe ₂ (CH ₂) ₃ -SiMe ₂]	(dmpe)Pd[CH ₂ CH ₂ CH ₂ Si-Ph ₂] + –Me ₂ SiSiMe ₂ (CH ₂) ₃ –	129–130	C ₆ D ₆		–70 °C –15 (dd) –1.9 (d)	¹³ C ³¹ P EA X-ray	417 ⁵
*19-5 C ₂₅ H ₅₁ N ₃ Pd ₂ Si ₃	(^t BuNC) ₂ Pd + 1,1,6,6-tetramethyl-1,5,6-trisilasp[4.4]nonane	92% orange	C ₆ D ₆		3.1 96.0	¹ H ¹³ C EA X-ray	418
*19-6 C ₁₈ H ₃₄ PdSi ₃	CpPd(<i>η</i> ³ -allyl) + 1,1,6,6-tetramethyl-1,5,6-trisilasp[4.4]nonane	85% white	C ₆ D ₆		19.9 25.6	¹ H ¹³ C EA X-ray	418
19-7 (Ph ₃ P)Pt[PPh ₂ CH ₂ SiMe ₂]- (SiPh ₃)	(Ph ₃ P) ₂ Pt(C ₂ H ₄) + Ph ₂ PCH ₂ SiMe ₂ SiPh ₃	87% 69 °C	C ₆ D ₆		–26 (dd, SiMe ₃) 2.7 (dd, SiPh ₃)	¹³ C ³¹ P EA X-ray	428
19-8 (Ph ₃ P)Pt[PPh ₂ (CH ₂) ₂ SiMe ₂]- (SiPh ₃)	(Ph ₃ P) ₂ Pt(C ₂ H ₄) + Ph ₂ P(CH ₂) ₂ SiMe ₂ SiPh ₃ ⁸	85% pale yel 78 (d)	C ₆ D ₆		32.5 (dd, SiMe ₂) 9.38 (dd, SiPh ₃)	¹³ C ³¹ P EA	428
19-9 (Ph ₃ P) ₂ Pt[SiMePh(CH ₂) ₄ - SiMePh] ⁹	(Ph ₃ P) ₂ Pt(C ₂ H ₄) + <i>cis</i> -1,2-dimethyl-1,2-diphenyl-1,2-disilacyclohexane						547c
19-10 (Et ₃ P) ₂ Pt(Me ₂ SiC ₂ B ₁₀ H ₁₀ - SiMe ₂)	(Et ₃ P) ₃ Pt + [(C ₂ B ₁₀ H ₁₁)Me ₂ Si–] ₂	75 white 173–175	C ₆ D ₆		38.4 (dd) <i>J</i> _{PtSi} = 1285	¹ H ³¹ P IR EA X-ray	424
19-11 [R ₃ SiCu] ¹⁰	[CuOTf] + 2 ⁿ Bu ₃ P + DMF + PhMe ₂ SiSiMe ₂ Ph		C ₇ D ₈				548
Si–C bonds							
*19-12 4:5-benzo-1-cobalta-2,2-diphenyl-2-silacyclopentene ¹¹	CpCo(CO) ₂ + 1,1-diphenylbenzosilacyclobutene	88 yellow 47 (dec)	CDCl ₃		48.1	¹³ C MS(Cl) IR EA DFT	448b
19-13 (<i>μ</i> ² - <i>η</i> ⁷ -C ₇ H ₆ -C)-(<i>μ</i> ² - <i>η</i> ⁵ -Me ₂ - Si(C ₅ H ₄)TiPt(PEt ₃) ₂)	Me ₂ Si(<i>η</i> ⁷ -C ₇ H ₆)Ti(<i>η</i> ⁵ -C ₅ - H ₄) + Pt(PEt ₃) ₃	26 green	C ₆ D ₆			¹³ C ³¹ P EA X-ray	549
19-14 (<i>μ</i> ² - <i>η</i> ⁷ -C ₇ H ₆ -C)-(<i>μ</i> ² - <i>η</i> ⁵ - Me ₂ - Si(C ₅ H ₄)(Et ₃ P) ₂)Pt–V	Me ₂ Si(<i>η</i> ⁷ -C ₇ H ₆)V(<i>η</i> ⁵ -C ₅ - H ₄) + Pt(PEt ₃) ₃	33 blue–grey				EA ESR X-ray	549
19-15 [(<i>η</i> ⁵ -C ₅ H ₄)-SiMe ₂ –Pt- (PEt ₃) ₂ -(<i>η</i> ⁷ -C ₇ H ₆)Cr]	Me ₂ Si(<i>η</i> ⁷ -C ₇ H ₆)Cr(<i>η</i> ⁵ -C ₅ - H ₄) + Pt(PEt ₃) ₄	76 green	C ₆ D ₆		115 (<i>J</i> _{SiPt} = 1392)	¹³ C ³¹ P X-ray	434
19-16 (Cy ₃ P) ₂ (OC)(Cl)RuSiCl ₃ ¹²	(Cy ₃ P) ₂ (OC)(Cl)RuH + CH ₂ =CHSiCl ₃		CD ₂ Cl ₂			¹³ C ³¹ P	550
19-17 (Ph ₃ P) ₂ (OC)(Cl)RuSiMe ₂ Ph	(Ph ₃ P) ₃ (OC)(Cl)RuH + CH ₂ =CHSiMe ₂ Ph	37% orange	CDCl ₃			³¹ P IR EA	199
19-18 (Cp*Ru) ₂ (<i>μ</i> -SiMe ₂)(<i>μ</i> - C- CH ₃)(<i>μ</i> -H)	(<i>η</i> ⁵ -C ₅ Me ₅)Ru(<i>μ</i> -H) ₄ - Ru(<i>η</i> ⁵ -C ₅ Me ₅) + CH ₂ =CHSiMe ₃ (Δ)	71 % dk brown	C ₇ D ₈ ¹ H, –10 ¹ H, –60 ²⁹ Si, 23	–17.94 –17.78 (s) <i>J</i> _{SiH} = 22	197.8 (d) <i>J</i> _{SiH} = 22.7	¹³ C IR EA	214
19-19 [(<i>η</i> ⁶ -C ₆ Me ₆)Ru{=HN ^{<i>i</i>} Pr- C(Me)= ^{<i>i</i>} Pr}(SiMe ₃)] ⁺ X [–] X [–] = PF ₆ ^{–13}	[(<i>η</i> ⁶ -C ₆ Me ₆)Ru{ <i>η</i> - ^{<i>i</i>} Pr- NC(Me)= ^{<i>i</i>} Pr}] ⁺ PF ₆ [–] + Me ₃ SiCHN ₂	91 % red 169 (d)	CD ₂ Cl ₂		24.23 (s)	¹³ C FAB-MS EA X-ray	404 ⁵

Table 19a. Continued

compound	reactants	% yield, color m.p., °C	NMR			
			solvent (temp.) ²	¹ H M–H ³	²⁹ Si ^{1,3}	other ⁴ ref ⁵
19-20 (dmpe)Pd[(CH ₂) ₃ SiPh ₂] + CH ₂ =CHCH ₂ SiMePh ₂	(dmpe)PdMe ₂ or (dmpe)Pd(CH ₂ =CHPh) + [CH ₂ CH ₂ CH ₂ SiPh ₂] ¹⁴	75 % pale yellow 108–109	C ₆ D ₆		47.1 (dd)	¹³ C ³¹ P EA X-ray 551
19-21 [Ph ₂ PCH ₂ CH ₂ SiPh ₂]Pt- (Ph)(PPh ₂ CH ₂ CH ₂ SiPh ₃)	(Ph ₃ P) ₃ Pt(C ₂ H ₄) + Ph ₂ PCH ₂ CH ₂ SiPh ₃ ¹⁵	52 % yellow	C ₆ D ₆		28.7 (dd)	¹³ C 28.7 552
19-22 Fe(η ⁵ -C ₅ H ₄) ₂ Pt[(PEt ₃) ₂ - SiMe ₂]	Pt(PEt ₃) ₄ + Fe(η ⁵ -C ₅ H ₄) ₂ SiMe ₂	80 % orange	C ₆ D ₆		5.18 (m)	¹³ C ³¹ P ¹⁹⁵ Pt EA 552
19-23 Fe(η ⁵ -C ₅ H ₄) ₂ Pt[(PEt ₃) ₂ - SiMeC≡CPh]	Pt(PEt ₃) ₃ + Fe(η ⁵ -C ₅ H ₄) ₂ - Si(Me)C≡CPh	55 % orange–red	C ₆ D ₆		–16.8 ¹ J _{SiPt} = 1433	¹³ C EA X-ray 426b
19-24 (‘Pr ₂ PCH ₂ CH ₂ NMe ₂)Pt- (C≡CPh)SiMe ₃	Pt(COD) ₂ + PhC≡CSiMe ₃ + ‘Pr ₂ PCH ₂ CH ₂ NMe ₂	62 colorless	C ₆ D ₆		0.03 (d)	¹³ C ³¹ P EA X-ray 423
19-25 (C ₂ yPCH ₂ CH ₂ PCy ₂)Pt- (C≡CPh)SiMe ₃	(dcpe)Pt(η ² -Me ₃ SiC≡C- Ph) + hν	70 pale yellow	C ₆ D ₆		0.03 (dd)	¹³ C ³¹ P EA X-ray 423
19-26 (PN)Pt(SiMe ₃)C≡C–C≡C–Pt- (SiMe ₃) (PN)	[(COD)Pt] ₂ Pt(SiMe ₃) ₂ C ₄ + PN	58 yellow	C ₄ D ₈ O		–16.61	¹³ C ³¹ P EA X-ray 423
Si–El 19-27 <i>cis</i> -(PhMe ₂ P) ₂ Pt(SiPh ₃)- SnMe ₃ ¹⁶	Pt(cod) ₂ + PMe ₂ Ph + Ph ₃ SiSnMe ₃	38% yellow	CD ₂ Cl ₂ (–50 °C)			¹³ C ³¹ P EA X-ray 426c, 553
19-28 <i>cis</i> -L ₂ Pt(SiPhMe ₂)(SnMe ₃) L = PMe ₃	Pt(cod) ₂ + L + PhMe ₂ SiSnMe ₃	35%	CD ₂ Cl ₂ (–50 °C)			¹³ C ³¹ P EA X-ray 426c
19-29 <i>cis</i> -(Me ₃ P) ₂ Pt(BX ₂)SiMe ₂ Ph X ₂ = –OCMe ₂ CMe ₂ O– ¹⁷	Pt(cod) ₂ + PMe ₃ + PhMe ₂ SiBX ₂	yellow 51	CD ₂ Cl ₂ (–50 °C)			¹³ C ³¹ P EA 429
19-30 <i>trans</i> -(Et ₃ P) ₂ Pt(SPh)(SiCl ₃) Si–X (X = halogen)	Pt(PEt ₃) ₄ + PhSSiCl ₃	orange oil ¹⁸	C ₆ D ₆			³¹ P EA 554
19-31 [N ₃](Cl)Ru(SiCl)(N,N) ¹⁹	[η ² -N ₃]Ru(η ² -MeC ₆ H ₅) + Cl ₂ Si{NN}	50	THF-d ₈		–10.42 (s)	¹³ C 213b
19-32 [N ₃]Ru(N ₂){SiNN} + [N ₃]Ru(Cl) ₂ (THF)	[η ² -N ₃]Ru(η ² -MeC ₆ H ₅) + N ₂ + 19-31	1:1	THF-d ₈			¹ H 213b
19-33 [N ₃]Ru(Cl) ₂ {Si(NN)}	[N ₃](Cl) ₂ Ru(C ₂ H ₄) + Si{N,N}	dark purple 80	C ₆ D ₆ , CDCl ₃ THF-d ₈		111.75 (s) ²⁰	213b
19-34 [PNP](Cl)Rh(SiMe ₂ Cl)	[PNP]Rh[S(‘Pr) ₂] + ClSiMe ₂ Cl	47	C ₆ D ₆		66.7 (dt) <i>J</i> _{RhSi} = 39	¹ H ¹³ C ³¹ P EA X-ray 254c
19-35 [PNP](Br)Rh(SiMe ₃)	[PNP]Rh[S(‘Pr) ₂] + BrSiMe ₃	40 green	C ₆ D ₆		59.5 (dt) <i>J</i> _{RhSi} = 28	¹ H ¹³ C ³¹ P EA X-ray 254c
19-36 [PNP](I)Rh(SiMe ₃)	[PNP]Rh[S(‘Pr) ₂] + ISiMe ₃	60 green	C ₆ D ₆		60.7 (dt) <i>J</i> _{RhSi} = 28	¹ H ¹³ C ³¹ P EA 254c
19-37 [PC ₃ N]Pt(Me) ¹²¹	[PC ₃ N]PtMe ₂ + Me ₃ SiI	78	CDCl ₃			¹³ C ³¹ P MS EA 292

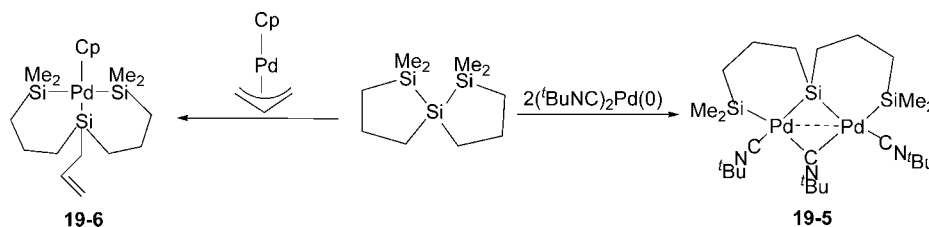
†



[†] dmpe = 1,2-Bis(dimethylphosphino)ethane; [N₃] = 2,6-(MesN=CMe)₂C₅H₃N; Si{NN} = *N,N'*-bis(neopentyl)-1,2-phenylenedi(amino)silylene; PC₃N = Ph₂P(CH₂)₃NMe₂. ^{†29}Si may have been determined by direct observation, INEPT or DEPT, or 2D ²⁹Si–¹H correlation. These methods are not distinguished in the table. ² Ambient temperature unless otherwise noted. Temperatures in °C. ³ In ppm. Coupling constants in Hz. Assignments: s, singlet; d, doublet; t, triplet; q, quartet; quin, quintet; sept, septet; m, multiplet; br, broad; vt, virtual triplet. ⁴ Will contain other characterization methods including spectroscopic, X-ray, and calculations if reported. If elemental analyses were reported, this will be indicated by EA. If analysis is outside ±0.5% of calculated percentage value for carbon, this will be indicated by the symbolism [EA]. The ¹³C NMR data are proton decoupled unless indicated otherwise. ⁵ Some data have been retrieved from the Supplemental Data associated with the indicated reference. ⁶ Deuterium analogue, (dcpe)Pd(SiMe₂H)₂, also mentioned. ^{120a} ⁷ Complex **19-3** was previously prepared from [(dcpe)Pd]₂(μ-H)₂ and characterized (except for ²⁹Si NMR) including an X-ray structure. ^{120b} ⁸ Reaction also performed with Ph₂P(CH₂)₂SiR'₂ER₃ (R' = Me, Ph, ER₃ = SiMePh₂; R' = Me, ER₃ = SnPh₃).⁴²⁸

Table 19b. Continued

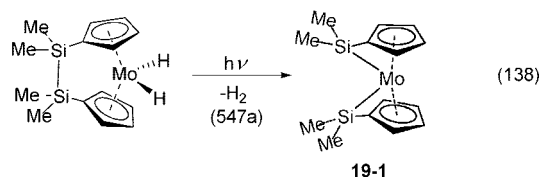
⁹ Proposed as an intermediate in the reaction of 1,2-dimethyl-1,2-diphenyl-1,2-disilacyclohexane. Product isolated, *cis*-1,2-dimethyl-1,2,3,4-tetraphenyl-1,4-disilacyclooct-2-ene, was from reaction of the presumed Pt species (**19-9**) with PhC≡CPh.^{547c, 10} Proposed intermediate in the copper(I)-catalyzed disilylation of alkylidene malonates.^{548, 11} Additional derivatives prepared from the (*p*-MeOC₆H₄)₂Si and ¹Pr₂Si analogues.^{448b, 12} Observed in solution. Removal of solvent gave an insoluble white solid that decomposed.^{550, 13} Also prepared was the TFPB[−] salt [TFPB[−] = tetrakis{3,5-bis(trifluoromethyl)phenyl}borate].^{404, 14} Reaction also performed with 1,1-dimethylsilacyclobutane.^{417, 15} Reaction also performed with Ph₂PCH₂CH₂SiPh₂Me.⁵⁵¹ No reaction occurs with Ph₂PCH₂CH₂SiMe₃.¹⁶ Related derivatives prepared from Me₃SiSnMe₃, PhMe₂SiSnMe₃, and Ph₂MeSiSnMe₃.^{553, 17} Additional derivatives, *cis*-Pt(SiMe₂Ph)(BX₂)L₂; X₂ = −OCMe₂CMe₂O−, L = PMe₂Ph, PEt₃; X₂ = −NMeCH₂CH₂NMe−, L = PMe₃.^{429, 18} Predominant product formed in >95% by NMR. A similar reaction of Pt(PPh₃)₃ and PhSSiCl₃ also was reported, but PhSSiMe₃ did not react with Pt(PEt₃)₄.^{554, 19} Product that is formed in the absence of N₂. Under N₂, the product formed was [N₃]Ru(Cl)₂(THF). [N₃] = 2,6-(Me₂N=CMe₂C₃H₃N), Si(NN) = *N,N'*-bisneopentyl-1,2-phenylenediaminosilylene.^{213b, 20} Data recorded in CDCl₃.^{213b, 21} Reactions of other LPtMe₂ complexes are reported for L = PN, *o*-Me₂NC₆H₄NMe₂; PCN, *o*-Me₂N.²⁹²

**Figure 44.** Formal insertion of Pd(0) and Pd(II) into the Si–Si bonds of a trisilane.⁴¹⁸

formation of (OC)₃Co(μ-SiMe₂)₂Co(CO)₃, **3-172**, formed from HSi(SiMe₃)₃ and Co₂(CO)₈. The formation of **3-172** was rationalized through a silyl–silylene rearrangement.²³³

Nikonov has discussed aspects of potential complexation of Si–Si σ-bonds to metals.⁵⁵⁹ The direct identification of a complex with a Si–Si bond coordinated to a metal center has been a problem. In an early case, Tanaka and co-workers¹²³ reported a Pd(VI) complex, **2-84**, with six Si–Pd σ-bonds, but theoretical calculations provided convincing arguments that there were two Si–Si σ-bonds present, which would result in the more common +2 oxidation state (see section 7.3.7.5). In accord with this assignment, two Si–Si distances of 2.49 and 2.59 Å are present in the solid-state structure. Such distances are similar to those found in the disilane, Ph₃Si–SiPh₃ (2.52 Å⁵²⁹). The nickel complex, [(1,2-C₆H₄SiH₂)(SiH)₂Ni₂(dmpe)₂], **2-76**, also reported by the Tanaka group,⁶⁴ has two short Si–Si contacts of 2.693(2) and 2.685(1) Å, and consequently, one view of **2-76** could be as a “stretched” σ-complex.

Transition metal catalyzed additions of Si–Si bonds to unsaturated organic systems have been reviewed by Beletskaya and Moberg^{560a} as well as by Sugimoto and Ito.^{560b} The Beletskaya/Moberg review contains a section on insertion of Ni, Pd, and Pt complexes into Si–Si bonds, but the references predate the period covered by the current review. A novel intramolecular insertion of Mo into a Si–Si bond occurred on photolysis of disila[2]molybdenocenophane dihydride, as illustrated in eq 138. The complex, **19-1**, was characterized by X-ray crystallography.^{547a}



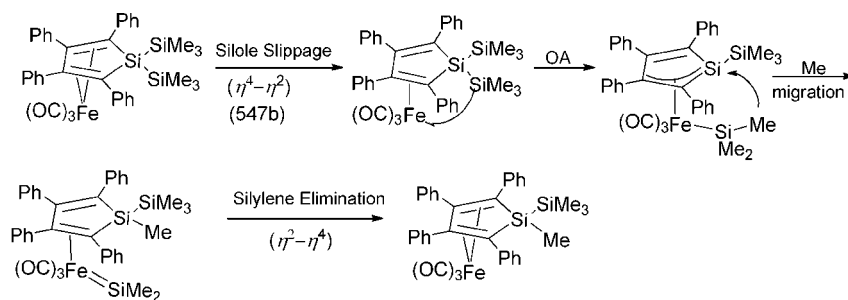
A DFT (B3LYP) computational study of the bis-silylation of acetylene has been modeled using HC≡CH, H₃Si–SiH₃, and Pd(PH₃)₂.^{561b} The mechanism contained three major steps: (i) OA of Si–Si to Pd(PH₃)₂; (ii) transfer of the two SiH₃ groups to the C–C triple bond; and (iii) RE of disilylacetylene and regeneration of Pd(PH₃)₂. The OA reaction was calculated to proceed through several transition

states, occurring first through an interaction of one H–Si^a bond with the Pd center then a second H–Si^b bond from the other silicon of the disilane before formation of the final two Si–Pd bonds, which required Si–Si cleavage to form *cis*-(H₃P)₂Pd(SiH₃)₂. A channel giving *trans*-(H₃P)₂Pd(SiH₃)₂ was also calculated. The transfer of the silyl groups to HC≡CH did not occur in a concerted process but involved several steps. The transfer of the second silyl group required an isomerization from the *cis*-channel to the *trans*-channel to place the Si and C in adjacent positions. The entire catalytic process is exothermic by 41.73 kcal/mol, in good agreement with the experimental estimate of ~40 kcal/mol.^{561b}

8.2.2. Si–C bonds

Activation of Si–C bonds is not uncommon, particularly for more strained systems. Overall, about 40% of the metal complexes in Table 19 contain Pt(0) such as Pt(PEt₃)_x (x = 3, 4), (LL)Pt(olefin), or Pt(COD)₂. Insertion of “Pt(PEt₃)₂” preferentially into the 7-membered ring of the *ansa*-metallocenes, Me₂Si(C₇H₆)(C₅H₄)M (Ti, **19-13**; V, **19-14**, Cr, **19-15**)^{434, 549} and also into silicon-bridged ferrocenophanes (**19-22**, **19-23**)^{426b, 552} has been demonstrated. In the case of the ferrocenophanes, insertion of Pt(0) into the strained Si–Cp ring occurs preferentially to coordination to the alkynyl substituent on silicon.^{426b} The Pd(0) precursor, (dmpe)Pd(CH₂=CHPh), inserts into the Si–C bond of silacyclobutanes (also a strained silacycle) to give **19-20**.⁴¹⁷ Oxidative addition (or its reaction equivalent) to nonactivated Si–C bonds has also been demonstrated in a thermal process with Pt(0) using the “chelate” approach described previously for Si–Si bond activation. The silane, Ph₂PCH₂CH₂SiPh₃, reacts with (Ph₃P)₂Pt(C₂H₄) to give **19-21**, where a Ph group has migrated from the Si center to the Pt center.⁵⁵¹ The related silane Ph₂PCH₂CH₂SiMe₃ did not transfer a Me group. Jones and co-workers have demonstrated that reaction of Pt(COD)₂ with PN (PN = ¹Pr₂PCH₂CH₂NMe₂) and the alkyne, PhC≡CSiMe₃, gave the alkyne complex (PN)Pt(PhC≡CSiMe₃), which quantitatively rearranged to (PN)-Pt(SiMe₃)(C≡CPh) (**19-24**; SiMe₃ is *trans* to the N of PN) at room temperature.⁴²³ A similar reaction of (dcpe)Pt with the same alkyne gave a stable (isolable) alkyne complex that

Scheme 32



required photolysis to give the Si–C cleavage product (dcpe)Pt(SiMe₃)(C≡CPh) (**19-25**).⁴²³ One of the more novel transformations involved reaction of the bis (COD)Pt adduct of 1,4-bis(trimethylsilyl)-1,3-butadiyne with PN, which then gave the bisplatinum complex (PN)Pt(SiMe₃)C≡C–C≡C–Pt(SiMe₃)(PN) (**19-26**).⁴²³ Another rearrangement of Me₃Si from carbon to an electrophilic platinum(IV) center occurred upon protonation (or deuteration) of the Pt(II) center of [(NN)Pt(CH₂SiMe₃)₂] (NN = 4,4'-di-*tert*-butyl-2,2'-bipyridine).^{561a} After protonation, rearrangement to a Me(Me₃Si)Pt(IV) intermediate or reductive coupling to Me₄Si took place. When the protonation was conducted with HBr at low temperature, the intermediate [(NN)(Br)Me₂PtSiMe₃] was identified, thus supporting an α -migration of the Me₃Si group from carbon to the cationic Pt center. The authors suggested that Si–C bond activation by an electrophilic Pt(II) complex could be an alternative to C–H activation.^{561a}

Although most recently reported insertions into a Si–C bond involve Pt, a reaction of Fe(CO)₅ with the silole, [Ph₄C₄]Si(SiMe₃)₂, may be an exception. The final product, **19-2**, contains an exocyclic Me substituent but no Si–Fe bond. The mechanism proposed by the authors is shown in Scheme 32 and features a sequence involving silole slippage (η^4 to η^2), oxidative addition of a Si–SiMe₃ bond, Me migration from Fe–SiMe₃ group to the ring Si, which generates an intermediate silylene followed by elimination of the silylene, and return to an η^4 -coordination.^{547b} In a more straightforward example, insertion of CpCo(CO) (produced from photolysis of CpCo(CO)₂) into the strained ring of a benzosilacyclobutene provided examples of the benzo-1-cobalta-2-silacyclopentene system such as **19-12** (see structure section of Table 19). The mechanism of the reaction was studied through DFT calculations (model used SiH₂ in place of SiPh₂). There was no associative pathway between CpCo(CO)₂ and the benzosilacyclobutene, and the authors proposed a spin change from ¹[CpCo(CO)₂] to ³[CpCo(CO)] prior to the Si–C insertion, leading to the product through the intermediate shown in Figure 45.^{448b}

The reaction of vinylsilanes with the ruthenium complexes L_x(OC)(Cl)RuH (L = PCy₃, *x* = 2; L = PPh₃, *x* = 3) were used in dehydrosilylation⁵⁵⁰ and hydrosilylation¹⁹⁹ studies. Reaction of these Ru precursors with VinSiR₃ gave L₂(OC)(Cl)RuSiR₃ (**19-16**,⁵⁵⁰ **19-17**¹⁹⁹) and C₂H₄, which gives the appearance of OA of Si–C to the Ru center followed by RE of C₂H₄. However, the more likely course

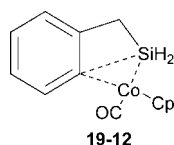


Figure 45. Intermediate proposed in reaction of CpCo(CO)₂ with benzosilacyclobutene.^{448b}

is insertion of the vinyl group into the Ru–H bond followed by a β -silyl elimination. It is a rather unusual method for the synthesis of complexes with Ru–Si bonds. The reaction of Cp*Ru(μ -H)₄RuCp* with VinSiMe₃ does involve the cleavage of two different Si–C bonds in the formation of **19-18**, (Cp*Ru)₂(μ -SiMe₂)(μ -CCH₃)(μ -H).²¹⁴ Another example involved reaction of the coordinatively unsaturated cationic ruthenium complex [(η^6 -C₆Me₆)Ru{ η^1 -PrNC(Me)=NⁱPr}]⁺ with Me₃SiCHN₂.⁴⁰⁴ The product, **19-19**, contained a Ru–Si bond whose formation required cleavage of the C–SiMe₃ bond. This was proposed to occur through migration of a trimethylsilyl group from an intermediate carbene ligand. Thus, the reactions of the Ru complexes basically do not involve insertion of a Ru moiety directly into a Si–C bond, which seems to dominate the Pt(0) and Pd(0) reactions.

The theoretical aspects of OA/RE of Si–C bonds were included in section 7.3.7 as it pertained to hydrosilylation mechanisms. However, there was a DFT (B3LYP) study that posed a different type of question concerning Si–C bond activation: how does the incoming substrate, HC≡CSiH₃, approach the metal in (H₃P)₂Pd?^{561c} Although the report focused primarily on the reactions of HC≡CSnH₃, the comments here will be confined to the silane. The interaction of HC≡CSiH₃ occurred through donation of a C≡C π -orbital to a Pd sp-hybridized orbital and back-donation from a Pd d π -orbital located in the P–Pd–P plane into the π^* -orbital as in a typical CDC model. The Pd d-orbital that is perpendicular to the P–Pd–P sequence does not participate in the activation reaction. In the TS, the C–Si σ -bond donates to the Pd sp-orbital and back-donation of the Pd d π -orbital in the P–Pd–P plane interacts with the C–Si σ^* . The Pd–C–Si twists from the P–Pd–P plane about 25° to avoid electronic repulsion between the C≡C π -orbital and the Pd d π -orbital in the P–Pd–P plane.

Although the reactions described in this section involve “insertion” (or the overall equivalent) into a Si–C bond by a metal unit, the reverse process would involve RE of Si–C from the metal center. As a type of model for this process, Ozawa and co-workers reported kinetic studies for RE of MeElPh₃ (El = Si, Ge) from thermolysis of *cis*-(PhMe₂P)₂Pt(Me)(ElPh₃) in the presence of excess PhC≡CPh.^{562a} The reaction proceeds by replacement of one of the phosphine ligands by the acetylene followed by elimination of MeElPh₃. The observed order of reactivity for elimination was C–Si > C–Ge \gg C–C. The complexes, *cis*-(PhMe₂P)₂Pt(C≡CAr)SiAr'₃, undergo C–Si RE under mild conditions to give [(PhMe₂P)₂Pt(ArC≡CSiAr'₃)].^{(Ni-90) 562b} The kinetic studies indicated that a concerted reaction process occurred from the 4-coordinate complex through partial bonding between Pt...C...Si atoms. The corresponding RE from *cis*-(PhMe₂P)₂Pt(CH=CH₂)SiR₃ also gave Pt(0) com-

plexes coordinated to vinylsilanes.^{562c} First-order kinetics were observed and addition of PMe_2Ph did not retard the rate, thus demonstrating that the direct RE occurs without prior dissociation of PhMe_2P from the Pt center.

8.2.3. Si–Ei (Ei = Sn, B, S)

Activation of Si–heteroatom bonds by transition metals has been studied particularly with regard to development of organic methodology. The earlier work (prior to 1998) has been the subject of several reviews.^{560a,b,563,564} The transition metal catalyzed additions of Si–Ge and Si–Sn bonds to unsaturated substrates was included in both refs 560a and 560b, and those of Si–S were briefly included in refs 563 and 564.

Ozawa and co-workers prepared a number of complexes of the type $\text{cis-L}_2\text{Pt}(\text{SiR}_3)(\text{SnMe}_3)$ ($\text{R} = \text{Ph}$, $\text{L} = \text{PPhMe}_2\text{P}$, **19-27**;⁵⁵³ $\text{R}_3 = \text{PhMe}_2$, $\text{L} = \text{PMe}_3$, **19-28**^{426c}) by oxidative addition of $\text{R}_3\text{SiSnMe}_3$ to $\text{Pt}(\text{cod})_2$ in the presence of 2 equiv of the phosphine. The complexes exhibited two sets of doublets in the $^3\text{P}\{^1\text{H}\}$ NMR spectrum at -50°C with ^{117}Sn , ^{119}Sn , and ^{195}Pt satellites. These signals broaden and coalesce at 35°C , and the process causing the line broadening was assigned to a twist-rotation via a pseudo-tetrahedral transition state (see Scheme 31). In line with this observation, the crystal structure of **19-28** showed that the Pt–Si and Pt–Sn bonds are tilted from the PtP_2 plane with a twist angle between the P–Pt–P plane and the Si–Pt–Sn plane of 32° .⁵⁶⁵ A similar process was described earlier in section 6.3 for the related complexes $\text{cis}-(\text{PhMe}_2\text{P})_2\text{Pt}(\text{SiR}_3)_2$ ($\text{R}_3 = \text{FMe}_2$,¹²⁵ MePh_2 ^{282a}) and twist angles were reported for $\text{R}_3 = \text{SiMe}_2\text{Ph}$ (22.8°),²⁸¹ SiMePh_2 (38.1°),^{282a} and SiPh_3 (28.3°).²⁸¹ The mechanism of alkyne insertion into the $\text{cis-bis}(\text{silyl})\text{platinum(II)}$ complexes²⁸¹ and into the $\text{cis-silyl}(\text{stannyl})\text{platinum complexes}$ ^{426c,553} was also reported.

Insertion of a variety of unsaturated organic reagents into Si–B bonds was summarized briefly in reviews.^{560a,b,563} Ozawa and co-workers reported four complexes from the reaction of $\text{Pt}(\text{cod})_2$, phosphines (PMe_3 , PEt_3 and PMe_2Ph), and $\text{PhMe}_2\text{Si-BX}_2$ ($\text{X}_2 = -\text{OCMe}_2\text{CMe}_2\text{O}-$, $-\text{NMeCH}_2\text{CH}_2\text{NMe}-$) to give the complex $\text{cis-L}_2\text{Pt}(\text{SiR}_3)(\text{BX}_2)$ [**19-29**, $\text{L} = \text{Me}_3\text{P}$, $\text{SiR}_3 = \text{SiMe}_2\text{Ph}$, $\text{X}_2 = -\text{OCMe}_2\text{CMe}_2\text{O}-$].⁴²⁹ Silyl(boryl)platinum(II) complexes have been assumed to be key intermediates in catalytic silylborylation but had not previously been observed prior to this study. The insertion of $\text{PhC}\equiv\text{CH}$ occurred exclusively into the Pt–B bond of the complexes, and RE of Si–C provides the silylborylation products. In another study, the silaboration of $\text{RCH}=\text{C}=\text{CH}_2$ and $\text{Me}_2\text{C}=\text{C}=\text{CH}_2$ in the presence of ArI , I_2 , or Me_3SiI and a Pd catalyst gave silaboration products with the silyl group on the central carbon and the boryl group on the terminal carbon of the allene.⁵⁶⁶ In the absence of the iodide, a different regiochemistry was observed. In the presence of an iodide, Pd(0) is converted to Pd(II) on reaction with R_3SiI followed by coordination of the allene to the Pd(II) and delivery of the R_3Si group to the central carbon of the allene. The cycle continues with the reaction of the siladioxaborolane reagent, which delivers the boron unit to the terminal carbon of the allene and provides R_3SiI to continue the cycle. Borylation studies of trialkylsilane Si–H bonds have been reported by Boebel and Hartwig with the catalyst system, $[\text{Ir}(\text{cod})\text{OMe}]_2$ and 4,4'-di-*tert*-butylbipyridine (dtbpy), B_2pin_2 , and R_3SiH .^[HSi-3(08)] The sterically hindered $^i\text{Pr}_3\text{SiH}$ did not react nor did

R_2SiH_2 or aryl-functionalized hydrosilanes. The authors did not speculate on the route that led to the R_3SiBpin product.

The reaction of $\text{Pt}(\text{PEt}_3)_4$ with PhSSiCl_3 provided $\text{trans}-(\text{Et}_3\text{P})_2\text{Pt}(\text{SPh})(\text{SiCl}_3)$ (**19-30**) in >95% by NMR.⁵⁵⁴ Although not common, Pt(0) appeared to catalyze the addition of Si–S bonds to alkynes when a mixture of $(\text{ArS})_2$ and Si_2Cl_6 was heated with a terminal alkyne in the presence of $(\text{Ph}_3\text{P})_2\text{Pt}(\text{CH}_2=\text{CH}_2)$. The silyl group appears on the terminal carbon center in the addition product.⁵⁵⁴ It was also demonstrated that a small concentration of **19-30** was in equilibrium with $\text{trans}-(\text{Et}_3\text{P})_2\text{Pt}(\text{SPh})_2$, and thus, it was concluded that it was PhSSiCl_3 that selectively added to the Pt(0) center.

8.2.4. SiX (X = Halogen)

Reports of activation of Si–halogen bonds were relatively rare during this review period. Schubert and co-workers examined the reactions of $\text{cis}-(\text{P}\backslash\text{N})\text{PtMe}_2$ with Me_3SiI where $\text{P}\backslash\text{N}$ are the hemilabile chelating ligands, $\text{Ph}_2\text{P}(\text{CH}_2)_x\text{NMe}_2$, $o\text{-Ph}_2\text{PC}_6\text{H}_4\text{NMe}_2$, and $o\text{-Ph}_2\text{C}_6\text{H}_4\text{-CH}_2\text{NMe}_2$.²⁹² Although no reaction occurred at room temperature, heating produced Me_4Si and $\text{cis}-(\text{P}\backslash\text{N})\text{PtMeI}$ (**19-37**, $\text{P}\backslash\text{N} = \text{Ph}_2\text{P}(\text{CH}_2)_3\text{NMe}_2$). The reaction was assumed to take place through OA of Me_3SiI to the Pt(II) center and RE of Me_4Si , although the Pt(IV) species was not observed by NMR spectroscopy. The reaction of $(\text{dppe})\text{PtMe}_2$ and Me_3SiI occurred to give the related $(\text{dppe})\text{Pt}(\text{Me})\text{I}$ complex, but at a much slower rate than observed for the $\text{P}\backslash\text{N}$ chelates. The faster reactivity for the hemilabile ligands was presumed to occur by reversible dissociation of the N-arm from the Pt center.

The activation of Si–Cl bonds by Ru(0) complexes, $[\eta^2\text{-N}_3]\text{Ru}(\eta^6\text{-Ar})$ or $\{[\text{N}_3]\text{Ru}\}_2(\mu\text{-N}_2)$ ($\text{Ar} = \text{C}_6\text{H}_6$, $\text{C}_6\text{H}_5\text{Me}$; $\text{N}_3 = 2,6\text{-(MesN=CMe)}_2\text{C}_5\text{H}_3\text{N}$) has been demonstrated for the N-heterocyclic silanes $(\text{X})(\text{Cl})\text{Si}(\text{NN})$ [$\text{NN} = (\text{NCH}_2\text{Bu})_2\text{C}_6\text{H}_4\text{-1,2}$].^{213b} The silane, where $\text{X} = \text{H}$, produced **3-134e**, which was presumed to form by OA of SiH to Ru(0) followed by migration of Cl from Si to Ru to give the silylene complex **3-134e**, $[\text{N}_3]\text{Ru}(\text{H})(\text{Cl})\{\text{Si}(\text{NN})\}$.^{213b} The fluxional properties of **3-134e** were described in section 6.3. When $\text{X} = \text{Cl}$, the reaction of $\text{Cl}_2\text{Si}\{\text{N},\text{N}\}$ with $[\eta^2\text{-N}_3]\text{Ru}(\eta^2\text{-MeC}_6\text{H}_5)$, in the absence of N_2 , produced **19-31**, $[\text{N}_3](\text{Cl})\text{RuSi}(\text{Cl})\{\text{N},\text{N}\}$, where SiCl has oxidatively added to the Ru(0) center and which could be isolated.^{213b} When, however, the reaction was performed under N_2 , the product was a mixture of $[\text{N}_3]\text{Ru}(\text{N}_2)\text{Si}\{\text{N},\text{N}\}$ and $[\text{N}_3]\text{Ru}(\text{Cl})_2(\text{THF})$. The formation of $[\text{N}_3]\text{Ru}(\text{Cl})_2(\text{THF})$ implied a 1,2-migration of Cl from Si to Ru followed by dissociation of the silylene from the intermediate complex, $[\text{N}_3]\text{Ru}(\text{Cl})_2\{\text{Si}(\text{NN})\}$, **19-32**. The intermediate complex was not observed in the reaction but could be generated from $[\text{N}_3](\text{Cl})_2\text{Ru}(\text{C}_2\text{H}_4)$ and the free silylene, $\text{Si}\{\text{N},\text{N}\}$.^{213b}

The hemilabile complexes $[\text{P}\backslash\text{N}]\text{PtMe}_2$ (particularly $\text{P}\backslash\text{N} = \text{Ph}_2\text{PCH}_2\text{CH}_2\text{NR}_2$, $\text{R} = \text{Me}$, Et , ^iPr) have been shown to activate a Si–Cl bond. Reaction of $[\text{P}\backslash\text{N}]\text{PtMe}_2$ with PhMe_2SiCl gave quantitative yields of the disilane, $\text{PhMe}_2\text{SiSiMe}_2\text{Ph}$. Oxidative addition of PhMe_2SiCl and RE elimination of MeCl was presumed to give the intermediate $[\text{P}\backslash\text{N}]\text{PtMe}(\text{SiMe}_2\text{Ph})$, which reacted with a second mole of PhMe_2SiCl to give the disilane.⁵⁶⁷

The mechanistic evidence developed for reactions that involve $[\text{P}\backslash\text{N}]\text{Pt(II)}$ species with organosilanes suggests that the 4-coordinate Pt(II) center becomes 3-coordinate during the reaction course as the hemilabile ligand opens at the N

center. Ab initio calculations (DFT/B3LYP) of the T-shaped model, $(\text{H}_3\text{P})\text{Pt}(\text{SiH}_3)\text{X}$ ($\text{X} = \text{Cl}, \text{CH}_3$), showed that the isomer with SiH_3 *cis* to PH_3 is the more stable isomer in both cases.⁵⁶⁸ The following *trans* influence was established for the ligands, $\text{Cl} < \text{CH}_3 < \text{SiH}_3$, and the authors proposed that the ligand with the lower *trans* influence would be *trans* to the PH_3 ligand. In the square-planar complex, *cis*- $(\text{R}_3\text{P})_2\text{PtXY}$, the phosphine ligand in the *trans* position to the ligand with the larger *trans* influence would be more readily eliminated and when eliminated would give the more energetically favored 3-coordinate complex. In a second study, the reactivity of the chlorosilanes SiCl_4 and SiH_3Cl towards $[(\text{PH}_3)\text{Pt}(\text{SiH}_3)\text{Me}]$ (as a model for $[\text{PtMe}(\text{SiH}_3)\{\kappa^2\text{-(P,N)}\text{-Ph}_2\text{PCH}_2\text{CH}_2\text{NMe}_2\}]$) was studied by DFT(B3LYP) calculations.⁵⁶⁹ The reaction with SiCl_4 proceeded through a 5-coordinate Pt(IV) square-pyramidal intermediate with SiH_3 in the apical position and Me/PH_3 *trans* to each other in the square plane. Reductive elimination of SiH_3Cl occurred to give the equivalent of exchange of SiCl_3 for SiH_3 . In the reaction of SiH_3Cl , a distorted trigonal-bipyramidal complex was formed (PH_3 and CH_3 apical). Reductive elimination, however, gave Si_2H_6 , which paralleled the results described in the previous paragraph.

The reactions of Me_3SiX with the pincer ligand complex, $(\text{PNP})\text{Rh}(\text{SPr}^i_2)$ [$\text{PNP} = \text{bis}(o\text{-diisopropylphosphinophenyl})\text{-amide}$], provided some interesting comparisons as a function of the halide.^{254c} No reaction with Me_3SiCl was observed, and that with Me_3SiBr was nearly isoergic with that of the SPr^i_2 ligand (producing an equilibrium between $(\text{PNP})\text{Rh}-\text{SPr}^i_2$ and the OA product $(\text{PNP})\text{Rh}(\text{Br})(\text{SiMe}_3)$ with $K \approx 0.8$ (65°C), although the OA product could be isolated. In contrast to Me_3SiCl , OA addition occurred with both MeSiCl_3 and SiCl_4 , although Me_2SiCl_2 produced an equilibrium similar to that observed with Me_3SiBr , but the complex **19-34** $(\text{PNP})\text{Rh}(\text{Cl})(\text{SiMe}_2\text{Cl})$ was isolated. The complexes were characterized by ^1H , ^{13}C , ^{31}P , and ^{29}Si NMR and **19-34** by X-ray diffraction. An interesting comparison was provided in the reaction of Me_2SiHCl with $(\text{PNP})\text{Rh}(\text{SPr}^i_2)$ where the only product isolated was $[(\text{PNP})\text{Rh}(\text{H})(\text{SiMe}_2\text{Cl})]$. The authors suggested that the complex could be described as either a classical OA product or as an $\eta^2\text{-H-Si}$ product. The Si center shows coupling to the hydride in the ^{29}Si NMR spectrum. The hydride distances determined in the solid were 1.50(2) and 1.93(2) Å for Rh-H and Si-H , respectively. The $\text{Si}\cdots\text{H}$ distance is in the range of an IHI interaction, which often occurs between M-H and SiMe_2Cl substituents (section 5.5.1 and Table 9), although a *trans*-orientation for $\text{H}\cdots\text{Si-Cl}$ would be necessary. In the present case, there is rotational disorder for the Me_2SiCl group that was reported; thus, an assignment of an IHI interaction is precluded in this case.^{254c}

9. Conclusion

A considerable expansion in studies of reactions of hydrosilanes with transition metal complexes has occurred over the years since our first review was published in 1999.^{1a} Tertiary silanes still remain the bulk of the silanes that have been studied, but some of the most interesting results in terms of variations of structures have come from studies of the reactions of primary and secondary silanes. It is the use of silanes with more than one Si-H bond that has produced most of the silyl-metal complexes reported to contain “nonclassical” interactions.

In contrast to the first review, the reactions of the silanes have been organized in section 3 not by primary, secondary, and tertiary silanes but first by ligand loss from the reacting metal complex (neutral or “anionic”) and then in smaller groupings such as low-valent metals and polynuclear complexes. Whether the silane oxidatively adds to the metal center or reacts through a σ -bond metathesis pathway, there must be an open coordination site at the metal center. If the silane oxidatively adds, then the metal center also needs to be electronically unsaturated ($<18e$ count). If a “saturated” metal complex is the starting point in the study, then loss of a neutral ligand, most commonly PR_3 , CO , or a coordinated olefin (see section 3.2), occurs, and this is accomplished, generally, by photolysis or thermolysis. Many such examples appear in Tables 1–3 and are summarized in Charts 1 (PR_3), 2 (CO), and 3 (unsaturated molecules) in section 3.2. In a second type of “ligand loss”, the hydrosilane adds to $[\text{TM}]-\text{R}$ and HR is eliminated to give the silyl-metal complex. The R group is typically Me (loss of methane) or Ph (loss of benzene) but can also be $[\text{TM}]-\text{H}$ (loss of H_2) or $[\text{TM}]-\text{SiR}_3$ (loss of HSiR_3). In the latter case, the most useful is $\text{R} = \text{Me}$ (i.e., HSiMe_3), which is volatile and may be removed from the system, providing the driving force for a silyl-exchange substitution at the metal. Since an important target of some studies has been formation of metal-silylenes, section 3.6.1 features reactions where this was successfully accomplished from a hydrosilane. Some reactions of hydrosilanes lead to transfer of hydride from silicon to the metal, and such cases are summarized in section 3.7.

An important characterization method in organometallic chemistry is the determination of the solid-state structure by X-ray diffraction (common) or by neutron diffraction (rare). Table 6 provides the parameters for Si-M , M-H , and Si-H distances (if reported for the latter two) for the complexes listed in Tables 1, 2, and 3 as well as for the examples that appear in the footnotes to these tables. In addition, Si-M distances for complexes prepared by routes other than by reaction of a silane are included in a footnote that appears at the end of each triad section (most of the data were obtained from the CDB). Also included in the tables is the temperature of the data collection if provided in the original report or in the CDB. Most structures are now determined at low temperature and presumably provide more reliable bond-distance data. The Si-M bond-distance range observed for each metal is provided in Table 7 and includes $2e/2c$ bonds, multicenter bonds, and metal silylenes. The extent of the range for an individual metal can vary from 0.07 to 0.79 Å. The ranges observed in the structurally characterized silylene complexes are summarized in Table 8 and compared to the range reported in Table 7. The Si-to-M distances in metal silylenes are not necessarily clustered in the short end of a range. The specific examples of metal silylenes used to establish the ranges are given in Supporting Information Table S1 (supplement to Table 7). A serious difficulty with this characterization method is the problem of establishing a reliable hydride distance in the presence of a heavy metal and also the fact that the hydrides cannot always be located in the structure. In addition, several complexes are disordered, precluding placement of hydrides.

When a silane approaches a metal center and the H-Si distance begins to exceed 1.50 Å, how should the interaction between the metal center, the silicon center, and the hydrogen be described? A possible classification, as well as the

attendant problems of characterization, is described in section 5. The complexes in this category are summarized with the characterization data in Table 9. Nonclassical interactions of hydrosilanes can be loosely described either as a metal hydride interacting with the silicon of the silyl substituent ($M-H\cdots Si$) or as a silyl hydrogen interacting with a metal center ($Si-H\cdots M$) and are described in section 5.4 as σ -complexes or as agostic interactions for the latter and as IHI or SISHA interactions in section 5.5 in the former. In general, the $Si-H$ separation (summarized in Scheme 15) has varied from just below 1.6 to ~ 2.4 Å in such complexes. The $Si-H\cdots M$ interactions have been found to vary from a nearly "head-on" entry of $H-Si$ with the metal ($Si-H-M$ angle near 180°) to a remote agostic interaction between the metal and an $H-Si$ bond in an ε -position. The $M-H\cdots Si$ interactions are generally longer, and the range with hydride-to-silicon separations were ~ 2 Å (IHI) and >2 Å (SISHA). Distances >2.5 Å for $H\cdots Si$ are considered nonbonding, although the sum of the van der Waals radii for Si and H is 3.4 Å. Important methods of characterization include X-ray, NMR, and IR data, and the problems that attend these methods are described in sections 5.1 and 5.2. To illustrate how the characterization data fit together, six representative examples of nonclassical interactions are discussed in section 5.3. A growing feature in "proof of structure" for the nonclassical interaction is a DFT calculation, and where appropriate, selected examples have been incorporated into section 5, although the majority of calculations (in general) appear in section 7. There is no uniformly adopted convention for describing the various bonding possibilities within the indicated assignments for a nonclassical complex. For the most part, the representations that are used are those provided by the respective authors. Furthermore, the complexes that have been reported form a continuum in $M\cdots H\cdots Si$ interactions, and clear borders between types of identified interactions and our attempts to classify these interactions can only be considered approximate. Another problem in efforts to describe the interactions is the lack of characterization data. A glance at Table 9 and the number of blank sites gives an idea of how much data are missing.

A key feature in the identification of an "agostic" interaction appears to be a shift of the normal SiH 1H NMR resonance upfield and generally upfield of the TMS signal. Is the presence of an upfield signal a reliable indicator of the nonclassical interaction? In order to answer this, it is important to determine whether the nonclassical interaction persists in solution. Since the nonclassical interaction is often revealed in the X-ray structure, the question could also be whether the structure in the solid is the same in solution. Since many examples of nonclassical interactions rely only on solution NMR data, this is an important determination. For the most part, the answer to this last question appears to be yes. However, both monometallic and bimetallic silyl-metal complexes, especially those with a $HMSiH$ sequence, exhibit fluxional properties in solution, and thus, room-temperature spectral data may not reveal the appropriate or expected signals. In section 6, systems that are fluxional are described first for monometallic hydride complexes (section 6.1) and then for bimetallic metal hydrides (section 6.2). There are at least six types of fluxional processes involving exchange of hydrides in monometallic complexes and four types of cases that have been identified in bimetallic complexes. In several examples, the thermodynamic parameters have been determined, and such data are included in section 6. The

interpretation of what causes the fluxional behavior is more of a problem and is often not addressed. However, in some cases, DFT calculations have provided a rationale for the observed behavior, and such examples are discussed and illustrated in this section. Other fluxional cases were collected in section 6.3 and include exchange through $M=Si$ intermediates, hindered $M-Si$ rotation, and isomerization within 4-, 5-, and 6-coordinate geometries.

A major difference between the current review and the previous review^{1a} was the increased use of calculations (primarily DFT) both as support for complexes that have been generated and in predicting new systems (section 7). With few exceptions, the calculations use simplified, model systems where phosphines and silyl groups are represented by PH_3 and $-SiH_3$, respectively, and Cp' (substituted Cp ring) is replaced by C_5H_5 . Usually the minimized, gas-phase structure from the calculation is compared to the actual complex whose parameters are obtained from the solid-state structure. In this way, hydride distances to both metal and silicon can be proposed for complexes where the hydrides could not be located. Since distances for $M-H$ and $M-H\cdots Si$ bonds are less precise for X-ray determinations, the calculations provide a possible value for consideration. Neutron diffraction measurements are superior for the determination of hydride distances, but only five structures have been determined by this method that contain both an $M-H$ and an $M-Si$ bond (section 4). How close do the calculated distances (angles) and the experimental distances (angles) have to be for the calculated structure to be considered in agreement with parameters measured for an actual complex? A second group of papers addresses calculations for unknown molecules. For instance, is it possible to stabilize an unstable or reactive silicon compound such as the valence isomers of Si_2R_2 through the formation of a metal complex? Of course, the calculation is performed with $R = H$, which is unrealistic to attempt in the laboratory. Thus, if $R \neq H$, how would this affect the conclusions derived from the calculations? Two recent publications relative to theoretical calculations are interesting to consider, although neither deals with silicon-metal chemistry: the first concerns the sources of error in DFT computations of C-C bond-formation thermochemistries⁵⁷⁰ and the second asks for more realism in predicting molecules.⁵⁷¹

This review deals with activation of $Si-H$ bonds and the myriad types of bonding interactions that have been observed upon reaction with transition metal complexes. Are other metals (such as lanthanides) or other $Si-El$ bonds activated by metals in a similar way? Section 8.1 described the relatively few reactions of lanthanide/actinide complexes with silanes. The reactions of $PhSiH_3$, for instance, exhibited $Si-C$ cleavage particularly when $R = Ph$. Similar to the hydride transfer reactions reported in section 3.7, silanes can transfer hydride to a lanthanide center. The introduction of the $-N(SiHMe_2)_2$ ligand in lanthanide complexes has demonstrated a prevalence of products with $Si-H\cdots Ln$ β -agostic interactions (see Table 18) as described earlier for nonclassical interactions in section 5.4.2. Since the $Ln(III)$ center (in Cp_2LnX) has an empty 5d-shell and a stabilized 4f-shell, activation of SiH bonds does not proceed by an OA mechanism. The bond transformations through a 4-centered σ -bond metathesis route have been the subject of theoretical calculations.

There are other $Si-El$ bonds that are activated by metals, and selected examples are summarized in section 8.2 (and

Table 19) for Si–Si, Si–C, Si–E(Sn, B, or S), and Si–X (halogen). Low-valent metals insert into Si–Si bonds, and such species have been proposed in catalytic cycles. The isolation of a metal complex that exhibits an interaction with a Si–Si single bond has yet to be verified, although there are some examples reported in this review (section 8.2.1) that appear to be consistent with that possibility, but the direct identification of a complex with a Si–Si bond coordinated to a metal center has yet to be achieved and remains, at this point, a proposal based on calculations. It remains a challenge for future work.

A common rationale for the study of reactions of hydrosilanes with transition metal complexes is that the hydrosilanes, which undergo SiH activation more easily than do alkanes, can function as a model for CH activation. Direct observation of a σ -bonded alkane molecule is rare outside of alkane matrix studies, but recent success has been achieved by Goldberg and Brookhart in reactions utilizing the pincer ligand, PONOP = 2,6-(Bu_2PO) $_2\text{C}_5\text{H}_3\text{N}$, in the M(I) complexes (PONOP)MCH $_3$ (M = Rh,^{572a} Ir^{572b}). Protonation of (PONOP)IrCH $_3$ provided [(PONOP)Ir(H)CH $_3$] $^+$ (isolated and crystallographically characterized as the BAR_4F_4^- salt), which undergoes rapid exchange between IrH and IrCH $_3$ protons and implies the reversible formation of a transient σ -CH $_4$ complex. A similar protonation of the rhodium analogue gave, at low temperatures, (PONOP)Rh–CH $_4^+$, which was characterized by various NMR experiments and also undergoes rapid exchange, giving a J_{CH} that is a weighted average of $^1J_{\text{CH}}$ and $^3J_{\text{CH}}$ coupling constants. The facile exchange (computed barrier <1 kcal/mol) was proposed to occur through a symmetric $\eta^2\text{-H}_2$ coordination mode. The exchange is similar to that proposed by Heinekey and depicted in Scheme 24 for exchange of a MH and a SiH in HMSiHR_2 (section 6.1.1). Thus, the hydrosilane as a model for an alkane seems to be warranted, and the results depicted in this review may provide hints for future work in CH activation.

10. Acknowledgments

I thank Dr. Nigam Rath for help in obtaining data from the Cambridge Data Base and Dr. Janet Braddock-Wilking for assistance in the earliest stages of the project for inputting data for the Co and Ni triads into Tables 1, 2, 3, and 6.

11. Supporting Information Available

Supplemental data for Tables 7 and 8. This material is available free of charge via the Internet at <http://pubs.acs.org>.

12. References

- (a) Corey, J. Y.; Braddock-Wilking, J. *Chem. Rev.* **1999**, 99, 175, and earlier reviews cited therein. (b) Eisen, M. S. *The Chemistry of Organic Silicon Compounds*; Patai, S., Rappoport, Z., Eds.; John Wiley and Sons: New York, 1998; Vol. 2 (Pt. 3), p 2037.
- Collman, J. P.; Hegedus, L. S.; Norton, J. R.; Finke, R. G. *Principles and Applications of Organotransition Metal Chemistry*; University Science Books: Mill Valley, CA, 1987; Chapter 5.
- (a) Walsh, R. In *The Chemistry of Organic Silicon Compounds*; Patai, S., Rappoport, Z., Eds.; John Wiley and Sons: New York, 1989; Chapter 5. (b) Müller, U.; Popowski, E. *Z. Phys. Chem. Leipzig* **1990**, 271, 703. *Chem. Abstr.* 1991, 114, 185603n. (c) Ding, L.; Marshall, P. *J. Am. Chem. Soc.* **1992**, 114, 5754.
- Schubert, U. *Adv. Organomet. Chem.* **1990**, 30, 151.
- (a) Nikonov, G. I. *Angew. Chem., Int. Ed.* **2001**, 40, 3353. (b) Braunstein, P.; Boag, N. M. *Angew. Chem., Int. Ed.* **2001**, 40, 2427. (c) Nikonov, G. I. *J. Organomet. Chem.* **2001**, 635, 24. (d) Kubas, G. J. *J. Organomet. Chem.* **2001**, 635, 37. (e) Kubas, G. J. *Metal Dihydrogen and σ -Bond Complexes: Structure, Theory, and Reactivity*; Kluwer Academic/Plenum Publishers: New York, 2001; Chapter 11. (f) Nikonov, G. I. *Adv. Organomet. Chem.* **2005**, 53, 217.
- Crabtree, R. H. *Angew. Chem., Int. Ed. Engl.* **1993**, 35, 789.
- Stadelmann, B.; Lassacher, P.; Stüger, H.; Hengge, E. *J. Organomet. Chem.* **1994**, 482, 201.
- (a) Sadow, A. D.; Tilley, T. D. *J. Am. Chem. Soc.* **2002**, 124, 6814. (b) Frank, D.; Baumgartner, J.; Marschner, C. *Chem. Commun.* **2002**, 1190 (see also ref 353).
- Hashimoto, H.; Sekiguchi, Y.; Iwamoto, T.; Kabuto, C.; Kira, M. *Organometallics* **2002**, 21, 454.
- Hashimoto, H.; Suzuki, K.; Setaka, W.; Kabuto, C.; Kira, M. *J. Am. Chem. Soc.* **2004**, 126, 13628.
- Feldman, J. D.; Mitchell, G. P.; Nolte, J.-O.; Tilley, T. D. *J. Am. Chem. Soc.* **1998**, 120, 11184.
- Feldman, J. D.; Mitchell, G. P.; Nolte, J.-O.; Tilley, T. D. *Can. J. Chem.* **2003**, 81, 1127.
- Fürstner, A.; Krause, H.; Lehmann, C. W. *Chem. Comm.* **2001**, 2372.
- Herrmann, W. A.; Härter, P.; Gstöttmayr, C. W. K.; Bielef, F.; Seeboth, N.; Sirsch, P. *J. Organomet. Chem.* **2002**, 649, 141.
- Petri, S. H. A.; Eikenberg, D.; Jutzi, P. *Organosilicon Chemistry IV, 4th ed.* **2000**, p 76. *Chem. Abstr.* 2000, 133, 89611.
- Gehrhuis, B.; Hitchcock, P. B.; Lappert, M. F.; Maciejewski, H. *Organometallics* **1998**, 17, 5599.
- Jutzi, P.; Petri, S. H. A. *Organosilicon Chem. III, 3rd ed.* **1998**, p 275. *Chem. Abstr.* 1998: 179492.
- Freeman, S. T. N.; Lofton, L. L.; Lemke, F. R. *Organometallics* **2002**, 21, 4776.
- Hao, L.; Lebus, A.-M.; Harrod, J. F. *Chem. Commun.* **1998**, 1089.
- (a) Bihlmeier, A.; Greene, T. M.; Himmel, H.-J. *Organometallics* **2004**, 23, 2350. (b) Ignatov, S. K.; Rees, N. H.; Tyrell, B. R.; Dubberley, S. R.; Razuvaev, A. G.; Mountford, P.; Nikonov, G. I. *Chem.—Eur. J.* **2004**, 10, 4991.
- (a) Wang, X.; Andrews, L. *J. Am. Chem. Soc.* **2008**, 130, 6766. (b) Vincent, J. L.; Luo, S.; Scott, B. L.; Butcher, R.; Unkefer, C. J.; Burns, C. J.; Kubas, G. J.; Lledós, A.; Maseras, F.; Tomás, J. *Organometallics* **2003**, 22, 5307.
- (a) Glaser, P. B.; Tilley, T. D. *Organometallics* **2004**, 23, 5799. (b) Tobita, H.; Matsuda, A.; Hashimoto, H.; Ueno, K.; Ogino, H. *Angew. Chem., Int. Ed.* **2004**, 43, 221.
- Himmel, H.-J. *Chem.—Eur. J.* **2004**, 10, 2851.
- (a) Stahl, S. S.; Labinger, J. A.; Bercaw, J. E. *Inorg. Chem.* **1998**, 37, 2422. (b) Ebsworth, E. A.; Marganian, V. M.; Reed, F. J. S.; Gould, R. O. *J. Chem. Soc., Dalton Trans.* **1978**, 1167.
- Macrae, V. A.; Greene, T. M.; Downs, A. J. *J. Phys. Chem. A* **2004**, 108, 1393.
- (a) Sadow, A. D.; Tilley, T. D. *Angew. Chem., Int. Ed.* **2003**, 42, 803. (b) Sadow, A. D.; Tilley, T. D. *J. Am. Chem. Soc.* **2005**, 127, 643. (c) Tardif, O.; Kurazumi, J.; Nishiura, M.; Horiuchi, A. *Kidorui* **2003**, 42, 50. *Chem. Abstr.* 2004, 140, 321452d.
- Hao, L.; Harrod, J. F.; Lebus, A.-M.; Mu, Y.; Shu, R.; Samuel, E. *Angew. Chem., Int. Ed.* **1998**, 37, 3126.
- Shu, R.; Hao, L.; Harrod, J. F.; Woo, H.-G.; Samuel, E. *J. Am. Chem. Soc.* **1998**, 120, 12988.
- (a) Muhoro, C. N.; He, X.; Hartwig, J. F. *J. Am. Chem. Soc.* **1999**, 121, 5033. (b) Spencer, M. D.; Shelby, Q.; Girolami, G. S. *J. Am. Chem. Soc.* **2007**, 129, 1860.
- Dioumaev, V. K.; Harrod, J. F. *Organometallics* **2000**, 19, 583.
- (a) Wu, F.; Jordan, R. F. *Organometallics* **2005**, 24, 2688. (b) Shinohara, A.; McBee, J.; Waterman, R.; Tilley, T. D. *Organometallics* **2008**, 27, 5717.
- (a) Ignatov, S. K.; Rees, N. H.; Merkoulou, A. A.; Dubberley, S. R.; Razuvaev, A. G.; Mountford, P.; Nikonov, G. I. *Chem.—Eur. J.* **2008**, 14, 296. (b) Gountchev, T. I.; Tilley, T. D. *J. Am. Chem. Soc.* **1997**, 119, 12831.
- Burckhardt, U.; Casty, L.; Tilley, T. D.; Woo, T. K.; Rothlisberger, U. *Organometallics* **2000**, 19, 3830.
- (a) Fryzuk, M. D.; MacKay, B. A.; Patrick, B. O. *J. Am. Chem. Soc.* **2003**, 125, 3234. (b) Hirotsu, M.; Fontaine, P. P.; Epshteyn, A.; Zavalij, P. Y.; Sita, L. R. *J. Am. Chem. Soc.* **2007**, 129, 9284.
- Petri, S. H. A.; Neumann, B.; Stammeler, H.-G.; Jutzi, P. *J. Organomet. Chem.* **1998**, 553, 317.
- (a) Mork, B. V.; Tilley, T. D.; Schultz, A. J.; Cowan, J. A. *J. Am. Chem. Soc.* **2004**, 126, 10428. (b) Khalimon, A. Y.; Simionescu, R.; Kuzmina, L.; Howard, J. A. K.; Nikonov, G. I. *Angew. Chem., Int. Ed.* **2008**, 47, 7701.
- (a) Zhou, D.-Y.; Zhang, L.-B.; Minato, M.; Ito, T.; Osakada, K. *Chem. Lett.* **1998**, 187. (b) Minato, M.; Zhou, D.-Y.; Zhang, L.-B.; Hirabayashi, R.; Takeya, M.; Matsumoto, T.; Harakawa, A.; Kikut-suji, G.; Ito, T. *Organometallics* **2005**, 24, 3434.
- (a) Watanabe, T.; Hashimoto, H.; Tobita, H. *Angew. Chem., Int. Ed.* **2004**, 43, 218. (b) Sakaba, H.; Hirata, T.; Kabuto, C.; Kabuto, K. *Organometallics* **2006**, 25, 5145; see ref 477.

- (39) Mork, V.; Tilley, T. D. *J. Am. Chem. Soc.* **2004**, *126*, 4375.
- (40) Butts, M. D.; Bryan, J.; Luo, X.-L.; Kubas, G. J. *Inorg. Chem.* **1997**, *36*, 3341.
- (41) Gavenonis, J.; Tilley, T. D. *Inorg. Chem.* **2004**, *43*, 4353.
- (42) (a) Gutsulyak, D. V.; Kuzmina, L. G.; Howard, J. A. K.; Vyboishchikov, S. F.; Nikonov, G. I. *J. Am. Chem. Soc.* **2008**, *130*, 3732. (b) Luh, L.-S.; Wen, Y.-S.; Tobita, H.; Ogino, H. *Bull. Chem. Soc. Jpn.* **1998**, *71*, 2865.
- (43) (a) Luh, L.-S.; Wen, Y.-S.; Tobita, H.; Ogino, H. *Bull. Chem. Soc. Jpn.* **1997**, *70*, 2193. (b) Braunstein, P.; Stahrfeldt, T.; Fischer, J. C. *R. S. Acad. Sci., Ser. Ilc* **1999**, *2*, 273.
- (44) (a) Bart, S. C.; Lobkovsky, E.; Chirik, P. J. *J. Am. Chem. Soc.* **2004**, *126*, 13794. (b) Man, M. L.; Zhou, Z.; Ng, S. M.; Lau, C. P. *Dalton Trans.* **2003**, 3727.
- (45) Thomas, C. M.; Peters, J. C. *Angew. Chem., Int. Ed.* **2006**, *45*, 776.
- (46) (a) Trovitch, R. J.; Lobkovsky, E.; Chirik, P. J. *Inorg. Chem.* **2006**, *45*, 7252. (b) Hirotsu, M.; Nishida, T.; Sasaki, H.; Muraoka, T.; Yoshimura, T.; Ueno, K. *Organometallics* **2007**, *26*, 2495.
- (47) (a) Grumbine, S. K.; Mitchell, G. P.; Straus, D. A.; Tilley, T. D.; Rheingold, A. L. *Organometallics* **1998**, *17*, 5607. (b) Rankin, M. A.; MacLean, D. F.; Schatte, G.; McDonald, R.; Stradiotto, M. *J. Am. Chem. Soc.* **2007**, *129*, 15855. (c) Rankin, M. A.; Hesp, K. D.; Schatte, G.; McDonald, R.; Stradiotto, M. *Chem. Commun.* **2008**, 250. (d) Rankin, M. A.; Schatte, G.; McDonald, R.; Stradiotto, M. *J. Am. Chem. Soc.* **2007**, *129*, 6390.
- (48) (a) Ng, S. M.; Lau, C. P.; Fan, M. F.; Lin, Z. *Organometallics* **1999**, *18*, 2484. (b) Chen, Y.-Z.; Chan, W. C.; Lau, C. P.; Chu, H. S.; Lee, H. L.; Jia, G. *Organometallics* **1997**, *16*, 1241.
- (49) Dioumaev, V. K.; Yoo, B. R.; Procopio, L. J.; Carroll, P. J.; Berry, D. H. *J. Am. Chem. Soc.* **2003**, *125*, 8936.
- (50) Gusev, D. G.; Fontaine, F.-G.; Lough, A. J.; Zargarian, D. *Angew. Chem., Int. Ed.* **2003**, *42*, 216.
- (51) (a) Dysard, J. M.; Tilley, T. D. *Organometallics* **2000**, *19*, 4726. (b) Campion, B. K.; Heyn, R. H.; Tilley, T. D. *J. Chem. Soc., Chem. Commun.* **1988**, 278.
- (52) Baya, M.; Crochet, P.; Esteruelas, M. A.; Gutiérrez-Puebla, E.; Ruiz, N. *Organometallics* **1999**, *18*, 5034.
- (53) Glaser, P. B.; Tilley, T. D. *Eur. J. Inorg. Chem.* **2001**, 2747.
- (54) Glaser, P. B.; Tilley, T. D. *J. Am. Chem. Soc.* **2003**, *125*, 13640.
- (55) Hayes, P. G.; Beddie, C.; Hall, M. B.; Waterman, R.; Tilley, T. D. *J. Am. Chem. Soc.* **2006**, *128*, 428.
- (56) Yong, L.; Hofer, E.; Wartchow, R.; Butenschön, H. *Organometallics* **2003**, *22*, 5463.
- (57) (a) Ingleson, M.; Fan, H.; Pink, M.; Tomaszewski, J.; Caulton, K. G. *J. Am. Chem. Soc.* **2006**, *128*, 1804. (b) Ingleson, M. J.; Pink, M.; Fan, H.; Caulton, K. G. *J. Am. Chem. Soc.* **2008**, *130*, 4262. (c) Doherty, M. D.; Grant, B.; White, P. S.; Brookhart, M. *Organometallics* **2007**, *26*, 5950. (d) Sangtrirutnugul, P.; Tilley, T. D. *Organometallics* **2007**, *26*, 5557.
- (58) Simons, R. S.; Gallucci, J. C.; Tessier, C. A.; Youngs, W. J. *J. Organomet. Chem.* **2002**, *654*, 224.
- (59) Simons, R. S.; Panzer, M. J.; Tessier, C. A.; Youngs, W. J. *J. Organomet. Chem.* **2003**, *681*, 1.
- (60) (a) Peters, J. C.; Feldman, J. D.; Tilley, T. D. *J. Am. Chem. Soc.* **1999**, *121*, 9871. (b) Feldman, J. D.; Peters, J. C.; Tilley, T. D. *Organometallics* **2002**, *21*, 4065.
- (61) Calimano, E.; Tilley, T. D. *J. Am. Chem. Soc.* **2008**, *130*, 9226.
- (62) (a) Zhang, L.; Chan, K. S. *Organometallics* **2006**, *25*, 4822. (b) Li, B.; Chan, K. S. *Organometallics* **2008**, *27*, 4034.
- (63) Shimada, S.; Rao, M. L. N.; Tanaka, M. *Organometallics* **1999**, *18*, 291.
- (64) Shimada, S.; Rao, M. L. N.; Hayashi, T.; Tanaka, M. *Angew. Chem., Int. Ed.* **2001**, *40*, 213.
- (65) Chen, W.; Shimada, S.; Tanaka, M.; Kobayashi, Y.; Saigo, K. *J. Am. Chem. Soc.* **2004**, *126*, 8072.
- (66) (a) Chen, W.; Shimada, S.; Hayashi, T.; Tanaka, M. *Chem. Lett.* **2001**, 1096. (b) Shimada, S.; Li, Y.-H.; Choe, Y.-K.; Tanaka, M.; Bao, M.; Uchimar, T. *PNAS* **2007**, *104*, 7758. (c) Shimada, S.; Rao, M. L. N.; Li, Y.-H.; Tanaka, M. *Organometallics* **2005**, *24*, 6029.
- (67) Simons, R. S.; Sanow, L. M.; Galat, K. J.; Tessier, C. A.; Youngs, W. J. *Organometallics* **2000**, *19*, 3994.
- (68) (a) Braddock-Wilking, J.; Levchinsky, Y.; Rath, N. P. *Organometallics* **2000**, *19*, 5500. (b) Levchinsky, Y.; Rath, N. P.; Braddock-Wilking, J. *Organometallics* **1999**, *18*, 2583.
- (69) Sanow, L. M.; Chai, M.; McConville, D. B.; Galat, K. J.; Simons, R. S.; Rinaldi, P. L.; Youngs, W. J.; Tessier, C. A. *Organometallics* **2000**, *19*, 192.
- (70) Braddock-Wilking, J.; Levchinsky, Y.; Rath, N. P. *Organometallics* **2001**, *20*, 474.
- (71) (a) Owens, T. M.; Nicholson, K. T.; Banaszak Holl, M. M.; Süzer, S. *J. Am. Chem. Soc.* **2002**, *124*, 6800. (b) Owens, T. M.; Süzer, S.; Banaszak Holl, M. M. *J. Phys. Chem. B* **2003**, *107*, 3177. (c) Schneider, K. S.; Lu, W.; Owens, T. M.; Fosnacht, D. R.; Banaszak Holl, M. M.; Orr, B. G. *Phys. Rev. Lett.* **2004**, *93*, 166104. (d) Schneider, K. S.; Lu, W.; Fosnacht, D. R.; Orr, B. G.; Banaszak Holl, M. M. *Langmuir* **2004**, *20*, 1258. (e) Chen, Y.; Banaszak Holl, M. M.; Orr, B. G. *Surf. Sci.* **2007**, *601*, 1937.
- (72) Castillo, I.; Tilley, T. D. *Organometallics* **2000**, *19*, 4733.
- (73) Castillo, I.; Tilley, T. D. *J. Am. Chem. Soc.* **2001**, *123*, 10526.
- (74) Castillo, I.; Tilley, T. D. *Organometallics* **2001**, *20*, 5598.
- (75) (a) Hou, Z.; Zhang, Y.; Nishiura, M.; Wakatsuki, Y. *Organometallics* **2003**, *22*, 129. (b) Shima, T.; Hou, Z. *Chem. Lett.* **2008**, 298.
- (76) Tardif, O.; Kurazumi, J.; Nishiura, M.; Horiuchi, A.; Hou, Z. *Kidorui* **2003**, *42*, 50. *Chem. Abstr.* 2003, 604895 (see ref 26c).
- (77) Harrod, J. F.; Shu, R.; Woo, H.-G.; Samuel, E. *Can. J. Chem.* **2001**, *79*, 1075.
- (78) (a) Dubberley, S. R.; Ignatov, S. K.; Rees, N. H.; Razuvaev, A. G.; Mountford, P.; Nikonov, G. I. *J. Am. Chem. Soc.* **2003**, *125*, 642. (b) Ignatov, S. K.; Rees, N. H.; Merkoulou, A. A.; Dubberley, S. R.; Razuvaev, A. G.; Mountford, P.; Nikonov, G. I. *Organometallics* **2008**, *27*, 5968.
- (79) Diminnie, J. B.; Xue, Z. *J. Am. Chem. Soc.* **1997**, *119*, 12657.
- (80) (a) Lang, H.; Meichel, E.; Weinmann, M.; Melter, M. *Organosilicon Chemistry III, 3rd ed.* **1998**, pp 423–428. (b) Weinmann, M.; Rheinwald, G.; Zsolnai, L.; Walter, O.; Büchner, M.; Schiemenz, B.; Huttner, G.; Lang, H. *Organometallics* **1998**, *17*, 3299.
- (81) Matthews, S. I.; Pons, V.; Heinekey, D. M. *Inorg. Chem.* **2006**, *45*, 6453.
- (82) (a) Mork, B. V.; Tilley, T. D. *Angew. Chem., Int. Ed.* **2003**, *42*, 357. (b) Stosur, M.; Szymańska-Buzar, T. *J. Mol. Catal. A: Chem.* **2008**, *286*, 98.
- (83) (a) Kotz, K. T.; Yang, H.; Snee, P. T.; Payne, C. K.; Harris, C. B. *J. Organomet. Chem.* **2000**, *596*, 183. (b) Ladogana, S.; Nayak, S. K.; Smit, J. P.; Dobson, G. R. *Inorg. Chem.* **1997**, *36*, 650. (c) Xie, X.; Simon, J. D. *J. Am. Chem. Soc.* **1990**, *112*, 1130.
- (84) Stosur, M.; Kochel, A.; Keller, A.; Szymańska-Buzar, T. *Organometallics* **2006**, *25*, 3791.
- (85) (a) Sakaba, H.; Tsukamoto, M.; Hirata, T.; Kabuto, C.; Horino, H. *J. Am. Chem. Soc.* **2000**, *122*, 11511. (b) Sakaba, H.; Hirata, T.; Kabuto, C.; Horino, H. *Chem. Lett.* **2001**, 1078.
- (86) Mork, B. V.; Tilley, T. D. *J. Am. Chem. Soc.* **2001**, *123*, 9702.
- (87) (a) Gadek, A.; Kochel, A.; Szymańska-Buzar, T. *Organometallics* **2003**, *22*, 4869. (b) Adrjan, B.; Szymańska-Buzar, T. *J. Organomet. Chem.* **2008**, *693*, 2163. (c) Gadek, A.; Kochel, A.; Szymańska-Buzar, T. *J. Organomet. Chem.* **2007**, *692*, 3765.
- (88) Bepalova, N. B.; Bovina, M. A.; Popov, A. V.; Mol, J. C. *J. Mol. Catal. A: Chem.* **2000**, *160*, 157.
- (89) (a) Scherer, W.; Eicklerling, G.; Tafipolsky, M.; McGrady, G. S.; Sirsch, P.; Chatterton, N. P. *Chem. Commun.* **2006**, 2986. (b) Schubert, U.; Wörle, B.; Jandik, P. *Angew. Chem., Int. Ed.* **1981**, *20*, 695. (c) Schubert, U.; Wörle, B.; Jandik, P. *Angew. Chem., Int. Ed.* **1981**, *20*, 695. (d) McGrady, G. S.; Sirsch, P.; Chatterton, N. P.; Ostermann, A.; Gatti, C.; Altmannshofer, S.; Herz, V.; Eicklerling, G.; Scherer, W. *arXiv.org, e-Print Archive, Physics* **2008**, 1, arXiv:0811.0451v1. *Chem. Abstr.* 2008, 1359475.
- (90) Weinmann, M.; Rheinwald, G.; Zsolnai, L.; Walter, O.; Büchner, M.; Schiemenz, B.; Huttner, G.; Lang, H. *Organometallics* **1998**, *17*, 3299.
- (91) Kayser, B.; Eichberg, M. J.; Vollhardt, K. P. C. *Organometallics* **2000**, *19*, 2389.
- (92) Yao, Z.; Klabunde, K. J.; Hupton, A. C. *Inorg. Chim. Acta* **1997**, *259*, 119.
- (93) Ohki, Y.; Kojima, T.; Oshima, M.; Suzuki, H. *Organometallics* **2001**, *20*, 2654.
- (94) Ohki, Y.; Suzuki, H. *Angew. Chem., Int. Ed.* **2000**, *39*, 3120.
- (95) (a) Malisch, W.; Vögler, M.; Käb, H.; Wekel, H.-U. *Organometallics* **2002**, *21*, 2830. (b) Malisch, W.; Wekel, H. U.; Grob, I.; Koehler, F. H. Z. *Naturforsch.* **1982**, *37B*, 601. (c) Heiden, Z. M.; Zampella, G.; De Gioia, L.; Rauchfuss, T. B. *Angew. Chem., Int. Ed.* **2008**, *47*, 9756.
- (96) Montiel-Palma, V.; Perutz, R. N.; George, M. W.; Jina, O. S.; Sabo-Etienne, S. *Chem. Commun.* **2000**, 1175.
- (97) Dioumaev, V. K.; Procopio, L. J.; Carroll, P. J.; Berry, D. H. *J. Am. Chem. Soc.* **2003**, *125*, 8043.
- (98) Takao, T.; Amako, M.-a.; Suzuki, H. *Organometallics* **2003**, *22*, 3855.
- (99) Hashimoto, H.; Hayashi, Y.; Aratani, I.; Kabuto, C.; Kira, M. *Organometallics* **2002**, *21*, 1534.
- (100) Atheaux, I.; Donnadiou, B.; Rodrigue, V.; Sabo-Etienne, S.; Chaudret, B.; Hussein, K.; Barthelat, J.-C. *J. Am. Chem. Soc.* **2000**, *122*, 5664.
- (101) Said, R. B.; Hussein, K.; Barthelat, J.-C.; Atheaux, I.; Sabo-Etienne, S.; Grellier, M.; Connadiou, B.; Chaudret, B. *Dalton Trans.* **2003**, 4139.
- (102) Ampt, K. A. M.; Duckett, S. B.; Perutz, R. N. *Dalton Trans.* **2004**, 3331.
- (103) Brookhart, M.; Grant, B. E.; Lenges, C. P.; Prosenc, M. H.; White, P. S. *Angew. Chem., Int. Ed.* **2000**, *39*, 1676.

- (104) Bourg, S.; Roury, B.; Carré, F.; Corriu, R. J. P. *Organometallics* **1997**, *16*, 3097.
- (105) Bourg, S.; Roury, B.; Carré, F. H.; Corriu, R. J. P. *Organometallics* **1998**, *17*, 167.
- (106) Câmpian, M. V.; Harris, J. L.; Jasim, N.; Perutz, R. N.; Marder, T. B.; Whitwood, A. C. *Organometallics* **2006**, *25*, 5093.
- (107) Mitchell, G. P.; Tilley, T. D. *Organometallics* **1998**, *17*, 2912.
- (108) Osakada, K.; Sarai, S.; Koizumi, T.-a.; Yamamoto, T. *Organometallics* **1997**, *16*, 3973.
- (109) Osakada, K.; Hataya, K.; Yamamoto, T. *Inorg. Chim. Acta* **1997**, *259*, 203.
- (110) Osakada, K.; Hataya, K.; Yamamoto, T. *Bull. Chem. Soc. Jpn.* **1998**, *71*, 2853.
- (111) Turculet, L.; Feldman, J. D.; Tilley, T. D. *Organometallics* **2004**, *23*, 2488.
- (112) Jackson, S. M.; Hughes, C. E.; Monfette, S.; Rosenberg, L. *Inorg. Chim. Acta* **2006**, *359*, 2966.
- (113) (a) Goikhman, R.; Milstein, D. *Chem.—Eur. J.* **2005**, *11*, 2983. (b) Geier, S. J.; Stephan, D. W. *Chem. Commun.* **2008**, 99.
- (114) Rosenberg, L.; Fryzuk, M. D.; Rettig, S. J. *Organometallics* **1999**, *18*, 958.
- (115) Cunningham, J. L.; Duckett, S. B. *J. Chem. Soc.* **2005**, 744.
- (116) Klei, S. R.; Tilley, T. D.; Bergman, R. G. *J. Am. Chem. Soc.* **2000**, *122*, 1816.
- (117) (a) Klei, S. R.; Tilley, T. D.; Bergman, R. C. *Organometallics* **2002**, *21*, 3376. (b) Arndtsen, B. A.; Bergman, R. G. *Science* **1995**, *270*, 1970.
- (118) Okazaki, M.; Tobita, H.; Kawano, Y.; Inomata, S.; Ogino, H. *J. Organomet. Chem.* **1998**, *553*, 1.
- (119) Iluc, V. M.; Hillhouse, G. L. *Tetrahedron* **2006**, *26*, 7577.
- (120) (a) Boyle, R. C.; Pool, D.; Jacobsen, H.; Fink, M. J. *J. Am. Chem. Soc.* **2006**, *128*, 9054. (b) Pan, Y.; Mague, J. T.; Fink, M. J. *Organometallics* **1992**, *11*, 3495. (c) Tanabe, M.; Mawatari, A.; Osakada, K. *Organometallics* **2007**, *26*, 2937.
- (121) (a) Kim, Y.-J.; Lee, S.-C.; Park, J.-I.; Osakada, K.; Choi, J.-C.; Yamamoto, T. *Organometallics* **1998**, *17*, 4929. (b) Kim, Y.-J.; Lee, S.-C.; Park, J.-I.; Osakada, K.; Choi, J.-C.; Yamamoto, T. *J. Chem. Soc., Dalton Trans.* **2000**, 417.
- (122) Tanabe, M.; Yamada, T.; Osakada, K. *Organometallics* **2003**, *22*, 2190.
- (123) Chen, W.; Shimada, S.; Tanaka, M. *Science* **2002**, *295*, 308.
- (124) Tanabe, M.; Osakada, K. *J. Am. Chem. Soc.* **2002**, *124*, 4550.
- (125) Kim, Y.-J.; Park, J.-I.; Lee, S.-C.; Osakada, K.; Tanabe, M.; Choi, J.-C.; Koizumi, T.-a.; Yamamoto, T. *Organometallics* **1999**, *18*, 1249.
- (126) Tanabe, M.; Yamazawa, H.; Osakada, K. *Organometallics* **2001**, *20*, 4451.
- (127) (a) Tanabe, M.; Ito, D.; Osakada, K. *Organometallics* **2008**, *27*, 2258. (b) Tanabe, M.; Ito, D.; Osakada, K. *Organometallics* **2007**, *26*, 459. (c) Braddock-Wilking, J.; Corey, J. Y.; Trankler, K. A.; Xu, H.; French, L. M.; Praingam, N.; White, C.; Rath, N. P. *Organometallics* **2006**, *25*, 2859. (d) White, C. P.; Braddock-Wilking, J.; Corey, J. Y.; Xu, H.; Redekop, E.; Sedinkin, S.; Rath, N. P. *Organometallics* **2007**, *26*, 1996.
- (128) Schubert, U.; Kalt, D.; Gilges, H. *Monatsh. Chem.* **1999**, *130*, 207.
- (129) Chan, D.; Duckett, S. B.; Heath, S. L.; Khazal, I. G.; Perutz, R. N.; Sabo-Etienne, S.; Timmins, P. L. *Organometallics* **2004**, *23*, 5744.
- (130) (a) Yamashita, H.; Tanaka, M.; Goto, M. *Organometallics* **1997**, *16*, 4696. (b) Korshin, E. E.; Leitus, G.; Shimon, L. J. W.; Konstantinovskii, L.; Milstein, D. *Inorg. Chem.* **2008**, *47*, 7177.
- (131) Braddock-Wilking, J.; Corey, J. Y.; French, L. M.; Choi, E.; Speedie, V. J.; Rutherford, M. F.; Yao, S.; Xu, H.; Rath, N. P. *Organometallics* **2006**, *25*, 3974.
- (132) Braddock-Wilking, J.; Corey, J. Y.; Dill, K.; Rath, N. P. *Organometallics* **2002**, *21*, 5467.
- (133) Shimada, S.; Li, Y.-H.; Rao, M. L. N.; Tanaka, M. *Organometallics* **2006**, *25*, 3796.
- (134) Braddock-Wilking, J.; Corey, J. Y.; Trankler, K. A.; Dill, K. M.; French, L. M.; Rath, N. P. *Organometallics* **2004**, *23*, 4576.
- (135) Itazaki, M.; Nishihara, Y.; Osakada, K. *Organometallics* **2004**, *23*, 1610.
- (136) (a) Bravo-Zhivotovskii, D.; Dobrovetsky, R.; Nemirovsky, D.; Molev, V.; Bendikov, M.; Molev, G.; Botoshansky, M.; Apeloig, Y. *Angew. Chem., Int. Ed.* **2008**, *47*, 4343. (b) Bravo-Zhivotovskii, D.; Yuzefovich, M.; Sigal, N.; Korogodsky, G.; Klinkhammer, K.; Tumanskii, B.; Shames, A.; Apeloig, Y. *Angew. Chem., Int. Ed.* **2002**, *41*, 649.
- (137) Bravo-Zhivotovskii, D.; Ruderfer, I.; Yuzefovich, M.; Kosa, M.; Botoshansky, M.; Tumanskii, B.; Apeloig, Y. *Organometallics* **2005**, *24*, 2698.
- (138) Hao, L.; Lebus, A.-M.; Harrod, J. F.; Woo, H.-G.; Samuel, E. *Chem. Commun.* **1998**, 2013.
- (139) Peulecke, N.; Ohff, A.; Kosse, P.; Tillack, A.; Spannenberg, A.; Kempe, R.; Baumann, W.; Burlakov, V. V.; Rosenthal, U. *Chem.—Eur. J.* **1998**, *4*, 1852.
- (140) Ciruelo, G.; Cuenca, T.; Gomez, R.; Gomez-Sal, P.; Martin, A. *J. Chem. Soc., Dalton Trans.* **2001**, 1657.
- (141) Snee, P. T.; Yang, H.; Kotz, K. T.; Payne, C. K.; Harris, C. B. *J. Phys. Chem. A* **1999**, *103*, 10426.
- (142) Nikonov, G. I.; Kuzmina, L. G.; Vybishchikov, S. F.; Lemenovskii, D. A.; Howard, J. A. K. *Chem.—Eur. J.* **1999**, *5*, 2947.
- (143) Dorogov, K. Yu.; Churakov, A. V.; Kuzmina, L. G.; Howard, J. A. K.; Nikonov, G. I. *Eur. J. Inorg. Chem.* **2004**, 771.
- (144) Nikonov, G. I.; Kuzmina, L. G.; Howard, J. A. K. *J. Chem. Soc., Dalton Trans.* **2002**, 3037.
- (145) (a) Bakhmutov, V. I.; Howard, J. A. K.; Keen, D. A.; Kuzminia, L. G.; Leech, M. A.; Nikonov, G. I.; Vorontsov, E. V.; Wilson, C. C. *J. Chem. Soc., Dalton Trans.* **2000**, 1631. (b) Nikonov, G. I.; Kuzmina, L. G.; Lemenovskii, D. A.; Kotov, V. V. *J. Am. Chem. Soc.* **1996**, *118*, 6333.
- (146) Nikonov, G. I.; Mountford, P.; Green, J. C.; Cooke, P. A.; Leech, M. A.; Blake, A. J.; Howard, J. A. K. *Eur. J. Inorg. Chem.* **2000**, 1917.
- (147) (a) Nikonov, G. I.; Mountford, P.; Ignatov, S. K.; Green, J. C.; Leech, M. A.; Kuzmina, L. G.; Razuvaev, A. G.; Rees, N. H.; Blake, A. J.; Howard, J. A. K.; Lemenovskii, D. A. *J. Chem. Soc., Dalton Trans.* **2001**, 2903. (b) Ignatov, S. K.; Rees, N. H.; Merkoulou, A. A.; Dubberley, S. R.; Razuvaev, A. G.; Mountford, P.; Nikonov, G. I. *Organometallics* **2008**, *27*, 5968.
- (148) Merkulov, A. A.; Nikonov, G. I.; Mountford, P. *Organosilicon Chemistry V: From Molecules to Materials* **2003**, 451. *Chem. Abstr.* 2004, 762243.
- (149) Nikonov, G. I.; Mountford, P.; Dubberley, S. R. *Inorg. Chem.* **2003**, *42*, 258.
- (150) Koshikawa, H.; Okazaki, M.; Matsumoto, S.-i.; Ueno, K.; Tobita, H.; Ogino, H. *Chem. Lett.* **2005**, *34*, 1412.
- (151) Ueno, K.; Masuko, A.; Ogino, H. *Organometallics* **1999**, *18*, 2694.
- (152) Bengali, A. A.; Rehnel, R. *Organometallics* **2005**, *24*, 1156.
- (153) Hirotsu, M.; Nunokawa, T.; Ueno, K. *Organometallics* **2006**, *25*, 1554.
- (154) Begum, R.; Komuro, T.; Tobita, H. *Chem. Commun.* **2006**, 432.
- (155) (a) Ignatov, S. K.; Rees, N. H.; Dubberley, S. R.; Razuvaev, A. G.; Mountford, P.; Nikonov, G. I. *Chem. Commun.* **2004**, 952. (b) Bent, H. A. *Chem. Rev.* **1961**, *61*, 275. (c) Chen, D.; Guo, J.; Xu, S.; Song, H.; Wang, B. *Organometallics* **2007**, *26*, 4212.
- (156) Ueno, K.; Asami, S.; Watanabe, N.; Ogino, H. *Organometallics* **2002**, *21*, 1326.
- (157) (a) Okazaki, M.; Suzuki, E.; Miyajima, N.; Tobita, H.; Ogino, H. *Organometallics* **2003**, *22*, 4633. (b) Suzuki, E.; Komuro, T.; Okazaki, M.; Tobita, H. *Organometallics* **2007**, *26*, 4379.
- (158) Suzuki, E.; Okazaki, M.; Tobita, H. *Chem. Lett.* **2005**, 1026.
- (159) (a) Sakaba, H.; Watanabe, S.; Kabuto, C.; Kabuto, K. *J. Am. Chem. Soc.* **2003**, *125*, 2842. (b) Sakaba, H.; Ishida, K.; Horino, H. *Chem. Lett.* **1995**, 1145.
- (160) (a) Sakaba, H.; Yoshida, M.; Kabuto, C.; Kabuto, K. *J. Am. Chem. Soc.* **2005**, *127*, 7276. (b) Osakada, K.; Tanabe, M. *Bull. Chem. Soc. Jpn.* **2005**, *78*, 1887.
- (161) Sakaba, H.; Ishida, K.; Horino, H. *Chem. Lett.* **1998**, 149.
- (162) Gadek, A.; Kochel, A.; Szymańska-Buzar, T. *J. Organomet. Chem.* **2005**, *690*, 685.
- (163) Karch, R.; Gilges, H.; Schubert, U. *Organosilicon Chemistry III, 3rd ed.* **1998**, p 271. *Chem. Abstr.* 1998, 179479.
- (164) Schwarz, M.; Kickelbick, G.; Schubert, U. *Eur. J. Inorg. Chem.* **2000**, 1811.
- (165) (a) Yang, H.; Asplund, M. C.; Kotz, K. T.; Wilkens, M. J.; Frei, H.; Harris, C. B. *J. Am. Chem. Soc.* **1998**, *120*, 10154. (b) Yang, H.; Kotz, K. T.; Asplund, M. C.; Wilkens, M. J.; Harris, C. B. *Acc. Chem. Res.* **1999**, *32*, 551.
- (166) Karch, R.; Schubert, U. *Inorg. Chim. Acta* **1997**, *259*, 151.
- (167) Schubert, U.; Grubert, S. *Monatsh. Chem.* **1998**, *129*, 437.
- (168) Fang, X.; Huhmann-Vincent, J.; Scott, B. L.; Kubas, G. J. *J. Organomet. Chem.* **2000**, *609*, 95.
- (169) Matthews, S. I.; Pons, V.; Heinekey, D. M. *Inorg. Chem.* **2006**, *45*, 6453.
- (170) Huhmann-Vincent, J.; Scott, B. L.; Kubas, G. J. *Inorg. Chim. Acta* **1999**, *294*, 240.
- (171) Fang, X.; Scott, B. L.; John, K. D.; Kubas, G. J. *Organometallics* **2000**, *19*, 4141.
- (172) Lee, Y.-J.; Lee, J.-D.; Kim, S.-J.; Ko, J.; Suh, I.-H.; Cheong, M.; Kang, S. O. *Organometallics* **2004**, *23*, 135.
- (173) Adams, R. D.; Smith, J. L., Jr. *Organometallics* **2005**, *24*, 4489.
- (174) (a) Chang, S.; Scharrer, E.; Brookhart, M. J. *Mol. Catal.* **1998**, *130*, 107. (b) Okazaki, M.; Iwata, M.; Tobita, H.; Ogino, H. *Dalton Trans.* **2003**, 1114.
- (175) Hashimoto, H.; Matsuda, A.; Tobita, H. *Chem. Lett.* **2005**, 1374.
- (176) Semenov, V. V.; Ladilina, E. Yu.; Khorshev, S. Ya.; Markarenko, N. P.; Kurskii, Yu. A.; Buchkova, O. A. *Russ. Chem. Bull.* **1998**, *47*, 2455.

- (177) (a) Sato, T.; Okazaki, M.; Tobita, H. *Chem. Lett.* **2004**, 33, 868. (b) Minglana, J. J. G.; Okazaki, M.; Hasegawa, K.; Luh, L.-S.; Yamahira, N.; Komuro, T.; Ogino, H.; Tobita, H. *Organometallics* **2007**, 26, 5859. (c) Beckmann, J.; Hesse, M. Z. *Anorg. Allg. Chem.* **2007**, 633, 1233.
- (178) (a) Semenov, V. V.; Cherepennikova, N. F.; Makarenko, N. P. *Russ. J. Gen. Chem.* **1999**, 69, 910. *Chem. Abstr.* 1999, 737783. (b) Mankad, N. P.; Whited, M. T.; Peters, J. C. *Angew. Chem., Int. Ed.* **2007**, 46, 5768.
- (179) Malisch, W.; Hofmann, M.; Kaupp, G.; Käß, H.; Reising, J. *Eur. J. Inorg. Chem.* **2002**, 3235. (see ref 232).
- (180) Reising, J.; Malisch, W.; Lankat, R. *Organosilicon Chemistry III, 3rd ed.* **1998**, p 412.
- (181) (a) Xue, P.; Zhu, J.; Liu, S. H.; Huang, X.; Ng, W. S.; Sung, H. H. Y.; Williams, I. D.; Lin, Z.; Jia, G. *Organometallics* **2006**, 25, 2344. (b) Gutsulyak, D. V.; Osipov, A. L.; Kuzmina, L. G.; Howard, J. A. K.; Nikonov, G. I. *Dalton Trans.* **2008**, 6843. (c) Gutsulyak, D. V.; Osipov, A. L.; Kuzmina, L. G.; Howard, J. A. K.; Nikonov, G. I. *Dalton Trans.* **2008**, 6843.
- (182) Freeman, S. T. N.; Lemke, F. R.; Brammer, L. *Organometallics* **2002**, 21, 2030.
- (183) Klei, S. R.; Tilley, T. D.; Bergman, R. G. *Organometallics* **2002**, 21, 4648.
- (184) Rodriguez, V.; Donnadieu, B.; Sabo-Etienne, S.; Chaudret, B. *Organometallics* **1998**, 17, 3809.
- (185) Duckett, S. B.; Kuzmina, L. G.; Nikonov, G. I. *Inorg. Chem. Commun.* **2000**, 3, 126.
- (186) Osipov, A. L.; Gerdov, S. M.; Kuzmina, L. G.; Howard, J. A. K.; Nikonov, G. I. *Organometallics* **2005**, 24, 587.
- (187) Osipov, A. L.; Vyboishchikov, S. F.; Dorogov, K. Y.; Kuzmina, L. G.; Howard, J. A. K.; Lemovskii, D. A.; Nikonov, G. I. *Chem. Commun.* **2005**, 3349.
- (188) Iwata, M.; Okazaki, M.; Tobita, H. *Organometallics* **2006**, 25, 6115.
- (189) (a) Dysard, J. M.; Tilley, T. D.; Woo, T. K. *Organometallics* **2001**, 20, 1195. (b) Derrah, E. J.; Pantazis, D. A.; McDonald, R.; Rosenberg, L. *Organometallics* **2007**, 26, 1473.
- (190) Burgio, J.; Yardy, N. M.; Petersen, J. L.; Lemke, F. R. *Organometallics* **2003**, 22, 4928.
- (191) Lee, M.; Ko, S.; Chang, S. J. *Am. Chem. Soc.* **2000**, 122, 12011.
- (192) Tobita, H.; Hasegawa, K.; Minglana, J. J. G.; Luh, L.-S.; Okazaki, M.; Ogino, H. *Organometallics* **1999**, 18, 2058.
- (193) (a) Minglana, J. J. G.; Okazaki, M.; Tobita, H.; Ogino, H. *Chem. Lett.* **2002**, 406. (b) Okazaki, M.; Minglana, J. J. G.; Yamahira, N.; Tobita, H.; Ogino, H. *Can. J. Chem.* **2003**, 81, 1350.
- (194) Brost, R. D.; Bruce, G. C.; Joslin, F. L.; Stobart, S. R. *Organometallics* **1997**, 16, 5669.
- (195) (a) Zhou, X.; Stobart, S. R. *Organometallics* **2001**, 20, 1898. (b) Brost, R. D.; Bruce, G. C.; Joslin, F. L.; Stobart, S. R. *Organometallics* **1997**, 16, 1898.
- (196) Kwok, W.-H.; Lu, G.-L.; Rickard, C. E. F.; Roper, W. R.; Wright, L. J. *J. Organomet. Chem.* **2004**, 689, 2511.
- (197) Montiel-Palma, V.; Pattison, D. I.; Perutz, R. N.; Turner, C. *Organometallics* **2004**, 23, 4034.
- (198) Maruyama, Y.; Yamamura, K.; Ozawa, F. *Chem. Lett.* **1998**, 905.
- (199) Maruyama, Y.; Yamamura, K.; Nakayama, I.; Keigo, Y.; Ozawa, F. *J. Am. Chem. Soc.* **1998**, 120, 1421.
- (200) Maruyama, Y.; Yamamura, K.; Sagawa, T.; Katayama, H.; Ozawa, F. *Organometallics* **2000**, 19, 1308.
- (201) Choo, T. N.; Kwok, W.-H.; Rickard, C. E. F.; Roper, W. R.; Wright, L. J. *J. Organomet. Chem.* **2002**, 645, 235.
- (202) Kwok, W.-H.; Lu, G.-L.; Rickard, C. E. F.; Roper, W. R.; Wright, L. J. *J. Organomet. Chem.* **2004**, 689, 2979.
- (203) Yi, C. S.; Lee, D. W.; He, Z.; Rheingold, A. L.; Lam, K.-C.; Concolino, T. E. *Organometallics* **2000**, 19, 2909.
- (204) Bushnell, G. W.; Casado, M. A.; Stobart, S. R. *Organometallics* **2001**, 20, 601.
- (205) Dioumaev, V. K.; Carroll, P. J.; Berry, D. H. *Angew. Chem., Int. Ed.* **2003**, 42, 3947.
- (206) Yardy, N. M.; Lemke, F. R.; Brammer, L. *Organometallics* **2001**, 20, 5670.
- (207) (a) Lachaize, S.; Sabo-Etienne, S.; Donnadieu, B.; Chaudret, B. *Chem. Commun.* **2003**, 214. (b) Lachaize, S.; Caballero, A.; Vendier, L.; Sabo-Etienne, S. *Organometallics* **2007**, 26, 3713.
- (208) Delpech, F.; Sabo-Etienne, S.; Daran, J.-C.; Chaudret, B.; Hussein, K.; Marsden, C. J.; Barthelat, J.-C. *J. Am. Chem. Soc.* **1999**, 121, 6668.
- (209) Delpech, F.; Sabo-Etienne, S.; Chaudret, B.; Daran, J.-C. *J. Am. Chem. Soc.* **1997**, 119, 3167.
- (210) (a) Hussein, K.; Marsden, C. J.; Barthelat, J.-C.; Rodriguez, V.; Conejero, S.; Sabo-Etienne, S.; Donnadieu, B.; Chaudret, B. *Chem. Commun.* **1999**, 1315. (b) Hussein, K.; Sabo-Etienne, S.; Hernandez, M.; Chung, G.; Chaudret, B.; Castel, A. *New J. Chem.* **1994**, 18, 175.
- (211) (a) Delpech, F.; Sabo-Etienne, S.; Donnadieu, B.; Chaudret, B. *Organometallics* **1998**, 17, 4926. (b) Montiel-Palma, V.; Piechaczkyk, O.; Picot, A.; Auffrant, A.; Vendier, L.; Le Floch, P.; Sabo-Etienne, S. *Inorg. Chem.* **2008**, 47, 8601.
- (212) Ayed, T.; Barthelat, J.-C.; Tangour, B.; Pradère, C.; Donnadieu, B.; Grellier, M.; Sabo-Etienne, S. *Organometallics* **2005**, 24, 3824.
- (213) (a) MacInnis, M. C.; MacLean, D. F.; Lundgren, R. J.; McDonald, R.; Turculet, L. *Organometallics* **2007**, 26, 6522. (b) Yoo, J.; Carroll, P. J.; Berry, D. H. *J. Am. Chem. Soc.* **2006**, 128, 6038. (c) Montiel-Palma, V.; Muñoz-Hernández, M. A.; Ayed, T.; Barthelat, J.-C.; Grellier, M.; Vendier, L.; Sabo-Etienne, S. *Chem. Commun.* **2007**, 3963. (d) Berthoud, R.; Baudouin, A.; Fenet, B.; Lukens, W.; Pelzer, K.; Basset, J.-M.; Candy, J.-P.; Copéret, J.-M. *Eur. J. Chem.* **2008**, 14, 3523. (e) Hameau, A.; Guyon, F.; Knorr, M.; Däschlein, C.; Strohmman, C.; Avarvari, N. *Dalton Trans.* **2008**, 4866.
- (214) Takao, T.; Amako, M.-a.; Suzuki, H. *Organometallics* **2001**, 20, 3406.
- (215) Matsubara, K.; Ryu, K.; Maki, T.; Iura, T.; Nagashima, H. *Organometallics* **2002**, 21, 3023.
- (216) Nombel, P.; Hatanaka, Y.; Shimada, S. *Chem. Lett.* **1999**, 159.
- (217) Martin, M.; Sola, E.; Lahoz, F. J.; Oro, L. A. *Organometallics* **2002**, 21, 4027.
- (218) Nagashima, H.; Suzuki, A.; Iura, T.; Ryu, K.; Matsubara, K. *Organometallics* **2000**, 19, 3579.
- (219) Adams, R. D.; Captain, B.; Fu, W. *Organometallics* **2000**, 19, 3670.
- (220) Glaser, P. B.; Wanandi, P. W.; Tilley, T. D. *Organometallics* **2004**, 23, 693.
- (221) Rickard, C. E. F.; Roper, W. R.; Woodgate, S. D.; Wright, L. J. *J. Organomet. Chem.* **2000**, 609, 177.
- (222) Möhlen, M.; Rickard, C. E. F.; Roper, W. R.; Salter, D. M.; Wright, L. F. *J. Organomet. Chem.* **2000**, 593–594, 458.
- (223) Kwok, W.-H.; Lu, G.-L.; Rickard, C. E. F.; Roper, W. R.; Wright, L. J. *J. Organomet. Chem.* **2006**, 691, 2593.
- (224) Albrecht, M.; Rickard, C. E. F.; Roper, W. R.; Williamson, A.; Woodgate, S. D.; Wright, L. J. *J. Organomet. Chem.* **2001**, 625, 77.
- (225) Attar-Bashi, M. T.; Rickard, C. E. F.; Roper, W. R.; Wright, L. J.; Woodgate, S. D. *Organometallics* **1998**, 17, 504.
- (226) Hall, R. J.; Sergueevski, P.; Keister, J. B. *Organometallics* **2000**, 19, 4499.
- (227) Deeming, A. J.; Hassan, Md. M.; Kabir, S. E.; Nordlander, E.; Toucher, D. A. *Dalton Trans.* **2004**, 3709.
- (228) Cavanaugh DiBiase, M.; Gregg, B. T.; Chiulli, R. J.; Cutler, A. R. *J. Organomet. Chem.* **1997**, 547, 173.
- (229) McIndoe, J. S.; Nicholson, B. K. *J. Organomet. Chem.* **1999**, 577, 181.
- (230) (a) Si, T. S.; Koo, S. M. *Polym. Int.* **2005**, 54, 891. (b) Mautz, J.; Heinze, K.; Wadepohl, H.; Huttner, G. *Eur. J. Inorg. Chem.* **2008**, 1413.
- (231) Berenbaum, A.; Jäkle, F.; Lough, A. J.; Manners, I. *Organometallics* **2001**, 20, 834.
- (232) Malisch, W.; Vogler, M. *Organosilicon Chemistry IV*, 4th ed.; Auner N., Weiss J., Eds.; Wiley-VCH Verlag GmbH: Weinheim, Germany, 2000; p 442.
- (233) Zirngast, M.; Marschner, C.; Baumgartner, J. *Organometallics* **2006**, 25, 4897.
- (234) Cuadrado, I.; Moran, M.; Moya, A.; Casado, C.; Barranco, M.; Alonso, B. *Inorg. Chim. Acta* **1996**, 251, 5.
- (235) Rattay, M.; Fenske, D.; Jutzi, P. *Organometallics* **1998**, 17, 2930.
- (236) Dunwoody, N.; Sun, S.-S.; Lees, A. G. *J. Inorg. Chem.* **2000**, 39, 4442.
- (237) Heaton, S. N.; Partridge, M. G.; Perutz, R. N.; Parsons, S. J.; Zimmermann, F. J. *Chem. Soc., Dalton Trans.* **1998**, 2515.
- (238) Taw, F. L.; White, P. S.; Bergman, R. G.; Brookhart, M. *J. Am. Chem. Soc.* **2002**, 124, 4192.
- (239) Taw, F. L.; Bergman, R. G.; Brookhart, M. *Organometallics* **2004**, 23, 886.
- (240) Aizenberg, M.; Ott, J.; Elsevier, C. J.; Milstein, D. *J. Organomet. Chem.* **1998**, 551, 81.
- (241) Novecki, D.; Braun, T.; Schulte, M.; Neumann, B.; Stammler, H.-G. *Dalton Trans.* **2003**, 4075.
- (242) Okazaki, M.; Ohshitanai, S.; Tobita, H.; Ogino, H. *Chem. Lett.* **2001**, 952.
- (243) Osakada, K.; Koizumi, T.-a.; Sarai, S.; Yamamoto, T. *Organometallics* **1998**, 17, 1868.
- (244) Tanabe, M.; Osakada, K. *Inorg. Chim. Acta* **2003**, 350, 201.
- (245) Goikhman, R.; Aizenberg, M.; Ben-David, Y.; Shimon, L. J. W.; Milstein, D. *Organometallics* **2002**, 21, 5060.
- (246) Okazaki, M.; Ohshitanai, S.; Tobita, H.; Ogino, H. *J. Chem. Soc., Dalton Trans.* **2002**, 2061.
- (247) (a) Duckett, S. B.; Gálvez-López, M.-D.; Perutz, R. N.; Schott, D. *Dalton Trans.* **2004**, 2746. (b) Sunada, Y.; Fujimura, Y.; Nagashima, H. *Organometallics* **2008**, 27, 3502.
- (248) (a) Goikhman, R.; Aizenberg, M.; Shimon, L. J. W.; Milstein, D. *Organometallics* **2003**, 22, 4020. (b) Ogata, K.; Toyota, A. J. *J. Organomet. Chem.* **2007**, 692, 4139.

- (249) Osakada, K.; Koizumi, T.-a.; Yamamoto, T. *Bull. Chem. Soc. Jpn.* **1997**, *70*, 189.
- (250) Muraoka, T.; Matsuda, I.; Itoh, K. *Tetrahedron Lett.* **1998**, *39*, 7325.
- (251) Muraoka, T.; Matsuda, I.; Itoh, K. *Organometallics* **2002**, *21*, 3650.
- (252) Nishihara, Y.; Takemura, M.; Osakada, K. *Organometallics* **2002**, *21*, 825.
- (253) de Wolf, E.; Speets, E.; Deelman, B.-J.; van Koten, G. *Organometallics* **2001**, *20*, 3686.
- (254) (a) Sangtrirutnugul, P.; Stradiotto, M.; Tilley, T. D. *Organometallics* **2006**, *25*, 1607. (b) MacLean, D. F.; McDonald, R.; Ferguson, M. J.; Caddell, A. J.; Turculet, L. *Chem. Commun.* **2008**, 5146. (c) Gatard, S.; Chen, C.-H.; Foxman, B. M.; Ozerov, O. V. *Organometallics* **2008**, *27*, 6257.
- (255) Karshtedt, A.; Bell, T.; Tilley, T. D. *Organometallics* **2006**, *25*, 4471.
- (256) Koizumi, T.-a.; Osakada, K.; Yamamoto, T. *Organometallics* **1998**, *17*, 5721.
- (257) Osakada, K.; Koizumi, T.; Yamamoto, T. *Angew. Chem., Int. Ed.* **1998**, *37*, 349.
- (258) Tanabe, M.; Osakada, K. *Chem. Lett.* **2001**, 962.
- (259) Diversi, P.; Marchetti, F.; Ermini, V.; Matteoni, S. *J. Organomet. Chem.* **2000**, 593–594, 154.
- (260) Esteruelas, M. A.; Fernández-Alvarez, F. J.; López, A. M.; Oñate, E.; Ruiz-Sánchez, P. *Organometallics* **2006**, *25*, 5131.
- (261) (a) Okazaki, M.; Iwata, M.; Tobita, H.; Ogino, H. *Sci. Rep. Tohoku Univ., First Ser.: Chem.* **2003**, *80*, 11. *Chem. Abstr.* 2004, 702436. (b) Bleeke, J. R.; Thananathanachon, T.; Rath, N. P. *Organometallics* **2007**, *26*, 3904. (c) Bleeke, J. R.; Thananathanachon, T.; Rath, N. P. *Organometallics* **2008**, *27*, 2436.
- (262) Okazaki, M.; Tobita, H.; Ogino, H. *J. Chem. Soc., Dalton Trans.* **1997**, 3531.
- (263) Martin, M.; Sola, E.; Torres, O.; Plou, P.; Oro, L. A. *Organometallics* **2003**, *22*, 5406.
- (264) (a) Gutiérrez-Puebla, E.; Monge, A.; Paneque, M.; Poveda, M. L.; Taboada, S.; Trujillo, M.; Carmona, E. *J. Am. Chem. Soc.* **1999**, *121*, 346. (b) Carlton, L.; Tetana, Z. N.; Fernandes, M. A. *Polyhedron* **2008**, *27*, 1959.
- (265) Stradiotto, M.; Fajdala, K. L.; Tilley, T. D. *Chem. Commun.* **2001**, 1200.
- (266) (a) Yang, J.; White, P. S.; Schauer, C. K.; Brookhart, M. *Angew. Chem. Int. Ed.* **2008**, *47*, 4141. (b) Carlton, L.; Molapisi, J. J. *J. Organomet. Chem.* **2000**, 609, 60.
- (267) Vicent, C.; Viciano, M.; Mas-Marzá, E.; Sanaú, M.; Peris, E. *Organometallics* **2006**, *25*, 3713.
- (268) Kang, Y.; Lee, J.; Kong, Y. K.; Kang, S. O.; Ko, J. *Chem. Commun.* **1998**, 2343.
- (269) Kang, Y.; Lee, J.; Kong, Y. K.; Kang, S. O.; Ko, J. *Organometallics* **2000**, *19*, 1722.
- (270) Maciejewski, H.; Sydor, A.; Marciniec, B.; Kubicki, M.; Hitchcock, P. B. *Inorg. Chim. Acta* **2006**, *359*, 2989.
- (271) Iluc, V. M.; Hillhouse, G. L. *Tetrahedron* **2006**, *26*, 7577 (see ref 119).
- (272) Maciejewski, H.; Marciniec, B.; Kownacki, I. *J. Organomet. Chem.* **2000**, *597*, 175.
- (273) Steinke, T.; Gemel, C.; Cokoja, M.; Winter, M.; Fischer, R. A. *Angew. Chem., Int. Ed.* **2004**, *43*, 2299.
- (274) Boyle, R. C.; Mague, J. T.; Fink, M. J. *J. Am. Chem. Soc.* **2003**, *125*, 3228.
- (275) Lee, Y.-J.; Bae, J.-Y.; Kim, S.-J.; Ko, J.; Choi, M.-G.; Kang, S. O. *Organometallics* **2000**, *19*, 5546.
- (276) (a) Lee, Y.-J.; Lee, J. D.; Kim, S.-J.; Keum, S.; Ko, J.; Suh, I.-H.; Cheong, M.; Kang, S. O. *Organometallics* **2004**, *23*, 203. (b) Sangtrirutnugul, P.; Tilley, T. D. *Organometallics* **2008**, *27*, 2223. (c) Carr, C. A. M.; Gribble, C. W.; Gibson, I. *Acta Cryst.* **2008**, *E64*, m472.
- (277) Woo, T. K.; Pioda, G.; Rothlisberger, U.; Togni, A. *Organometallics* **2000**, *19*, 2144.
- (278) Fang, X.; Scott, B. L.; Watkin, J. G.; Kubas, G. J. *Organometallics* **2000**, *19*, 4193.
- (279) Yamada, T.; Tanabe, M.; Osakada, K.; Kim, Y.-J. *Organometallics* **2004**, *23*, 4771.
- (280) Koizumi, T.-a.; Osakada, K.; Yamamoto, T. *Organometallics* **1997**, *16*, 6014.
- (281) Ozawa, F.; Kamite, J. *Organometallics* **1998**, *17*, 5630.
- (282) (a) Tsuji, Y.; Nishiyama, K.; Hori, S.-i.; Ebihara, M.; Kawamura, T. *Organometallics* **1998**, *17*, 507. (b) Tsuji, Y.; Obora, Y. *J. Organomet. Chem.* **2000**, 611, 343.
- (283) Kalt, D.; Schubert, U. *Inorg. Chim. Acta* **2000**, *306*, 211.
- (284) (a) Knorr, M.; Kneifel, S.; Strohmman, C. *Organosilicon Chemistry III, 3rd ed.* **1998**, p 211. (b) Knorr, M.; Guyon, F.; Jourdain, I.; Kneifel, S.; Frenzel, J.; Strohmman, C. *Inorg. Chim. Acta* **2003**, *350*, 455. (c) Aarii, H.; Takahashi, M.; Noda, A.; Nanjo, M.; Mochida, K. *Organometallics* **2008**, *27*, 1929.
- (285) Kang, Y.; Kang, S. O.; Ko, J. *Organometallics* **1999**, *18*, 1818.
- (286) Kang, Y.; Kang, S. O.; Ko, J. *Organometallics* **2000**, *19*, 1216.
- (287) Jayaswal, M. N.; Peindy, H. N.; Guyon, F.; Knorr, M.; Avarvari, N.; Fourmigué, M. *Eur. J. Inorg. Chem.* **2004**, 2646.
- (288) Goikman, R.; Karakuz, T.; Shimon, L. J. W.; Leitens, G.; Milstein, D. *Can. J. Chem.* **2005**, *83*, 786.
- (289) Reinartz, S.; White, P. S.; Brookhart, M.; Templeton, J. L. *J. Am. Chem. Soc.* **2001**, *123*, 6425.
- (290) Thompson, S. M.; Stöhr, F.; Strumayr, D.; Kickelbick, G.; Schubert, U. *J. Organomet. Chem.* **2003**, *686*, 183.
- (291) Pfeiffer, J.; Schubert, U. *Organometallics* **1999**, *18*, 3245.
- (292) Pfeiffer, J.; Kickelbick, G.; Schubert, U. *Organometallics* **2000**, *19*, 62.
- (293) Pfeiffer, J.; Kickelbick, G.; Schubert, U. *Organometallics* **2000**, *19*, 957.
- (294) (a) Stöhr, F.; Thompson, S.; Sturmayer, D.; Pfeiffer, J.; Schubert, U. *Organosilicon Chemistry V: From Molecules to Materials* **2003**, p 456. *Chem. Abstr.* 2004, 762244. (b) Schubert, U.; Pfeiffer, J.; Stöhr, F.; Sturmayer, D.; Thompson, S. *J. Organomet. Chem.* **2002**, *646*, 53.
- (295) Reinartz, S.; White, P. S.; Brookhart, M.; Templeton, J. L. *Organometallics* **2000**, *19*, 3748.
- (296) Roy, A. K.; Taylor, R. B. *J. Am. Chem. Soc.* **2002**, *124*, 9510.
- (297) Guyon, F.; Jayaswal, M. N.; Peindy, H. N.; Hameau, A.; Knorr, M.; Avarvari, N. *Synth. Met.* **2005**, *151*, 186.
- (298) (a) Kempter, A.; Gemel, C.; Fischer, R. A. *Chem.—Eur. J.* **2007**, *13*, 2990. (b) Osakada, K.; Tanabe, M.; Tanase, T. *Angew. Chem., Int. Ed.* **2000**, *39*, 4053.
- (299) Bender, R.; Braunstein, P.; Bouaoud, S.-E.; Merabet, N.; Rouag, D.; Zanello, P.; Fontani, M. *New J. Chem.* **1999**, *23*, 1045.
- (300) Itazaki, M.; Kitami, O.; Tanabe, M.; Nishihara, Y.; Osakada, K. *J. Organomet. Chem.* **2005**, *690*, 3957.
- (301) Nicholson, K. T.; Zhang, K.; Banaszak-Holl, M. *J. Am. Chem. Soc.* **1999**, *121*, 3232.
- (302) Hirayama, M. K. N.; Caseri, W. R.; Suter, U. W. *J. Colloid Interface Sci.* **1999**, *216*, 250.
- (303) Bravo-Zhivotovskii, D.; Yuzefovich, M.; Bendikov, M.; Klinkhamer, K.; Apeloig, Y. *Angew. Chem., Int. Ed.* **1999**, *38*, 1100.
- (304) Wang, Q.; Corey, J. Y. *Can. J. Chem.* **2000**, *78*, 1434.
- (305) Liu, Z.; Wu, Z.; Peng, Z.; Wu, Y.-D.; Xue, Z. *J. Am. Chem. Soc.* **1999**, *121*, 5350.
- (306) Liu, X.; Wu, Z.; Cai, H.; Yang, Y.; Chen, T.; Vallet, C. E.; Zuh, R. A.; Beach, D. B.; Peng, Z.-X.; Wu, Y.-D.; Concolino, T. E.; Rheingold, A. L.; Xue, Z. *J. Am. Chem. Soc.* **2001**, *123*, 8011.
- (307) (a) Sadow, A. D.; Tilley, T. D. *Organometallics* **2001**, *20*, 4457. (b) Sadow, A. D.; Tilley, T. D. *Organometallics* **2003**, *22*, 3577. (c) Sadow, A. D.; Tilley, T. D. *J. Am. Chem. Soc.* **2003**, *125*, 9462.
- (308) (a) Cai, H.; Chen, T.; Wang, X.; Schultz, A. J.; Koetzle, T. F.; Xue, Z. *Chem. Commun.* **2002**, 230. (b) Bond, D. G.; Fanwick, P. E.; Abu-Omar, M. M. *J. Am. Chem. Soc.* **2007**, *129*, 5180.
- (309) Vela, J.; Smith, J. M.; Yu, Y.; Ketterer, N. A.; Flaschenriem, C. J.; Lachicotte, R. J.; Holland, P. L. *J. Am. Chem. Soc.* **2005**, *127*, 7857.
- (310) Man, M. L.; Zhou, Z.; Ng, S. M.; Lau, C. P. *Dalton Trans.* **2003**, 3727.
- (311) Esteruelas, M. A.; Herrero, J.; Oliván, M. *Organometallics* **2004**, *23*, 3891.
- (312) Tanaka, S.; Akita, M. *Angew. Chem., Int. Ed.* **2001**, *40*, 2865.
- (313) Lee, Y.; Seomoon, D.; Kim, S.; Han, H.; Chang, S.; Lee, P. H. *J. Org. Chem.* **2004**, *69*, 1741.
- (314) Holland, P. L.; Andersen, R. A.; Bergman, R. G.; Huang, J.; Nolan, S. P. *J. Am. Chem. Soc.* **1997**, *119*, 12800.
- (315) Chung, M.-K.; Orlova, G.; Goddard, J. D.; Schlaf, M.; Harris, R.; Beveridge, T. J.; White, G.; Hallett, F. R. *J. Am. Chem. Soc.* **2002**, *124*, 10508.
- (316) Chung, M.-K.; Schlaf, M. *J. Am. Chem. Soc.* **2004**, *126*, 7386.
- (317) (a) Chauhan, B. P. S.; Rathore, J. S.; Chauhan, M.; Krawicz, A. *J. Am. Chem. Soc.* **2003**, *125*, 2876. (b) Chauhan, B. P. S.; Rathore, J. S.; Bando, T. *J. Am. Chem. Soc.* **2004**, *126*, 8493.
- (318) Huber, C.; Kokil, A.; Caseri, W. R.; Weder, C. *Organometallics* **2002**, *21*, 3817.
- (319) Itazaki, M.; Nishihara, Y.; Osakada, K. *J. Org. Chem.* **2002**, *67*, 6889.
- (320) van der Boom, M. E.; Ott, J.; Milstein, D. *Organometallics* **1998**, *17*, 4263.
- (321) Mori, A.; Fujita, A.; Nishihara, Y.; Hiyama, T. *Chem. Commun.* **1997**, 8887.
- (322) Ito, H.; Ishizuka, T.; Arimoto, K.; Miura, K.; Hosomi, A. *Tetrahedron* **1997**, *38*, 8887.
- (323) Ito, H.; Yamanaka, H.; Ishizuka, T.; Tateiwa, J.-i.; Hosomi, A. *Synlett* **2000**, 479.
- (324) Mankad, N. P.; Laitar, D. S.; Sadighi, J. P. *Organometallics* **2004**, *23*, 3369.
- (325) Kaur, H.; Zinn, F. K.; Stevens, E. D.; Nolan, S. P. *Organometallics* **2004**, *23*, 1157.

- (326) Hao, H.; Cui, C.; Roesky, H. W.; Bai, G.; Schmidt, H.-G.; Noltemeyer, M. *Chem. Commun.* **2001**, 1118.
- (327) Mimoun, H.; de Saint Laumer, J. Y.; Giannini, L.; Scopelliti, R.; Floriani, C. *J. Am. Chem. Soc.* **1999**, 121, 6158.
- (328) Hou, Z.; Zhang, Y.; Tardif, O.; Wakatsuki, Y. *J. Am. Chem. Soc.* **2001**, 123, 9216.
- (329) Arndt, S.; Voth, P.; Spaniol, T. P.; Okuda, J. *Organometallics* **2000**, 19, 4690.
- (330) (a) Tardif, O.; Hishiura, M.; Hou, Z. *Organometallics* **2003**, 22, 1171. (b) Trifonov, A. A.; Fedorova, E. A.; Fukin, G. K.; Bochkarev, M. N. *Eur. J. Inorg. Chem.* **2004**, 4396.
- (331) (a) Gountchev, T. I.; Tilley, T. D. *Organometallics* **1999**, 18, 2896. (b) Wang, J.; Gurevich, Y.; Botoshansky, M.; Eisen, M. S. *Organometallics* **2008**, 27, 4494.
- (332) (a) Gountchev, T. I.; Tilley, T. D. *Organometallics* **1999**, 18, 5661. (b) Kirillov, E.; Lehmann, C. W.; Razavi, A.; Carpentier, J.-F. *Organometallics* **2004**, 23, 2768.
- (333) Shimada, S.; Tanaka, M. *Coord. Chem. Rev.* **2006**, 250, 991.
- (334) Kang, S. O.; Lee, J.; Ko, J. *Coord. Chem. Rev.* **2002**, 231, 47.
- (335) Okazaki, M.; Ohshitanai, S.; Iwata, M.; Tobita, H.; Ogino, H. *Coord. Chem. Rev.* **2002**, 226, 167.
- (336) (a) Malisch, W.; Jehle, H.; Möller, S.; Thum, G.; Reising, J.; Gbureck, A.; Nagel, V.; Fickert, C.; Kiefer, W.; Nieger, M. *Eur. J. Inorg. Chem.* **1999**, 1597. (b) Nguyen, T.-I.; Scheschke, D. J. *Am. Chem. Soc.* **2005**, 127, 10174.
- (337) (a) Ogino, H. *Chem. Rev.* **2002**, 2 (5), 291. (b) Braunstein, P.; Knorr, M.; Stern, C. *Coord. Chem. Rev.* **1998**, 178–180, 903.
- (338) (a) Ray, M.; Nakao, Y.; Sato, H.; Sakaba, H.; Sakaki, S. *J. Am. Chem. Soc.* **2006**, 128, 11927. (b) Ray, M.; Nakao, Y.; Sato, H.; Sakaki, S. *Organometallics* **2007**, 26, 4413. (c) Koloski, T. S.; Carroll, P. J.; Berry, D. H. *J. Am. Chem. Soc.* **1990**, 112, 6405. (d) Bi, S.; Zhu, S.; Zhang, Z.; Yuan, Z. *J. Organomet. Chem.* **2007**, 692, 3454.
- (339) Avent, A. G.; Gehrhus, B.; Hitchcock, P. B.; Lappert, M. F.; Maciejewski, H. J. *Organomet. Chem.* **2003**, 686, 321.
- (340) (a) Neumann, E.; Pfaltz, A. *Organometallics* **2005**, 24, 2008. (b) Lalov, A. V.; Egorov, M. P.; Nefedov, O. M.; Cherkasov, V. K.; Ermolaev, N. L.; Piskunov, A. V. *Russ. Chem. Bull. Int. Ed.* **2005**, 54, 807.
- (341) Okazaki, M.; Tobita, H.; Ogino, H. *Dalton Trans.* **2003**, 493.
- (342) Wanandi, P. W.; Glaser, P. B.; Tilley, T. D. *J. Am. Chem. Soc.* **2000**, 122, 972.
- (343) (a) Klei, S. R.; Tilley, T. D.; Bergman, R. G. *Organometallics* **2001**, 20, 3220. (b) Tanaka, I.; Ohhara, T.; Nimura, N.; Ohashi, Y.; Jiang, Q.; Berry, D. H. *J. Chem. Res.* **1999**, 4, 14.
- (344) Sharma, H. K.; Pannell, K. H. *Organometallics* **2001**, 20, 7.
- (345) (a) Cai, X.; Gehrhus, B.; Hitchcock, P. B.; Lappert, M. F. *Can. J. Chem.* **2000**, 78, 1484. (b) Klimpel, M. G.; Gorlitzer, M.; Tafipolsky, M.; Spiegler, W.; Scherer, R.; Anwender, J. *Organomet. Chem.* **2002**, 647, 236; see ref 540b. (c) Dietrich, H. M.; Meermann, C.; Törnroos, K. W.; Anwender, R. *Organometallics* **2006**, 25, 4316.
- (346) Amgoun, A.; Thomas, C. M.; Roisnel, T.; Carpentier, J.-F. *Chem.—Eur. J.* **2006**, 12, 169.
- (347) (a) Wu, Z.; Diminnie, J. B.; Xue, Z. *Inorg. Chem.* **1998**, 37, 6366. (b) Zirngast, M.; Baumgartner, J.; Marschner, C. *Eur. J. Inorg. Chem.* **2008**, 1078.
- (348) (a) Wu, Z.; McAlexander, L. H.; Diminnie, J. B.; Xue, Z. *Organometallics* **1998**, 17, 4853. (b) Nguyen, T.-I.; Scheschke, D. J. *Am. Chem. Soc.* **2005**, 127, 10174.
- (349) (a) Fischer, R.; Frank, D.; Gaderbauer, W.; Kayser, C.; Mechtler, C.; Baumgartner, J.; Marschner, C. *Organometallics* **2003**, 22, 3723. (b) Zhang, Y.; Keaton, R. J.; Sita, L. R. *J. Am. Chem. Soc.* **2003**, 125, 8746. (c) Kayser, C.; Kickelbick, G.; Marschner, C. *Angew. Chem., Int. Ed.* **2002**, 41, 989. (d) Kayser, C.; Frank, D.; Baumgartner, J.; Marschner, C. *J. Organomet. Chem.* **2003**, 667, 149. (e) Frank, D.; Baumgartner, J.; Marschner, C. *Chem. Commun.* **2002**, 1190.
- (350) Wu, Z.; Diminnie, J. B.; Xue, Z. *Organometallics* **1998**, 17, 2971.
- (351) (a) Qiu, H.; Cai, H.; Woods, J. B.; Wu, Z.; Chen, T.; Yu, X.; Xue, Z.-L. *Organometallics* **2005**, 24, 4190. (b) Wu, Z.; Diminnie, J. B.; Xue, Z. *J. Am. Chem. Soc.* **1999**, 121, 4300. (c) Yu, X.; Cai, H.; Guzei, I. A.; Xue, Z. *J. Am. Chem. Soc.* **2004**, 126, 4472. (d) Nakata, N.; Fujita, T.; Sekiguchi, A. *J. Am. Chem. Soc.* **2006**, 128, 16024. (e) Wagner, H.; Baumgartner, J.; Marschner, C. *Organometallics* **2007**, 26, 1762.
- (352) (a) Galsworthy, J. R.; Green, M. L. H.; Maxted, M.; Muller, M. *J. Chem. Soc., Dalton Trans.* **1998**, 387. (b) Cai, H.; Yu, X.; Chen, S.; Qiu, H.; Guzei, I. A.; Xue, Z.-L. *Inorg. Chem.* **2007**, 46, 8071.
- (353) Fischer, R.; Zingast, M.; Flock, M.; Baumgartner, J.; Marschner, C. *J. Am. Chem. Soc.* **2005**, 127, 70.
- (354) Castillo, I.; Tilley, T. D. *J. Organomet. Chem.* **2002**, 643, 431.
- (355) Tanaka, I.; Ohhara, T.; Nimura, N.; Ohashi, Y.; Jiang, Q.; Berry, D. H. *J. Chem. Res. (S)* **1999**, 4, 14. *J. Chem. Res. (S)*, 1999, 180.
- (356) (a) Dorogov, K. Yu.; Dumont, E.; Ho, N.-N.; Churakov, A. V.; Kuzmina, L. G.; Poblet, J.-M.; Schultz, A. J.; Howard, J. A. K.; Bau, R.; Lledós, A.; Nikonov, G. I. *Organometallics* **2004**, 23, 2845. (b) Dorogov, K. Yu.; Yousufuddin, M.; Ho, N.-N.; Churakov, A. V.; Kuzmina, L. G.; Schultz, A. J.; Mason, S. A.; Howard, J. A. K.; Lemenovskii, D. A.; Bau, R.; Nikonov, G. I. *Inorg. Chem.* **2007**, 46, 147.
- (357) Wesemann, L.; Trinkaus, M.; Ruck, M. *Angew. Chem., Int. Ed. Engl.* **1999**, 38, 2375.
- (358) Nikonov, G. I.; Vyboishchikov, S. F.; Kuzmina, L. G.; Howard, J. A. K. *Chem. Commun.* **2002**, 568.
- (359) Liu, X.; Li, L.; Diminnie, J. B.; Yap, G. P. A.; Rheingold, A. L.; Xue, Z. *Organometallics* **1998**, 17, 4597.
- (360) Burckhardt, U.; Casty, G. L.; Gavenonis, J.; Tilley, T. D. *Organometallics* **2002**, 21, 3108.
- (361) Wu, Z.; Cai, H.; Yu, X.; Blanton, J. R.; Diminnie, J. B.; Pan, H.-J.; Xue, Z. *Organometallics* **2002**, 21, 3973.
- (362) Burckhardt, U.; Tilley, T. D. *J. Am. Chem. Soc.* **1999**, 121, 6328.
- (363) Schmedake, T. A.; Haaf, M.; Paradise, B. J.; Millevolte, A. J.; Powell, D. R.; West, R. *J. Organomet. Chem.* **2001**, 636, 17.
- (364) Shinohara, A.; Takeda, N.; Sasamori, T.; Matsumoto, T.; Tokitoh, N. *Organometallics* **2005**, 24, 6141.
- (365) (a) Petri, S. H. A.; Eikenberg, D.; Neumann, B.; Stammeler, H.-G.; Jutzi, P. *Organometallics* **1999**, 18, 2615. (b) Clendenning, S. B.; Gehrhus, B.; Hitchcock, P. B.; Moser, D. F.; Nixon, J. F.; West, R. *J. Chem. Soc., Dalton Trans.* **2002**, 484.
- (366) (a) Minato, M.; Nishiuchi, J.-y.; Kakeya, M.; Matsumoto, T.; Yamaguchi, Y.; Ito, T. *Dalton Trans.* **2003**, 483. (b) Chen, T.; Sorasane, K. R.; Wu, Z.; Diminnie, J. B.; Xue, Z. *Inorg. Chim. Acta* **2003**, 345, 113.
- (367) Ito, T.; Shimada, K.; Ono, T.; Minato, M.; Yamaguchi, Y. *J. Organomet. Chem.* **2000**, 611, 308.
- (368) (a) Palitzsch, W.; Bohme, U.; Beyer, C.; Roewer, G. *Organometallics* **1998**, 17, 2965. (b) Watanabe, T.; Hashimoto, H.; Tobita, H. *J. Am. Chem. Soc.* **2006**, 128, 2176. (c) Begum, R.; Komuro, T.; Tobita, H. *Chem. Lett.* **2007**, 36, 650. (d) Hashimoto, H.; Ochiai, M.; Tobita, H. *J. Organomet. Chem.* **2007**, 692, 36. (e) Sakaba, H.; Hirata, T.; Kabuto, C.; Kabuto, K. *J. Organomet. Chem.* **2007**, 692, 402.
- (369) (a) Ueno, K.; Sakai, M.; Ogino, H. *Organometallics* **1998**, 17, 2138. (b) Wang, B.; Zhu, B.; Xu, S.; Zhou, X. *Organometallics* **2003**, 22, 4842. (c) Wagner, W.; Baumgartner, J.; Marschner, C. *Organometallics* **2005**, 24, 4649.
- (370) (a) Palitzsch, W.; Beyer, C.; Bohme, U.; Rittmeister, R.; Roewer, G. *Eur. J. Inorg. Chem.* **1999**, 1813. (b) Heyn, R. H.; Tilley, T. D. *Inorg. Chim. Acta* **2002**, 341, 91.
- (371) (a) Lebus, A.-M.; Christendat, D.; Gilson, D. F. R.; Butler, I. S. *Acta Crystallogr., Sect. C: Cryst. Struct. Commun.* **1997**, C53, 1206. (b) Weber, H. P.; Bryan, R. F. *Acta Cryst.* **1967**, 22, C-34.
- (372) Petri, S. H. A.; Eikenberg, D.; Neumann, B.; Stammeler, H.-G.; Jutzi, P. *Organometallics* **1999**, 18, 2015.
- (373) (a) Tobita, H.; Sato, T.; Okazaki, M.; Ogino, H. *J. Organomet. Chem.* **2000**, 611, 314. (b) Malisch, W.; Jehle, H.; Schumacher, D.; Binnewies, W.; Soger, N. *J. Organomet. Chem.* **2003**, 667, 35.
- (374) Yamaguchi, K.; Ueno, K.; Ogino, H. *Chem. Lett.* **1998**, 247.
- (375) (a) Malisch, W.; Jehle, H.; Möller, S.; Thum, G.; Reising, J.; Gbureck, A.; Nagel, V.; Fickert, C.; Kiefer, W.; Nieger, M. *Eur. J. Inorg. Chem.* **1999**, 1597. (b) Zhang, Y.; Cervantes-Lee, F.; Pannell, K. H. *Organometallics* **2003**, 22, 2517. (c) Watanabe, T.; Hashimoto, H.; Tobita, H. *Organometallics* **2004**, 23, 4150. (d) Braunstein, P.; Cossy, J.; Knorr, M.; Strohmman, C.; Vogel, P. *New J. Chem.* **1999**, 23, 1215. (e) Sato, T.; Okazaki, M.; Tobita, H.; Ogino, H. *J. Organomet. Chem.* **2003**, 669, 189.
- (376) (a) Simons, R. S.; Galat, K. J.; Bradshaw, J. D.; Youngs, W. J.; Tessier, C. A.; Aullón, G.; Alvarez, S. *J. Organomet. Chem.* **2001**, 628, 241. (b) Hoffmann, F.; Bohme, U.; Roewer, G. *Organosilicon Chem.: From Mol. To Mater.* **2005**, 6, 445.
- (377) (a) Zhang, Y.; Sun, X.; Wang, B.; Xu, S.; Zhou, X. *Organometallics* **1999**, 18, 4493. (b) Knorr, M.; Jourdain, I.; Villafañe, F.; Strohmman, C. *J. Organomet. Chem.* **2005**, 690, 1456. (c) Kückmann, T. I.; Dornhaus, F.; Bolte, M.; Lerner, H.-W.; Holthausen, M. C.; Wagner, M. *Eur. J. Inorg. Chem.* **2007**, 1989.
- (378) (a) Braunstein, P.; Veith, M.; Blin, J.; Huch, V. *Organometallics* **2001**, 20, 627. (b) Vögler, M.; Pavel, I.; Hofmann, M.; Moigno, D.; Nieger, M.; Kiefer, W.; Malisch, W. *Inorg. Chem.* **2003**, 42, 3274.
- (379) (a) McIndoe, J. S.; Nicholson, B. K. *J. Organomet. Chem.* **2002**, 648, 237. (b) Kawamura, K.; Nakazawa, H.; Miyoshi, K. *Organometallics* **1999**, 18, 1517.
- (380) Freeman, S. T. N.; Petersen, J. L.; Lemke, F. R. *Organometallics* **2004**, 23, 1153.
- (381) Kobayashi, H.; Ueno, K.; Ogino, H. *Chem. Lett.* **1999**, 239.
- (382) (a) Okazaki, M.; Jung, K. A.; Satoh, K.; Okada, H.; Naito, J.; Akagi, T.; Tobita, H.; Ogino, H. *J. Am. Chem. Soc.* **2004**, 126, 5060. (b) Dufour, P.; Dartiguenave, M.; Dartiguenave, Y.; Simard, M.; Beauchamp, A. L. *J. Organomet. Chem.* **1998**, 563, 53. (c) Okazaki,

- M.; Jung, K. A.; Tobita, H. *Organometallics* **2005**, *24*, 659. (d) Nakazawa, H.; Itazaki, M.; Kamata, K.; Ueda, K. *Chem. Asian J.* **2007**, *2*, 882.
- (383) (a) Okada, H.; Okazaki, M.; Tobita, H.; Ogino, H. *Chem. Lett.* **2003**, *32*, 876. (b) Knorr, M.; Strohmman, C. *Eur. J. Inorg. Chem.* **2000**, 241. (c) Okazaki, M.; Jung, K. A.; Tobita, H. *Chem. Commun.* **2005**, 912.
- (384) Schuh, W.; Braunstein, P.; Benard, M.; Rohmer, M.-M.; Welter, R. *Angew. Chem., Int. Ed.* **2003**, *42*, 2161.
- (385) (a) Sun, H.; Teng, X.; Huang, X.; Hu, Z.; Pan, Y. *J. Organomet. Chem.* **2000**, *595*, 268. (b) Sun, H.; Liu, Q.; Gu, J.; Zhang, C.; Zhang, Z.; Wang, Q. *Organometallics* **2008**, *27*, 4505.
- (386) (a) Zhang, Y.; Xu, S.; Tian, G.; Zhou, X.; Sun, J. *Organometallics* **1998**, *17*, 1122. (b) Schuh, W.; Braunstein, P.; Welter, R. C. R. *Chim.* **2003**, *6*, 59. (c) Malisch, W.; Schumacher, D.; Schmiedeskamp, B.; Jehle, H.; Eisner, D.; Schoeller, W. W.; Nieger, M. *Eur. J. Inorg. Chem.* **2003**, 2133. (d) Marsh, R. E. *Acta Crystallogr., Sect. B: Struct. Sci.* **2004**, *60*, 252. (e) Sun, H.; Huang, X.; Hu, Z.; Zhang, Z.; Leng, X.; Weng, L. *Inorg. Chim. Acta* **2003**, *348*, 8. (f) Schuh, W.; Braunstein, P.; Bénard, M.; Rohmer, M.-M.; Welter, R. *J. Am. Chem. Soc.* **2005**, *127*, 10250. (g) Sun, H.; Pan, Y.; Huang, X.; Guo, Z.; Zhang, Z.; Zhang, H.; Li, J.; Wang, F. *Organometallics* **2006**, *25*, 133.
- (387) (a) Sun, H.; Pan, Y.; Huang, X.; Guo, Z.; Zhang, Z.; Zhang, H.; Li, J.; Wang, F. *Organometallics* **2006**, *25*, 133. (b) Xie, W.-H.; Wang, B. Q.; Xu, S.-S.; Zhou, X.-Z.; Cheung, K.-K. *Polyhedron* **1999**, *18*, 2645. (c) Braunstein, P.; Durand, J.; Morise, X.; Tiripicchio, A.; Ugozzoli, F. *Organometallics* **2000**, *19*, 444. (d) Wang, B.; Zhu, B.; Zhang, J.; Xu, S.; Zhou, X.; Weng, L. *Organometallics* **2003**, *22*, 5543. (e) Liu, S.-Y.; Hills, I. D.; Fu, G. C. *J. Am. Chem. Soc.* **2005**, *127*, 15352. (f) Grogger, C.; Fallmann, H.; Furpass, G.; Stuger, H.; Kickelbick, G. *J. Organomet. Chem.* **2003**, *665*, 186. (g) Okazaki, M.; Satoh, K.; Jung, K. A.; Tobita, H.; Ogino, H. *Organometallics* **2004**, *23*, 1971. (h) Knorr, M.; Braunstein, P.; Messaoudi, A.; Tiripicchio, A.; Ugozzoli, F. *J. Cluster Sci.* **2007**, *18*, 289. (i) Iwata, M.; Okazaki, M.; Tobita, H. *Chem. Commun.* **2003**, 2744.
- (388) (a) Braunstein, P.; Knorr, M.; Reinhard, G.; Schubert, U.; Stahrfeldt, T. *Chem.—Eur. J.* **2002**, *6*, 4265. (b) Malisch, W.; Vögler, M.; Schumacher, D.; Nieger, M. *Organometallics* **2002**, *21*, 2891.
- (389) (a) Pannell, K. H.; Kobayashi, T.; Cervantes-Lee, F.; Zhang, Y. *Organometallics* **2000**, *19*, 1. (b) Sharma, H. K.; Cervantes-Lee, F.; Pannell, K. H. *Organometallics* **2006**, *25*, 3969. (c) Lee, V. Ya.; Kato, R.; Sekiguchi, A.; Krapp, A.; Frenking, G. *J. Am. Chem. Soc.* **2007**, *129*, 10340. (d) Takanashi, K.; Lee, V. Y.; Ichinohe, M.; Sekiguchi, A. *Angew. Chem., Int. Ed.* **2006**, *45*, 3269.
- (390) Pfister, H.; Fenske, D. *Z. Anorg. Allg. Chem.* **2001**, *627*, 575.
- (391) Fox, T.; Burger, P. *Eur. J. Inorg. Chem.* **2001**, 795.
- (392) (a) Meyer, M.; Noth, H.; Jutzi, P. Private communication cited in Cambridge Data Base, REFC=RUF01. (b) Hashimoto, H.; Aratani, L.; Kabuto, C.; Kira, M. *Organometallics* **2003**, *22*, 2199.
- (393) (a) Ochiai, M.; Hashimoto, H.; Tobita, H. *Angew. Chem., Int. Ed.* **2007**, *46*, 8192. (b) Amoroso, D.; Haaf, M.; Yap, G. P. A.; West, R.; Fogg, D. E. *Organometallics* **2002**, *21*, 534.
- (394) Tobita, H.; Kurita, H.; Ogino, H. *Organometallics* **1998**, *17*, 2850.
- (395) Takao, T.; Yoshida, S.; Suzuki, H. *Organometallics* **2005**, *24*, 521.
- (396) Tobita, H.; Kurita, H.; Ogino, H. *Organometallics* **1998**, *17*, 2844.
- (397) (a) Jiang, F.; Male, J. L.; Biradha, K.; Leong, W. K.; Pomeroy, R. K.; Zaworotko, M. J. *Organometallics* **1998**, *17*, 5810. (b) Takao, T.; Amako, M.; Suzuki, H. *Organometallics* **2003**, *22*, 3855. (c) Dioumaev, V. K.; Plössel, K.; Carroll, P. J.; Berry, D. H. *Organometallics* **2000**, *19*, 3374. (d) Stüger, H.; Braunwarth, M.; Fuerpass, G.; Baumgartner, J.; Saf, R. *Monatsh. Chem.* **2006**, *137*, 595.
- (398) Atheaux, I.; Delpech, F.; Donnadiou, B.; Sabo-Etienne, S.; Chaudret, B.; Hussein, K.; Barthelat, J. C.; Braun, T.; Duckett, S. B.; Perutz, R. N. *Organometallics* **2002**, *21*, 5347.
- (399) (a) Berenbaum, A.; Lough, A. J.; Manners, I. *Acta Crystallogr., Sect. E: Struct. Rep. Online* **2002**, *E58*, 679. (b) Chen, D.; Mu, B.; Xu, S.; Wang, B. *J. Organomet. Chem.* **2006**, *691*, 3823.
- (400) Wesemann, L.; Ramjoie, Y.; Trinkaus, M.; Spaniol, T. P. *Eur. J. Inorg. Chem.* **1998**, 1263.
- (401) (a) Dioumaev, V. K.; Plossl, K.; Carroll, P. J.; Berry, D. H. *J. Am. Chem. Soc.* **1999**, *121*, 8391. (b) Stüger, H.; Braunwarth, M.; Fuerpass, G.; Baumgartner, J.; Saf, R. *Monatsh. Chem.* **2006**, *137*, 595.
- (402) Zhang, Y.; Wang, B.; Xu, S.; Zhou, X.; Sun, J. *J. Organomet. Chem.* **1999**, *584*, 356.
- (403) Takao, T.; Yoshida, S.; Suzuki, H. *Chem. Lett.* **2001**, 1100.
- (404) Hayashida, T.; Nagashima, H. *Organometallics* **2001**, *20*, 4996.
- (405) Okazaki, M.; Yamahira, N.; Minglana, J. J. G.; Tobita, H. *Organometallics* **2004**, *23*, 4531.
- (406) (a) Attar-Bashi, M. T.; Rickard, C. E. F.; Roper, W. R.; Wright, L. J.; Woodgate, S. D. *Organometallics* **1998**, *17*, 504. (b) Albrecht, M.; Kwok, W.-H.; Lu, G.-L.; Roper, W. R.; Wright, L. J. *Inorg. Chim. Acta* **2005**, *358*, 1407. (c) Clark, G. R.; Lu, G.-L.; Rickard, C. E. F.; Roper, W. R.; Wright, L. J. *J. Organomet. Chem.* **2005**, *690*, 3309. (d) Takanashi, K.; Lee, V. Ya.; Ichinohe, M.; Sekiguchi, A. *Eur. J. Inorg. Chem.* **2007**, 5471.
- (407) Rickard, C. E. F.; Roper, W. R.; Woodman, T. J.; Wright, L. J. *Chem. Commun.* **1999**, 837.
- (408) Mohlen, M.; Rickard, C. E. F.; Roper, W. R.; Salter, D. M.; Wright, L. J. *J. Organomet. Chem.* **2000**, *593*, 458.
- (409) Kon, Y.; Sakamoto, K.; Kabuto, C.; Kira, M. *Organometallics* **2005**, *24*, 1407.
- (410) (a) Harfoot, G. J.; Nicholson, B. K. *J. Organomet. Chem.* **2003**, *669*, 106. (b) Evans, C.; Nicholson, B. K. *J. Organomet. Chem.* **2003**, *665*, 95. (c) Evans, C.; Harfoot, G. J.; McIndoe, J. S.; McAdam, C. J.; MacKay, K. M.; Nicholson, B. K.; Robinson, B. H.; Van Tiel, M. L. *J. Chem. Soc., Dalton Trans.* **2002**, 4678. (d) Gunale, D.; Steiner, D.; Schweikart, D.; Pritzkow, H.; Berndt, A.; Siebert, W. *Chem.—Eur. J.* **1998**, *4*, 44. (e) Takanashi, K.; Lee, V. Ya.; Matsuno, T.; Ichinohe, M.; Sekiguchi, A. *J. Am. Chem. Soc.* **2005**, *127*, 5768.
- (411) Tse, A. K.-S.; Wu, B.-M.; Mak, T. C. W.; Chan, K. S. *J. Organomet. Chem.* **1998**, *568*, 257.
- (412) Cook, K. S.; Incarvito, C. D.; Webster, C. E.; Fan, Y.; Hall, M. B.; Hartwig, J. F. *Angew. Chem., Int. Ed.* **2004**, *43*, 5474.
- (413) Lenges, C. P.; White, P. S.; Brookhart, M. *J. Am. Chem. Soc.* **1999**, *121*, 4385.
- (414) Gutierrez, E.; Puebla, A.; Monge, A.; Paneque, M.; Poveda, M. L.; Taboada, S.; Trujillo, M.; Carmona, E. *J. Am. Chem. Soc.* **1999**, *121*, 346.
- (415) (a) Gehrhus, B.; Hitchcock, P. B.; Lappert, M. F.; Maciejewski, H. *Organometallics* **1998**, *17*, 5599. (b) Theil, M.; Jutzi, P.; Neumann, B.; Stammli, A.; Stammli, H.-G. *J. Organomet. Chem.* **2002**, *662*, 34.
- (416) (a) Ozawa, F.; Sugawara, M.; Hasebe, K.; Hayashi, T. *Inorg. Chim. Acta* **1999**, *296*, 19. (b) Li, Y.-H.; Zhang, Y.; Zhao, M.-M.; Yuan, Y.-Y. *Acta Crystallogr., Sect. E: Struct. Rep. Online* **2008**, *E64*, m1271.
- (417) Tanaka, Y.; Yamashita, H.; Shimada, S.; Tanaka, M. *Organometallics* **1997**, *16*, 3246.
- (418) Sugimoto, M.; Kato, Y.; Takeda, N.; Oike, H.; Ito, Y. *Organometallics* **1998**, *17*, 495.
- (419) Kira, M.; Sekiguchi, Y.; Iwamoto, T.; Kabuto, C. *J. Am. Chem. Soc.* **2004**, *126*, 12778.
- (420) Iwamoto, T.; Sekiguchi, Y.; Yoshida, N.; Kabuto, C.; Kira, M. *Dalton Trans.* **2006**, 177.
- (421) (a) Schmedake, T. A.; Haaf, M.; Paradise, B. J.; Powell, D.; West, R. *Organometallics* **2000**, *19*, 3263. (b) Braunschweig, H.; Gross, M.; Radacki, K. *Organometallics* **2007**, *26*, 6688. (c) Schaub, T.; Döring, C.; Radius, U. *Dalton Trans.* **2007**, 1993. (d) Watanabe, C.; Iwamoto, T.; Kabuto, C.; Kira, M. *Angew. Chem., Int. Ed.* **2008**, *47*, 5386.
- (422) (a) Li, Y.-H.; Zhang, Y.; Zhao, M.-M.; Li, Z. *Acta Crystallogr., Sect. E: Struct. Rep. Online* **2008**, *E64*, m1272. (b) Bravo-Zhivotovskii, D.; Peleg-Vasserman, H.; Kosa, M.; Molev, G.; Botoshanskii, M.; Apeloig, Y. *Angew. Chem., Int. Ed.* **2004**, *43*, 745.
- (423) Müller, C.; Lachicotte, R. J.; Jones, W. D. *Organometallics* **2002**, *21*, 1190.
- (424) Lee, Y.-J.; Lee, J.-D.; Kim, S.-J.; Yoo, B. W.; Ko, J.; Suh, I.-H.; Cheong, M.; Kang, S. O. *Organometallics* **2004**, *23*, 490.
- (425) (a) Knorr, M.; Guyon, F.; Jourdain, I.; Kneff, S.; Frenzel, J.; Strohmman, C. *Inorg. Chem. Acta* **2003**, *350*, 455. (b) Ozawa, F.; Sakamoto, Y.; Sagawa, T.; Tanaka, R.; Katayama, H. *Chem. Lett.* **1999**, 1307.
- (426) (a) Kim, Y.-J.; Choi, E.-H.; Lee, S. W. *Organometallics* **2003**, *22*, 3316. (b) Chan, W. Y.; Berenbaum, A.; Clendenning, S. B.; Lough, A. J.; Manners, I. *Organometallics* **2003**, *22*, 3796. (c) Sagawa, T.; Sakamoto, Y.; Tanaka, R.; Katayama, H.; Ozawa, F. *Organometallics* **2003**, *22*, 4433.
- (427) Hasebe, K.; Kamite, J.; Mori, T.; Katayama, H.; Ozawa, F. *Organometallics* **2000**, *19*, 2022. see ref. ⁵⁵⁷.
- (428) Gilges, H.; Kickelbick, G.; Schubert, U. *J. Organomet. Chem.* **1997**, *548*, 57.
- (429) Sagawa, T.; Asano, Y.; Ozawa, F. *Organometallics* **2002**, *21*, 5879.
- (430) Mullica, D. F.; Leschnitzer, D.; Sappenfield, E. L. *J. Chem. Crystallogr.* **1997**, *27*, 435.
- (431) Mitchell, G. P.; Tilley, T. D. *Angew. Chem., Int. Ed.* **1998**, *37*, 2524.
- (432) Tamm, M.; Kunst, A.; Herdweck, E. *Chem. Commun.* **2005**, 1729; see ref 549.
- (433) Hashimoto, H.; Sekiguchi, Y.; Sekiguchi, Y.; Iwamoto, T.; Kabuto, C.; Kira, M. *Can. J. Chem.* **2003**, *81*, 1241.
- (434) Bartole-Scott, A.; Braunschweig, H.; Kupfer, T.; Lutz, M.; Manners, I.; Nguyen, T.-I.; Radacki, K.; Seeler, F. *Chem.—Eur. J.* **2006**, *12*, 1266.
- (435) (a) Klinkhammer, K. W.; Klett, J.; Xiong, Y.; Yao, S. *Eur. J. Inorg. Chem.* **2003**, 3417. (b) Klett, J.; Klinkhammer, K. W.; Niemeyer,

- M. Chem.—Eur. J.* **1999**, *5*, 2531. (c) Klinkhammer, K. W. Z. *Anorg. Allg. Chem.* **2000**, 626, 1217. (d) Farwell, J. D.; Hitchcock, P. B.; Lappert, M. F.; Protchenko, A. V. *J. Organomet. Chem.* **2007**, 692, 4953.
- (436) Oroz, M. M.; Schier, A.; Schmidbaur, H. Z. *Naturforsch., B: Chem. Sci.* **1999**, *54*, 26.
- (437) (a) Klinkhammer, K. W. Thesis, University of Stuttgart, Stuttgart, Germany, 1998. (b) Nanjo, M.; Oda, T.; Mochida, K. *J. Organomet. Chem.* **2003**, 672, 100.
- (438) (a) Wiberg, N.; Niedermayer, W.; Lerner, H.-W.; Bolte, M. Z. *Anorg. Allg. Chem.* **2001**, 627, 1043. (b) Goicoechea, J. M.; Sevov, S. *Organometallics* **2006**, 25, 4530.
- (439) Anantharaman, G.; Roesky, H. W.; Magull, J. *Angew. Chem., Int. Ed.* **2002**, *41*, 1226.
- (440) (a) Bravo-Zhivotovskii, D.; Yuzefovich, M.; Bendikov, M.; Klinkhammer, K. W.; Apeloig, Y. *Angew. Chem., Int. Ed. Engl.* **1999**, *38*, 1100. (b) Farwell, J. D.; Fernandes, M. A.; Hitchcock, P. B.; Lappert, M. F.; Layh, M.; Omondi, B. *Dalton Trans.* **2003**, 1719.
- (441) Pickett, N. L.; Just, O.; VanDerveer, D. G.; Rees, W. S., Jr. *Acta Crystallogr., Sect. C: Cryst. Struct. Commun.* **2000**, *56*, 412.
- (442) Evans, W. J.; Perotti, J. M.; Ziller, J. W.; Moser, D. F.; West, R. *Organometallics* **2003**, 22, 1160.
- (443) (a) Cao, X.; Gehrhus, B.; Hitchcock, P. B.; Lappert, M. F. *Can. J. Chem.* **2000**, *78*, 1484; see ref 345a. (b) Diaconescu, P. L.; Odom, A. L.; Agapie, T.; Cummins, C. C. *Organometallics* **2001**, 20, 4993.
- (444) Lukevics, E.; Arsenyan, P.; Pudova, O. *Main Group Metal Chem.* **2002**, 25, 415.
- (445) Lukevics, E.; Arsenyan, P.; Pudova, O. *Main Group Metal Chem.* **2002**, 25, 541.
- (446) Lukevics, E.; Pudova, O. *Main Group Metal Chem.* **2000**, 23, 207.
- (447) Lukevics, E.; Pudova, O. *Main Group Metal Chem.* **1999**, 22, 385.
- (448) (a) Gossage, R. A. *J. Organomet. Chem.* **2000**, 608, 164. (b) Agenet, N.; Mirebeau, J.-H.; Petit, M.; Thouvenot, R.; Gandon, V.; Malacria, M.; Aubert, C. *Organometallics* **2007**, 26, 819.
- (449) (a) Jacobsen, H.; Fink, M. J. *Organometallics* **2006**, 25, 1945. (b) Jacobsen, H.; Ziegler, T. *Comments Inorg. Chem.* **1995**, 17, 301.
- (450) (a) Tilley, T. D. Transition-metal silyl derivatives and Appendix to "Transition-metal silyl derivatives". In *The silicon heteroatom bond*; Patai, S.; Rappoport, Zvi, Eds.; John Wiley & Sons: New York, 1991; Chapters 9 and 10. (b) Zybail, Ch. The Coordination Chemistry of Low Valent Silicon. In *Transition Metal Coordination Chemistry*; Herrmann, W. A., Ed.; Topics in Current Chemistry; Springer-Verlag: Berlin, 1992; Vol. 160, p 1.
- (451) (a) Bau, R.; Drabnis, M. H. *Inorg. Chim. Acta* **1997**, 259, 27. (b) Koetzle, T. F. *Trans. Am. Crystallogr. Assoc.* **1995**, 31, 57 CAN 130: 345169.
- (452) Lachaize, S.; Sabo-Etienne, S. *Eur. J. Inorg. Chem.* **2006**, 2115.
- (453) Takao, T.; Yoshida, S.; Suzuki, H. *Organometallics* **2005**, 24, 521.
- (454) Tanabe, M.; Osakada, K. *Chem.—Eur. J.* **2004**, 10, 416.
- (455) Kubas, G. J. *PNAS* **2007**, 6901.
- (456) Nakajima, S.; Sumimoto, M.; Nakao, Y.; Sato, H.; Sakaki, S.; Osakada, K. *Organometallics* **2005**, 25, 4029.
- (457) (a) Kawachi, A.; Tanaka, Y.; Tamao, K. *Organometallics* **1997**, 16, 5102. (b) Commonly assumed value.
- (458) Choi, S.-H.; Feng, J.; Lin, Z. *Organometallics* **2000**, 19, 2051.
- (459) (a) Luo, X.-L. L.; Kubas, G. J.; Bryan, J. C.; Burns, C. J.; Unkefer, C. J. *J. Am. Chem. Soc.* **1994**, 116, 10312. (b) Takao, T.; Yoshida, S.; Suzuki, H.; Tanaka, M. *Organometallics* **1995**, 14, 3855.
- (460) (a) Kubas, G. J. *Catal. Lett.* **2005**, 104, 79. (b) Numbers used in Scheme 15A are from ref 455.
- (461) Schubert, U.; Ackermann, K.; Wörle, B. *J. Am. Chem. Soc.* **1982**, 104, 7378.
- (462) Lemke, F. R.; Galat, K. J.; Youngs, W. J. *Organometallics* **1999**, 18, 1419.
- (463) Schultz, A. J.; Stearley, K. L.; Williams, J. M.; Mink, R.; Stucky, G. D. *Inorg. Chem.* **1977**, 16, 3303.
- (464) Hoyano, J. K.; Elder, M.; Graham, W. A. G. *J. Am. Chem. Soc.* **1969**, 91, 4568.
- (465) *NMR and the Periodic Table*; Harris, R. K., Mann, B. E., Eds.; Academic Press: London, 1978.
- (466) Besora, M.; Maseras, F.; Lledós, A.; Eisenstein, O. *Inorg. Chem.* **2002**, 41, 7105.
- (467) Corral, I.; Mó, O.; Yáñez, M. *New J. Chem.* **2003**, 27, 1657; see ref 50.
- (468) Corral, I.; Mó, O.; Yáñez, M. *Int. J. Mass Spectrom.* **2003**, 227, 401.
- (469) Corral, I.; Mó, O.; Yáñez, M. *J. Phys. Chem. A* **2003**, 107, 1370.
- (470) Corral, I.; Mó, O.; Yáñez, M. *J. Phys. Org. Chem.* **2006**, 19, 495.
- (471) Vyboishchikov, S. F.; Nikonov, G. I. *Chem.—Eur. J.* **2006**, 12, 8518.
- (472) Bent, H. A. *Chem. Rev.* **1961**, 61, 275; see ref 155b.
- (473) (a) Krishner, L. C.; Pierce, L. J. *Chem. Phys.* **1960**, 32, 1619. (b) Zeil, W.; Gegenheimer, R.; Pferrer, S.; Dakouri, M. Z. *Naturforsch.* **1972**, 27a, 1150. (c) Harmony, M. D.; Strand, M. R. *J. Mol. Spectrosc.* **1980**, 81, 308. (d) Kewley, R.; McKinney, P. M.; Robiette, A. G. *J. Mol. Spectrosc.* **1970**, 34, 309. (e) Kanazachi, M. *Bull. Chem. Soc. Jpn.* **1953**, 26, 493. (f) O'Reilly, J. M.; Pierce, L. J. *Chem. Phys.* **1961**, 34, 2276. (g) Takeo, H.; Matsumara, C. *Bull. Chem. Soc. Jpn.* **1965**, 50, 1633. (h) Glidewell, C.; Pinder, P. M.; Robiette, A. G.; Sheldrick, G. M. *J. Chem. Soc., Dalton Trans.* **1972**, 1402. (i) Allen, F. H.; Kennard, O. *Chem. Des. Autom. News* **1993**, 8, 31.
- (474) Campion, B. K.; Heyn, R. H.; Tilley, T. D. *Chem. Commun.* **1992**, 1201.
- (475) Pandey, K. K.; Lein, M.; Frenking, G. *Organometallics* **2004**, 23, 2944.
- (476) (a) Beddie, C.; Hall, M. B. *J. Am. Chem. Soc.* **2004**, 126, 13564. (b) Beddie, C.; Hall, M. B. *J. Phys. Chem.* **2006**, 110, 1416.
- (477) Sakaba, H.; Hirata, T.; Kabuto, C.; Kabuto, K. *Organometallics* **2006**, 25, 5145; see ref 38b.
- (478) Ogino, H.; Tobita, G. *Adv. Organomet. Chem.* **1998**, 42, 223.
- (479) Perutz, R.; Sabo-Etienne, S. *Angew. Chem., Int. Ed.* **2007**, 46, 2578.
- (480) Rosenberg, L.; Davis, C. W.; Yao, J. J. *Am. Chem. Soc.* **2001**, 123, 5120.
- (481) References cited in ref 151. Ueno, K.; Masuko, A.; Ogino, H. *Organometallics* **1997**, 16, 5023.
- (482) Maseras, F.; Lledós, A.; Clot, E.; Eisenstein, O. *Chem. Rev.* **2000**, 100, 601.
- (483) Lin, Z. *Chem. Soc. Rev.* **2002**, 31, 239.
- (484) Heinekey, D. M.; Lledós, A.; Lluch, J. M. *Chem. Soc. Rev.* **2004**, 33, 175.
- (485) Sakaki, S.; Biswas, B.; Musashi, Y.; Sugimoto, M. *J. Organomet. Chem.* **2000**, 611, 288.
- (486) Frenking, G.; Fröhlich, N. *Chem. Rev.* **2000**, 100, 7171.
- (487) Fan, M.-F.; Lin, Z. *Organometallics* **1998**, 17, 1092.
- (488) (a) Wang, C.; Ye, S. *Int. J. Quantum Chem.* **1999**, 75, 47. (b) Wang, C.; Xu, X.; Cao, Z.; Ye, S.; Zhang, Q. *J. Phys. Chem. A* **2003**, 107, 6681.
- (489) (a) Sakaki, S.; Takayama, T.; Sumimoto, M.; Sugimoto, M. *J. Am. Chem. Soc.* **2004**, 126, 3332. (b) Sakaki, S.; Takayama, T.; Sugimoto, M. *Chem. Lett.* **2001**, 1222.
- (490) (a) Chung, G.; Gordon, M. S. *Organometallics* **2003**, 22, 42. (b) Zhang, X.-H.; Chung, L. W.; Lin, Z.; Wu, Y.-D. *J. Org. Chem.* **2008**, 73, 820.
- (491) Fehner, T. P. *J. Organomet. Chem.* **2001**, 635, 92.
- (492) (a) Lichtenberger, D. L.; Rai-Chaudhuri, A. *J. Am. Chem. Soc.* **1989**, 111, 3583. (b) Lichtenberger, D.; Rai-Chaudhuri, A. *J. Am. Chem. Soc.* **1990**, 112, 2492. (c) Lichtenberger, D. L.; Rai-Chaudhuri, A. *Inorg. Chem.* **1990**, 29, 975.
- (493) Lichtenberger, D. L. *Organometallics* **2003**, 22, 1599.
- (494) Bader, R. F. W.; Matta, C. F.; Cortés-Guzmán, F. *Organometallics* **2004**, 23, 6253.
- (495) Paterson, M. J.; Chatterton, N. P.; McGrady, G. S. *New J. Chem.* **2004**, 28, 1434.
- (496) (a) Schubert, U.; Schwarz, M.; Möller, F. *Organometallics* **1994**, 13, 1554. (b) Costa, P. J.; Romão, C. C.; Fernandes, A. C.; Royo, B.; Reis, P. M.; Calhorda, M. J. *Chem.—Eur. J.* **2007**, 13, 3934.
- (497) (a) Nikonov, G. I. *Organometallics* **2003**, 22, 1597. (b) Royo, B.; Romão, C. C. *J. Mol. Catal. A: Chem.* **2005**, 236, 107. (c) Ison, E. A.; Trivedi, E. R.; Corbin, R. A.; Abu-Omar, M. M. *J. Am. Chem. Soc.* **2005**, 127, 15374. (d) Du, G.; Abu-Omar, M. M. *Organometallics* **2006**, 25, 4920. (e) Chung, L. W.; Lee, H. G.; Lin, Z.; Wu, Y.-D. *J. Org. Chem.* **2006**, 71, 6000.
- (498) Jetz, W.; Graham, W. A. G. *Inorg. Chem.* **1971**, 10, 1159.
- (499) (a) Bühl, M.; Mauschick, F. T. *Organometallics* **2003**, 22, 1422. (b) Schubert, U.; Scholz, G.; Müller, J.; Ackermann, K.; Worle, B.; Stansfield, R. F. D. *J. Organomet. Chem.* **1986**, 306, 303. (c) Grumbine, S. K.; Tilley, T. D.; Arnold, F. P.; Rheingold, A. L. *J. Am. Chem. Soc.* **1994**, 116, 5495.
- (500) Fan, M.-F.; Lin, Z. *Organometallics* **1999**, 18, 286.
- (501) (a) Arnold, F. P., Jr. *Organometallics* **1999**, 18, 4800. (b) Hratchian, H. P.; Prendergast, T.; Milletti, M. C. *Polyhedron* **2001**, 20, 209. (c) Grumbine, S. D.; Tilley, T. D.; Rheingold, A. L. *J. Am. Chem. Soc.* **1993**, 115, 358. (d) Bi, S.; Zhao, Y.; Kong, X.; Zhao, X.; Xie, Q. *J. Organomet. Chem.* **2008**, 693, 639.
- (502) (a) Chung, L. W.; Wu, Y.-D.; Trost, B. M.; Ball, Z. T. *J. Am. Chem. Soc.* **2003**, 125, 11578. (b) Tuttle, T.; Wang, D.; Thiel, W.; Köhler, J.; Hofmann, M.; Weis, J. J. *Organomet. Chem.* **2007**, 692, 2282. (c) Tuttle, T.; Wang, D.; Thiel, W.; Köhler, J.; Hofmann, M.; Weis, J. *Organometallics* **2006**, 25, 4504. (d) Böhme, U. *J. Organomet. Chem.* **2006**, 691, 4400. (e) Valliant-Saunders, K.; Gunn, E.; Shelton, G. R.; Hrovat, D. A.; Borden, W. T.; Mayer, J. M. *Inorg. Chem.* **2007**, 46, 5212.
- (503) Besora, M.; Maseras, F.; Lledós, A.; Eisenstein, O. *Organometallics* **2006**, 25, 4748.
- (504) (a) Webster, C. E.; Hall, M. B. *Coord. Chem. Rev.* **2003**, 238–239, 315. (b) Vyboishchikov, S. F.; Nikonov, G. I. *Organometallics* **2007**, 26, 4160.

- (505) Kuramoto, Y.; Sawai, N.; Fujiwara, Y.; Sumimoto, M.; Nakao, Y.; Sato, H.; Sakaki, S. *Organometallics* **2005**, *24*, 3655.
- (506) Nakajima, S.; Yokogawa, D.; Nakao, Y.; Sato, H.; Sakaki, S. *Organometallics* **2004**, *23*, 4672.
- (507) Sakaki, S.; Yamaguchi, S.; Musashi, Y.; Sugimoto, M. *J. Organomet. Chem.* **2001**, *635*, 173.
- (508) Choi, S.-H.; Lin, Z. *J. Organomet. Chem.* **2000**, *608*, 42.
- (509) Auburn, M.; Ciriano, M.; Howard, J. A. K.; Murray, M.; Pugh, N. J.; Spencer, J. L.; Stone, F. G. A.; Woodward, P. *J. Chem. Soc., Dalton Trans.* **1980**, 659.
- (510) Tsipis, C. A.; Kefalidis, C. E. *Organometallics* **2006**, *25*, 1696.
- (511) Sakaki, S.; Mizoe, N.; Musashi, Y.; Biswas, B.; Sugimoto, M. *J. Phys. Chem. A* **1998**, *102*, 8027.
- (512) Sakaki, S.; Mizoe, N.; Sugimoto, M. *Organometallics* **1998**, *17*, 2510.
- (513) (a) Sakaki, S.; Mizoe, N.; Musashi, Y.; Sugimoto, M. *THEOCHEM* **1999**, *461–462*, 533. (b) Ozawa, F. *J. Organomet. Chem.* **2000**, *611*, 332.
- (514) Biswas, G.; Sugimoto, M.; Sakaki, S. *Organometallics* **1999**, *18*, 4015.
- (515) (a) Sakaki, S.; Mizoe, N.; Sugimoto, M.; Musashi, Y. *Coord. Chem. Rev.* **1999**, *190*, 933. (b) van Stralen, J. N. P.; Bickelhaupt, F. M. *Organometallics* **2006**, *25*, 4260. (c) Sakaki, S.; Ogawa, M.; Kinoshita, M. *J. Phys. Chem.* **1995**, *99*, 9933.
- (516) Giorgi, F.; De Angelis, N. Re.; Sgamellotti, A. *Chem. Phys. Lett.* **2002**, *364*, 87.
- (517) Jagadeesh, M. N.; Thiel, W.; Köhler, J.; Fehn, A. *Organometallics* **2002**, *21*, 2076.
- (518) Beste, A.; Frenking, G. *Z. Anorg. Allg. Chem.* **2000**, *626*, 381.
- (519) (a) Ozawa, F.; Hikida, T.; Hayashi, T. *J. Am. Chem. Soc.* **1994**, *116*, 2844. (b) Ozawa, F.; Hikida, T.; Hasebe, K.; Mori, T. *Organometallics* **1998**, *17*, 1018.
- (520) Sakurai, H.; Sugimoto, M. *J. Organomet. Chem.* **2004**, *689*, 2236.
- (521) Stöhr, F.; Sturmayer, D.; Schubert, U. *Chem. Commun.* **2002**, 2222.
- (522) Sturmayer, D.; Schubert, U. *Eur. J. Inorg. Chem.* **2004**, 2658.
- (523) Zeller, A.; Bielert, F.; Haerter, P.; Herrmann, W. A.; Strassner, T. *J. Organomet. Chem.* **2005**, *690*, 3292.
- (524) McGuinness, D. S.; Yates, B. F.; Cavell, K. J. *Organometallics* **2002**, *21*, 5408.
- (525) Matsubara, T.; Hirao, K. *J. Am. Chem. Soc.* **2002**, *124*, 679.
- (526) Wendt, O. F.; Deeth, R. J.; Elding, L. I. *Inorg. Chem.* **2000**, *39*, 5271.
- (527) Sherer, E. C.; Kinsinger, C. R.; Kormos, B. L.; Thompson, J. D.; Cramer, C. J. *Angew. Chem., Int. Ed.* **2002**, *41*, 1953.
- (528) Aullón, G.; Lledós, A.; Alvarez, S. *Angew. Chem., Int. Ed.* **2002**, *41*, 1956.
- (529) Kleiner, N.; Drager, M. *J. Organomet. Chem.* **1984**, *270*, 151.
- (530) Kostic, N. M. *Chemtracts* **2003**, *16*, 42.
- (531) Corral, I.; Mó, O.; Yáñez, M. *New J. Chem.* **2003**, *27*, 1657; see ref 467.
- (532) Boehme, C.; Frenking, G. *Organometallics* **1998**, *17*, 5801.
- (533) Radu, N. S.; Hollander, F. J.; Tilley, T. D.; Rheingold, A. L. *Chem. Commun.* **1996**, 2459.
- (534) Takaki, K.; Kamata, T.; Miura, Y.; Shishido, T.; Takehira, K. *J. Org. Chem.* **1999**, *64*, 3891.
- (535) Horino, Y.; Livinghouse, T. *Organometallics* **2004**, *23*, 12.
- (536) Takaki, K.; Sonoda, K.; Kousaka, T.; Koshiji, G.; Shishido, T.; Takehira, K. *Tetrahedron Lett.* **2001**, *42*, 9211.
- (537) Tardif, O.; Nishiura, M.; Hou, Z. *Tetrahedron* **2003**, *59*, 10525.
- (538) Wang, J. X.; Dash, A. K.; Berthet, J. C.; Ephritikine, M.; Eisen, M. S. *J. Organomet. Chem.* **2000**, *610*, 49.
- (539) Eppinger, J.; Spiegler, M.; Hieringer, W.; Herrmann, W. A.; Anwender, R. *J. Am. Chem. Soc.* **2000**, *122*, 3080.
- (540) Spiegler, M.; Scherer, W.; Anwender, R. *J. Organomet. Chem.* **2002**, *647*, 236; see ref 345.
- (541) (a) Nagl, I.; Scherer, W.; Tafipolsky, M.; Anwender, R. *Eur. J. Inorg. Chem.* **1999**, 1405. (b) Meermann, C.; Gerstberger, G.; Spiegler, M.; Törnroos, K. W.; Anwender, R. *Eur. J. Inorg. Chem.* **2008**, 2014.
- (c) Dietrich, H. M.; Meermann, C.; Törnroos, K. W.; Anwender, R. *Organometallics* **2006**, *25*, 4316. (d) Tardif, O.; Kaita, S. *Dalton Trans.* **2008**, 2531.
- (542) Maron, L.; Eisenstein, O. *New J. Chem.* **2001**, *25*, 255.
- (543) (a) Maron, L.; Eisenstein, O. *Inorg. Chem.* **2002**, *41*, 4363. (b) Perrin, L.; Eisenstein, O.; Maron, L. *New J. Chem.* **2007**, *31*, 549.
- (544) Hieringer, W.; Eppinger, J.; Anwender, R.; Herrmann, W. A. *J. Am. Chem. Soc.* **2000**, *122*, 11983.
- (545) Clark, D. L.; Gordon, J. C.; Hay, P. J.; Martin, R. L.; Poli, R. *Organometallics* **2002**, *21*, 5000.
- (546) Hitchcock, P. B.; Lappert, M. F.; Smith, R. G.; Bartlett, R. A.; Power, P. P. *J. Chem. Soc., Chem. Commun.* **1988**, 1007.
- (547) (a) Braunschweig, H.; Gross, M.; Radacki, K.; Rothgaengel, C. *Angew. Chem., Int. Ed.* **2008**, *47*, 9979. (b) Zhang, Z.; Gu, J.; Zhang, C.; Sun, H. *Organometallics* **2008**, *27*, 2149. (c) Cha, S.-H.; Lee, K.-K.; Kwak, Y.-W.; Choi, H.-J.; Park, Y. S.; Naka, A.; Ishikawa, M. *Organometallics* **2001**, *20*, 3718.
- (548) Clark, C. T.; Lake, J. F.; Scheidt, K. A. *J. Am. Chem. Soc.* **2004**, *126*, 84.
- (549) Tamm, M.; Kunst, A.; Herdweck, E. *Chem. Commun.* **2005**, 1729; see ref 432.
- (550) Yi, C. S.; He, Z.; Lee, D. W.; Rheingold, A. L.; Lam, K. C. *Organometallics* **2000**, *19*, 2036.
- (551) Gilges, H.; Schubert, U. *Organometallics* **1998**, *17*, 4760.
- (552) Temple, K.; Lough, A. J.; Sheridan, J. B.; Manners, I. *J. Chem. Soc., Dalton Trans.* **1998**, 2799.
- (553) Ozawa, F.; Sakamoto, Y.; Sagawa, T.; Tanaka, R.; Katayama, H. *Chem. Lett.* **1999**, 1307.
- (554) Han, L.-B.; Tanaka, M. *J. Am. Chem. Soc.* **1998**, *120*, 8249.
- (555) Suginome, M.; Ito, Y. *J. Chem. Soc., Dalton Trans.* **1998**, 1925.
- (556) Suginome, M.; Ito, Y. *Topics in Organometallic Chemistry*; Murai, S., Ed.; Springer-Verlag: Berlin, 1999; Vol. 3, p 131.
- (557) Lee, Y.-J.; Lee, J.-D.; Kim, S.-J.; Yoo, B. W.; Ko, J.; Suh, I.-H.; Cheong, M.; Kang, S. O. *Organometallics* **2004**, *23*, 490; see ref 424.
- (558) Yoshida, H.; Ikadai, J.; Shudo, M.; Ohshita, J.; Kunai, A. *Organometallics* **2005**, *24*, 156.
- (559) Nikonov, G. I. *Angew. Chem., Int. Ed.* **2003**, *42*, 1335.
- (560) (a) Beletskaya, I.; Moberg, C. *Chem. Rev.* **1999**, *99*, 3435. (b) Suginome, M.; Ito, Y. *Chem. Rev.* **2000**, *100*, 3221.
- (561) (a) Ong, C. M.; Burchell, T. J.; Puddephatt, R. J. *Organometallics* **2004**, *23*, 1493. (b) Bottoni, A.; Higuero, A. P.; Miscione, G. P. *J. Am. Chem. Soc.* **2002**, *124*, 5506. (c) Matsubara, T.; Hirao, K. *Organometallics* **2002**, *21*, 4482.
- (562) (a) Ozawa, F.; Hidida, T.; Hasebe, K.; Mori, T. *Organometallics* **1998**, *17*, 1018. (b) Ozawa, F.; Mori, T. *Organometallics* **2003**, *22*, 3593. (c) Ozawa, R.; Tani, T.; Katayama, H. *Organometallics* **2005**, *24*, 2511.
- (563) Han, L.-B.; Tanaka, M. *Chem. Commun.* **1999**, 395.
- (564) Kondo, T.; Mitsudo, T.-a. *Chem. Rev.* **2000**, *100*, 3205.
- (565) Interplane angle calculated from coordinates for the complex (YAS-QIS in the CDB).
- (566) Chang, K.-J.; Rayabarapu, D. K.; Yang, F.-Y.; Cheng, C.-H. *J. Am. Chem. Soc.* **2005**, *127*, 126.
- (567) Unpublished work cited in ref 264b.
- (568) Sturmayer, D.; Schubert, U. *Monatsh. Chem.* **2003**, *134*, 791.
- (569) Sturmayer, D.; Schubert, U. *Eur. J. Inorg. Chem.* **2004**, 776.
- (570) Pieniazek, S. N.; Clemente, F. R.; Houk, K. N. *Angew. Chem., Int. Ed.* **2008**, *47*, 7746.
- (571) Hoffmann, R.; von Ragué, S.; Schaefer, H. F., III *Angew. Chem., Int. Ed.* **2008**, *47*, 7164.
- (572) (a) Bernskoetter, W. H.; Schauer, C. K.; Goldberg, K. I.; Brookhart, M. *Science* **2009**, *326*, 553. (b) Bernskoetter, W. H.; Schauer, C. K.; Goldberg, K. I.; Brookhart, M. *J. Am. Chem. Soc.* **2009**, *131*, 8603.